Norwegian University of Science and Technology

Department of Energy and Process Technology

HIGH-FREQUENCY PRESSURE MEASUREMENTS IN THE REFINING ZONE OF A HIGH-CONSISTENCY REFINER

Oddbjørn Eriksen

NTNU
Norwegian University of
Science and Technology

Thesis submitted in partial fulfilment of the doktor ingeniør degree

June 2003

URN:NBN:no-6437

URN:NBN:no-6437

ABSTRACT

This thesis is based on an experimental study of the pressure conditions in the refining zone of high-consistency refiners used in paper making. The work presents the findings from two different mill-scale experiments in addition to results obtained from a pilot refiner study. The experiments have been performed using two different types of pressure sensors:

- Fibre-optic pressure sensors based on extrinsic Fabry Perot interferometer (EFPI).
- Piezoresistive temperature and pressure transducers.

This study has shown that it is possible to establish high-frequency pressure measurements in the refining zone of high-consistency refiners. Data have been collected at rates up to 20 million samples per second. The fibre-optic sensors seem to be preferable to the piezoresistive transducers as the fibre-optic sensors were working well after long exposure to the harsh environment inside the refining zone. Reliable measurements were still obtained after 1000 operating hours. On the other hand, the piezoresistive sensors suffered from problems caused by the wet environment inside the refiner as well as from the electrical dependent circuits and transmission cables. However, in the pilot refiner under less harsh environment, the piezoresistive transducer functioned well.

The main focus in this thesis has been related to the second mill-scale experiment which used fibre-optic pressure sensors. The results obtained from this experiment are considered to be more valuable than those from the first mill-scale experiment which used combined piezoresistive pressure and temperature transducers. Furthermore, pulp samples were collected during the second mill-scale experiment allowing an even more comprehensive analysis. However, the results from the first mill-scale experiment are shown as a comparison and in order to demonstrate the challenge of selecting the appropriate technology. Results from a successfully test performed in the pilot refiner, which also used a combined piezoresistive pressure and temperature transducer, are shown as well. In addition, as a supplement to the results from the mill-scale experiment with fibre-optic sensors, an experiment which employed external accelerometers for measuring the high-frequency vibrations in the mill refiner is discussed. Another supplement was made through an experiment measuring the deviation of the rotational speed of the refiner shaft.

The main objective of this study has been to find out how to make high-frequency pressure measurements in the refining zone of a mill-scale high-consistency TMP refiner. The study has particularly focused on the signal analyses and the reliability of the pressure measurements. Since the investigations have been focused on the experimental issues, assessments are primarily made regarding the recorded data and the related process observations.

URN:NBN:no-6437

One of the challenges was to find suitable technology for use in a harsh environment. Obtaining and selecting an appropriate sensor was extremely important. A fast responding sensor was prerequisite. It was of particular interest to investigate the pressure pulses generated from the squeezing of wood particles between the sensor surface and the bars on the opposite disc. In addition, the dimension of the sensor surface had to be small so that the peak pressures could be determined. The size should preferably be smaller than a width of a bar. Especially the fibre-optic sensors met this criterion as they had a surface diameter of approximately 1 mm. The piezoresistive sensors had a surface diameter of 3.8 mm.

Mill-scale experiments were conducted to test the sensors in a realistic environment. The design of the experiments was important in the assessment of the performance of the sensors during different controlled conditions. Collecting of pulp samples to assess the pulp quality of the primary refining in comparison to the process behaviour and the pressure signals were matters of additional interest.

The analyses of the experiment should give conclusions about the reliability of the sensors. A goal of the present work has also been to examine the behaviour and the properties of the pressure signals, and investigate the origin of the pressure pulses.

Most of the results are from high-frequency measurements of pressure in the refining zone of a high-consistency TMP refiner. Combined temperature and pressure measurements are shown from the test in the pilot refiner. The fast development within sensor and computer technology has made it possible to achieve measurements that have not been performed earlier. The use of fibre-optic sensor technology in chip refiners has not been reported earlier. The high-frequency recordings using sample rates of up to 20 MSamples/s suffered from the lack of demodulation technology such that the accuracy of the absolute pressure readings is limited. However, this study indicates average pressures between 20 and 30 bar in the intermediate zone.

Even more interesting is the fast pressure changes obtained using frequency analysis. Common frequencies indicating vibrations in the discs appearing from the pressure pulses when the pulp is squeezed between the bars of the stator and rotor disc have been observed. This observation was supported by vibration analysis using external accelerometers. It is claimed that there is a relationship between vibrations in the refiner discs and the pressure pulses that are generated from the squeezing of pulp between bars on the rotor and stator disc. However, nobody has investigated this particular relationship although this study strongly indicates that this relationship exists. Furthermore, it is shown that the pressure sensors were not affected by vibrations operating in resonance. This strongly supports the conclusion that the fibre-optic pressure sensors were solely measuring the activities in the refining zone.

The frequency analysis of the different recordings gave firm evidence of the process related influences of the pressure readings. The reliability of the performance of the sensors was clearly visible through this analysis technique. Several analyses found that the shift in the bar crossing frequencies was directly proportional to and caused by fluctuations in the rotational speed of the refiner. However, local bar crossing

frequencies were generally not as clear as expected. The measurements indicated that some specific radial positions determined by the tapered plate pattern, dominated the responses. Among the most dominating frequencies were periodicities associated with the rotational speed of the refiner, the number of bars in the breaker bar and coarse zones as well as the transition zone between the intermediate and fine bar zones. When the plates were new, a 25.2 kHz periodicity that arose from a bar-to-bar passage in the fine bar zone dominated the pressure readings. These pulses probably propagated in the disc so that the whole disc vibrated. It is not assumed that these vibrations generated large plate gap variations. However, these fluctuations were predominant compared with the local generated pressure pulses. The pressure variations probably propagated through the steam and pulp pad as pressure waves. Thus the pulp and steam flow through the whole refining zone was affected. The local bar crossing frequencies were suppressed and only visible to a minor extent. It is conceivable that the steam and pulp interacts through a two-phase flow. Thus the steam may have a repressive effect on the interaction between the pulp pad and the bar patterns on the discs.

Recordings during different controlled operating conditions were used to study the reliability of the sensors. The relationship between the pressure signals and the process variables has been investigated as well. The most reliable relationship was obtained when changing the chip flow to the refining zone after 1000 hours of operating time. The motor load and acceleration variables were strongly correlated with the pressure readings. No strong correlations were found between the data from the pressure sensors and the process variables shortly after start-up using new plates. The pulp samples that were collected and analysed did not give a good relationship between the pressure signals and the quality data. However, during this period other process disturbances affected the conditions in the refining zone more than the randomized manipulation of the control variables. This was observed as time dependent variations in the pressure recordings as well as several process variables. The most probable disturbance was the amount of chips fed to the refiner and subsequent changes of the plate gap. Further indications imply that the pressure sensors were sensitive to variations in the incoming stream of chips. Besides the successful test when changing the chip flow to the refining zone, frequency analyses have showed that the sensors also were affected by periodicities in the pulp flow that were related to the inner part of the refining zone and the breaker bar section. This was shown both as sideband effects as well as plain peak frequencies. Sideband effects are interpreted as periodic waves of pulp flow propagated through the refining zone.

This study indicates that the average pressure in the intermediate zone of the refining zone of the mill-scale TMP refiner was as high as 20-30 bar. This was somewhat higher than expected from the theoretical considerations. However, the theoretical calculations have some limiting factors, which there are some disagreement in the literature. The area where the energy is applied in the refining zone as well as the tangential friction coefficient is not clearly determined. Both are included in one of the theoretical approaches. Thus there are some uncertainties associated with the models. However, some uncertainties are related to the determination of the pressure levels for the measurements using the fibre-optic sensors as well. This is mainly due to the lack of

well-established demodulation techniques for the sinusoidal relation between the sensor signal and the pressure. This is the greatest weakness in this part of the investigation.

The pressure levels obtained using the piezoresistive sensors were to some extent agreeable with the fibre-optic measurements. However, there was greater uncertainty in the piezoresistive measurements due to probable disturbances related to electromagnetic noise or moisture having a detrimental influence on electric circuits in the sensors. The most interesting results obtained using the piezoresistive sensors in the mill-scale experiment have been observations of process relevant periodic signal patterns.

Stable average pressures between 2 and 4.5 bar were found in the atmospheric pilot refiner during normal operating conditions. Since the local bar crossing frequency did not dominate the periodicities obtained from these recordings it is assumed that the steam affected the pressure conditions in the refining zone. This is assumed despite the fact that the refiner was atmospheric. Pressure peaks above 10 bar were observed frequently. When the plate gap decreased, the pressure pulses were considerably higher. Pressure peaks up to 60 bar were observed during operation with a small plate clearance. The local bar crossing frequency was clearly visible under such conditions, not otherwise.

PREFACE

This thesis is submitted in partial fulfilment of the *doktor ingeniør* (dr.ing.) degree at the Norwegian University of Science and Technology (NTNU). The work has been carried out at PFI – Norwegian Pulp and Paper Research Institute and Department of Energy and Process Technology, NTNU with Professor Per-Åge Krogstad as supervisor. Professor Erling Hammer, Department of Physics at the University of Bergen and Professor Øyvind Gregersen, Department of Chemical Engineering, NTNU have been engaged as co-supervisors.

Planning of the work started in the autumn in 1997 as a result of discussions between Göran Dahlqvist, the former head of the Mechanical Pulp Department in Norske Skog Research, Alfred Holmberg, Norske Skog Skogn, Professor Torbjørn Helle, Department of Chemical Engineering, NTNU and the late Professor Odd Andreas Asbjørnsen, Department of Thermal Energy and Hydro-Power. Professor Asbjørnsen was the first supervisor of this study.

Norske Skog ASA has been the main industrial partner in this project. The mill-scale experiments have been conducted at the Norske Skog Follum mill where Erik Muggerud, head of the TMP plant, and his co-workers have made it possible to accomplish the experiments. The first experiment was carried out in December 2000, while the second mill-scale experiment was performed in February 2002. During planning, performing and assessment of the last mill-scale experiment Norske Skog Research through Jan Hill, the head of the Mechanical Pulp Department and senior R&D engineer Karl Mosbye have been strongly involved. Furthermore, J&L Fiber Services Inc. has contributed to a large extent in the experimental work through Technical Director Ola Johansson and his co-workers. The project has further received financial support from the Research Council of Norway through the PROSMAT programme between 1998 and 2001.

The topic of the thesis was considered relevant to the pulp and paper industry as well as the plate manufacturer since the knowledge of the pressure conditions in the refining zone of high-consistency refiners was limited. Atack and Stationwala (1975) were pioneers within this field. However, further experimental investigations about this issue have been limited due to the difficulties associated with the pressure measurements. The fast development within sensor and computer technology has made it possible to achieve new and valuable results. Despite the academic and scientific form, the results should primarily lead to increased interest and improved knowledge of the prevailing conditions inside the refiner. Plate geometry improvements as well as improved solutions for chip feeding may be the prime results. This may lead to improvements in the operating conditions and energy savings as well as the possibilities for composing more tailor-made pulps.

ACKNOWLEDGEMENTS

I would like to express my deepest respect for my first supervisor, Professor Odd Andreas Asbjørnsen, who died 26th May 1999 only 68 years old. His family lost a warm and friendly father. His encouragement and scientific support has been of great value for me.

I will express my greatest thanks to my present supervisor, Professor Per-Åge Krogstad, Department of Energy and Process Technology, NTNU, for his contribution and help during the course of this work.

The author is indebted to Professor Erling Hammer, Department of Physics, University of Bergen and former head of the Paper Department at the Norwegian Pulp and Paper Research Institute, Professor Øyvind Gregersen, Department of Chemical Engineering, NTNU, for their scientific advice, discussions and inspirations through this study.

A special recognition is given to Karl Mosbye, senior R&D engineer at Norske Skog Research for stimulating discussions, invaluable advices and good friendship. Karl has been my nearest professional colleague during this work despite the distance of 700 km between our offices.

Jan Hill, head of the Mechanical Pulp Department in Norske Skog Research, is recognized for his interest and participation in this project. His enormous professional skills have been of great value for the outcome of this project.

Without the contribution from Ola Johansson, Technical Director in J&L Fiber Services, Inc. and his co-workers, the last and most valuable mill-scale experiment would not have been conducted. I am grateful for J&L's contribution. Ola Johansson is recognized for his engagement and participation.

Erik Muggerud, head of the TMP plant at Norske Skog Follum, and his present and former co-workers are acknowledged for their participation in this project.

I would also like to express my thanks to Luna Innovations, Inc. through Steve Poland, Trevor Rice, Clark Boyd and their co-workers for making tailor-made fibre-optic sensors and for their contribution in the second mill-scale experiment.

The author has received financial support from Norske Skog ASA and the Research Council of Norway through the PROSMAT programme. This financial support is gratefully acknowledged.

Professor Emeritus Torbjørn Helle, Department of Chemical Engineering, NTNU, Göran Dahlqvist, former head of the Mechanical Pulp Department, Norske Skog Research, Alfred Holmberg, Norske Skog Skogn and former head of the Mechanical Pulp Department at PFI, Ingunn Omholt are acknowledged for their support in the early part of this project.

English language adviser, Stewart Clark, Office of International Relations, NTNU, is thanked for his editing work and his tips on English usage.

Lars Strand, Norske Skog Skogn has been to great help in translating articles from French. He is acknowledged for support and good friendship.

Andritz, Inc. through Nichlas Kavander and Michael J. Kraft is acknowledged for obtaining and permitting me to print sketches and images of the Twin refiner, plates and other process equipments.

I would like to thank all my present and former colleagues at PFI for making the inspiring atmosphere at the institute. Trond Karlsen and Iver Johnsen are in addition acknowledged for their support during the pilot refiner trials. I would also express special thanks to John Mosbye and Lars Johansson for their social attitude and friendship.

Former colleagues and superiors, Dag Arne Skjærholt, Christen Jønsberg and Gunnar (GW) Pettersen are acknowledged for contributions in the early stage of the project and for their friendship.

I am especially grateful for support from my nearest family. My dear wife Anne Kirsti and my lovely children Mari (9) and Helle (5) have maintained a warm and lovely home.

TABLE OF CONTENTS

CHAPTER 6

CHAPTER 7

CHAPTER 8

NOMENCLATURE AND DEFINITIONS

Nomenclature

A/D	Analog-to-digital converter
BNC	Coaxial cable connector
CAN	Controller Area Network
DAQ	Data acquisition card
DC	Direct current (voltage)
DCS	Distributed control system
CP	Centre point
DS	Drive (motor) side of the refiner
EFPI	Extrinsic Fabry-Perot Interferometer
F1, F2, F3	Flange number
FFT	Fast Fourier Transform
FOSS	Fiber Optic Support System
FS	Front side of the refiner
I/O	Input-Output card
LSB	Least significant bit
LSC	Load sense conveyor
LWC	Lightweight coated paper grade
MS-DOS	Microsoft Disk Operating System
NA	Not available
NI	National Instruments
PCI	Peripheral component interconnect (bus architecture)
PHD	Process history database
pmf	Probability mass function
PQM	Pulp quality monitoring
PXI	PCI extensions for instrumentation
RMP	Refined mechanical pulp
ROP	Type of the pilot refiner manufactured by Defibrator
rpm	Revolutions per minute
rps	Revolution per second
SC	Uncoated super calendared magazine paper
SNR	Signal-to-Noise ratio
TMP	Thermomechanical pulp

Definitions

- The two terms sensor and transducer are not differentiated. In this study they mean the same. They are both used to describe the same part of the measurement equipment. Physically they describe the small piece that incorporates the surface, sensing element, as well as the housing from which the signal transmission cable is led. Furthermore, the term sensor signal or the transducer signal is understood as the signal that is captured from the amplifier unit. This appears as a voltage output signal.
- Pressure values are given in relation to atmospheric pressure, which is denoted gauge pressure. Thus zero bar is atmospheric pressure.

CHAPTER 1

INTRODUCTION

1.1 Background

A more detailed knowledge about the basic properties in the refining process is required because the thermomechanical pulping (TMP) process determines the properties of wood containing printing paper to a large extent. Primarily the quality of the mechanical pulp fibres affects the paper through surface smoothness and optical properties. In addition, the refining process is an expensive process in the pulp and paper industry due to its considerable primary energy consumption. The recovery rate of the steam makes the total account less cost demanding. However, improvements in both the pulp quality and the energy efficiency are sought. A prerequisite here is to improve the control of the refining operation, which will require better understanding of pulp flow behaviour and the refining action between the discs in the refiner.

Basic controllers for freeness and consistency are commonly used. However, as there is still a lack of control strategies, this makes the refiner operation exposed to large variations. It is common that refiners have frequent load variations with a coefficient of variation of more than five per cent. Thus, short-term load variations of large mill-scale refiners can be higher than 2 MW peak-to-peak. Such variations obviously affect the quality of the produced pulp. Extensive and frequent variations are also a challenge to control. Since the lack of well-fitted measurements is the main drawback, improvements are impossible until the fundamental variables can be measured. In addition, high frequency measurements are necessary to gain fundamental knowledge and improve theoretical models of refiner behaviour.

Pressure measurements in the refining zone of high-consistency refiners are important for the development of theoretical models that can be used in control strategies. The lack of experimental investigations regarding pressure measurements despite their importance represents a challenge. More than 25 years have passed since the first and only report from an experimental study of pressure measurements in a high-consistency refiner was published by Atack and Stationwala (1975). In experimental studies, others have followed different and spectacular approaches to gain more detailed knowledge about the secrets of the refining process, for instance the residence time measurements reported by Ouellet *et al.* (1995b) and Härkönen *et al.* (2000). A lot has changed since Atack and Stationwala presented their work. The fast developments within sensor and

computer technology make previously unsolved tasks possible and past challenges are now addressable using improved equipment.

1.2 Objectives of the study

The main objective of this study has been to find out how to make high-frequency pressure measurements in the refining zone of a mill-scale high-consistency TMP-refiner. The study has particularly focused on the signal analysis and the reliability of the pressure measurements. It has mainly been an experimental study, which means that assessments are made primarily regarding the recordings and the related process observations. Extensive theoretical judgements or model considerations are not included in this work.

The main objective can be split into three goals:

- Goal number one was to find suitable technology for use in the harsh environment. Here obtaining and selecting an appropriate sensor was extremely important. Fast responding sensors were required such that the expected pressure pulses generated from the squeezing of wood particles between the sensor surface and the bars on the opposite disc could be detected. In addition, the dimension of the surface of the sensors had to be small so that the peak pressures could be determined. The size should preferably be smaller than the width of a bar. In connection with the fast responding sensors, high-speed data acquisition board and sufficient data storage capacity were also necessary.
- Goal two was that a mill-scale experiment should be planned and completed. The design was important in the assessment of the performance of the sensors under different and controlled conditions. Collecting of pulp samples to assess the pulp quality of the primary refining in comparison to the process behaviour and the pressure signals were matters of additional interest.
- Goal three was that the analyses of the experiment should give conclusions about the reliability of the sensors. The present work has examined the behaviour and the properties of the pressure signals and investigated the origin of the pressure pulses. It was of particular interest to assess the contribution from the steam pressure and from the mechanical pressure generated by the pulp pad. Another matter was to investigate the pulp flow behaviour through an appropriate design of the location of the sensors and using cross-correlation analysis. This investigation was necessary to assess the pulp flow movement between different locations in the refining zone. The interrelation obtained from the cross-correlation can be used in the determination of the velocity and direction of the pulp flow or the pressure wave propagation between two simultaneously captured sensor signals.

A further objective was to simultaneously measure the temperature in the refining zone and examine the relationship between the measured pressure and temperature. This investigation was done in order to assess the water vapour pressure. The goal was to find out whether there were saturated or superheated conditions in the refining zone.

1.3 Outline of the thesis

This thesis presents the findings from two different mill-scale experiments in addition to the results obtained from a pilot refiner study. Two different types of pressure sensors have been tested. These are respectively based on piezoresistive and fibre-optic technology. The main focus in this thesis has been on the mill-scale experiment where fibre-optic pressure sensors were used. The results obtained from this experiment, which was the second mill-scale experiment, are more valuable than the results from the other mill-scale experiment using combined piezoresistive pressure and temperature transducers. It is assessed whether the behaviour of the fibre-optic sensors was better than the piezoresistive transducers. The behaviour of the latter sensors was related to uncertainties associated with influence of power hum and moisture. Furthermore, pulp samples were collected and variations of the rotational speed of the refiner shaft were captured during the second experiment allowing an even more comprehensive analysis to be made. However, the results from the first mill-scale experiment are shown as a comparison and demonstrate the challenge in selecting the appropriate technology.

The results from a successful test made in the pilot refiner, using a combined piezoresistive pressure and temperature transducer, are also presented. In addition, as a supplement to the results obtained from the mill-scale experiment containing fibre-optic sensors, an experiment is discussed that used external accelerometers for measuring the high frequency vibrations in the mill-scale refiner.

Chapter 2 reviews the most relevant literature covering the following main topics:

- Fundamental mechanisms in thermomechanical refining.
- Theoretical approaches of the pulp flow behaviour in the refining zone.
- Refining zone measurements with the focus on pressure and vibration. Few pressure measurements in high-consistency refiners are reported, and therefore similar measurements made in low-consistency refiners are presented.

Chapter 3 comprises descriptive information about the refiners and sensors. Plate patterns and sensor locations are discussed. Overviews of the experimental procedures of the experiments are also given. Theoretical estimates of the expected pressures in the refining zone are also discussed in this chapter. The data analysis methods that have been used are described as well.
Chapter 4 discusses the results obtained in the first mill-scale experiment using piezoresistive sensors.
Chapter 5 discusses the results obtained in the test performed in the pilot refiner where data were collected from one single combined piezoresistive pressure and temperature transducer.
Chapter 6 comprises results and discussions related to the pressure measurements using the fibre-optic sensors. Thus the main part of the experimental work is treated in this chapter.
Chapter 7 gives the results obtained using external accelerometers in the investigation of vibrations in the refiner. Chapters 6 and 7 are closely related since both of the experiments were carried out when the refiner was using the same plates.
Chapter 8 summarizes the major conclusions of this study,
Chapter 9 deals with proposals and improvements for further work.

CHAPTER 2

OVERVIEW OF THEORY AND RELATED EXPERIMENTAL STUDIES

2.1 Introduction

The thermomechanical refining process is the dominating process for the production of pulp for wood containing paper. Mechanical pulps constitute the main component in newsprint and in higher grades both uncoated magazine paper (SC-paper) and coated grades like LWC. The objective for the TMP process is to break down wood into pulp of smaller particles. Fibres constitute the main part of the pulp and further development of the fibres makes them well suited for papermaking.

The main constituent parts of the TMP process are the refiner and the wood chips. The refiner is restricted to its dimensions and running conditions. The wood chips have material properties that determine their behaviour in the refiner. The interconnection between the properties and behaviour of the refiner and the wood chips lead to the energy-quality relationship in the created pulp. The prevailing theories and mathematical models describe this interconnection.

General descriptions of the TMP process are covered well in textbooks such as Sundholm (1999) and Kappel (1999). The following literature survey is particularly focused on the two constituent parts and the link between them. The refiner is deemed as the operating unit determining the peripheral frame, while the wood chips determine restrictions related to interior framework. The interconnection is reflected through discussions about the properties of the pulp behaviour in the refining zone during influence of cyclic compression and shear forces. This discussion will give an overview of the prevailing knowledge about this part of the TMP process. The focus is related to the origin and the level of the pressures both as static and high frequency components.

2.2 Wood chips

The discussions about the wood chips are mainly connected to their internal properties as a viscoelastic material and their behaviour during refining. Although, a lot of prominent scientific work has been made in the field of wood, mechanical pulp and fibre characterization, these themes are not discussed in this thesis. Among the studies within that field, the following can be mentioned: Rydholm (1965), Forgacs (1963), Karnis (1994), Höglund *et al.* (1976, 1997), Stationwala *et al.* (1979, 1991, 1993), Corson (1989, 1997), Corson *et al.* (1996, 1997), Mohlin (1997), Heikkurinen *et al.* (1993), Sabourin *et al.* (1997, 2002), Tyrväinen (1995a, 1995b, 1997a, 1997b), Braaten (1996), Kure (1999) and Reme (2000).

The wood material response to mechanical treatment is greatly affected by temperature, moisture and time under load. Under water-soaked conditions it is the lignin softening that is important since the cellulose and hemicellulose parts of the fibres are softened already at room temperature (Salmén *et al.* (1983)). It is well known that at conditions above the softening temperature of lignin the force required to cause rupture in the wood structure decreases drastically (Koran (1981). Arne Asplund utilized this effect during development of the process for fibreboard production in 1930s (Höglund *et al.* (1997), Asplund (1953)). The fibres can be separated from each other without being damaged too much providing the lignin is partly softened. Then the main separation appears in the lignin rich parts of the fibres. The degree of softening is influenced by temperature, moisture and frequency of strain. The glass transition of lignin in water-saturated spruce occurs at approximately 80 ∀C (Björqvist *et al.* (1997)). With increasing frequency, which occurs in refining, the lignin softening is shifted to even higher temperatures. When the wood is heated beyond 140 ∀C, the viscoelastic behaviour of wood changes gradually to plastic. According to Koran (1981) the separation energy has the steepest decreasing trend between 150 ∀C and 170 ∀C. Problems occur if the refining process keeps the pulp at too high temperature for too long time so that the lignin is transformed to plastic conditions. When the lignin is too soft defibration occurs to a large extent in the middle lamella, and when the temperature decreases the fibres are covered with lignin. The lignin will thus be deposited as a *lignin-suite* outside the fibre. The high temperature darkens the pulp. In addition, the fibres lose the much-needed fibre-bonding properties (Sundholm (1999, Ch. 4)).

Salmén and co-workers have contributed to a large extent in the development of the research related to deformation properties of wood in recent decades. They have studied the fatigue properties of wood, which imply the study of permanent structural changes in the wood under plastic deformation. The viscoelastic character of wood describes how energy is absorbed in large plastic deformations and in small reversible viscoelastic deformation. Only a small portion of the energy is used in the structural deformations of the wood, while to a large extent the energy is transferred to heat through the viscoelastic character of the wood (Salmén *et al.* (1983)). Leider and Nissan (1977) have stated that 98.5 % of the energy used in the refining is transformed into heat. The rest is used to increase the pressure and the pulp velocity. Salmén *et al.* (1997) estimated that 10000 repeated compressions consume approximately the same amount of energy as consumed in commercial refiners. Estimation by Miles (1991) indicates a

corresponding number of impacts on fibres in refining. The role of the wood as a heterogeneous material composed of thick-walled latewood fibres and thin-walled earlywood fibres should also get attention due to different requirements during refining such as the required number of impacts needed to make fibres well suited for papermaking (Salmén *et al.* (1997)).

Previous conclusions made by Salmén and co-workers (1983) and Salmén and Fellers (1982) are that the higher the stress amplitude the fewer cycles that are needed to failure. It is also claimed that, above a certain amplitude limit, the breakdown of the wood per cycle is greater in the first cycle. Also Thiruvengadaswamy and Ouellet (1997) found that the elastic modulus was strongly reduced after the first cycle in a laboratory test. In addition, the higher the frequency, the higher the softening temperature of the polymer. Measurements at different frequencies between 0.2 and 20 Hz show a shift of the mechanical loss maximum towards higher temperatures of approximately 8.5 ∀C per decade of frequency (Salmén and Fellers (1982), Becker *et al.* (1977)). This should indicate a shift in the glass transition of the wet lignin by approximately 40 ∀C while the frequency of the load is in the range of 20 kHz.

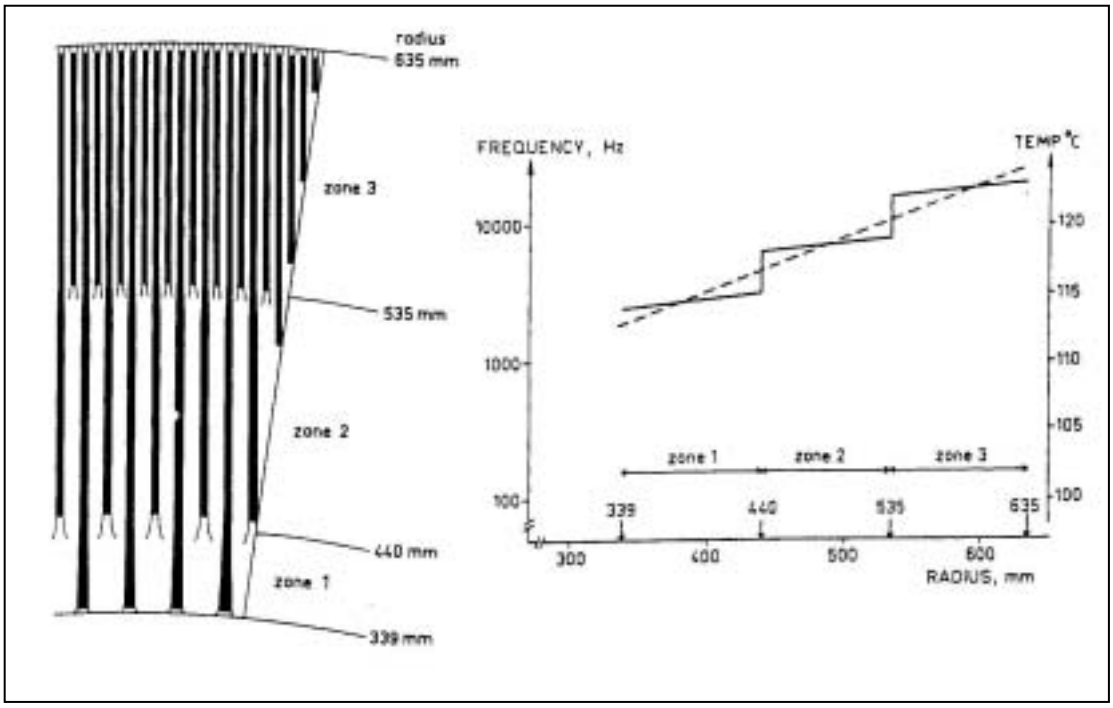

Figure 2.1: A typical refiner plate pattern together with a frequency-temperature relationship as a function of the radius reported by Becker *et al.* (1977).

The bar-crossing frequencies in commercial single disc refiners are increasing along the radius from some few hundred Hertz at the inlet to beyond 25 kHz at the periphery. In double disc refiners the frequencies are twice as high when assuming the same disc size and plate patterns. The latter is true for Europe where all motors operate at 1500 rpm. In

North America, single disc refiners generally run at 1800 rpm, and double disc refiners have 1200 rpm motors, so the ratio is not 2:1 here, but rather 4:3. However, a rise in frequency has to be compensated for by a rise in temperature to maintain the same efficiency in structural breakdown. This is due to the fact that the stiffness of the viscoelastic fibre material increases as a function of the square of the frequency, while a temperature rise decreases the stiffness (Höglund *et al.* (1973)). It is further claimed by Höglund *et al.* (1973) that an increase in frequency leads to an increased energy loss only when the wood particles are held at a temperature somewhat above the transition temperature.

The results from an experimental study performed by Johansson *et al.* (2001) indicated that both the energy requirements and the pulp quality were improved when the temperature-frequency relationship followed the theoretical assumptions. The particular case aimed to decrease the temperature in the early stage of the refining zone where the frequencies related to the bar-to-bar passage is relatively low. The opposite action through increasing of the temperature was performed in the outer part of the refining zone where the bar crossing frequency is high.

Sundholm *et al.* (1987) tested the role of rate of rotation and frequency in refiner mechanical pulping. It was claimed that the frequency of the impacts of the bars acting on the wood substance in refining appears to be of great importance with respect to defibration. They found that an increase in the rate of rotation of the disc reduces the energy consumption. This was primarily due to the resulting increase in impulse moment of the bars. It could also be related to the higher contribution from the force connected to the centripetal acceleration. However, increasing the impact frequency of the bars that were changed by the plate pattern (more bars per radian of the disc) gave the opposite effect, but to a smaller extent.

A contrary proposal concerning reduced impact frequency from the bar movement was proposed by Gullichsen (1989). He claimed that a new refining concept where the steam from the heating caused by the energy losses in the refining of the viscoelastic wood, was separated already in the refining zone could benefit through longer residence time of the pulp. Together with adapted refining plates such that the impact frequency was decreased this refining concept could save significantly amount of energy. The new design was proven as a pilot project in the middle of the 1980s (Gavelin *et al.* (1996)).

When considering the frequencies that the pulp is exposed for through cyclic compressions it is clear that the highest frequencies are operating in the lower region of the ultrasound frequency area. Originally mechanical pressure pulses have arisen from these bar-crossings actions, which in turn generate pressure waves that appear as sound waves. In the outer part of the refining zone it should be expected that ultrasound waves are present. It can be considered that the high-frequency mechanical pressure and the propagation of the pressure waves are two interdependent and in basic different modes. However, without discussing the origin of ultrasound in detail or how the two different modes influence the defibration, it should be mentioned that ultrasound itself contributes to internal fibrillation (Giertz (1964)). Moreover, ultrasound treatment of wood material implemented in defibration processes is described in the literature. In

1977 Laine and co-workers summarized the use of sonic and ultrasonic energy for this purpose (Laine *et al.* (1977)).

2.3 Refining mechanisms

The refining of wood chips is an empirically developed process. During the last 40 years a lot of research have been made to identify the real mechanisms of the refining action. Since Luhde (1962) proposed his theory Atack and co-workers (1963), (1980), (1981), (1983), (1989) have further developed the main ideas. This is later visualized and enhanced by other studies reported by Stationwala *et al.* (1992), Ouellet *et al.* (1995a) and Alahautala *et al.* (1999). The prevailing main opinion about the refining action in a first stage refiner is about as follows:

Wood in the form of chips is feed into the first stage refiner using a plug screw. This is a volumetric feeding process and the flow rate is determined by the speed of the plug screw. The feeding of chips is done through the centre region of the refiner along the rotational shaft. The wood chips are broken down into coarse fibres and shives already ahead of the breaker bar section. Considerable recirculation of fibrous materials occurs in the breaker bar section influenced by the back flowing steam. Fibres and agglomerates of fibres also termed as flocs[1] are stapled in a tangential orientation on the bars in the coarse zone before they are further defibrated and developed in the fine bar section.

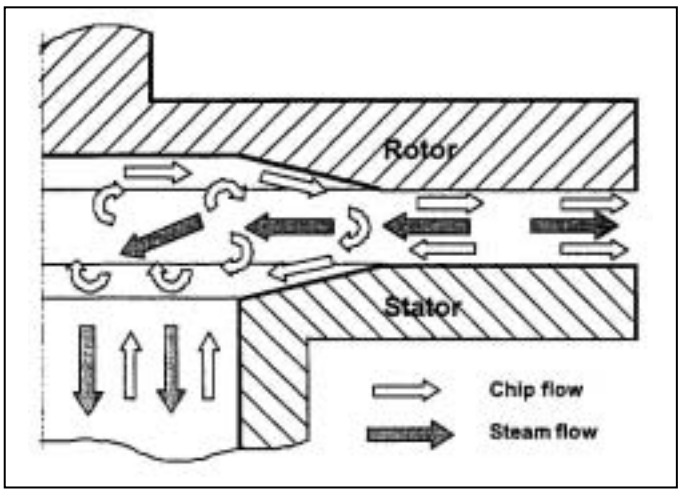

Figure 2.2: This sketch of the refining process shown by Härkönen and Tienviere (2001), illustrates the fibre and steam flows that appear in the refining.

[1] According to Hietanen and Ebeling (1990) references to fibre flocs and flocculation effects have appeared in the literature since the 1920s. A chronological overview is made in this reference.

In single disc refiners the main material flow follows a spiral form out of the refining zone influenced by radial directed forces and imposed by shear from the rotating disc. However, it is assumed that fibres and flocs are stapled to the rotor bars in short time periods (Atack (1980), Ouellet *et al.* (1995a)). Thus, it is expected that the fibre flow is a randomised process that proceeds in leaps and bounds.

The papermaking fibres are made by repeated or cyclic influence of compressive and shear forces executed by passing bars of the rotating disc. The changes in fibre morphology have been studied in detail by several researchers. The main opinion is that the primary refiner is largely responsible for establishing the characteristic properties of the papermaking pulp (Karnis (1994), Stationwala *et al.* (1993), Heikkurinen *et al.* (1993)). According to Karnis (1994), the refining process can be considered as consisting of two main actions. These are the fibre separation and the fibre development stages. The first action appears early in the process, in the innermost part of the primary refining stage. The fibre length seems to be determined by the actions that appear already in the first stage (Corson and Ekstam (1995), Karnis (1994), Mohlin (1997)). The second action starts in the small plate gap in the primary refiner and continues in the second stage. Most of the energy that is consumed in the refining is used to develop the fibres such that the pulp is suitable for papermaking. Fibre development involves decreasing of the fibre wall thickness through efficient delamination or fibrillation. Johnsen *et al.* (1995) proved the decrease in cross-sectional area of the fibres. The peeling of material from the fibre surface will increase the fibre flexibility and the degree of bonding in the sheet. Abundant fines in the length proportion of 1-50 μm generated from the peeling off from the middle lamella and the outer fibre wall layers provides good optical properties because of their light scattering properties. Pulp strength and optical properties of mechanical pulps are governed by fibre length and fibre bonding ability, as shown by Forgacs (1963).

2.3.1 Theoretical approach

Despite a general opinion about the main refining mechanisms the prevailing theoretical model about the pulp flow behaviour in the refining zone is the object of discussion. A theoretical model was established by Miles and May during the late 1980s (Miles and May (1990), (1991)). In some reports this work is termed as the Paprican model. However, the authors use one of the following terms: the Miles and May model or the Miles and May equations (May (1998)). This model is widely accepted as a theory that has furthered the understanding of the refining. Miles and May were honoured for their scientifically work through the Marcus Wallenberg award in 1998. Their speeches from this event are reported as May (1998) and Miles (1998).

Among the criticisms that are raised against the Paprican model is that it is only concerned with steady state operation and thus neglects dynamic effects (Fan *et al.* (1997)). In addition, several measurements of the residence time of the pulp in the refining zone show discrepancy with the calculated residence time (Murton *et al.* (2002), Härkönen *et al.* (2000), Ouellet *et al.* (1995b)). However, the discrepancy shown in the latter reference was explained through the use of kraft pulp (Senger *et al.* (1998)). Härkönen and Tienvieri (2001) claimed that the descriptions of TMP refining so far have been made using empirical terms. In their paper, Härkönen and Tienvieri

(2001) have proposed a set of equations describing the phenomena in the plate gap by using unambiguous physical concepts. Moreover, Allison *et al.* (1995) have found divergence between the Paprican model and their simulations regarding the steam pressure profile. While Isaksson *et al.* (1997) and Senger and Ouellet (2002) show discrepancies between the size and distribution of friction forces in the model compare with their independent studies. In addition, Sabourin *et al.* (2001) claimed that the model is restricted for practical use because of too many unknown factors and the limited ability to predict pulp properties.

Because of the Paprican model's rigorous approach in the understanding of the refining mechanisms it is useful to discuss it even closer. In this study the prevailing theory will be contrasted with other opinions and experimental experience to come closer to the main aspect as the proportion of the pressure in the refining zone.

The high-consistency refining process is built on knowledge generated in connection with low-consistency refining and beating of chemical pulp a couple of decades before the first high-consistency refining plant was developed. In 1968 the first TMP plant was started (Leask (1981)). Fundamental researchers in the field of low-consistency refining were Wultsch and Flucher. They were the originators of the well-known specific edge load theory, which is a tool to calculate the intensity of the refining (Wultsch and Flucher (1958)). Another widely used theory is the C-factor developed by Kerekes (1990). The C-factor is used to estimate the number and intensity of impacts imposed on fibres. According to Welch (1999), high-consistency refining can be seen as a specialized case of the C-factor application. There is no further presentation of models which are developed in connection with low-consistency refining. General views on the different theories are given in Welch (1999), Baker (1995), Stevens (1992) and Pearson (1990). The papers by Leider and Rihs (1977) and Leider and Nissan (1977) also contain comprehensive mathematical analysis regarding the low-consistency disc refiners.

The theories and mathematical analyses behind the low-consistency refining process are interesting. However, according to May *et al.* (1988) and Sundholm (1999, Ch. 7) the approaches used in the low-consistency refining theories cannot be applied to chip refiners because of major differences in the processes. One of the most important differences is that the refining zone in a low-consistency refiner is filled with water in which the pulp is dispersed. The flow of pulp through the refiner is determined by the flow of water. The refiner acts like a low speed, low efficient centrifugal pump and the pulp slurry behaves like a Newtonian fluid (Leider and Rihs (1977)). The plate gap clearance is much smaller in the low-consistency refiners. Typical gap sizes in low consistency refiners are 0.06-0.2 mm (Martinez *et al.* (1997)). In high-consistency refiners the gap is approximate ten times wider. According to May *et al.* (1988) the refining zone in a chip refiner can never be packed full of pulp because much of the available volume is filled with the copious amount of steam produced by the process. Gullichsen (1989) stated that 99.5 % of the volume between the refiner plates is occupied by steam. As for the rest, the steam and the pulp in a high-consistency refiner travel at different speeds and even in opposite directions in the inner part of the refining zone. In large refiners the speed of steam leaving the refining zone at the periphery

approaches sonic velocity (Miles *et al.* (1980)) or even higher (supersonic) as claimed by Newman *et al.* (1985).

The Paprican model is associated with the flow of pulp in the refining zone of chip refiners. Miles and May introduced the concept of refining *intensity* at the same time (Miles and May (1990)). The equation for the radial velocity of the pulp in a high-consistency refiner is based on theoretical calculations of the forces that influence the flow of pulp. According to the authors, the mathematical analysis is based on knowledge, which was obtained by use of high-speed photography as shown by Atack *et al.* (1983). The mathematical model consists of hydrodynamic as well as aerodynamic considerations. The result of this analysis is a set of equations that connects the radial velocity and the residence time of the pulp to the refiner's design and operation parameters.

Miles and May focus on the residence time as an important parameter. They claim that the number of impacts between the fibrous material and the bars on the plates depend on the time the material needs to pass through the refining zone, the volume between the plates, the plate pattern and the rotational speed of the refiner. The residence time only depends on the radial component of the velocity of the fibrous material. The radial velocity of the pulp is deduced from three forces: the centrifugal[2] force, the friction forces and the drag force from the steam flow. The net accelerating force on the pulp in radial direction is given by Equation (2.1).

$$F = C + F_{r1} + F_{r2} + b \cdot S \quad ; [N] \tag{2.1}$$

C : *centrifugal force [N].*
F_{r1} : *Radial friction force between pulp and disc 1(stator); [N].*
F_{r2} : *Radial friction force between pulp and disc 2 (rotor); [N].*
S : *Drag force on the pulp from the steam; [N].*
b : *Steam force direction coefficient (+1 in outer part where the steam is flowing forward, 0 at stagnation point and -1 in inner part).*

The forces acting upon the pulp as deduced by Miles and May are illustrated in Figure 2.3.

Steam force
The theory of steam flow in chip refiners consists of equations which describe the generation and subsequent velocity of the steam in the refining zone. The pressure and temperature gradient that develops there are described as well. The theory also comprises the interference of the pulp in the refining zone to the flow of steam. Dana *et al.* (1975) developed a preliminary theory, while an extended version was attempted by Miles *et al.* (1980).

[2] According to general literature within physics the term centrifugal is just a convenient concept. The pertinent concept is that the particles move as a result of influence by an effective potential energy derived from the conservation of angular momentum (Alonso and Finn (1980)).

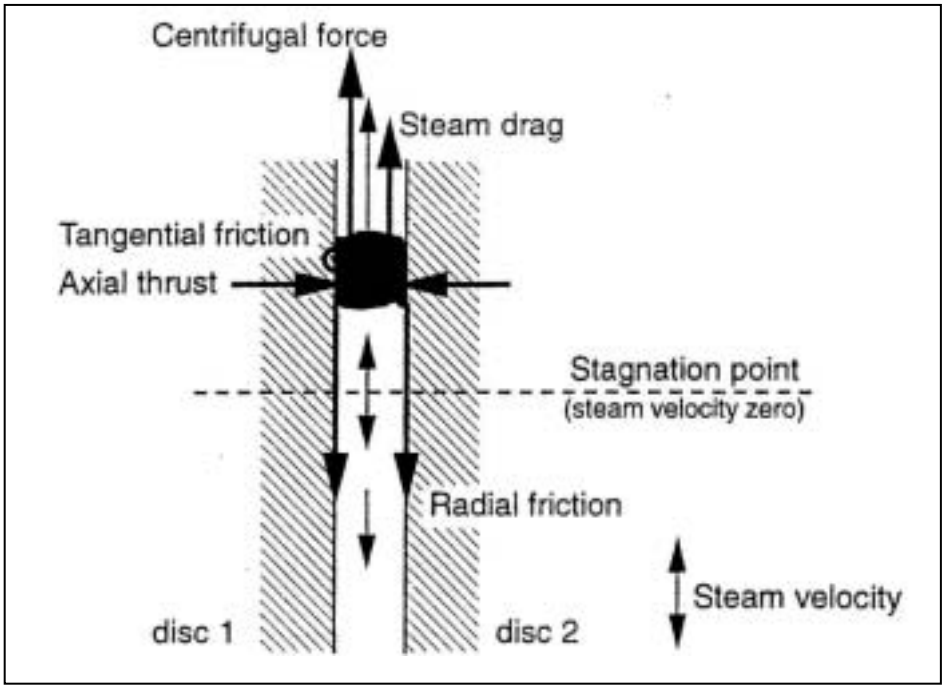

Figure 2.3: The forces acting upon the pulp in the refining zone as shown by May (1998).

The steam flow is a driving force in the outer part of the refining zone where the pressure in the radial direction is decreasing from a maximum pressure peak. In the inner refining zone, the pressure is increasing in a radial direction until a maximum pressure peak is obtained. This is the force from the steam flow acting against the pulp flow. It is claimed that the amount of back-flowing and forward-flowing steam in commercial refiners is remarkably balanced (Miles *et al.* (1980)). The point between the inlet and the periphery of the refining zone where the maximum pressure is obtained and the steam velocity is balanced to be zero is called the stagnation point. Miles and May claim that the location of the stagnation point is quite stable in spite of different process variations. Engstrand *et al.* (1995) indicated that the stagnation point is shifted inwards as the plate clearance decreases.

According to Miles and May the structure of the fibrous material is a dynamic network that changes continuously. This ensures a uniform application of total energy to the fibres in the network. However, it is claimed that the distribution of energy is uniform in the effective part of the refining zone. The fine bar area is assumed to be excluded from this effective part (Miles *et al.* (1980)). Miles and May (1990) also assume that all the dilution water is absorbed in the network and does not separate despite of the centrifugal forces acting on it. Thus, the centrifugal force depends on the consistency of the pulp. The generated steam is assumed to penetrate the network. There is cyclic variation in the forces acting on the pulp because of the volume variation created by the bar and groove position on the plates on the two opposite discs. When a bar is opposite a groove it is expected that some of the forces will be reduced, depending on the amount

of packed pulp trapped in the groove. In the Paprican model these cyclic variations are averaged, and a mean value of the forces acting upon the pulp is used.

The drag force from the steam is influenced by parameters such as the plate gap, plate taper, plate pattern and degree of filling in the grooves. Compressibility of the fibre network is an implicit determining factor. It affects the plate clearance needed to draw a given amount of specific energy. The steam drag force is shown as Equation (2.2).

$$S = \frac{1}{2} \int C_f \int \psi_s / r 0 \int U(r)^2 \int A_p(r) \int dm(r) \qquad ; [N] \tag{2.2}$$

C_f : *frictional drag coefficient of steam on pulp; [kg^{-1}].*
$\psi_s(r)$: *density of the steam at radius r; [kg/m^3].*
$U(r)$: *velocity of the steam at radius r; [m/s].*
$A_p(r)$: *aerodynamic specific surface of the pulp; [m^2].*
$dm(r)$: *oven dry mass of pulp in the annulus dr; [kg].*

According to Miles and May (1990) the steam flow term in the analysis is the most complex factor. It is derived from Navier-Stokes equations and the Kozeny-Carman equation. This matter is considered further in Miles *et al.* (1980) and Dana *et al.* (1975). The effect of the steam velocity can be derived from the steam flow equations, which is treated in the above references. Using the steam flow equation depends on knowing the plate gap and the temperature distribution through the refining zone. According to Sundholm (1999, Ch. 4) the steam flow model only concerns the rotor and it is one-dimensional, describing the motion in the plate gap in a radial direction. The authors claim that studies have shown that the predicted values of self-pressurization, which are pressure generated in the steam, are close to the measured values. The results suggest that the depth of the pulp packing in the grooves has an important effect on the amount of self-pressurization and further on steam flow in the refining zone.

Results from a study reported by Allison *et al.* (1995) indicated a bad fit between the model and simulated data regarding the steam pressure profile across the refining zone. The authors indicated that three circumstances could lead to the discrepancy:

- The open area available for steam is not known and differs from the assumption made in the Paprican model.
- The assumption of a continuous network seems to be incorrect as Stationwala *et al.* (1992), observed that as much as 50 % of the total bar surface was free of pulp.
- The energy distribution is assumed to be even across the refining zone. Based on visual inspection of the plates that showed uneven wear, the authors were doubtful to this assumption. However, another experimental study using strain gauges mounted on the refiner plates made it possible to estimate the energy consumed at an arbitrary point along the disc radius. This work is reported in Gradin *et al.* (1999). The results showed that the power per unit area was roughly constant. The change in measured sensor strain correlated well with the measured total applied electrical power to the refiner.

Mechanical forces

The mechanical forces involved in the Paprican model are less complex. These are the force connected to the centripetal acceleration, Equation (2.3), and the friction forces Equation (2.4). They contain two operating parameters, the specific energy and the inlet consistency, as well as four design parameters through rotational speed, plate size, refiner type specified by single or double discs and friction coefficients in radial and tangential direction.

Centrifugal force, Equation (2.3):

$$C/r0| \; dM(r) \; (\varpi^2 \; (r \qquad ; [N] \tag{2.3}$$

dM(r) : *wet mass of pulp in the annulus dr; [kg].*
ϖ : *angular velocity of disc 2 (rotor); [s^{-1}].*
r : *radius; [m].*

Total radial friction force, Equation (2.4):

$$F_r \; | \; F_{r1} \; 2 \; F_{r2} \; | \; 4 \; (\phi \; (\sigma_r \; (r \; (P_m(r) \; (dr \qquad ; [N] \tag{2.4}$$

σ_r : *average of the two radial coefficients of friction.*
$P_m(r)$: *average mechanical pressure over the annulus dr; [Pa].*

Miles and May assumed that the radial and tangential friction coefficients are constant, 0.25 and 0.75 respectively. Isaksson *et al.* (1997) stated that there is no reason to believe that the friction coefficients should be constant. Their experiment performed in mill scale refiners showed that the tangential friction coefficient was much lower than the corresponding value assumed by Miles and May. However, this result should be interpreted with caution, since this work has not been published in a peer-reviewed journal. In addition, they found that the tangential friction coefficient was higher in the primary refiner compared with the findings related to the refiner in the second stage. Based on this discrepancy they assumed that the tangential friction coefficient decreases across the refining zone.

Senger and Ouellet (2002) showed that the tangential friction coefficient rose with increasing consistency, and the plate wear affected the coefficient value as well. The latter results were obtained through an experiment in a single bar laboratory refiner during the measurement of normal and shear forces. The reason for the increased friction is assumed to be related to strengthening of the fibre network. The drier fibre network creates higher resistance when the bar encounters it. Based on experiments reported by Karnis *et al.* (1985), the consistency increases across the refining zone. According to Senger and Ouellet this should lead to increasing tangential friction across the refining zone. Thus, the indication in Isaksson *et al.* (1997) of decreasing tangential friction between the inlet and periphery of the discs is to the contrary.

Another result reported by Senger and Ouellet (2002) indicated that the tangential friction coefficient decreases as refining zone temperature increases. This result was obtained by investigation of data published by Miles and May (1990) and Atack and

Stationwala (1975). Their interpretation was that higher temperature creates more flexible fibres which offer less resistance to the bar edge, as it ploughed its way through the floc.

The axial pressure arisen from the fibres, Equation (2.7), is determined by considering the power dissipated as given by equalizing the powers given by Equation (2.5) and Equation (2.6). These equations are derived for a single disc refiner.

The power dissipated against the tangential friction force, Equation (2.5):

$$W(r) = F_{t1}\,\omega\,r = \sigma_{t1}\,P_m(r)\,dA\,\omega\,r \quad ; [J/s] \tag{2.5}$$

σ_{t1} : *tangential coefficients of friction between the pulp and the rotor disc.*
dA : *area of the annulus dr; [m^2].*

The power dissipated per unit area is assumed constant and leads to Equation (2.6):

$$P(r) = \frac{\dot{m}\,E\,dA}{\phi\,(r_2^2 - r_1^2)} \quad ; [J/s] \tag{2.6}$$

$\dot{m}$: *oven dry throughput; [kg/s]*
E : *total specific energy applied to the refiner; [J/kg].*

The axial pressure (mechanical pressure) from the pulp as quoted in Miles and May (1991) Equation (2.7):

$$P_m(r) = \frac{\dot{m}\,E}{\phi\,(r_2^2 - r_1^2)\,\sigma_{t1}\,\omega\,r} \quad ; [Pa] \tag{2.7}$$

$\dot{m}\,E$: *total motor load, evenly distributed across the refining zone; [J/s]*

The axial thrust from the chips or pulp pad as shown by Isaksson *et al.* (1997) Equation (2.8):

$$F_m = \int_{r_1}^{r_2} 2\phi\,r\,P_m\,dr \quad ; [N] \tag{2.8}$$

The total axial thrust (Isaksson *et al.* (1997)) Equation (2.9):

$$F_{hyd.} = F_{steam} - 2\,F_m \quad ; [N] \tag{2.9}$$

F_{steam} : *axial thrust from the contribution of steam; [N]*

Consistency

Miles and May have focused on consistency as an important variable as it determines some important quality properties of the pulp that can be obtained for a given total of specific energy. The results that they present compare consistency with tear strength. Figure 2.4 shows tear strength as a function of consistency. Due to size, every refiner has an optimum level of consistency to reach an optimum level of this pulp quality parameter. Large refiners need higher consistency to reach the optimum tear strength level as shown in Figure 2.4. This clear relationship is obtained when other process variables such as rotational speed and plate pattern are the same. The only changeable variable is therefore the refiner size.

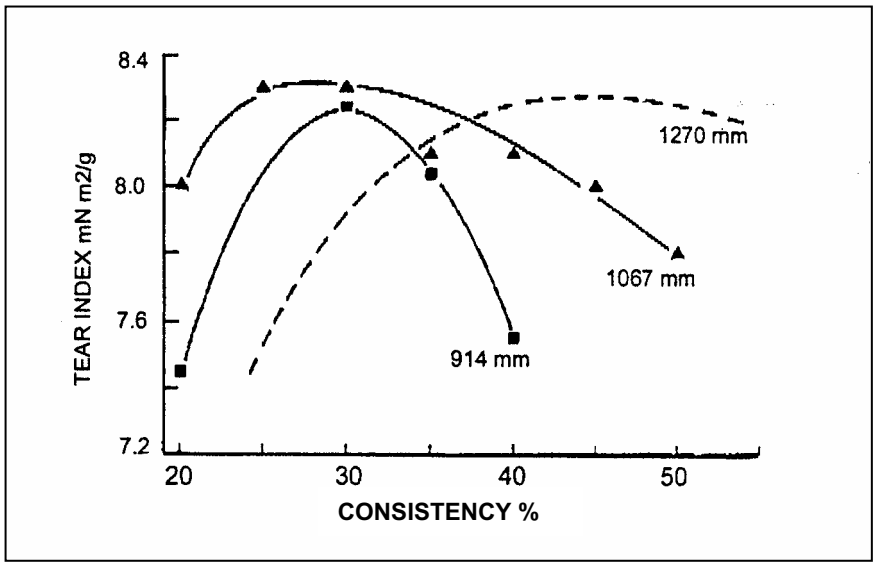

Figure 2.4: Tear strength increases with consistency until a maximum, and then decreases. The size of the refiners defines the optimum tear-consistency point (Miles and May (1990)).

Consistency changes due to the conversion of water to steam. The relationship between consistency and radius is shown in Equation (2.10).

$$c(r) = \frac{c_i \cdot L \cdot (r_2^2 - r_1^2)}{L \cdot (r_2^2 - r_1^2) + c_i \cdot E \cdot (r_2^2 - r_1^2)} \quad ; [\%] \tag{2.10}$$

c_i : *inlet consistency; [%].*
L : *latent heat of steam; [J/kg].*
E : *total specific energy applied to the refiner; [J/kg].*

The reason why the consistency is important is related to the centripetal acceleration and the corresponding force, which is proportional to the wet mass of the pulp. Low consistency gives a high value of this force. The residence time will be shorter and the refining intensity increases for a given specific energy. In addition, the lower residence time reduces the amount of pulp present in the refining zone, which in turn leads to smaller plate gap.

Strand and Hartler (1985) also claimed that the consistency was important for the residence time of the pulp in the refiner. Their interpretation was related to the volumetric flow rate. They stated that the refiner consistency has a double effect on the (relative) residence time. Lower consistency results in smaller plate clearance, which in turn reduces the refiner volume and in addition increases the volumetric flow rate. Both effects reduce the residence time. Furthermore, Strand and Hartler claimed that the residence time rather than consistency is the variable that controls pulp quality.

Too high consistency is undesirable as it makes the refiner unstable. The unstable condition occurs when the centrifugal force becomes weaker than the frictional forces, which is assumed independent of the consistency (Miles and May (1990)). Then the feeding mechanisms in the refiner begin to break down. The consistency that equalizes the centrifugal force and the frictional force is defined as the maximum operating value. The latter is based on the fact that the drag force term is removed from the steam, which is not of present interest in a pressurized refiner. Forward-flowing steam will help to maintain stability, while back-flowing steam, which tends to decelerate the pulp, will contribute to instability. An example from Miles and May (1990) shows that a small refiner (914 mm, 1200 rpm) will be unstable with an inlet consistency above 17 %. A refiner with larger centrifugal forces (914 mm, 1800 rpm) tends to be unstable when the inlet consistency is above 23 %.

Larger refiners can operate at a higher consistency than smaller ones before becoming unstable. This is also due to the large size that generates higher centripetal acceleration, but also lower frictional forces than smaller ones. However, it is not clear why a larger refiner would generate lower frictional forces than a smaller one. In addition, the velocity of the forward-flowing steam is higher in larger refiners that operate at higher power per unit area of refining zone. Hence high-consistency chip refining is typically done at inlet consistencies between 18-30 % (Miles and May (1990)). Inlet consistency levels are seldom used because of the difficulties connected to measures of this value. Therefore the outlet consistency is the more usual notion. The outlet consistency in mill scale refiners is typically in the area of 40-50 % (Sundholm (1999, Ch. 7)).

The change of pulp velocity across the refining zone is given by the above equations and furthers their derivation. It can be expressed in the following implicit form Equation (2.11):

$$\frac{dv}{dr} = \frac{r\,\omega^2}{v} - 4a\left(\frac{\sigma_r}{\sigma_t}\right)\left(\frac{E\,c(r)}{\omega\,(r_2^2 - r_1^2)}\right) - 2\frac{b}{2}\,C_f\,i_s(r)\,U(r)^2\,A_p(r)\left(\frac{c(r)}{v}\right) \quad ; [s^{-1}] \tag{2.11}$$

v : *pulp velocity; [m/s].*
a : *constant due to refiner type (a=4 for SD, a=2 for DD).*
μ_t : *tangential coefficient of friction between the pulp and the disc it is slipping over (in this case the stator).*
c(r) : *average consistency of pulp in the annulus dr; [%].*

The residence time can be determined from the velocity equation as shown in Equation (2.12).

$$\vartheta = \int_{r1}^{r2} \frac{1}{v} dr \qquad ;[s] \tag{2.12}$$

Miles and May's paper *"Predicting the performance of a chip refiner; a constitutive approach."* from 1991 deals with theoretical aspects of the flow of pulp and steam through a refiner. This paper also contains information from an experimental study, which supports the theoretical work. Their work provides useful descriptions of how the refiners react under different conditions such as:

- When the specific energy is increased, the amount of pulp in the refining zone increases, despite the reduced plate gap.
- When the consistency is increased, the plate gap must be widened to maintain constant specific energy.
- At higher consistency the self-pressurization will be weaker, because there is less wet mass, slower pulp flow, higher mass concentration and more fibre network. This reduces the steam velocity and the self-pressurization becomes smaller.
- When throughput is increased, the plate gap has to be reduced in order to maintain a constant specific energy level.
- When the casing pressure is increased in a pressurized refiner, the plate gap must be increased to maintain the constant specific energy.

The constitutive model predicts these and other descriptions. The model consists of a set of equations shown as Equations (2.13), (2.17) and (2.18).

The change of pulp velocity across the refining zone, Equation (2.13):

$$\frac{dv}{dr} = \text{Equation (2.11)} \cdot 2 \cdot \sigma_r \cdot \omega \qquad ; [s^{-1}] \tag{2.13}$$

The last term in Equation (2.13) is the effect from the Coriolis force[3].

The rate of change of the flow area with radius, Equation (2.14):

$$\frac{dA_F}{dr} = A_F \left(\frac{1}{\kappa} \left(\frac{d\kappa}{dr} \right) + \frac{1}{v} \left(\frac{dv}{dr} \right) + \frac{1}{\eta} \left(\frac{d\eta}{dr} \right) \right) \qquad ; [m] \tag{2.14a}$$

A_F : *cross-sectional area available for steam flow at radius r; [m²].*
κ : *porosity of the flowing pulp network.*
η : *density of the pulp network at radius r; [kg/m³].*

[3] Coriolis force ($F = 2 m \omega v$; [N]). An apparent force experienced by a body (m) that moves (v) along a radius of a rotating frame (ω), and opposing the rotation of the body relative to the stationary frame. (Source: Borowski and Borwein: "*Collins Dictionary of Mathematics*.", HarperCollins Publisher, UK, 1989)

Cross-sectional area available for steam flow, Equation (2.14b):

$$A_F = \frac{\kappa \dot{m}}{\eta v} \quad ; [m^2] \tag{2.14b}$$

$\dot{m}$: *throughput; [kg/s]*

Density of the pulp network, Equation (2.14c), derived from experiments reported by May *et al.* (1988):

$$\eta = a P_R^d \quad ; [kg/m^3] \tag{2.14c}$$

P_R : *average mechanical pressure applied to the pulp at radius r; [Pa].*
a, d : *constants.*

The plate gap at radius r, Equation (2.15), and the amount of fibres per area, Equation (2.16), are given below:

$$G = \frac{M_c}{\eta} \quad ; [m] \tag{2.15}$$

M_c : *local mass concentration; [kg/m^2].*

$$M_c = \frac{\dot{m}}{2\phi r v} \quad ; [kg/m^2] \tag{2.16}$$

The radial steam pressure gradient, Equation (2.17):

$$\frac{dP}{dr} = \frac{\iota_s}{A_F (1 - k_1 U^2)} \left(\frac{dA_F}{dr} r \omega^2 - \frac{4\phi r m_s U}{\iota} - 2U^2 \frac{dA_F}{dr} - \frac{b}{2} C_f U^2 A_p \frac{\dot{m}}{v} \right) \tag{2.17}$$

k_1 : *constant relating steam density to steam pressure.*
m_s : *rate of steam generation per unit area at radius r; [kg/m^2].*

The radial velocity gradient of the steam, Equation (2.18):

$$\frac{dU}{dr} = \frac{1}{\iota_s A_F} \left(2\phi r m_s - k_1 U A_F \frac{dP}{dr} - \iota_s U \frac{dA_F}{dr} \right) \quad ; [s^{-1}] \tag{2.18}$$

The constitutive equations are solved numerically by the iterative procedure in which the inlet back-flow velocity of the steam is adjusted until the stipulated casing pressure

is obtained. The solution produces the steam pressure and velocity, the pulp velocity, the plate gap, the groove depth, and the refining intensity as a function of radial position. It also produces the pulp residence time, the average refining intensity, and the axial thrust load of the refiner.

Miles and May introduced some assumptions in order to get satisfactory results. These state that the pulp and steam flow begins to scour out a passage in the partial filled grooves if the average mechanical pressure applied to the pulp pad rises above a certain level. This will be associated with a critical mass concentration. They have further assumed that the critical mass concentration cannot be exceeded between the bars, while the pressure can rise beyond its critical value. The steam velocity is assumed to increase when the mechanical pressure increases. The pulp is assumed to flow along the grooves at the same average velocity as it does along the bars.

The depth to which the grooves have been opened is given by Equation (2.19). According to the authors a model is necessary because there is no way of measuring the unpacked depth of the grooves.

$$D = \frac{1}{\phi} \int_r^R \left(\frac{A_F}{\kappa} \right) 2\phi \, dr \qquad ; [m] \tag{2.19}$$

Other assumptions are that the porosity of the pulp network is constant, and the density of the pulp is a function of the mechanical pressure exerted on it by the discs. The mechanical pressure is in turn dependent on the dynamic compressive modulus of the pulp and the local temperature.

Refining intensity

Refining intensity is defined as the total amount of energy applied to the pulp in the refiner divided by the number of impacts the pulp gets as it passes through the refiner as shown by Equation (2.22). The concept of refining intensity is derived in Miles and May (1990). According to May (1998) the refining intensity has a crucial effect on the energy-quality relationship. Thus it is assessed to be an important variable in the refining process. Its recognition came when the Miles and May equations made it possible to calculate the residence time (May (1998)).

However, a similar approach was introduced earlier by May *et al.* (1988) and it is also found in the literature related to low-consistency refiners too (Leider and Nissan (1977)). The approach made by May *et al.* (1988) has obviously been further developed before it ended as the derived relationship presented in Miles and May (1990).

The refining intensity is calculated from the power input and the residence time. The latter is determined by the pulp velocity, which is stated in Miles and May (1990) and further simplified as derived in Miles (1991).

The algebraic equations, which are introduced from the simplified assumptions, state that the effect of steam on the average pulp velocity and residence time is small. See Equations (2.20) and (2.21).

The analytic expression of radial velocity of pulp, Equation (2.20):

$$v = \frac{\sigma_t}{\sigma_r} \cdot \frac{r \cdot \omega^3 \cdot (r_2^2 - r_1^2)}{a \cdot E \cdot c(r)} \quad ; [m/s] \tag{2.20}$$

An algebraic equation for the residence time, Equation (2.21):

$$\vartheta = \frac{\sigma_r}{\sigma_t} \cdot \left(\frac{a \cdot E \cdot c_i \cdot L}{\omega^3 \cdot (L \cdot (r_2^2 - r_1^2) - 2 \cdot c_i \cdot E \cdot (r_1^2 - \left(\ln \frac{r_2}{r_1} - \frac{1}{2} \ln \frac{L - 4 \cdot c_i \cdot E}{L} \right) \right) \quad ; [s] \tag{2.21}$$

The refining intensity, Equation (2.22):

$$e = \frac{E}{n} \quad ; [J/kg / impacts] \tag{2.22}$$

n : number of impacts.

The number of impacts, Equation (2.23):

$$n = N \cdot h \cdot \omega \cdot \left(\frac{r_1 - r_2}{2} \right) \cdot \vartheta \text{; number of impacts.} \tag{2.23}$$

N : number of bars per unit length of arc.
h : constant (1 for single disc, 2 for double disc).

The solution of the algebraic equations shows that the refining intensity and the residence time are highly sensitive to the speed of the refiner and the disc diameter. The refining intensity is proportional to the square of the rotational speed of the refiner, and the residence time decreases rapidly as the diameter increases. The residence time is also proportional to the ratio of the radial and tangential friction coefficients while the refining intensity is inversely proportional to the same ratio. For instance a decrease in the tangential friction coefficient due to wear of the plates, will give an increase in the residence time. This is caused by the effect that more axial thrust is required to generate the same motor load. The pulp will then be squeezed more tightly between the plates and does not escape as quickly.

According to Miles (1991), the algebraic equations give satisfactory results for the average radial pulp velocity and residence time compared to the numeric solutions of the differential equations. It should be mentioned that the local pulp velocity is greatly affected by the assumption that the effect of steam can be neglected. When the steam

flow is included, the pulp velocity is lower in the region before the stagnation point because of deceleration by the back-flowing steam and higher beyond the stagnation point because of acceleration by the forward-flowing steam. See Figure 2.5.

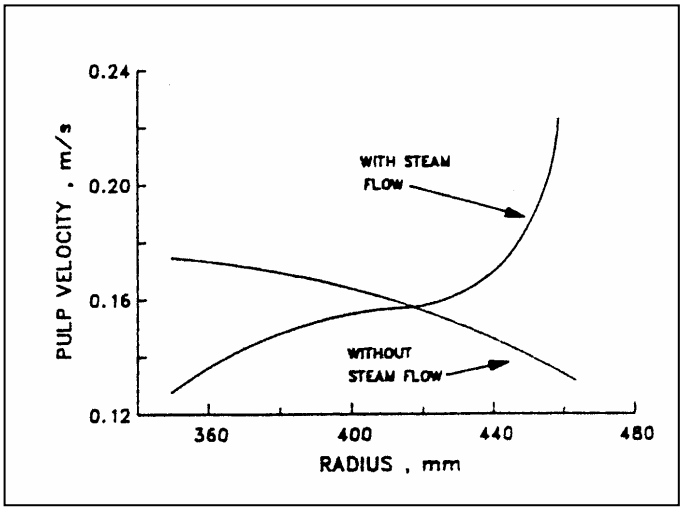

Figure 2.5: Pulp velocity in the refining zone computed with and without influence of drag force from the steam as shown by Miles (1991).

An increase in specific energy leads to a decrease in the radial velocity of the pulp (Equation (2.20)) and the number of impacts decreases (Equation (2.23)), while the intensity remains constant (Equation (2.22)). According to Miles (1998) this relationship reveals the most significant feature of the high-consistency disc refiner because by increasing the number of impacts there is no need to increase the specific energy per impact when the process demands for higher energy input. Thus the pulp quality depends on the refining intensity and not only the specific energy and the refining consistency. Miles *et al.* (1991) claimed that a higher refining intensity in the first stage produces pulps with better strength and optical properties for the same consumption of energy. Miles has concluded that the essence of high consistency refining is that the intensity of the process is independent of the specific energy. This unique feature is what enables fibre development to proceed while fibre length is preserved (Miles (1998)).

Furthermore, assuming that the energy distribution and impact frequency are taken into account Miles (1998) shows that the velocity equation, Equation (2.20), is derived to an expression for the refining intensity as shown in Equation (2.24).

$$e \propto \frac{1}{2N} \left(\frac{\sigma_t}{\sigma_r}\right) \left(\frac{r\omega^2}{c(r)}\right) \tag{2.24}$$

The rotational speed of the refiner is the most significant factor in Equation (2.24). However, the number of bars per unit length of arc affects the refining intensity as well.

Fewer bars on each plate should also lead to higher refining intensity. This factor is given little attention.

Alami *et al.* (1997) have discussed the refining intensity and related them as follows:

- A change in the residence time of the pulp flow across the refining zone implies a change in the number of impacts available to supply a given total specific energy. This, in turn, implies a change in the specific energy per impact, or refining intensity.
- Refining intensity rises through an increase in the centrifugal force applied to the fibre feed relative to the restraining forces required for energy application. At a given rotational speed, the impulsion force applied to each unit mass of fibre is determined by its total mass and therefore inversely proportional to the refining consistency. Reducing the consistency may therefore increase the refining intensity.
- The specific refining energy required to obtain a given pulp quality may be reduced by increasing refining intensity.

According to Sundholm (1999, Ch. 4) the notation refining intensity has a limited applicability as a quantitative concept. The reason for this is the limited possibility to measure the residence time and the power dissipation distribution in a regular refiner. Such measurements require special arrangements and techniques. Härkönen and Tienvieri (2001) support this criticism and state that the concepts high or low refining intensity are used in many connections to describe harsh or gentle refining. In these connections the concept has only a qualitative meaning and it is no longer a precise numerical expression to specify refining conditions.

Another approach for description of the refining mechanisms

The description by Härkönen and Tienvieri (2001) about the phenomena in the refiner takes another approach to the Miles and May equations. Some aspects of this description are given in the following discussion.

The power consumption is given by Equation (2.25):

$$P = M \cdot \omega \quad ; [J/s] \tag{2.25}$$

M : *torque; [Nm].*
ω : *angular velocity[rad/s].*

The torque as a function of the shear force between the pulp and the discs is given by Equation (2.26):

$$M = \int r \cdot \vartheta \, dA \quad ; [Nm] \tag{2.26}$$

A : *surface area of plates (intersecting area due to bar crossing); [m^2].*
r ; *radius of the plates [m].*
ϑ ; *shear stress between the pulp and the rotating disc [Pa] ([N/m^2]).*

The authors claimed that the amount of fibres in the pulp pad is so large that compression of the pulp pad must be included in the model. The compression of the

fibre mat defines the free volume that is available for steam flow. In addition the compression defines the proportion of the shear force needed to deform the fibre mat. They further claimed that there is limited knowledge of the compression behaviour in the refiner. Equation (2.27) shows the volume fraction of fibres as function of the pressure.

$$\kappa = \kappa_0 + (\kappa_{lim} - \kappa_0)\left(1 - e^{-\frac{4P}{P_0}}\right) \qquad (2.27)$$

κ_0 : *volume fraction of fibres when continuous network is formed.*
κ_{lim} : *maximum volume fraction of fibres under compression.*
P : *pressure on the fibres [Pa].*
P_0 : *specific value for the pressure (pressure corresponding to κ_{0}) [Pa].*

The reliability of Equation (2.27) was tested during static conditions for various refining pulps. Coefficients were found for specific conditions, but it is not sure that they are transferable to the conditions in the plate gap. Similar tests were made by May *et al.* (1988) in a laboratory press. They measured the pad thickness of different amount of fibres per area, specified as mass concentration (kg/m^2), versus applied stress. They found fibre pad densities increasing from approximately 140 kg/m^3 to approximately 300 kg/m^3 when increasing the applied gauge pressure from 0 to 200 kPa (0-2 bar).

Härkönen and Tienvieri (2001) stated that there are unknown factors of the phenomena in the plate gap. Particularly the behaviour of the shear stress is not known. However, a hypothesis was put forward to describe the shear force and the corresponding tangential friction. Two different mechanisms were assumed. The first involved only a velocity gradient in the pulp pad between the stator disc and the rotor disc. All the energy dissipation occurs in the pulp pad. This mechanism was described as gentle refining. The second mechanism assumed a velocity gradient between the rotor disc and the pulp pad. All the energy is dissipated as a result of friction between the surface of the plate and the fibres in direct contact with the plates. This mechanism was described as harsh. The authors indicated that both mechanisms probably occur during normal operation.

Härkönen and Tienvieri (2001) also derived an equation for the residence time. It has some similarities with an approach reported by May *et al.* (1988) and Strand and Hartler (1985). They have further adopted the expression for the intensity introduced by Miles and May (1990) and used their own terms to describe the intensity in another way.

In 1997 Härkönen and co-workers launched a dynamic simulation model, which calculates the flow phenomena in a conical disc refiner (Härkönen *et al.* (1997)). According to Sundholm (1999, Ch. 4) this model is comprehensive and it contains the fibre and steam velocities, fibre and steam pressures, fibre and steam temperatures, and dry content of pulp and power dissipation in the plate gap. The model is rotationally symmetric and includes the rotor, stator and the plate gap. The model contains all the physical factors needed to describe the steam and fibre motion as well as the different power dissipation mechanisms. However, little information was given about these factors in the described paper. According to Sundholm (1999) this model contains

several parameters, which must be determined by testing. An interesting result obtained from this study was that the maximum values of the steam pressure and the fibre pressure did not occur at the same location in the refining zone. The maximum fibre pressure was related to the conical zone where the main contribution to the axial thrust was produced. The steam pressure had the maximum value located to the inner part of the plane zone.

A stochastic approach of fibre movement

Among other model considerations the work reported by Fan and co-workers is indeed interesting (Fan (1987), (1995) and Fan *et al.* (1994), (1997)). Fan and co-workers have developed an extended model for the residence time in a single-disc refiner. This is reported in Fan *et al.* (1994). The work is based on results from experimental studies, which were reported by Stationwala *et al.* (1992). The results from the experimental work, which are acquired using high-speed photographic techniques and image analysis, have shown that 50-85 % of the bar surfaces are covered by pulp, and the pulp appears in the form of flocs. The pulp flow model developed by Fan *et al.* (1994) is a stochastic approach to fibre movement. The degree of fibre movement in the refining zone is based on probability factors. Thus, the model gives a distribution of residence time. This model is a kinematic model, which does not take the forces acting on the pulp explicitly into account.

The results from this study showed that the observed and model-computed minimum residence times became close providing the probability parameters obtained values that force most of the pulp flocs to the rotor. Thus the distribution of the residence time becomes almost symmetrical about the maximum values, which indicates that the means and the medians of the distribution are approximately equal. Here, the asymmetry of the residence time distribution could be accentuated by forcing the probability parameters to take extreme values. This arises if there is small probability of the pulp changing location from a stator groove to the gap or vice versa. Then the pulp will stay for a longer period in the refining zone and the residence time distribution will be skew. Murton *et al.* (2002) and Härkönen *et al.* (2000) have both shown that the measured distribution of the residence time is skew. However, this skewness may be an effect of mixing in the entrance zone, rather than a proof of the mechanism postulated by Fan *et al.* (1994).

A further extended model has been developed to allow the prediction of short-term variations in pulp discharge and radial density profile of pulp in the refining zone. The modified model is reported in Fan *et al.* (1997). The new condition in the model is that a mass is assigned to the flocs. Expressions are introduced to estimate the radial pulp density profile in the refining zone, so that fluctuations in density and production rate can be predicted. As a result the model predicts that the average pulp density in the refining zone decreases steadily from the inner to the outer periphery. The pulp residence time still becomes a random variable, and the model can predict its distribution. The model is implemented as a computer model as well as a stochastic model.

The assumptions are as follows and some of these are illustrated in Figure 2.6:

- The pulp moves inside a refiner in the form of discrete flocs, instead of the assumption of a continuous mass flow.
- The pulp in the grooves behaves differently from the pulp in the gap.
- The extended model divides the refining zone into three regions, which are the grooves on the stator plate, the grooves on the rotor plate and the gap between the plates.
- The pulp velocity is assumed to be constant in each of the three regions, denoted as u in the rotor grooves and $u/2$ in the gap, stapled either on a stator or a rotor bar. The velocity in the stator grooves is assumed to be zero.
- The pulp movement from one region to another is treated as a stochastic process with different probabilities to change region.

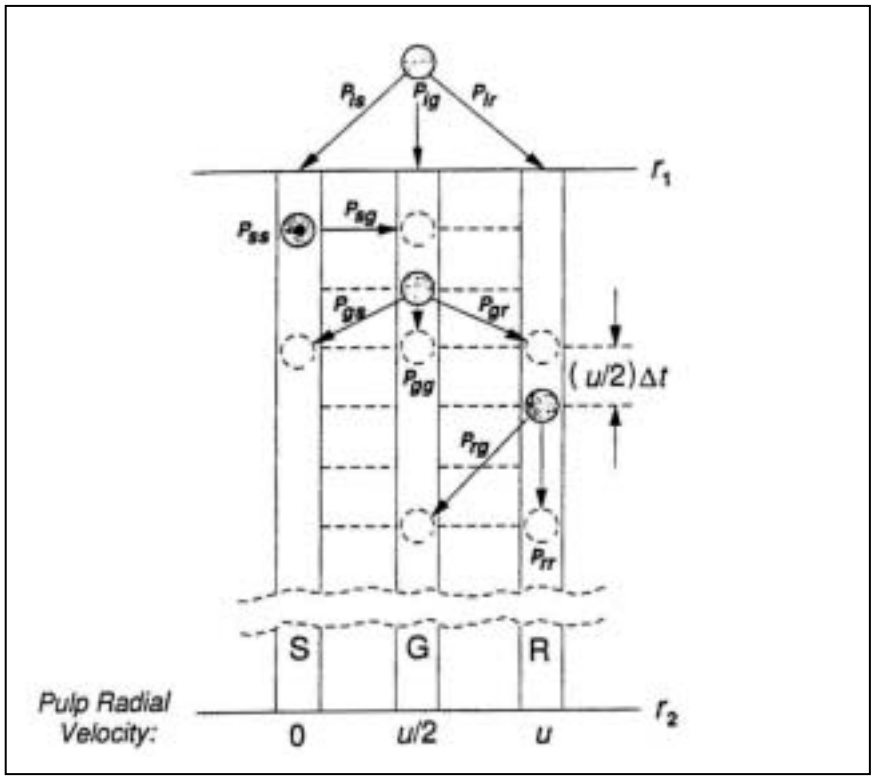

Figure 2.6: The mechanism of floc exchange between the three defined regions and floc velocities as used in the stochastic model composed by Fan and co-workers (Fan *et al.* (1997)).

The model does not include factors such as the recirculation of pulp, steam flow, plate taper and changes in the cross-sectional area of the groove, which will influence the pulp density profile. The authors claim that there are no data in the literature, which could be directly compared with the predicted values of the pulp densities in the gap.

The predicted values are in the order of 180-580 kg/m^3. A discussion about the use of information from Stationwala *et al.* (1992) and May *et al.* (1988) concludes that the predictions seem acceptable. As mentioned earlier, the pulp pad densities in the study reported by May *et al.* (1988), indicated pulp density variations between approximately 140 kg/m^3 to 300 kg/m^3 under influence of different compressive loads. As a remark, the density of the fibre cell wall is approximately 1530 kg/m^3 (Braaten (1996)) and the basic density for Norway spruce (*Picea abies*) is 410 kg/m^3 (Rydholm (1965)). The latter value is approximate since it varies over a wider range due to the age of the wood. As a comparison MacDonald and Guthrie (1987) measured the dry chip bulk density of softwood species and found it to vary between 138 and 154 kg/m^3. Similar values are reported by Mosbye *et al.* (2001) regarding mill-produced chips from Norway spruce. However, sawmill chips had a larger variation and were stated to be in the range 140-180 kg/m^3.

2.3.2 Visualization of the pulp flow behaviour

Two different research groups seem to have achieved very good results using photographic methods for visualization of pulp in the refining zone of high-consistency refiners. Researchers at Paprican, especially, Atack and Stationwala have contributed important information to the theoretical framework and the results from their studies are based on high-speed photography and image analysis. Their work has been reported since the early 1980s. This report has referenced two of their publications: Stationwala *et al.* (1992) and Atack *et al.* (1989). The other group, which seems to have created good results in the work with visualization of pulp in the refiner, is located at the Tampere University of Technology in Finland. Their work is reported recently by Alahautala *et al.* (1997) and (1999). In addition, it can be mentioned that similar research has been performed in low-consistency refiners showing interesting results (Fox *et al.* (1979), (1982)).

Stationwala *et al.* (1992) describe two techniques, which produce blur-free photography of the fibre flow inside a refiner. The two techniques are cinestroboscopic photography and a high-speed electronic image-converter, IMACON-camera. The trials were conducted on a single disc, second stage refiner. A transparent refiner plate segment, machined out of high-temperature polycarbonate sheet stock, was placed in a window cut in the stationary plate. The measurements were taken at three radial locations in the refining zone. An image-converting camera operating at 100 000 pictures per second was used to record the movement of pulp during one bar crossing of the refiner plates. The exposure time for the individual frame was 1 μs.

Analysis of the photos showed that 50-70 % of the mid-region of the refining zone was covered with pulp. The inner section was covered with 70-80 % of pulp and the outer section was covered even more. This means that there is a considerably higher amount of pulp between the refiner plates at the beginning of the refining zone than the nominal throughput. This is assumed to be caused by considerable back-flow and recirculation of pulp in the inner half of the refining zone. The higher amount of pulp in the outer periphery is probably caused by the restriction to radial pulp flow by the fine plate pattern in this region and the narrow gap due to the taper. The authors discussed their results and compared them to the theoretical values obtained by May *et al.* (1988),

which found that only 16 % of the bar intersecting area was covered by pulp in a primary refiner. In the second stage refiner May *et al.* (1988) found that only 5 % of the bar area was covered. Assuming that the various types of refiners in these experiments behaved differently, Stationwala *et al.* (1992) indicated that, despite of the different results, these values appeared to agree fairly well.

The image analysis showed that pulp appears in the form of flocs. The flocs move tangentially, driven by the rotor, across the bar width. The flocs change shape and are disrupted in the process. Flocs can also be trapped on bar edges. It seems likely that the material on the bars is aligned in the tangential direction. According to the authors the pictures support the refining mechanism described by Atack (1980), namely that refining is accomplished by a moving bar working along the length of fibres trapped momentarily on the stationary bar.

Atack *et al.* (1989) measured the pulp flow pattern in a second-stage pressurized single-disc refiner. The pulp-flow velocity both as forward flow and back flow was determined for different plate patterns. Back-flow velocities up to 30 m/s were observed in the coarse (breaker bar) zone. Forward-flow had velocities up to 20 m/s in the fine bar zone. Tangential flow of pulp was observed in the transition zone between the intermediate and fine zone with a velocity of approximately 20 m/s. The direction of tangential flow was the same as the rotational direction. The tangential velocity of the disc at the radius of 0.7 metre was approximately 110 m/s. The rotational speed of the refiner was 1500 rpm.

Alahautala *et al.* (1999) and (1997) took images inside the refiner with a CCD-camera, light stroboscope and endoscope optics to come close to the pulp. Their experimental study was performed on a first-stage refiner at four different radial locations: 537 mm, 607 mm, 669 mm and 797 mm. The measurements were focused on pulp velocity (both magnitude and direction), pulp orientation, pulp coverage and the presence of fibre flocs. The measurements were executed through windows in the stator plate with a diameter of 20 mm. The endoscope diameter and thus the effective optical aperture, was 12 mm. All windows had a plate pattern, which corresponded to their locations, manufactured onto the sapphire surface.

Results from this study showed that back-flow velocity in the crush zone i.e. outer part of the breaker bar zone or inner part of the refiner plate, was found to be surprisingly small, only a few centimetres per second. The velocity above the bars was much higher (0.2-0.4 m/s) than in the grooves. It was also observed that this zone was full of pulp. Furthermore, it was indicated that there was some free water in the coarse zone. An increase of dilution water raised the back-flow velocities. This is agreeable with Miles and May (1991), who stated that lower consistency leads to higher steam velocity and higher self-pressurization (increased steam production). Increasing the dilution water flow leads to reduced power consumption. According to Miles and May (1991) the plate gap must be smaller to maintain a constant specific energy.

Pulp flow in the intermediate zone grooves was very turbulent, and the back-flow velocity was about 1 m/s. Approximately 60 % of the area of the grooves was covered

with pulp. It was observed that the amount of water was very high in this zone. In the refining zone grooves the pulp velocity was about 30 m/s[4]. When the amount of dilution water was increased, the pulp velocity decreased to approximately 20 m/s. This is contrary to the response observed in the coarse zone when the consistency decreased. Observations showed that there were few flocs and a low fibre coverage ratio in the grooves in the fine bar zone, which indicated low volume consistency.

2.3.3 Measurements of pressure and forces in refining

It is necessary to measure the steam pressure in the plate gap in order to control the axial force balance in the refiner given by Equation (2.28):

$$F_{axial} = F_{steam} + F_m \quad ; [N] \tag{2.28}$$

F_{axial} : *Total axial (gap closing) thrust; [N].*
F_{steam} : *Total reaction steam thrust; [N].*
F_m : *Total reaction mechanical thrust from chips (pulp); [N].*

According to Miles and May (1990), it is possible to calculate the mechanical thrust from chips or pulp as shown in Equation (2.7). Equation (2.29) shows the derived equation of the mechanical thrust as quoted from Isaksson *et al.* (1997).

Mechanical thrust from chips or pulp, Equation (2.29):

$$F_m = \frac{2 \cdot W}{h \cdot \mu_{t1} \cdot \omega \cdot (r_1 + r_2)} \quad ; [N] \tag{2.29}$$

W : *Motor load; [J/s].*
h : *Constant due to refiner type (h=1 for SD, h=2 for DD).*
μ_{t1} : *Tangential friction coefficient against the rotor disc.*
ω : *Angular velocity; [rad/s].*
$r_{1,2}$: *Inlet and outlet of the refining zone; [m].*

If it can be assumed that the steam is saturated, then the steam pressure can be obtained from measurements of the temperature in the refining zone. Di Ruscio and Holmberg (1996) reported some algebraic relations for saturated steam with reference to earlier work reported in Di Ruscio (1993). The relations consist of three equations, Equations (2.30), (2.31) and (2.32), which relate density and temperature and latent heat of saturated steam to pressure. The denomination of pressure used in these equations is bar. According to Di Rusico, the expressions are sufficiently accurate for the pressure range 2-10 bar.

[4] 30 m/s is a good approximation to the assumed blow line velocity if the assumption is made that the pulp velocity in the blow line is mainly driven by the refiner housing pressure, which is assumed to be approximately 4 bar gauge pressure. The approximated blow line velocity is calculated from the energy balance, which states that the kinetic energy is due to the potential energy. In Sutinen and Joensuu (1996) the blow line velocity is typically assumed to be around 40 m/s.

Density as a function of pressure, Equation (2.30):

$$\rho = 0.145 + 0.493\sqrt{p} \quad ; [kg/m^3] \tag{2.30}$$

Temperature as a function of pressure, Equation (2.31):

$$T = 92.53 + 36.91\ln(p) \quad ; [°C] \tag{2.31}$$

Latent heat of saturated steam, Equation (2.32):

$$L = 2288.6 - 114.2\ln(p) \quad ; [kJ/kg] \tag{2.32}$$

Temperature measurements are widely used. Such measurements have been reported since 1973 (May *et al.* (1973)). Among the many reports the following can be mentioned Johansson *et al.* (2001), Mosbye *et al.* (2001), Engstrand *et al.* (1995), Stationwala *et al.* (1979), (1991), Lunan *et al.* (1983) and Atack and Stationwala (1975). A typical temperature profile for the measured temperatures in first and second stage mill scale refiners is shown in Figure 2.7.

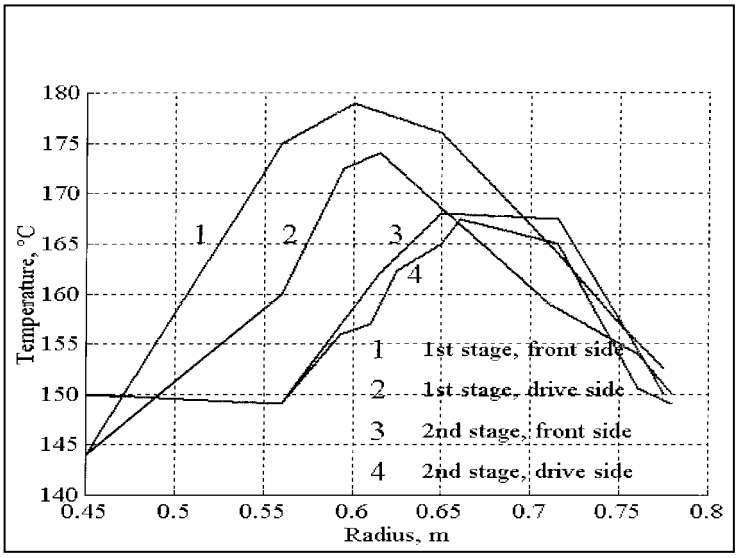

Figure 2.7: The illustration shows curves, which are plotted according to measurements of the temperature profile in the refining zones in 60 inch (1524 mm) twin refiners (Sundholm (1999, Ch. 4)).

According to Miles *et al.* (1980) a sharp peak of the temperature profile, related to the middle of the refining zone as shown in Figure 2.7 (first stage refiner), indicates that the least energy is applied in the fine bar section as well as close to the inlet. The position of the maximum temperature indicates the position of the turning point of the steam flow, which Miles and May (1990) termed the stagnation point. The steam velocity is zero at this point. The steam flows in opposite directions from the stagnation point. According

to Sundholm (1999, Ch. 4) it seems to be a difficult technical task to measure pressure and temperature at the same point. The same textbook reports that several trials have been conducted to measure the superheating of steam. These show that superheating is less than 5 ∀C. A Norwegian study has reported superheating to be three times larger (Holmberg (1992)).

Pressure measurement in a high-consistency refiner
Atack and Stationwala (1975) have shown that it is possible to put small sensors into the refining zone of a high-consistency refiner. Their work dealt with measurement of temperature and pressure in an open discharge refiner. The main purpose of the study was to obtain quantitative data on the magnitude and distribution of steam pressures generated in commercial refiners.

The trials were conducted on a 1.5 MW single disc refiner operating at 1800 rpm. The size of the refiner was 42 inch (1067 mm). This refiner was producing newsgrade pulp. The normal operating condition for this atmospheric refiner was a specific energy level at 1.8 MWh/tonne and a consistency of 30 %. The temperature in the refining zone was measured by copper-constantan thermocouples with a diameter of 0.25 mm. The cylindrical sheath of the temperature sensor had a diameter of 1.25 mm. The rise time of the sensor was found to be about 0.2 seconds. Miniature metal diaphragm transducers made by Kulite Semiconductor Products Inc. measured the refining zone pressures. The sensing element of the transducer was a semiconductor bridge network, and the outer diameter of the sensor was 3.75 mm. The natural frequency of the diaphragm was 80 kHz, and the rated pressure range was 0-7 bar with a maximum allowable pressure of 14 bar. Both the temperature and pressure sensors were mounted into a common hole in the refining plate.

The study was divided into two trials. First the instrumentation and the durability of the sensors was tested through the use of one set of sensors with an oscilloscope as the data-recording instrument. The second trial was extended to contain five sets of transducers. These were inserted in three of the refiner plates at different radial distances. The angle between the three plates was 120∀. A temperature recorder and a magnetic tape recorder collected the data. All the pressure transducers, except one, failed at some point during the last part of the second trial. All the temperature sensors worked satisfactorily.

The results showed a very stable temperature in the range of 120-135 ∀C under normal operating conditions. The radial temperature distribution was found to be roughly parabolic. The temperature of 132 ∀C corresponds to a saturated steam pressure of 1.85 bar. The pressure measurements showed a somewhat irregular, but periodic, pattern of variation of up to ∂ 0.28 bar around the value of the saturated steam pressure at the measured refining zone temperature. This variation was ascribed to local changes in the refining plate clearance. The periodicity of the varying signal was related to the period of rotation of the rotor disc. The rise time of the temperature sensor was not fast enough to explain whether the pressure fluctuations corresponded to fluctuations in the saturated steam pressure.

Intermittent pressure spikes up to 6.2 bar gauge pressure were observed with a frequency of approximately 14 kHz. This frequency corresponded to the bar frequency of the moving refiner plate. The spikes were ascribed to localized mechanical pressure resulting from the movement of large fragments of wood, which passed through this part of the refining zone. The second trial containing five pressure sensors showed random pressure spikes of approximately the same frequency. However, pressure spikes appearing at this frequency were obtained by all of the sensors located in different radial positions.

The following results were obtained from runs under different operating conditions:

- Increasing specific energy gave increasing temperatures in the refining zone. The consistency and motor load were held constant.
- Increasing consistency gave a decreasing temperature in the refining zone. The specific energy and motor load were held constant.
- Increasing consistency gave an increasing temperature in the breaker bar zone. The specific energy and motor load were held constant.
- Steam pressure generated in the refining zone accounted for between 50-70 % of the reaction force, which balances the axial load of the refiner disc. The rest of the reactive force is mechanical and originates from the wood fragments trapped between the refiner plates.

Additional information was given by the authors in a later article (Stationwala *et al.* (1979)). This article is based on results from a new and longer mill study. The latter article is related to measurements of the temperature in the refining zone and the plate clearance. The investigation has been focused on relationship between the measured variables and the process variables. However, the study has also been related to the relationship between the measured variables and the pulp quality. One of the conclusions was that no evidence was found of any large effects of refining zone temperature on the pulp quality.

Based on Equation (2.29), Isaksson *et al.* (1997) found that the steam pressure accounted for 68-75 % of the total axial thrust in the primary refiner, while approximately 60 % of the axial thrust appeared from the steam pressure in the second stage refiner.

An internal Norske Skog report from 1992 was based on an experimental study done by a research group at Norske Skog and provided some interesting results (Holmberg (1992)). The report states that their measurements indicated superheating in the refining zone. Therefore it is not so certain that a saturated condition can be assumed. If it is present, deviation will occur when computing the pressure in the refining zone directly from temperature measurements. The temperature and pressure measurements were made in a first stage TMP refiner. A TDC - True Disc Clearance - transmitter was modified and extended with a pressure sensor in the middle and two temperature sensors were placed diametrically. The sensors were placed in the bottom of the plate grooves.

The idea behind this study was to show whether it is possible to compute fast pressure changes using temperature measurements at the bars on the plates. The use of temperature measurement data in modelling work is common, but the measurements are used without checking the real pressure level. The question asked, was whether the Mollier diagram for water and steam in equilibrium can be used in connection with fast pressure changes.

The results showed that the computed saturated steam temperature was lower than the measured value. The difference was in the order of 10 % or approximately 15 °C. In addition, different pressure peak frequencies were obtained. The frequencies were assumed to be related to different process parameters. The bar frequency of the moving refiner plate was not obtained because the sampling frequency was too low. But an alias pattern was observed. It was assumed to be created by the bar frequency at the location of the sensors, which should be in the order of 10.8 kHz. Furthermore, other low frequency components were found. Both the angular velocity of the rotor disc appearing at 25 Hz in the frequency spectrum as well as two frequencies related to the revolution speed of the feeding screws at 10 and 11 Hz were observed. One frequency at 900 Hz was assumed to be related to the number of plates in the conical zone. A second trial was done after a period under ordinary operating conditions. The results from this period showed damped pressure peaks that were assumed caused by pulp packing in the space in front of the sensors.

Pressure measurement in low-consistency refiners

Nordman and co-workers reported in 1981 from an experimental study containing temperature and pressure measurements as well as plate clearance measurements. The pressure measurements were made using similar sensors as reported by Atack and Stationwala (1975). The pressure sensors were mounted both in a groove and a bar. The pressure that was measured had average amplitudes between 0.1 and 0.5 bar. However, these average values were calculated based on measurements captured from several revolutions of the rotor disc. No high peak values were found, but the authors indicated that shives and fibre knots damaged several of the pressure transducers. Results from a frequency analysis showed that the angular velocity of the rotor disc and its harmonic signals was observed as well as some higher frequencies. The latter were related to the bar crossing frequencies. In addition, the amplitudes were higher in the high frequency region than in the lower region.

Both Martinez *et al.* (1997) and Caucal *et al.* (1991), (1992a) and (1992b) have reported from Goncharov (1971). They claimed that Goncharov measured the pressure distribution over the bar surface in a low-consistency laboratory refiner and that the peak pressures were as high as 35 bar. Such high peak pressures were obtained at the edge of the bars. The average pressure reported by Goncharov was approximately 13 times lower than the peak pressures. Results from a study performed by Caucal *et al.* (1992b) indicated average pressures arisen from the fibres of approximately 8 bar. The authors claimed that this result corresponded with similar results obtained by Goncharov (1971) and Hietanen (1991). The measurements made by Caucal and co-workers were based on axial thrust measurements and the pressure values were accordingly calculated. The effective pressure on the fibre mat increased with increasing

axial thrust and thus decreasing plate clearance. Hietanen (1991) reported similar results. Furthermore, he measured pressures as high as 26.6 bar when the plate gap was only 15 μm. Refining during such extreme conditions led to a high degree of fibre cutting. In an earlier study, Hietanen and Ebeling (1990) discussed the energy inefficiency of low-consistency refining, the heterogeneous nature of refining and the role of flocs. One assumption that was related to the magnitude of the pressure pulses should give further attention. They referred to Ebeling (1980), who claimed that the pressure acting on flocs during a bar crossing may be as high as 100 bar. This assumption was made based on fairly low coverage of the bar intersecting area with fibres and that the fibres are treated as flocs. A coverage rate of 10 % was mentioned, and the pressure acting on a single floc could be up to 100 times the average refining pressure.

In two earlier reports Caucal *et al.* (1991) and (1992a) another measurement is described. In this work remotely mounted piezoelectric transducers were used. The pressure was assumed to be transferred through water in a pipe binding the transducer to the medium in the refining zone. A hole of 1.5 mm in diameter in a bar was made and the hole was tied to the tube at the back of the plate. Different tube lengths between 120 mm and 460 mm were tested and the authors found that the signals were damped when the tube length was increased. Reported pressure pulses were in the range of 0.5 bar to 1 bar. However, the frequency analysis showed that the bar-to-bar frequency was clearly visible. In addition, the number of plates and the number of bolt holes in the plates made significant periodic signal patterns especially when the plate clearance was small. A couple of frequencies that were of unknown origin were also observed. When the plate gap was high, no particular frequencies related to known process conditions were found. It was concluded that the bolt holes affected the pulp flow in the refining zone when the plate gap was small. The peak-to-peak value of this periodic pattern was as high as 3.5 bar, while the bar passage created pressure peaks of approximately 1 bar. Another conclusion was that the average hydraulic pressure was independent of the gap variations. It was indicated that only the flow of suspension was responsible of the internal pressure variations (Caucal *et al.* 1992a).

Normal and shear forces in low- and high-consistency refining

Researchers at the University of British Columbia and Paprican in Vancouver have reported a lot of interesting work related to studies of normal and shear forces imposed on fibres during refining. Their single bar laboratory refiner has been used to increase the knowledge about the influence of the forces. Among several articles the following references are particularly relevant: Martinez and Kerekes (1994), Martinez *et al.* (1997), Batchelor *et al.* (1997), Senger and Ouellet (2001) and (2002).

The normal and shear forces acting on the fibres and flocs of fibres play an important role of the final pulp quality. According to Senger and Ouellet (2002), which have referred to other sources, the normal force has been shown to contribute to internal fibrillation of the fibre wall through transverse compression and bending of fibres. On the other hand the shear force has been shown to cause external fibrillation and thus the production of fines. Thiruvengadaswamy and Ouellet (1997) claimed that shear stress induced by compression is more effective for structural breakdown of wood than

compression forces alone. Brought forward to refining, Hattula and Mannström (1981) stated that shear forces are most important in the innermost part of the refining, while the compression becomes more important in the outermost part because of the small plate gap.

Martinez *et al.* (1997) claimed that none of earlier reported measurements regarding pressure have been linked to the force applied to individual fibres or the size, structure and compressibility of flocs. In this article the authors describe the relationship between the strain imposed on a floc and individual fibre properties such as coarseness and diameter, floc consistency, compressibility. It was found that the effect of gap size on the peak force is strongly dependent on the size of the floc, the mass of fibres caught between the gap and the compressive modulus of the floc. As a result a theoretical and experimental force distribution as the bars passed over one another is shown. The authors claimed that the shape of this distribution is similar to the normal force distribution curve reported by Goncharov (1971).

In an earlier report, Martinez and Kerekes (1994), describe the behaviour of flocs during bar crossing. Flocs were found to remain intact at larger gap sizes, but ruptured into two parts at very small gap sizes. Luhde (1962) illustrated the latter phenomena as well. The authors indicated that the latter effect might be the similar effect that causes pad collapse and consequent plate clash in refiners. Such effect as a function of applied power and plate clearance is shown among several by Dumont and Åström (1988) and Dumont (1982).

An expression has also been derived to predict the shear force acting on an ideal floc (Batchelor *et al.* (1997)). The results from this study indicated that the shear force increased to a peak over the first part of the bar surface and then decreased to an even level over the remaining width of the bar. The shear force was strongly dependent on the magnitude of the normal force acting on the floc. However, the peak of the shear force was related to a corner force or as termed by Page (1989) a ploughing force (Batchelor *et al.* (1997)). Luhde (1962) also illustrated this phenomenon as an additional effect related to the leading edge of a bar.

Senger and Ouellet (2002) have used a similar approach as Batchelor *et al.* (1997), but they investigated the behaviour of shear forces upon high-consistency pulp flocs. One illustration of the forces acting upon a trapped floc and in addition a experimental result obtained by Senger and Ouellet (2002) showing the progress of the normal force and the shear force during a bar crossing are displayed in Figure 2.8.

Senger and Ouellet (2002) discussed the tangential coefficient of friction. Based on the asymmetry of the shear force profile over a bar width, which is assumed caused by the ploughing or corner force in the region of the leading bar edge, the authors introduced a new term of the tangential friction coefficient. They called it the equivalent tangential coefficient of friction and stated that the shear force is not simply a friction component of the normal force. Experimental results obtained from the single bar laboratory refiner showed that the equivalent tangential coefficient of friction increased with increasing floc consistency. In addition, for the higher grammage flocs, there was a substantial

drop in tangential friction when the bar was worn. Another indication was that the normal force did not appear to be influenced significantly by the degree of bar wear. The reason for the relationship between the tangential coefficient of friction and the consistency is related to the higher strength properties of the drier fibre network. The effect of wear is assumed related to the decreasing size of the ploughing force when the bars got rounded edges.

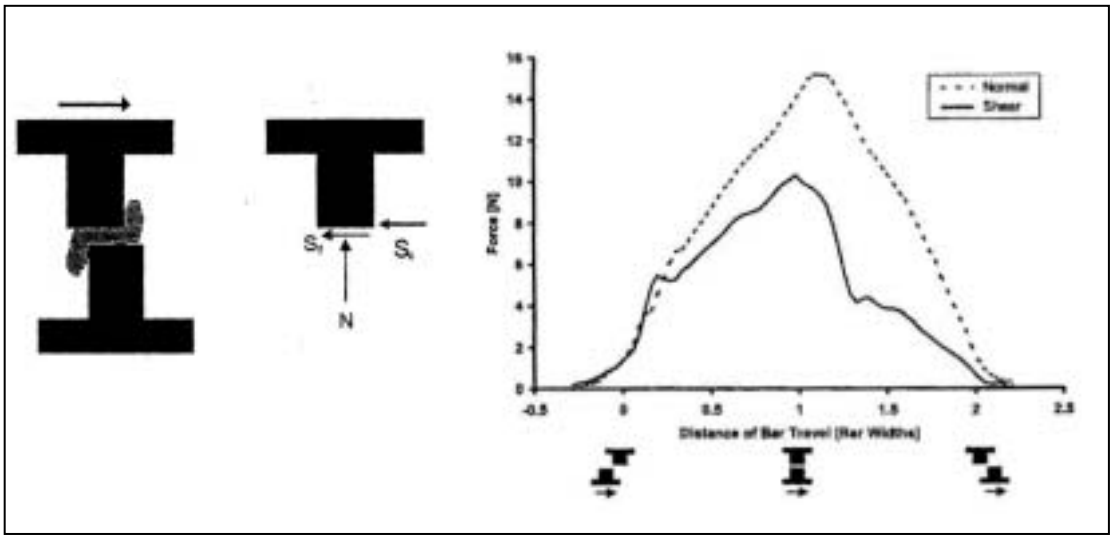

Figure 2.8: Illustration of the trapped floc and the forces acting upon it, and an experimental obtained result of the shape of the normal and shear forces during a bar crossing (Senger and Ouellet (2001) and (2002)).

2.3.4 Influence of dynamic conditions in the refining zone

The previous investigations of the pressure in the refining zone have revealed periodic signal patterns that can be related to particular process conditions. Both Atack and Stationwala (1975) and Caucal *et al.* (1992a) have identified the bar crossing frequencies. Furthermore, Atack and Stationwala (1975) indicated that one particular bar crossing frequency was detected by several sensors irrespective of radial location. In addition, the angular velocity of the rotor disc was clearly visible in several studies (Atack and Stationwala (1975), Nordman *et al.* (1981), Holmberg (1992)). Observations of frequencies related to the number of bolt holes and the number of plates in the refining zone have also been made (Caucal *et al.* (1991), Holmberg (1992)).

Vibrations in disc refiners

It is known from fundamental vibration theory that motion of a linear system resulting from an applied sinusoidal force will always be sinusoidal at the same frequency as the force (Petrusewicz and Longmore (1974)). Based on this knowledge a study related to investigations of the relationship between high frequency vibrations in a disc refiner and the pulp quality has been reported by Strand and Hartler (1985) and Strand and Mokvist (1987). They indicated that the origin of vibrations is directly related to the intensity of the pressure pulses resulting from the passing of rotor and stator bars. Thus, Strand and

Mokvist (1987) assumed that the intensity of the vibrations corresponding to the refiner bar frequencies could be used to characterize the dynamic forces applied to the fibres. In this article they showed one frequency spectrum based on a vibration analysis made on one refiner and another spectrum showed the frequencies obtained from the corresponding bar intersecting area (bar pass area). The similarities between these spectra are striking. The former study was performed using a special designed accelerometer mounted on the back of a stator plate. The frequencies related to the accelerometer signal could be divided into four definite regions, as shown in Figure 2.9, corresponding to the breaker bar, coarse bar and fine bar sections in addition to vibrational overtones as equivalent termed harmonics (Strand and Hartler (1985)).

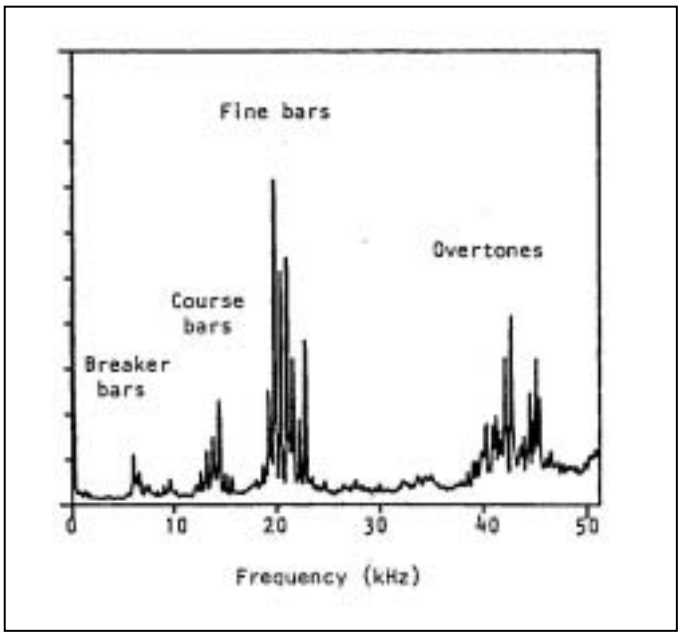

Figure 2.9: The frequency spectrum made on measurements of vibrations obtained by Strand and Hartler (1985) shows four distinct regions corresponding to the different sections of the refiner plates.

Another interesting result from this study was that the vibrational energy, obtained using the accelerometer, increased with increased radial position. Maximum energy was obtained approximately 20 mm from the plate periphery indicating that energy is applied throughout the entire fine bar section. According to the authors, this is contrary to the assumptions made by Miles *et al.* (1980) in their work related to modelling of the steam flow behaviour. Furthermore, the vibrational energy was strongly affected by plate wear both as damped amplitudes and as change in radial distribution. After 900 operating hours no peaks were obtained in the radial distribution of the vibrational energy thus indicating that the applied energy was distributed more evenly across the refining zone. Both vibrational energy distributions are shown in Figure 2.10. In the region of the high vibrational energy that was measured on the new plates, a particularly high degree of plate wear was observed. An additional result was that the vibrational

energy together with the specific energy and the residence time predicted pulp quality very well (Strand and Hartler (1985)).

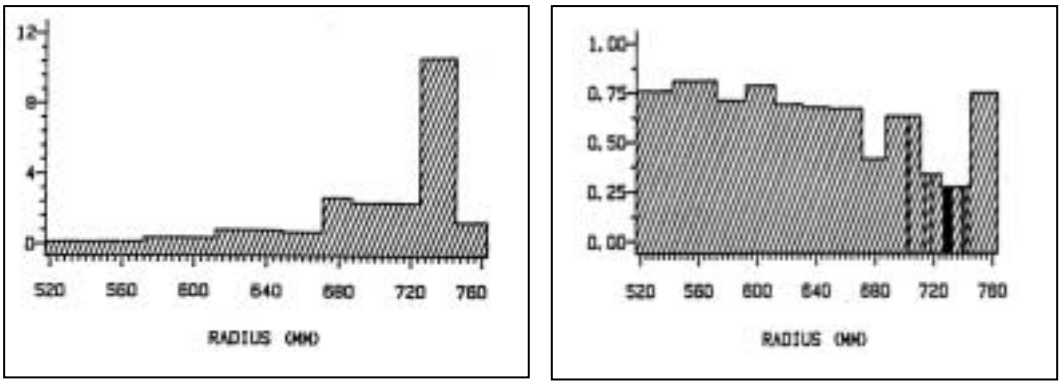

Figure 2.10: Results obtained by Strand and Hartler (1985) show that the relative vibrational energy per unit area ($10^6/s^4$) was strongly shifted towards the periphery (left-hand plot) when the plates were new. When the plates were worn the vibrational energy distribution was more even (right-hand plot). The dark vertical lines indicate positions on the plate that showed clearly visible wear after removal of the plates.

Both Wultsch and Flucher (1958) and Pettersen and Gunstrøm (1980) have used phonometric measurements on the refiner housing. They have related the noise and vibration measurements to be in direct connection with the motor load of the refiner. The latter report was related to noise and vibration analysis from conical beaters and disc refiners. Among the conclusions was that pressure pulses generated from bar crossing created vibrations both in the stator and the rotor disc. Thus, the vibrations generated acoustic oscillations. Furthermore, the analyses have revealed that the peak frequencies were shifted towards lower frequencies when the motor load was increased. The shift was not large. The different power spectra indicated a shift of only a few Hertz. This phenomenon was assumed to be due to lag in the motor related to its synchronized rotational speed.

Additional results reported by Pettersen and Gunstrøm (1980) were as follows:

- New plates generated more noise and larger vibrational energy than worn plates.
- Higher axial thrust gave increased vibration amplitudes. In addition, the peak frequencies related to the region closer to the inlet (lower frequencies) were more dominating compared to the predominant higher frequencies, related to the outer part of the refining zone, when the axial thrust was lower.
- Sideband effects were observed. These were obtained as frequency peaks on both sides of the bar crossing frequencies. Especially the rotational speed and its multiple frequencies were obtained as sidebands. Some of the sideband frequencies had higher amplitude values than the bar crossing frequencies. Such sideband effects

were ascribed to irregularities in plate clearance and whirling of the disc-shaft assembly.

- Harmonic frequencies related to the bar crossing frequencies were also observed.
- Vibration analyses related to radial position showed a parabolic curve indicating a parabolic distribution of the applied energy. Similarities related to temperature measurements are apparently obvious.
- These investigations also showed that the beaters had several natural frequencies especially in the regions between 700-1600 Hz and between 2-4 kHz. The most powerful natural frequencies were found in the latter region.
- Wave patterns in the surface structure of the housing were also detected when the housing was put in vibrations.
- One experiment performed on a stator plate in conical beater showed a shift in radial direction up to 0.02 mm. This indicated that the clearance between the stator and rotor varied during operation because of wave propagation in the stator and rotor. Assuming that similar wave propagation occurs in disc refiners similar variations between the stator and rotor disc would appear in axial direction causing fluctuating plate clearance.

Periodic oscillations

Oscillation effects related to variations in plate clearance in disc refiners have been observed and reported during the past decades (May (1970), May *et al.* (1973), Breck *et al.* (1975), Ohls and Syrjänen (1976), Miles and May (1977), Stationwala and Atack (1980), Stationwala *et al.* (1979), (1991)). According to Miles and May (1977) dynamic fluctuations in plate clearance might have a positive effect on pulp properties, but these might have negative effect on plate life and machine durability.

The most common oscillation effects are described in terms of run-out, out-of-tram and oscillations associated with shaft whirl arising from out-of balance mass (Stationwala and Atack (1980)). Out-of-tram refers to the condition where the shafts of the refiner are tilted with respect to each other, while run-out refers to the condition where the disc is not at right angles to the axis of the shaft. Both effects represent non-parallelism of the planes of the disc. In the out-of-tram state the plate clearance is constant at any fixed point in space, while in a run-out condition the clearance varies cyclically (May (1970)). It is seen that the variations of plate separation arising from out-of-tram misalignment occur at a frequency related to the rotational speed whereas those arising from run-out and whirl occur at the double frequency (Stationwala and Atack (1980)).

The phenomenon wherein the discs are tilted by passage of the pulp flow has been called dynamic-out-of-tram. Normal out-of-tram due to misalignment of the shaft bearings has been called static-out-of-tram. The dynamic effect can cause several times as large deflections as the static generated deflections (May (1970)). May also showed that as soon as chips entered the refiner the imbalance was decreased. He could not conclude whether the imbalance was prevented, or the pulp formed a mechanical link between the discs that made them both tilt in phase with each other. Frazier (1985) claimed that the refining process can tolerate large changes in the gap and will also tolerate a certain amount of lack of tram or run-out by whirling of the disc-shaft assembly. However, the presence of non-parallelism is claimed to contribute towards

load fluctuations (Ohls and Syrjänen (1976)). Ohls and Syrjänen have shown that there appears to be no correlation between the swing in motor load and the axial movement of the rotor despite of high correlation between the load and the axial force. They proposed a hypothesis that steam blow-out is a localized phenomenon, causing momentary gap emptying, which is measured as a sudden change in both motor load and axial force rather than as rotor movement. They claimed that the rotor movement is only in the order of 0.5 µm when the refiner is loaded. Larger gap variations, in the order of several millimetres, have been reported by Miles and May (1977) and May *et al.* (1973). The latter report showed that the disc oscillation was accompanied by a rise in temperature towards the periphery. A temperature of 130 ∀C towards the periphery in an atmospheric refiner was obtained. The reason for this high temperature was related to plate touching.

Ouellet and Weiss (1994) have reported a very interesting theoretical approach related to axial vibrations of the rotor assembly in a disc refiner. Based on initial investigations showing that the reaction force from the pulp in the refining zone can vary in a deterministic way, and that this force can vary randomly because of changes in the distribution of material inside the refiner, a model was proposed. Since the reaction thrust from the pulp pad can vary with time the authors expected that it could be a driving force for axial vibrations.

The equation of motion for a single-rotating disc with the stator plate as reference position is shown in Equation (2.33):

$$M\frac{d^2x}{dt^2} 4 F_P 4 F_S 2 F_B \mid 0 \qquad ; [N] \tag{2.33}$$

M : *Mass of the rotor assembly; [kg]*
x : *Plate gap; [m]*
t :*Time; [s]*
F_P : *Total reaction mechanical thrust from chips (pulp); [N]*
F_S : *Total reaction thrust from steam; [N].*
F_M : *Total axial (hydraulic) thrust supported by the bearing; [N].*

This theoretical investigation aimed at modelling the total reaction force from the pulp pad. The assumptions for the model were as follows:

∉ The rotor assembly is a rigid body.
∉ The rotor and stator plates are parallel.
∉ A viscoelastic stress-strain relation can describe the pulp behaviour.
∉ Only pulp caught between two intersecting bars could support a load. Pulp in the grooves is neglected as contributing to the reaction force.
∉ Also forces originating from the breaker bar region were neglected because of the larger plate clearance.

A four-parameter non-linear model for the pulp pad was proposed. The differential equation for the total stress was solved numerically. The authors pointed out that

evaluation of the involved parameters was difficult because of lack of available data in the literature. Values of mechanical thrust reported by Atack and Stationwala (1975) were used to represent the average reaction force from the pulp pad. Furthermore, experimental data related to dynamic compression of pulp under constant strain rate reported by Goncharov and Zyulkov (1974) were used as reference data. According to Ouellet and Weiss, this article showed that the stress developed during compression was not a linear function of strain.

A strain model was proposed to determine the total load supported by the pulp pad. It involved an initial pulp pad thickness of height $h + x$ above the stator bar surface, and a final thickness x when the pulp pad was trapped and compressed between the bars. The resulting strain was expressed as Equation (2.34):

$$\kappa | \frac{h}{h 2 x} \quad ; \tag{2.34}$$

h : Part of the pulp pad thickness greater than the plate gap; [m]
x : Plate gap; [m]

The following assumptions were made regarding input values in the simulation model of the stress behaviour:

- Plate gap: 0.1-0.68 mm.
- Pad thickness beyond the plate gap thickness: 0.4-1.0 mm.
- Fibre coverage factor: 50-80 %. (Based on observations made by Atack and Stationwala (1990)).
- Total reaction force from the steam is based on the assumption that 50-70 % of the total axial thrust is resisted by the steam force (Atack and Stationwala (1975)). A value of 50 % was used.
- Data regarding tilting-pad thrust bearings were also included in an extended total force from the bearing.

The simulation results from this study indicated that bar coverage variations could significantly contribute to axial vibrations. However, the peak-to-peak amplitudes were to a large extent very small. Simulation results indicated variations up to approximately 1 μm. The response was also dominated by a resonant component in the low frequency band (below 200 Hz). This was assumed to be related to a resonance effect. The natural frequency of the rotor assembly was assumed to be approximately 300 Hz. Therefore, a new test was run to check if a driving force in the low frequency range could make any differences. A sinusoidal force with a frequency similar to the lowest bar crossing frequency in the breaker bar section was used as the excitation force. The simulated gap variations exceeded 6 μm indicating that low frequency driving forces can generate larger vibrations than the high frequency components alone. This will presumably be true when the frequencies of the driving forces are close to the natural frequencies of the system.

The absence of high frequency plate gap variations despite the high frequency components related to the variations of the bar intersecting area, which was claimed limited to 15 kHz as the lowest strong frequency component, was probably related to the large mass of the system. According to Petrusewicz and Longmore (1974), when the frequency of the force is very high, the system does not have time to respond so the displacement amplitude is very small. The applied force simply accelerates the mass. The acceleration of the mass is proportional to, and hence in phase with the applied force, while the displacement of the mass will be 180∀out of phase with its acceleration.

Ouellet and Weiss (1994) also discussed the damping effect introduced by the hydrodynamic bearing. They concluded that under normal operating conditions, the damping from the bearing should keep vibrations at a sufficiently low level. When discussing observations made by Ohls and Syrjänen (1976) that indicated gap variations in the order of 0.5 μm in an industrial refiner, Ouellet and Weiss claimed that such variations could also result from dynamic out-of-tram. This study indicated that there are only small axial vibrations resulting from deterministic variations of bar intersecting area and random variations of bar coverage by pulp.

2.4 Summing up

This literature review has revealed a lot of interesting features about the refiners and furthermore within the refining zone as should be considered important for the present study. The following results are extracted from the previous discussions:

- The response of the wood material to mechanical treatment is greatly affected by temperature, moisture and time under load.
- Only a small portion of the energy is used in the structurally deformations of the wood, while to a large extent the energy is transferred to heat through the viscoelastic character of the wood.
- A rise in frequency has to be compensated for by a rise in temperature to maintain the same efficiency in the structural breakdown.
- The papermaking fibres are made by repeated or cyclic influence of compressive and shear forces executed by passing bars of the rotating disc.
- Despite a general opinion about the main refining mechanisms the prevailing theoretical model, Miles and May equations, about the pulp flow behaviour in the refiner is the object for discussion.
- Visual inspection of the pulp flow behaviour has showed that 50-70 % of the mid-region of the refining zone was covered with pulp. The inner section was covered with 70-80 % of pulp and the outer section was covered even more.
- Back-flow velocities up to 30 m/s were observed in the coarse (breaker bar) zone. Forward-flow had velocities up to 20 m/s in the fine bar zone. Tangential flow of pulp was observed in the transition zone between the intermediate and fine zone with a velocity of approximately 20 m/s.
- Pulp flow in the intermediate zone grooves was very turbulent. The back-flow velocity was about 1 m/s. Approximately 60 % of the area of the grooves was

covered with pulp. It was observed that the amount of water was high in the intermediate zone. In the refining zone grooves the pulp velocity was about 30 m/s.

- A theoretical approach showed that it is possible to calculate the mechanical thrust from chips or pulp as a function of the motor load.
- If it can be assumed that the steam is saturated, then the steam pressure can be obtained from measurements of the temperature in the refining zone.
- Steam pressure generated in the refining zone is assumed to be accounted for between 50-70 % of the total reaction force.
- Pressure measurements in a high-consistency refiner have shown a periodic pattern of variation of up to ∂ 0.28 bar around the value of the saturated steam pressure. Pressure spikes up to 6.2 bar gauge pressure were observed.
- In low-consistency refiners several measurements are reported. The measured pressures have shown large variations. One study showed average amplitudes between 0.1 and 0.5 bar.
- Another study reported peak pressures up to 35 bar obtained at the leading edge of the bar. The average pressure was approximately 13 times lower than the peak pressure.
- A third study showed that increasing axial thrust and thus decreasing the plate clearance leaded to increasing pressure. Pressure as high as 26.6 bar was measured.
- A theoretical study indicated that the pressure acting on flocs during a bar crossing may be as high as 100 bar. This assumption was made based on fairly low pulp coverage of the bar intersecting area.
- The equivalent tangential coefficient of friction has been introduced based on results showing that the shear force is not simply a friction component of the normal force.
- The previous investigations of the pressure in the refining zone have revealed periodic signal patterns that can be related to particular process conditions. The bar crossing frequencies have been observed. In addition, one particular bar crossing frequency was detected by several sensors irrespective of radial location. The angular velocity of the rotor disc was clearly visible in several studies. Observations of frequencies related to the number of bolt holes and the number of plates in the refining zone have been made.
- Indications about the origin of vibrations in disc refiners have been made. It has been claimed that vibrations are directly related to the intensity of the pressure pulses resulting from the passing of rotor and stator bars.
- The frequencies related to collected accelerometer signals could be divided into four definite regions corresponding to the breaker bar, coarse bar and fine bar sections of the plates in addition to vibrational overtones.
- Peak frequencies obtained by vibration analyses were observed shifting towards lower frequencies when the motor load increased. The shift was of only a few Hertz. This phenomenon was assumed related to lag in the motor load.
- New plates generate more noise and larger vibrational energy than worn plates.
- Higher axial thrust gave increased vibration amplitudes. In addition, the peak frequencies related to the region closer to the inlet were more dominating at high loads compared to the predominant higher frequencies, appearing from the outer part of the refining zone, when the axial thrust was lower.

- Sideband effects have been observed through vibration analyses. These were obtained as frequency peaks on both sides of the bar crossing frequencies. Especially the rotational speed and its multiple frequencies were obtained as sidebands. Some of the sideband frequencies had higher amplitudes than the amplitudes of the bar crossing frequencies. Such sideband effects were ascribed to irregularities in plate clearance and whirling of the disc-shaft assembly.
- Harmonic frequencies related to the bar crossing frequencies have been observed.
- Vibration analyses related to radial position showed a parabolic curve indicating a parabolic distribution of the applied energy. Similar shapes are typically for temperature distributions as well.
- Vibration analyses showed that conical beaters had several natural frequencies.
- Wave patterns in the surface structure on the housing of conical beaters were detected when the housing was subject to vibrations.
- The plate clearance between the stator and rotor has been observed to vary during operation.
- It has been seen that the variations of plate separation arising from out-of-tram misalignment occurs at a frequency related to the rotational speed whereas those arising from run-out and whirl occur at double the rotational frequency.
- There appears to be no correlation between the swing in motor load and the axial movement of the rotor despite high correlation between the load and the axial force. A hypothesis has been proposed indicating that steam blow out is a localized phenomenon causing momentary gap emptying. This has been measured as a sudden change in both motor load and axial force rather than as rotor movement.
- A simulation result indicated that axial vibrations resulting from deterministic variations of bar intersecting area and random variations of bar coverage by pulp are small. However, this effect might contribute to axial vibrations and hence plate gap variations.

CHAPTER 3

MATERIALS AND METHODS

3.1 Introduction

This chapter describes the refining system and the conditions during the experiments. The refiners and plates both in mill-scale and pilot-scale are described in Section 3.2 and Section 3.3. Since both mill-scale experiments were performed in the same refiner, parts of the following descriptions are divided into two subsections: a mill-scale and a pilot-scale. However, sometimes the differences between the two mill-scale experiments were distinct and demand particular attention. This is especially related to the plate patterns and the sensors and their location.

Descriptions of conditions in this case mean typical running conditions related to chip treatment, feeding, consistencies, power and energy consumption. The current plates and their bar-groove patterns are described in the sense of cyclic treatments of the chips and pulp. In connection with the mill-scale experiment using fibre-optic sensors the rotor plate is shown together with the corresponding location of the sensors and the corresponding bar crossing frequencies. This is shown in Section 3.3.3. The bar passing frequencies are given by the number of bars at the associated radial location. Moreover, the bar and groove widths and the tangential speed at the corresponding radial location can be used to determine the bar crossing frequencies. The effect of the broaden plate clearance related to the tapers of the plates is also shown in this section.

Section 3.4 is devoted to discussions about the expected pressures in the refining zone. An intuitive approach is made and compared with theoretical assumptions and experimental experience shown in the literature. Furthermore, the sensors and data acquisition equipments are described in Section 3.5. The external accelerometers used as supplement to the second mill-scale experiment are described in this section as well. The experimental procedures and the data analysis methods are described in Section 3.6 and Section 3.7.

3.2 Process descriptions

3.2.1 Mill refiner

The mill-scale experiments were performed in the TMP2 plant at the Norske Skog Follum mill in Norway during production of newsgrade pulp. TMP2 comprises two similar lines, A and B, with Andritz Twin 60 inch (1524 mm) refiners in two stages. The reject is sent back to the second stage refiner. The primary refiner in line B, equipped with 62 inch (1575 mm) plates, was used as the case refiner in these studies. This refiner was driven by a 16 MW synchronous motor denoted GBA 1000 from ABB Inc. An illustration of the Twin refiner is shown in Figure 3.1.

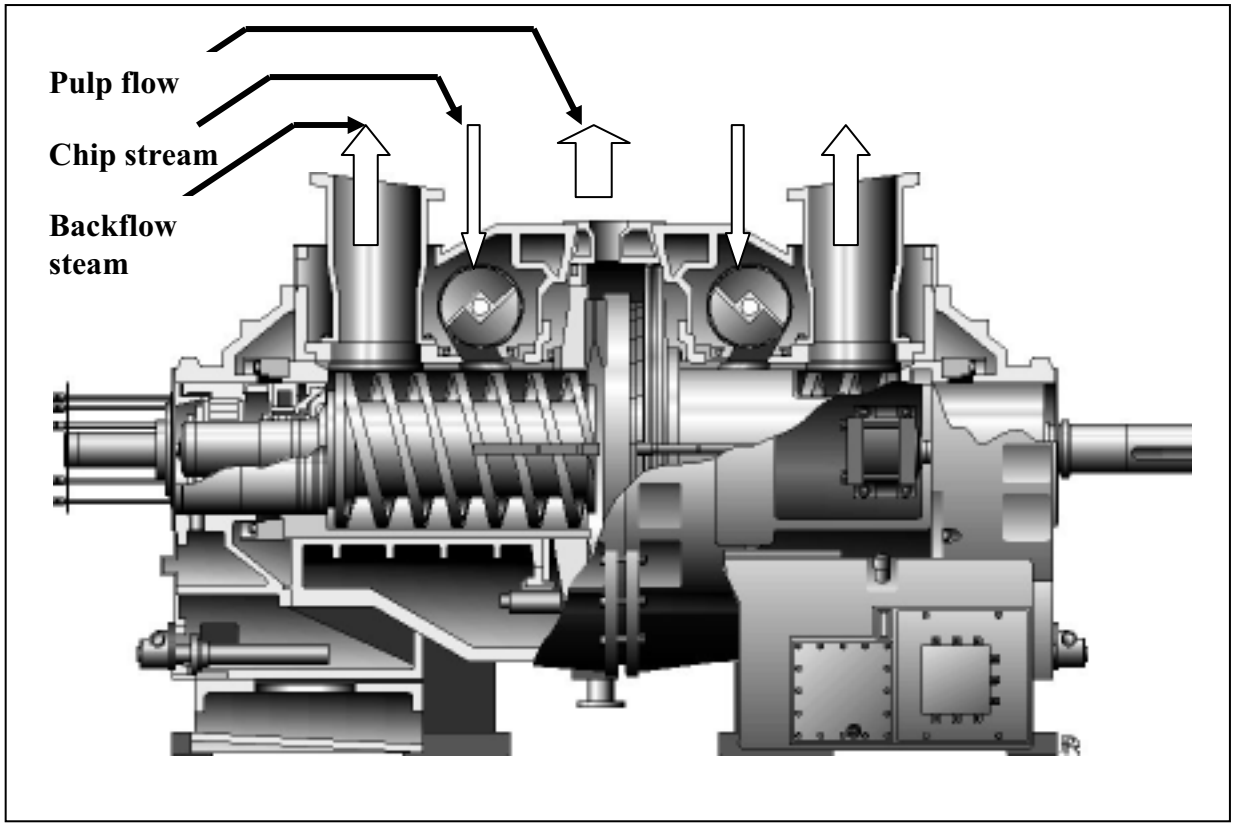

Figure 3.1: Twin-60 refiner from Andritz Inc.

The Twin refiner is designed for a large production capacity and contains two flat stationary discs and a double-sided rotor disc in between. In this way, axial thrust is balanced on both sides of the rotating disc. According to Sundholm (1999, Ch. 7), the symmetry related to the balanced axial forces maintains a good parallelism of the refining zones. Four hydraulic cylinders, two cylinders on each stator disc, accomplish the loading of the refiner. Equal loading on both sides are assured through the hydraulic system (Sundholm (1999, Ch. 7)). However, the rotor disc in this specific refiner is equipped with apparently a fix bearing that has a slack up to 0.4 mm[5]. Furthermore, the

[5] Jan Hill, Norske Skog Research. Private communication (2002).

chip distribution in the two refining zones is to a certain degree manual controlled. Thus the loading of the refiner is not completely equally distributed on both sides despite the hydraulic trust being similar on both sides.

The plate protecting system contains accelerometers located in each stator disc. The acceleration measurements measure the vibrations that are generated when the refiner plate bars pass each other. This provides signals that can be used to indicate the gap clearance between the plates. However, both the accelerations and the loads of the load-sense conveyors are used to anticipate plate contact and consequently unload the refiner when it is necessary. At the Norske Skog Follum mill acceleration values are given in per cent of a rated range of the number of g (acceleration of gravity) [6].

Chips are presteamed in an open atmospheric chip bin and fed by means of a plug screw feeder with a rated maximum rotational speed of approximately 140 rpm. The chip stream is divided in two separate streams through the load-sensing conveyors that transfer the presteamed chips into two refiner inlets. A sketch of the two power screws of the load sense conveyor is shown in Figure 3.2.

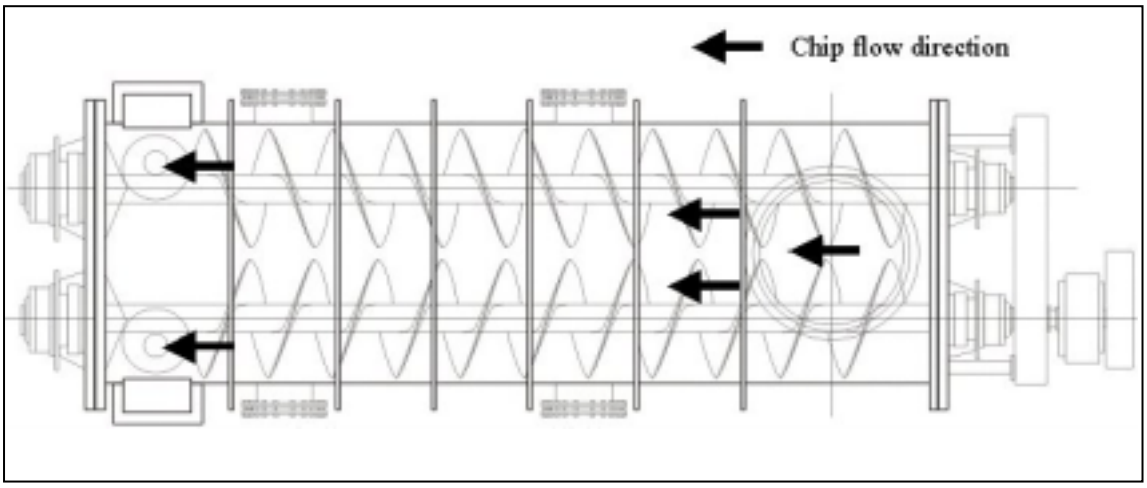

Figure 3.2: The power screws of the load-sense conveyor.

The chip distribution in the two refining zones of the Twin refiner is to some extent determined by the difference in the angular position of the two screws feeding the refiner. The angle variations are obtained through adjusting an actuating device on the stream splitter called Giri-gari. Through a manual switch the Giri-gari device adjusts the angle of one of the power screws. The other power screw is fixed in one position. The total number of positions is 262 thus one-step change causes an angle shift of approximately 1.4∀ The positions of the two power screws determine how the chips from the plug screw are fed in and filled up in the two parallel screws feeding each of the refining zones. However, the Giri-gari value is not a measurement of the chip distribution in the two refining zones of the Twin refiner. It is an indication of the

[6] 0-100 %: 0-20 g (1 g = 9.8 m/s^2).

difference in the angular position, and it can be used to equalize the refining zone properties in the two zones (Mosbye *et al.* (2001)).

The refiner's feed screws on both sides of the rotating disc are of the ribbon-type design as shown in Figure 3.3. The ribbon is attached to the main shaft; hence the ribbon feeder rotates at the same speed as the shaft and the rotor disc. The chips are imposed by the centripetal acceleration that force the wood material to the periphery of the feeder barrel, thus allowing back flowing steam to escape in the middle along the shaft. In this way, steam does not disturb the feed of chips into the refiner. Pressurized dilution water is fed in through valves in the center of the refiner together with the chips. Pulp and steam are flung out at the periphery of the refining zone into the casing and further into the blow line located at the top of the refiner. Before entering the second stage refiner, steam and pulp are separated in cyclones.

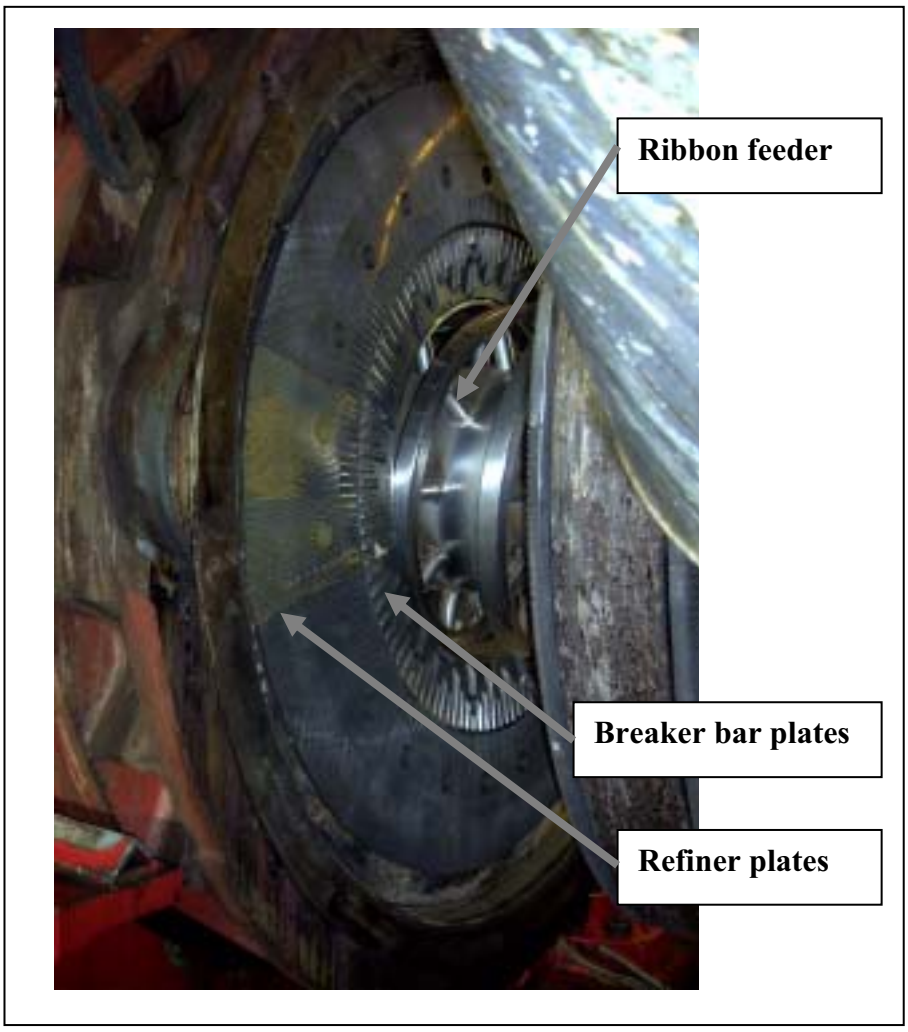

Figure 3.3: Image of the drive side stator disc attached with breaker bar and refiner plates. The ribbon feeder attached to the refiner shaft is visible in the centre of the refiner.

Normally 25 % of the chips used in this TMP plant are sawmill chips from Norway spruce (*Picea abies*). However, during both of the experimental periods only on-site produced chips from Norway spruce were used. Based on experience the moisture content of these chips varies between 40 and 50 % and the bulk density is in the range of 145 to 155 kg/m^3 (Mosbye *et al.* (2001)).

Typical operation conditions are as follows:
- Rotational speed: 1500 rpm (25 rps).
- Casing and inlet pressure: 4 bar gauge. The refiner's inlet and outlet (casing) is short-circuited by the steam.
- Motor load: 13-15 MW. The motor load is rated to 16 MW.
- Plug screw speed: 64-72 %[7] (90-100 rpm). Maximum rotational speed is 140 rpm.
- Production rate: approximately 280 tonnes per day (1.6 kg/s in each refining zone).
- Specific energy consumption of the primary refiner: 1100-1200 kWh/tonne.
- Axial thrust: 1200-1300 kN on each stator disc provided by approximately 110 bar differential pressure across each of two hydraulic cylinders on each stator disc. In Section 3.4 the thrust balance is described in more detail.
- Dilution water: approximately 2.0 l/s on each side.
- Pulp consistency: 35-40 %.

3.2.2 Pilot refiner

The test run performed in the pilot refiner was done on a 20 inch (510 mm) atmospheric single disc refiner at the Norwegian University of Science and Technology in Trondheim, Norway. The pilot refiner was used as a first-stage high-consistency refiner producing refined mechanical pulp (RMP). The refiner characteristics were:
- ROP Defibrator Asplund Raffinator AB, Stockholm 1968.
- Maximum motor power: 132 kW.
- Refiner speed: 1500 rpm.
- Plug screw speed: 69 rpm.

Chips of Norway spruce prepared by the Norske Skog Skogn mill were used in the experiment. The following preparation steps were made:
- Impregnation of the chips in water for approximately 12 hours.
- Pre-steaming of the chips for approximately 20 minutes at 1 bar gauge pressure.
- The dry content of the chips after the steaming was approximately 47 %.

The refiner was pre-heated by using dilution water.
- The temperature of the dilution water was approximately 53 ∀C.
- The pre-heating lasted for approximately 30 minutes, and included calibration of the refiner disc clearance.

Typical operation conditions were as follows:
- Net refining power: 30-50 kW.
- Plate clearance: 0.5-1.0 mm.

[7] Norske Skog Follum uses per cent of the rated maximum rotational speed.

- Production rate: approximately 1.4 tonnes per day (0.015 kg/s)
- Specific energy consumption: 500-1000 kWh/tonne.
- Pulp consistency: approximately 20 %.

3.3 Refiner plates and the radial location of the sensors

3.3.1 Mill-scale experiment – piezoresistive sensors

The first mill-scale experiment was performed using piezoresistive sensors mounted into a plate manufactured by J&L Fiber Services Inc. A description of the experimental procedure is shown in Section 3.6, while the specifications of the sensors are recorded in Section 3.5.

The rotor and stator discs were equipped with plates of the type 62SWP 114/115. Each set contains 12 plates, which form the complete ring of plates. One of the stator plates at the drive side of the refiner was modified in a small area allowing the interleaving of the sensors. A stator plate is shown in Figure 3.4. The holes shown to the left in Figure 3.4 were equipped with temperature sensors provided by J&L Fiber Services Inc. The temperature data were available as a part of the process data. Apart from the angle of the bars the stator plate is similar to the rotor plates that were used.

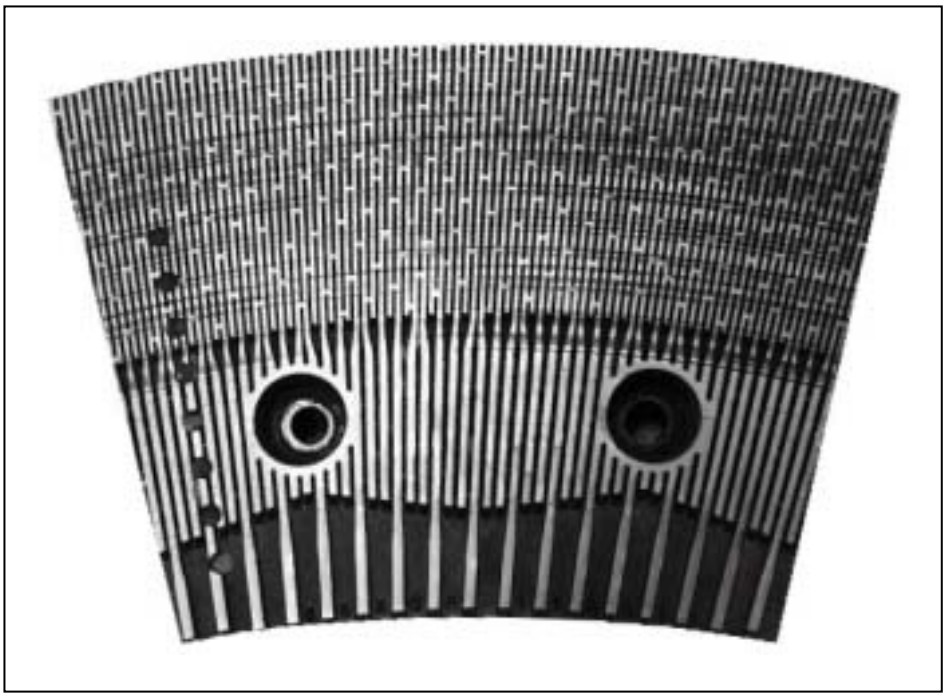

Figure 3.4: This is a stator plate provided by J & L Fiber Services, Inc. In both mill-scale experiments this type of plate was used. In the first mill-scale experiment a similar type was used on the rotor side as well.

Figure 3.5 shows the modified part of the stator plate where the piezoresistive transducers were mounted.

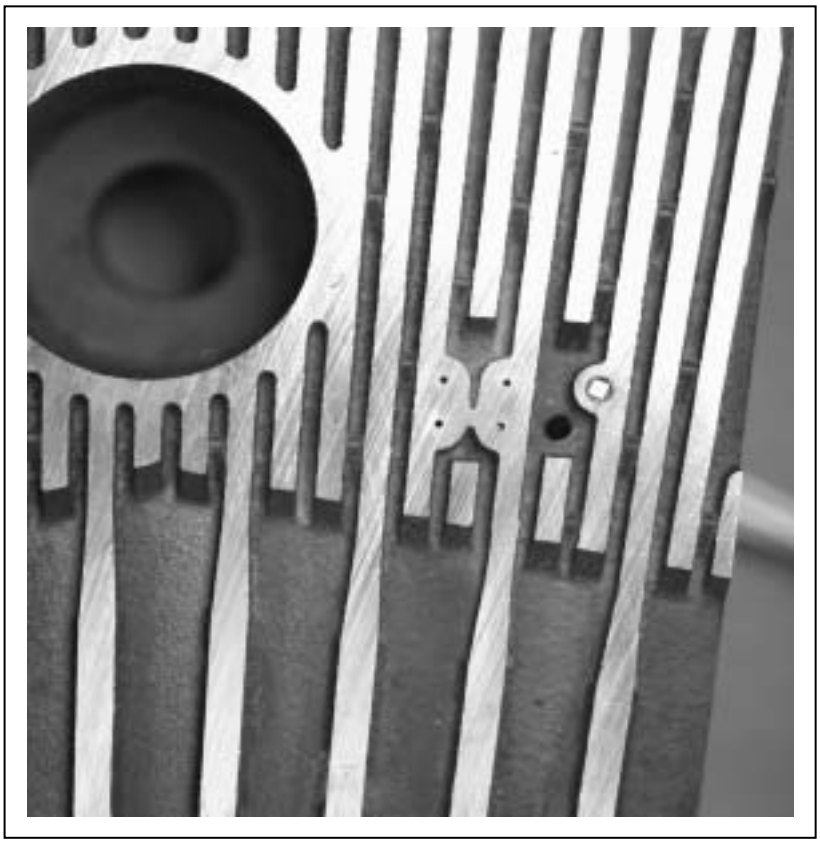

Figure 3.5: The modified part of the stator plate equipped with the piezoresistive transducers used in the first mill-scale experiment.

The breaker bar section consists of six plates. None of these are shown as a separate picture. However, the breaker bar section is visible in Figure 3.3.

Characteristic data related to the different zones and corresponding number of bars in the rotor plates are displayed in Table 3.1.

Table 3.1: Data related to the rotor plates used in the first mill-scale experiment.

Zones of the rotor plates	Radial location		No. of bars per plate [Bars/plate]	No. of bars per revolution [Bars/rev.]	Bar crossing frequency [kHz]
	Start [mm]	End [mm]			
Breaker bar	305		2	12	0.3
			6	36	0.9
		508	20	120	3.0
Coarse	508	560	17	204	5.1
Intermediate	560	650	52	624	15.6
Fine bar	650	788	90	1080	27.0

Notice that the bar crossing frequencies related to the number of bars in the different zones, right column in Table 3.1, are constant within each zone. The breaker bar plates can be divided into three zones as well, each zone gives a constant bar crossing frequency as shown in Table 3.1. Furthermore, the pulp flow might be affected by additional geometrical conditions concerning the plates and the chip feeding mechanism. It can be mentioned that the plates are attached to the disc by large bolts. The refiner plates have two bolt holes each. These bolt holes might disturb the flow of pulp through the refining zone, hence it should be realized that the bolt holes can be associated with frequencies at 300 Hz and 600 Hz in the frequency spectra. The first frequency is related to the bolt holes in the breaker bar plates, while the latter appears as a result of the number of bolt holes in the main refiner plates. The bolt holes in the main refiner plates are located in the intermediate zone at a radial distance of 610 mm. Each of the holes has a diameter of 39 mm. As shown in Figure 3.4, the bolt holes in the rotor plates partly covered the location of the transducers. Furthermore, the ribbon feeder consists of 12 ribbons that might affect the pulp flow through the refining zone. In that case, an influence of the pulp flow, which might be picked up by the transducers, would occur at a frequency of 300 Hz. The frequency related to the rotational speed, which is 25 Hz, is another periodicity that is important to be aware of.

Four of the holes in the plate shown in Figure 3.5 were equipped with piezoresistive sensors, three from Kulite Semiconductor Inc. and one from Presens AS, a Norwegian manufacturer. Further details regarding the sensors and their locations are given in Section 3.5. The sensors were mounted in the intermediate zone at radial locations of approximately 575 mm and 585 mm from the center of the refiner.

3.3.2 Pilot-scale experiment – piezoresistive sensor

In the pilot refiner the plates both at the stator and rotor discs were made of one piece, consequently they were not divided into several segments. A picture of the stator plate is shown in Figure 3.6. The rotor plate was identical to the stator plate.

Characteristic numbers related to the rotor plate are displayed in Table 3.2.

Table 3.2: Data related to the rotor plate used in the pilot-scale experiment.

Zones of the refiner plate	Radial location		No. of bars per revolution		Bar crossing frequency	
	Start [mm]	End [mm]	[Bars/rev.]	[Bars/rev.]	[kHz]	[kHz]
Breaker bar	100	140	18	18	0.45	0.45
Coarse	140	170	90	90	2.25	2.25
Intermediate	170	210	90	126	2.25	3.15
Fine bar	210	255	270	288	6.75	7.20

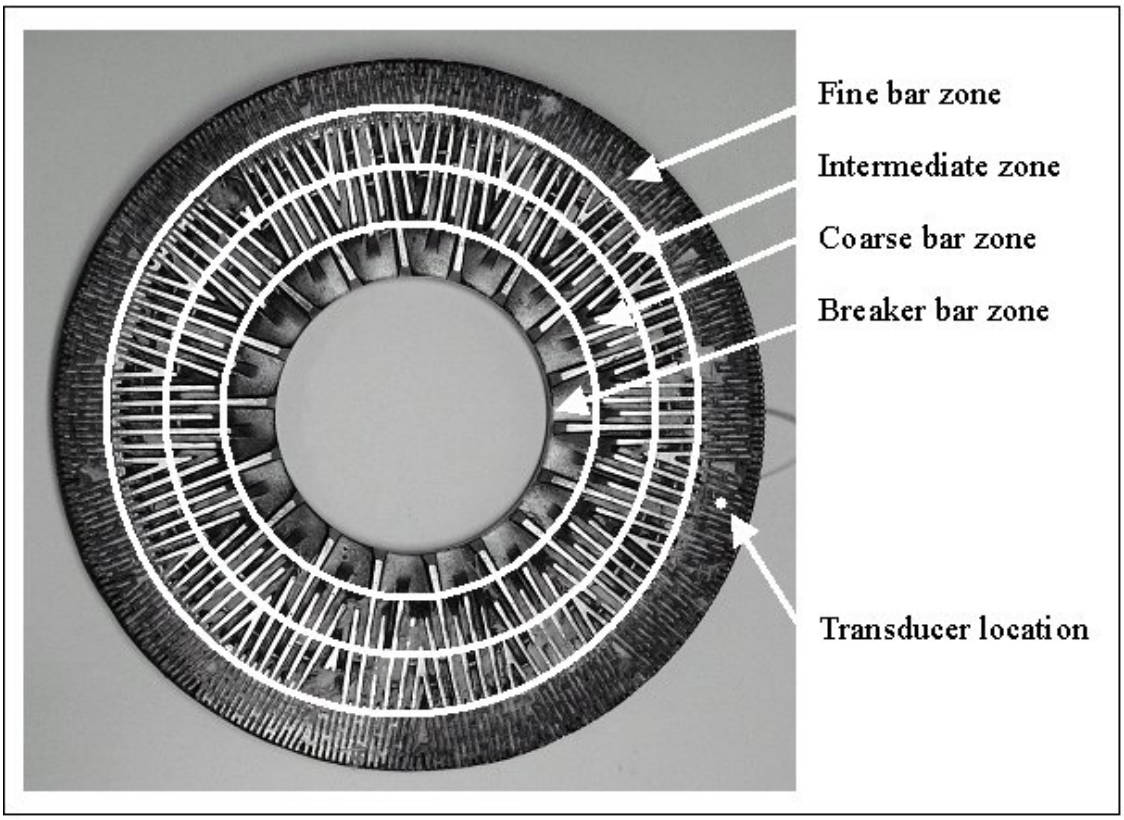

Figure 3.6: The stator plate as used in the pilot-scale experiment.

In the pilot refiner only three bolt holes per plate-ring were necessary to keep the plate attached to the disc. The bolt holes were located at a radial position of 205 mm from the centre of the refiner. They could be associated with a frequency of 75 Hz. In addition, the plate pattern had different larger V-formed grooves that appeared nine times per revolution or at 225 Hz if the term of frequency is used.

Only one piezoresistive sensor from Kulite Semiconductor Inc. was tested in this pilot experiment. It was located at a radial position of approximately 231 mm. It was attached to the plate using a stainless steel tube and set screws. In addition, a flexible combined rubber adhesive and sealant, Silastic 744 RTV, was added to the back of the sensor housing. This was added to provide appropriate sealing of the cable insertion hence protecting the sensor housing against penetration of steam and water from the back of the refiner plate.

3.3.3 Mill-scale experiment – fibre-optic sensors

The second mill-scale experiment was performed using fibre-optic sensors from Luna Innovations, Inc. mounted into a stator plate from J&L Fiber Services, Inc. The stator discs were equipped with similar plates as shown in Figure 3.4. The holes in the plate on the left-hand side were fitted with temperature sensors provided by J&L Fiber Services Inc. during this experiment. No surface modifications of the plate, that kept the sensors, were necessary except for the small holes of approximately 1 mm in diameter

through the bars. A part of the stator plate for mounting the sensors is shown in Figure 3.7. The rotor plates that were used in this experiment were different than the stator plates. Durametal Inc. had manufactured the rotor plates. The type of plates is termed Andritz 62200/201. Figure 3.8 shows the rotor plate. The breaker bar section at the rotor side was termed D33-169.

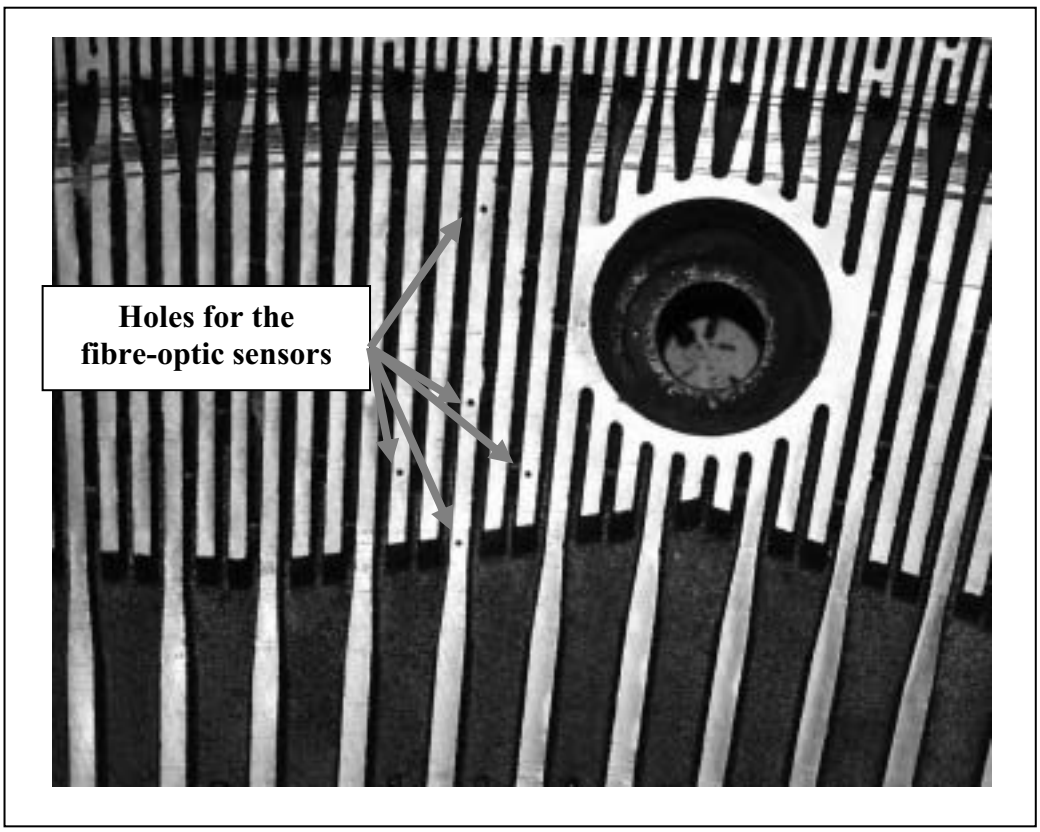

Figure 3.7: Part of the stator plate showing five of the nine holes through the surface where the fibre-optic sensors were installed. This plate was used in the second mill-scale experiment.

Characteristic data related to the rotor plates are displayed in Table 3.3.

Table 3.3: Data of the rotor plates used in the second mill-scale experiment.

Zones of the rotor plates	Radial location		No. of bars per plate [Bars/plate]	No. of bars per revolution [Bars/rev.]	Bar crossing frequency [kHz]
	Start [mm]	End [mm]			
Breaker bar	305	508	8 36	48 216	1.2 5.4
Coarse	508	560	20	240	6.0
Intermediate	560	650	44 48	528 576	13.2 14.4
Fine bar	650	788	74 92	888 1104	22.2 27.6

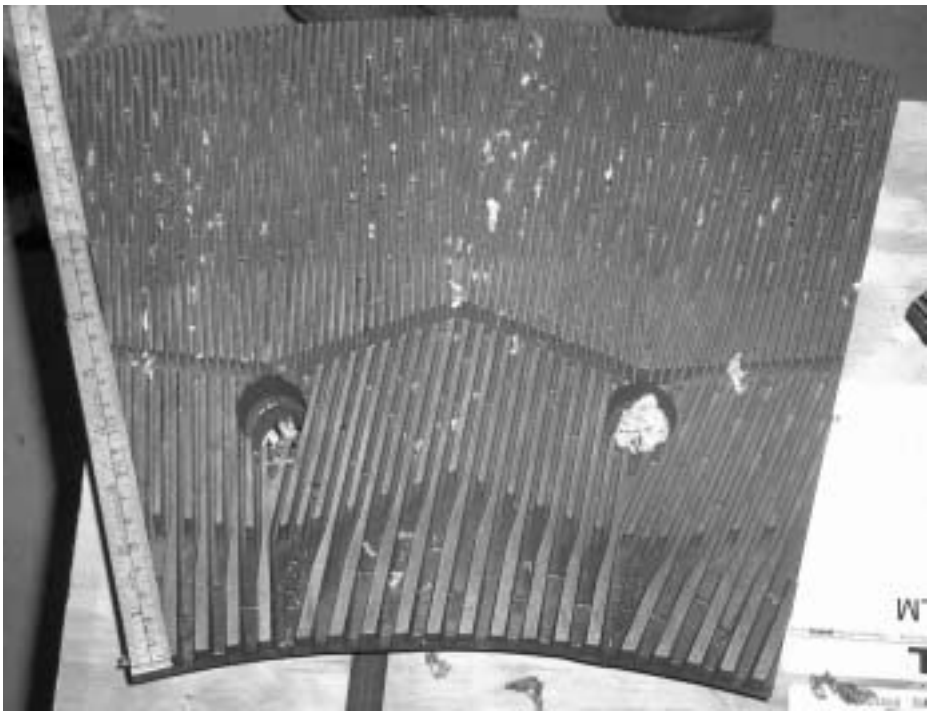

Figure 3.8: One of the rotor plates that was used in the second mill-scale experiment.

Table 3.3 shows that the intermediate and fine bar zones of the refiner plates give several different bar crossing frequencies. The numbers displayed in the right column in Table 3.3 determine intervals where the bar crossing frequencies belong. This is on the contrary compared to the rotor plates used in the first mill-scale experiment, which had a constant number of bars in each zone. However, the same potential distortions of the pulp flow through the refiner can be created by the bolt holes and the ribbon feeder as mention in Section 3.3.1. The sketch in Figure 3.9 illustrates the different periodicities appearing from the rotational movement of the ribbon feeder and the rotor disc.

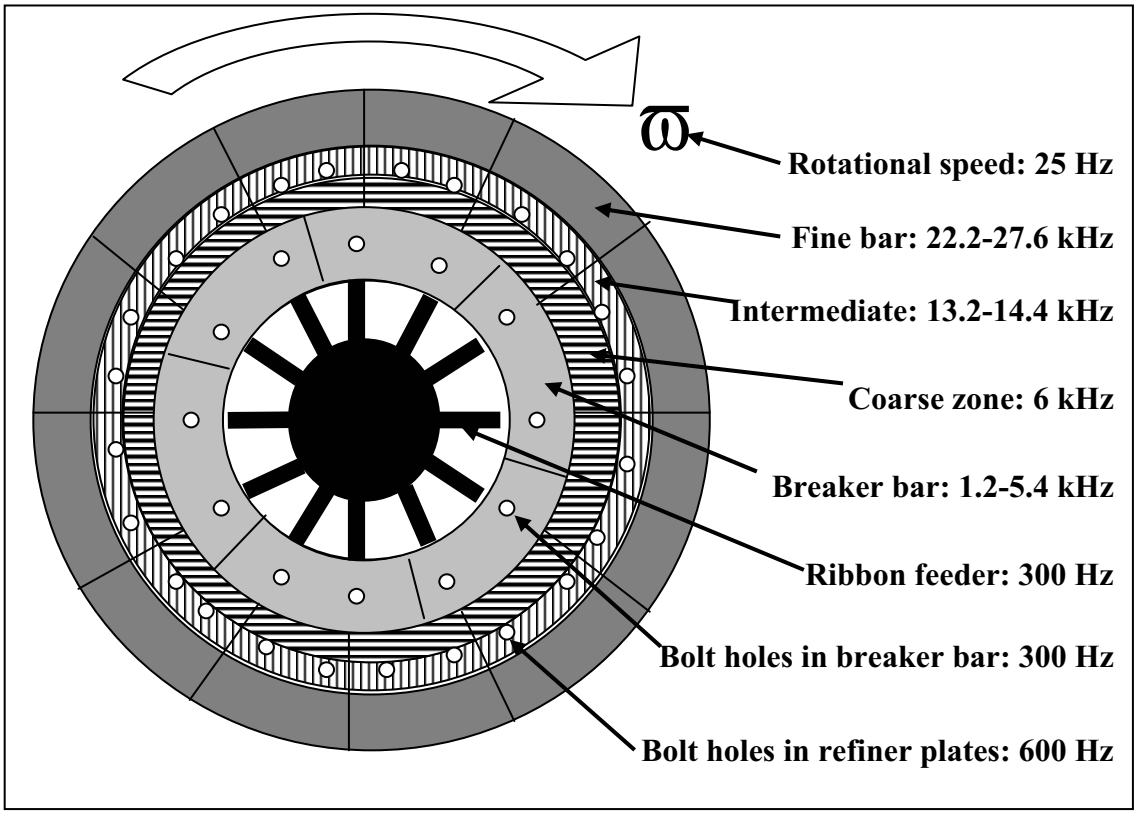

Figure 3.9: Illustration of the refiner's inlet and rotor disc with its different zones. Their corresponding periodic frequencies that generate the refining actions and distortions of the chips and pulp flow are labelled as well.

Nine fibre-optic sensors working basically as extrinsic Fabry-Perot interferometers were mounted into separate holes in the plate. More details about the sensors' structure and manner of operation are given in Section 3.5. The sensors were located in different geometric positions in the plate as shown in Figure 3.10. Five of the sensors (No. 1, 4, 5, 6, and No. 9) were located at the same radial line, but in different radial positions from 567 mm to 720 mm from the centre of the refiner, see Table 3.4. The two inner positioned sensors at the same radial line (No. 1 and No. 4), were located with an inherent distance of 25.4 mm. These sensors formed a square together with two other sensors (No. 2 and No. 7). A similar square was formed in the outer part of the refining zone. Sensor No. 6 and No. 9 were located at the same radial line, while sensor No. 3 and No. 8 were located at each side of the straight line through sensor No. 6 and No. 9. The last sensor, sensor No. 5, was located between the two squares of sensors in a radial position where the maximum temperature was expected to be and thus the stagnation point. Originally nine sensors were attached to the plate. However, the fibre-optic cable of sensor No. 3 broke during installation, and hence eight sensors were available from the start of the experiment.

The times of the different bar-to-bar passages and the corresponding frequency figures are quoted in Table 3.4. These figures are based on the measured bar and groove widths

and the corresponding radial positions that determine the tangential velocities of the rotor disc. In addition, the numbers of bars and grooves in the corresponding locations on the rotor plate are also quoted. Furthermore, the illustrations both in Figure 3.9 and in Figure 3.10 show the associated bar crossing frequencies.

Table 3.4: Sensor locations and the bar-to-bar passage time and frequency.

Sensor	Radial Location [mm]	Rotor plate pattern			Bar-to-bar passage time [μs]	Bar-to-bar passage frequency [kHz]	No. of bars per plate [No.]	Bar-to-bar passage frequency [kHz]
		Bar-groove width [mm]	Bar width [mm]	Groove width [mm]				
1	566.6	6.5	3	3.5	73	13.69	44	13.2
2	579.3	6.5	3	3.5	71	14.00	44	13.2
7	579.3	6.5	3	3.5	71	14.00	44	13.2
4	592.0	6.5	3	3.5	70	14.31	46	13.8
5	626.9	6.5	3	3.5	66	15.15	48	14.4
6	694.6	4.4	2	2.4	40	24.74	84	24.3
8	707.3	4.4	2	2.4	40	25.20	84	25.2
9	720.0	4.4	2	2.4	39	25.64	84	25.2

Small divergences in the results from the two different methods to determine the bar crossing frequencies were obtained. The uncertainties are related to the measures of the bar and groove widths and in addition the counting of the number of bars per plate. The latter uncertainty is related to the discontinuity of the bars at the edges of the plates and through the bolt holes. Despite uncertainties related to the absolute frequencies of the locale bar crossings, the main frequency regions of the sensors' positions are determined.

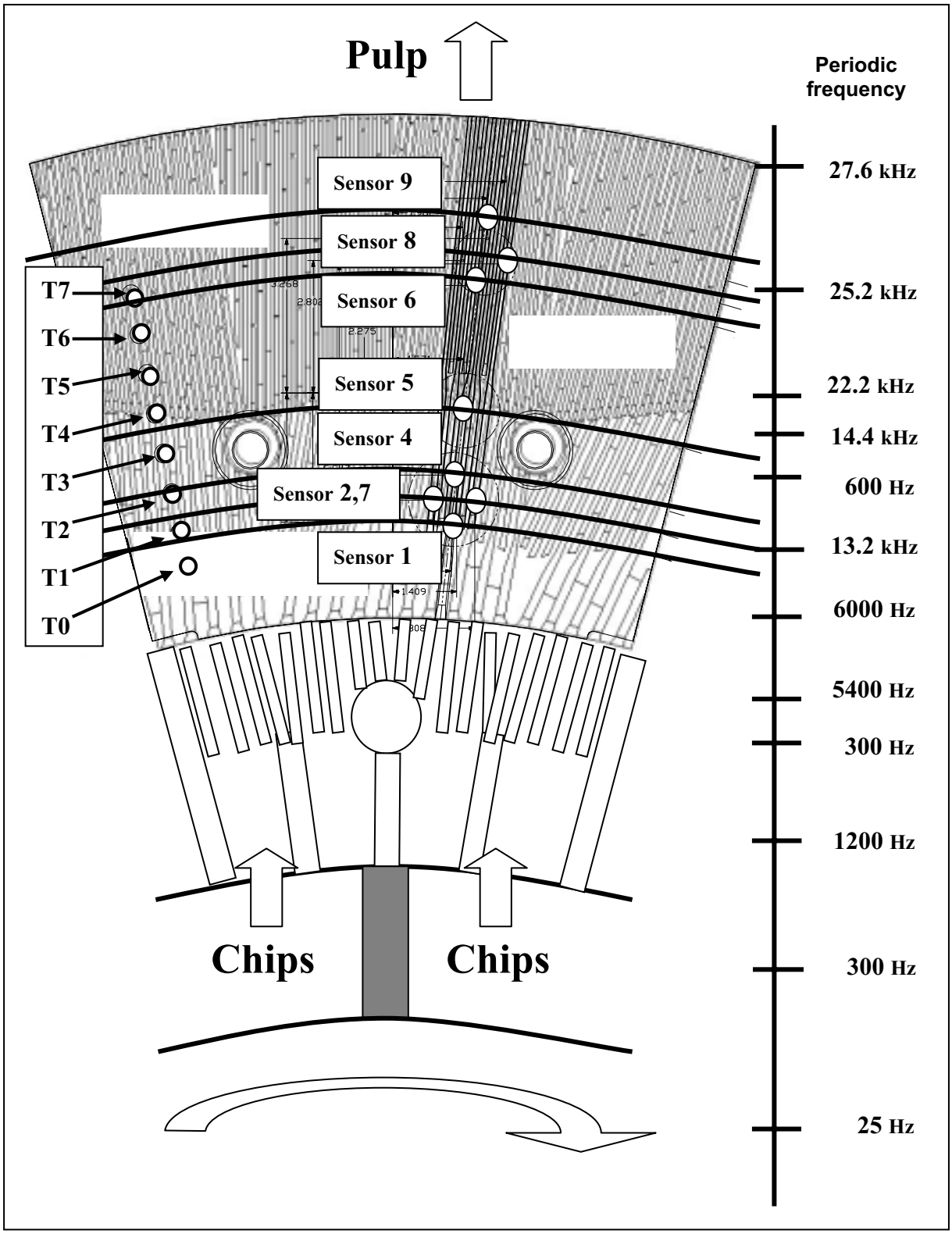

Figure 3.10: The locations of the fibre-optic sensors in the stator plate superimposed on a sketch of the rotor plate are shown. In addition, the breaker bar plate and the ribbon feeder are illustrated. The temperature sensors are labelled as T0 to T7.

Other details that should be considered, when the pulp flow behaviour is investigated, are the tapers of the plates. The tapers of the plates used in the second mill-scale experiment are illustrated in Figure 3.11.

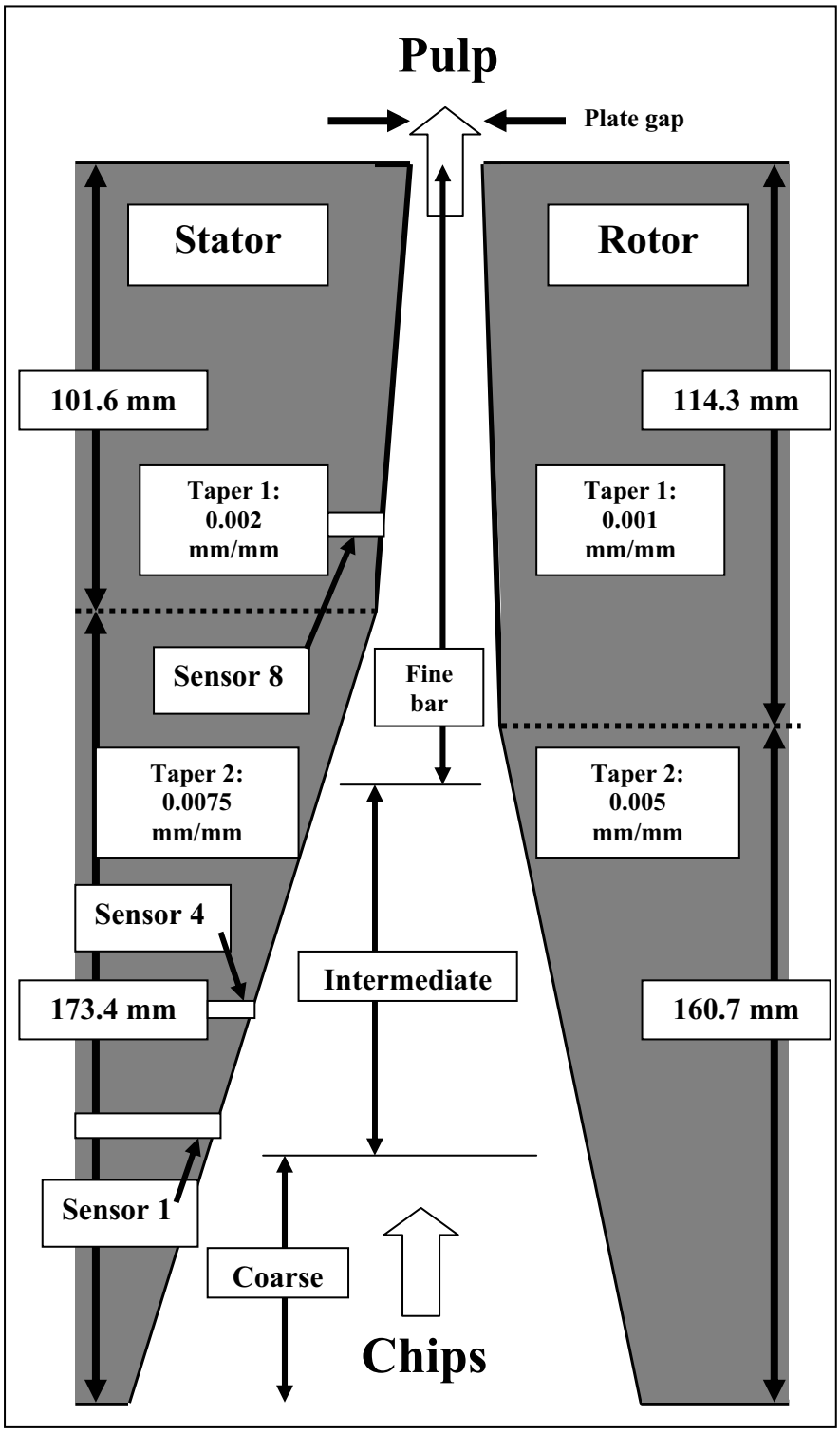

Figure 3.11: The tapers in the stator and the rotor plates.

The tapers indicate that the refining zone is approximately 2.4 mm wider at the entrance of the refiner plate compared with the periphery clearance when no deflection of the plates is assumed. The apparent deflection on the rotor related to the large torque is equalized in the Twin refiners because of the two refining zones. Assuming that the stator discs are rigid enough no deflections are accounted for. Thus the plate clearance follows the ratios given by the tapers of the plates. The following relative gaps at the different locations of the sensors are calculated and shown in Table 3.5.

Table 3.5: The plate clearance as a function of the tapers of the plates.

Sensor No.	Radial location [mm]	Relative plate gap [mm]
Periphery	788	0
9	720	0.20
8	707	0.24
6	695	0.28
5	627	0.98
4	592	1.41
2	579	1.58
7	579	1.58
1	567	1.72
Start refining zone	508	2.44

3.4 Theoretical estimates of expected pressure

3.4.1 Approach I: mill-scale refiner

A simple intuitive model of the expected pressure in the refining zone during refining is proposed in this section. An axial force balance is used in the model. This is partly based on similar considerations as Isaksson *et al.* (1997) used in their investigation on the same type of refiner as discussed in this thesis.

The axial force balance is given by Equation (3.1):

$$F_{axial} = F_{steam} + F_{mech} \tag{3.1}$$

The pressures applied on two hydraulic cylinders on each stator disc constitute the main axial closing force, which the steam and the pulp pad must resist to avoid plate clash. The sketches in Figures 3.12 and 3.13 show the geometric figures. The size of the hydraulic cylinders and the area of the stator disc together give the distribution of the hydraulic thrust that is applied. In addition, a minor contribution from the casing pressure is present. This is due to the overhang associated with the difference between the size of the plates (62 inch) and the discs (60 inch). Behind the stator plates in the Twin refiner atmospheric condition is present.

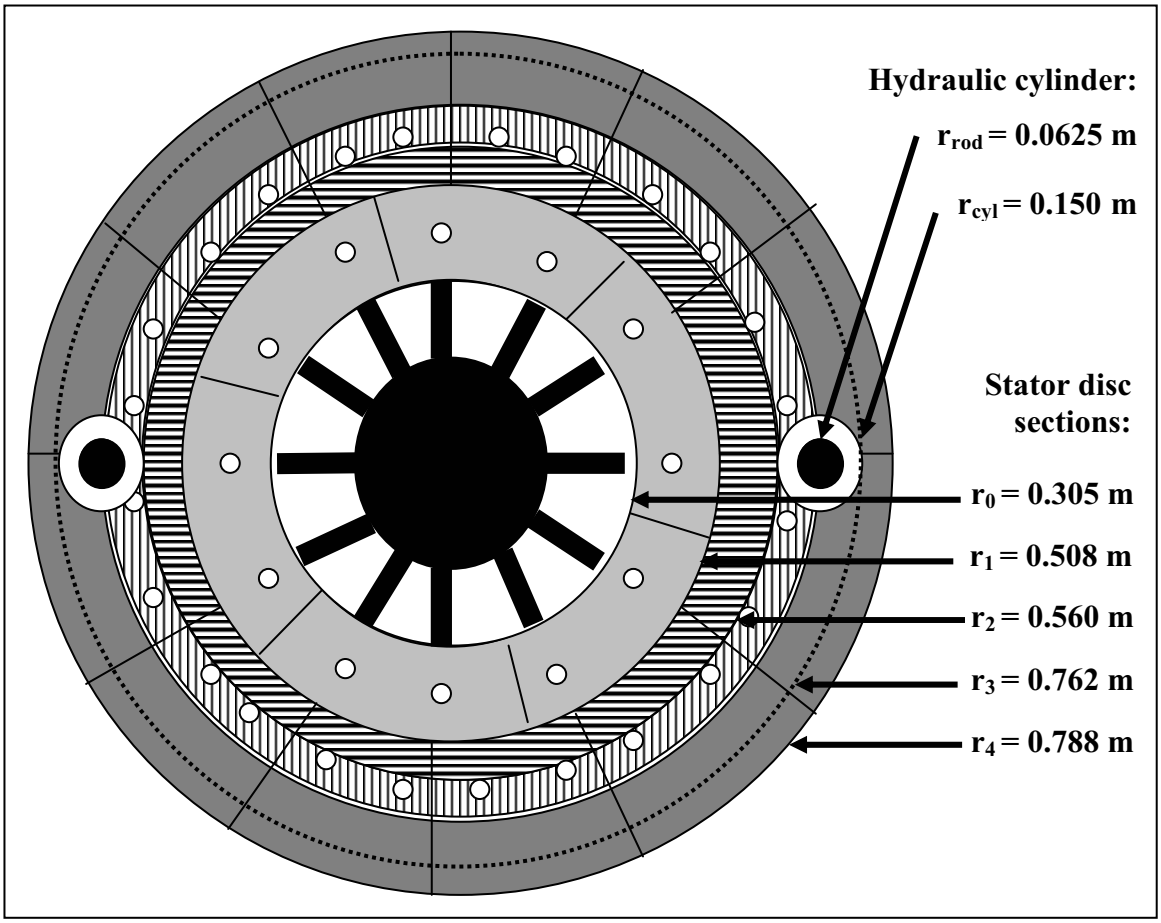

Figure 3.12: Illustration of the stator disc and the hydraulic cylinders.

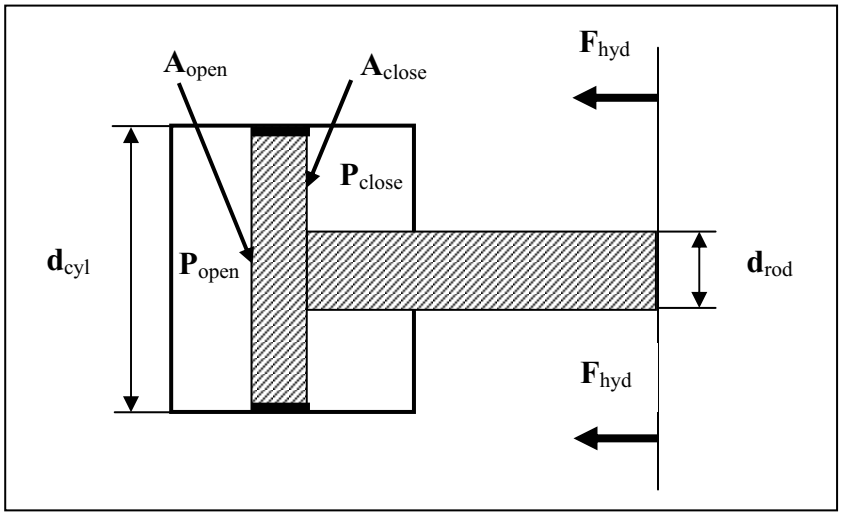

Figure 3.13: Illustration of the hydraulic cylinder[8] (Isaksson *et al.* (1997)).

[8] The cylinder is attached to the stationary side of the refiner casing and the piston rod is fixed to the plate holder (moving part) (Michael Kraft, Andritz Inc. Private communication (2003)).

The hydraulic thrust applied to the stator disc is then determined by the following equations. In this example a typical value of 110 bar (11 MPa) as the differential hydraulic pressure applied on each cylinder, is chosen. This pressure represents the measured value, which is given from the mill's DCS. Norske Skog Follum operates with a constant closing pressure of 145 bar (14.5 MPa) thus 35 bar (3.5 MPa) is the opening pressure in this example. Moreover, because of safety reasons 13 bar (1.3 MPa) is the minimum opening pressure that is permitted. A typical value for the casing pressure is 4 bar (400 kPa).

Differential pressure: $\div P_{hyd} = P_{close} - P_{open}$ (3.2)

Cylinder closing area: $A_{close} = (r_{cyl}^2 - r_{rod}^2)\cdot\phi = 0.058\ m^2$ (3.3)

Cylinder opening area: $A_{open} = r_{cyl}^2\cdot\phi = 0.071\ m^2$ (3.4)

Hydraulic thrust: $F_{hyd} = 2\cdot(P_{close}\cdot A_{close} - P_{open}\cdot A_{open}) = 1200\ kN$ (3.5)

Steam closing area: $A_{cas\text{-}close} = (r_4^2 - r_3^2)\cdot\phi = 0.127\ m^2$ (3.6)

Steam closing thrust: $F_{cas\text{-}close} = P_{casing}\cdot A_{cas\text{-}close} = 51\ kN$ (3.7)

Axial thrust: $F_{axial} = F_{hyd} + F_{cas\text{-}close} = 1251\ kN$ (3.8)

The contribution from the steam to the opening of the plate gap is assumed equally distributed over the whole disc area. No rigorous calculation based on the steam pressure distribution as shown by Isaksson *et al.* (1997) is made. The steam pressures chosen are based on typical average temperatures in this refiner and the assumption that saturated water vapour pressure condition is present. The relationship between the temperature and the saturated water vapour pressure is easily found by using Equation (2.31) reported by Di Ruscio and Holmberg (1996). However, the relationship shown in Figure 3.14 is based on table values[9].

The average temperature in the refining zone does not seem to change much during normal operating conditions. Based on experience from this particular refiner, despite the maximum temperature varying within a relative large range of approximately 10 ∀C, the temperatures closer to the breaker bar and plate periphery are relatively constant (Mosbye *et al.* (2001)). However, assuming that the average temperature in the refining zone is between 160 and 170 ∀C this represents the majority of the operating conditions. Figure 3.14 shows that this temperature range corresponds to saturated water vapour pressures between approximately 5.2 and 7.2 bar. Measured temperature distributions for this refiner are shown in Figures 4.10 and 6.34. The steam thrust values calculated by Isaksson *et al.* (1997) represent average values of the saturated water vapour pressure in the order of 5 to 6 bar. Simple integration of the saturated water vapour pressures

[9] Hodgman, C.D: *"Handbook of Chemistry and Physics"*, 31st Edition, Chemical Rubber Publishing Co., USA, pp. 1855-1856, 1949.

corresponding to the temperature distributions in Figures 4.10 and 6.34 gives average pressures between 5.1 and 5.6 bar, which are in the same order as reported by Isaksson *et al.* (1997).

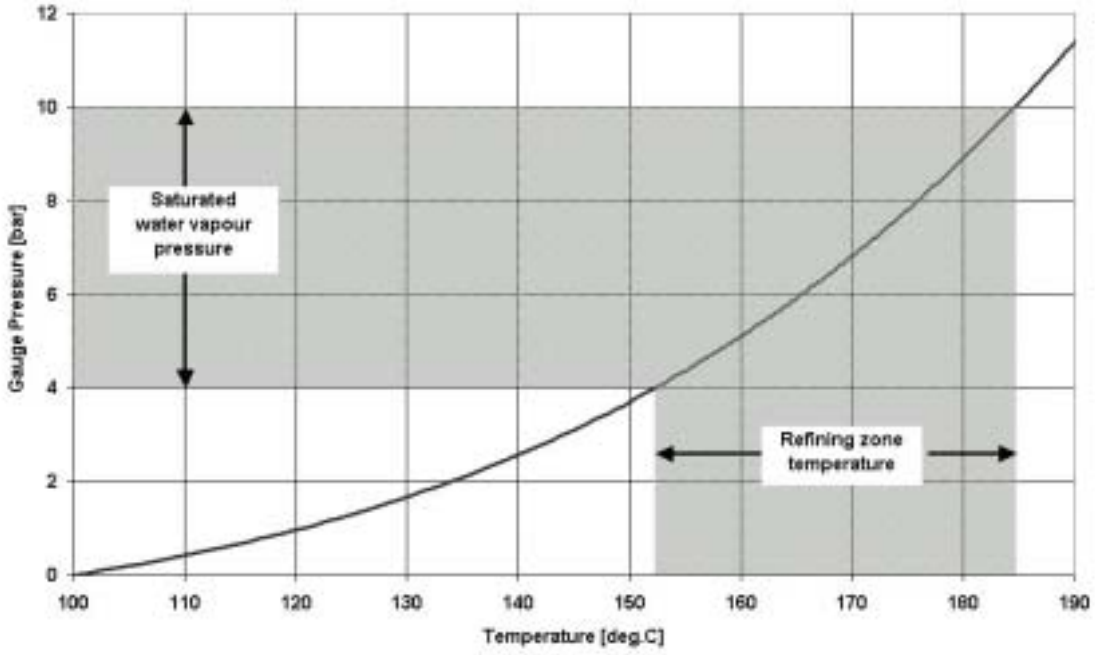

Figure 3.14: The relationship between temperature and saturated water vapour pressure.

The following equations are used for the part of the counteracting thrust that represents the steam:

Steam opening area: $A_{steam} = (r_4^2 - r_0^2)\cdot\phi = 1.66\ m^2$ (3.9)

Steam opening thrust: $F_{steam} = P_{steam} \cdot A_{steam}$ (3.10)

The amount of fibres on the bars is an important factor as they withstand the pressure and keep the discs separate. This model is based on the part of the area of the stator disc that contributes to balance the axial thrust. Regarding the mechanical thrust appearing from the fibres or the pulp pad, this area is denoted the bar intersecting area, *ba*. Assuming that 50 % of the disc area is covered by bars i.e. bar-groove ratio (*bgr*) is 0.5, then the bar intersecting area is 0.25 (May *et al.* (1988)). In addition, the amount of pulp or fibres that cover the bar intersecting area also called the fibre coverage ratio, *fcr*, is considered in the model. These restrictions are based on the assumptions that the pulp in the grooves does not contribute to resist the axial thrust, and that the pulp pad in the refining zone is not continuous. Both May *et al.* (1988) and Ouellet and Weiss (1994) have made similar assumptions. Another consideration is that the area where the mechanical pressure is working is reduced compared with the total disc area. Because of the taper of the plates it is assumed that the pulp in the breaker bar section does not contribute to the mechanical trust balance. According to Miles *et al.* (1980) as well as

Allison *et al.* (1995) the applied power is assumed to be small in both the inner and outer parts of the refining zone. Thus, in this model the area where the mechanical pressure is assumed to occur is limited to the intermediate zone and the fine bar zone except for a part of the outer fine bar section.

The following equations are used for the part of the counteracting thrust that is carried by the fibres:

Mechanical thrust area: $A_{mech} = (r_3^2 - r_2^2) \cdot \phi$ (3.11)

Fibre coverage area: $A_{fca} = A_{mech} \cdot ba \cdot fcr$ (3.12)

Mechanical thrust: $F_{mech} = P_{mech} \cdot A_{fca}$ (3.13)

Equations (3.1) to (3.13) give an expression for the mechanical pressure appearing from the fibres in the refining zone as a function of the bar intersecting area and the fibre coverage ratio. This expression is shown as Equation (3.14).

Mechanical pressure: $$P_{mech} = \frac{F_{axial} - 4 (P_{steam} \cdot A_{steam})}{A_{mech} \cdot ba \cdot fcr} \quad (3.14)$$

Furthermore, it is also assumed that the fibre coverage ratio determines the probability of how often the bar intersecting area is fully covered by pulp. If *fcr* is 0.8 then during 80 % of the time the bars are covered by pulp. In the remaining time (1-*fcr*) it is assumed that the bar area is free of pulp. Thus the average pressure in the refining zone, seen from a stator bar, during a certain time period can be derived from Equation (3.15). It is assumed that the sensor located flush to a bar surface, measures the steam pressure when a rotor groove is opposite the sensor surface. When a rotor bar is opposite the sensor surface it measures the sum of the steam and mechanical pressure. Hence the bar-groove ratio, *bgr*, is included in this expression.

$$P_{ave\text{-}bar} = P_{steam} + P_{mech} \cdot bgr \cdot fcr \quad (3.15)$$

There are several parameters in the earlier equations in this section that can be reconsidered for assessment and adjustment. The fibre coverage ratio and the contribution from the steam thrust are the two main factors. However, the area that is associated with the mechanical pressure is another factor that should be subject for further investigations. It can also be discussed whether the area where the steam pressure is working, is independent on the fibre coverage ratio. If the steam penetrates the fibre network everywhere in the refining zone, it is independent on the *fcr*. This is assumed here. However, if the fibres trapped between two opposite bars do not permit the steam to penetrate, then the area where the steam is working is somewhat smaller. In that case the steam thrust is restricted from working in the same area as the thrust from the fibres. Furthermore, it is clear that the derived expressions represent the average values of the pressures. It is expected that high-pressure spikes related to large fragments of wood will be present. This is not included in these calculations.

Figure 3.15 shows two sets of curves representing the mechanical pressure as well as the average pressure for three different values of the steam pressure.

Figure 3.15 shows that the pressure on the bar intersecting area increases when the fibre coverage ratio decreases. When the temperature in the refining zone increases, shown by an increased steam pressure, the mechanical pressure decreases. The validity of the assumed independent relationship between the fibre coverage ratio and the steam pressure is not evaluated closer. The average pressure, as assumed measured on the stator bar surface, is dependent on the fibre coverage ratio to a minor extent. However, when the fibre coverage ratio is small, a large extent of the pressure readings will give small pressure values limited to the steam pressure. Hence a corresponding small extent of the recordings will give large pressure values. A high fibre coverage ratio will lead to a periodic variation related to the locale bar crossing frequency.

Another simplification that was made is that the estimated pressures are the average values in that part of the refining zone where the mechanical pressure on the fibres is present. The taper and the expected different sizes of the particles in the inner and outer parts of the refining zone as well as different fibre coverage ratios in different parts of the refining zone as reported by Stationwala *et al.* (1992) would probably lead to more differentiated pressure estimates. Obviously, this means that the pressure in the refining zone is much more complex than indicated in Figure 3.15.

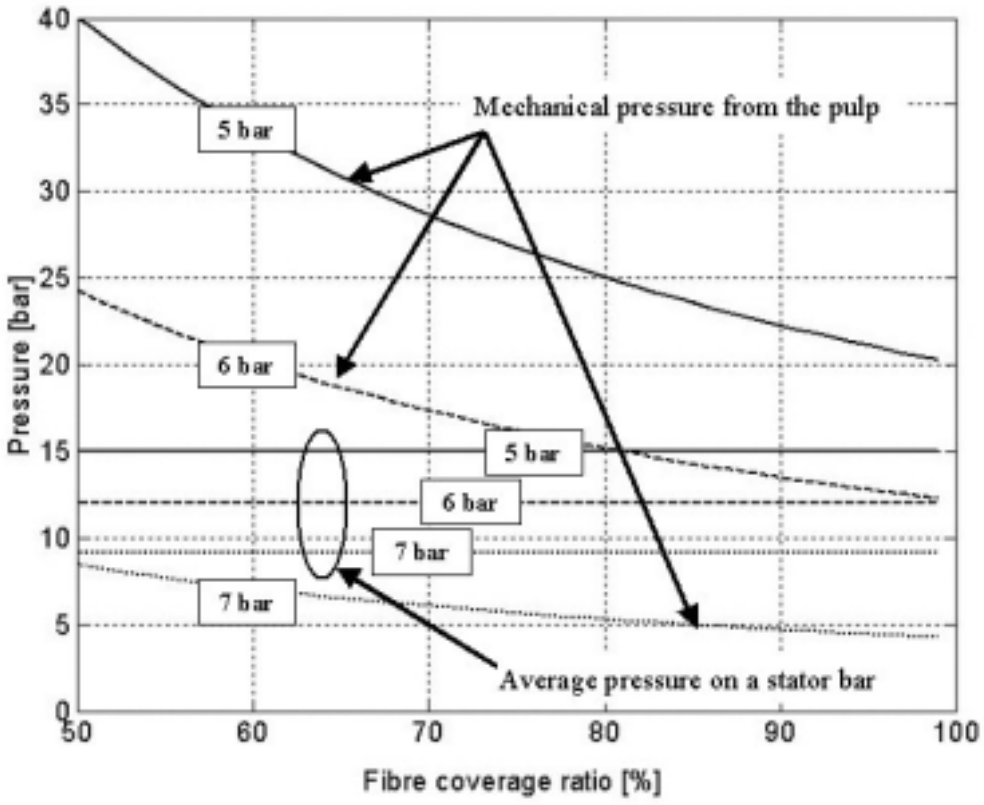

Figure 3.15: The mechanical pressure from the fibres and the associated average pressure on a stator bar calculated for three different steam pressures (5, 6 and 7 bar) and for increasing fibre coverage ratio.

3.4.2 Approach II: mill-scale refiner

A different approach is made to confirm the previous estimated pressures. The following calculations are made based on Miles and May's theoretical approach (1990) related to the mechanical thrust arisen from the pulp pad, Equation (2.7), and further derived by Isaksson *et al.* (1997), Equation (2.29). The latter equation is repeated as Equation (3.16).

Mechanical thrust from chips or pulp, Equation (3.16):

$$F_{mech} = \frac{2 \cdot W}{h \cdot \mu_{t1} \cdot \omega \cdot (r_1 - r_2)} \quad ; [N] \tag{3.16}$$

W : *Motor load; [J/s].*
h : *Constant due to refiner type (h=1 for SD, h=2 for DD).*
μ_{t1} : *Tangential friction coefficient between the fibres and the rotor disc.*
ω : *Angular velocity; [rad/s].*
$r_{1,2}$: *Inlet and outlet radius of the refining zone; [m].*

The calculations are based on the same operating conditions that gave the results shown in Figure 3.15. The difference between these methods is the different process values used in the calculation. While Miles and May's equation uses the motor load and the tangential friction coefficient, assumed constant at 0.75, to calculate the mechanical pressure, the previous estimates were based on the hydraulic thrust. In the previous estimations the hydraulic thrust was assumed a typical value (110 bar applied at each hydraulic cylinder). During operation with the same level of hydraulic thrust, the following operating conditions are assumed:

- Specific energy consumption: 1120 kWh/t.
- Production: 280 tonnes/day (1.6 kg/s per refining zone).

These production values lead to:

- Motor load: 13.1 MW (MJ/s).
- Motor load per refining zone: 6.5 MW (MJ/s).

Inserting Equation (3.16) into Equation (3.13) the mechanical pressure on the fibres can easily be estimated. However, the tangential friction coefficient is the uncertain parameter in Equation (3.16). Isaksson *et al.* (1997) estimated the tangential friction coefficient in a mill-scale refiner to be in the order of 0.22 to 0.32. This result differs a lot from the estimated value of 0.75 given by Miles and May (1990). In this study it is interesting to estimate the tangential friction coefficient related to typical operating conditions in the present refiner. Based on the method of Isaksson *et al.* (1997) the tangential friction coefficient is found using Equation (3.17) for a set of different assumed average steam pressures. Equation (3.17) is derived from Equations (3.1), (3.10) and (3.16).

Tangential friction coefficient, Equation (3.17):

$$\sigma_{t1} = \frac{2 \cdot W}{(F_{axial} - 4 \cdot (P_{steam} \cdot A_{steam})) \cdot \omega \cdot (r_2 - r_3)} \qquad (3.17)$$

The calculated tangential friction coefficient is shown in Figure 3.16 for steam pressures between 5-7 bar. Figure 3.16 indicates that the tangential friction coefficient in a mill-scale refiner is smaller than 0.75 as claimed by Miles and May (1990). Miles and May's assumption is based on experiments performed in small refiners. However, the present estimates of the tangential friction coefficient are somewhat lower compared to the result obtained by Isaksson *et al.* (1997) as well. They performed their experiment in a similar primary stage mill-scale refiner as used in this study. The results obtained by Isaksson *et al.* (1997) were based on steam thrust values that correspond to average steam pressures between 5-6 bar. The associated friction coefficients were in the order of 0.22 to 0.32. The differences between their results and the present calculations are due to the different process conditions. The data used in this text are based on prevailing conditions in the refiner using new refiner plates. Which conditions the plates in the experiment performed by Isaksson *et al.* (1997) were in, are not clarified. However, it is expected that the tangential friction coefficient decreases as the plates wear. The reported process values from their study differed somewhat compare to the values used here. The hydraulic thrust was smaller in the study performed by Isaksson *et al.* (1997) despite the motor power being approximately the same.

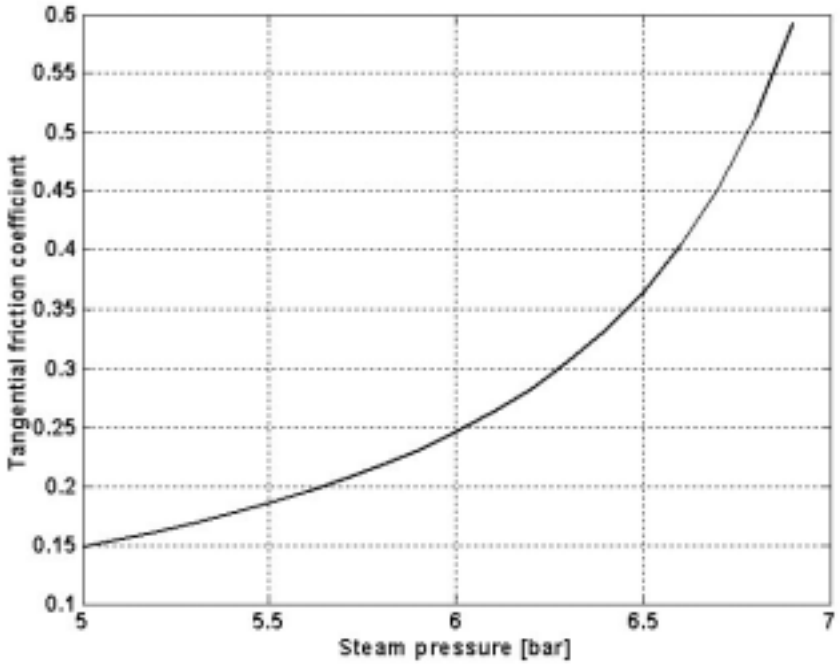

Figure 3.16: The tangential friction coefficient calculated for increasing steam pressure.

The estimated mechanical pressures in the refining zone using the mechanical thrust approach are determined using Equation (3.18). This equation is derived from Equations (3.13) and (3.16).

$$P_{mech} = \frac{2 \pi W}{A_{mech} \beta a \gamma fcr \sigma_{t1} \omega \rho r_2 2 r_3 0} \tag{3.18}$$

Two sets of pressure curves as a function of the fibre coverage ratio are shown in Figure 3.17. One of the sets shows simulated results of the mechanical pressures for three different tangential friction coefficients. The second set of curves shows the average pressures using the associated steam pressures obtained from the relationship between the steam pressures and the tangential friction coefficients. The average pressures are determined using Equation (3.15).

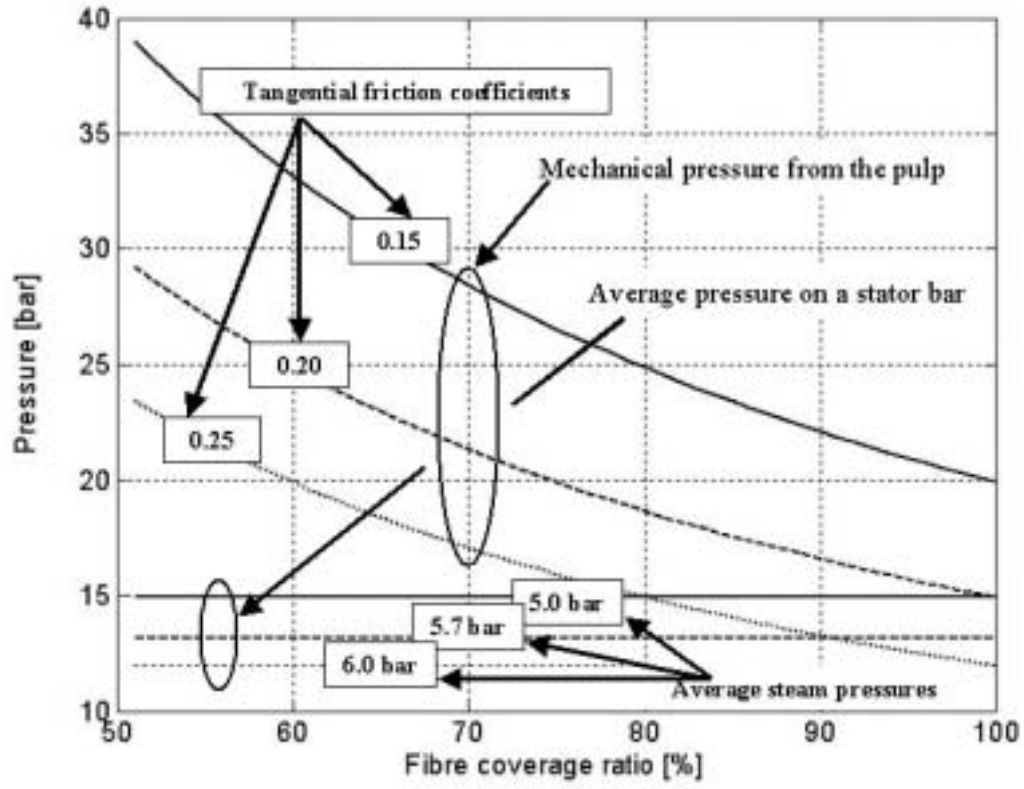

Figure 3.17: The mechanical pressure from the fibres and the associated average pressure on a stator bar as a function of the fibre coverage ratio. The mechanical pressure is calculated for three different tangential friction coefficients, while the average pressure is based on the associated steam pressures.

Assuming a low tangential friction coefficient the two discussed theoretical approaches give pressures in the same order. High mechanical pressures above 20 bar can be

expected, especially when the lack of fully covered disc area is taken into consideration. Expected average pressures seem to be in the same order. Average pressure between 10 and 20 bar seems to be realistic. Furthermore, high and frequent pressure variations associated with the bar crossing frequency can be expected, especially if the fibre coverage ratio is high.

3.4.3 Pilot refiner

A similar approach using the friction coefficient is made to estimate pressures in the pilot refiner. The first approach cannot be used, as the hydraulic thrust cannot be measured in the pilot refiner. The pilot refiner is gap controlled in contrary to the Twin, which is controlled by hydraulic thrust. The calculations of the pressure caused by the pulp pad can be made using Equation (3.18). The following experienced process conditions have to be included:

- Specific energy consumption: 900 kWh/t
- Production: 0.85 kg/min. (0.014 kg/s)
- Motor load: 46 kW (kJ/s)

In addition to these process values, an area where the mechanical thrust is working has to be defined. This is indicated in Figure 3.18.

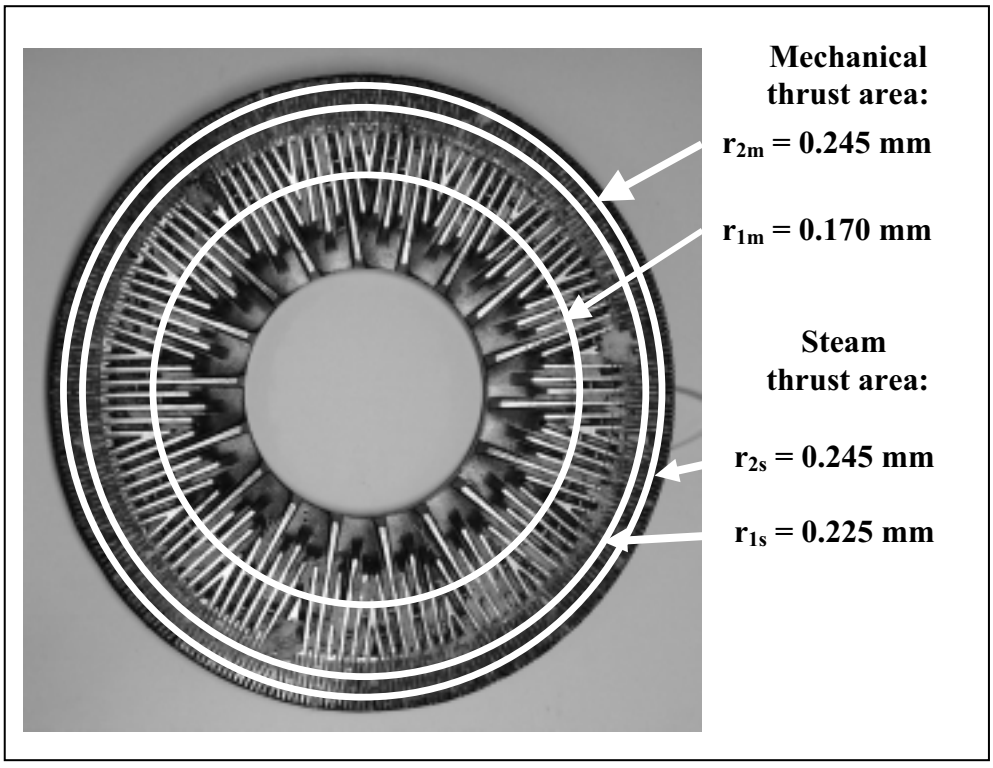

Figure 3.18: The refining zone of the pilot refiner.

Furthermore, to estimate an average pressure seen from a stator bar as in accordance with Equation (3.15), it is necessary to assess the contribution of steam pressure. Despite that the pilot refiner being atmospheric it is assumed that the steam pressure contributes somewhat to balance the axial thrust. However, the extent of the axial thrust that is resisted by the contribution from the steam is not closely assessed. It is observed that there is a steam flow out of the pilot refiner. This steam flow is obviously affected by the centripetal acceleration, but it is conceivable that a pressure gradient contributes to an increased steam flow. A possible contribution from the steam might be related to a small area where the steam is restricted from flowing freely because of a small open volume. Such area can be associated with the fine bar zone. For instance if the grooves in the fine bar zone are covered by pulp the open areas are strongly limited. Then the pulp and steam flows are mainly dependent on the small plate gap.

Atack and Stationwala (1975) claimed that the thrust contributed from the steam was in the order of 50-70 % of the total axial thrust. These figures were obtained from a self-pressurized open discharge refiner operating with a temperature above 120 ∀C. If it is assumed that the steam contributed to balance the axial thrust in the pilot refiner is comparable with the lowest level of this thrust balance then 50 % of the axial thrust is balanced by the steam. This might be a starting point for this approach. The parts of the refining zone of the pilot refiner where the mechanical and the steam thrusts are assumed working are sketched in Figure 3.18.

The estimated pressures in the pilot refiner within the area where it is assumed that both mechanical and steam thrusts are working are shown in Figure 3.19. The mechanical pressure is based on a tangential friction coefficient of 0.75. This value was found by Miles and May (1990) after several trials in small refiners.

Figure 3.19 shows that the steam pressure is small, despite the fact that a small area is chosen for the steam thrust. A large area would make the steam pressure contribution even smaller, and then it could be neglected. However, if the tangential friction coefficient is lower than 0.75, all of the pressure curves are shifted towards higher pressure levels. Assuming that the fibre coverage ratio is low as claimed by May *et al.* (1988), which estimated the fibre coverage ratio in a small primary refiner to be 16 %, the expected pressures should be as shown in the left part of the plot. Then it should be expected few, but high pressure peaks, while the average pressure should be at a low level. This is in accordance with Atack and Stationwala (1975). They measured the pressure in the refining zone of a self-pressurized high-consistency refiner and found that the average pressure was fluctuating across the saturated water vapour pressure by only ± 0.27 bar. The steam pressure was assumed to be approximately 1.9 bar. Furthermore, they measured pressure peaks as high as 6.2 bar.

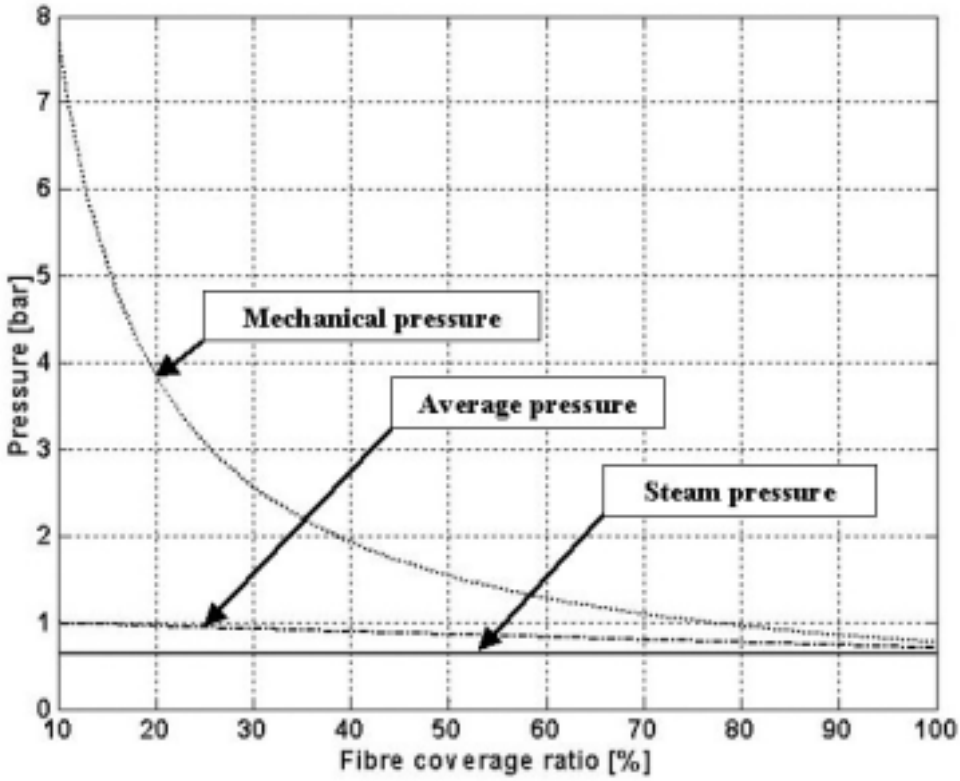

Figure 3.19: The estimated pressures in the pilot refiner in one area where it is assumed that both mechanical and steam thrusts are working.

3.5 Sensors and measurement equipment

The measuring systems used in these experiments were built up of several components. Based on previous experience new components replaced old ones. The process was started with small size combined piezoresistive pressure and temperature transducers and ended using fibre-optic pressure sensors. Also some changes were made during the process regarding the use of amplifiers and data acquisition cards.

The size of the transducer's casing and the reliability in the harsh environment in the refining zone were among the important criteria for the transducers that should be selected. In addition, it was necessary to have transducers capable of measuring very fast pressure variations. A dynamic response time corresponding to a few hundred kHz was desirable. The size of the transducers is important when they are to fit into the bar-groove pattern of the refiner plates. Modifications of the plates should be avoided to minimize the distortion of the pulp flow pattern. It was desirable to have transducers that were smaller than two millimetres wide. In addition, the hot and wet environment inside the refiner made it important to get transducers suited for such conditions. Much effort was put into the selection of potential transducer suppliers. Very few producers could satisfy such criteria. The subsequent sections describe the sensors and the measurement equipment.

3.5.1 Mill-scale experiment – piezoresistive sensors

Four piezoresistive combined pressure and temperature sensors were used in the first mill-scale experiment. Three out of four were delivered from Kulite Semiconductor Inc. Presens AS, a Norwegian producer, manufactured the fourth. The transducers' characteristic data were as follows:

- Kulite model No.: XCL-1-152-35BARSG. (Figure 3.20 and Figure 3.22).
  - Circular size: 3.8 mm in diameter (casing), 3.2 mm in diameter (diaphragm).
  - Length of 25.4 mm. See Figure 3.24.
  - Natural frequency: 840 kHz.
  - Rated pressure range: 0-35 bar. (Maximum: 70 bar.)
  - Compensated temperature range: 150-200 ºC.
  - Pressure and temperature sensitivity:
    - Sensor 1: 2.456 mV/bar, 4.202 mV/ºC.
    - Sensor 2: 2.411 mV/bar, 4.040 mV/ºC.
    - Sensor 3: 2.437 mV/bar, 4.024 mV/ºC.

- Presens model No.: PT-30bar 160-190C.
  - Circular size: 3.8 mm in diameter (casing), 2.0 mm in diameter (diaphragm).
  - Length of 28.5 mm.
  - Natural frequency: NA.
  - Rated pressure range: 0-30 bar. (Maximum: NA.)
  - Compensated temperature range: 160-190 ºC.
  - Pressure and temperature sensitivity:
    - Presens: 1.2 mV/bar, 0.56 mV/ºC.

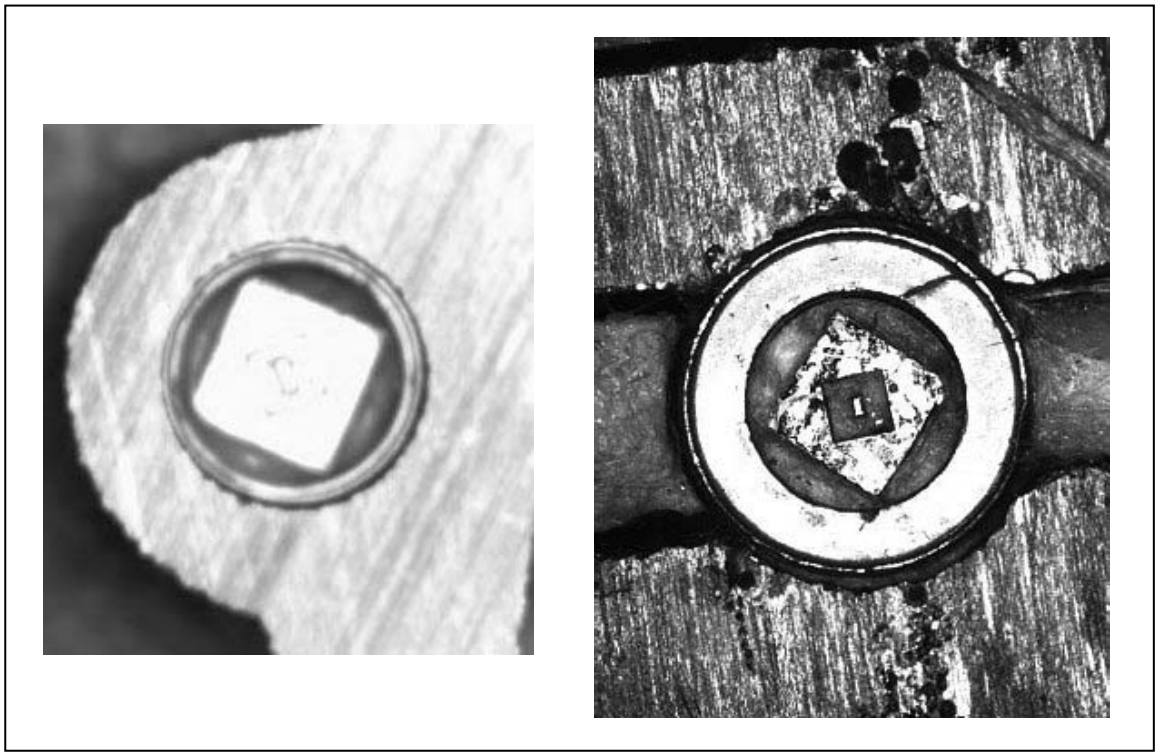

Figure 3.20: The diaphragm of the Kulite transducer. Four piezoresistive strain elements are incorporated in the inner square. The transducer shown in the left-hand picture was used in the first mill-scale experiment, while the transducer to the right was used in the pilot test. The thickness of the tubular metal housing was different between these transducers.

The basic operating principle was similar for both types of transducers. It is based on the piezoresistive effect, which is defined as the change in electrical resistivity with applied stress. Piezoresistivity is a material property. Certain semiconductors are utilized as sensing devices because of their large piezoresistive effect (Ainsworth *et al.* (2000), Elgamel (1995)). The sensing element of the transducers was an elastic silicon diaphragm as shown in Figure 3.20. The diaphragm incorporated four piezoresistive strain elements connected in a Wheatstone bridge network. A fifth resistor was connected in series with the deflection bridge. The temperature was measured as a linear combination of the voltage readings over the fifth resistor. As the diaphragm deflects under pressure, the resistances of the piezoresistive element change in value, causing the Wheatstone bridge network to move out of balance. The output signal from this sensing device was a voltage signal proportional to the applied pressure. A stable external power supply, which was an integrated part of the amplifier unit, was required. This ensured that the bridge and series resistor was excited (10 V) in order to give a highly reproducible voltage output signal.

The temperature measurement system was an integrated part of the pressure transducer. One opposite pair of the strain gauges in the deflection bridge responded equally to the

tension forced on the diaphragm. The other pair worked in compression mode. Moreover all four strain gauges responded with the same change in resistance to temperature changes. The deflection bridge was still in balance when the temperature changes despite the fact that the voltage over the bridge changed. The pressure signals were therefore not affected by temperature changes. The temperature change was measured as the voltage change over the total bridge or alternatively over the series resistor. However, the response of the temperature measurement was expected to be much slower than the response of the pressure measurements due to the thermal inertia of the silicon diaphragm. The manufacturer of the transducers assumed a response time of approximately 2 milliseconds for the temperature measurements.

The four strain elements in the transducers from Kulite had resistance values of approximately 1.3 kT each, while the series resistor had a resistance value of approximately 1 kT. Corresponding values for the Presens transducer were respectively 5.9 kT and 47 T. A principle sketch of the electrical circuit of the piezoresistive transducer from Kulite is shown in Figure 3.21. In addition, the electrical circuit comprises of temperature compensating resistors. Discussions about this subject are assessed to be outside the scope of this thesis. For the Presens transducer the earth and excitation voltage were in opposite position. However, the functionality of the transducer is not affected by the location of the series resistor.

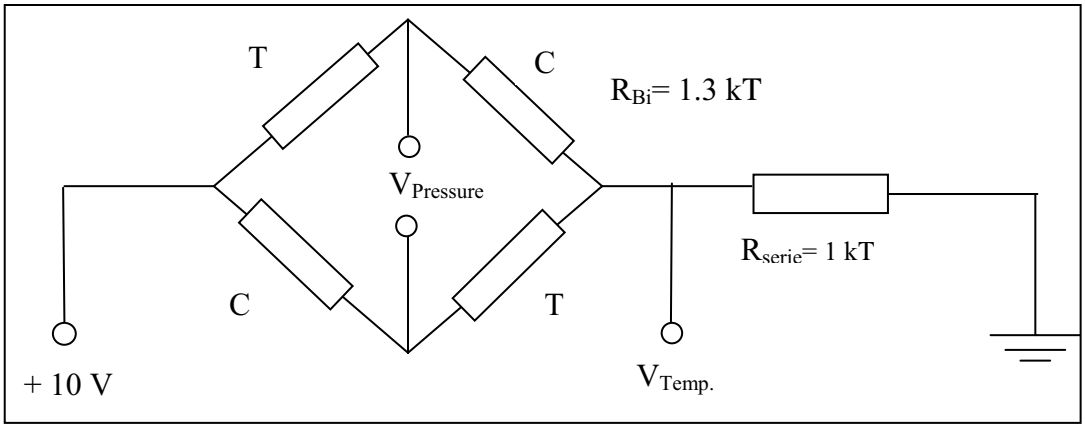

Figure 3.21: A principle sketch of the sensor Wheatstone bridge with elements in tension (T) and compression (C) and the excitation and measurement set up of a Kulite transducer is shown.

Several laboratory tests were performed as preparatory work. This was done to prepare for the mill-scale experiment. It was important to be familiar with the transducers and the rest of the instrumentation. The following tests were performed:

- Water (20-100 ∀C) and heat chamber (100-170 ∀C) tests.
- Calibration test in a pressure (7-32 bar) and temperature (20-180 ∀C) chamber.
- Dynamic pressure response test using a falling-weight test rig mounted in a water-filled chest.

Actually, several transducers were tested in the different laboratory tests. Some of the results are shown in Appendix A. Not all of the tested transducers survived. Originally five similar transducers from Kulite were tested. Only two of the five transducers were still working after the calibration test in the combined pressure and temperature chamber. New sensors of similar type were re-ordered. In addition, during the dynamic response test the original high-speed data acquisition card failed. Only low-speed (500 Samples/s) recordings were obtained from this test as shown in Appendix A3.

The preliminary tests revealed some weak points. The main uncertainty was related to the behaviour of the output signals when the transducers were exposed to a wet environment. Increased signal variation was observed during and after water exposure. An attempt to reduce the risk for failure was made. The cable insertion to the sensor housing was sealed using Epoxy.

When the Kulite transducer cables were assembled to the seal plug in the refiner's casing, it was necessary to cut off the series resistors from the transducers. This was done because of the large size of the tube surrounding the resistors almost at the end of the cables. The series resistors were replaced by new series resistors of approximately the same resistance value as the originally resistors. Static values of both temperature and pressure under no-stress conditions were observed before and after the replacement of the series resistors. The replacement caused offsets in the voltage output signals that were taken into account in the calibration models for the sensors.

Furthermore, during calibration of the transducers from Presens it was observed that one of the signal cables sometimes was in contact with the transducer's casing caused by lack of insulation. This had no effect on the preliminary calibration made by the manufacturer. The functionality of the transducer should not be affected provided that the transducer's casing was not conducting any noise currents. However, the transducer casing was not insulated from the refiner plate and consequently not insulated from the refiner's casing, which earthed the power supply from the refiner motor. Another uncertainty was that the connection points of the transducer cables were exposed to the environment on the back of the plate apart from only a thin plastic coating. Non-conducting Epoxy was inserted over the plastic coating and the connection points to prevent short-circuiting as far as possible.

Location of the sensors

Six holes were made for the transducers in the modified plate, as shown in Figure 3.22. Only four of them were used. Five of the holes were made in three neighbouring bars. One of these was made for a surface location, while the others were located in cavities approximately 1-2 mm subsurface with a smaller hole of approximately 1 mm diameter extending up to the surface. The last hole was located in the groove in surface position. This was not used in the experimental trial. Two of the Kulite transducers, as termed sensor No. 1 and sensor No. 2, together with the Presens-transducer were located sub-surfaced in the cavities. Sensor No. 3 from Kulite was located in the hole in the bar with the surface position. All of the transducers were glued into the holes by a high-strength, high-temperature Epoxy from Devcon Inc.

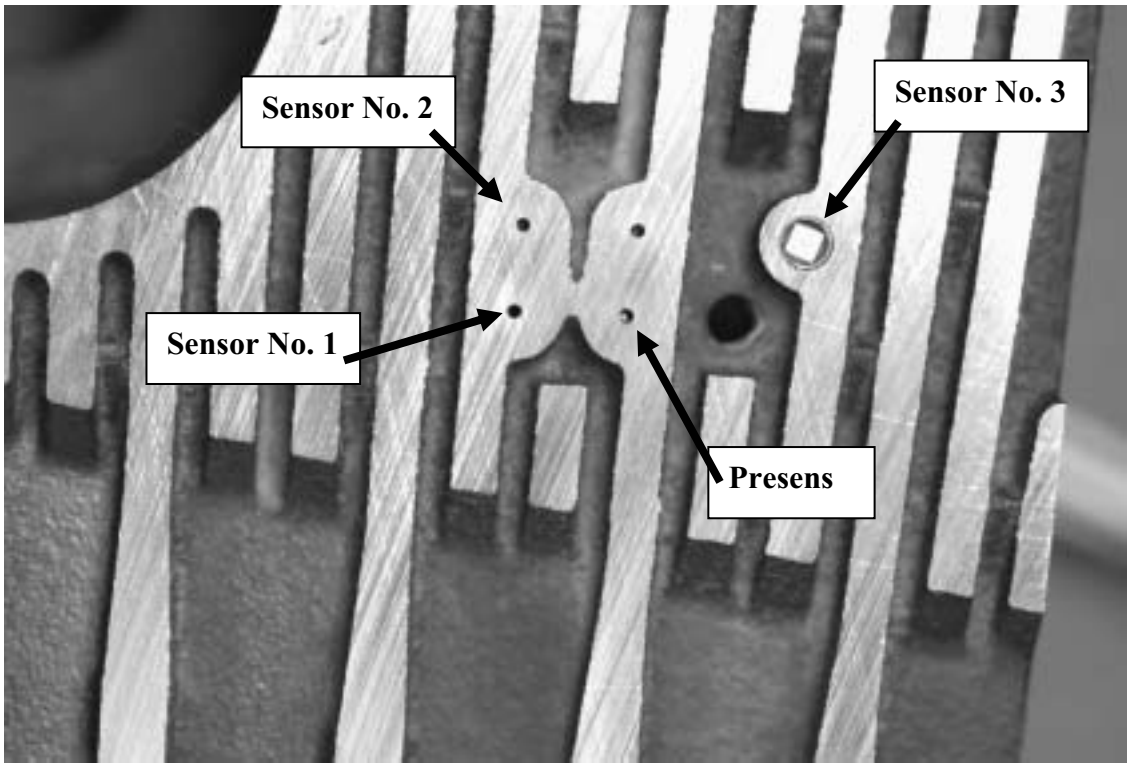

Figure 3.22: The location of the sensors in the modified plate as used in the first mill-scale experiment.

Amplifier unit

Three amplifier-boards comprising two amplifier channels each and a common external power supply formed the amplifier unit termed D486 from Kulite. The transducers produced an output signal (mV/V) in relation to the power voltage signal of the deflection bridge, which emerge from the external power supply. A highly stable 10 V external voltage signal was used to power the strain gauges and the series resistor. The amplifiers were calibrated together with the Kulite transducers at Kulite's plant in the Netherlands. The amplifiers were originally built for an output range of ∂ 10 volt and a bandwidth of 100 kHz. However, only the pressure signals were amplified through this device. The temperature signals were not amplified, which resulted in a poor resolution of the temperature output signals.

DAQ-cards

Another important part of the measurement system was the data acquisition equipment. The criteria of such units were high-speed capacity, high resolution of the A/D-converters, and a large data storage capability. A 12-bit high-speed DAQ-card, IS-16 from RC Electronics, Inc., was used as the main component of the data acquisition system in this experiment. However, two other data acquisition equipments were used in addition to the stand-alone high-speed DAQ-card. One of the other cards was an 8-bit PC-Scope card with a limited data storage capacity, while the second card was a low-speed I/O-card used with the CAN-bus (Controller Area Network). The two latter items of equipment were running on a CompactPCI-bus using a standard PC with a hard

disk capacity of approximately 80 Gbyte and with an internal memory of 256 Mbyte. LabVIEW software from National Instruments was used together with these DAQ-systems.

The high-speed DAQ-card was a standalone system with a separate PC as limiting unit i.e. internal memory and data storage capacity. The data acquisition of this system was controlled by MS-DOS developed software from RC Electronics. It was used as a single or two channels data-recording unit because of the desire of a high sampling rate. This device was a 16 channels unipolar DAQ-card. However, the restriction of a unipolar mode was not consequently followed. When collecting data from more than one sensor at a time, the high-speed DAQ-card was sometimes used as a differential input channel board. A maximum sample frequency of 200 kHz and a recording time of up to approximately seven minutes per recording were used during the experiment.

The PC-Scope was a 20 MSamples/seconds Digital Oscilloscope, PXI-5102, having two simultaneously sampling input channels. Only 8-bit resolution was a limitation of this PC-Scope. In addition, the limited storage capability range of 663 kSamples, in the available measuring system, made this DAQ-equipment most useful for visual considerations of the input signals on site. This PC-Scope worked together with LabVIEW through the software application VirtualBench.

The main idea behind the use of the CAN-bus system was to record all of the signals simultaneously at a low sampling rate, both pressure and temperature, to supervise the transducers output signals. The low-speed I/O-board termed as CAN-A analog I/O board could either be used as a 8-channel differential or a 16-channel unipolar DAQ-card. It had 12-bit resolution and a built-in 40 kHz A/D converter. The input signal could either be voltage (∂ 10 V) or current (∂ 20 mA). For the use in this experiment two such devices operating as voltage units were available. Both devices were used as differential input channels. A ground signal referencing the input voltage should be connected to the ground of the analog input.

On-site location

The rig with the combined amplifier-boards and the external power supply was positioned beside the refiner. The limiting factor for the location was the cable length of the transducers, which was approximately 5 metres. A sketch of the cable structure and equipment locations is shown in Figure 3.23.

Two types of signal cables were directed from the amplifier-unit to the data acquisition equipment. The data acquisition equipment was located in the control room of the TMP-mill, 20-25 metres from the amplifier unit. The pressure channels on the amplifier unit were connected to the data acquisition equipment by coaxial cables with BNC-connectors at both sides. A six pair twisted and shielded cable was directed from the back plane of the amplifier unit, where the temperature signals were extracted, to the data acquisition equipment. The series resistors of the transducers were assembled at the 15-pin D-sub-connectors at the input of the amplifier unit, at the end of the 5 metres long transducer cable.

The shields of the transducer cables were roughly assembled to the casing of the amplifier unit. This was also the case for the shield of the six pair twisted cables. At the data equipment side of the cable, the shield was not connected. The 15-pin D-sub-connectors were open during the experiment to ease the supervision of the points of solder.

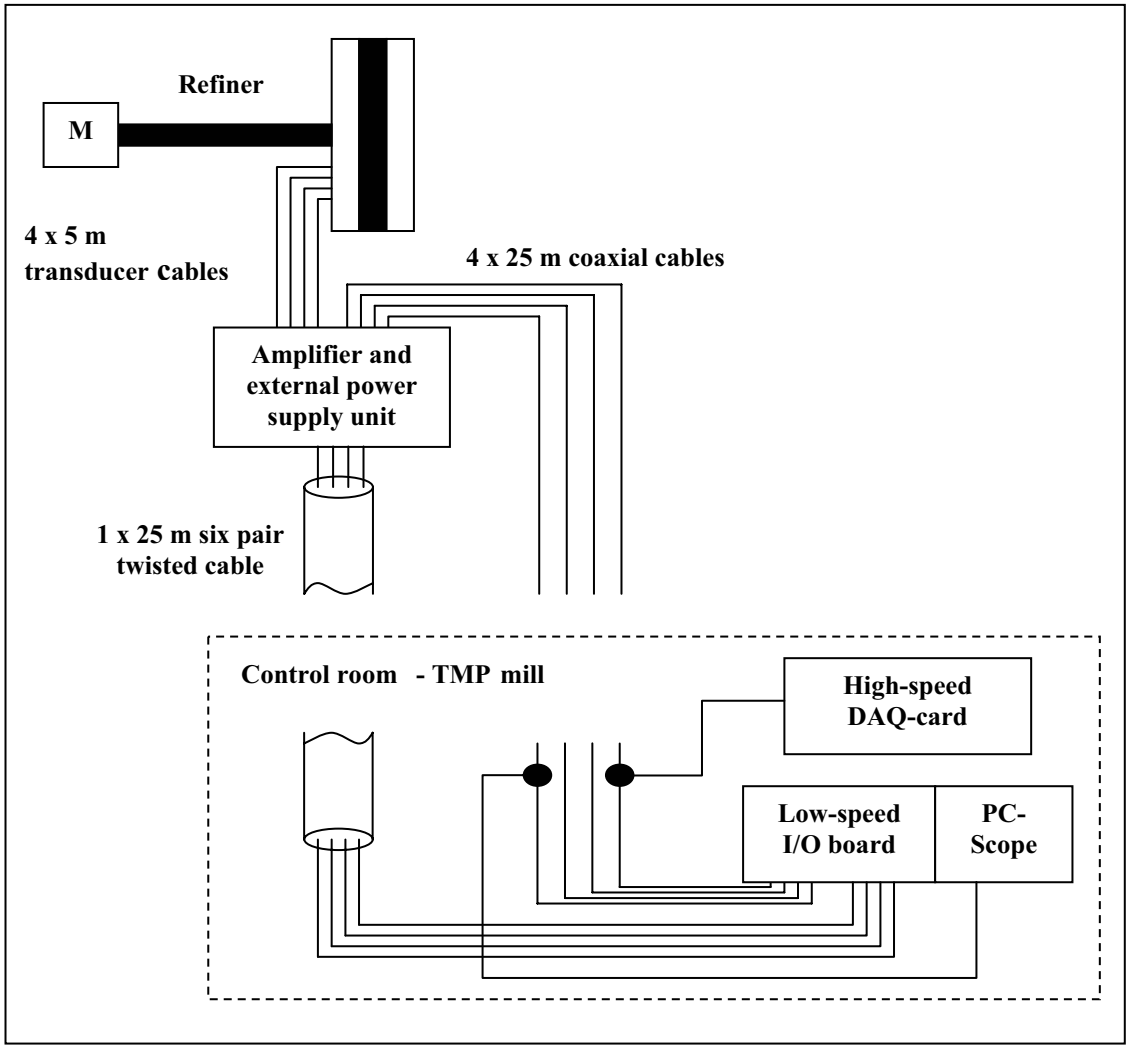

Figure 3.23: On-site location of the amplifier unit and the data acquisition equipment and the cable structures between the different devices.

3.5.2 Pilot-scale experiment – piezoresistive sensor

A single combined piezoresistive pressure and temperature transducer was used in the pilot-scale experiment. It was of the same type as manufactured by Kulite for the first mill-scale experiment. However, this sensor was one of the re-ordered transducers, which was different from the others through a thicker wall of the tubular metal housing as shown in Figure 3.20. It was mounted flush to the surface of a dam at a radial distance of 231 mm from the centre of the refiner. The mounted transducer in the plate and a similar one lying on the plate are shown in Figure 3.24. The bar-groove width in

that region was 5.1 mm. The bar and groove widths were respectively 2.5 mm and 2.6 mm. Essential data associated with the transducer are:

- Kulite model No.: XCL-1-152-35BARSG. (Figure 3.20 and Figure 3.24).
  - Circular size: 3.8 mm in diameter (casing), 2.5 mm in diameter (diaphragm).
  - Length of 25.4 mm. See Figure 3.24.
  - Natural frequency: 840 kHz.
  - Rated pressure range: 0-35 bar. (Maximum: 70 bar.)
  - Compensated temperature range: 150-200 ºC.
  - Pressure sensitivity: 3.450 mV/bar.
  - Temperature sensitivity: 3.440 mV/ºC.

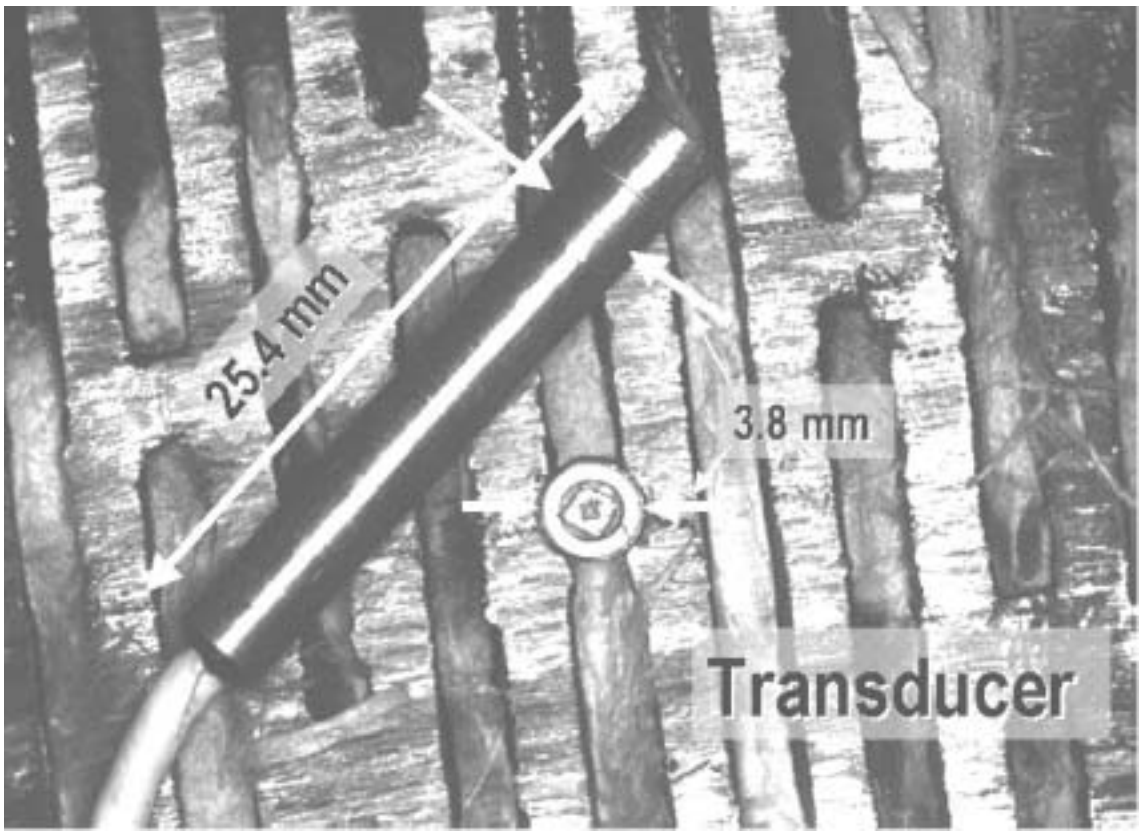

Figure 3.24: The sensor was mounted flush to the surface of a dam between two bars. A similar transducer is lying at the top of the plate.

The pressure signals were amplified by the same amplifier from Kulite, denoted D486 with a bandwidth of 100 kHz, as used in the previous experiment. However, the data acquisition was performed using another high-speed DAQ-card. A data acquisition card from National Instruments Corp. was used with the following data:

- Type: NI-6115, 4 channel multifunction DAQ-Card.
  - Resolution: 12 bits.
  - Internal gain: 0.2-50.
  - Sampling rate: max. 10 MSamples/s. (1.25 MSamples/s simultaneous on 4 channels.)

The temperature signals were not amplified, neither externally nor internally, because of the large DC component. This resulted in a poor resolution of the temperature output signal. The 12 bit resolution of the data acquisition card resulted in a bit resolution (LSB) of 4.88 mV, which corresponded to a temperature resolution of approximately 1.5 °C.

Some laboratory tests were performed as preparatory work also for this sensor. The following tests were performed:

- Static measurements of the output signals as well as resistance measurements.
- Heat chamber (25-185 °C) tests. These tests revealed a slight divergence in temperature sensitivity. A new value was obtained to be 3.15 mV/°C. Results from one test are shown in Appendix B1.
- Dynamic response test in a falling-weight test rig mounted in a water-filled chest. Response curves were obtained as shown in Appendix B2. However, a transfer function was not derived due to insufficient generation of a pure impulse.

In addition to these tests, the amplifier channel was tested with a dummy to confirm the gain. Assuming the original pressure sensitivity the amplified output signal ratio was 0.235 V/bar. Furthermore, the data acquisition system was tested using a signal generator (Krohn-Hite model 5100).

3.5.3 Mill-scale experiment – fibre-optic sensors

The measurement system contained nine fibre-optic pressure transducers from Luna Innovations Inc. The sensor surface was about 1 mm in diameter. The transducers are called EFPI fibre-optic strain sensors. EFPI is the abbreviations for Extrinsic Fabry-Perot Interferometer, which is the functional principle of the sensors. In other words, the sensor is based on interference between reflected light waves. The output signals from the interferometer are the phase differences of the light that appear when the gap between the reflecting surfaces alters as a function of the pressure imposed on the sensor surface. One of the reflecting surfaces is the optic fibre itself and the other is the reflecting surface in the end of a sliding gap also called Fabry-Perot cavity, which the light is transmitted into. A sketch of the EFPI pressure sensor is shown in Figure 3.25.

The EFPI system consists of a single mode laser diode operating with a wavelength of 1310 nm. The light from the laser diode illuminates a Fabry-Perot cavity through an optic coupler. The cavity is formed between an input single mode fibre and a reflecting single mode or multimode fibre. A glass tube aligns the input fibre and the reflecting fibre. For uncoated fibre ends, a 4 % Fresnel reflection results at both ends of the cavity, thus the EFPI can be approximated as a two-beam interferometer. The first reflection

denoted R1, called the reference reflection, is independent on the applied perturbation. However, the second reflection denoted R2 and called the sensing reflection, is dependent on the length of the cavity, which in turn is modulated by the applied pressure. These two reflecting light waves interfere provided that the path difference is within the coherence length of the source (Murphy (1996), Meller (1996)).

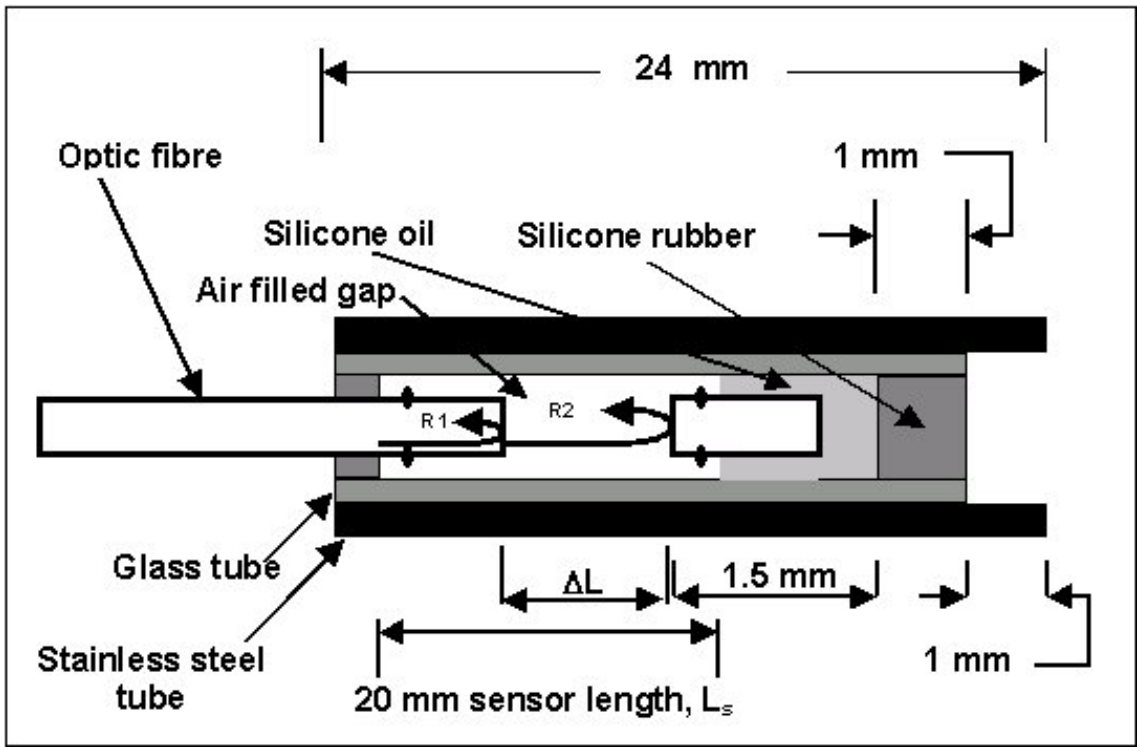

Figure 3.25: The Extrinsic Fabry-Perot Interferometer pressure sensor as manufactured for the second mill-scale experiment.

Either the intensity as a measure of the energy or the power of the light can be expressed as a simple function of the cavity length. Equation (3.19) shows the intensity.

$$I \mid I_0 \left[\cos\left(\frac{4\phi \div L}{\varsigma}\right)\right] \qquad (3.19)$$

I_0 : Maximum value of output intensity; [W/m^2].
$\div L$: Length of the Fabry-Perot cavity; [m].
ς : The laser diode centre wavelength; [m].

A phase change corresponding to a cavity length of $\varsigma/2$ is denoted a *fringe* period. Using an infrared laser diode with a wavelength of 1.3 μm as the light source, only 0.65 μm gap variation leads to a phase change of 2ϕ. In the following a gap change corresponding to $\varsigma/4$ will be called a *flange* provided that the half fringe period starts in a maximum or a minimum point of the periodic intensity pattern. Moreover, the terms fringe and flange are illustrated in Figure 3.26.

For more detailed information about theoretical equations connected to the Fabry-Perot interferometer, the book by Andonovic and Uttamchandani (1989) is recommended. An analogous detection system is also described in Eriksen (1995).

The illustration displayed in Figure 3.25 shows a sketch of the pressure sensor, which was used in the second mill-scale experiment. The stainless steel tube, protecting the remaining sensor housing, was fitted into a hole in the stator plate of approximately 1.2 mm in diameter. The stainless steel tube was mounted 1 mm sub-surface in a bar. Furthermore, a quartz tube surrounding the primary sensor parts ensures that the fused silica fibres that constitute the Fabry-Perot cavity are aligned. The optical fibre within the alignment tube is free to float such that the surrounding tube does not have to deform for strain transfer to occur (Murphy *et al.* (1996)). The imposed strain from the steam and pulp pad in the refining zone is firstly forced upon the high strength mould making silicon rubber, denoted Dow Corning HSIII, which appeared as a diaphragm. The intention behind the use of this silicon surface was that it should protect the even more sensitive silicone oil, DOT 5 silicone brake fluid, surrounding the reflecting fibre. It is assumed that the silicon rubber behave like a spring transferring the imposed pressure without damping. However, the sensors were calibrated with this silicone rubber diaphragm applied on the surface. No dynamic step-response test was done in advance. However, the manufacturer of the EFPI pressure sensors claims that the natural frequency of the sensor is approximately 80 kHz with the frequency response close to that. A frequency response between 72 and 76 kHz is indicated. In a former reference, the inventor of the EFPI sensor stated that the response to frequency was flat between 10 Hz and 10 kHz as well as the transducers did not require any temperature compensation. The latter was obtained by testing in environmental conditions up to 1100 ºC (Murphy (1996)).

The strain is determined by dividing the changes in gap distance by the gauge length (sensor length) as shown by Equation (3.20) (Singh and Shukla (1996)).

$$\kappa = \frac{N \zeta}{2 L_S} \tag{3.20}$$

N : Number of fringes.
L_S : Length of the sensor; [m].
ζ : The laser diode centre wavelength; [m].

The applied pressure is a function of the strain. A simple relationship is given by Hooke's law, which states that the normal stress is proportional to the normal strain as shown by Equation (3.21).

$$\omega = E \kappa \tag{3.21}$$

E : Young's modulus of elasticity; [Pa].
κ : Strain.

Since the sensor length is constant the resulting strain is negatively correlated with applied pressure. Thus, when the diaphragm is exposed to compressive forces the silicon oil moves the reflecting fibre such that the gap between the fibres decreases and

the phase of the interfering light waves vary. The phase variation affects the light intensity of the light brought back to the detector and the amplifier, as shown by Equation (3.19). Hence, the EFPI sensor is a phase-based sensor providing differential rather than an absolute measurement. It requires demodulation of some form in order to extract meaningful information. The most basic form of demodulation requires counting and tracking the fringes recorded during an experiment (Murphy (1996), Sing and Shukla (1996)). However, the sensors were delivered with calibration curves such that the absolute pressure was possible to extract from the measurements.

In addition to the sensors, the measurement system from Luna Innovations consisted of a laser diode light source and a photo diode, light-intensity detector, with supplementing devices as drivers and amplifiers. This system is called FOSS I, Fiber Optic Support System. Its output signal is a voltage signal proportional to the interferometric optical signal. The interferometric signal is a sinusoidal function of the pressure as shown by the calibration curves. Figure 3.26 shows two of the nine sinusoidal transfer function curves. The remaining calibration curves are shown in Appendix C. Figure 3.26 indicates that to move the output signal between two adjacent maximum points or two adjacent minimum points, denoted a fringe, the pressure has to increase or decrease approximately 20 bar. Hence, one flange of the sinusoidal signal i.e. between a maximum and the adjacent minimum point or vice versa, corresponds to a pressure change of about 10 bar. At the quadrature points i.e. when the second order derivative of the sinusoidal function is zero, the highest sensitivity of the sensor system is obtained.

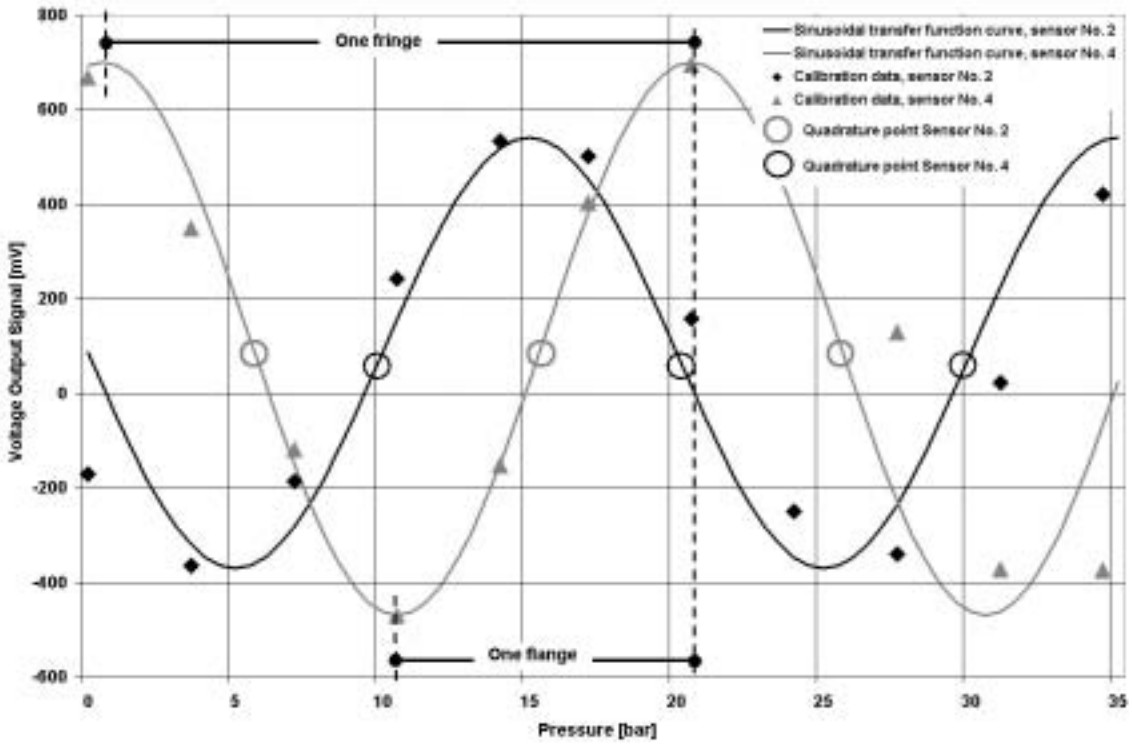

Figure 3.26: Sinusoidal transfer function curves for sensor No. 2 and sensor No. 4.

The EFPI sensor is widely used as reported by Murphy (1996). It is not intended in this thesis to discuss theoretical limitations. It is assumed that limitations regarding coherence length versus Fabry-Perot cavity length and non-ideal sinusoidal interference signal because of multiple reflections in the cavity are well treated by the manufacturer. Damping of the output signal occurs if the gap of the Fabry-Perot cavity is large compare to the coherence property of the light source. Then it does not give satisfactorily fringe visibility. The fringe visibility must then be accounted for. However, in this specific case such limitations are assumed to be negligible. Furthermore, calibration curves of the prevailing sensors were obtained between 0 and approximately 35 bar. Within this range the experimentally obtained calibration points secure the fringe visibility and the voltage output range from the measurements. If the pressure is increased beyond 40 bar an approximate calibration curve based on the sinusoidal relationship between the voltage output signals and the pressure gives a satisfactory transfer function.

The combined laser driver and light intensity-to-voltage converting unit, FOSS I, is the central unit in the measurement system. The laser driver provides transmitted light of a very stable wavelength to the sensor heads. The incoming interference light waves are converted through photo detectors and amplified. FOSS I has two incoming and outgoing channels such that two and two sensors are illuminated and are thus ready for pressure measurements. The bandwidth of the amplifying unit is claimed to be approximately 250 kHz.

The amplified signals were transmitted via coaxial cables to the data acquisition system. In the beginning of the experiment two DAQ-systems were recording simultaneously. Luna Innovations' high-speed data recorder provided a sampling rate up to 20 MSamples per second, while the other used data acquisition system comprised a four channel analog input card from National Instruments denoted NI-6115. It provided a sample rate up to 1.25 MSamples/s simultaneously at all the channels. Luna Innovations' DAQ-system was used as a backup system and for comparison between the systems. The sensors were originally calibrated using Luna Innovations' system. The main difference between the two systems was a constant offset of approximately 50 mV, which is incorporated in the recalibration curves of the sensors. Only data recorded with the NI-6115 DAQ-card are used in the presentation of the results in this study.

In addition to recording two pressure signals simultaneously, the two other channels on the DAQ-systems were used to record supporting data. A magnetic induction signal from a small magnet attached to the shaft of the refiner and the motor load signal directed from the mill's DCS were recorded simultaneously at the same high sample rate. All the signals were transmitted via cables from the refiner to the measurement equipment located in the control room of the mill. Figure 3.27 shows the on-site location of the measurement system.

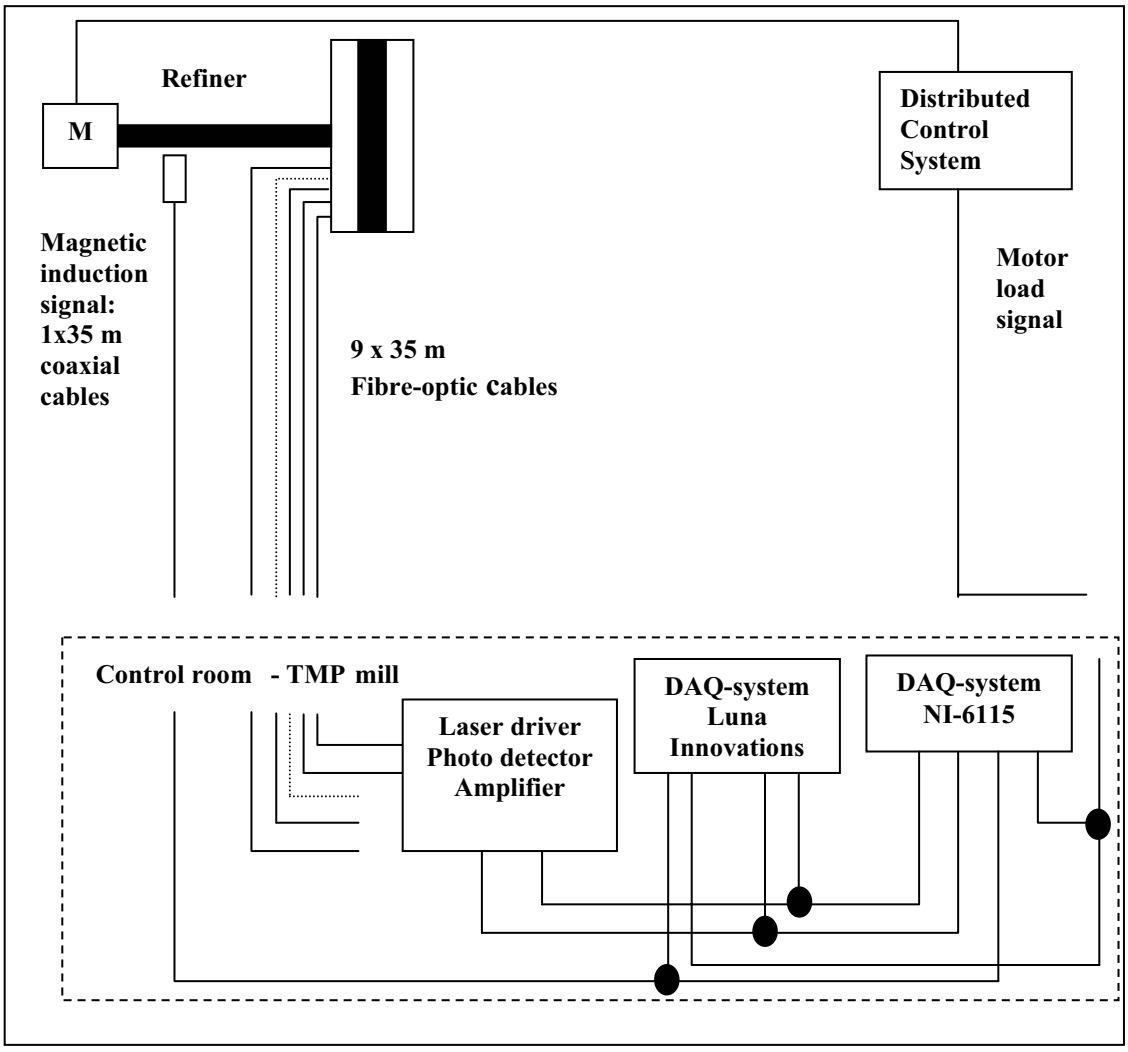

Figure 3.27: On-site location of the amplifier unit and the data acquisition equipment and the cable structures between the different devices.

3.5.4 Mill-scale experiment – external accelerometers

Two similar accelerometers were used in one part of the second mill-scale experiment. Brüel & Kjær manufactured the piezoelectric accelerometers already in 1987. The accelerometers were attached to the refiner housing, measuring the vibrations in axial direction. Recordings were made both on the motor side and the front side of the refiner. The accelerometers were used together with Brüel & Kjær's charge amplifier and the high-speed data acquisition card from National Instruments, NI-6115. Essential data were:

- Accelerometer No. 1: Brüel & Kjær type 4384, serial No. 1390386.
- Accelerometer No. 2: Brüel & Kjær type 4384, serial No. 1390387.
  - Circular size: 14 mm in diameter, length of 24.5 mm.
  - Weigth: 11 grams.
  - Piezoelectrial, natural frequency: 45 kHz.
    - Flat transfer function between 0.1 Hz – 10 kHz.
    - Gain below 6 dB: 10-35 kHz.
- Charge amplifiers: Brüel & Kjær type 2635.

The accelerometers were tested in advance using Brüel & Kjær Calibration Exciter type 4294. The calibration tests were satisfactorily showing expected level (10 mm/s) for a given frequency (159.2 Hz) as shown in Appendix D.

During the mill test recording was done from one accelerometer at a time. The amplifier was located a short distance of approximately 1-2 metres from the accelerometer. Furthermore, the data acquisition system was also located close to the refiner. The coaxial cable between the amplifier and NI-6115 was approximately 5-10 metres long. The shortest distance was when the accelerations on the drive side were measured.

Most of the recordings were made when the accelerometers were attached to the refiner housing in the shortest distance from the refining zone. The refiner housing has cavities on both sides where holes into the back of the refiner plates on the stator discs are accessible. These holes were used as throughput for the sensor cables both for the external temperature measuring system and the pressure sensors. In a short distance (50-100 mm) below these holes the accelerometers were attached using magnets and attachment screws.

3.6 Experimental procedures

This section considers the procedures for the different recordings. Primarily it was sought to measure the pressure and temperatures under normal operating conditions. In addition, it was intended to investigate which effect changes of different process parameters had upon the pressure and temperature readings. Furthermore, because of the uncertainty regarding the survival of the sensors the recordings and the follow-ups were performed during the preheating as well.

Both of the mill-scale experiments were performed in connection with the replacement of the plates. All the assembly work related to the sensors and measurement equipment was made before the start-up procedure was started. Both mill-scale experiments had the same start-up procedure that can be described as follows:

- First, a preheating period using steam was initiated. It lasted for approximately 30 minutes. The refiner was running with an open bottom valve allowing condensate to escape. The pressure condition was atmospheric.

- Second, an offset adjustment of the plate gap was performed during standstill. Because of the shutdown of the refiner and the subsequent rollout, this period lasted for approximately 30 minutes.
- Third, a second preheating period was started. This lasted for approximately one hour. It incorporated two distinct, but dependent sub processes classified as preheating and pressure built-up. In the beginning steam was transported through the refiner and condensate was removed through a valve in the bottom of the refiner. After a while the valve was closed and a casing pressure of 2.5-3 bar gauge pressure was built up.

Soon before the initial chip feeding, dilution water was turned on and the discs were moved towards each other providing an initial plate clearance. When the chips were entered the hydraulic thrust was gradually increased. The chips were subjected to compressive and shear forces that defibrated the wood matrix. The steam pressure increased because this work was performed through the contact between the chips and the bar and groove pattern of the plates i.e. the friction work increases the steam production. When the steam pressure had reached 4 bar gauge pressure, the valve in the blow line controlled the refiner housing pressure. Moreover, the effect that brings the steam pressure in the refining zone to increase above the casing pressure is called self-pressurization.

3.6.1 Mill-scale experiment – piezoresistive sensors

Some gigabytes of data were collected by all of the data acquisition units during the experimental period, which lasted for three days. The PC-Scope-card and the high-speed data acquisition card were in turns recording data together with the low-speed data acquisition boards (CAN-A I/O-boards). Thus two DAQ-systems were simultaneously collecting data. Parallel signals were allowed through a BNC T-plug connector located only a short distance, some 1-2 metres from the data acquisition equipment. However, some changes were made in the measurement set-up during the experimental period as are now described:

- The referencing signal of the CAN-A I/O device for the Kulite pressure signals was disconnected approximately three hours after initial chip feeding took place. This was done because of observations of unexpected large signal variations and an effort was made to prevent potential ground loop introduced noise. The change made no clear improvement.
- On the second day, data recordings were performed separately on the different data acquisition systems. The use of single data acquisition systems was done to prevent any common interactions between the different devices..

The measurement set-up during the preheating was as follows: Both temperature and pressure from all of the four piezoresistive transducers were recorded in the CAN-A I/O-board system. The pressure signals were amplified while the temperature signals were recorded without amplifying. The signals from the Presens transducer were recorded both with and without amplification for both the temperature and pressure signals. The data were recorded using a sample rate of 100 Hz. The measurement set-up on the CAN-A I/O-devices was separated to allow the three Kulite transducers, both

temperature and pressure signals, to be connected to the same device (six channels). Signals from the Presens transducer were connected to the other CAN-A I/O-unit (four channels). Only the device with the Kulite transducers was connected with a reference signal to the ground of the CAN-A board. The low level analog input was used as a reference signal. The PC-Scope-card recorded data simultaneously to check the signals from different transducers.

The initial period of chip feeding was accurately recorded using the high-speed data acquisition card with a sample rate of 83.3 kHz. Two channels were recorded. One of the recorded signals was the pressure signal from Kulite sensor No. 3, which was mounted in the surface position on a bar. The second channel recorded the amplified pressure signal from the Presens transducer. In addition, the CAN-A I/O-boards were recording signals as during the preheating.

Only a few minutes after the initial production start-up the refiner was running under stable conditions, which represented:

- Motor load: 12-15 MW.
- Hydraulic thrust: 100-110 bar. (Differential pressure applied on each of the two hydraulic cylinders.)
- Dilution water flow: 2.1 - 2.2 l/s (in each gap).
- Casing pressure: 4 bar gauge pressure.
- Feed screw speed: 64-65 % (approximately 260-270 tonnes/day (33 kg/second)).
- Temperature: 180 C (at the radial position where the transducers were installed).

The second day of data recording some experiments were done with different step-responses. Recording of both temperature and pressure were performed during the change of some process variables in the following way:

- The first step-response test firstly involved a decrease of the hydraulic thrust (- 2 bar). Secondly, after the process had been stabilized after approximately two minutes, an increase in the dilution water flow rate (+ 0.1 l/s in each refining zone) was made.
- The second step-response test comprised of a decrease of the hydraulic thrust (- 2 bar) and a subsequent increase in the dilution water flow rate (+0.1 l/s). The last change was performed after the process had been stabilized after approximately two minutes.
- The third step-response test involved an increase of the hydraulic thrust (+ 2 bar), while the dilution water flow rate was reduced (- 0.1 l/s) after approximately two minutes.
- The fourth step-response test comprised of two subsequent changes of the feed screw speed. The first step was a decrease in the rotational speed (- 2 %). Two minutes later, there was an increase in the feed screw speed (+ 2 %).

The high-speed data acquisition board was used for recording data during these four step-response tests. Only signals from the Kulite transducers were recorded. In the first and fourth tests both temperature and pressure signals from sensor No. 1 were recorded.

Temperature and pressure signals from sensor No. 2 were recorded in the second test, while the two signals from sensor No. 3 were recorded in the third test. All tests were recorded using an 83.3 kHz sample rate.

Lack of time-synchronization between the data acquisition systems and the mills' DCS made it necessary to keep an accurate log. All occasions during the experimental period were carefully registered. Thus the refining zone measurements could be compared with the process behaviour showed by the data in the DCS. The communication with the process operators went well. Every procedure and process modification was well informed allowing the data acquisition to be planned and initiated at proper time periods. Hence, the synchronizing of the recorded data with the data from the process variables stored in the mill's process database was to a certain degree well attended.

3.6.2 Pilot-scale experiment – piezoresistive sensor

This experiment was a test run that was designed to take measurements under different operational conditions. The plate gap and the dilution water flow rate were changed during the test run. However, the experiment was carried out in such a way that it was not possible to separate the influence of the disc clearance and the dilution water content in the recorded pressure and temperature signals.

The plate gap was approximately 1 mm when chips were initially fed into the refiner. Later the disc clearance was changed in steps of 0.25 mm to a minimum of approximately 0.25 mm, while at the same time the dilution water flow rate was increased from 3.8 to 7.1 litres per minute. Pulp samples were taken out for determination of production rate and pulp consistency during the three following operating conditions:

- Plate clearance: 0.75 mm. Dilution water flow rate: 3.8 litres per minute.
- Plate clearance: 0.5 mm. Dilution water flow rate: 6.0 litres per minute.
- Plate clearance: 0.25 mm. Dilution water flow rate: 7.1 litres per minute.

During the last running conditions with the smallest plate gap, the refiner operation became unstable and the feed screw was blocked. Recording of this extra ordinary occasion was made as well.

3.6.3 Mill-scale experiment – fibre-optic sensors

The fibre-optic sensors were tested and calibrated at Luna Innovations locations before they were fitted into the plate. Testing and recalibration of the sensors were performed on site before installation of the plates in the refiner. Zero bar gauge pressure was tested as well as tests in a water pressure chamber. Results from the latter tests are shown together with the different calibration curves in Appendix C. Data from these pre-tests gave input to the recalibration of the sensors. Further testing of the sensors was performed until the refiner start-up took place.

As opposed to the first mill-scale experiment, the data acquisition systems were carefully synchronized with the mill's DCS. The clocks on the measuring units were adjusted to fit the time on the DCS. In addition, a battery driven electric circuit with a

power switch was connected to an external process database, which stored both process data from the DCS and data from the temperature sensors. This power switch was manually activated each time a high-frequency pressure recording was started ensuring that the pressure readings were collected at known process conditions.

Data recordings were made during the warm-up process as well as the initial chip feeding. However, maintenance problems in the mill made it necessary to shut down the process before the refiner achieved a stable production level. A new start-up took place the day after. Also at this time the preheating and the initial chip feeding periods were properly recorded.

After a few hours of stable operation it was possible to start the test run series as part of the experiment. This part consisted of 30 tests during which the refiner was operated under different set points. Moreover, this set of test runs was an extended factorial designed experiment at two levels in addition to centre points that formed a third level. Four process variables were used to manipulate the refiner: the hydraulic thrust, the plug screw speed, the dilution water flow and the casing pressure. The factorial design, as a central composite design, is illustrated in Figure 3.28, and it is shown in Tables 3.6a and 3.6b.

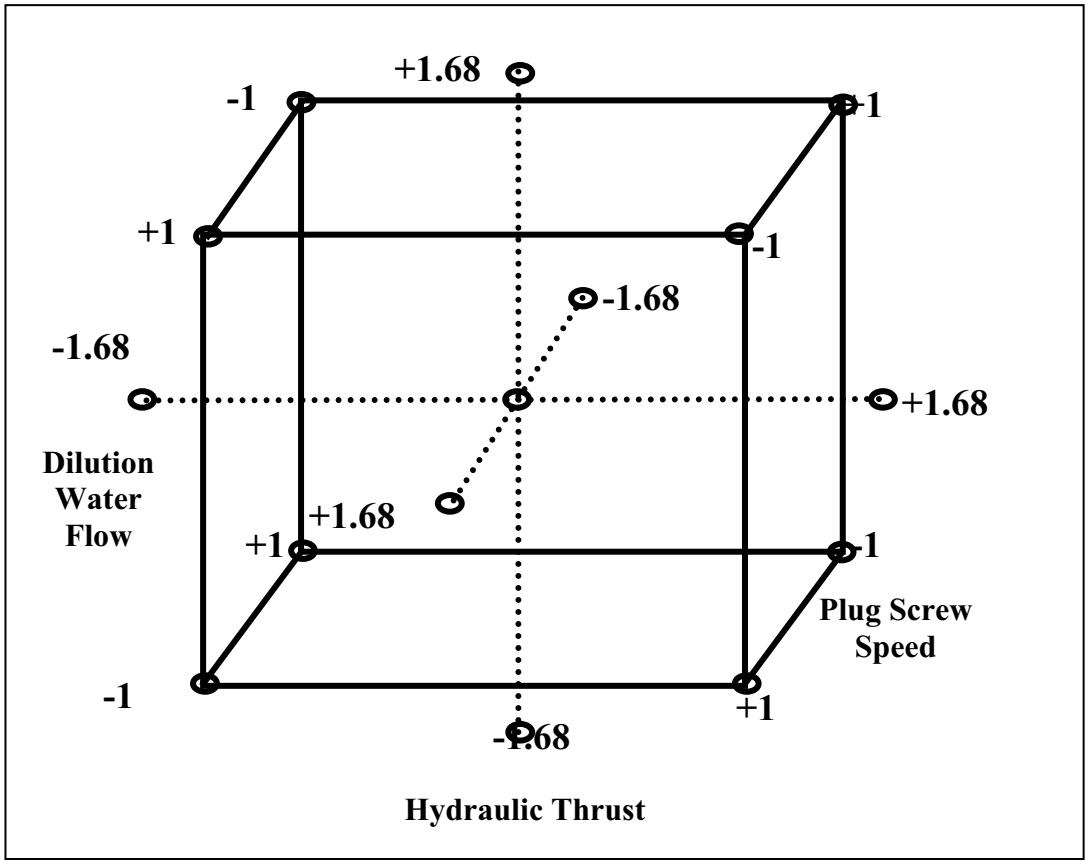

Figure 3.28: Illustration of the central composite design in three factors.

Table 3.6a: A central composite design in four variables.

Run No.	Hydraulic thrust	Plug screw speed	Dilution water flow	Casing pressure
1	-1	-1	-1	-1
2	1	-1	-1	-1
3	-1	1	-1	-1
4	1	1	-1	-1
5	-1	-1	1	-1
6	1	-1	1	-1
7	-1	1	1	-1
8	1	1	1	-1
9	-1	-1	-1	1
10	1	-1	-1	1
11	-1	1	-1	1
12	1	1	-1	1
13	-1	-1	1	1
14	1	-1	1	1
15	-1	1	1	1
16	1	1	1	1
17	0	0	0	0
18	0	0	0	0
19	0	0	0	0
20	0	0	0	0
21	*-1*	*0*	*0*	*0*
22	*1*	*0*	*0*	*0*
23	*0*	*-1*	*0*	*0*
24	*0*	*1*	*0*	*0*
25	*0*	*0*	*-1*	*0*
26	*0*	*0*	*1*	*0*
27	*0*	*0*	*0*	*-1*
28	*0*	*0*	*0*	*1*
29	*0*	*0*	*0*	*0*
30	*0*	*0*	*0*	*0*

Table 3.6b: Values of the manipulated variables of the factorial experiment.

Factor	Low level (-1)	Centre (0)	High level (+1)
Hydraulic thrust [bar]	104	108	112
Plug screw speed [%]	64	68	72
Dilution water flow[1] [l/s]	1.70	1.85	2.0
Casing pressure [bar]	3.9	4	4.1

1 Dilution water flow related to the feed rate fed into one of the refining zones.

The experimental set-up was organized in randomized order as shown in Chapter 6, Table 6.8, as opposed to the standard order design shown in Table 3.6a. Randomizing avoids correlated errors between the recordings. The use of factorial designs and analysis techniques as a part of the response surface methodology is related to arranging the experimental trials such that the effect of changing each factor can be measured and separated from the effects of other factors that were changed. Effect is understood as the change in the response caused by the change in one factor or combination of factors. Some features with the chosen design are described in Appendix E. Moreover, in the literature factorial designed experiment and analysis techniques are closely treated (Box *et al.* (1978), Box and Draper (1987)).

A part of this factorial designed experiment was performed with investigations of the pulp quality as well as recording of the pressure. Pulp samples were collected during 10 of the test runs where the casing pressure was at the low level except for the centre point runs. The test conditions for this part of the experiment are given in Table 3.7.

Table 3.7: The factorial designed experiment for pulp samples analyses.

Standard run [No.]	Hydraulic thrust (Centre point: 108 bar) ∂ [bar]	Plug screw speed (Centre point: 68 %) ∂ [%]	Dilution water flow (Centre point: 1.85 l/s) ∂ [l/s]
1	- 4	- 4	- 0.15
2	+ 4	- 4	- 0.15
3	- 4	+ 4	- 0.15
4	+ 4	+ 4	- 0.15
5	- 4	- 4	+ 0.15
6	+ 4	- 4	+ 0.15
7	- 4	+ 4	+ 0.15
8	+ 4	+ 4	+ 0.15
17	0	0	0
18	0	0	0

Pressure readings were collected with a sample rate of 500 kSamples/s. Each recording lasted for 10 seconds, while each run lasted for approximately 3 to 15 minutes. The latter was dependent on how many pressure sensors that were recorded. One sensor, sensor No. 4, was followed up more accurately than the others. At least three recordings in each run were made with sensor No. 4. Also signals from sensor No. 1, sensor No. 6 and sensor No. 9 were recorded in all 30 runs. During the same 10 runs as the pulp samples were collected, signals from all the pressure sensors were recorded at least once. The choice of sensor No. 4 as the sensor that was followed up more accurately was related to the results from the pre-tests that were performed before the production start-up and the responses from the measurements made before the test runs started. The choice was also based on an initial request, because sensor No. 4 was mounted close to a radial position where it was expected that the pressure peak would be obtained.

The data recording continued in short periods after the factorial designed experiment was completed (day three). Furthermore, the fourth day of data recording a new planned

short shutdown and the following start-up was carefully recorded. The measurement equipment was decoupled after these last recordings. However, the fibre-optic sensors were still attached to the refiner plate, which was not replaced.

Data recording was carried out during a second period as well. After approximately 1000 hours operating time the measurement equipment was again hooked up, and new time series were collected. However, only the fibre-optic measurement system was assembled. The power switch for synchronizing of recorded data with the process database and the magnetic sensor for capturing of the rotational speed of the refiner shaft were not connected. The primary objective behind these last pressure measurements was to assess the signals from the sensors after that long period in the harsh environment inside the refiner. However, the second day of the second main data-recording period was used to investigate the responses from the pressure sensors when changing the chip flow rates to the two refining zones of this Twin refiner. This was achieved by changing the angle – step by step - of one of the power screws in the load sense conveyor. The angle variations, approximately 1.4∀step, were obtained by adjusting the actuating device on the stream splitter called Giri gari.

The chip stream splitter test was performed in such a way that the adjusting of the Giri gari was closely related to the observations of the process behaviour made by the operators. Adjusting one step was followed by a stabilizing period of some seconds (10-20 seconds). This was repeated until the operators observed a large acceleration deviation between the two refining zones. A reverse action was made as well. The test ended with adjusting the Giri gari value such that the acceleration values in the two zones were almost even.

3.6.4 Mill-scale experiment – external vibration measurements

In connection with the subsequent change of the plates some tests were performed to measure the axial vibrations on the refiner. This was achieved using external accelerometers attached to the refiner housing. It was important to compare the vibrations on the refiner when it was equipped with the plate sets used during the experiment with the fibre-optic sensors with similar vibrations when the new plates were used. Thus tests were performed both before the worn plates were removed and after the new ones were installed. The latter was performed during operation with another type of stator plates. Simultaneously measurements of the pressure in the refining zone were not accessible because the laser driver and amplifier unit, FOSS I, was returned to the manufacturer of the fibre-optic sensors.

The first tests were performed during the last day using the plates, which are described in Section 3.3.3. High-frequency (500 kSamples/s) acceleration measurements were recorded. These measurements used the external accelerometers, which are described in Section 3.5.4.

The plates were replaced in the second day of this experimental period. The new plates both on the stator and the rotor discs were of the same type as previously attached to the rotor disc as shown in Figure 3.8. Recordings were made both under unloaded non-spinning conditions and under unloaded spinning conditions. After the first preheating

period and before the refiner was restarted, measurements were performed while exciting resonance in the refiner housing. One of the accelerometers (No. 2) was attached to the front side of the refiner while a soft hammer was used to hit the refiner housing in axial direction every fifth to tenth second in a short period lasting for approximately 60 seconds. Further measurements were obtained during initial chip feeding and during normal operation. The last measurements were performed on the drive side of the refiner approximately 75 minutes after the initial chip feeding.

3.7 Data analysis methods

The recorded data were analysed mainly using applications in LabVIEW and Matlab. Analyses of the central composite designed experiment were made using Minitab. Mainly the same investigations were performed after all experiments as will be described in this section. However, the analyses of the second mill-scale experiment using the fibre-optic pressure sensors had to be carried out more carefully because of the sinusoidal transfer function curves. Before the data analysis methods are described the challenge regarding the determination of the pressure signals is illustrated. Figure 3.29 shows this illustration, which is divided into three subplots.

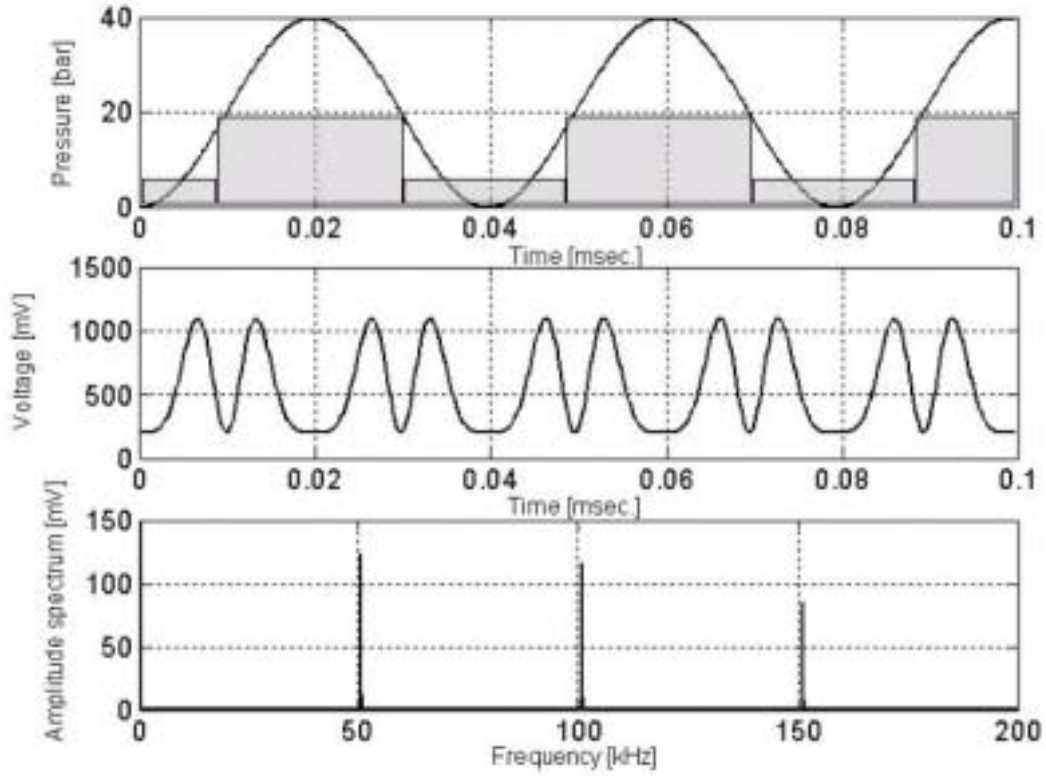

Figure 3.29: Illustration of a pressure signal created by a bar-groove pattern (upper plot). The corresponding measured signal is shown in the plot in the middle and its frequency spectrum is shown in the lower plot.

The upper plot in Figure 3.29 simulates an idealized pressure signal as a sinus wave with a frequency (25.2 kHz) given by a bar-groove pattern. The plot in the middle shows the corresponding output signal (voltage) from the measurement system, while the lower plot shows the frequency spectrum appearing from the voltage signal.

The challenge is to determine the development or the form of the pressure signal (upper plot) based on the measured information (plot in the middle) and data analysis tools as frequency analysis (lower plot). The plot in the middle shows that the output signal cover two sinusoidal periods (two fringes) between 0 and 40 bar and additional two sinusoidal periods when the pressure decreases to zero. Four sinusoidal periods corresponding to four times the fundamental frequency will be obtained by the measurement system while the real pressure signal has swept through one bar-groove period only. The four sinusoidal periods are retrieved as the peak frequency at approximately 100 kHz in the frequency spectrum in the lower plot in Figure 3.29. The peak frequency at 50 kHz has appeared as a result of the parts of the sinusoidal curve that have flattened out at its maximum (40 bar) and minimum (0 bar) corresponding with the low voltage level of the transfer function curve. The transfer function curves are shown in Appendix C.

In addition to visual evaluation of the measured signal patterns, frequency analyses as well as assessment of the probability mass function (*pmf*) curves (histograms) are considered useful as data analysis tools. Measured signals that correspond to large pressure variations as shown in Figure 3.29 will give saddle shaped *pmf*-curves because more samples appear from the less steep parts round the turning points of the transfer function curve.

The following part of this section describes the analyses that were made:

- Time series analysis. Data were visually inspected and analysed statistically on data sets of 1 MSamples. This investigation was performed to get an overview of the different batches of samples and the sensors functionality. The following parameters of the output signals have been estimated:

  - Average and standard deviation values.
  - Maximum and minimum values (one of each per data set).
  - Correlation coefficient between simultaneously recorded signals.

- Histograms (*pmf*) of the recordings gave an overview of the distribution of the voltage output signals i.e. the number of samples for each voltage value. The resolution of the histograms, which determined the number of bins, was mainly equal to the resolution (LSB) of the recorded time series. Especially for the measurements using the fibre-optic sensors it was important to check the distribution of the voltage output signals. This was important when considering the output signals with the sinusoidal transfer function curves. Thus, this check was useful while determining if the output signals crossed the minimum or maximum points of a fringe. See also Appendix F3 for additional discussion about the evaluation of the histograms

∉ Frequency analysis was the most important analysis method performed in this study. The normalized amplitude spectrum analysis performed using FFT (Fast Fourier Transform) was used to find out if the output signals carried some periodic patterns. The normalized term was used to show the relationship between the amplitudes in the frequency domain with the corresponding amplitudes in the time domain. A unit sinusoid in the time domain corresponds to unit amplitude in the frequency domain. The FFT-routine in Matlab was used in the calculations. Equation (3.22) shows the equation for the normalized amplitude spectrum.

$$A_n \mid abs(fft(x)\ \Gamma\frac{2}{N}) \tag{3.22}$$

N : total number of samples included in the FFT-calculation.

The total number of samples included is determined by 2^n. For data series containing 1 MSamples the maximum number of samples (N) in one FFT-calculation were 2^{19} (524 288) samples[10]. The frequency spectrum produced by this N point FFT consists of N/2+1 samples equally spaced between zero and one-half of the sampling frequency (Smith (1999)). Assuming a sample rate of 500 kSamples/s i.e. sampling frequency of 500 kHz, this gives a frequency resolution of approximately 1 Hz. Moreover, the spectral resolution can be expressed as shown by Equation (3.23) (Fairchild (1982)).

$$\div f \mid \frac{f_s}{N} \tag{3.23}$$

f_s : the sampling frequency.

4 Amplitude spectra averaging were implemented in many of the analyses. This was done to smooth out the spectrum and reduce statistical errors that are inherent in recorded signal measurements where they appear as noise. The random noise reduces in proportion to the square root of the number of segments when utilizing the segment averaging method (Smith (1999)). The averaging was performed such that amplitude spectra of sequential blocks of samples were calculated and averaged. The random frequency peaks were cancelled out. Inherent periodic patterns derived advantage from this averaging and became even more visible. For instance, 1 MSamples comprises 30 blocks of 2^{15} (32 768) samples each. Thus, the averaging spectrum is based on 30 amplitude spectra. However, the spectral resolution is reduced. Using the same figures as in previous example, the resolution reduces from 1 Hz to 15 Hz.

4 Peak frequency determination has been performed. This is based on FFT-analysis of a number of small data sets until the whole time series is analysed. Thus it gives additional information compared to the straight FFT-analysis

[10] The total number of 2^{20} (1 048 576) samples, for example, could be used by adding zeros to the extra number of samples beyond 1 MSamples. This zero-padding would not change the shape of the frequency spectrum (Smith (1999)).

because the peak frequency determination gives information of where in the recorded time series the different peak frequencies were dominating. This analysis was primarily used on data sets obtained in the first mill-scale experiment as discussed in Chapter 4.

4 For support of the visual impression of the FFT spectra a phase average analysis was used, particularly regarding the data recorded in the pilot refiner as treated in Chapter 5. This analysis is based on dividing a large data set into smaller sets of a given length i.e. the length of the periodic signal pattern. The mean values of the synchronized samples in each small data set form the phase average values. Mathematically it can be expressed as in Equation (3.24):

$$\overline{X}_j = \frac{1}{(n+1)} \sum_{i=0}^{n} X_{j+i(m)}, \qquad j = 1,\ldots,m \tag{3.24}$$

X : Sample (measured value).
i : Phase number (synchronized period).
j : Sample number in each period.

For instance, if a bar-groove period consisted of 70 samples (m), the phase average analysis of such period over one revolution of the rotating refiner disc (288 bar-groove periods per disc in the pilot refiner) consisted of 70 mean values determined by 288 phases or synchronized periods ($n+1$).

4 Signal-to-noise ratio (SNR) is another term that has been used in the present study. According to Smith (1999) SNR is equal to the mean represented by the average value, divided by the standard deviation. Moreover this representation is closely related to the term coefficient-of-variations, which is defined as the standard deviation divided by the mean, multiplied by 100 per cent. Better data mean a higher value for the SNR and a lower value for the coefficient-of-variation.

It is common to use signal-to-noise ratio in connection with frequency peaks in spectrum analyses. Then the signal-to-noise ratio is defined in decibels as shown in Equation (3.25) (Bentley (1995)).

$$SNR = 20 \left[\log \left(\frac{V_{peak}}{V_{noise}} \right) \right] \; ; \; [dB] \tag{3.25}$$

V_{peak} : Amplitude (peak) value in the amplitude spectrum.
V_{noise} : Value of the noise level.

The noise level (white noise) to a signal, which is represented in the frequency domain, is associated with the relative flat region in the frequency range above approximately 100 Hz. Below this frequency, the noise rapidly increases. This

noise is called 1/f noise (Smith (1999)). SNR is associated with the white noise level. However, in this study a modified meaning of SNR is used. SNR is determined from the noise level that is present in the surrounding frequency range at the current frequency peak. Thus it can be described as an *amplitude ratio*. Especially in the low-frequency range, where the 1/f noise is present, the modified SNR gives lower values than an SNR derived from the white noise.

- In connection with the fibre-optic measurements a moving average analysis was carried out on some recordings. Moving average values were determined for batches of samples corresponding to the number of samples collected in one bar-groove period. In addition, each batch gave one maximum and one minimum value. This analysis was helpful when the output signal should be localized to a certain flange on the sinusoidal transfer function curve. As a supplement to the histograms this analysis also gave information about the calibration offset. This method has been used in connection with some analyses, which is discussed in Section 6.5.

- Cross-correlation analysis was done between output signals from fibre-optic sensors that were located in the same square pattern in the plate. The results are shown in Section 6.4. This investigation was intended to give causal information about the flow of pulp in parts of the refining zone. However, the speed and direction of the pressure waves were probably more visible than the pulp flow behaviour using this method.

For two signals, x(t) and y(t), the cross-correlation is defined as Equation (3.26) (Bentley (1995)):

$$R_{xy}(\eta) = \lim_{T\Downarrow\leftarrow}\frac{1}{T}\int_0^T x(t-\eta)\,y(t)dt \qquad (3.26)$$

The discrete mathematical function of the cross-correlation is expressed as a function of the covariance and the individual standard deviations. The estimated cross-correlation function is thus given by Equation (3.27) (Wei (1994)):

$$\hat{\rho}_{xy}(k) = \frac{\hat{\gamma}_{xy}(k)}{S_x S_y} \qquad k = 0, \pm 1, \pm 2, \ldots, \qquad (3.27a)$$

$$\hat{\gamma}_{xy}(k) = \frac{1}{n}\sum_{t=1}^{n-k}(x_t - \bar{x})(y_t - \bar{y}) \quad k \geq 0;\ k < 0\ (t = 1-k \Downarrow\ t = n) \qquad (3.27b)$$

$$S_x = \sqrt{\hat{\gamma}_{xx}(0)},\ S_y = \sqrt{\hat{\gamma}_{yy}(0)} \qquad (3.27c)$$

The discrete cross correlation function was used by utilizing the unbiased *xcov*-function in Matlab together with the determined standard deviation values of the two time series of interest. The unbiased option of the covariance function in Matlab

assures that the cross-correlation coefficients are lying between -1 and 1. Hence, the cross-correlation coefficient for zero-lag (k=0) for two identical time series is 1.

4 The lack of information regarding standing wave patterns from the cross-correlation analysis was overcome when a low pass filter was included in the analysis. Both an ordinary averaging procedure, averaging the number of samples corresponding to one bar and one groove, and a moving average routine were tested as well as an inherent low pass filter function in Matlab. No large deviations were found between these three methods. However, the low pass filter function in Matlab based on the Butterworth filter was selected in this analysis. A filter order of 9 and a cut-off frequency of 15 kHz were chosen. Thus an ordinary one-dimensional digital filter based on implementation of the standard difference equation was used. This filter is denoted *Filter* in Matlab. A zero-phase forward and reverse digital filtering function denoted *Filtfilt* in Matlab was tested as well. No differences were observed.

∉ Linear regression analysis was preferred before the factorial analysis in this study. The reason was that one of the 30 runs was performed differently from the designed experimental plan as shown in Tables 3.6a and 3.6b. However, linear regression gives the same results as the factorial analysis, which is described in Appendix E.

The four manipulated variables were investigated to explore how they influenced other process variables and some pulp quality variables. The pressure and temperature measurements were also tested as response variables. The results are given in Section 6.6. Multiple linear regression models as shown by Equations (3.28)-(3.30) were tested.

Multiple linear regression:

$$y_j = \eta_0 + \eta_1 x_{j1} + \eta_2 x_{j2} + \eta_3 x_{j3} + \eta_4 x_{j4} + \kappa_j \qquad (3.28)$$

Multiple regression with interactions:

$$y_j = \eta_0 + \sum_{i=1}^{4} \eta_i x_{ji} + \sum_{i=1}^{4} \eta_{ji} x_{ji} x_{j(i+1)} + \kappa_j \qquad (3.29)$$

Multiple regression with interactions and polynomial:

$$y_j = \eta_0 + \sum_{i=1}^{4} \eta_i x_{ji} + \sum_{i=1}^{4} \eta_{ji} x_{ji} x_{j(i+1)} + \sum_{i=1}^{4} \eta_{ii} x_{ji}^{2} + \kappa_j \qquad (3.30)$$

In addition, models comprising other process variables as manipulated variables for instance the motor load were tested to find which influence they had on different response variables. Simple linear regression models were mainly used.

∉ The time deviation of the rotational speed of the refiner, observed in the second mill-scale experiment and presented in Section 6.8, was analysed through the following steps:

- The magnetic induction that appeared when the magnet attached to the refiner shaft passed by the sensor head, gave a signal as shown in Figure 3.30. The raw data from this induction signal were filtered by a moving average method resulting in a smoother appearance. Ten samples were consecutively averaged to reduce random noise.
- The number of samples between two adjacent maximum points in the data from the filtered magnetic induction signal and the corresponding number of samples between two adjacent minimum points was averaged. The averaged number of samples corresponded to the time of one revolution of the refiner rotor disc. The refiner made 50 revolutions during a recording lasting for two seconds. The first and the last values were not included in this analysis.

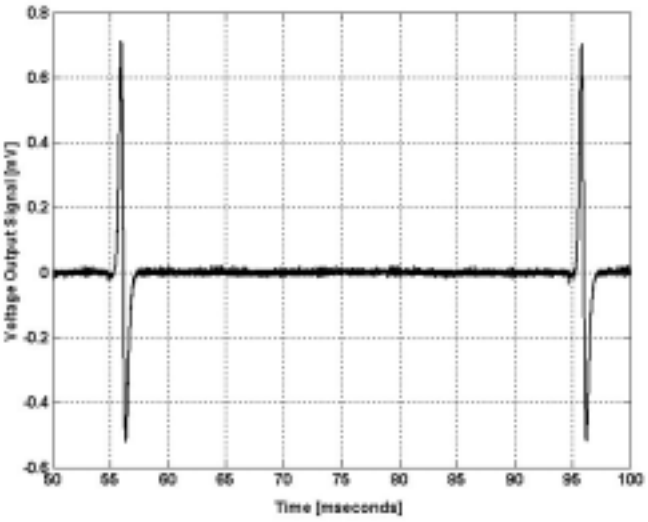

Figure 3.30: The magnetic induction signal from two passages of the magnet attached to the refiner shaft.

- Instead of displaying the total time per revolution the average value was subtracted giving a zero mean distribution of the time of one revolution. Thus the analysis showed the time deviation from the average time per revolution.
- Further analysis involved the motor load variation as well. The corresponding high-frequency recording of the motor load was divided into a number of average values associated with the number of revolutions. The number of samples recorded in a period lasting for 40 milliseconds i.e. the time of one revolution, was averaged. Accordingly, the total number of average values in a period lasting for two seconds was 50.
- A cross-correlation analysis between the time deviation per revolution and the average motor load per revolution was performed on the 48 corresponding obtained values.

∉ Evaluations of special signal patterns as sideband effects, that have been observed when the fibre-optic sensors were used, have been made using simple simulation. Descriptions of the simulation procedures are made in Section 6.9.

CHAPTER 4

RESULTS AND DISCUSSION PIEZORESISTIVE SENSORS MILL REFINER

4.1 Introduction

This chapter contains the results and assessments about the recordings that were made in the first mill-scale experiment. The experiments comprised of four combined piezoresistive pressure and temperature transducers mounted into a modified part of one stator plate as shown in Figure 3.5.

The results that are shown in the following sections mainly comprise recordings undertaken during normal operating conditions. Because the results are associated with a certain degree of uncertainty different recordings showing different shape and pressure levels are displayed. The assessments are related to the credibility of the readings and the probable causes of the appearance of the different recordings. Amplitude spectrum analysis has been an important tool in this work. It will be shown that it is the frequency spectra that probably contain the most valuable results from this experimental period.

Plots of different time series of the raw data are partly shown with the voltage output values as well as the corresponding measuring unit of the pressure. The output signals converted from voltage to pressure values were based on simple linear calibration curves. The calibration curves were obtained using the amplifiers' gradient figures fitted to the sensitivity data of the transducers. Recordings of the non-stress conditions (20∀C / 1 bar) made after the sensors and the plates were installed in the refiner were used to fit the readings as well.

4.2 Pre-chip feeding observations

The first recordings were undertaken during the preheating phase. The lack of consistent data readings was already observed then. Some simultaneous level shifts and offsets from pre-calibrated output values appeared. The Presens-sensor was clearly affected by

power hum noise. Large 50 Hz signal variations were visible. This signal disturbance was probably power hum coupled through the transducer's casing. It was probably caused by the lack of insulation between the casing and one of the connecting points for the signal cables. Furthermore, shortly after the refiner was pressurized the recorded output signals from the Presens transducer made a large and sudden level shift. This was not reasonable, and the readings indicated that the transducer instantly broke down. The reason was probably due to penetration of high-pressure steam behind the plates. Such water vapour penetration resulted in a situation where the contact areas of the cable ends were surrounded by steam. This probably caused a resistive coupling and eventually a final total collapse of the deflection bridge circuit. Further assessments regarding the Presens-sensor are not included in the present thesis.

No temperature recordings from the Kulite transducers are included either. This is because of the uncertainties observed during the preheating. Large signal deflections and readings that did not fit well into the pre-registered sensitivity data caused this decision. A possible reason for the uncertainties might be connected to the replacement of the series resistors made during the assembly work. New series resistors that were not delivered by the manufacturer were soldered to the connectors that were interconnected to the amplifiers. Small divergences between the original resistors and the new resistors might have had a negative influence on the readings. In addition, partly wrong use of the data acquisition system, as discussed in Section 4.6, could lead to offsets and saturation effects.

The pressure readings from the Kulite transducers during the preheating process were not consistent. Thus, already early in the experiment there was an apparent lack of credible recordings. Then it became necessary to change the original targets. Troubleshooting was initiated and some efforts were made to find the causes of the uncertainties. This led to more consistent data recordings, and some interesting features were observed during the experiment as shown in the following sections.

4.3 Initial chip feeding

While initiating the chip feeding, there are interesting readings of the pressure output signal from Kulite sensor No. 3, as shown in Figure 4.1. The low-level pressure readings are shown to be 2.7 bar. The rise in pressure lasted for approximately four seconds before it flattened off at an average pressure between 30 and 35 bar. Both the low-level pressure readings and the rise time coincided well with the measured process variables, especially the motor load and the casing pressure. The corresponding motor load and casing pressure signals collected from the mill's distributed control system (DCS) are shown in Figure 4.2.

The current pressure recording was made by the high-speed data acquisition system at a sampling frequency of 83 kHz. During a short period lasting for 12 seconds as shown in the left-hand plot in Figure 4.1, the measurements appeared to fit well with the process. More alarming, the rest of the measurements of this time series, shown in the right-hand plot of Figure 4.1, revealed a sudden level shift towards saturation followed by a rapid variation of the output signal, which indicates a lack of credibility. This unexpected

signal behaviour was probably caused by some earthing or ground loop noise problems. Perhaps there were some interactions between the different data acquisition systems since these were not properly decoupled. That is to say that the high-speed measurements also corresponded well with the simultaneous data recorded by the low-speed DAQ-board, as shown in Figure 4.3. These plot show data that has been sampled at a frequency of 100 Hz. The left-hand plot in Figure 4.3 corresponds well with the right-hand plot in Figure 4.1, while the right-hand plot shows the whole data set of this time series. Except for short periods, for instance during the first 15 minutes, this recording completely lacked consistent readings.

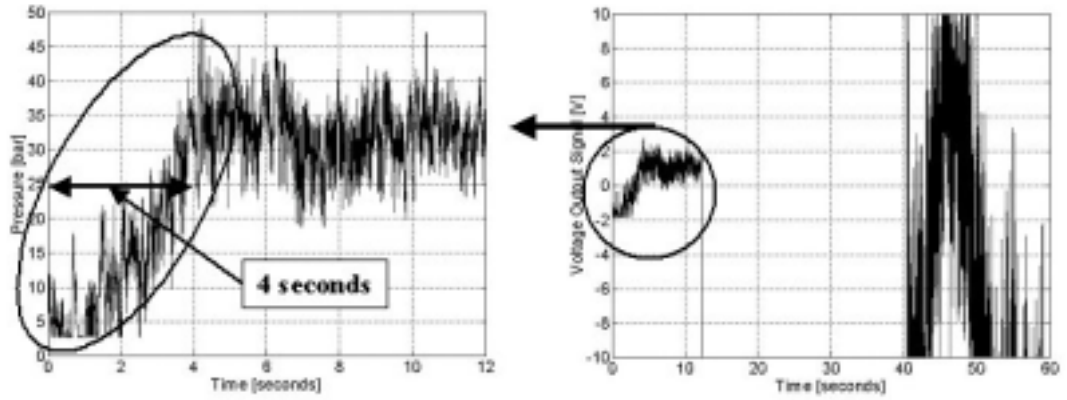

Figure 4.1: The pressure output signal from sensor No. 3, recorded by the high-speed DAQ-card, while initiating the chip feeding.

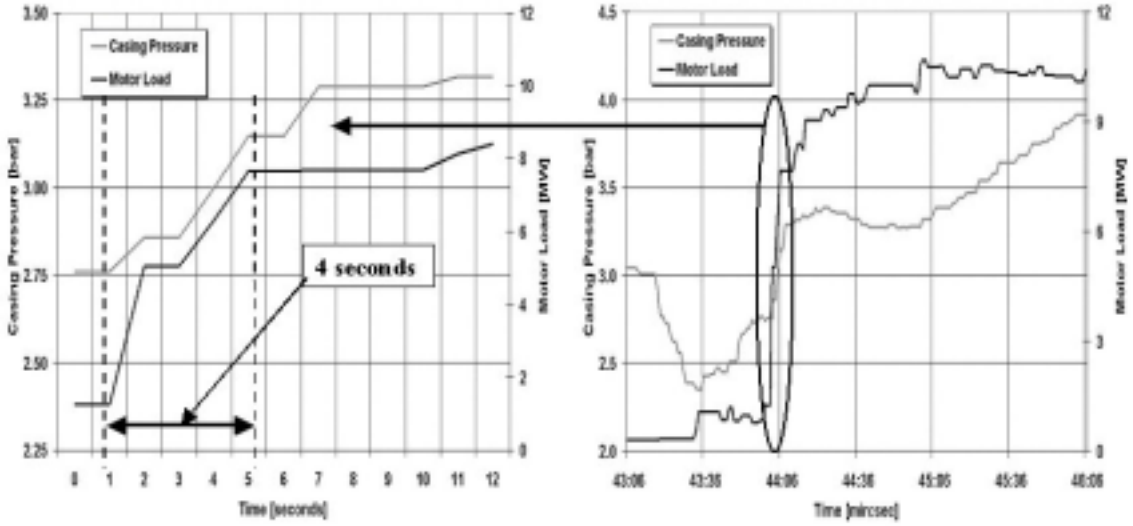

Figure 4.2: The motor load and casing pressure readings, taken from the mill's DCS, show a increasing level for about four seconds while initiating the chip feeding.

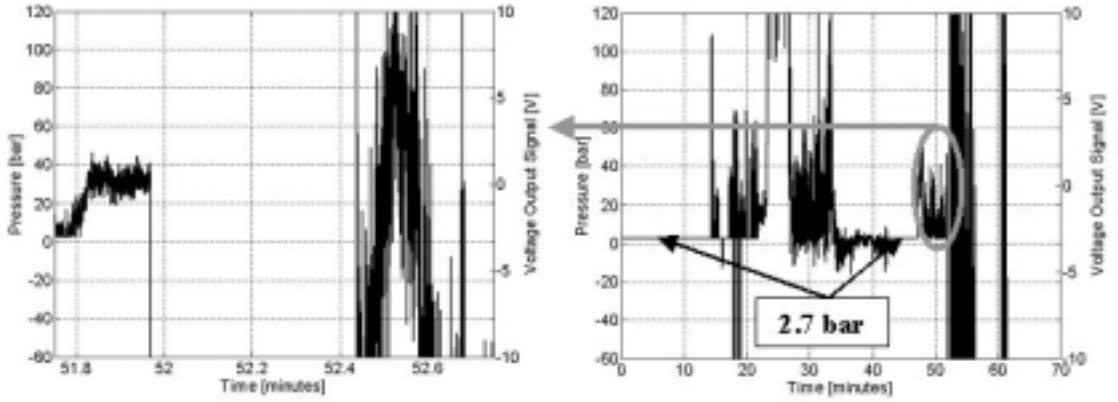

Figure 4.3: The pressure output signal from sensor No. 3, recorded by the low-speed DAQ-board, while initiating the chip feeding (left-hand plot) and over long periods before and after this event (right-hand plot).

The strange and noisy signal pattern recorded by the low-speed DAQ-system showing large fluctuations and saturated readings occurred probably as a result of improper earthing. Furthermore, the connection between the different data acquisition systems probably affected the recordings made by the high-speed DAQ-card as well. It is clearly evident that the high-speed data readings shown in the right-hand plot of Figure 4.1 have great similarities with the readings shown in the left-hand plot in Figure 4.3. Because of this negative influence, there is obviously reason to question the validity of the readings. The low-level pressure readings (2.7 bar) that appeared meaningful, at first glance, can also be questioned. This is because the low-speed recording showed 2.7 bar already before the refiner was pressurized as displayed in the beginning of the right-hand plot in Figure 4.3.

However, the FFT-analysis of the time series recorded by the high-speed data acquisition card during a short time period just after the initiating the chip feeding, between 4 and 12 seconds of the left-hand plot shown in Figure 4.1, reveals interesting peak frequencies. These amplitude spectra with normalized amplitude values are shown in Figure 4.4. The left-hand plot shows a single spectrum based on 2^{19} samples, while the right-hand plot is an averaging spectrum based on the average of 40 subsequent time series containing 2^{14} samples each.

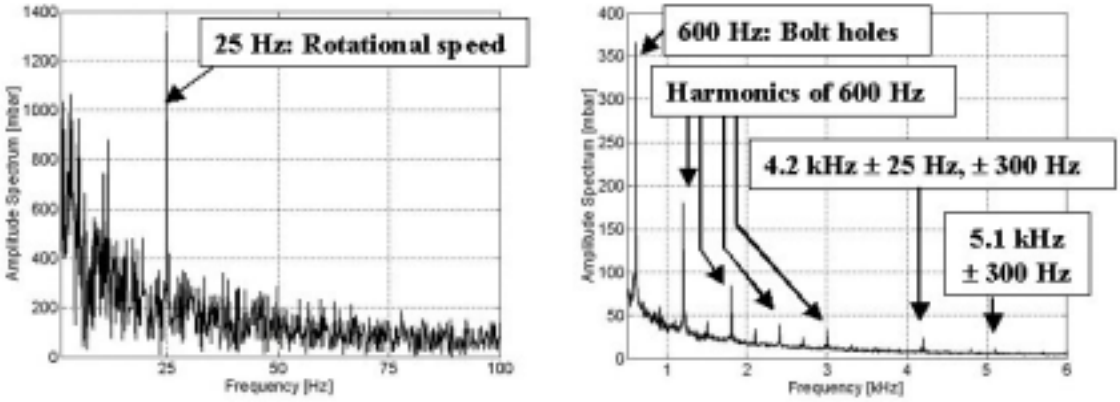

Figure 4.4: The normalized amplitude spectra from sensor No. 3 based on readings between 4 and 12 seconds of the recording shown in the left-hand plot in Figure 4.1.

Several of the frequencies shown in Figure 4.4 may be related to the process. The peak frequency at 25 Hz, not shown here, which had a amplitude ratio of 17 dB, is given by the refiner's rotational speed as one revolution of the rotor disc. The 600 Hz (14 dB) can be associated with the number of holes for assembling the plates to the disc. In addition, the peak frequencies at 3.0 kHz (9 dB) and 5.1 kHz (5 dB) can be respectively related to the number of bars in the outer part of the breaker bar plates and the number of bars in the coarse zone of the rotating plates. Other frequencies shown are harmonic frequencies of the peak at 600 Hz. The peak frequency at 4.2 kHz (10 dB) can also be a harmonic signal of the 600 Hz, but the link (3.6 kHz) between the other harmonics is missing. Furthermore, the 4.2 kHz had additional sideband frequencies that were missing around the other harmonics. These sideband frequencies at 25 and 300 Hz had small amplitudes. However, sideband effects represent typical peak frequencies in measurements and analyses regarding rotating machinery (Wowk (1991), Pettersen and Gunstrøm (1980)). The origin of the 4.2 kHz signal remains unidentified.

The frequencies that are observed, except for the frequency of the rotational speed, can be related to the transmission zone between the breaker bar plates and the bolt holes. The bolt holes were located in the intermediate zone just beside the location of the sensors. A frequency associated with the ribbon feeder has not been observed. It should appear as a peak at 300 Hz if the ribbon feeder had some influence on the pressure measurements. This frequency could be connected to the number of plates as well. The bar-crossing frequency especially related to the number of bars at the radial location of the sensors, which have been identified to be 15.6 kHz, was not visible. A peak frequency at 27.0 kHz related to the bar-to-bar passage in the outer part of the refining zone was not observed. The reason why these bar-crossing frequencies were not found can probably be ascribed to the low hydraulic thrust applied in this period. It was less than 70 bar compared to more than 100 bar under normal operation. Thus it is likely that the plate gap was too wide, making the local bar-to-bar frequency to be invisible. In addition, the clean plates probably affected the flow pattern through the refining zone in such a way that more pulp flowed through the grooves because of the lack of stagnant pulp here.

4.4 Stable operation

4.4.1 Recording shortly after the process was stabilized

Another recording is shown in Figure 4.5. It was captured approximately 15 minutes after the initial chip feeding. The readings of the pressure output signal from the Kulite sensor No. 1 were acquired using the high-speed data acquisition card. A sample rate of 83 kSamples/s was chosen, and the data collecting lasted for approximately 2 minutes. The process was stabilized at the following operation conditions:

- Motor load: 12.5 MW.
- Hydraulic thrust: 100 bar x 2 hydraulic cylinders per stator disc.
- Casing Pressure: 4 bar.
- Production rate: 266 tonnes/day.
- Dilution water flow rate: 2.1 l/s in each refining zone.
- Acceleration DS: 3 %.
- Acceleration FS: 4 %.
- Refining zone temperatures: NA.

The output signal as shown in the left-hand plot in Figure 4.5 had a slow level shift, which is remarkable. The pressure readings reveal that the pressure reached the upper saturation point of the amplifier unit (+10 Volt) at a pressure of 74 bar gauge pressure, which was much higher than expected. Therefore, it is appropriately to question the validity of the acquired data and especially this level change. The absolute lowest pressure was obtained to be 0.7 bar. No saturation effect was observed in this region. The average pressure in the first 90 seconds was 11.5 bar (± 5.5 bar), while it increased to 52 bar (± 11 bar) in the last 20 seconds of the recording.

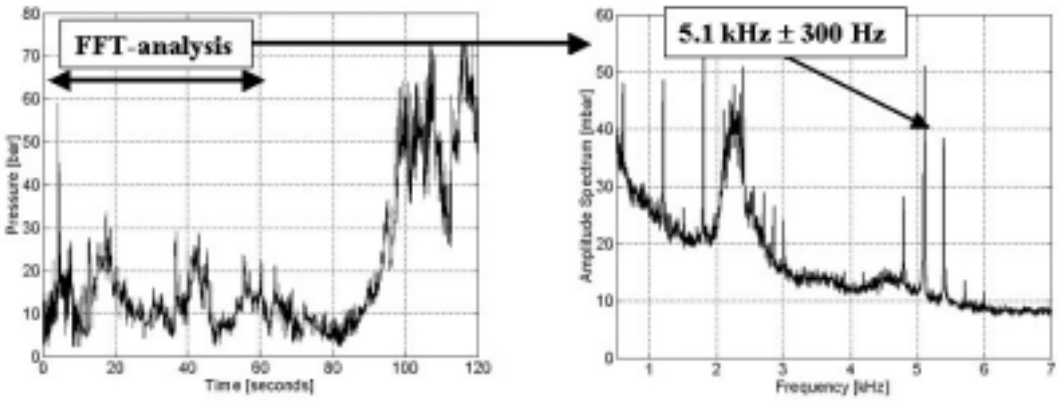

Figure 4.5: The pressure output signal from sensor No. 1 recorded by the high-speed DAQ-card, approximately 15 minutes after the initial chip feeding. The time series is shown in the left-hand plot, while the power spectrum is shown in the right-hand plot.

The amplitude spectrum, as shown in the right-hand plot of Figure 4.5, which is based on the data set of the first 5 MSamples (60 seconds), is an averaged spectrum of 305 subsequent periods of 2^{14} samples. It clearly shows the peak frequency at 5.1 kHz (15 dB) with additional sideband frequencies at ∂ 300 Hz. This peak frequency has been related to the coarse bar zone indicating that the refining action in this zone affected the measurements. However, the peak amplitude was not very high. The figure of the normalized amplitude is approximately 50 mbar. The presence of the peak frequency at 25 Hz was strongly reduced compared with the recording during the initial chip feeding. The latter can be explained through the time of operation and the running conditions. The running conditions reached were more typical of the level which the refiner was designed for. This stabilized the process and reduced the apparently out-of-tram misalignment, which can be reflected in periodical disturbances related to the rotational speed of the refiner (Stationwala and Atack (1980)). The time of operation assured that the refining zone was filled up with pulp, thus the effect related to the bolt holes also might be reduced because the holes were filled with pulp. However, the peak frequency at 600 Hz (3 dB) and its additional harmonics at 1.2 kHz (6 dB) and 1.8 kHz (9 dB) were present as shown as the three peak frequencies to the left in Figure 4.5.

Other interesting frequencies revealed in the amplitude spectrum in Figure 4.5 are the peak frequencies between 2 and 3 kHz. The relatively broad frequency band between 2.1 and 2.4 kHz contained a lot of power. The origin of these frequencies is not completely identified. However, they can be related to harmonics or sideband frequencies. The number of bars in the outer breaker bar zone has been identified to give a periodicity of 3 kHz as shown in Table 3.1. Whether the frequency band between 2.1 and 2.4 kHz is related to this frequency or the harmonics of 600 Hz is not clarified.

4.4.2 Recording during a near plate clash period

The recording shown in Figure 4.6 was captured during a period when a disc-to-disc clash nearly happened. Data were recorded from sensor No. 1 by the high-speed data acquisition card. The displayed time series represents 30 MSamples of the pressure measurements. However, the readings have been low-pass filtered[11] to clearly show the shape of the time series. Thus, it is easier to compare the signal pattern against the progress of the process variables shown in Figure 4.7.

[11] Butterworth filter of order 5 and a cutoff frequency of 200 Hz.

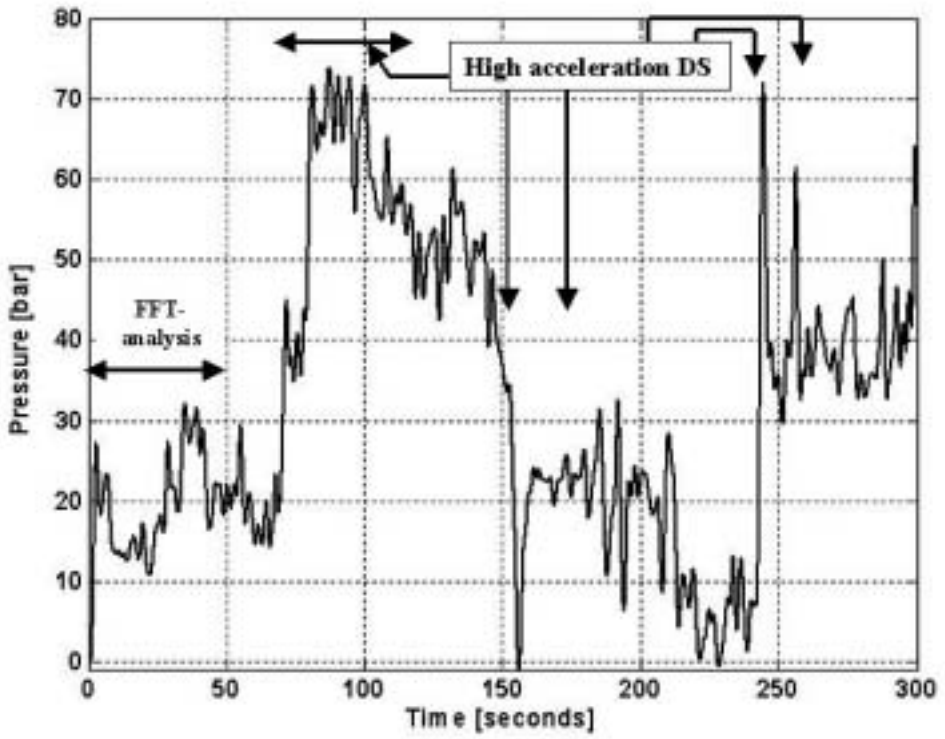

Figure 4.6: **The low-pass filtered pressure output signal from sensor No. 1 recorded before and during a period where the discs almost clashed.**

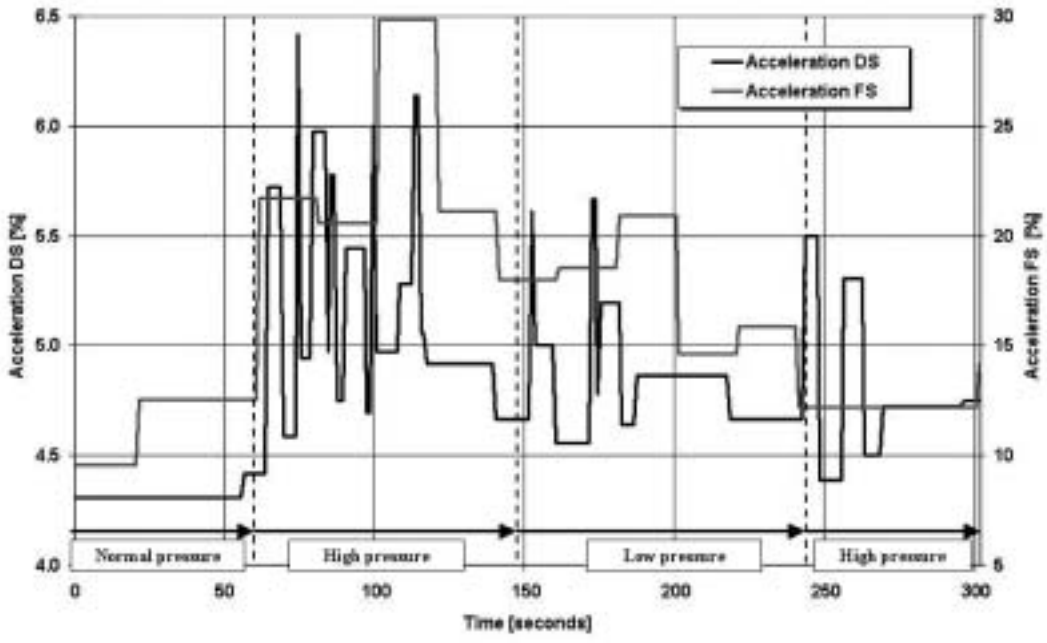

Figure 4.7: **The acceleration variables given by the mill's DCS showed increased values during the same period as the pressure signal fluctuated.**

The acceleration variables as visualized in Figure 4.7 show high values, which indicate that the discs were moving towards each other. Since both measurements show increased values in the same period it was apparently the lack of pulp that created empty spaces between the stators and rotor discs. Thus there were fewer fibres in the bar intersecting area that could counteract the hydraulic thrust applied. The pressure measurements (Figure 4.6) showed that the pressure increased rapidly from a relative stable pressure level at 20 bar (∂ 8 bar), which was the average value in the first 60 seconds of the recording. This pressure increase occurred at the same time as the acceleration values increased as shown in Figure 4.7. A step drop followed the high pressures before the pressure was stabilized for a period. A new drop followed before the readings were stabilized at a high level towards the end of the recording.

Figures 4.6 and 4.7 are interesting diagrams since they indicate that a common cause, probably lack of chips fed in, affected both the process data as well as the pressure readings. However, the validity of the pressure measurements may be questioned. The pressure readings were very high in some periods so that they reached the amplifier's saturation level. After approximately 150 seconds duration when the pressure shifted towards zero gauge pressure the readings reached the low-level saturation. It might be questioned if these measurements were showing proper pressures, or if the data acquisition was affected by some unidentified or DAQ-interconnection disturbances. Lack of synchronized data capturing between the high-speed pressure measurements and the mill's DCS make the uncertainty greater. However, the coincidence with the process measurements was there and was logged manually during the recording.

The validity of the rapid pressure measurements was also reinforced through the FFT-analysis made on the data readings from the first part (60 seconds) of the recording. This is shown in the two plots in Figure 4.8.

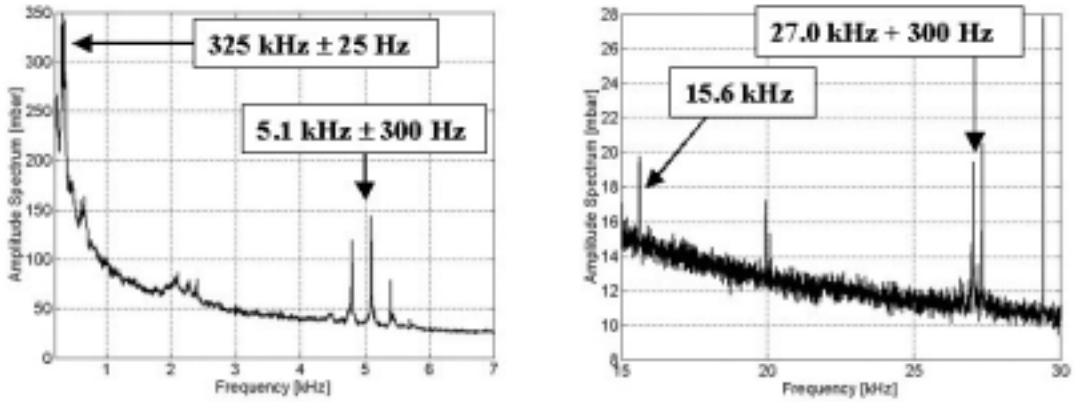

Figure 4.8: Two amplitude spectra obtained from the recording of sensor No. 1, as shown in Figure 4.6, in a relative stable period just before a nearly plate clash period.

The peak frequencies at 5.1 kHz (14 dB) and 300 Hz (6 dB), as shown in the left-hand plot in Figure 4.8, indicate that periodic effects appeared from the process have affected the measurements. The sideband frequencies shown as 25 and 300 Hz on both sides of

the respective peak frequencies at 300 Hz and 5.1 kHz reinforce the assumption about the process influence of the pressure measurements. This is further confirmed through the additional peak frequencies shown in the right-hand plot of Figure 4.8. Here the bar-crossing frequencies arisen from the intermediate and fine bar zones are present. The bar-to-bar passage in the intermediate zone was represented by the peak frequency at 15.6 kHz (3 dB). A 600 Hz sideband frequency at 15.0 kHz (3 dB) was also observed. The latter probably appeared due to the bolt holes located in this zone. In the fine bar zone the bar-crossing frequency at 27.0 kHz (5 dB) was found. In addition, a sideband frequency at 27.3 kHz (6 dB) was present. Additional frequencies were clearly visible as two peak frequencies close to 20 kHz as well as one peak frequency at 29.4 kHz. These frequencies are not identified. Furthermore, the frequency related to the rotational speed (25 Hz) was present (6 dB), while the frequency related to the noise generated from the power hum was absent.

4.4.3 Recording of a non-stationary pressure signal

The pressure output signal from sensor No. 1 was recorded during a period, which the refiner was running under relative low and stable conditions, approximately 30 minutes after a short shutdown and a subsequent start-up. This is shown in Figures 4.9 and 4.11. The plot shown in Figure 4.9 is a filtered time series of original 20 MSamples. It is filtered with a low-pass Butterworth filter of order 5 and a cut-off frequency of 200 Hz. Figure 4.11 shows the unfiltered data of the first 5 MSamples and in addition the corresponding amplitude spectrum.

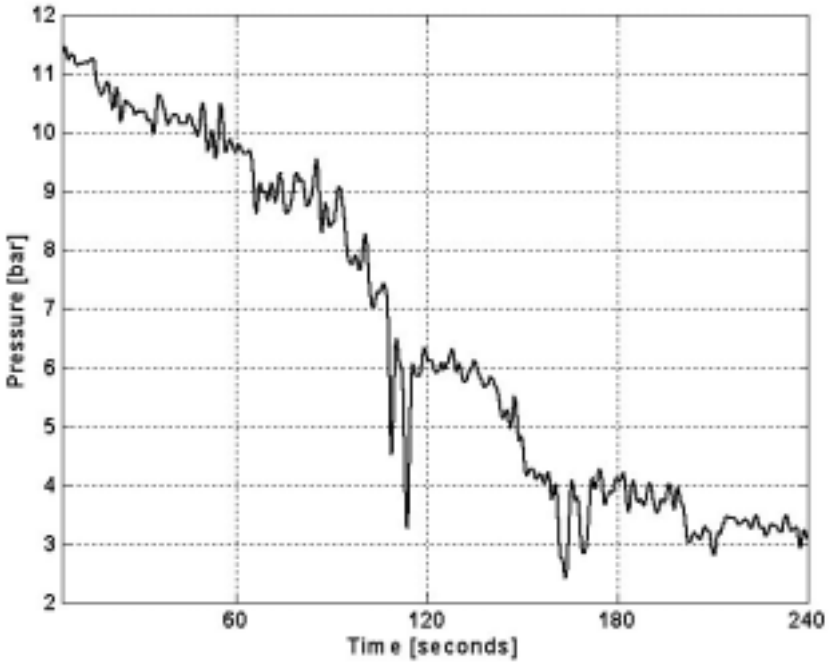

Figure 4.9: The low-pass filtered pressure signal from sensor No. 1 shows clearly the non-stationary behaviour of the recorded signal.

The process was running under the following operation conditions, which were particularly stable, as additionally was confirmed by the low acceleration values:

- Motor load: 12.0 MW.
- Hydraulic thrust: 100 bar x 2 hydraulic cylinders per stator disc.
- Casing Pressure: 4 bar.
- Production rate: 263 tonnes/day.
- Dilution water flow rate: 1.8 l/s in each refining zone.
- Acceleration DS: 2.8 %.
- Acceleration FS: 2.9 %.
- Temperature T2-DS (588 mm): 175.5 ∀C.

The readings were apparently not affected by any large disturbances created by the interconnection of the data acquisition systems. No saturation levels were reached. The recorded pressure values shown in the beginning of the time series in Figure 4.9 could be expected. The pressure level of 10-12 bar was approximately 1-4 bar higher than the saturated water vapour pressure (8.7 bar at 176.3 ∀C). However, the decreasing trend towards a level below the casing pressure of 4 bar was surprising. The refiner was running under relatively low specific energy consumption (1100 kWh/tonne), but anyway, the pressure should not decrease below the casing pressure. It is also known that the refiner is steam-wise short-circuited, and the sensor was located close to the stagnation point as shown in Figure 4.10. Thus higher pressure than the casing pressure would be expected.

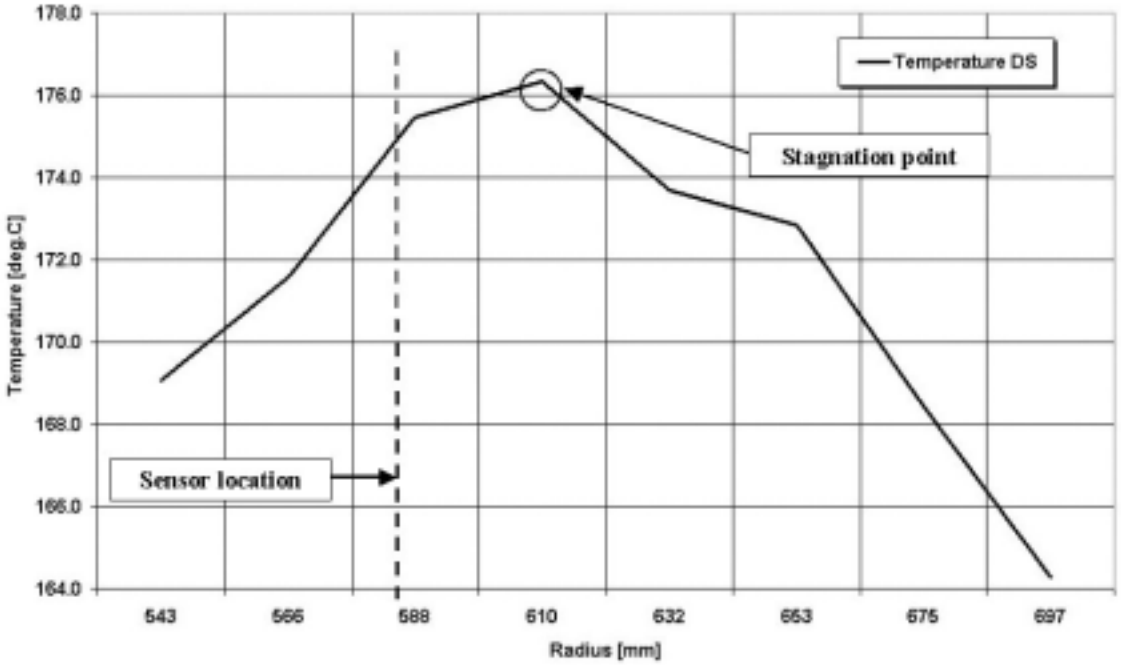

Figure 4.10: Averaged temperatures distributed along the radius recorded by an external measuring system. The average is based on readings from a period of 10 minutes when the pressure measurements shown in Figure 4.9 were made.

The unfiltered data is shown in Figure 4.11. The left-hand plot shows the time series captured in the beginning of the recording. The amplitude spectrum of the corresponding time series is shown in the right-hand plot of Figure 4.11. The latter is built up by the average of 305 subsequent spectra, which each contained 2^{14} samples.

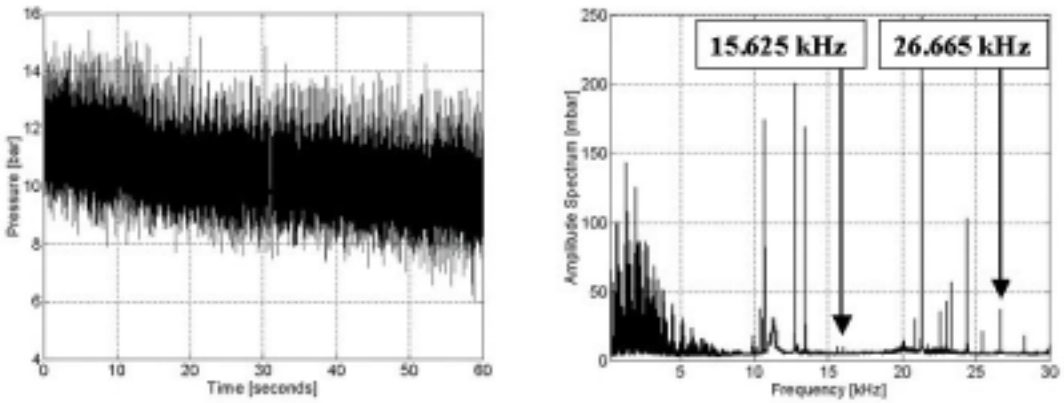

Figure 4.11: The unfiltered pressure readings from sensor No. 1 in the first 60 seconds (left-hand plot) of the recording shown in Figure 4.9 and the averaged spectrum of the corresponding time series (right-hand plot).

The amplitude spectrum reveals that the bar-crossing frequency from the intermediate zone was present. The peak frequency at 15.6 kHz (10 dB) had a small amplitude value of only 9 mbar. The peak frequency at 26.665 kHz (18 dB) might be associated with the bar-to-bar passage of the fine bar zone. However, there are several peak frequencies that are not identified. Among these the following below 30 kHz are: 24.4 kHz (24 dB), 21.34 kHz (32 dB), 13.4 kHz (29 dB), 12.7 kHz (30 dB) and 10.66 kHz (30 dB). In addition and different from the previous recordings, the peak frequencies at 50 and 150 Hz were clearly visible. Both of these can be related to the power hum. It indicates that the noise from the power hum was affecting the recording. Thus several of the additional unidentified peak frequencies might be connected to external noise sources picked up by the DAQ-system.

4.4.4 Noise affected recording

The next recording shown was captured on the second day of the experiment. Figure 4.12 shows that this particular recording was strongly affected by noise. However, in between the noisy readings there were periods containing information about the process.

The process was operated under stable conditions with the following values:

- Motor load: 13.7 MW.
- Hydraulic thrust: 110 bar x 2 hydraulic cylinders per stator disc.
- Casing Pressure: 4 bar.
- Production rate: 263 tonnes/day.

- Dilution water flow rate: 2.15 l/s per refining zone.
- Acceleration DS: 4 %.
- Acceleration FS: 4 %.
- Temperature T2-DS (610 mm): 181 ∀C.

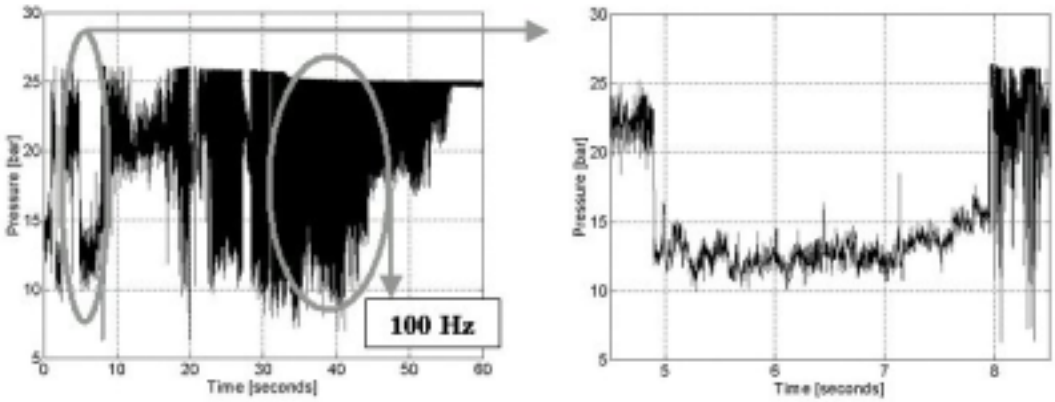

Figure 4.12: Pressure readings from sensor No. 1 as shown as a long and noise affected recording (left-hand plot) and a short period corresponding to the readings between 4.5 and 8.5 seconds (right-hand plot).

Apparently the whole time series was influenced by noise or sensor failure. The major part of the recording was dominated by a 100 Hz signal probably related to the rectifier in the amplifier unit. However, in short periods as shown in the right-hand plot in Figure 4.12, it was possible to find process related information. This was obtained using the peak frequency analysis as described in Section 3.7. The peak frequency analysis calculates the amplitudes of one selected peak frequency in subsequent periods of the recording as shown in Figure 4.13. In this particular investigation the whole time series was divided into 305 subsequent periods, which was analysed one at a time by an FFT-analysis containing 2^{14} samples.

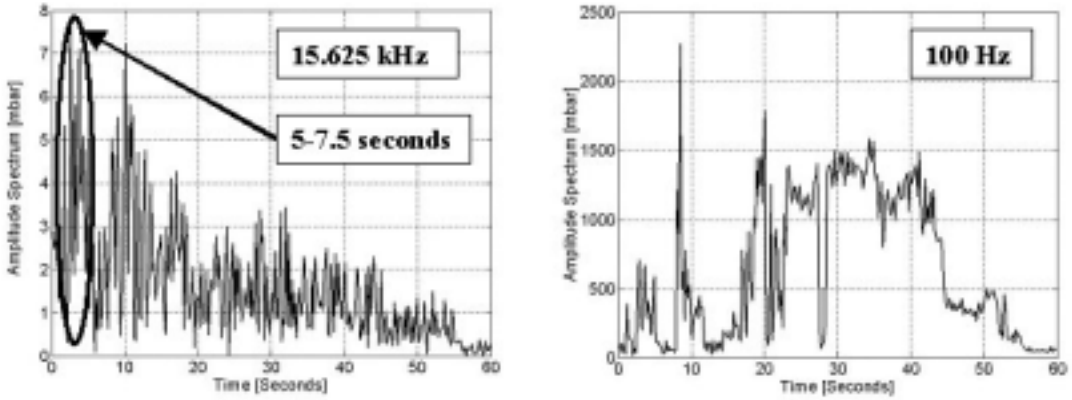

Figure 4.13: The peak frequency analysis shows that 15.625 kHz (left-hand plot) was more present in the first part of the recording compare to the last part. The 100 Hz noise signal was dominating much of the recording especially between 20 and 40 seconds (right-hand plot).

Two normalized amplitude spectra corresponding to the short time series in the right-hand plot in Figure 4.12 are shown in Figure 4.14. They are obtained from averaging of 14 subsequent spectra each containing 2^{14} samples.

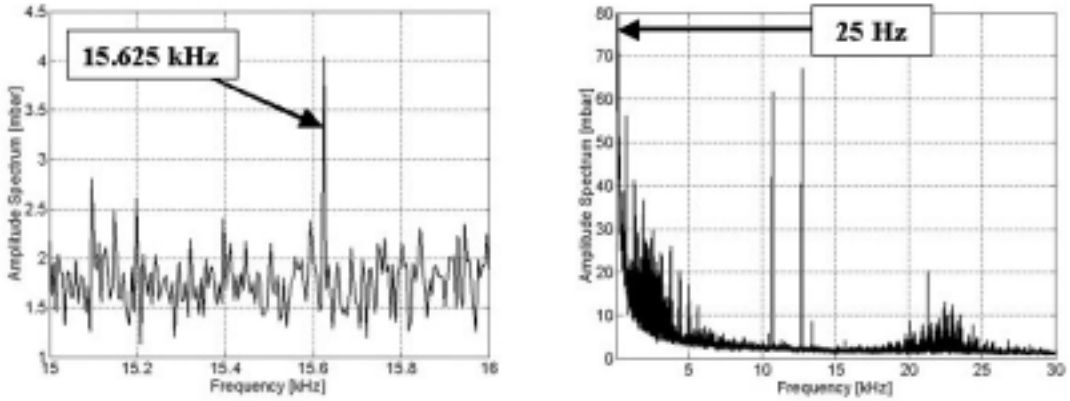

Figure 4.14: In the short time series containing readings between 5 and 7.5 seconds as shown in the right-hand plot in Figure 4.12 the peak frequency at 15.6 kHz was visible (left-hand plot) while the peak frequency at 25 Hz was dominating in the low frequency range (right-hand plot).

The peak frequency at 15.6 kHz (11 dB) was visible, but it was not dominating the spectrum. Also the bar-crossing frequency in the fine bar zone (27.0 kHz) was present with a signal-to-noise ratio of 10 dB. In addition, 25 Hz sideband frequencies were lying at each side of the 27.0 kHz. In the low frequency region the frequency related to the rotational speed was dominating. Compared to the amplitude spectrum in Figure 4.11, the most interesting difference is the relatively broad frequency band between 20 and 25 kHz. Despite the low amplitudes these frequencies jointly represent more power than one single peak frequency. The reason for their origin is not identified. However, because of the broad frequency range it is likely that some effect of random nature was causing their presence. Fibre motion or fibre rolling over the sensor surface may have caused it.

4.4.5 Saturation-like recordings

Some unexpected time series were captured on the third day of data acquisition. Saturation-like signal patterns were observed in recordings of the pressure signal from sensor No. 3. The saturation levels of the amplifier were not reached. Neither it is likely that the process produced these effects, which is shown in Figures 4.15 and 4.16. The process was operated under stable conditions with the following values:

- Motor load: 14.1 MW.
- Hydraulic thrust: 109 bar x 2 hydraulic cylinders per stator disc.
- Casing Pressure: 4 bar.
- Production rate: 263 tonnes/day.
- Dilution water flow rate: 2.15 l/s per refining zone.

∉ Acceleration DS: 5.5 %.
∉ Acceleration FS: 5.5 %.
∉ Temperature T2-DS (610 mm): 181 ∀C.

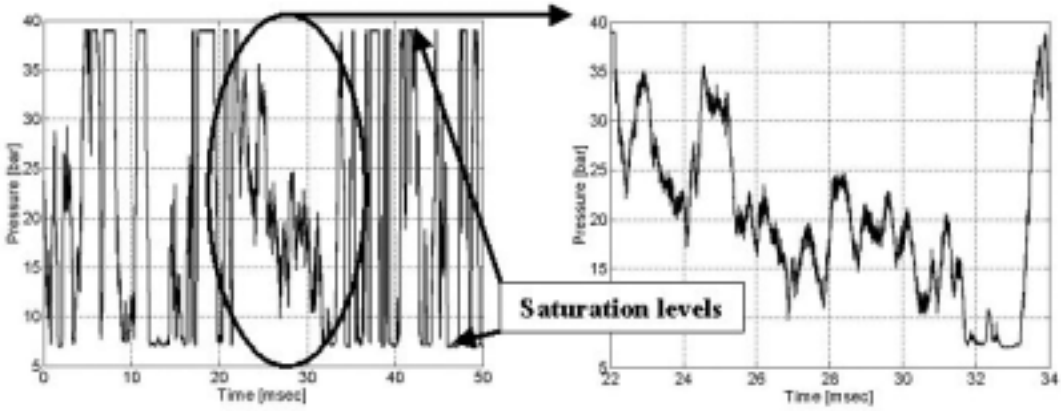

Figure 4.15: The pressure output signal from sensor No. 3 recorded on the third day with a sample rate of 200 kSamples/s. The left-hand plot shows 10 000 samples, while the right-hand plot shows 2 400 samples from the middle part of the left-hand plot.

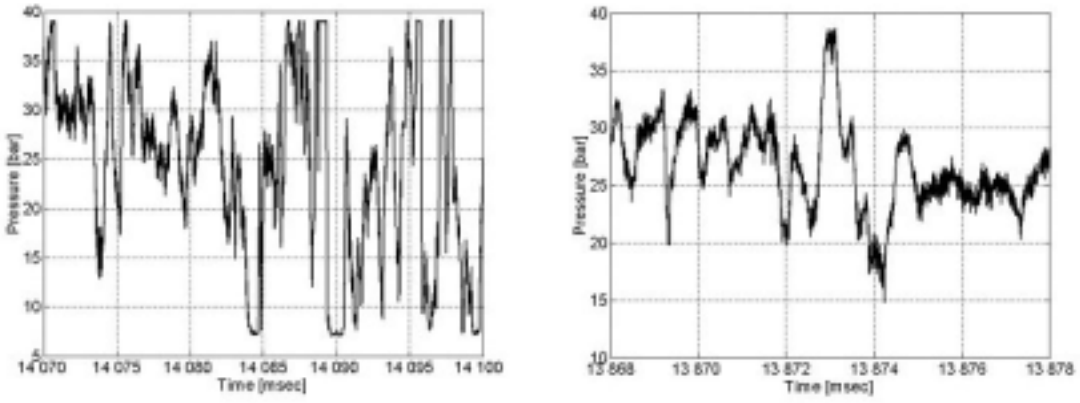

Figure 4.16: The pressure output signal from sensor No. 3 as part of the same recording as shown in Figure 4.15. The left-hand plot shows readings from a period lasting for 30 milliseconds captured after 14 seconds, while the left-hand plot shows readings from a period lasting for 10 milliseconds captured after 13.8 milliseconds.

The recording, partly shown in Figures 4.15 and 4.16, was different from the recordings made on the previous days of the experiment. However, several similar recordings were made on the same day. Both the high-speed data acquisition card used with sampling rates from 83.3 to 200 kSamples/s, and the PC-scope-card using a sample rate of 5 MSamples/s were giving similar results. Furthermore, each recording was made on single DAQ-systems decoupled from each other to prevent interconnected noise.

There are still some questions with respect to the measurements. All measurements lie between two levels at approximately the same values. The low level was lying at approximately 7 bar gauge pressure, which represents a temperature of 175 ∀C assuming saturated water vapour conditions. The absolutely lowest pressure value measured was 3.9 bar. The latter corresponded well with the casing pressure in the refiner. However, only 25 samples had this pressure level. The high-pressure level was approximately 39 bar gauge pressure. The pressure variations related to the saturation-like levels corresponded to only a few bits resolution (4.88 mV/bit corresponded to 48.8 mbar/bit). Calculations have revealed that approximately 15 % of the total number of samples was lying within the pressure range of 38.6 to 39.2 bar (11 bits). A similar proportion of samples were related to the low-pressure region. Approximately 12 % of the readings were lying between 6.9 and 7.1 bar, while only 28 samples showed pressure values below 6.9 bar. However, more than 70 % of the readings fluctuated between these saturation-like levels. The average pressure was measured to be approximately 21 bar with a huge standard deviation value of approximately 12 bar.

Assuming that the pressure readings reflected the real conditions in the refining zone these results are to some extent comparable with the theoretical calculations made in Section 3.4.1. Figure 3.14 shows that a steam pressure corresponding to 6 bar gauge pressure leads to a mechanical arisen pressure of approximately 40 bar when the fibre coverage ratio is assumed to be 50 %. The corresponding average pressure was calculated to be approximately 15 bar. However, it was not expected such apparently saturation-like pressure levels, especially at the high-pressure side. This may be due to the particle sizes, which is expected to vary to some extent and therefore giving larger variation of the peak pressures. If the saturation-like pressure level was trustworthy then the measurements appeared to be weakly affected by the different particle sizes. Or taking the contrary approach, it could be indicated that the particles moving over the bars were not very heterogeneous.

Based on the readings that were collected this day, it is reasonable to believe that some saturation effects influenced the measurements. But what types of effects would cause such saturation levels? The process itself as discussed, might have been the source, or the instrumentation including the transducer might have caused it. The influence by the instrumentation was reduced since the data acquisition systems were decoupled from each other. However, there is some uncertainty related to the amplifier unit, which was located close to the refiner (approximately 5 metres from the refiner motor) and approximately 25 metres from the DAQ-cards. Some noise from the power hum was picked up as shown in Figure 4.17. Both 50 Hz disturbances as well as high-frequency noise appearing as peak frequencies at 70.6 (35.3) kHz and 72.6 kHz were recorded. The origin of the latter frequencies is discussed in Section 6.3.5. Furthermore, it cannot be excluded that additional effects, which remain unidentified, have arisen from the amplifier unit. The sensors should not be considered capable of measuring the real conditions perfectly. It should be remembered that the environment inside a refiner is harsh with a large amount of steam. The wet environment could have affected the electrical circuits in the sensors.

Another important issue was the assembly of the sensors. Sensor No. 3, whose readings have been discussed in this section, was located almost flush to the surface of one bar. Furthermore, it was attached to the stator plate using Epoxy. When the plates were removed from the refiner after approximately 10 weeks, this transducer had been moved approximately 10 millimetres backwards. When this happened or if this movement occurred instantaneously or continuously has not been possible to find out. Apparently the high-pressure pulses applied, in addition to a gradual weakness of the Epoxy were probably the reasons for the movement of the transducer. One of the sensors located in the cavities had been moved approximately 3 mm, while the others had not been moved. Assuming that the movement did not take place immediately after start-up or during the experimental period, it is remarkable that the recordings from the first two days differed that much compare to the presently discussed recording. Assuming that the sensor's movement took place between day two and day three of the experimental period this might have been the cause for the saturation-like recordings. However, it is uncertain what effect the movement of the sensor had on the measurements, and no effort has been made to test it. It would be expected that the cavity over the sensor surface would be filled by fibrous material and thus damping the largest pressure peaks, but if this led to any saturation effects on the measurements is not known. Taking Helmholtz resonator theory (Morse and Ingard (1986)) into account, damping of the pressure wave frequency could be expected when the length of the cavity was increased. Thus the amplitude of the measured pressure could also decrease. Further discussion about theoretical restrictions concerning sound wave propagation is assumed to be out of the scope of this study.

The corresponding amplitude spectra, Figure 4.17, show the expected peak frequencies, which can be related to the process.

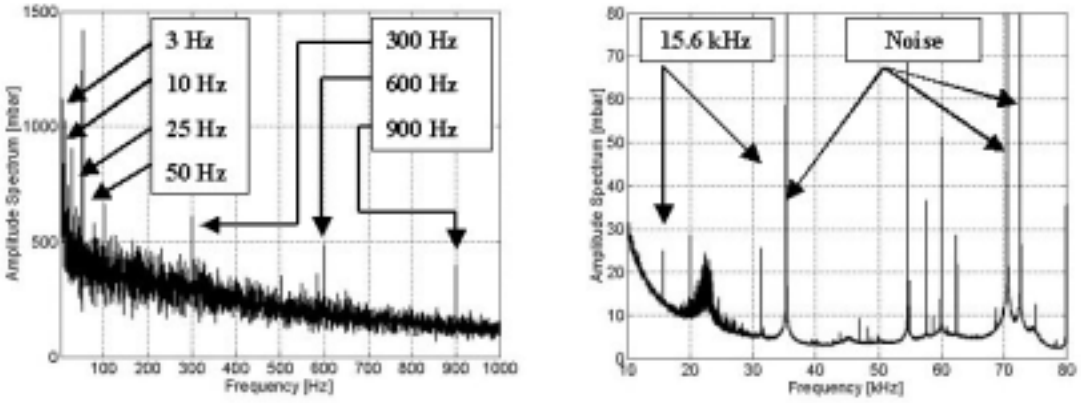

Figure 4.17: Two amplitude spectra of the pressure output signal from sensor No. 3 based on one recording containing 5 MSamples. Parts of the corresponding time series are shown in Figures 4.15 and 4.16.

The right-hand plot in Figure 4.17 shows that the peak frequencies related to the bar-crossings both in the intermediate zone (15.6 kHz (9 dB)) and the fine bar zone (27.0 kHz (4 dB) ∂ 25 Hz) were visible. In addition, the harmonic of the peak

frequencies at 15.6 kHz (31.23 kHz (16 dB)) and 27.0 kHz (54.65 kHz (16 dB)) was even clearer than the fundamental frequencies. Other process related peak frequencies were found in the low-frequency region as 25, 300, 600 and 900 Hz as shown in the left-hand plot in Figure 4.17. In addition, the bar crossing frequency associated with the coarse zone (5.1 kHz (5 dB) ∂ 600 Hz) was present in the frequency analysis of this time series.

Frequencies that previously have been identified as noise, appearing at 35.3 (28 dB), 70.6 (36 dB) and 72.6 kHz (32 dB) respectively, were observed in this recording as well, as shown in Figure 4.17. Other unidentified peak frequencies were observed too. However, they were also common with previous observations as discussed regarding Figure 4.11. It is clear that some of these were harmonic frequencies. Hence, some of the frequencies definitely had common source. The frequency band between approximately 20 and 24 kHz, which was observed in previous recordings as shown in Figure 4.14, was clearly visible in this recording too.

Another consideration about the recording shown in this section was that the level shift between the saturation-like levels sometimes happened very fast. This is shown in Figure 4.18. A change between the low and high levels and vice versa occurred in less than 100 microseconds, which was close to the time of the bar-to-bar passage at 64 microseconds. If the recordings reflected the process conditions, it indicates that such a sudden level shift can be related to the time of one bar-to-bar passage. It can be interpreted that when one rotor bar was opposite of the sensor surface there was pulp in between, and during the time until the next bar was opposite the sensor surface the pulp was removed. In the first situation the sensor would measure a high pressure, while in the next situation the measured pressure would correspond to the steam pressure. A similar assumption was made in the theoretical considerations in Section 3.4. However, then the pressure change would appear even faster and the bar-crossing frequency would dominate. The latter is not observed in this experiment.

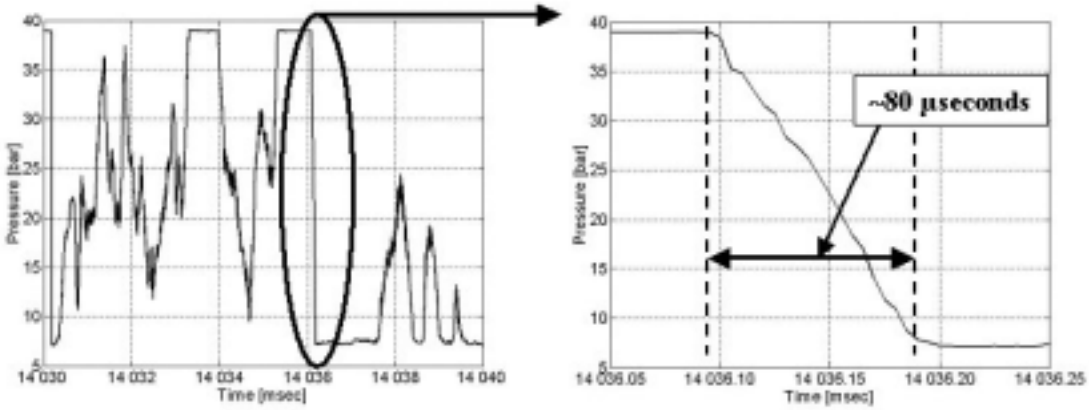

Figure 4.18: The pressure output signal from sensor No. 3 as a part of the same recording as shown in Figure 4.15. The left-hand plot shows readings from a period lasting for 10 milliseconds, while the right-hand plot shows readings from 0.2 milliseconds as a part of the left-hand plot.

4.5 Step-response tests

On the second day of data recording, a few step-response tests were performed. In the following sections the results from these tests are briefly discussed.

4.5.1 Hydraulic thrust and dilution water flow tests

Three subsequent recordings were undertaken when changing the hydraulic thrust and the dilution water flow rate. Each of the three Kulite sensors recorded separately one set of process changes. The first test was performed in such a way that the differential hydraulic pressure applied on the hydraulic cylinders was decreased from 111 to 109 bar during a few seconds. Approximately two minutes later the dilution water flow rate in each refining zone was increased by 0.1 litres per second. The recording was made using sensor No. 1 as shown in the left-hand plot of Figure 4.19. The right-hand plot reveals the averaging amplitude spectrum based on 305 subsequent spectra containing 2^{14} samples each. Hence the amplitude spectrum represents only the first 60 seconds of the recorded time series. The pertinent process variables are displayed in Figure 4.20.

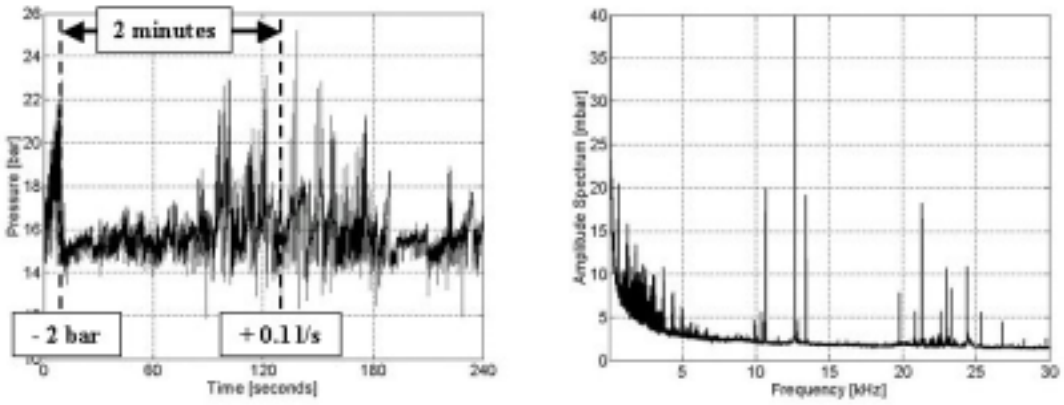

Figure 4.19: The first step-response test was recorded by sensor No. 1 (left-hand plot). The amplitude spectrum representing the first 60 seconds of the time series is shown in the right-hand plot.

At first glance the steep decrease in the hydraulic thrust (Figure 4.20) might have affected the pressure measurements as shown in Figure 4.19. However, the pressure drop was not a level change, but more a pressure peak lasting for some few seconds. The initial readings from the pressure sensor were approximately at the same level as after the hydraulic thrust alteration. Furthermore, there were some uncertainty related to the synchronizing of the pressure readings and the readings from the process. Lack of automatic synchronizing routines between the process database and the pressure measurements made the on-site communication between the process operator and the manual written time-stamp log the only form of control.

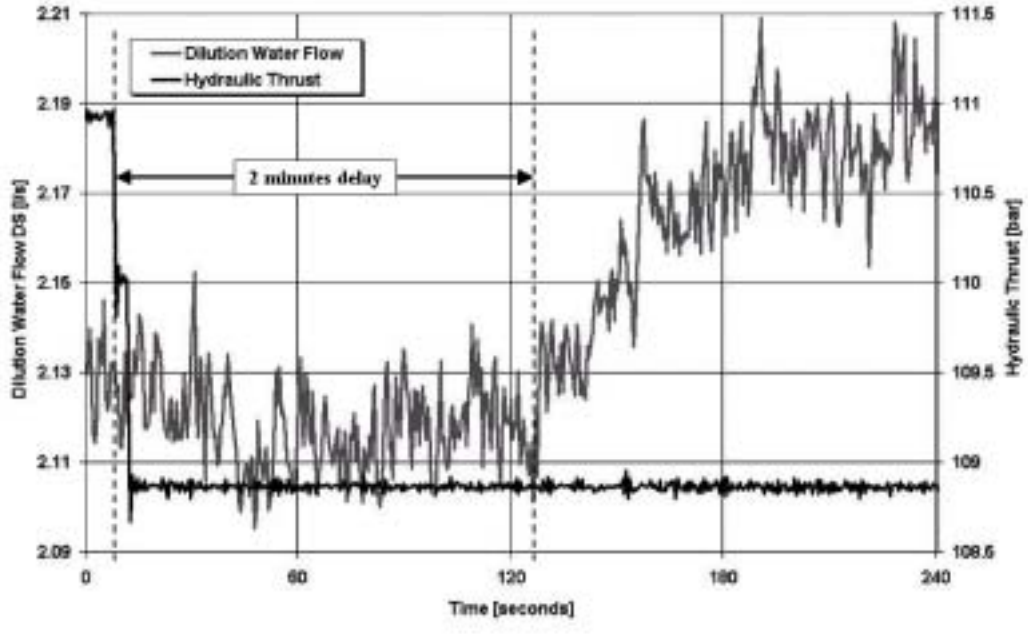

Figure 4.20: The first step-response test comprised a decrease in the hydraulic thrust as well as an increase in the dilution water flow rate. The latter was performed after a delay lasting for two minutes.

The following change in the dilution water flow, shown after 120 seconds in Figure 4.20, coincided with a period showing high-pressure readings as shown in Figure 4.19. However, there is no strong evidence that indicates any good correlation between the pressure readings and the process changes. It could signify that the measurements were not trustworthy, or that there was no substantial correlation between the pressure measurements and the current process variables. The latter would be correct also if the process changes that were made were too small to give any influence on the pressure measurements.

The next two step-response tests comprised similar process changes. The two other sensors recorded these tests as shown in Figures 4.21 and 4.22. However, these recordings did not reveal any better relationship between the pressure measurements and the process variables

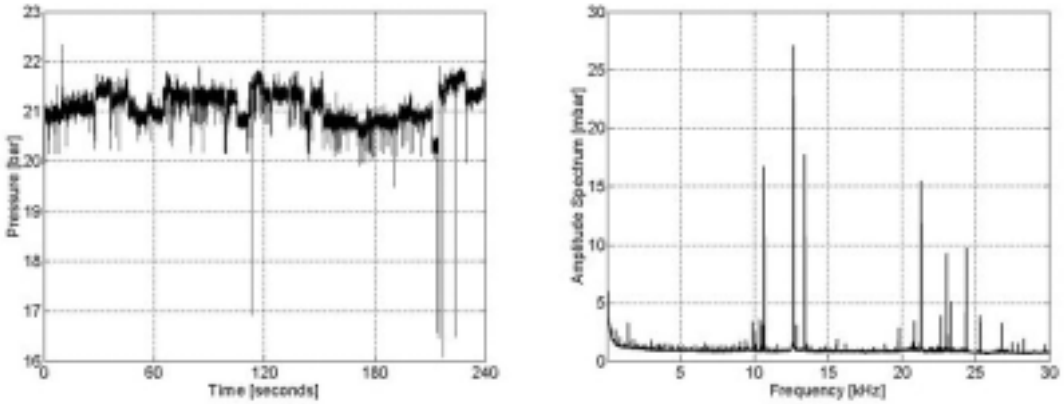

Figure 4.21: The second step-response test was recorded by sensor No. 2 (left-hand plot). The amplitude spectrum representing the first 60 seconds of the time series is shown in the right-hand plot.

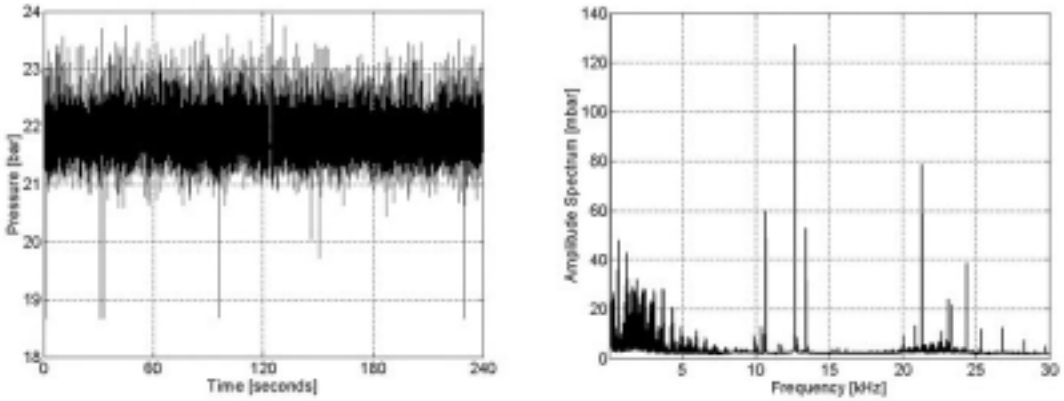

Figure 4.22: The third step-response test was recorded by sensor No. 3 (left-hand plot). The amplitude spectrum representing the first 60 seconds of the time series is shown in the right-hand plot.

4.5.2 Plug screw speed test

The last step-response test was performed in such a way that the plug screw speed was decreased from 64 to 62 %. This change corresponded with a change in production rate from approximately 262 to 254 tonnes/day. The reverse action was performed after a time delay of approximately two minutes. The recording was made using sensor No. 1 as shown in the left-hand plot of Figure 4.23. The right-hand plot shows the averaged amplitude spectrum. In addition, Figure 4.24 shows the plug screw speed and the simultaneously recorded motor load during the same period.

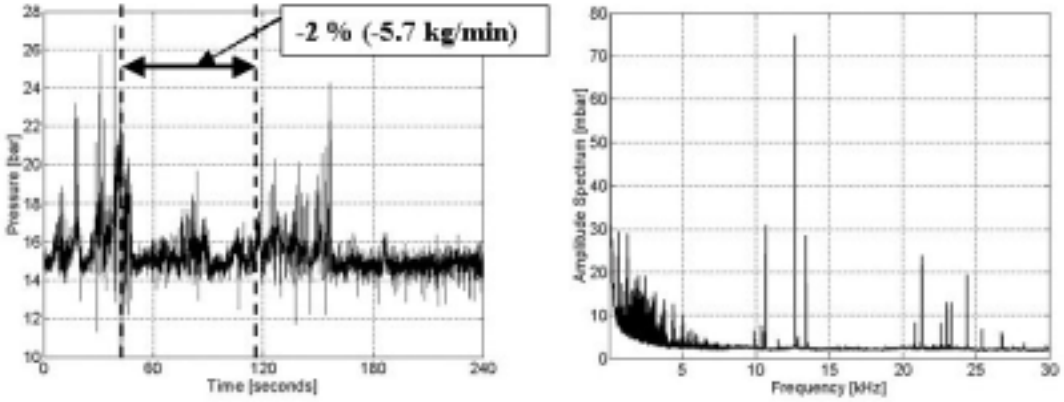

Figure 4.23: The last step-response test was recorded by sensor No. 1 (left-hand plot). The amplitude spectrum representing the first 60 seconds of the time series is shown in the right-hand plot.

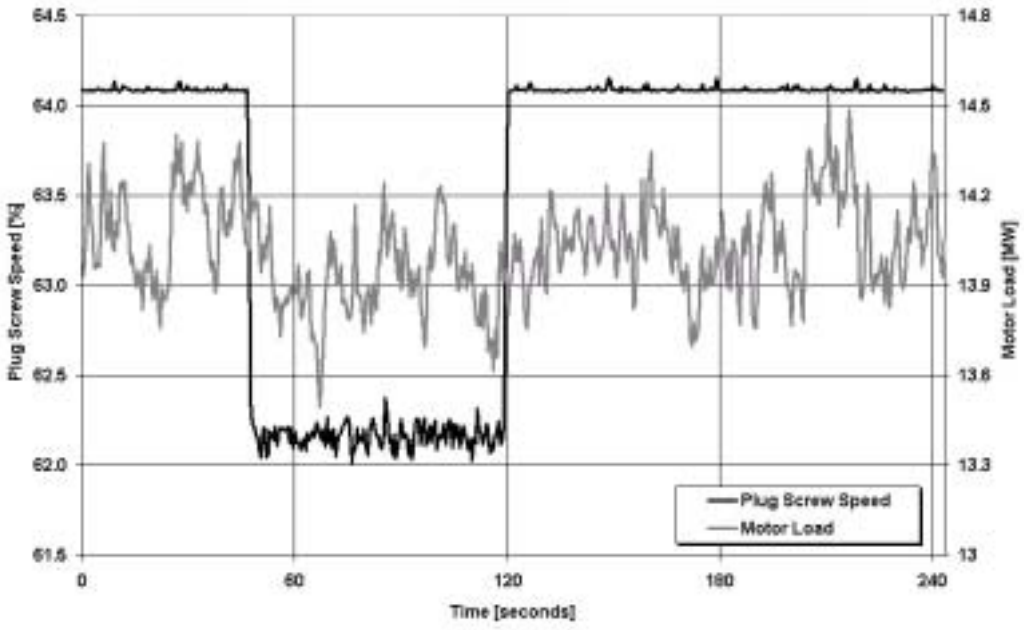

Figure 4.24: The last step-response test comprised both a decrease and an increase in the plug screw speed. In addition to the plug screw speed, the corresponding readings from the motor load are shown.

The pressure recording (Figure 4.23) undertaken during this test did not clarify the relationship between the pressure measurements and the plug screw speed. The only indication revealed from this measurement was that the pressure appeared to be more stable. It showed smaller variation in the same period as the plug screw was running at a lower speed. However, the low variation level was obtained towards the end of the recording when the plug screw speed was operating at a high level again. Thus, there is no strong evidence for a clear relationship between the pressure measurements and the

process variables. Why this was so, can be related to a few main conditions. The first is related to the uncertainty corresponding to the pressure measurements and the second is that the expected relationship is not present. A third choice is related to the process changes that might have been too small to give any clear effect on the pressure readings.

4.6 General discussion

The mill-scale experiment gave a large number of measurements. Some of the results were unexpected by being affected by high-pressure values, undefined disturbance sources, and the saturation like behaviour. However, all recorded files consisted of peak frequencies, which can be related to the process. It is unlikely that the peak frequencies are created randomly. Therefore, the results from this experiment are still interesting. It can be assumed that the pressure sensors have responded on the forces acting on the diaphragm. However, it is not evident that the calibrations of the sensors were trustworthy. Thus the measured pressure levels can be questioned.

There are many unclear experimental readings. Some of the disturbances, which appeared in some time series, have still undefined sources. The electromagnetic radiation from the powerful refiner motor, which was located only a couple of metres from the amplifier unit, was one of the potential sources for the noise. The 20-25 metres long signal cables might have received such noise as well as the open 15-pin D-sub connectors at the transducers' cable ends. The connectors should have been handled differently having proper shields. The measurement set-ups were not checked sufficiently considering the sources of error in connection with potential ground loops. The absence or incorrect use of a referencing signal to the earth when using the low-speed data acquisition boards might have caused undesirable effects as well. In accordance to Shah (2000) bias resistors must be provided when measuring floating signal sources in differential and single-ended no-referenced configurations. Failure to do so will result in erratic or saturated readings i.e. positive full-scale or negative full-scale readings. In some cases, the use of two input signals to the high-speed data acquisition card, which should be used as a single-ended analog input board, have probably caused undesirable effects. Fortunately, this data acquisition board was mainly used for one input signal, or with a probably non-working transducer in the other position. Thus the failures from this source were reduced considerably.

From the recorded and analysed data there appear to be especially two transducers, which have yielded signals of particular interest. The sensors labelled as No. 1 and 3 have shown interesting signal variations. Sensor No. 1 was mounted subsurface in a cavity in a bar, while sensor No. 3 was located flush to the surface in one bar. The locations might have affected the output signals, but the investigations have not revealed any conclusions of that. However, recordings from both of these transducers have given peak frequencies, which coincided with current process frequencies. The calculated pressure levels were sometimes higher than expected. Some time series show pressure levels exceeding 70 bar. Related to the theoretical estimates such pressure levels correspond to a low fibre coverage ratio. However, the majority of the recorded pressures shown in this chapter lay between 15 and 30 bar, which correspond fairly well with the theoretical approaches made in Section 3.4.

The atmospheric pressure signal from sensor No. 2 had already from the start a dubious and not trustworthy value. Mainly, the signal from this transducer gave little useful information. The Presens transducer seemed to work reasonably early in the warm-up phase. It is likely to assume that this transducer broke down because of too wet environment on the back of the plates. The connection points of the signal cables to the strain elements were only covered with non-conducting epoxy.

A possible reason for the unexpected output signals and the failures, even for the transducers that seemed to give interesting information, has been the wet environment surrounding the transducers. High-pressure steam might have penetrated behind the plates. Since the transducers were not hermetically sealed, this might have affected the operation of the transducers. After some time in the wet environment, it can be suspected that steam or water might have entered the transducer units along the cable ends thus ruining the calibration. The penetrated water or steam could have caused a resistive coupling, which in turn could have affected the bridge resistance and given failure. Whether this actually happened during the experimental period is not clear. Some of the transducers that were tested in the preparatory work broke down probably because of exposure to water and steam. Resistance measurements undertaken on the transducers after 10 weeks inside the refiner, after removing the plates, showed that all the transducers had broken down.

From the literature it is known that moisture affects the operation of piezoresistive transducers (Nakladal and Sager (1993), Sager *et al.* (1995), Gerlach *et al.* (1996)). According to Sager *et al.* (1995) the influence of humidity and moisture on the sensor behaviour cannot be neglected. They claimed that forming of condensed water on the sensor surface causes large changes in the sensor offset-voltage up to the nominal output voltage.

4.7 Concluding remarks

The most convincing results from this mill-scale experiment using four piezoresistive transducers were the peak frequencies obtained from the amplitude spectra. Some peak frequencies can be associated with process inherent features. The following recognized frequencies have been found:

- ∉ 25 Hz : Rotational speed of the refiner.
- ∉ 300 Hz : Ribbon feeder or the number of plates in the stator circle.
- ∉ 600 Hz : Bolt holes located close to the radial position of the sensors.
- ∉ 3.0 kHz : The number of bars in the outer part of the breaker bar plates.
- ∉ 5.1 kHz : The number of bars in the coarse zone.
- ∉ 15.6 kHz : The bar-crossing frequency in the intermediate zone.
- ∉ 27.0 kHz : The number of bars in the fine bar zone.
- ∉ Sideband frequencies of ∂ 25, ∂ 300 and ∂ 600 Hz.

It is unlikely that the peak frequencies are created randomly. It can be assumed that the pressure sensors have responded on the forces acting on the diaphragm. However, it is

not evident that the calibrations of the sensors were trustworthy. Lack of consistent recordings related to influence of noise and saturation effects appearing from the amplifier and the interconnection of the DAQ-systems have been observed. The wet environment may have affected the transducers as well. Some uncertainties can be related to the measurements, and especially the measured pressure levels can be questioned. The following results were obtained:

- The majority of the recordings showed average pressure between 15 and 30 bar, which correspond fairly well with the theoretical calculated pressure.
- One recording performed during the initiating chip feeding showed that the pressure increased from 2.7 bar gauge pressure to a level between 30 and 35 bar within four seconds.
- Large fluctuating pressure readings were observed during a nearly plate clash period. High pressures beyond 70 bar were observed as well as pressure readings that decreased below atmospheric.
- One recording was performed under severe influence of noise. Despite that, parts of the recording did give reasonable readings when the influence of noise was limited.
- Saturation-like recordings were observed. The features of these recordings were that the low-pressure level corresponded well with the saturated water vapour pressure, while the high-pressure level was approximately 39 bar. Between 12 and 15 % of the readings were located in each saturation-like region thus giving large pressure variations. The pressure levels were comparable with a theoretical approach assuming a fibre coverage ratio of approximately 50 %.
- Results from the step-response tests involving the hydraulic thrust, the dilution water flow rate and the plug screw speed did not show any good correlation between the pressure measurements and the process variables.

CHAPTER 5

RESULTS AND DISCUSSION PIEZORESISTIVE SENSOR PILOT REFINER

5.1 Introduction

This chapter contains results and discussions about the observations that were made in the pilot-scale experiment using one single combined piezoresistive pressure and temperature transducer. Most of the results are previously reported (Eriksen (2002)). However, here some extensions are made to further discuss the observed data.

The results comprise recordings from the test run, which was designed to take measurements under different operational conditions. The recordings related to the plate gap changes and readings from a period of initial chip feeding are given particular attention. Also recordings from a period when chip-feeding problems occurred are considered to be interesting.

As opposed to the measurements discussed in Chapter 4 the present results did not show any substantial irregularities. Therefore, there is greater confidence in the measured pressure levels in this part of the study compared to the first mill-scale experiment. In addition, the sensor responded as expected after the experiment was finished and the plate was removed from the refiner.

5.2 Pressure readings during normal operating conditions

After the pre-heating, chips were fed to the refiner. The refiner had clean plates without any pulp in the grooves. The responses of the high-frequency pressure and temperature signals during the initial chip feeding are shown in Figure 5.1. It is further displayed in Figure 5.2, which shows the two-second average values over a period of 390 seconds (195 MSamples). The average values of the data that are shown in Figure 5.1 form the data points at 39 seconds in Figure 5.2.

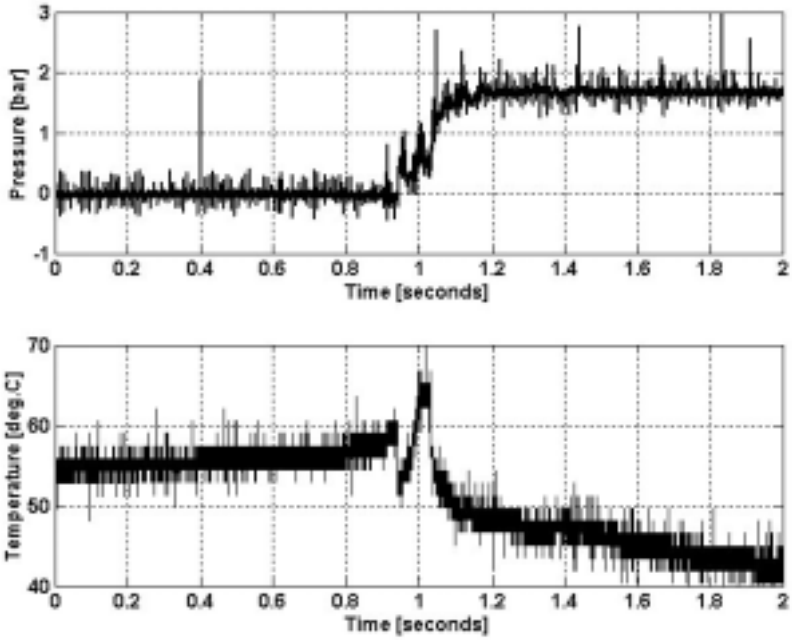

Figure 5.1: Pressure (top) and temperature (bottom) measurements when chips were fed to the refiner. These data were collected with a sample rate of 500 kSamples/s.

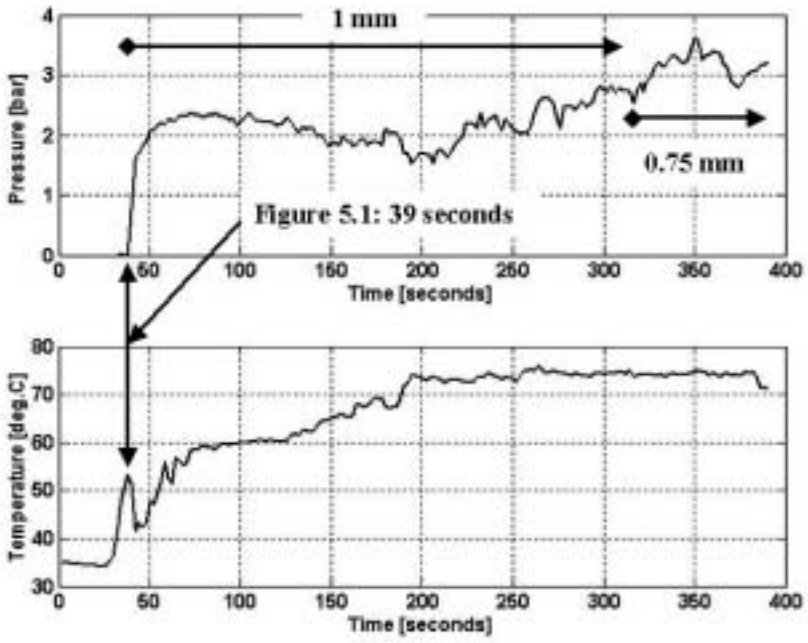

Figure 5.2: Pressure (top) and temperature (bottom) signals, averaged over a two-second window, are shown from a period during unloaded conditions to normal operation of the refiner.

The recording shown in Figures 5.1 and 5.2 started when the refiner was unloaded and continued with the initial chip-feeding phase. However, the majority of the readings were captured during a period when the refiner was operated under stable conditions. The initial plate gap was approximately 1 mm, while the measurement ended in a period with a smaller plate gap at 0.75 mm starting at approximately 320 seconds as shown in Figure 5.2.

Additional statistical information about this recording is shown in Figure 5.3. In this figure the statistically obtained variables represent the maximum, minimum, standard deviation and correlation coefficient. Each of the two-second periods gave one value of each of the statistical variables. Thus each line in Figure 5.3 as well as in Figure 5.2 contains 195 data points.

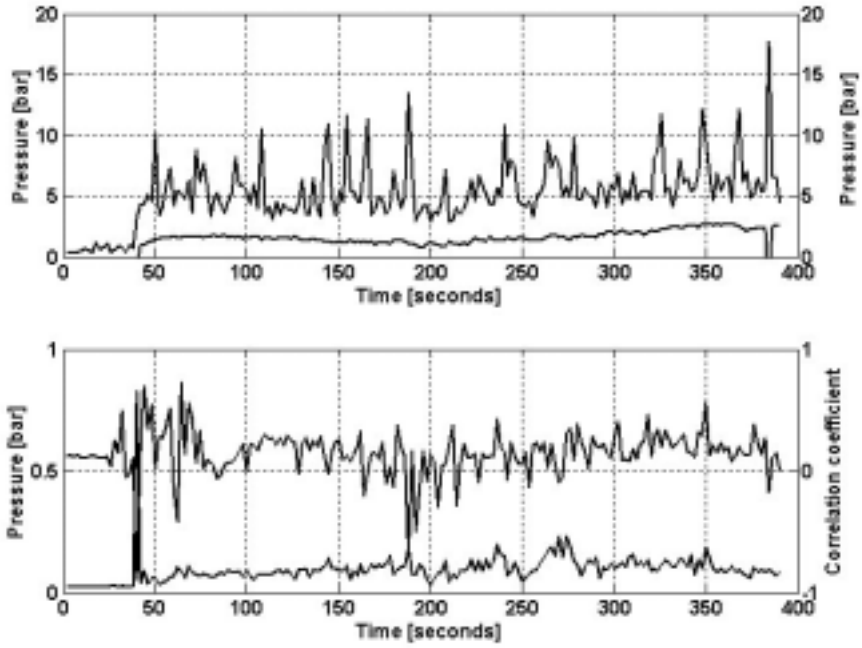

Figure 5.3: The maximum and minimum values of the pressure signals are shown in the top plot. The bottom plot shows the standard deviation of the pressure signals (lower line) and the correlation coefficient between the pressure and temperature signals (upper line).

As shown in Figure 5.1, the rise time from zero bar gauge pressure to approximately 1.7 bar lasted for approximately 0.2 seconds. This level shift has to be related to the filling of the refining zone with pulp. Thus, the time to fill this refiner can be associated with the pressure rise time. Simultaneously with the pressure increase, the temperature rose as well. This was expected. However, the following decrease in temperature was surprising. The reason seems to be related to the cold chips fed with a temperature of approximately 30-40 ∀C. Despite the pre-steaming of the chips, the delay in the chip bin, before the feed screw, cooled the chips. When the chips were forced towards the

surface of the transducer these might have cooled it. The temperature drop only lasted for some seconds as shown in Figure 5.2. Generally, increasing amounts of wood in the refining zone increase the friction and hence the heat in the refining zone implying an increase in temperature as shown in Figure 5.2 between 50 and 200 seconds.

The result from the statistical analysis, as shown in Figure 5.3, shows that intermittent pressure spikes between 5 and 15 bar were visible. However, the pressure readings mainly were very stable with standard deviation values between 0.1 and 0.2 bar. Also the values representing the minimum pressures were higher than atmospheric. These observations indicate that the measured pressure was shifted to a higher average level when the refiner was filled by pulp. It is important to discuss the reason for this observation.

The only study that the present investigation can be compared with is the report by Atack and Stationwala (1975). The pressure level of approximately 2 bar, which was obtained after the refiner was filled up with pulp and operated with approximately 1.0 mm disc clearance, as shown in Figure 5.2, is comparable with the measurements reported by Atack and Stationwala. However, one of the differences between their process and the pilot refiner was that the temperature in their refiner (open discharge refiner, 42 inch, 1492 kW) was higher. They measured temperatures in the order of 130 ∀C, which means that their refiner was self-pressurized. On the other hand, the temperature in the pilot refiner was mainly well below 100 ∀C. Atack and Stationwala assumed that their refiner was operating under saturated steam conditions. A conclusion from their study was that they measured a pressure level, which showed a variation of approximately ∂ 0.3 bar about the value of the saturated steam pressure. A temperature of 130 ∀C corresponds to a pressure value of 1.8 bar under saturated water steam conditions. Atack and Stationwala (1975) claimed that the steam pressure contributed to a large extent (50-70 %) of the reaction thrust on the refiner plates while the remaining 30-50 % was mechanical. Since the contribution to the reaction thrust in an atmospheric refiner probably has larger contribution from the chips and pulp compare to the steam, comparison between these different processes is more intricate.

It was expected that the pressure should vary with a frequency associated with the bar and groove pattern of the rotor plate. High pressure was expected when fibres were squeezed between two opposite bars, and low-pressure readings were expected when a rotor groove was opposite the sensor surface. Since atmospheric pressure was the prevailing condition in the pilot refiner, it could be expected zero bar when the sensor surface was opposite a groove. Assuming a low fibre coverage ratio, the majority of the pressure readings were expected to be zero bar as well as the local bar crossing frequency would be reduced or more or less disappear.

One apparent solution to the observed pressure shift may be found in the steam that is generated and thus have to flow out of the refining zone. Since the temperatures were below 100 ∀C it is not actual to discuss saturated water vapour pressure conditions. However, some contribution from the steam to balance the axial thrust may be expected. This was discussed in Section 3.4 when the theoretical estimated pressures in the refining zone were determined. It was shown in Section 3.4.3 that the contribution from

the steam on the estimated pressure was small. The steam pressure derived from a chosen contribution from steam (50 %) to the axial trust balance could be ignored if the steam was assumed distributed evenly across the refining zone. The steam could have some effect on the measured pressure when assuming that the steam was working only in a small part of the refining zone. In this particular part of the refining zone the low-pressure level would be greater than the atmospheric. This is a hypothesis that can be considered as an explanation of the measured pressure shift when the refiner was loaded.

The relative large size of the pressure transducer, compared to the bar and groove widths, is another approach to the explanation of the observed pressure shift. Its tubular metal housing (3.8 mm) was wider than a bar as shown in Figures 3.20 and 3.24. However, the diaphragm was approximately 2.5 mm, which was of the same size as the bar and groove widths. When a groove was opposite the sensor surface, parts of the tubular metal housing could be affected by pulp squeezed between two adjacent rotor bars. It is not clarified whether pressure applied on the tubular metal housing affected the pressure readings. It cannot be excluded that stresses could be induced into the silicon diaphragm under such conditions. This effect might have generated an apparent pressure. However, the small pressure variations shown in Figure 5.3 would imply that this effect was continuous. Thus a high fibre coverage ratio would be expected.

Another cause that can have created an unbalanced force on the sensor is that pulp in the stator groove has been pressed against the tubular metal housing of the transducer. The transducer was mounted flush to the surface of a dam in the refiner plate with no additional protection against the radial flow in the corresponding groove. It is known from the literature that radial outward flowing pulp in the stator grooves of mill-scale refiners is assumed to have velocities up to more than 30 m/s in the fine bar zone (Alahautala *et al.* (1999), Atack *et al.* (1989)).

This discussion whether a substantial pressure level shift as observed is trustworthy has to include the above mentioned conditions that are related to the pressure sensor's performance and physically size as well as the location. Furthermore, it cannot be excluded that the moisture in the refining zone of the pilot refiner affected the sensor behaviour. No evidence indicated that moisture distorted the readings. Failure associated with steam penetration through the cable end is excluded because the cable end from the sensor housing was forcibly sealed. However, these conditions remain as uncertain factors regarding the presented measurements.

5.2.1 Pressure readings from different operating conditions

Table 5.1 shows the measured pressure for different plate clearances. In addition to the average pressure and the corresponding standard deviation, the average maximum and minimum pressures with the corresponding standard deviation values are shown. The average pressure is derived from a huge number of readings with a sample rate of 500 kSamples/s. The number of data points used to calculate the average maximum and minimum pressures are based on one value for each two-second period.

Table 5.1: Average pressures for different plate gaps.

Plate gap [mm]	Time period [second]	Average Pressure [bar]	Standard deviation [bar]	Average Max. Pressure [bar]	Standard deviation [bar]	Average Min. Pressure [bar]	Standard deviation [bar]
1.00	162	2.0	0.2	5.3	2.2	1.4	0.2
0.75	76	3.2	0.2	7.2	2.8	2.3	1.0
0.50	82	4.5	0.4	8.1	4.4	2.8	0.7

Data from the recording performed when the refiner was operated with the smallest plate clearance (0.25 mm) are not included in this table. This recording contained few readings because during this part of the experiment the operational conditions created abnormal flow phenomena as shown in Section 5.4.

The result from this study shows that the pressure level increased when the plate gap decreased. Also the minimum and maximum pressures were shifted to a higher level. It seems to be reasonable that the pressure was shifted towards a higher value when the axial trust was increased. Hence the mechanical pressure on the fibres increased to counteract the closing force. In addition, the low-pressure readings were substantially higher than zero bar. Assuming that the steam pressure was a contributing part of the measured pressure, this result indicates that the steam pressure was affected by the decreasing plate gap too. Assuming that the pressure readings represented the real pressure conditions in the local part of the refining zone, these results show that the pressure was shifted to a higher level both when the refining zone was filled with pulp and when the plate gap decreased. In addition, the measurements may indicate that the steam pressure contributes to balance the axial thrust in an atmospheric refiner.

5.2.2 Observed periodicities in the pressure signal

The movement of the bars in the rotating disc should give a periodicity of approximately 0.14 milliseconds corresponding to a frequency of 7.15 kHz at the radial location of the sensor. However, the bar crossing frequency was almost absent in the pressure recordings performed during normal operating conditions. Figures 5.4 - 5.7 illustrate this observation.

Figure 5.4 shows a part of one recording performed during refining with a plate gap of approximately 0.5 mm. It gave a relative stable operation at first glance. No indications about irregular operation were made when the experiment was carried out. However, a closer investigation of the data shows that the measurements were partly affected by process instability as shown in Figure 5.4 and particularly in Figure 5.5.

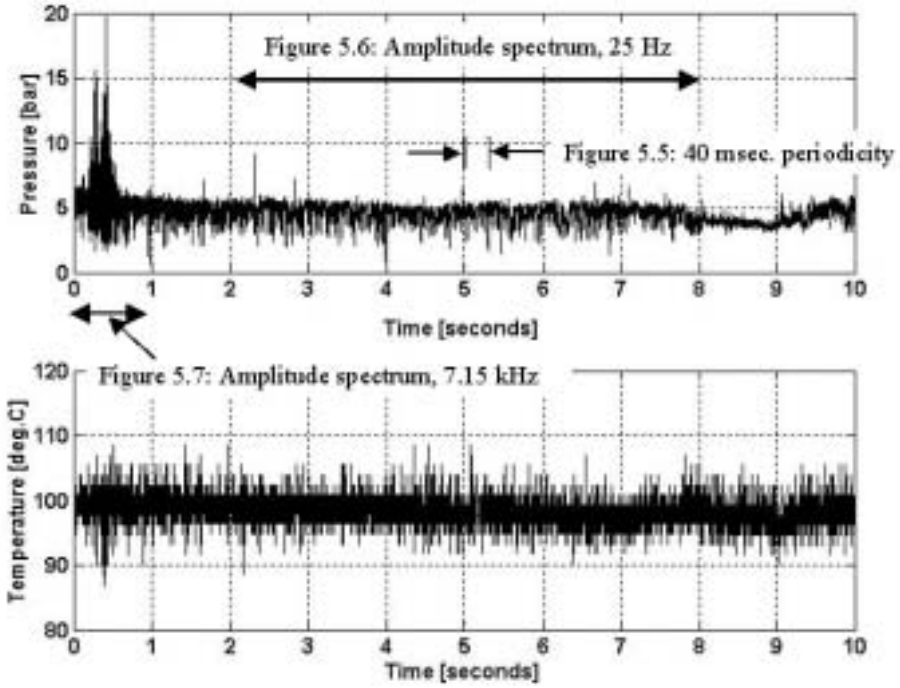

Figure 5.4: Pressure (top) and temperature (bottom) measurements when the refiner is operating with a plate gap of approximately 0.5 mm.

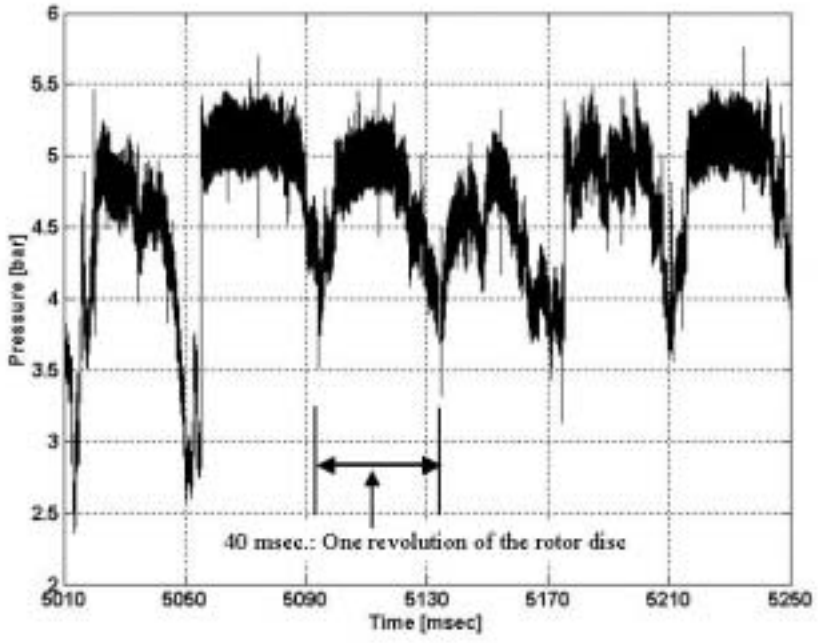

Figure 5.5: Pressure measurements after 5 seconds in Figure 5.4. A 25 Hz periodic pattern is clearly evident.

Figure 5.5 shows a selection of the data in Figure 5.4 after 5 seconds. The periodicity of 40 milliseconds is clearly visible. This is analog to a 25 Hz periodic signal, which can be related to the rotational velocity of the refiner rotor disc. It is common to relate such effects as out-of-tram misalignment (Stationwala and Atack (1980)). Out-of tram represents an imbalance in the refiner disc causing periodically variations of the plate separation. Probably such effect is revealed here too. The short time series in Figure 5.5 indicates a relative large periodical variation. Here the pressure fluctuated up to 2.5 bar. Atack and Stationwala (1975) made similar observations. They ascribed it to local changes in the refining plate clearance, which appeared once per revolution of the rotating disc. Their findings showed pressure variations in the order of ∂ 0.27 bar. This is agreeable with the amplitudes shown in the normalized amplitude spectrum in Figure 5.6.

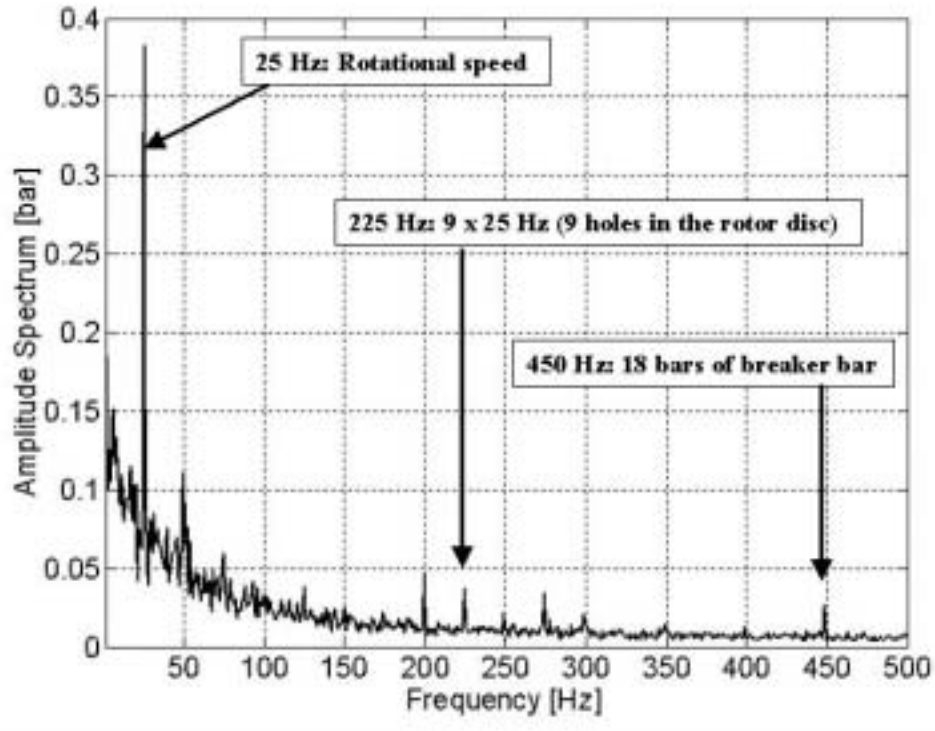

Figure 5.6: The amplitude spectrum of the pressure signals, which are shown in Figure 5.4 between 2 and 8 seconds (3 MSamples).

The frequency analysis shown in Figure 5.6 has revealed that the peak frequency at 25 Hz was dominating in the low-frequency range with an amplitude value of 0.38 bar and an amplitude ratio of 13 dB (modified SNR). Other interesting peak frequencies given by this analysis were the peak frequencies at 225 and 450 Hz. The former can be related to 9 holes in the rotor disc at the same radial distance from the centre of the refiner as the transducer was mounted. The amplitude value of this frequency was only 36 mbar (11 dB). The peak frequency at 450 Hz can have had its origin as a harmonic

frequency of 225 Hz. However, the number of bars in the breaker bar zone also corresponded with the peak frequency at 450 Hz.

The amplitude of the bar crossing frequency at 7.15 kHz (not shown in Figure 5.6) was almost absent with an amplitude value of only 0.7 mbar (7 dB). However, the bar-to-bar passage was much clearer when an FFT analysis was made on the readings from the first period of the measurements presented in Figure 5.4. The bar-to-bar passage was clearly observed in the period where the readings showed high peak values, between 0 and 0.5 second. This is shown in the amplitude spectrum in Figure 5.7.

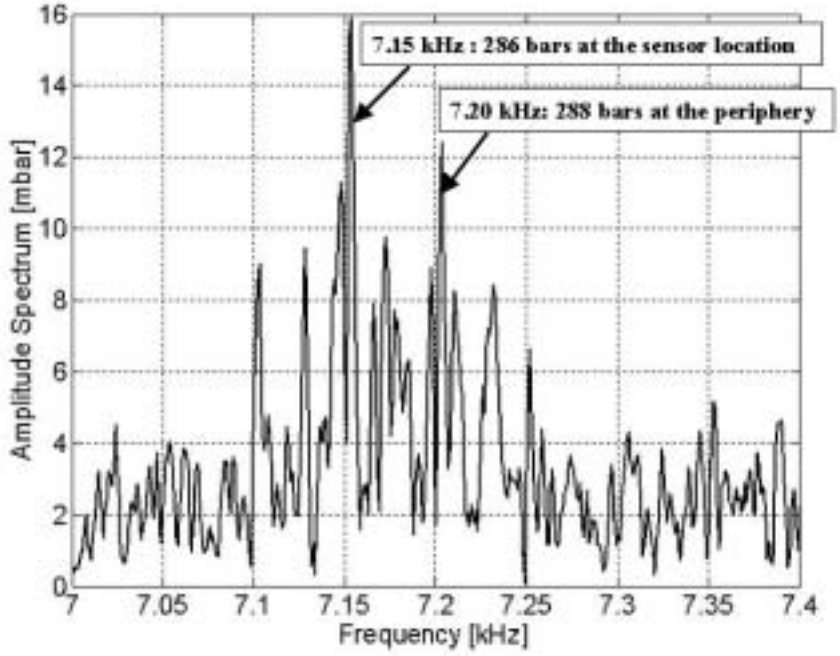

Figure 5.7: The amplitude spectrum of the pressure signals, which are shown between 0-0.5 seconds in Figure 5.4.

The amplitude spectrum in Figure 5.7 shows the frequency corresponding to the bar-to-bar passage at the sensor location. The additional peak frequencies can be identified as sideband effects. However, the frequency at 7.20 kHz can also be a result of the refining action that occurred at the periphery of the plate. The number of bars distributed along the periphery was 288, which corresponds to the periodicity of 7.2 kHz.

The frequency analysis of this small part of the recording revealed that the peak frequency at 25 Hz was dominating in the low-frequency range also here. Its amplitude value was 0.26 bar with an amplitude ratio of 8 dB. In addition, the peak frequencies at 225 and 450 Hz were visible too. The amplitude value of the frequency at 225 Hz was 0.16 bar giving an amplitude ratio of 12 dB.

The periodicities that are revealed in the Figures 5.4 to 5.7 indicate that the pressure sensors responded on inherent features in the process. Thus, these figures support the

assumption that the transducer responded fairly well. However, it is not clarified why the pressure readings shifted to a higher-pressure level when the refiner was filled up with pulp and the plate gap decreased. Furthermore, it was expected that the pressure readings were dominated by the fluctuations created by the bar pattern on the rotating plate. The reason why the bar crossing frequency was almost absent during stable operation remains unanswered. However, it is assumed that the plate gap and the amount of pulp in the refining zone as well as steam flow contributed in such way that the contact between the sensor surface and the pulp in the plate gap was gentle.

Another approach to the explanation of the measured pressure is the reaction thrust from the pulp in the grooves. Whether the packing of pulp in the plate grooves had any effect on the pressure readings can be discussed. Ouellet and Weiss (1994) assumed that the reaction thrust from the pulp in the grooves could be ignored when they considered axial vibrations and plate gap variations in disc refiners. Miles and May (1991) discussed the cyclic changes in the forces generated by the bar pattern. They indicated that some of the forces would be reduced when a groove is opposite a bar. However, it was indicated that this reduction is dependent on the amount of packed pulp trapped in the groove. The latter can be interpreted that the pulp in the grooves affects the pressure so that the cyclic variations due to the bar and groove pattern is reduced. Thus the bar crossing frequency would be less visible. The packed pulp in the grooves would also make the volume available for the steam flow smaller. It is conceivable that the steam pressure would increase because of such effect. This may contribute to explain the pressure readings in this experiment. If the grooves in the plate were packed full of pulp the pressure would be less dependent on the bar pattern on the facing plate and the average pressure would show a higher level with a smaller variance. In addition, it is conceivable that the steam pressure could contribute more than previously expected because of a smaller volume available.

5.3 Pressure peaks

The pressure peak readings indicate that the pressure could be surprisingly high as shown in Figure 5.3. Pressure peaks in excess of 10 bar were frequently observed. Compared to the measurements that were reported by Atack and Stationwala (1975), these pressure peaks were almost twice as high. It is known that the refiner studied by Atack and Stationwala was self-pressurized, which means that the temperature was higher than in an atmospheric refiner as studied here. The fibres were probably much softer in the self-pressurized refiner and therefore it could be expected that this pulp transmitted a lower pressure to the sensor at a given compression. Thus, the measured pressure peaks would be smaller in the self-pressurized refiner, while the stiffer fibres, which could be expected in the pilot refiner, would give larger pressure peaks.

Additional information from the pilot refiner experiment is shown in Figure 5.8 where the averaged maximum pressure peaks (lower line) and the absolute maximum pressure peaks (upper line) observed at a given plate gap are shown. The average maximum pressures and their corresponding standard deviation values for the three largest plate gaps are shown in Table 5.1.

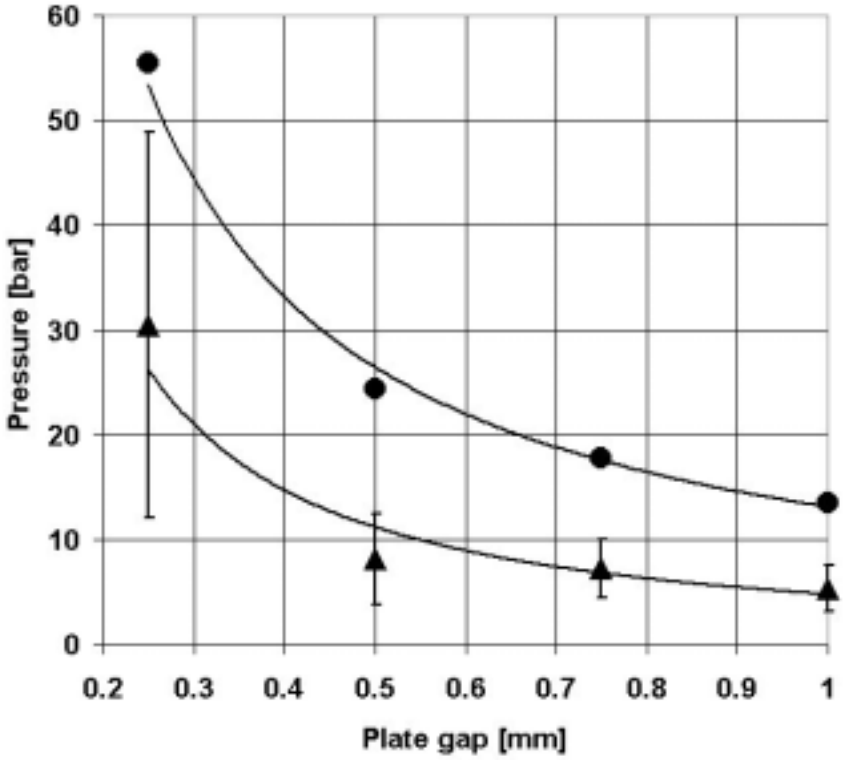

Figure 5.8: The absolute maximum values (upper line) and averaged maximum values (lower line) of the pressure signals for various plate gaps.

The tendency in Figure 5.8 supports the average pressure readings, which indicated a substantial level shift to higher pressures when the plate gap decreased. The average maximum pressures are added with the corresponding standard deviation values. It shows that the variations are too large to make any solid conclusion about the displayed trend. However, Hietanen (1991) reported a similar trend from a study performed in a low-consistency refiner. The pressures measured in the low-consistency refiner were somewhat lower with a maximum reading of approximately 30 bar at a plate gap of 15 μm. According to Ebeling (1980) pressure as high as 100 bar can be expected under particular circumstances in low-consistency refiners.

5.4 Pressure readings during chip feeding problems

The experiment performed in the pilot refiner was performed at the different operating conditions as shown in Table 5.2. This table gives the process data as well as data obtained from the collected pulp samples. In addition, the average and standard deviation values of the pressure and temperature signals are shown.

Table 5.2: Experimental data from the pilot refiner experiment.

Plate gap [mm]	Dil. water flow [l/min]	Time period [second]	Ave. press. [bar]	Std. dev. [bar]	Ave. temp. [∀C]	Std. dev. [∀C]	Pulp cons. [%]	Prod. [kg/min]	Specific energy consumpt. [kWh/t]
1.00	n.a	162	2.0	0.1	67	1	n.a	n.a	n.a
0.75	3.8	76	3.2	0.1	74	1	19.7	0.96	550
0.50	6.0	82	4.5	0.4	75	1	21.4	0.85	900
0.25	7.1	6	1.4	1.3	103	6	55.0	0.50	2300

An unexpected recording is shown in Table 5.2 for the smallest plate gap. The pressure value was unexpectedly low compared with the other readings. In addition, it had a very high standard deviation, which indicated unstable operation of the refiner. The corresponding consistency and specific energy consumption were very high as well. A possible reason for this unexpected and unstable measurement was unstable feeding of the refiner at the small plate gap. Such behaviour has been studied by Miles and May (1990) and (1991).

Two circumstances call attention to this assumption. First, the consistency was very high, and second, the plate clearance was small. High-consistency or equivalently very dry fibrous material gives less possibility for the centripetal force to build driving centrifugal potential energy to move the pulp through the refining zone. The result is that the residence time of the pulp increases. In addition, if the plate clearance is small, higher friction resists the outgoing flow. The final result in this part of the test run was that the feed screw was blocked and the feed screw motor stopped. The readings from this unstable period are shown in Figure 5.9, which represents 5 MSamples.

Figure 5.9 shows two strange and unexpected signal patterns. There are several phenomena that are hidden in these recordings. Because of the noisy signals it could be considered that there was no information of interest buried here. It was also conceivable that the sensor was broken. However, the sensor responded well after the experiment was finished. Instead, the data have been investigated critically to find reasonable explanations for different signal patterns.

These unexpected data occurred when the plate gap was decreased to 0.25 mm. It should be mentioned that the plate clearance was calibrated after a preheating period lasting for approximately 30 minutes. The preheating was conducted with hot water with a temperature of approximately 53 ºC. The real plate clearance after a period of pulp production and thus additional heating was not clarified.

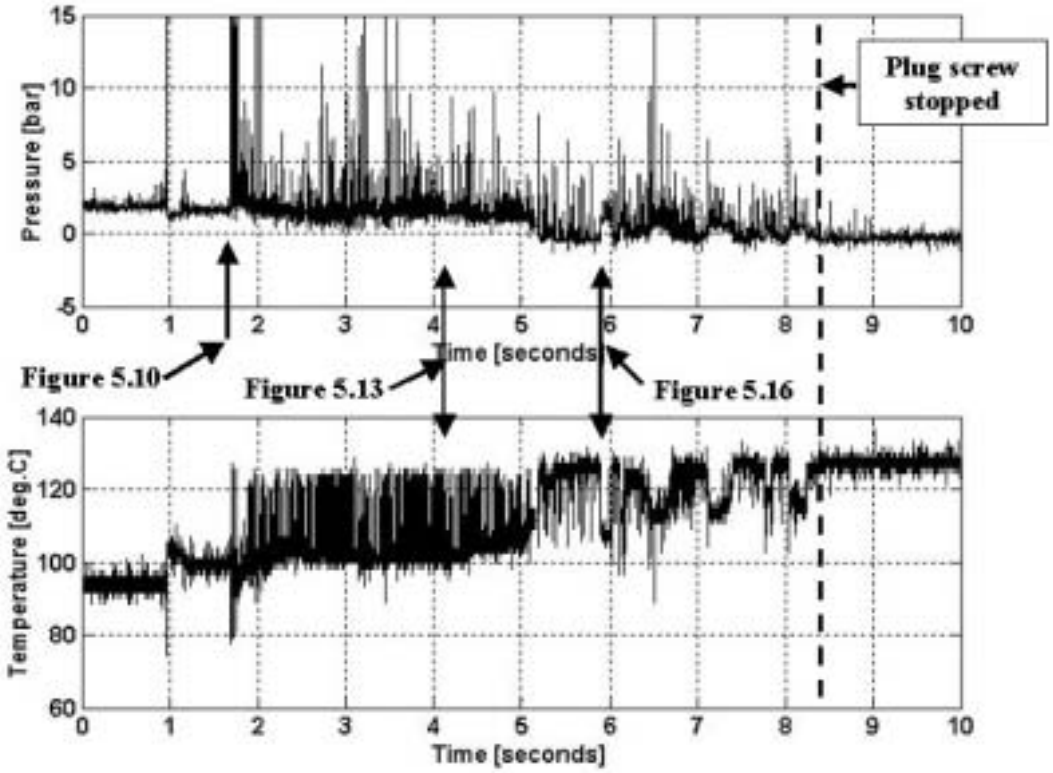

Figure 5.9: Pressure (top) and temperature (bottom) measurements when the refiner was operating at a very small plate gap of approximately 0.25 mm.

5.4.1 Bar crossing frequency

The first occasion occurred after approximately 1.7 seconds of the recording shown in Figure 5.9. This is shown in Figure 5.10. In other respects this plot shows the highest peak pressures that were observed in this experiment. The amplifier signal was saturated at pressure peaks corresponding to 55 bar. The real pressure readings would be even higher. Equally interesting is the periodic signal pattern revealed in Figure 5.10, which can be associated with the movement of the bars on the rotor disc. Figure 5.10 shows 14 peaks during a period lasting for 2 milliseconds, which clearly reveals the duration of the bar-to-bar passage to be approximately 0.14 milliseconds.

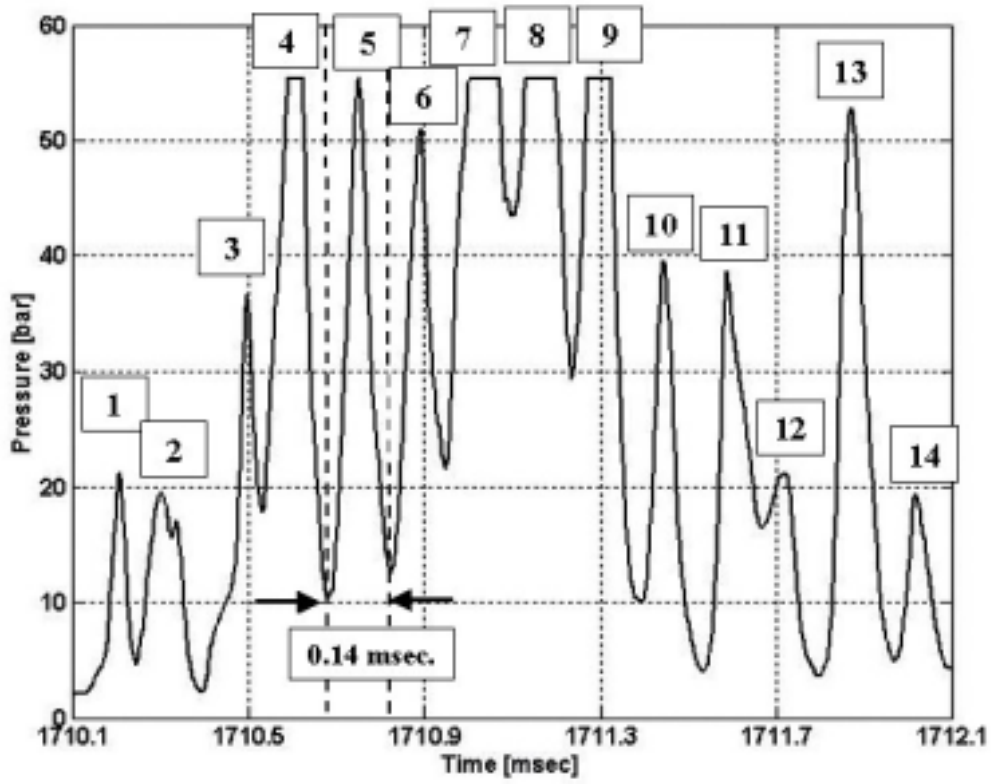

Figure 5.10: The pressure readings after about 1.7 seconds of the measurements showed in Figure 5.9.

It is obvious that the bar-to-bar passage was less visible in time series where the refiner was operating at stable conditions i.e. when the plate gap was relatively high and the chip feeding was working well. In the specific operation with a tight plate gap and problems with continuous feeding, the bar-to-bar passage was indeed present. A possible cause of this is that the discs were really close. Because of the expected disc misalignment it is appropriate to question if the discs were hitting each other during the time of one revolution. Moreover, the tight plate gap and the high consistency of the pulp might have reduced the radial pulp flow through the refining zone such that the wood material stayed in the refining zone for a longer time. When the wood material was squeezed in the small plate gap between the transducer's surface and the bars on the rotating disc, the pressure readings were very high. Another conceivable reason is that a possible disc-disc contact shocked the transducer such that irregular output signals were recorded.

A corresponding amplitude spectrum of part of the time series in Figure 5.9 including the data set of Figure 5.10 is shown in Figure 5.11. The present FFT analysis has been performed on readings between 1.68 and 1.75 seconds of the readings in Figure 5.9. The bar-to-bar passage corresponds to the peak frequency at 7.15 kHz with the amplitude value of 1 bar (14 dB). Two other peak frequencies at approximately 300 Hz (1.7 bar, 5 dB) and 2.9 kHz (1.2 bar, 5 dB) were observed as well. These frequencies

were not as clear in other FFT-analysed data sets under different operating conditions. The basic cause of their presence remains unidentified. However, the frequency at 2.9 kHz can be associated to the refining action in the intermediate zone, which comprised a number of bars between 90 and 126. Thus, periodically patterns can have been present in the range from 2.25 to 3.1 kHz.

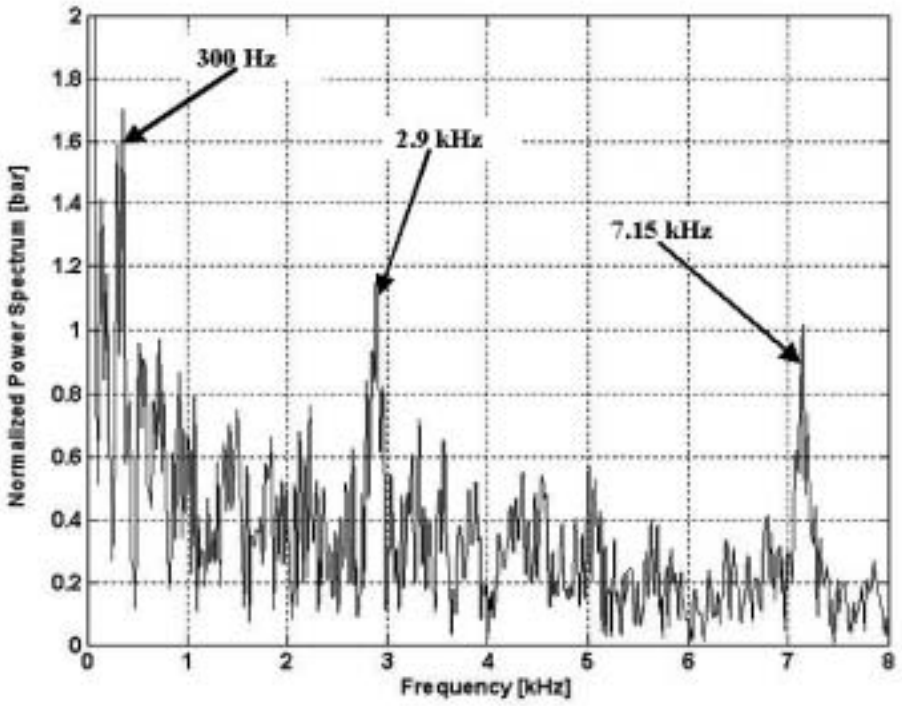

Figure 5.11: Normalized amplitude spectrum of the pressure readings between 1.68 and 1.75 seconds of the measurements shown in Figure 5.9.

5.4.2 Phase averaged bar-to-bar passage

To support the visualization of the amplitude spectrum in Figure 5.11, a plot of the phase-averaged analysis of the bar-to-bar passage during a period of about one revolution of the rotating disc is shown in Figure 5.12. The data set contains about 20 kSamples including the readings that formed the basis for the amplitude spectrum in Figure 5.11.

The curve in Figure 5.12 contains 70 data points each. Each point is an average value of 286 synchronized samples. A bar-groove pattern is sketched in the plot to illustrate a bar-groove passage of the moving refiner disc. However, there is no information that states that the sketch is appropriately fitted to the measurement. Figure 5.12 shows that the averaged pressure variation was in the order of ∂ 1.5 bar during the bar-groove passage. Compared to the high-pressure readings shown in Figure 5.10 this pressure variation is small. Thus additional periodical patterns have interfered with the pure bar

crossing signal. There have not been made any efforts to filter out additional signal patterns or anomalies in the readings.

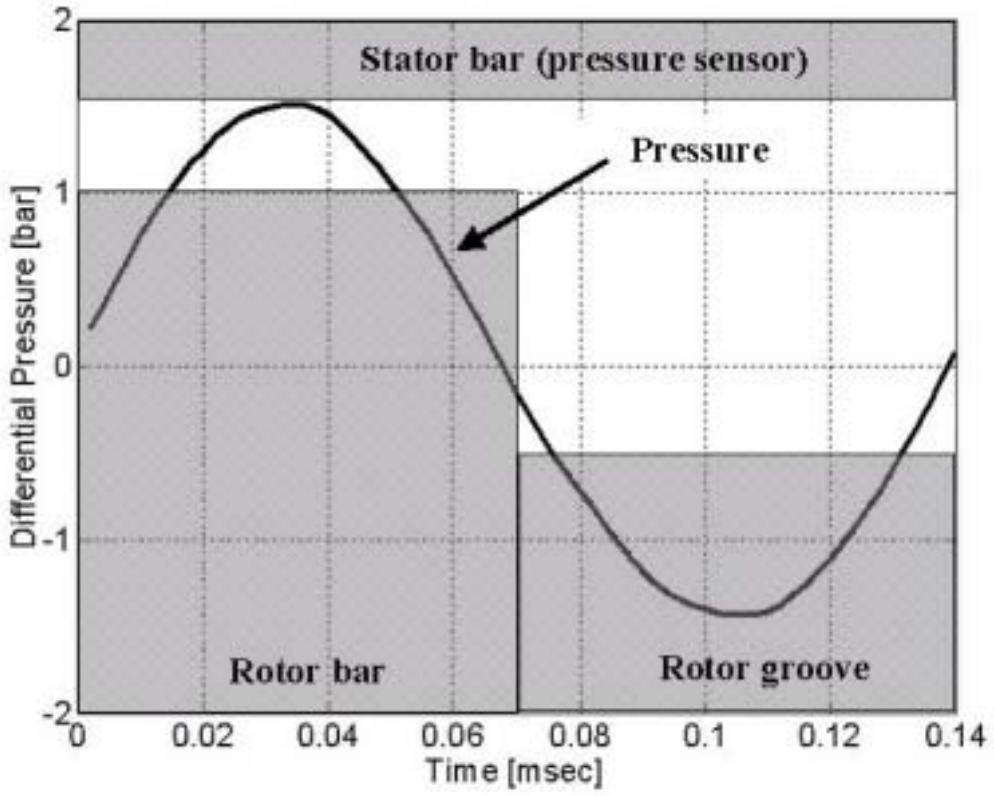

Figure 5.12: The phase-averaged analysis of a period corresponding to the bar-to-bar passage over a period of one revolutions of the rotating disc.

5.4.3 Relationship between pressure and temperature signals

The readings shown in Figure 5.13 were captured shortly after the plate gap was decreased to 0.25 mm, and the problems due to continuous chip feeding had started. The readings include one bar-to-bar passage as shown between the two dotted vertical lines in Figure 5.13. It is likely that the pressure increase was generated by pulp squeezed between the sensor surface and a rotor bar. The correlation between the temperature and the pressure is clearly visible. A cross-correlation analysis, not shown here, indicated that the highest (positive) correlation coefficient occurred at +50 μseconds when the temperature lagged the pressure. This is intuitively a natural course of the dependency. In addition, it should be remembered that the rise time for the temperature signal was 2 milliseconds as stated from the manufacturer. This should indicate that the real temperature, highest level, was not obtained before the signal decreased again.

The high temperature increase was unexpected at first glance. A temperature rise of approximately 25 ºC during such small time period was surprising. However, the simultaneously pressure increase was between 1 and 1.5 bar. A corresponding shift in saturated water vapour pressure (Figure 3.14) from 1.5 to 3 bar gives a temperature shift

of approximately 16 ºC. The temperature shift shown in Figure 5.13 was higher than that. However, it should not be concluded that the temperature readings were false. The stable readings before and after the recorded bar passing reinforce the reliability of this measurement. It should neither be excluded that any common sources caused these responses. This is conceivable since the temperature and pressure measurements were based on the same resistive bridge network.

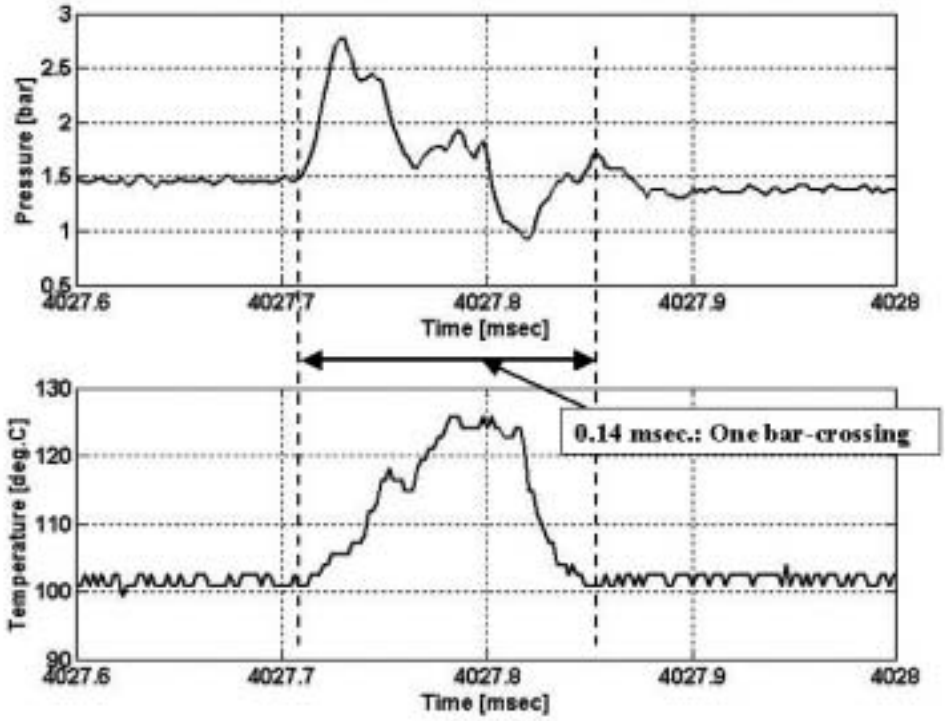

Figure 5.13: The pressure (upper plot) and the temperature (lower plot) readings as part of the recording shown in Figure 5.9 after 4 seconds.

All the temperature recordings did not show similar relationship as revealed in Figure 5.13. The temperature recording performed simultaneous with the highest-pressure peaks is shown in Figure 5.14. Thus the readings in Figure 5.10 are repeated together with the corresponding temperature readings. These temperature readings were fluctuating between approximately 80 and 110 ∀C as shown in Figure 5.14. There is no evidence for any sensor failures, because then larger signal fluctuations would be expected. However, the small plate gap and the readings of the high pressures indicated that the fibres between the sensor surface and the rotor bars were strongly squeezed. In the middle of the plot, when the pressure peaks were at their highest, the corresponding temperatures were relatively stable. This indicates that the pulp above the sensor surface had an even temperature, between 90 and 95 ∀C, and that the pulp prevented any temperature fluctuations. A further assumption is that when the fibres were removed from the sensor surface, high temperature steam affected the sensor resulting in a temperature rise.

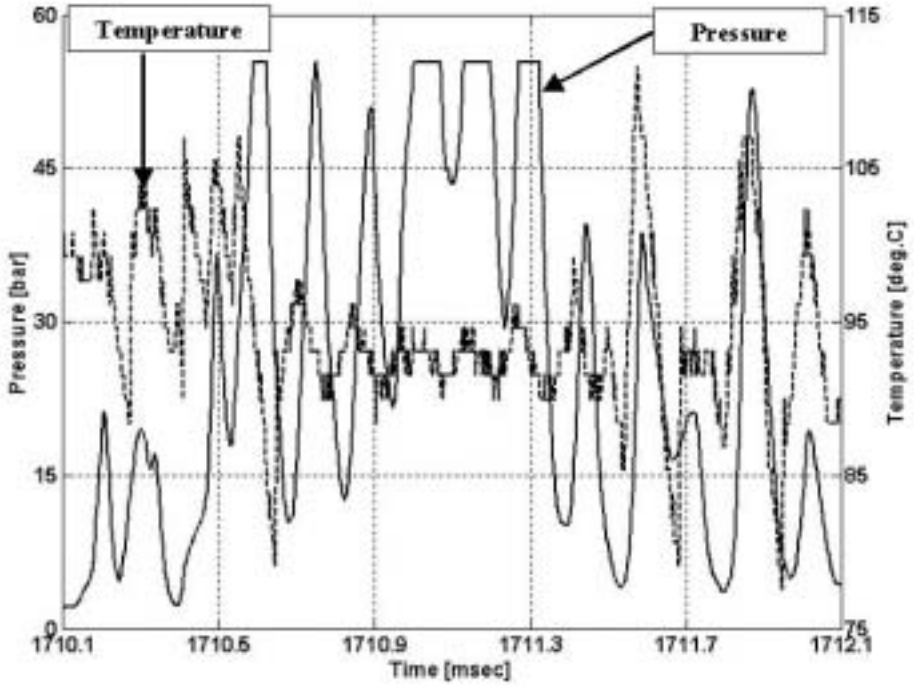

Figure 5.14: Temperature and pressure readings during 14 bar-crossings.

It is not easy to draw any categorical conclusions about the temperature and pressure dependency based on these readings. A cross-correlation analysis was therefore performed on the same readings as shown in Figure 5.14. See Figure 5.15.

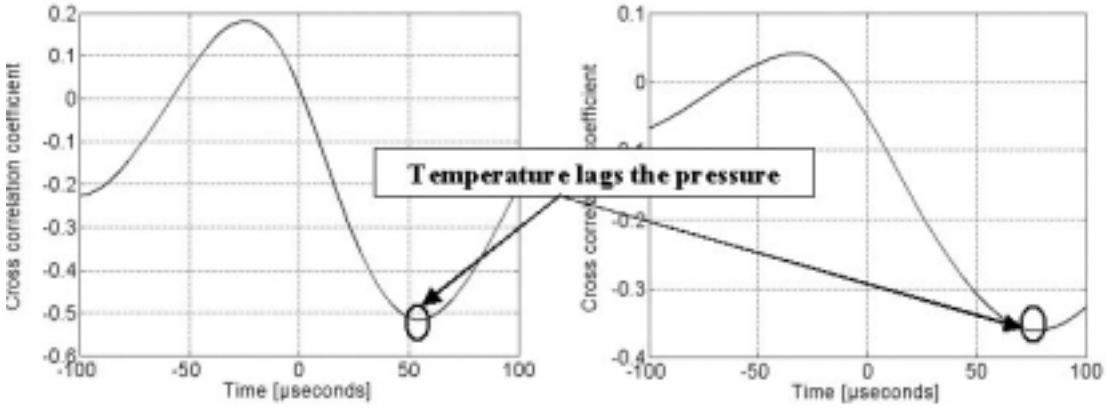

Figure 5.15: Cross-correlation between the temperature and the corresponding pressure values. Left-hand plot is the cross-correlation of the same readings as shown in Figure 5.14. The right-hand plot is a result of the readings shown in Figure 5.12.

In Figure 5.15 two cross-correlation plots are shown. The left-hand plot shows the cross-correlation between the temperature and the pressure for the same recordings as shown in Figure 5.14, while the right-hand plot represents the readings captured during an single revolution which the phase-averaged plot in Figure 5.12 is made from. These cross-correlation analyses showed that the highest correlation coefficient was obtained when the temperature lagged behind the pressure. However, then the correlation was negative.

The two cross-correlation plots in Figure 5.15 show that the lag was increasing when additional readings were used in the analysis indicating that there was no full harmonization. The higher correlation coefficient in the left-hand plot is due to fewer readings. Because of the very special operating conditions, there is some uncertainty related to the origin of these cross-correlation curves. Mainly positive correlation has been observed between the temperature and pressure signals as shown in Figure 5.3. However, negative correlation has been observed when the pressure spikes were high. This has to some extent been confirmed in the correlation analyses between the pressure and temperature signals as shown in Figure 5.3. The reason for this apparent relationship between the negative correlation coefficients and the high-pressure peaks may be associated with a direct connection between these signals. It is conceivable that when a strong force was applied on the sensor diaphragm the Wheatstone bridge was strongly imbalanced such that the bridge voltage and thus the temperature readings were affected.

Similar concerns have been associated with the signal patterns that are shown in Figure 5.16. This figure looks like a mirror image. This may indicate that some inherent features in the sensor have affected the pressure and temperature readings simultaneously. It is clearly evident that the correlation between these signals was high. Cross talk from one data acquisition channel to the other cannot be excluded. However, if cross talk was expected this should have given mirror images from other recordings as well. Such mirror images have not been observed elsewhere. The behaviour of the refiner during this abnormal operating is not proven. Further discussions follow next.

5.4.4 Pressure readings below atmospheric

Figure 5.16 shows an enlarged part of the recorded data in Figure 5.9 after 5.8 seconds of that time series. The high temperature readings and the corresponding low pressures are interesting. The pressure level was below atmospheric, which is remarkable. However, this observation was made when the feeding problems occurred and led to the feed screw stopping.

Probably too dry an environment caused the high temperature if all the water had evaporated and stagnant pulp in the grooves near the transducer was burnt. The latter was observed when the plates were removed. The stagnant pulp in the grooves was not carbonized, but parts of the remaining pulp had a dark brown colour. Looking closer at the end of Figure 5.9 after approximately 8.5 seconds, the output signals were stabilized at corresponding levels, high temperature (125 ∀C) and low pressure (-0.6 bar gauge pressure). The feed screw had stopped at that time. Low pressure readings, below

atmospheric might occur if the feed screw was packed full of chips and the periphery was open. The centripetal force may then create suction.

The first part of Figure 5.16 shows similar pressure and temperature conditions as assumed created by plugging of the feed screw. Shortly before the plug screw stopped the operation of the refiner was difficult. Probably the plug screw was plugged several times before the final chip-plug got stuck.

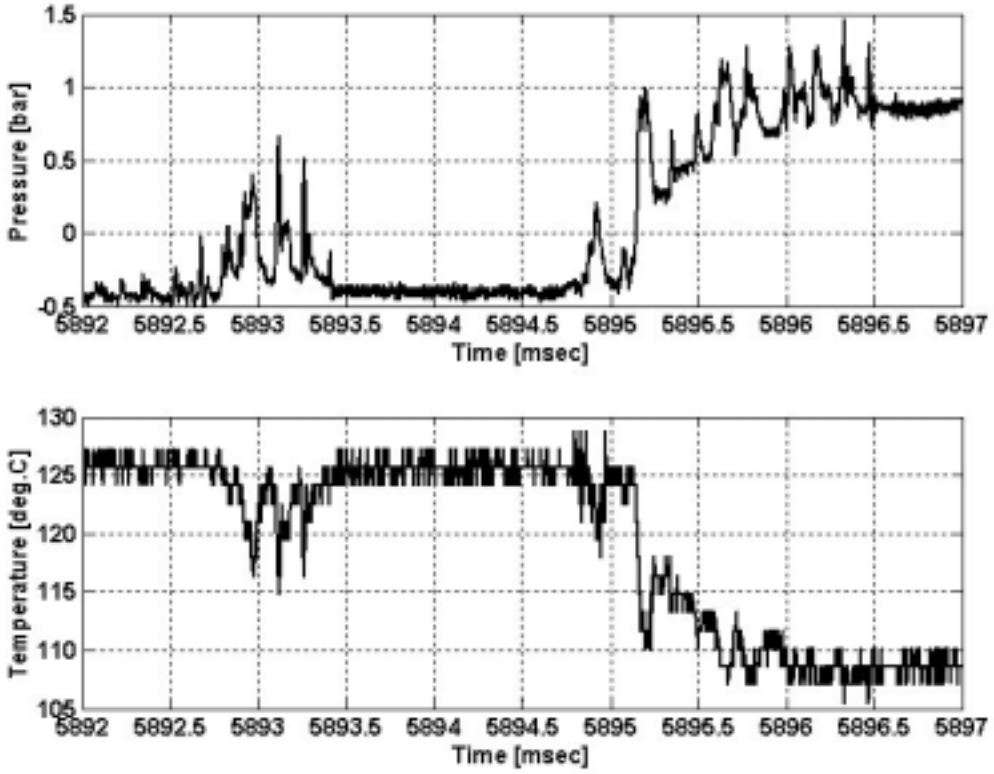

Figure 5.16: The change in pressure (top) and temperature (bottom) measurements when the plugging problems had occurred. These recorded data are showed in Figure 5.9 at about 5.89 seconds.

Another consideration that can be made from Figure 5.16 is that the high temperature generated more steam that opened the gap and simultaneously caused a pressure drop. However, a wider plate gap should cause a decrease in the temperature since smaller amount of friction would be generated. Thus the temperature and pressure would probably oscillate. Instead the pressure and temperature were stabilized at these abnormal levels. This makes the first approach more probable.

The high temperature may have another cause associated with disc-to-disc contact. Such observation of high temperature readings was reported by May *et al.* (1973). In an atmospheric refiner temperature up to 130 ∀C was observed close to the periphery. It was claimed that these abnormal readings were caused by plate touching. Such an effect

cannot be excluded in the present study based on the fact that the plate gap was decreased to an initial set point of 0.25 mm. The heating of the refiner might have created an offset in the plate clearance. In addition, if non-parallelism of the planes of the discs was present, the effect of plate touching cannot be excluded, as an additional effect to suction generated by the plugging.

5.5 Concluding remarks

- High-frequency pressure and temperature measurements were performed in a 20 inch (510 mm) atmospheric single disc pilot refiner using a combined piezoresistive pressure and temperature transducer.
- Pressure changes were observed during chip feeding and during step changes in refiner operating conditions. Decreasing plate clearance gave significantly increased pressure readings. Stable pressure readings between 2 and 4.5 bar were observed.
- Pressure peaks up to 60 bar were observed at a 0.25 mm plate gap.
- High and stable pressure readings indicate that the steam contribution for counteracting the axial thrust should not be ignored. Low-level pressure readings might be an indicator of that steam pressure was present to some extent. A possible reason for this may be related to stagnant pulp in the grooves that resisted the steam flow. Thus steam pressure could have been built up in small parts of the outer region of the refining zone. However, uncertainties associated with the relative large diameter transducer casing as well as unbalanced forces generated by radial flow in the stator groove where the transducer was located, cannot be excluded as factors that have generated apparent pressure readings.
- Periodic pressure variations were observed related to one revolution of the moving disc (25 Hz) of the refiner. This was probably caused by out-of tram misalignment representing an imbalance in the refiner disc.
- The bar-crossing frequency at 7.15 kHz related to the radial location of the sensor was observed when the plate clearance was small and the pressure readings were high. A phase-averaged sampling plot is shown in connection with observation of the bar crossing frequency.
- Other periodic signals were also observed. Peak frequencies at 225 and 450 Hz were visibly resulting from nine holes in the plate pattern of the rotor disc and the bars in the breaker bar region respectively. Periodicities associated with 300 Hz and 2.9 kHz were observed as well. The latter might be related to the bars in the intermediate zone, while the peak frequency at 300 Hz remains unidentified.
- A period of process instability caused by chip-feeding problems was recorded. A plausible explanation of these findings was that excessive friction occurred due to small plate clearance, and that too low outward driving forces were activated because of high pulp consistency. Pressures below atmospheric were recorded, as well as unexpected high temperature values. The latter might be related to plate touching.
- A relationship between the temperature and pressure signals was obtained. The temperature readings lagged behind the pressure by approximately 50 μseconds. Less clear dependencies were found during the abnormal running conditions.

CHAPTER 6

RESULTS AND DISCUSSION FIBRE-OPTIC SENSORS MILL REFINER

6.1 Introduction

This results chapter is built up as follows:

- The general performance of the fibre-optic pressure sensors is presented by some examples in Section 6.2.
- The dynamic responses of the sensor signals are outlined in Section 6.3. The time series and histograms are displayed together with amplitude spectra based on the FFT-analysis. The frequency analyses have formed an essential role in this study.
- Cross-correlation analyses for the investigation of the pulp flow movement and the pressure wave propagation have been performed. These are discussed in Section 6.4.
- Section 6.5 focuses on the validity and uncertainty of the transformation of the raw sensor signals to pressure. A main part of this section is related to the recalibration of the sensor signals.
- The basis of Section 6.6 is the results obtained during the factorial designed experiment. Additional information from the process data and regression analyses has been used to build the conclusions.
- Results from the test containing the changes in the amount of chips fed to the refining zones are discussed in Section 6.7.
- The fluctuations in the rotational velocity are discussed in Section 6.8. Both load variations and variations in bar-crossing frequency are shown.
- Section 6.9 contains discussions about captured signal patterns. Simulation results are introduced and compared with the original pressure signals.
- The last section summarizes the findings and the main results from the previous discussions.

6.2 Examples

This section contains results from particular running conditions like the heating of the refiner, the initial chip feeding and shutdown. Illustrative examples from these periods easily show the performance of the sensors. During the heating process the results were predictable because the process behaviour was not as complex as during production of pulp. Examples are also given from periods of initial chip feeding and shutdowns as well as an informative example from the test where the chip distribution between the refining zones were significantly affected.

6.2.1 Responses during warm-up and initial chip feeding

Figures 6.1 and 6.2 show the voltage output signals from the sensors No. 9 and 4 respectively during two separate initial chip-feeding periods. The readings shown in Figure 6.1 were captured during the very first start-up after the new plates were installed. This figure also shows the shutdown, which followed soon after. Plugging in the blow line caused this shutdown. Both figures show the simultaneously captured output signals from the motor load as the upper plot. Thus the lower plots show the high-frequency voltage output signals from the sensors.

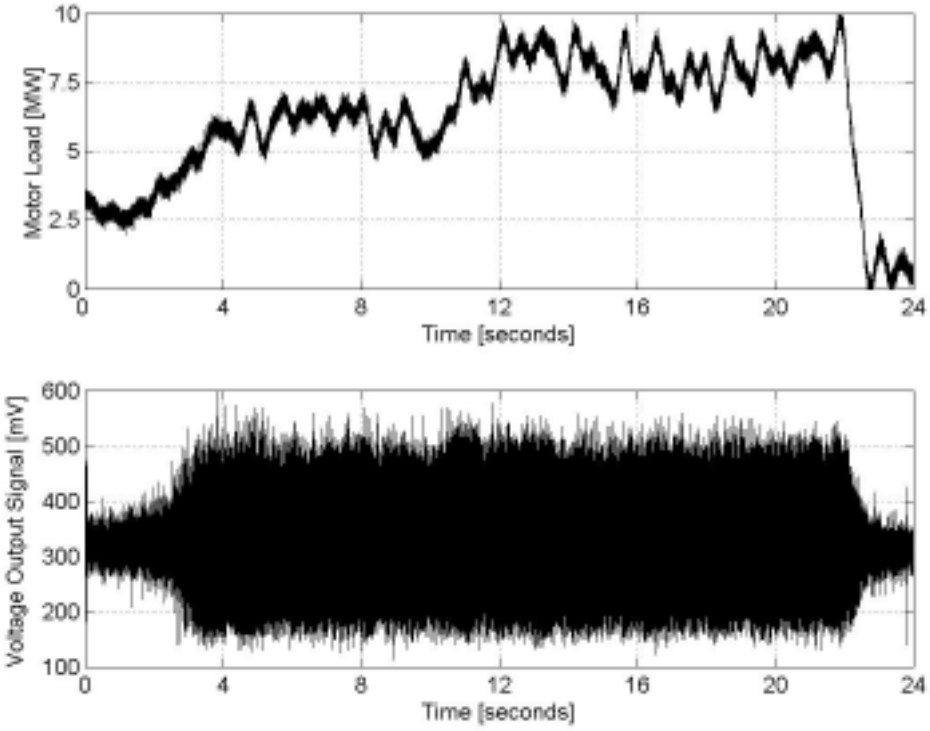

Figure 6.1: The motor load (upper plot) and the voltage output signals from sensor No. 9 (lower plot) during the initial chip feeding and the following shutdown on the first day of data recording.

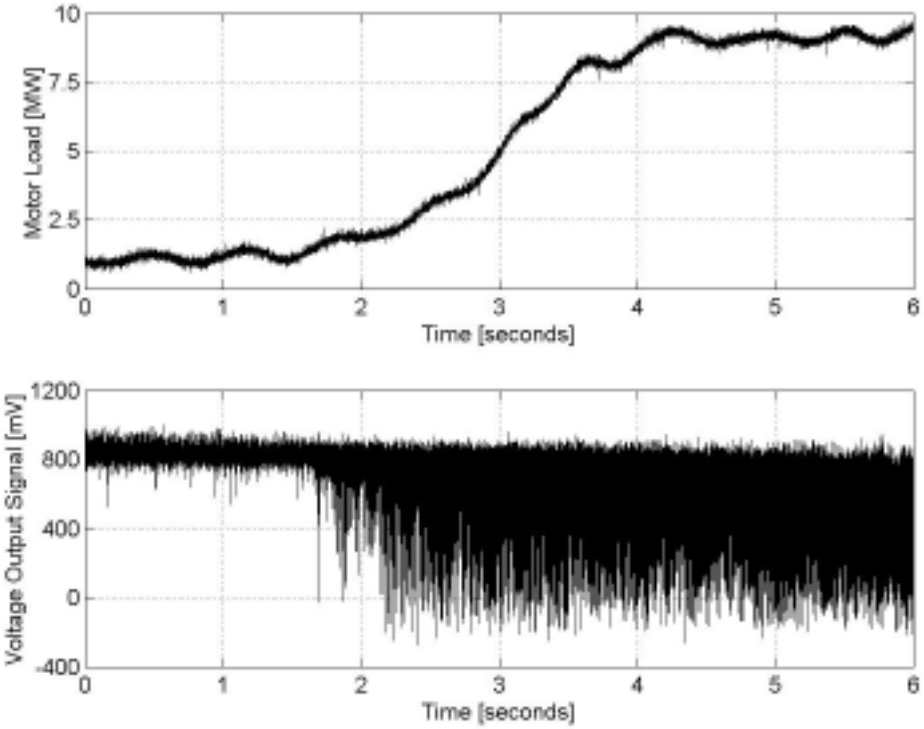

Figure 6.2: The motor load (upper plot) and the voltage output signals from sensor No. 4 (lower plot) during initial chip feeding on the second day.

The raw data signals behave as expected. When there were no chips fed in, the sensor signals were fluctuating about a stable DC-level. The fluctuations were comparable with the observed noise level. The chip feeding increased the amplitudes of the output signals and hence revealed the increase in pressure. The different shape of the sensor signals shown in Figures 6.1 and 6.2 indicates the different phases of the sinusoidal transfer function curves. While the recorded sensor signal in Figure 6.1 started at approximately 3 bar (320 mV), the recording in Figure 6.2 started at approximately 1 bar (900 mV). The shape of the latter signal shows that the voltage signal associated with 1 bar was located close to a maximum point of the sinusoidal transfer function curve. Moreover, the sinusoidal transfer function curves for the different sensors are shown in Appendix C

6.2.2 Average pressure and process data

The examples in this section show pressure readings converted from the voltage output signals. The raw data have been converted to pressure using calibration data as shown in Appendix C. The basis for the calibration data is discussed in Section 6.5. Figure 6.3 shows the average pressures, averaged over a one-second window i.e. 500 kSamples per average data point when the data were captured at a sample rate of 500 kSamples/s, from sensors No. 4 and 9 during a period lasting for 180 seconds. The refiner was preheated and the initial chip feeding started during this period. The process start-up

failed after about 20 seconds. Therefore, Figure 6.3 also shows the subsequent shutdown. The raw data shown in Figure 6.1 are basis for parts of these averaged pressure values. Additional raw data from sensors No. 4 and 9 captured shortly after the initial chip feeding started are shown in Figures F1 and F2. Together with the pressure signals the process data of the pressure in the refiner housing is also shown. In addition, it can be mentioned and further shown in Figure F3, that the temperature measurements were highly correlated, as expected, with the casing pressure and the average pressure in the refining zone.

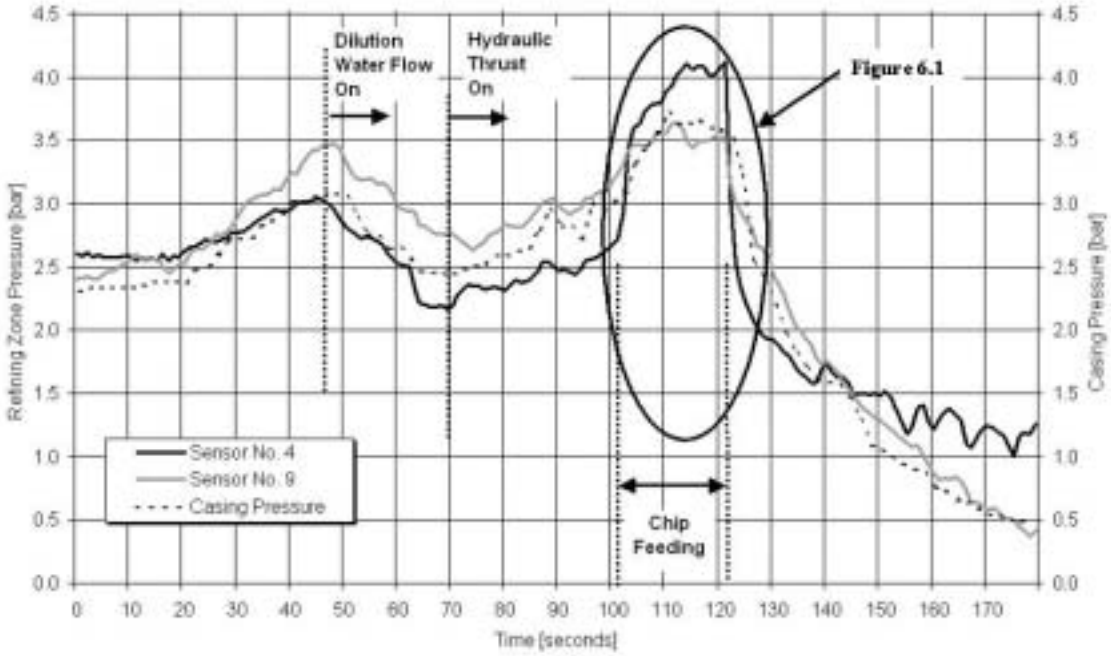

Figure 6.3: Average pressures measured by sensors No. 4 and 9 are shown together with the casing pressure from the mill's DCS during the preheating, the initial chip feeding and the subsequent shutdown on the first day of data recording.

Another start-up sequence is shown in Figure 6.4. This plot is based on data captured in two different recordings lasting for 60 seconds each. Non-continuous readings are shown as discontinuous lines. The separation lasted for about 30 seconds. The first part shows the last period of the preheating phase, while the second part shows the initial chip feeding. The pressure in the refining zone decreased below the casing pressure shortly before the initial chip feeding. This pressure drop was probably caused by the cooling effect of incoming dilution water and the force created by the centripetal acceleration on the water flow through the refining zone. The centripetal acceleration created a lower pressure in the refining zone than in the refiner housing where the casing pressure measures.

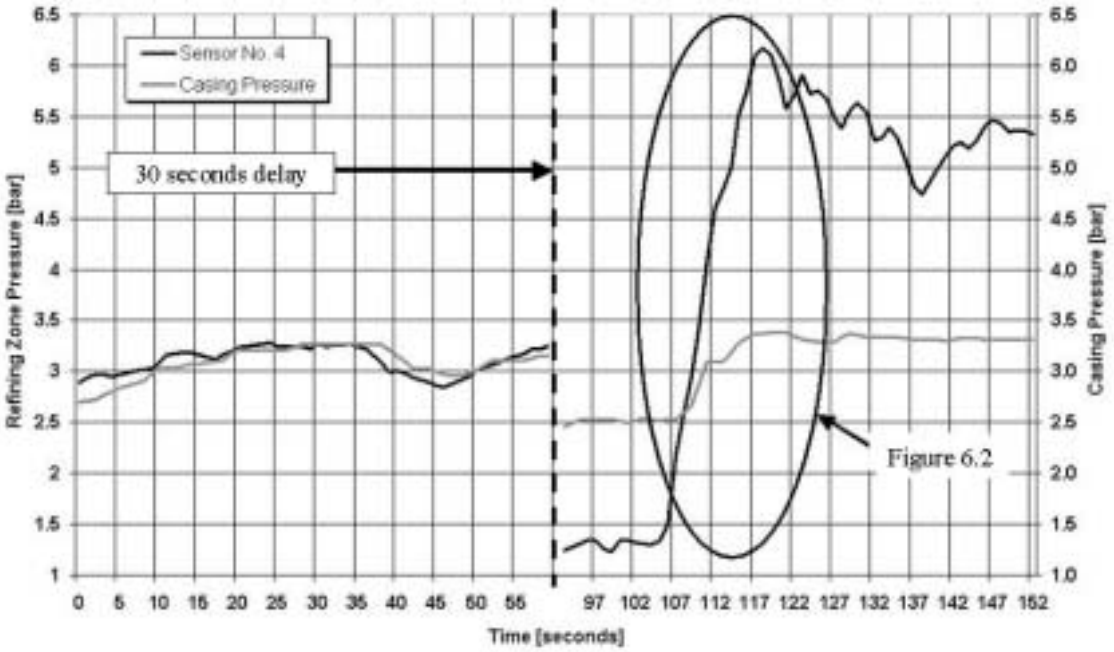

Figure 6.4: Average pressures measured by sensor No. 4 and the casing pressure from the mill's DCS are shown during the preheating and the initial chip feeding on the second day.

A third start-up sequence is shown in Figure 6.5 after a relatively short shutdown after 39 hours of work time. The figure reveals data captured in four different recordings separated by 40 to approximately 250 seconds, therefore the lack of continuous readings. The first recorded data lasted for 60 seconds while the rest were lasting for 30 seconds. The motor load, captured by the same fast data recording system as the pressure readings, has been averaged and is shown together with the average pressures in this figure.

Figure 6.5 indicates that the average pressure in the intermediate and fine bar regions of the refining zone can be in the order of 20-30 bar. However, the absolute pressure levels are not determined exactly. Lack of an appropriate demodulation technique has made the determination of the pressures difficult. The sinusoidal transfer function curves have given several possible pressure levels for a single voltage value. The challenge has been to deduce the most promising pressure for each sensor in each recording. A lot of effort has been done to manage this. Process data and theoretical considerations have been used. The present result is the best that is achieved through this investigation. However, there is related uncertainty to the stipulation of the pressures. This is discussed in more detail in Section 6.5.

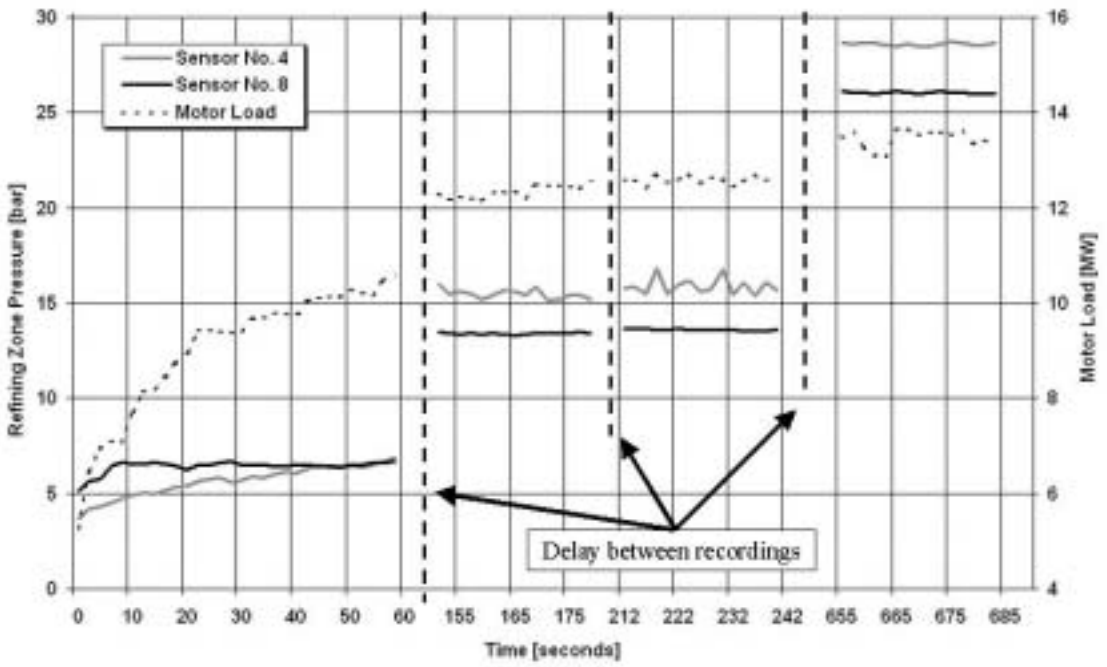

Figure 6.5: Average pressure measured by sensors No. 4 and 8 during the initial chip feeding on the third day, after 39 hours of operating time.

6.2.3 Chip-stream splitter test

Figure 6.6 shows the averaged pressure readings captured after 1000 operating hours during the test, where the aim was to change the amount of chips to the refining zones. The test is also labelled *Giri-gari* test. The data recording and the test lasted for about ten minutes. In this figure the motor load, collected from the mill's DCS, are shown together with the pressure readings. The pressure readings have been converted from voltage to pressure through the third flange of the calibration curve as discussed in Section 6.5. Details about the test run conditions and the results obtained are further discussed in Section 6.7.

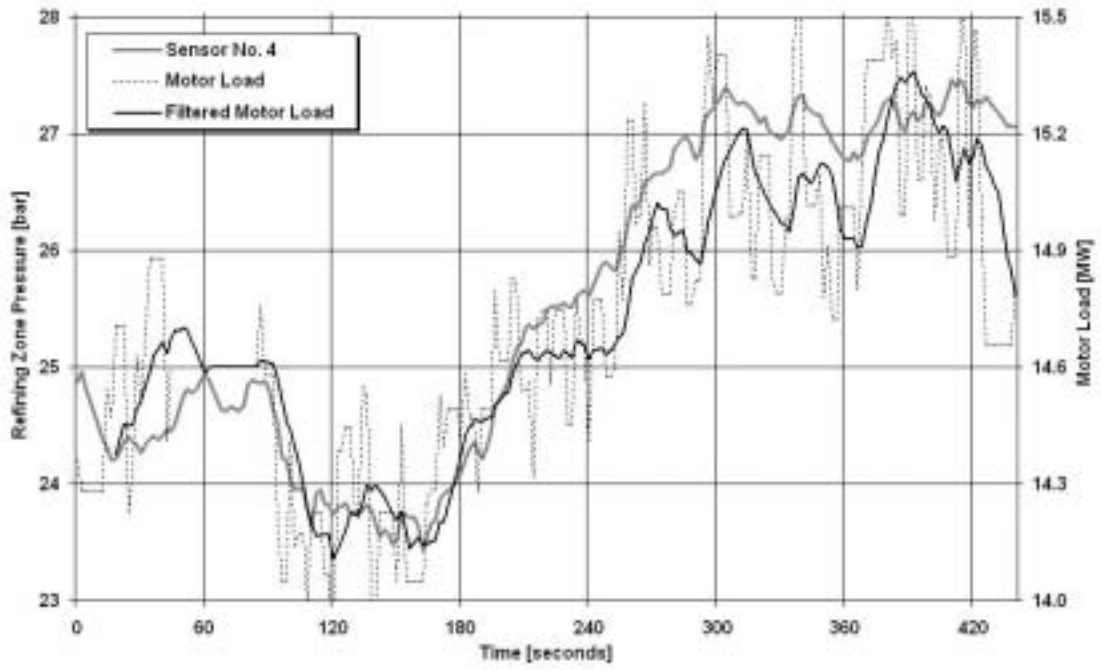

Figure 6.6: Average pressure measured by sensor No. 4 and the motor load obtained from the mill's DCS during the *Giri-gari* test, which was performed after 1000 operating hours.

6.2.4 Summing up

The plots shown in this section reveal that the pressure measurements have given the expected responses. The pressure signals have followed the casing pressure during the preheating process. The correlation between the pressure signal and the motor load were clearly visible when the distribution of chips to the refining zones was changed. High pressures are shown. Average pressures are indicated in the order of 20-30 bar measured by sensors located in the intermediate and fine bar zones. However, the pressure levels remain uncertain because the sinusoidal relationship between the pressures and the voltage output signals suffers from the lack of an appropriate demodulation scheme. Selection of the exact flange of the calibration curve is essential for determining the absolute pressure levels. The pressure levels chosen here have been based on the investigations of the signal fluctuations and the corresponding process data.

6.3 Dynamic properties of the voltage output signals

This section contains results from the analyses of the recorded data during different operational conditions. Pressure signals captured in the first main period of data recording are shown in the first section. These data were collected while the plates were new. The second section contains data series captured after approximately 1000 working hours of the plates. The sensors were not removed from the plates between these two main experimental periods.

The following figures display distinctive features from the response of the sensors. The selection of which data sets represent the responses from the sensors is based on subjective criteria. Both typical and special properties are shown to give an overview of the voltage output signals. This overview contains an extract of selected time series from each sensor recorded and the corresponding normalized amplitude spectrum. In addition, each selected recording, which contains 1 MSamples, is represented with a histogram.

Section 6.3.1 shows the data captured at sample rates of 0.5 or 1 MSamples/s. The amplitude spectra are based on the average of the FFT analyses made on 60 subsequent periods, each containing 2^{14} samples. The analysis results shown in Section 6.3.2 display data recorded at sample rates of 0.5, 1 or 5 MSamples/s. Here, the amplitude spectra are based on the average of the FFT analyses made on 2^{14} samples for data recorded at sample rates of 0.5 or 1 MSamples/s and 2^{17} samples for data recorded at a sample rate of 5 MSamples/s.

Each section contains a table summing up the results, Tables 6.1 and 6.2. These tables show the common observed frequencies, which can be related to the rotor plate geometry. The frequency analysis and the peak amplitudes for frequencies below 2 kHz are determined by FFT analysis of 2^{19} samples. In addition, the frequency analyses of the noise signals observed during unloaded conditions are quoted in a subsequent table, Table 6.3.

The text boxes on the opposite page from the diagrams give information about the recorded periods as well as characteristic properties of the prevailing process conditions. In addition, some assessments are made to explain what the analyses have revealed. The plots on the left-hand side correspond to the text box on the left-hand side and vice versa.

The reader can be helped through these sections by some descriptive figures. Figure 3.10, which shows the radial location of the sensors and in addition the periodic frequencies appeared from the plate geometry, is displayed in an extractable page in Appendix H. The sinusoidal transfer function curves are shown in Appendix C. Reference is also made to Section 6.9, in which some characteristic features known as harmonics and sideband frequencies are discussed. Several sensors have shown such effects as are illustrated in the figures below.

6.3.1 Measurements with new plates

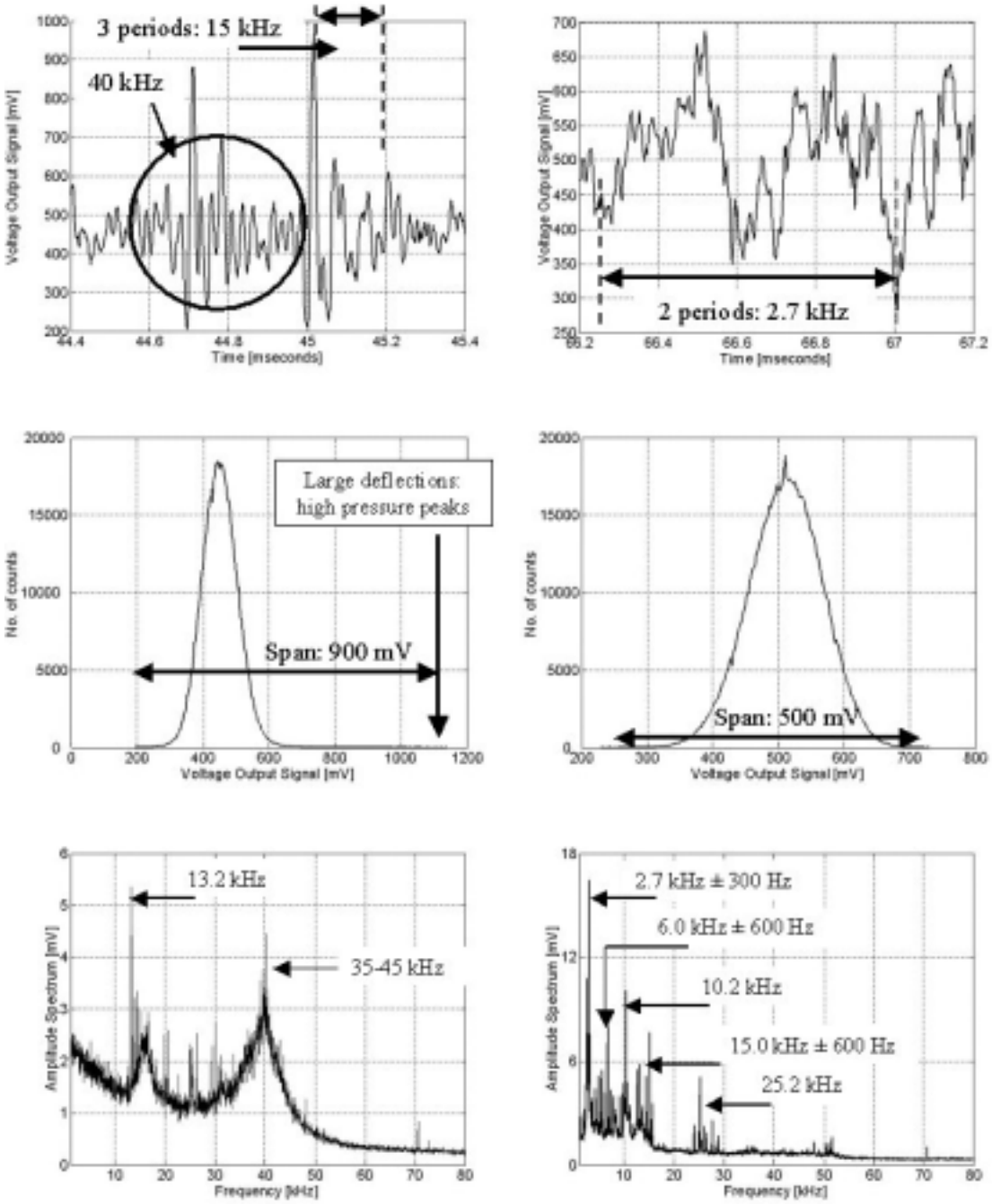

Figure 6.7: Sensor No. 1. Time series (upper plots), histograms (plots in the middle) and normalized amplitude spectra (lower plots).

Sensor No. 1 – radial loc. 567 mm
Recording period:
20 minutes after initial chip feeding.
Motor load: 12.5 MW
Hydraulic thrust: 113 bar
Production quantity: 280 tonnes/day
Dilution water flow: 1.55 litres/sec.
Temperature T0-DS: 158 ∀C

The process data were characteristic with the following properties:
- ∉ Low refining zone temperature. (Sat. water steam pressure: 5 bar)
- ∉ High hydraulic axial forces.
- ∉ Small amount of dilution water.

The readings from sensor No. 1 had the following properties:
- ∉ Large maximum span. Few readings outside a typical Gaussian distribution between 200 and 700 mV. Assumed average pressure: 4-5 bar. See Figure C1.
- ∉ The amplitude spectrum reveals small amplitudes. Frequencies:
  - 4 13.2 kHz: fit to the expected bar-crossing frequency at the location of the sensor and to the area between the coarse and the intermediate zones.
  - 4 25.2 kHz: observed by all the sensors (vibrations).
  - 4 35-45 kHz: a broad frequency band, assumed created by a stochastic variable (fibres).

It is assumed that large mechanical forces caused by the high axial thrust affected the readings. The low temperature indicates that the steam forces were weak. Thus, the bar-crossing frequency was visible and also the frequency band between 35 and 45 kHz, which is assumed, created by the pulp itself.

Sensor No. 1 – radial loc. 567 mm
Recording period:
6 hours after initial chip feeding.
Motor load: 12.9 MW
Hydraulic thrust: 103 bar
Production quantity: 296 tonnes/day
Dilution water flow: 2.0 litres/sec.
Temperature T0-DS: 170 ∀C

The process data were characteristic with the following properties:
- ∉ High refining zone temperature. (Sat. water steam pressure: 7 bar)
- ∉ Low hydraulic axial forces.
- ∉ High production rate.
- ∉ Large amount of dilution water.

The readings from sensor No. 1 had the following properties:
- ∉ Small span. Typical Gaussian distribution between 300 and 700 mV. Assumed average pressure: 5-6 bar. See Figure C1.
- ∉ The amplitude spectrum is dominated by frequencies arisen in the coarse zone as:
  - 4 2.7 kHz ∂ 300 Hz
  - 4 6.0 kHz ∂ 600 Hz
  - 4 10.2 kHz
  - 4 12.9 kHz ∂ 300 Hz
  - 4 15.0 kHz ∂ 600 Hz
- ∉ Additional frequencies:
  - 4 25.2 kHz ∂ 1200 Hz
  - 4 27.6 kHz: periphery or 2.4 kHz side frequency

It is assumed that the high production volume gave a thick pulp pad. The high temperature indicates that the steam forces were strong. Therefore, the mechanical forces were less dominating compared to the pulp flow activities shown by frequencies related to the coarse and the intermediate zones and the junction areas between these zones.

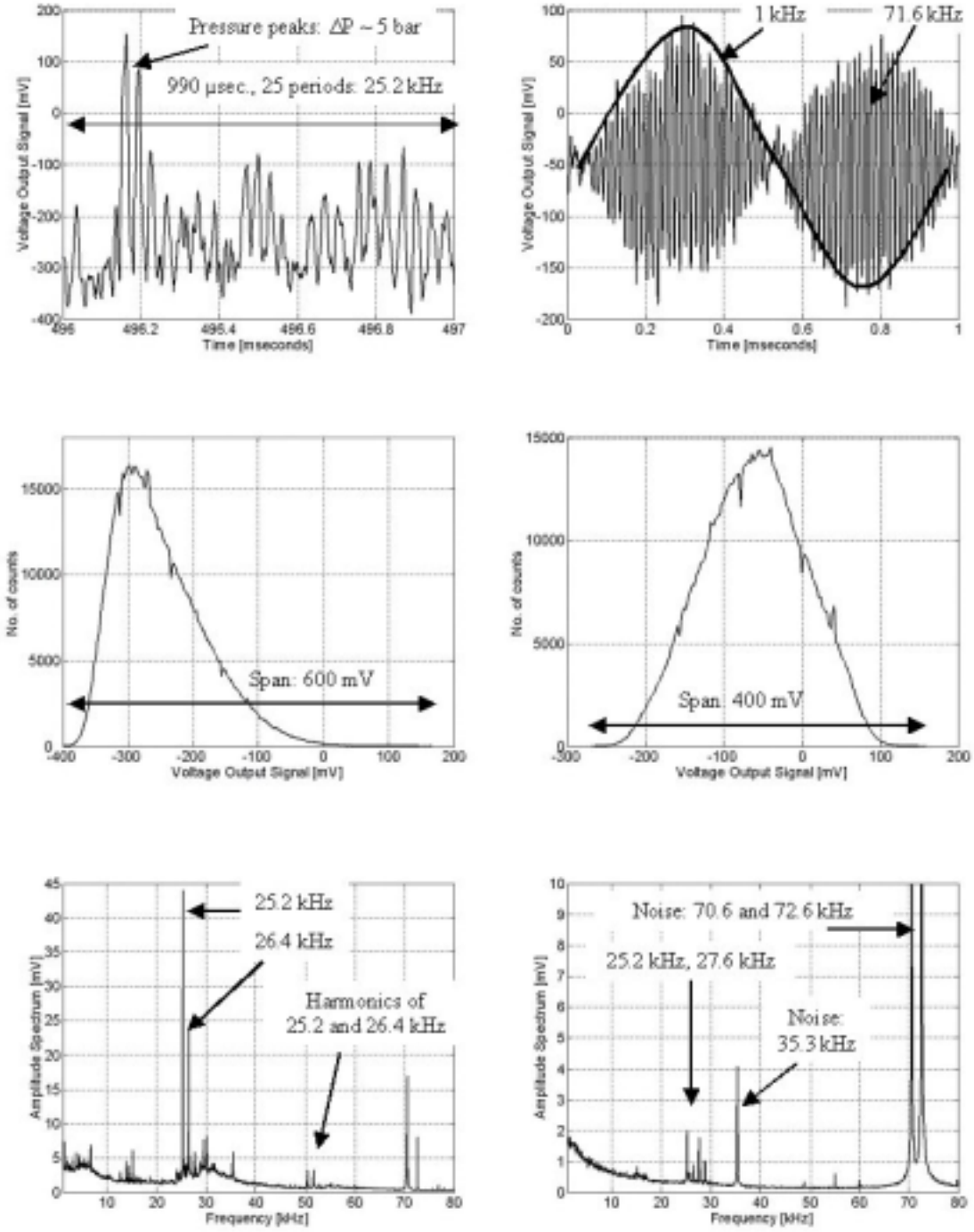

Figure 6.8: Sensor No. 2. Time series (upper plots), histograms (plots in the middle) and normalized amplitude spectra (lower plots).

Sensor No. 2 – radial loc. 579 mm
Recording period:
30 minutes after initial chip feeding.
Motor load: 12.8 MW
Hydraulic thrust: 114 bar
Production quantity: 280 tonnes/day
Dilution water flow: 1.7 litres/sec.
Temperature T1-DS: 157 ∀C

The process data were characteristic with the following properties:

- ∉ Low refining zone temperature. (Saturated water steam pressure: approximately 5 bar.)
- ∉ High hydraulic axial forces.

The readings from sensor No. 2 were characteristic with the following properties:

- ∉ Relative large maximum span. Some readings of high values. Distribution shifted towards minimum. Assumed average pressure of approximately 5-6 bar as indicated by Figure C2.
- ∉ The amplitude spectrum reveals relatively high amplitudes. The dominating frequencies are:
  - 4 25.2 kHz + 1200 Hz: observed by all the sensors (vibrations in the disc).
  - 4 50.4 kHz + 1200 Hz: harmonic frequency.
  - 4 1200 Hz.

The readings were dominated by the assumed vibrations in the disc, created by pressure pulses at the location that gives the 25.2 kHz bar-to-bar frequency. The low frequency of 1200 Hz probably appeared as a sideband effect caused by the ribbons in the breaker bar plates. The harmonic frequencies are visible probably because of the shift towards minimum of the calibration curve.

Sensor No. 2 – radial loc. 579 mm
Recording period:
20.5 hours after initial chip feeding.
Motor load: 14.1 MW
Hydraulic thrust: 107 bar
Production quantity: 269 tonnes/day
Dilution water flow: 2.0 litres/sec.
Temperature T1-DS: NA

The process data were characteristic with the following properties:

- ∉ Low hydraulic axial forces.
- ∉ Low production rate.
- ∉ Large amount of dilution water.

The readings from sensor No. 2 were characteristic with the following properties:

- ∉ Small span. Typical Gaussian distribution between -250 and 150 mV. Assumed average pressure of approximately 9 bar. See Figure C2.
- ∉ The amplitude spectrum is dominated by noise frequencies:
  - 4 71.6 kHz ∂ 1 kHz (70.6 and 72.6 kHz).
- ∉ Additional frequencies:
  - 4 25.2 kHz.
  - 4 27.6 kHz: periphery or 2.4 kHz side frequency.
  - 4 28.8 kHz: side frequency or harmonic of 14.4 kHz.

The recording was dominated by noise. The noise signal seems to be amplitude-modulated with a carrier frequency of 71.6 kHz and a modulation signal of 1 kHz or as contribution from two sources having 70.6 and 72.6 kHz signals. The mechanical pressure from the pulp is assumed to have contributed in a small extent. Assumed average pressure of approx. 9 bar corresponds to steam at a temperature of 180 ∀C.

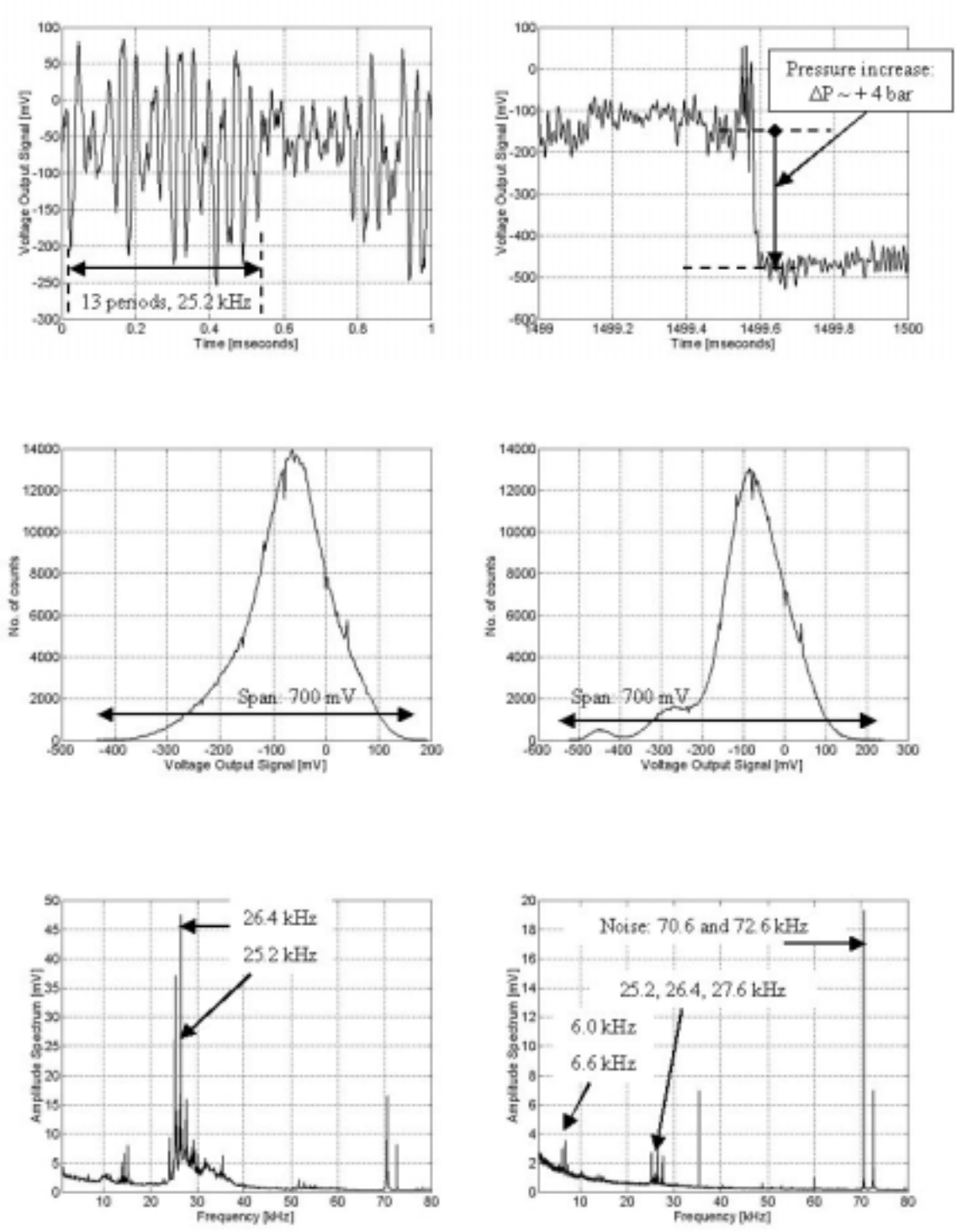

Figure 6.9: Sensor No. 7. Time series (upper plots), histograms (plots in the middle) and normalized amplitude spectra (lower plots).

Sensor No. 7 – radial loc. 579 mm

Recording period:
30 minutes after initial chip feeding.

Motor load:	12.6MW
Hydraulic thrust:	114 bar
Production quantity:	280 tonnes/day
Dilution water flow:	1.7 litres/sec.
Temperature T1-DS:	157∀C

The process data were characteristic with the following properties:

- ∉ Low refining zone temperature. (Saturated water steam pressure: approximately 5 bar)
- ∉ High hydraulic axial forces.

The readings from sensor No. 7 were characteristic with the following properties:

- ∉ Relative small span. Assumed average pressure of approx. 8 bar as indicated by Figure C3.
- ∉ The amplitude spectrum reveals relatively high amplitudes. The dominating frequencies were:
  - 4 25.2 kHz ∂ sideband frequencies, especially 1200 Hz.
  - 4 14.4 kHz ∂ 600 Hz

The assumed vibrations in the discs, created by pressure pulses at the location that gave the 25.2 kHz bar-to-bar frequency, dominated the measurements for this sensor too. The low frequencies of 600 and 1200 Hz appeared as sideband frequencies.

Sensor No. 7 – radial loc. 579 mm

Recording period:
7.5 hours after initial chip feeding.

Motor load:	14.5MW
Hydraulic thrust:	112 bar
Production quantity:	263 tonnes/day
Dilution water flow:	1.7 litres/sec.
Temperature T1-DS:	161 ∀C

The process data were characteristic with the following properties:

- ∉ Low refining zone temperature. (Saturated water steam pressure: approximately 5.5 bar)
- ∉ High hydraulic axial forces.
- ∉ Low production rate.

The readings from sensor No. 7 had the following properties:

- ∉ Small span. The distribution is split in one main and two smaller distributions shifted towards minimum. The shift towards minimum indicates higher pressure. The main distribution was moved a few mV towards minimum compared with the readings shown to the left. Assumed average pressure of approximately 9 bar, given by Figure C3.
- ∉ The amplitude spectrum was dominated by noise frequencies:
  - 4 70.6 and 72.6 kHz
- ∉ Additional frequencies:
  - 4 25.2 kHz
  - 4 26.4 kHz: 1200 Hz side frequency of 25.2 kHz
  - 4 27.6 kHz: periphery frequency or side frequency of 2.4 kHz from 25.2 kHz.

The recordings were weakly affected by the pulp and flow patterns. The steam pressure has been assumed to dominate the readings.

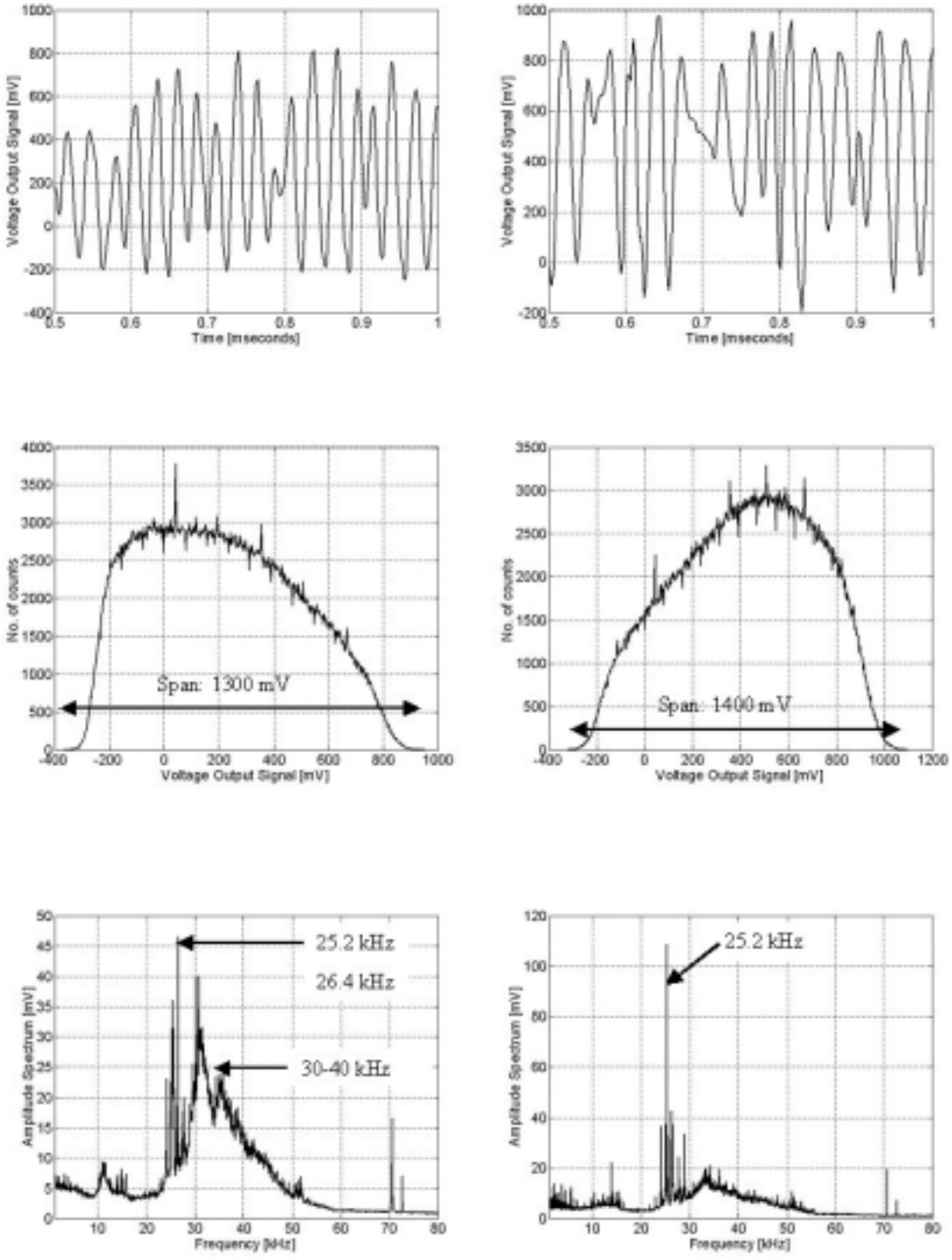

Figure 6.10: Sensor No. 4. Time series (upper plots), histograms (plots in the middle) and normalized amplitude spectra (lower plots).

Sensor No. 4 – radial loc. 592 mm
Recording period:
20 minutes after initial chip feeding.
Motor load: 12.7 MW
Hydraulic thrust: 114 bar
Production quantity: 280 tonnes/day
Dilution water flow: 1.6 litres/sec.
Temperature T2-DS: 163 ∀C

The process data were characteristic with the following properties:

- ∉ Low refining zone temperature. (Saturated water steam pressure: approximately 6 bar.)
- ∉ High hydraulic axial forces.
- ∉ Small amount of dilution water.

The readings from sensor No. 4 had the following properties:

- ∉ Large span. The distribution is shifted towards minimum. Pressure, peak–to-peak, variations of at least ∂ 5 bar (one flange of the calibration curve). Assumed average pressure: −13 or −26 bar, see Figure C4.
- ∉ The amplitude spectrum reveals relatively high amplitudes. The dominating frequencies are:
  - 4 25.2 kHz and sideband frequencies.
  - 4 30-40 kHz.

The assumed vibrations in the discs, created by pressure pulses at the location that gave the 25.2 kHz bar-to-bar frequency, dominated the signal. A frequency band between 30 and 40 kHz was clearly visible. The assumption is that a stochastic variable as the pulp, through the fibre and flocs, created this signal pattern. The assumed reason is related to the high hydraulic forces and the assumed small contribution of steam forces.

Sensor No. 4 – radial loc. 592 mm
Recording period:
9.5 hours after initial chip feeding.
Motor load: 13.8MW
Hydraulic thrust: 108 bar
Production quantity: 280 tonnes/day
Dilution water flow: 1.9 litres/sec.
Temperature T2-DS: 167 ∀C

The process data were characteristic with the following properties:

- ∉ Relative low refining zone temperature. (Saturated water steam pressure: approximately 7 bar.)

The readings from sensor No. 4 had the following properties:

- ∉ Large span. The distribution is shifted towards maximum. Pressure, peak-to-peak, variations of at least ∂ 5 bar. Assumed average pressure: −16 or −25 bar, see Figure C4.
- ∉ The amplitude spectrum was strongly dominated by the 25.2 kHz and additional sidebands.
- ∉ Additional frequencies:
  - 4 14.4 kHz ∂ 300 Hz
  - 4 13.8 kHz.
  - 4 600 Hz (bolt holes in the plates).

The recording was strongly affected by the common vibrations created by the pressure pulses in the fine bar pattern zone, located in the area dominated by the 25.2 kHz bar-crossing frequency.

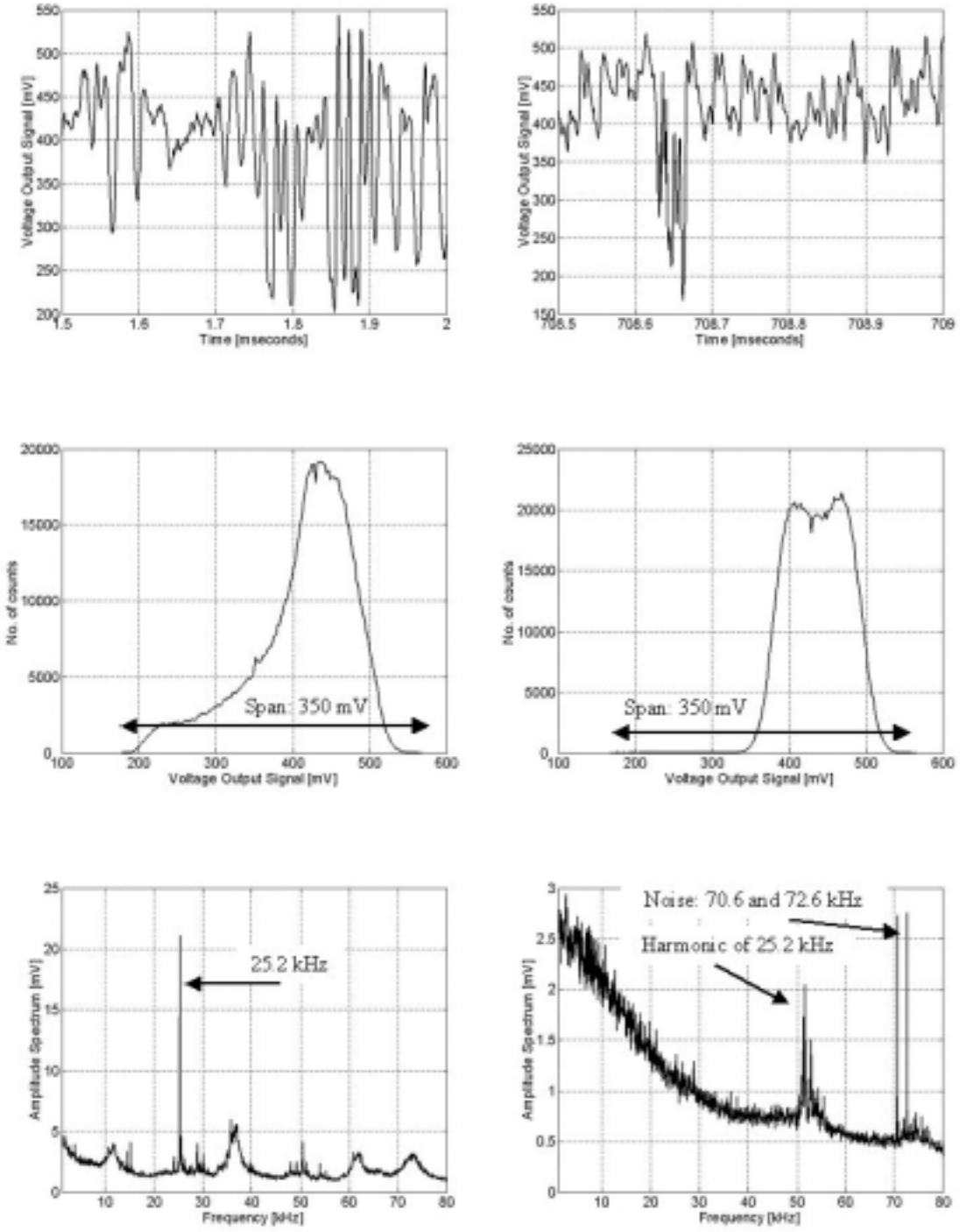

Figure 6.11: Sensor No. 5. Time series (upper plots), histograms (plots in the middle) and normalized amplitude spectra (lower plots).

Sensor No. 5 – radial loc. 627 mm
Recording period:
30 minutes after initial chip feeding.
Motor load: 12.8 MW
Hydraulic thrust: 114 bar
Production quantity: 280 tonnes/day
Dilution water flow: 1.7 litres/sec.
Temperature T3-DS: 160 ∀C

The process data were characteristic with the following properties:

- Low refining zone temperature. (Saturated water steam pressure: approximately 5 bar.)
- High hydraulic axial forces.
- Small amount of dilution water.

The readings from sensor No. 5 had the following properties:

- Small span. The distribution was shifted towards maximum. The readings from sensor No. 5 have not been fitted into a pressure range because of an unsatisfactory calibration curve, as shown in Figure C5.
- The amplitude spectrum reveals:
  - The 25.2 kHz vibration frequency.
  - A frequency band between 35 and 40 kHz.

The assumed common vibrations in the discs, shown as the 25.2 kHz bar-to-bar frequency, dominated the recording. Because of the faulty calibration curve, which is assumed caused by a too thick layer of protective silicon rubber on the sensor surface, it was assumed that this sensor should respond only when high-pressure pulses were present. In spite of that, it shows the 25.2 kHz clearly, indicating that these vibrations were powerful.

Sensor No. 5 – radial loc. 627 mm
Recording period:
19.5 hours after initial chip feeding.
Motor load: 13.9MW
Hydraulic thrust: 107 bar
Production quantity: 269 tonnes/day
Dilution water flow: 2.0 litres/sec.
Temperature T3-DS: NA

The process data were characteristic with the following properties:

- Low production rate.
- Relative large amount of dilution water.

The readings from sensor No. 5 had the following properties:

- Small span. The maximum span was about the same range as shown in the histogram to the left. However, a great majority of the readings was connected to a smaller part of the distribution.
- The amplitude spectrum does not show any high frequency peaks. The noise frequencies dominated the spectrum together with some frequencies that could be related to harmonic frequencies of the 25.2 kHz.

This recording was hardly affected by anything related to the actions in the refining zone. The lack of well-fitted surface layer on the sensor seems to have caused the weak responses. Some few high-pressure pulses might have been present as shown in the time series as well as indicated by the maximum span in the corresponding histogram.

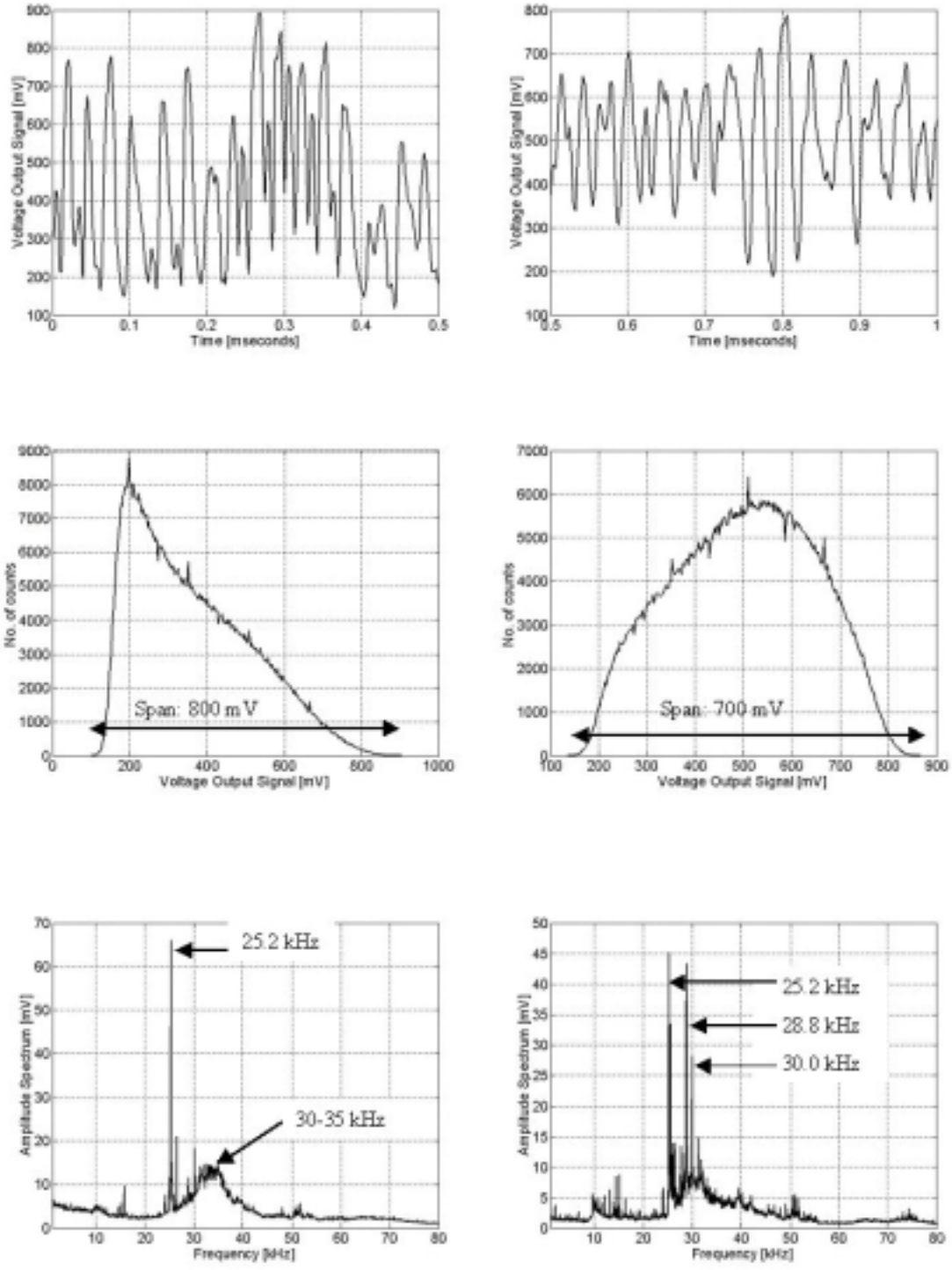

Figure 6.12: Sensor No. 6. Time series (upper plots), histograms (plots in the middle) and normalized amplitude spectra (lower plots).

Sensor No. 6 – radial loc. 695 mm
Recording period:
20 minutes after initial chip feeding.
Motor load: 12.4 MW
Hydraulic thrust: 113 bar
Production quantity: 280 tonnes/day
Dilution water flow: 1.6 litres/sec.
Temperature T5-DS: 162 ∀C

The process data were characteristic with the following properties:
- ∉ Low refining zone temperature. (Saturated water steam pressure: approximately 5.5 bar.)
- ∉ High hydraulic axial forces.
- ∉ Small amount of dilution water.

The readings from sensor No. 6 had the following properties:
- ∉ Large span. The distribution was shifted strongly towards minimum. The pressure variations (peak-to-peak) are assumed to be at least ∂ 5 bar (one flange of the calibration curve). Assumed average pressure: −13 or −27 bar, see Figure C6.
- ∉ The amplitude spectrum reveals relatively high amplitudes. The dominating frequencies were:
  - 4 25.2 kHz and its sideband frequencies.
  - 4 30-35 kHz frequency band.

The sensor has picked up the assumed vibrations in the discs, created by the pressure pulses at the location that gave the 25.2 kHz bar-to-bar frequency. The frequency band between approximately 30 and 35 kHz was clearly visible. The assumption is that the pulp, through the fibre and flocs, has created this signal pattern.

Sensor No. 6 – radial loc. 695 mm
Recording period:
7.5 hours after initial chip feeding.
Motor load: 14.4 MW
Hydraulic thrust: 112 bar
Production quantity: 263 tonnes/day
Dilution water flow: 1.7 litres/sec.
Temperature T5-DS: 173 ∀C

The process data were characteristic with the following properties:
- ∉ Relative high refining zone temperature. (Saturated water steam pressure: approx. 8 bar.)
- ∉ High hydraulic axial forces.
- ∉ Low production rate.

The readings from sensor No. 6 had the following properties:
- ∉ Large span. The distribution was symmetric. Based on the assumption that the readings covered the whole flange of the calibration curve the average value was lying approximately at the middle of the flange. The pressure variations (peak-to-peak) are assumed to be at least ∂ 5 bar. Assumed average pressure: −15 or −26 bar, see Figure C6.
- ∉ The amplitude spectrum is strongly dominated by the 25.2 kHz and its sidebands.
- ∉ Additional frequencies:
  - 4 28.8 kHz: sideband (3.6 kHz from 25.2 kHz) or harmonic of 14.4 kHz.
  - 4 30.0 kHz: sideband (4.8 kHz from 25.2 kHz) or harmonic of 15.0 kHz.

The recording was strongly affected by the common vibrations (25.2 kHz) created by the pressure pulses 12 mm outwards the location of sensor No. 6.

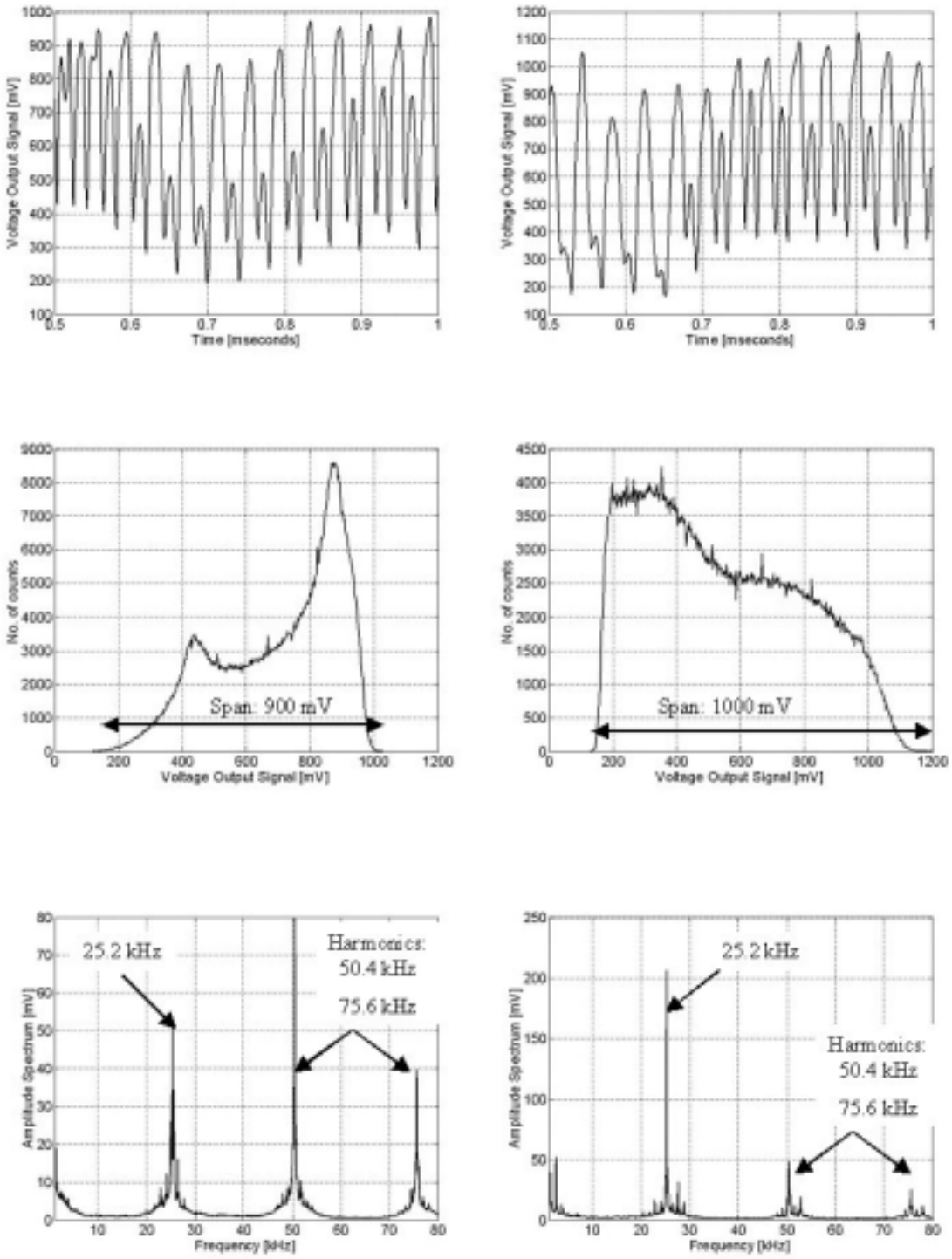

Figure 6.13: Sensor No. 8. Time series (upper plots), histograms (plots in the middle) and normalized amplitude spectra (lower plots).

Sensor No. 8 – radial loc. 707 mm
Recording period:
20 minutes after initial chip feeding.
Motor load: 12.7 MW
Hydraulic thrust: 114 bar
Production quantity: 280 tonnes/day
Dilution water flow: 1.6 litres/sec.
Temperature T6-DS: 163 ∀C

The process data were characteristic with the following properties:

- ∉ Low refining zone temperature. (Saturated water steam pressure: approximately 6 bar.)
- ∉ High hydraulic axial forces.
- ∉ Small amount of dilution water.

The readings from sensor No. 8 had the following properties:

- ∉ Relative large span. The distribution was influenced by a sinusoidal effect (saddle shape) shown as one peak at each side of the distribution. The distribution was shifted towards maximum. A conservative estimate is that the pressure variations (peak-to-peak) were approximately ∂ 5 bar (one flange of the calibration curve). Assumed average pressure: –14 or –26 bar, see Figure C7.
- ∉ The amplitude spectrum reveals high peak amplitudes. The dominating frequencies were:
  - 4 25.2 kHz and its harmonics.
- ∉ Additional frequencies:
  - 4 25, 300 and 1200 Hz as single and sideband frequencies.

The radial location of sensor No. 8 corresponded with the origin of the vibrations in the discs, assumed created by pulp squeezed between rotor and stator bars. Therefore, the high amplitude of this frequency has been shown.

Sensor No. 8 – radial loc. 707 mm
Recording period:
20.5 hours after initial chip feeding.
Motor load: 14.4 MW
Hydraulic thrust: 107 bar
Production quantity: 269 tonnes/day
Dilution water flow: 2.0 litres/sec.
Temperature T6-DS: NA

The process data were characteristic with the following properties:

- ∉ Low production rate.
- ∉ Large amount of dilution water.

The readings from sensor No. 8 had the following properties:

- ∉ Large span. The distribution was shifted towards minimum. The pressure variations (peak-to-peak) are assumed to be some higher than ∂ 5 bar because of the asymmetric distribution. Assumed average pressure: –17 or –23 bar, see Figure C7.
- ∉ The amplitude spectrum was strongly dominated by the 25.2 kHz (bar crossing frequency) and its sidebands.
- ∉ Additional frequencies:
  - 4 25, 300 and 1200 Hz as single and sideband frequencies.

The recording was strongly affected by the common vibrations created by the pressure pulses (bar-to-bar passage) approximately at the same location as this sensor. The pattern of the time series has given indication of a modulated signal, created by periodical fluctuations in the pulp flow and shown as sideband frequencies. This effect has probably affected the pressure. The harmonic and sideband frequencies probably appeared from modulation effects as discussed in Section 6.9.

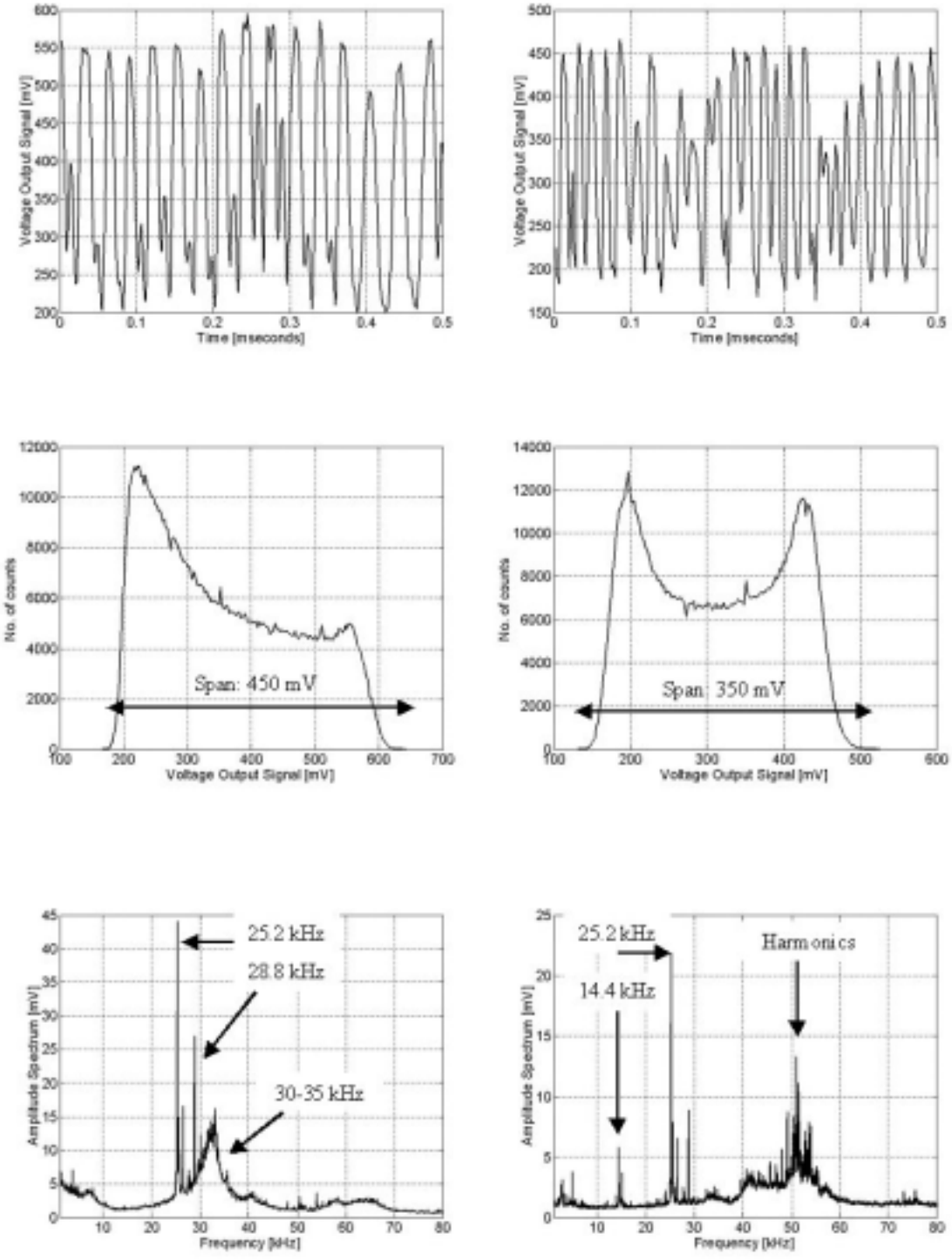

Figure 6.14: Sensor No. 9. Time series (upper plots), histograms (plots in the middle) and normalized amplitude spectra (lower plots).

Sensor No. 9 – radial loc. 720 mm
Recording period:
30 minutes after initial chip feeding.
Motor load: 12.8 MW
Hydraulic thrust: 114 bar
Production quantity: 280 tonnes/day
Dilution water flow: 1.7 litres/sec.
Temperature T7-DS: 162 ∀C

The process data were characteristic with the following properties:

- ∉ Low refining zone temperature. (Saturated water steam pressure: approximately 6 bar.)
- ∉ High hydraulic axial forces.
- ∉ Small amount of dilution water.

The readings from sensor No. 9 had the following properties:

- ∉ Relative large span. The distribution was shifted towards minimum. It is assumed that the pressure variations (peak-to-peak) were somewhat higher than ∂ 5 bar (if the signal crossed the minimum of the calibration curve). Assumed average pressure: −14 or −24 bar, see Figure C8.
- ∉ The amplitude spectrum reveals high peak amplitudes. The dominating frequencies were:
  - 4 25.2 kHz and its sidebands.
- ∉ Additional frequencies:
  - 4 28.8 kHz: sideband or harmonics of the 14.4 kHz.
  - 4 30-35 kHz frequency band.

The common frequency at 25.2 kHz dominated. The frequency band between 30-35 kHz indicates an effect created by a stochastic variable, which was assumed to be mechanical in origin.

Sensor No. 9 – radial loc. 720 mm
Recording period:
4.5 hours after initial chip feeding.
Motor load: 13.1 MW
Hydraulic thrust: 108 bar
Production quantity: 280 tonnes/day
Dilution water flow: 1.9 litres/sec.
Temperature T7-DS: 173 ∀C

The process data were characteristic with the following properties:

- ∉ High refining zone temperature (Saturated water steam pressure: approximately 8 bar.)
- ∉ Low hydraulic axial forces.
- ∉ Large amount of dilution water.

The readings from sensor No. 9 had the following properties:

- ∉ Relative large span. The distribution was influenced by a sinusoidal effect revealed as one peak at each side of the distribution. The distribution was symmetric. The pressure (peak-to-peak) variations are assumed to be somewhat higher than ∂ 5 bar because of the sharp edges of the histogram. Assumed average pressure: −14 or −24 bar, see Figure C8.
- ∉ The amplitude spectrum was strongly dominated by the 25.2 kHz and its first harmonic with their sideband frequencies.
- ∉ Additional frequency: 14.4 kHz.

The recording was strongly affected by the common vibrations of 25.2 kHz. However, the peak frequency at 14.4 kHz indicates that the pressure pulses generated in the intermediate zone affected the pressure measurements in this recording more than recordings performed earlier in the experiment.

Table 6.1: Amplitude spectrum peaks – 20-30 min. after initial chip feeding.

Sensor	25 [Hz]	300 [Hz]	600 [Hz]	1200 [Hz]	5.4 [kHz]	6.0 [kHz]	13.2 [kHz]	14.4 [kHz]	25.2 [kHz]	26.4 [kHz]	70.6 [kHz]
	[mV] [dB]	[mV] [dB]	[mV] [dB]	[mV] [dB]	[mV] [dB]	[mV] [dB]	[mV] [dB]	[mV] [dB]	[mV] [dB]	[mV] [dB]	[mV] [dB]
1	-	-	-	-	-	-	5.5 11	3.4 7	2.4 7	2.6 7	0.8 9
2	-	-	4.2 13	6.5 16	4.3 9	4.3 9	-	3.5 7	43 33	22 23	14 31
7	-	-	2 6	4 12	-	-	2 6	6.5 16	36 31	43 33	15 38
4	7 11	-	12 16	2 6	-	-	-	[1]	30 16	43 19	15 27
5	7.5 18	-	-	-	-	-	-	3 10	19 26	2 6	-
6	9.2 15	-	2.5 3	5.2 10	-	4.5 3	-	4.3 7	55 21	18 11	-
8	19 16	14 13	-	19 20	-	-	-	-	50 36	13 24	-
9	8.5 13	-	-	5 8	-	-	-	1.4 3	42 20	15 11	-

1) ∂ 600 Hz : 6-8 mV (6-8 dB).

Table 6.2: Amplitude spectrum peaks– 4.5–20.5 hours after initial chip feeding.

Sensor	25 [Hz]	300 [Hz]	600 [Hz]	1200 [Hz]	5.4 [kHz]	6.0 [kHz]	13.2 [kHz]	14.4 [kHz]	25.2 [kHz]	26.4 [kHz]	70.6 [kHz]
	[mV] [dB]	[mV] [dB]	[mV] [dB]	[mV] [dB]	[mV] [dB]	[mV] [dB]	[mV] [dB]	[mV] [dB]	[mV] [dB]	[mV] [dB]	[mV] [dB]
1	4.7 16	2.2 10	2.5 11	1.5 6	4.2 9	5.7 12	4.9 14	7 17	3.8 18	1.6 10	1 12
2	-	-	-	-	-	-	-	[2]	2.6 19	0.7 7	47 53
7	-	-	3.4 9	-	-	2.6 7	-	0.9 4	3.5 19	3 18	19 42
4	5.5 9	4 6	21 20	10 14	10.5 8	7 5	-	[3]	88 23	30 14	19 28
5	1.9 4	-	-	-	-	-	-	-	1.1 2	1 1	2.7 15
6	3.1 10	-	-	1.2 6	[4]	1.5 4	6 14	8.2 17	39 28	12 18	-
8	55 21	64 22	10 6	45 19	-	-	-	-	150 31	27 17	-
9	2.6 16	1.1 9	-	0.8 6	-	-	-	6.5 19	21 26	7 17	-

2) 15.0 kHz : 0.8 mV (6 dB), 3) ∂ 300 Hz : 10 mV (8 dB), 4) ∂ 600 Hz : 1.5-1.8 mV (4-5 dB), 5) ∂ 1200 Hz : 2.5-2.7 mV (8-9 dB).

6.3.2 Summing up

The findings can be summarized as follows:

- Several periodic patterns were common for data from all of the sensors. Atack and Stationwala (1975) made similar observations. In the present study, the frequencies related to fine bar pattern area (25.2 and 26.4 kHz) and the frequency related to the junction between the intermediate and the fine bar pattern zones (14.4 kHz.) was clearly visible. The 25.2 kHz peak frequency dominated in the amplitude spectra. This periodicity seems to have contributed as the main dynamic pressure signal.
- The signal pattern with a periodicity of 25.2 kHz coincided with the bar-to-bar passage at the radial location of sensor No. 8. Data recorded from this sensor showed the 25.2 kHz signal extremely clearly. In addition to sensor No. 8, sensors No. 6 and 9 were located within the same area in the refining zone as the common 25.2 kHz pressure pulse frequency. However, the other sensors located in the intermediate zone did not measure pressure signals that were dominated by their local bar crossing frequencies. A possible reason is that the tapered plate gap due to its width, prevented disruption of the pulp pad. It is conceivable that the bar pattern on the rotor disc disrupted the pulp pad on the rotor side, while the pulp pad on the stator side was changed to a minor extent. Thus, the sensors measured pressure fluctuations in the pulp pad that were predominant compared to the local generated pressure pulses. This assumption is probably close to the concept of gentle refining as described by Härkönen and Tienvieri (2001).
- The reason why the 25.2 kHz was detected by all the sensors independent of the radial location is probably vibrations in the refiner discs generated by the pressure pulses at this location. The radial location of sensor No. 8 and the basis area for the 25.2 kHz signal was lying about 26 mm outside the boundary line of the taper of the stator plates and 39 mm outside the corresponding point of the rotor plates. A hypothesis regarding why the signal occurred at this location may be that the pulp flow met a smaller plate gap and therefore resisted the outward pulp flow. As a consequence a denser pulp pad was probably built up and the pulp was beaten more continuously and harder. The vibrations propagated through the rigid discs causing vibrations as well as disturbances in the pulp flow. Thus, sensors in all locations picked up these periodic disturbances. This hypothesis is supported by vibration measurements as discussed in Chapter 7. Both Ouellet and Weiss (1994) and Ohls and Syrjänen (1976) have discussed vibration effects in disc refiners. From their studies it cannot be assumed that the vibrations generated large plate gap fluctuations.
- Another point of view is that the sensors have picked up vibrations in the disc that had nothing to do with the pulp flow. However, this is probably not the case. The sensors were built by two main parts as the end of the optic fibre itself and a mirror (another end of an optic fibre) separated by a distance smaller than 0.1 mm. A glass tube housed the main parts, which in addition was surrounded by silicon oil (brake fluid). Furthermore, these parts were protected by means of a stainless steel tube. In a hypothetic case the sensors could pick up vibrations that were not generated in front of the sensor surface. To do so, one of the main parts had to be affected by the vibrations while the other was at rest. It is not very likely that vibrations, which not synchronized the two main parts of the sensor, could be present. In addition, the amplitudes of the 25.2 kHz signals were very high indicating that the sensor surface

was exposed to strong forces. Furthermore, it is indicated in Section 7.4 that the pressure sensors were not affected by vibrations operating in resonance. This strongly supports the conclusion that the fibre-optic pressure sensors were solely measuring the activities in the refining zone. In addition, the manufacturer of the sensors has indicated that because of the small size of the sensors, large g forces have to be present if the sensor should be affected by vibrations[12].

- Shortly after start-up, a high-frequency band between 30-40 kHz was present in the data from several sensors (sensor Nos. 1, 4, 6, and 9). Similar signal patterns were observed in data sets recorded during the initial chip feeding too as shown in Figures F1 and F2. A relatively cold refiner may have caused this behaviour because the steam production had not risen to a level that could reduce gap fluctuations due to variations in the pulp flow. It can be assumed that the density of the pulp pad changed through the refining zone. A smaller amount of steam surrounding the pulp pad could cause larger influence on the measurements than a pulp pad surrounded and penetrated by higher temperature steam. It can be assumed that the steam had a damping effect on the density variations of the pulp pad. In addition, the hydraulic thrust was higher when the first data set of each sensor was captured than in the subsequent recordings. The higher axial pressure and the lack of steam to counteract the high hydraulic forces may be a reason for this observation. Another speculation is that the lack of enough steam and heat created less flexible chips and flocs of fibres. Any of these effects can have caused the differences shown in the amplitude spectra. A possible explanation for the frequency band between approximately 30 and 40 kHz may be associated with the mechanical forces acting on the flocs of fibres. The broad frequency band as distinctive from the plain peak frequencies, support the assumption that these observations have arisen from a source of random nature. Fibres and flocs of fibres can definitively be associated with such source. Therefore, this frequency range may be associated with the sizes of the flocs of fibres or the velocity of the fibres moving along the bars.
- The amplitude spectra contained several sideband effects, which are further discussed in Section 6.9. However, the sideband effect can be interpreted as various wave patterns. It is conceivable that the pulp flow propagates radially outwards in waves caused by low-frequency disturbances as feeding variations and interruptions by the ribbon feeder or coarse bars. The high frequency influence of the pulp flow by the fine bars appears as the carrier frequency in the modulated signal. Most common sidebands were related to frequencies, which can be found in the early stage of chip-flow interaction with the refiner. The rotational velocity, 25 revolutions per second, was visible as a periodic signal with the frequency of 25 Hz. In vibration analysis this is a well-known phenomenon regarding gears and vanes. The running speed occurs as sideband to the gear-mesh frequency respective the vane passing frequency (Wowk (1991)). Pettersen and Gunstrøm (1980) reported similar effects when they investigated the origin of noise and vibrations from beaters and refiners. Moreover, the frequency of 1200 Hz, which can be related to the number of coarse bars on the breaker bar plates (48 bars per revolution), was

[12] According to calculations by Luna Innovations Inc., for the sensor to see an equivalent of 1 bar of pressure from mechanical vibration, it would require accelerations roughly 31 000 times the force of gravity.

also pronounced. The frequencies of 300 and 600 Hz appeared as sidebands as well. These frequencies can be associated with the number of bolt holes in the breaker bar segments and the bolt holes in the plates respectively. The 300 Hz can also be related to the number of plates per circle.

- In several data sets, second and third harmonic frequencies have appeared. The second harmonic frequencies of the 25.2 kHz and its side frequencies appeared in several of the data sets. This was extremely clear in the data recorded from sensor No. 8 as shown in Figure 6.13. The non-linear calibration curve created the harmonic signals when the pressure variation was larger than one monotonically rising flange of the sinusoidal transfer function curve. However, variations of the output signals were distorted independent of the signal crossed a maximum or minimum of the sinusoidal curve because of the non-linearity. Harmonic effects are well-known phenomena in vibration analysis (Wowk (1991), Pettersen and Gunstrøm (1980)).
- Other peak frequencies that were observed, but not quoted in Tables 6.1 and 6.2 were typical harmonic and sideband frequencies such as 900, 1500, 1800, 2400, 2700 and 3600 Hz in the low-frequency band. In other frequency bands 6.6, 9.9, 10.2, 27.6 and 28.8 kHz were found. The frequency of 27.6 kHz may be a sideband frequency of the 25.2 kHz. However, the bar pattern at the plate periphery can also be associated with this frequency. In addition, the frequencies of 27.6 and 28.8 kHz can be related to harmonic frequencies of 13.8 and 14.4 kHz.
- Noise-generated signal patterns were present as well. In several data sets especially the 70.6 kHz and its half frequency of 35.3 kHz were visible. The frequency of 72.6 kHz, separated by 2 kHz from 70.6 kHz, was often visible too. These two highest frequencies occurred probably as an effect of amplitude modulation between a low frequency signal of 1 kHz and a high frequency signal of 71.6 kHz or as an effect of the combination of two separate frequencies (70.6 and 72.6 kHz) arising from two different sources that interfered and appeared as a common noise. The last effect is called beats in the vibration analysis (Wowk (1991)). The second time series from sensor No. 2, shown as the right-hand plot in Figure 6.8, was particularly affected by the amplitude-modulated noise signal. Table 6.4, shown in Section 6.3.5, gives an overview of the noise signals.

6.3.3 Measurements after 1000 working hours

The dynamic properties of the voltage output signals recorded after 1000 working hours are displayed in the same manner as previous plots and tables. Selected data sets are displayed to give an overview of similarities and differences between the responses of the sensors before and after the long exposure to the harsh environment. Signals from some sensors were in addition captured under different operational conditions during this part of the experiment. The latter is related to recordings undertaken before and after adjustment of the screw angle of the load sense conveyor. This adjustment can be used to equalize the refining conditions between the two refining zones of the Twin-refiner through changing the distribution of chips to the refining zones.

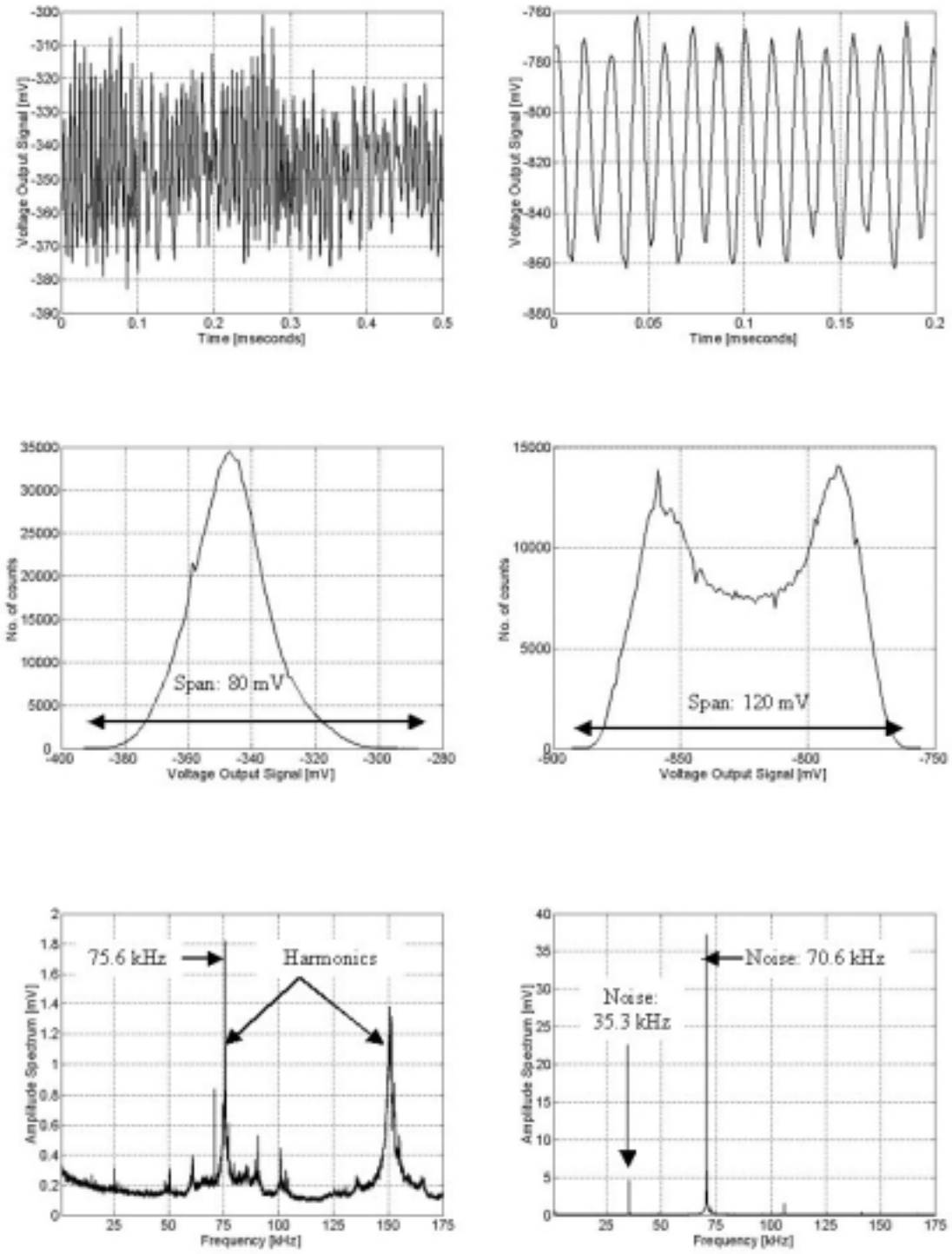

Figure 6.15: Sensor No. 1 (left) and sensor No. 2 (right). Time series (upper plots), histograms (plots in the middle) and ampltude spectra (lower plots).

Sensor No. 1 – radial loc. 567 mm

Recording period:
30 min. after the start of recording

Motor load:	14.6 MW
Hydraulic thrust:	118 bar
Production quantity:	285 tonnes/day
Dilution water flow:	2.0 litres/sec.
Acceleration-DS:	12.1 %

The process data were characteristic with the following properties:

- High hydraulic axial forces.
- Relative high acceleration.

The readings from sensor No. 1 had the following properties:

- Small span. The amplitudes of the output signals were strongly damped compared with the corresponding readings in the first main period.
- An offset had occurred compared with the recordings in the first main period.
- The amplitude spectrum reveals small peak amplitudes. The dominating frequencies were:
  - 75.6 kHz and its harmonic.
- Additional frequencies:
  - 25.2 kHz
  - 70.6 kHz (noise).

The readings showed that the sensor has picked up some process related signals. However, the amplitudes were strongly reduced. The source of damping may be connected to fibrous material built up in front of the sensor surface during the 1000 operating hours.

The plain peak frequencies associated with the harmonics of 25.2 kHz, especially the 75.6 kHz signal, were probably caused by the worn plate pattern.

Sensor No. 2 – radial loc. 579 mm

Recording period:
1 hour after the start of recording

Motor load:	14.6 MW
Hydraulic thrust:	118 bar
Production quantity:	285 tonnes/day
Dilution water flow:	2.0 litres/sec.
Acceleration-DS:	12.4 %

The process data were characteristic with the following properties:

- High hydraulic axial forces.
- Relative high acceleration.

The readings from sensor No. 2 had the following properties:

- Small span. The distribution was dominated by a sinusoidal effect shown as one peak at each side of the distribution. The distribution was symmetric.
- The amplitude spectrum contains of noise frequencies only.

The recording was solely noise signals. The level of the output signals showed a corresponding value as measured without any sensor connected to the data acquisition system as shown in Table 6.4. The sensor cable had probably been broken so that no light was transmitted between the sensor and the amplifier unit.

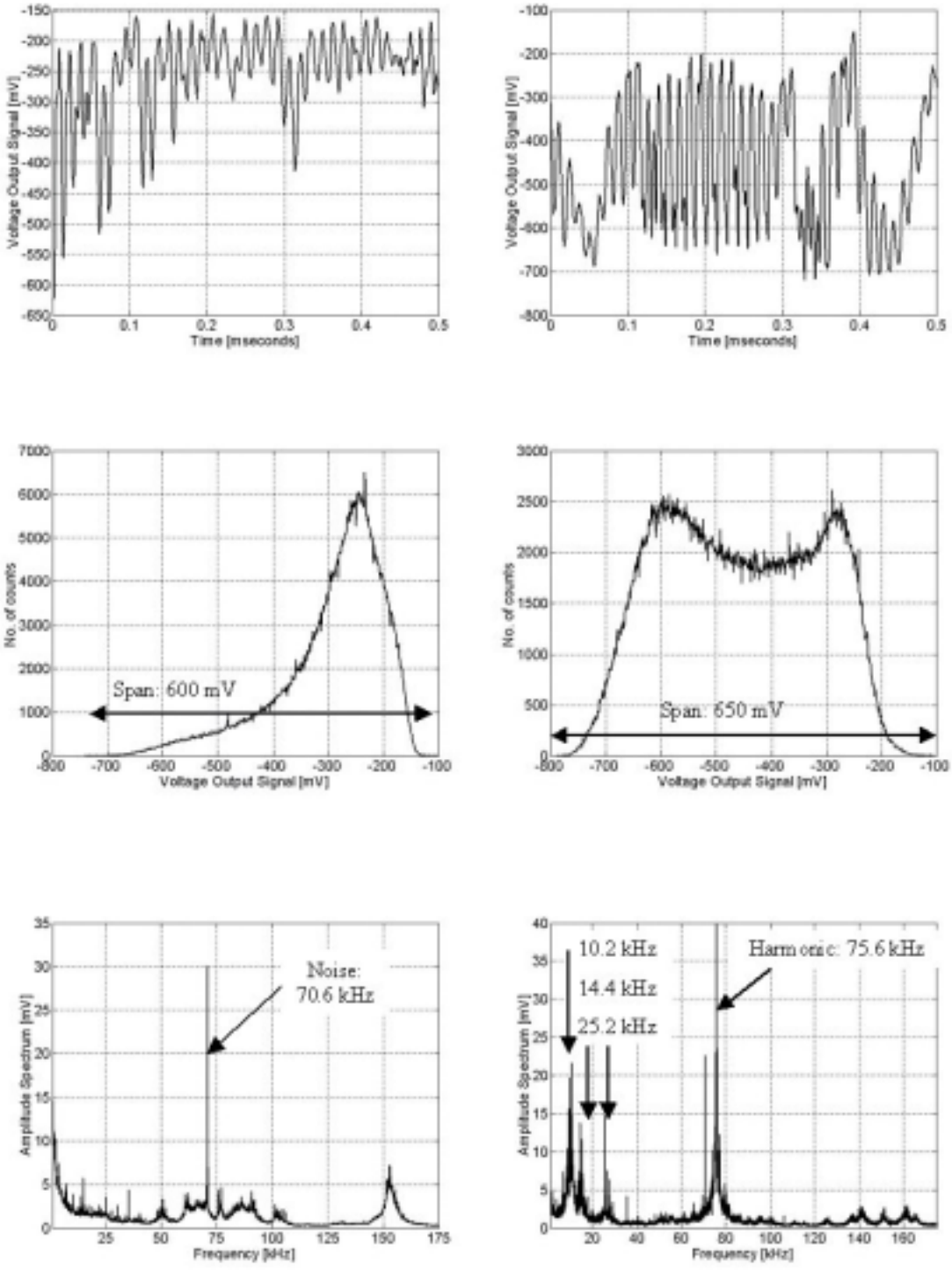

Figure 6.16: Sensor No. 7. Time series (upper plots), histograms (plots in the middle) and normalized amplitude spectra (lower plots).

Sensor No. 7 – radial loc. 579 mm
Recording period:
1 hour after the start of recording

Motor load:	14.5 MW
Hydraulic thrust:	118 bar
Production quantity:	285 tonnes/day
Dilution water flow:	2.0 litres/sec.
Acceleration DS:	12.4 %

The process data were characteristic with the following properties:

- High hydraulic axial forces.
- Relative high acceleration.

The readings from sensor No. 7 had the following properties:

- Relative large maximum span. However, the span was smaller for the great majority of the readings. The distribution was shifted towards maximum.
- An offset had occurred compared with the recordings in the first main period. The readings were shifted towards more negative values.
- The amplitude spectrum reveals small peak amplitudes from the process related effects. The dominating frequencies were:
  - 70.6 kHz (noise).
- Additional frequencies:
  - 25.2 kHz and its harmonics.
  - 14.4 kHz and sidebands.

It is assumed that the contribution from the mechanical pressure (fibres) was small in this recording. Probably smaller amount of chips was fed into this refining zone than the other because of the high acceleration value (small gap) as discussed in Section 6.7. Thus, it is assumed that the sensor was more seldom affected by fibrous material. In that case the steam pressure was measured.

Sensor No. 7 – radial loc. 579 mm
Recording period:
19.5 hours after the start of recording

Motor load:	14.8 MW
Hydraulic thrust:	117 bar
Production quantity:	285 tonnes/day
Dilution water flow:	2.1 litres/sec.
Acceleration DS:	10.3 %

The process data were characteristic with the following properties:

- High hydraulic axial forces.
- Acceleration DS equalized with the acceleration on the front side.

The readings from sensor No. 7 had the following properties:

- Large span. The distribution was dominated by a sinusoidal effect shown as one peak at each side of the distribution. The distribution was symmetric.
- The amplitude spectrum reveals:
  - 75.6 kHz (third harmonic)
  - 25.2 kHz and sidebands.
  - 14.4 kHz and sidebands.
  - 10.2 kHz as peak frequency in a frequency band between 9 and 11 kHz.

The recording was dominated by signal patterns, which have frequencies in a frequency band between 9 and 11 kHz. This remains unidentified. These frequencies can be associated with harmonic frequencies related to the junction between the breaker bar plates and the coarse zone. The frequency related to the junction between the intermediate zone and the fine bar zone (14.4 kHz) was clearly evident as well as the frequency from the fine bar pattern zone (25.2 kHz). The third harmonic of 25.2 kHz was especially clear.

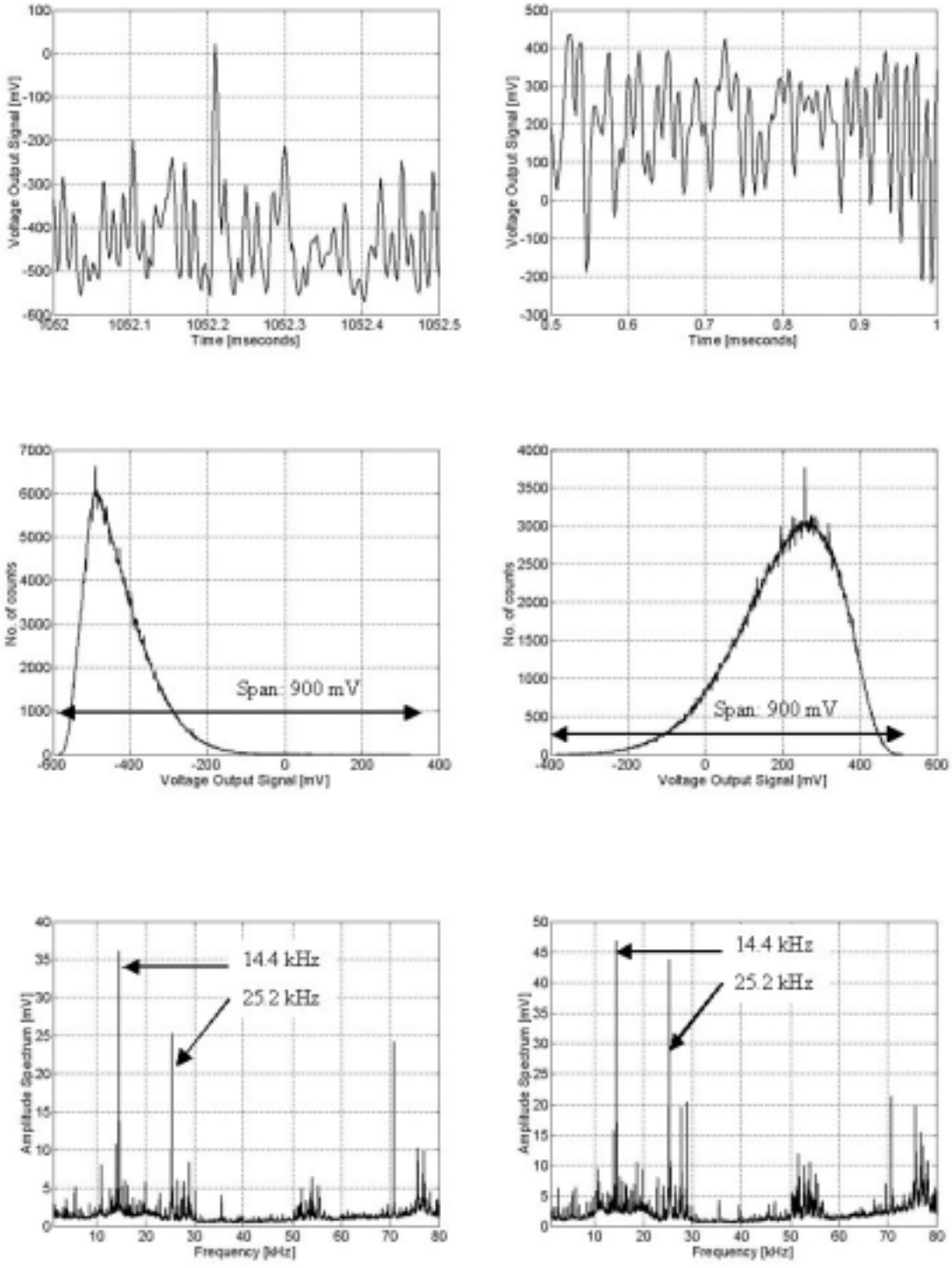

Figure 6.17: Sensor No. 4. Time series (upper plots), histograms (plots in the middle) and normalized amplitude spectra (lower plots).

Sensor No. 4 – radial loc. 592 mm
Recording period:
18.5 hours after the start of recording
LSC screw angle pos.: + 9.6∀
Motor load: 14.2 MW
Hydraulic thrust: 117 bar
Production quantity: 285 tonnes/day
Dilution water flow: 2.1 litres/sec.
Acceleration DS: 9.5 % (See Section 6.7).
The process data were characteristic with the following properties:

- ∉ High hydraulic axial forces.
- ∉ Low acceleration.

The readings from sensor No. 4 had the following properties:

- ∉ Relative large maximum span. The span was smaller for a great majority of the readings. The distribution was strongly shifted towards minimum.
- ∉ An offset had occurred compared with the recordings in the first main period. The readings were shifted towards more negative values.
- ∉ The amplitude spectrum reveals relatively large peak amplitudes. The main contribution was from process related effects. The dominating frequencies were:
  - 4 14.4 kHz and its sidebands.
  - 4 25.2 kHz and its harmonics.

The recording revealed that the contribution from the process behaviour was high. As opposed to corresponding recordings from the first main period, the frequency related to the junction between the intermediate and fine bar pattern zones dominated compared to the 25.2 kHz signal. This indicates that the process behaviour had changed during the two periods.

Sensor No. 4 – radial loc. 592 mm
Recording period:
18.5 hours after the start of recording
LSC screw angle pos.: - 4.1∀
Motor load: 15.0 MW
Hydraulic thrust: 117 bar
Production quantity: 285 tonnes/day
Dilution water flow: 2.1 litres/sec.
Acceleration DS: 14.3 % (See Section 6.7).
The process data were characteristic with the following properties:

- ∉ High hydraulic axial forces.
- ∉ High acceleration.

The readings from sensor No. 4 had the following properties:

- ∉ Relative large span. The distribution was dominated by a sinusoidal effect shown as one peak at each side of the distribution. The distribution was shifted towards maximum.
- ∉ The amplitude spectrum reveals relatively large peak amplitudes. The main contribution was from process related effects. The dominating frequencies were:
  - 4 14.4 kHz and its sidebands.
  - 4 25.2 kHz and its harmonics.

The distribution was shifted towards maximum and the shift was significantly compared to the recording shown to the left. Thus, the average pressure had shifted as a result of the changed process behaviour. However, the frequency spectrum has not changed much. This indicates that a similar flow pattern was present during these recordings.

This recording is part of a long time series captured during the stream splitter test and is further discussed in Section 6.7.

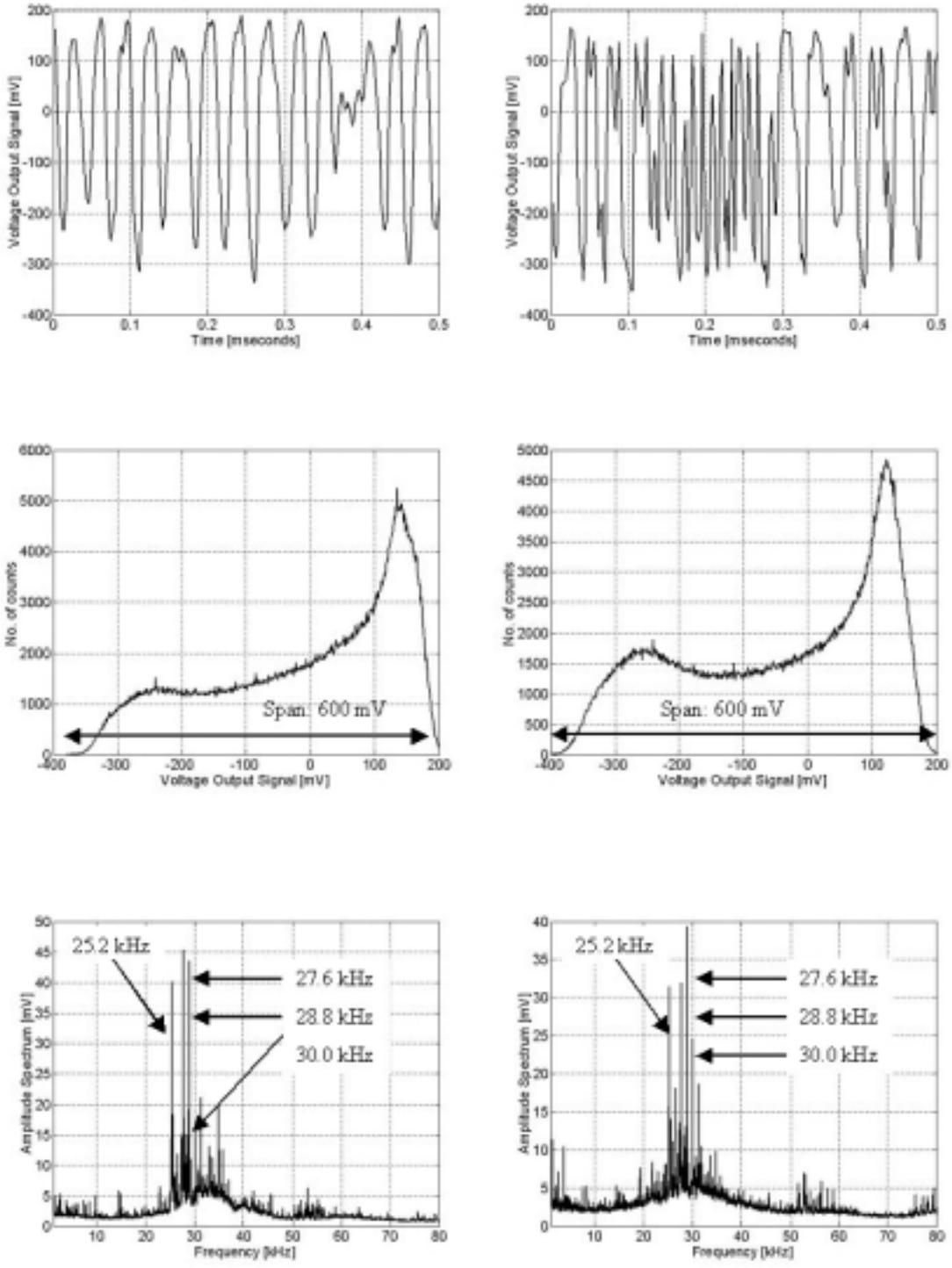

Figure 6.18: Sensor No. 6. Time series (upper plots), histograms (plots in the middle) and normalized amplitude spectra (lower plots).

Sensor No. 6 – radial loc. 695 mm
Recording period:
18.5 hours after the start of recording
LSC screw angle pos.: + 9.6∀
Motor load: 14.2 MW
Hydraulic thrust: 117 bar
Production quantity: 285 tonnes/day
Dilution water flow: 2.1 litres/sec.
Acceleration DS: 9.5 % (See Section 6.7).
The process data were characteristic with the following properties:

- ∉ High hydraulic axial forces.
- ∉ Low acceleration.

The readings from sensor No. 6 had the following properties:

- ∉ Large span. The distribution was shifted towards maximum.
- ∉ An offset had occurred compared with the recordings in the first main period. The readings were shifted towards more negative values.
- ∉ The amplitude spectrum reveals relatively large peak amplitudes. The main contribution was from process related effects. The dominating frequencies were:
  - 4 27.6 kHz.
  - 4 28.8 kHz.
  - 4 25.2 kHz.

The dominating frequencies of 27.6 and 28.8 kHz can have been sideband effects of 25.2 kHz, or they can have been the second harmonic frequencies of the 13.8 and 14.4 kHz respectively. The last assumption was reinforced by the fact that the recording from this sensor was captured simultaneously as the readings from sensor No. 4 as shown in previous figure. Figure 6.17 showed that 14.4 kHz and its sideband frequencies dominated.

Sensor No. 6 – radial loc. 695 mm
Recording period:
18.5 hours after the start of recording
LSC screw angle pos.: - 4.1∀
Motor load: 15.0 MW
Hydraulic thrust: 117 bar
Production quantity: 285 tonnes/day
Dilution water flow: 2.1 litres/sec.
Acceleration DS: 14.3 % (See Section 6.7).
The process data were characteristic with the following properties:

- ∉ High hydraulic axial forces.
- ∉ High acceleration.

The readings from sensor No. 6 had the following properties:

- ∉ Large span. The distribution was shifted towards maximum.
- ∉ The amplitude spectrum reveals relatively large peak amplitudes. The main contribution was from process related effects. The dominating frequencies were:
  - 4 27.6 kHz.
  - 4 28.8 kHz.
  - 4 25.2 kHz.

In contrast to the recordings from sensor No. 4 shown in Figure 6.17, the distribution of the two different recordings shown here did not differ much. This reveals that the average pressure was at the same level despite the changed process behaviour. The frequency spectra did not differ much indicating that the same flow patterns dominated the recordings. Compared with the recordings shown in Figure 6.17, it can be assumed that the pressure was not affected much in the outer part of the refining zone while the pressure change revealed by sensor No. 4 was approximately 3 bar as shown in Figure 6.57, Section 6.7.

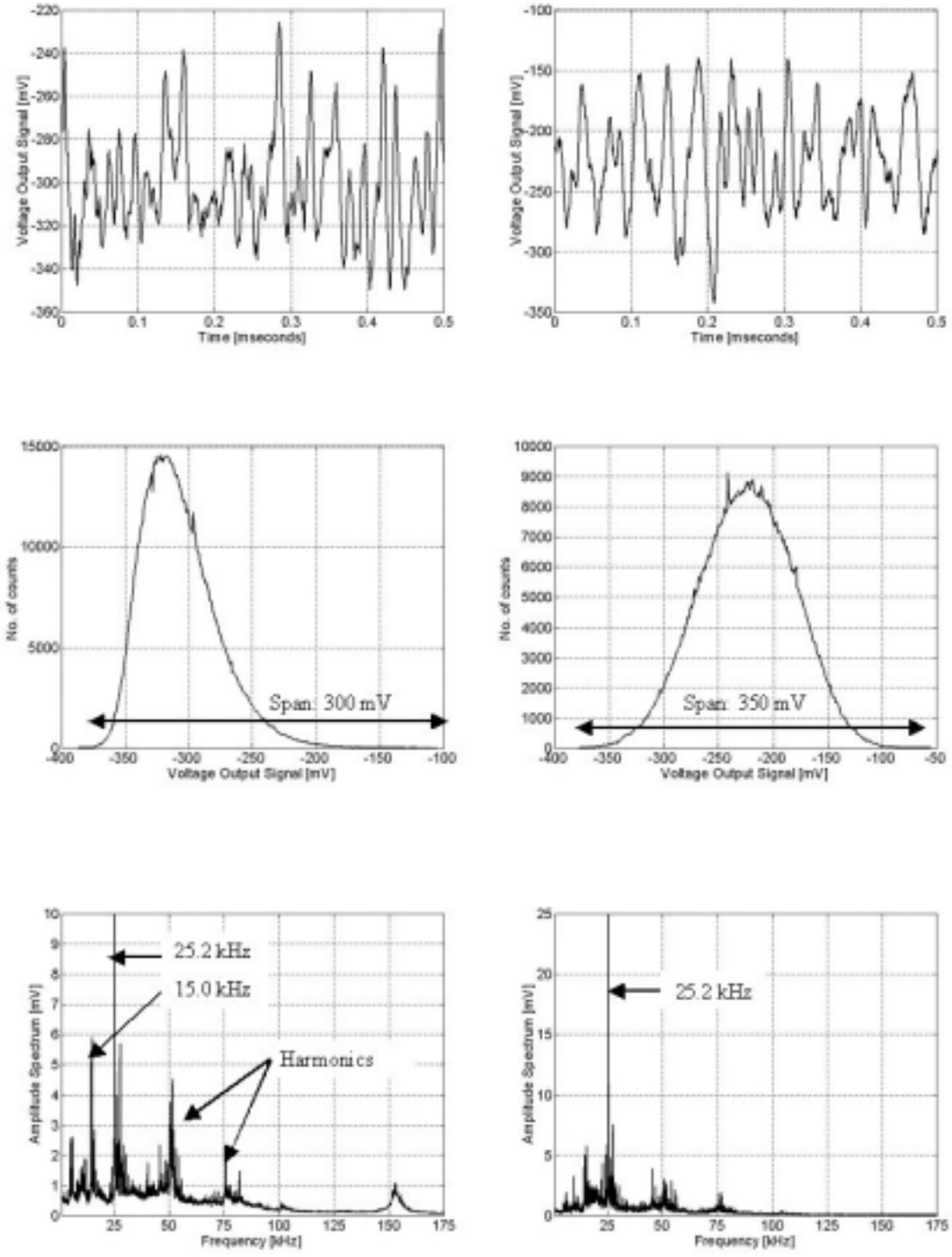

Figure 6.19: Sensor No. 8. Time series (upper plots), histograms (plots in the middle) and normalized amplitude spectra (lower plots).

Sensor No. 8 – radial loc. 707 mm
Recording period:
1 hour after the start of recording
Motor load: 14.5 MW
Hydraulic thrust: 118 bar
Production quantity: 285 tonnes/day
Dilution water flow: 2.0 litres/sec.
Acceleration DS: 12.4 %

The process data were characteristic with the following properties:
- ∉ High hydraulic axial forces.
- ∉ High acceleration.

The readings from sensor No. 8 had the following properties:
- ∉ Small span. The distribution was shifted towards minimum.
- ∉ The span was strongly reduced compared with the recordings in the first main period.
- ∉ The amplitude spectrum reveals relatively small peak amplitudes. The main contribution was from process related effects. The dominating frequencies were:
  - 4 25.2 kHz and its sidebands.
  - 4 27.6 kHz.
  - 4 15.0 kHz and its sideband.
  - 4 6.0 kHz.
  - 4 5.4 kHz.

The dominating frequency was 25.2 kHz, which can be identified as the bar-crossing frequency at the location of sensor No. 8. In contrast to the readings from the first main period the spectrum here also show other typical process related frequencies as the 14.4 kHz with its sidebands and in addition the 5.4 and 6.0 kHz. The last two frequencies can be associated with the junction between the breaker bar plate and the refiner plate.

Sensor No. 8 – radial loc. 707 mm
Recording period:
19.5 hours after the start of recording
Motor load: 14.7 MW
Hydraulic thrust: 117 bar
Production quantity: 285 tonnes/day
Dilution water flow: 2.1 litres/sec.
Acceleration DS: 10.4 %

The process data were characteristic with the following properties:
- ∉ High hydraulic axial forces.
- ∉ Relative low acceleration.

The readings from sensor No. 8 had the following properties:
- ∉ Small span. The distribution was symmetric.
- ∉ The amplitude spectrum reveals relatively large peak amplitudes. The main contribution was from process related effects. The dominating frequency was:
  - 4 25.2 kHz.

The symmetric distribution gave a clear peak frequency at 25.2 kHz, which was the local bar-crossing frequency. The shift in the distribution between the two recordings shown in this figure indicates that the average pressure has been shifted to another level.

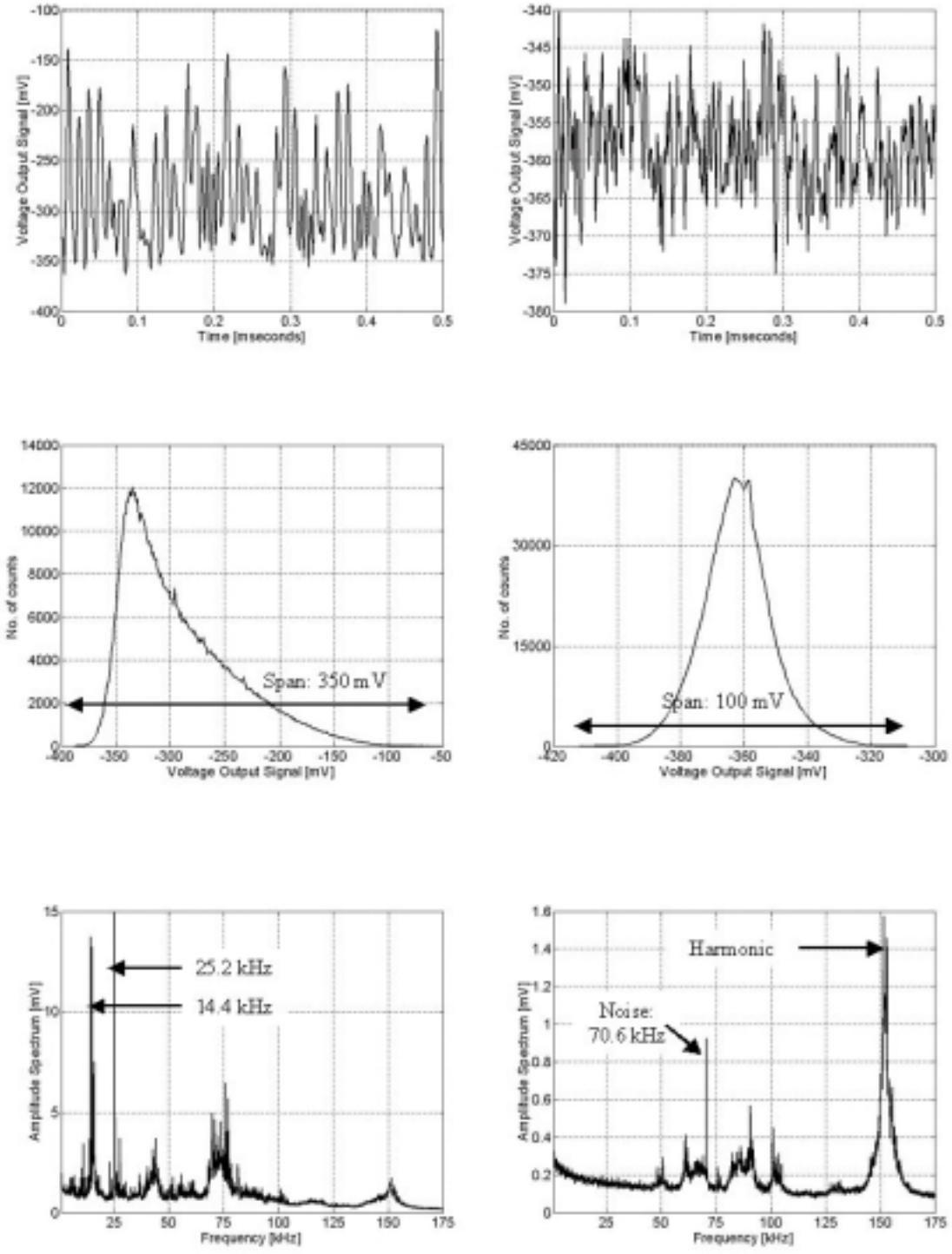

Figure 6.20: Sensor No. 5 (left) and sensor No. 9 (right). Time series (upper plots), histograms (plots in the middle) and normalized amplitude spectra (lower plots).

Sensor No. 5 – radial loc. 627 mm

Recording period:
30 min. after the start of recording

Motor load:	14.6 MW
Hydraulic thrust:	118 bar
Production quantity:	285 tonnes/day
Dilution water flow:	2.0 litres/sec.
Acceleration DS:	12.2 %

The process data were characteristic with the following properties:

- ∉ High hydraulic axial forces.
- ∉ Relative high acceleration.

The readings from sensor No. 5 had the following properties:

- ∉ Small span. The distribution was shifted towards minimum.
- ∉ The span did not differ much from the recordings captured in the first main period, but an offset had occurred.
- ∉ The amplitude spectrum reveals relatively small peak amplitudes. The main contribution was from process related effects. The dominating frequencies were:
  - 4 25.2 kHz and harmonics.
  - 4 14.4 kHz and its sidebands.

The output signal from sensor No. 5 did not differ much from the recordings made in the first main period. The main difference was due to the offset. The frequency spectrum has given process related frequencies through the peak frequencies at 25.2 and 14.4 kHz.

Sensor No. 9 – radial loc. 720 mm

Recording period:
1 hour after the start of recording

Motor load:	14.7 MW
Hydraulic thrust:	118 bar
Production quantity:	285 tonnes/day
Dilution water flow:	2.0 litres/sec.
Acceleration DS:	12.3 %

The process data were characteristic with the following properties:

- ∉ High hydraulic axial forces.
- ∉ Relative high acceleration.

The readings from sensor No. 9 had the following properties:

- ∉ Small span. The distribution was symmetric.
- ∉ The span was strongly reduced compared with the recordings performed in the first experimental period.
- ∉ The amplitude spectrum reveals small peak amplitudes. The main contribution was from the noise frequency of 70.6 kHz and from a high frequency signal about 150 kHz. The latter signal was probably a harmonic signal of 25.2 kHz.

The small span indicates that the output signal from sensor No. 9 had been strongly reduced. No indications have been made about any cable failures. If so, the noise signals should have dominated completely. However, the sensor signal from this recording gave no valuable information.

Table 6.3: Amplitude spectrum peaks – after 1000 working hours.

Sensor	25 [Hz]	300 [Hz]	600 [Hz]	1200 [Hz]	5.4 [kHz]	6.0 [kHz]	13.2 [kHz]	14.4 [kHz]	25.2 [kHz]	26.4 [kHz]	70.6 [kHz]
	[mV] [dB]	[mV] [dB]	[mV] [dB]	[mV] [dB]	[mV] [dB]	[mV] [dB]	[mV] [dB]	[mV] [dB]	[mV] [dB]	[mV] [dB]	[mV] [dB]
1[1]	-	-	-	-	0.22 1	-	-	-	0.27 6	0.17 2	0.8 12
2[2]	-	-	-	-	-	-	-	-	-	-	29 49
7[3]	-	-	7.5 5	4.5 1	-	-	-	14 19	15 20	8 15	23 24
4[4]	8 18	3.5 17	1.7 10	2 12	5.5 15	7.5 18	5 8	42 26	33 32	5 16	25 22
5[5]	4 16	1.4 11	2.8 17	1.3 10	[9]	1.4 6	-	14 27	14 27	-	6 18
6[6]	4.5 16	-	-	11 24	[10]	3.2 4	-	5 8	24 16	15 11	-
8[7]	1.2 6	0.7 7	0.8 9	-	2 12	2.8 15	-	4.5 18	8 26	3.5 19	1 10
9[8]	-	-	-	-	0.2 2	-	-	-	-	-	0.8 18

1) Amplitude spectrum from data recorded after 30 min.
2) Amplitude spectrum from data recorded after 1 hour.
3) Amplitude spectrum from data recorded after 19.5 hours.
4) Amplitude spectrum from data recorded after 18.5 hours. LSC screw angle position: -4.1∀
5) Amplitude spectrum from data recorded after 30 min.
6) Amplitude spectrum from data recorded after 18.5 hours. LSC screw angle position: -4.1∀
7) Amplitude spectrum from data recorded after 19.5 hours.
8) Amplitude spectrum from data recorded after 1 hour.
9) ∂ 600 Hz : 1.4-1.5 mV (6-7 dB).
10) ∂ 600 Hz : 3.2-3.7 mV (4-5 dB).

6.3.4 Summing up

The findings from the second main period of data recording have revealed that except for one, all the sensors have given responses that can be associated with fluctuations that occurred in the process. However, the periodicities in the pressure recordings have changed the pattern during the time between the two main experimental periods. Two main changes have been observed:

- ∉ The contribution from the high-frequency part of the signal identified as the 25.2 kHz periodicity has been smaller. The amplitude of this frequency has been reduced. The lower frequency at 14.4 kHz has been more visible.
- ∉ The span in most of the recorded signals has been reduced compared to the spans that were observed in the first experimental period.

The reasons for these changes are likely to be as follows:

- The periodic signal of 25.2 kHz, corresponding to the bar-to-bar passage at the radial location of approximately 707 mm from the centre of the refiner, seems to be more damped in the data recorded after 1000 working hours than in the first main period of data recording. On the other hand, the signals generated from the transition zone between the intermediate zone and the fine bar patter zone, identified with the frequency of 14.4 kHz, seems to have had stronger influence on the signal patterns. This indicates that the pulp flow pattern had changed during the time elapsed. Strand and Hartler (1985) observed similar phenomenon. They claimed that plate wear caused both damped vibration amplitudes and a change in the radial distribution of the vibration frequencies. This was further associated with the energy distribution in the refining zone. While a dominating high-frequency signal was assigned an energy distribution that was shifted outwards to the fine bar zone, a broader distributed frequency pattern was associated with the energy applied to the process being more evenly distributed. Further discussions about vibration measurements and any relationship between the pressure measurements are found in Chapter 7.

  Another study reporting vibration measurements in beaters and chip refiners indicated that higher motor loads shifted the dominating bar-crossing frequencies towards lower frequencies (Pettersen and Gunstrøm (1980)). This indicates that the main refining action appears in an earlier section of the refining zone when the motor load increases. Such indication is comparable with the results shown by the pressure measurements. The motor load was higher in the second main period of data recording compared with the first experimental period. Furthermore, the 14.4 kHz was more pronounced than the dominating frequency of 25.2 kHz in the first period. From a practical point of view, this frequency shift appears as a result of higher loads because the plate gap decreases. A smaller plate gap will probably resist the outward flowing pulp earlier in the refining zone. Thus, it can be assumed that higher-pressure pulses appearing from higher refining action occur earlier in the refining zone. In addition, a study reported by Stationwala *et al.* (1991) concluded that worn plates operate at lower refining zone temperature than new plates. This was ascribed to the fact that a larger proportion of steam is expelled, counter to the material flow, back through the feeder. This indicates that the outward flowing pulp can be resisted because of the backward flowing steam due to increased plate wear. Thus the main refining action may occur earlier in the refining zone.

- The spans of the output signals from a great majority of the sensors were smaller in the time series from the second main period compare with the readings in the first period. Only sensors No. 5 and 7 seem to have unchanged variation levels. Sensor No. 2 only measured noise as the plots in Figure 6.15 shows. The span reduction has been as follows:
  - Sensor No. 1: Span decreased to approximately 10 % of its previous level.
  - Sensor No. 4: Span decreased to approximately 50 % of its previous level.
  - Sensor No. 6: Span decreased to approximately 85 % of its previous level.
  - Sensor No. 8: Span decreased to approximately 30-40 % of its previous level.
  - Sensor No. 9: Span decreased to approximately 20-30 % of its previous level.

The spans of the output signals from sensors Nos. 1 and 9 were reduced to a level that corresponded to the noise level. However, their amplitude spectra did not indicate that the sensors were broken. A probable reason for the lack of benefited data is that the cavity in the front of the sensor surface was packed with fibrous material. As a result the pressure pulses have been strongly damped. The reduced amplitudes of the pressure signals may also be related to plate wear. Both Pettersen and Gunstrøm (1980) and Strand and Hartler (1985) showed that the amplitude values from the measured noise and vibrations decreased when the plates were worn. Some pictures of the replaced plate containing the fibre-optic sensors are shown in Appendix G.

Additional observations that have been made in the second experimental period are discussed next:

- The output signals from sensors Nos. 4, 7, and 6 have clearly given expected responses to different process conditions. While comparing the two recordings from each sensor in this experimental period, it can be indicated that the radial locations of the sensors have affected the average pressure readings. Sensor No. 4 has given an extremely clear shift in the distribution as shown in Figure 6.17, while sensor No. 6 was affected to a minor extent (Figure 6.18). The reason is probably that sensor No. 6 was located in the outer part of the refining zone while sensor No. 4 was located in the intermediate zone with a larger plate gap. The plate gap was approximately 1 mm wider at the radial location of sensor No. 4 compared with the plate clearance at the location of sensor No. 6. The latter is shown in Table 3.5. Thus it is assumed that changes in the amount of pulp into the refining zone affects the pressure measurements in the regions with a wider plate gap more than the measurements undertaken in a small plate gap region. This seems to be reasonable when the pulp flow is resisted earlier in the refining zone because of a small plate gap. Thus it can also be assumed that the energy applied in the outer part of the refining zone is limited as indicated by Strand and Hartler (1985) and Allison *et al.* (1995). See also Section 6.7.

- The recordings from Sensor No. 7, located in the transition zone between the coarse section and the intermediate zone, show similar shift in the distribution as revealed by sensor No. 4. The pressure readings from sensor No. 7, as shown in Figure 6.16, have probably been affected by the effect of larger plate gap and thereby a smaller amount of pulp squeezed between the discs at its radial location. The plots to the left in Figure 6.16 indicate a minor activity in the area round the sensor surface, while the activity has been more pronounced in the period shown in the other plot. Additional discussions about pressure changes due to variations in the amount of pulp are treated in Section 6.7.

- In spite of the large decrease in the span of the output signals from sensor No. 8, the sensor signal has revealed apparently reasonable amplitude spectra. The clear differences between the amplitude spectra representing the recording in the first period (Figure 6.13) of data recording compared with the frequency spectra obtained in the last experimental period (Figure 6.19) may indicate that the process behaviour has changed as discussed in the first point in this section.

- The frequency of 27.6 kHz, as shown in Figure 6.18, has been more visible in last period compared with the recordings undertaken in the first main period. This frequency can be associated with three different conditions as the bar-crossing frequency at the plate periphery, the harmonic of the 13.8 kHz signal or the 2400 Hz-sideband about 25.2 kHz. Assuming that the first condition represents this frequency, it can be conceived that the high loads and thereby a small plate clearance made the bar crossing frequency from the plate periphery more visible. The second condition is relevant when considering the frequency shift toward lower frequencies as the dominating periodicities in the recordings. The peak frequency at 14.4 kHz and its sideband frequencies seem to have had more influence on the recorded signals in the second period. Thus it is conceivable that 27.6 kHz was a harmonic frequency of 13.8 kHz. The third condition is considered possible too. However, no conclusion is drawn about the origin of this frequency.

6.3.5 Noise detection

In this section the contribution of noise signals in the recordings is revealed and analysed. The measurements were performed with and without the sensors connected to the amplifier unit. When the sensors were connected to the amplifier the refiner was unloaded i.e. spinning without pulp in the refining zone.

Table 6.4 clearly states that channel A on the combined amplifier and laser driver unit picked up more noise than channel B. A similar result was obtained when comparing the two channels of the data acquisition card. Channel No. 0 on the DAQ unit picked up more noise than channel No. 1. Such differences are clearly shown in data recorded during loaded conditions as well. Figure 6.21 shows analyses of the recordings from sensor No. 4 undertaken in the second main period of data recording. The output signal displayed in the plots on the left-hand side were recorded using channel A, while the plots on the right-hand side show the output signal, which was recorded using channel B. These recordings were separated in time by approximately 5 minutes. The main differences between these plots were caused by the different gain and the ability of channel A to pick up more noise. The noise frequencies of 70.6 and 35.3 kHz are visible in the amplitude spectrum on the left-hand side.

Table 6.4: Noise frequencies.

Sensor NO.	Amplifier Channel	DAQ Channel	Zero bar gauge pressure 20 ∀C, 25 rps		Normalized amplitude spectrum analysis (Peak frequencies and amplitude values.)				
			Ave.	St.dev.	70.6 35.3 [kHz]	72.6 [kHz]	26.4 [kHz]	50 150 250 [Hz]	25 100 [Hz]
			[mV]	[mV]	[mV] (dB)	[mV] (dB)	[mV] (dB)	[mV] (dB)	[mV] (dB)
1[1]	B	1	260	20	0.8 (22) 0.2 (7)	0.7 (21)			
2[1]	**A**	0	-22	31	26 (54) 7 (43)	22 (53)	3 (36)	7 (19) 6 (18) 3 (11)	3 (11)
7[1]	**A**	0	-150	33	27 (55) 9 (42)	22 (53)	3 (33)	6 (12) 6 (12) 3 (6)	
4[1]	**A**	0	880	38	18 (51) 9 (42)	15 (50)	3 (30)	7 (11) 7 (11)	4 (6)
5[1]	B	1	322	20	1.3 (25) 0.15 (4)	1 (23)			2 (6)
6[1]	B	1	666	35	1.3 (25) 0.2 (4)	1.1 (24)			
8[1]	B	1	240	21	1.2 (25) 0.2 (6)	1.1 (24)			
9[1]	B	1	255	20	1.2 (26) 0.2 (7)	1.1 (25)			1.3 (8)
N[2]	**A**	0	-866	20	27 (59) 5 (44)	0.7 (27)		5 (30) 4 (29) 2 (22)	
N[2]	B	1	-410	6	0.6 (20) 0.1 (4)			0.9 (13)	1.2 (16)
N[2]	N	0	0	2	0.8 (38) 0.2 (26)				
N[2]	N	1	0	0.5	0.2 (34) 0.05 (22)				

N: None connection.

1) The measurements were captured in the first main period of data recording, before the chips were fed in.
2) This noise test was performed in the second main period of data recording.

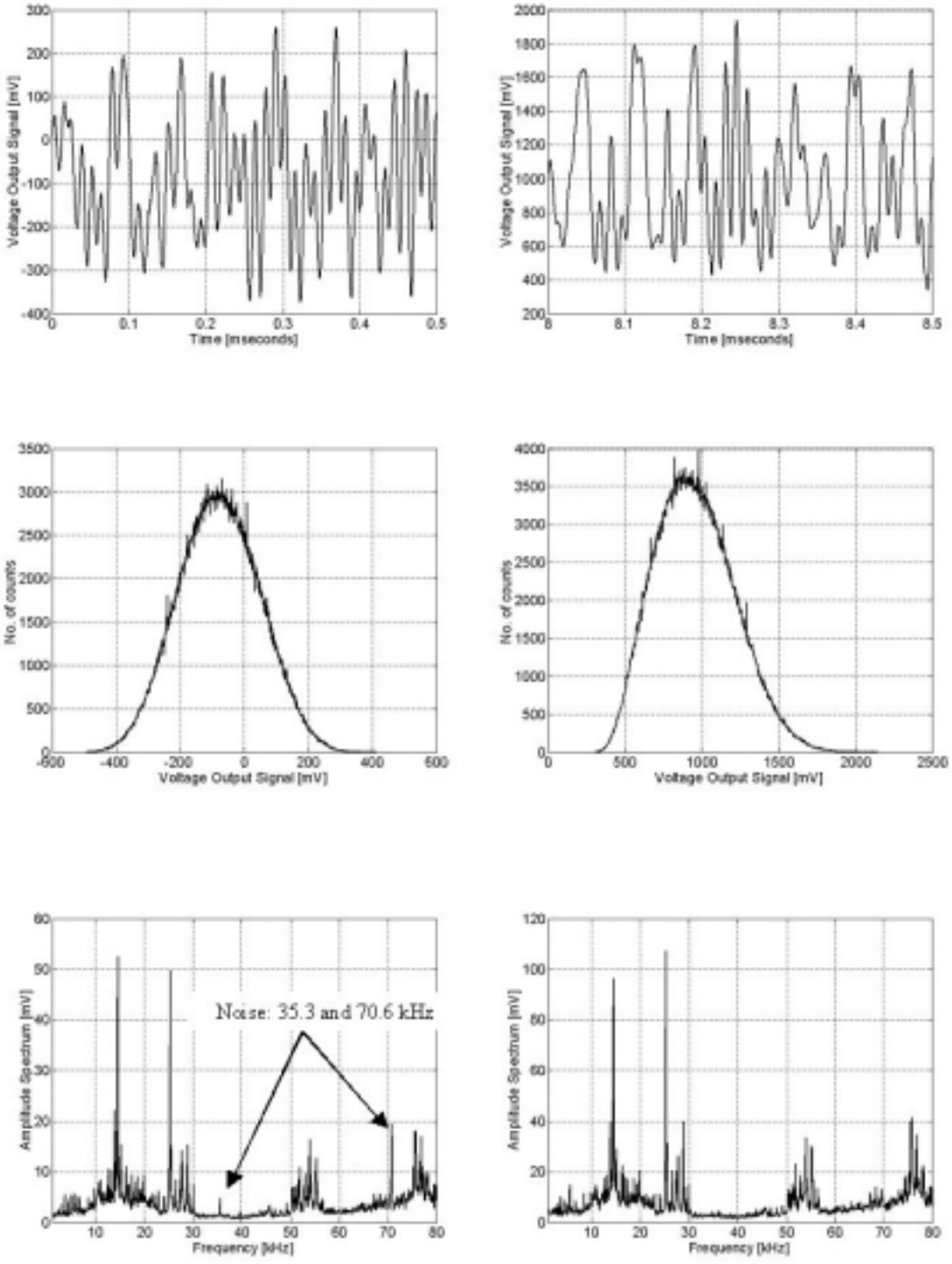

Figure 6.21: Sensor No. 4 recorded from channel A (left) and from channel B (right) during loaded conditions. Time series (upper plots), histograms (plots in the middle) and normalized amplitude spectra (lower plots).

6.4 Cross-correlation analysis

The particular design of the sensor's location in the plate was planned for extraction of information about the pulp flow in the refining zone. The intention was to investigate the relationship between the output signals from different sensors. The aim was to investigate if it was possible to measure the velocity of the pulp flow in different sections of the refining zone. Based on the literature survey it could be expected velocities in different directions up to about 30 m/s (Atack *et al.* (1989), Alahautala *et al.* (1999)). The hypothesis was that a short distance between the locations of the sensors could give responses that revealed a time-dependent relationship between simultaneously captured readings from different sensors. The cross-correlation analysis has been used to test this hypothesis. The following diagrams display the main findings regarding the analysis of the recorded data.

A great majority of the recordings contained periodic signals. Hence, in the cross-correlation analysis the periodic signals appeared as standing waves. Such cross-correlation patterns were difficult to decipher. To overcome these difficulties low-pass filtering of the original recordings was necessary. The analysis regarding the low-pass filtering is described in Section 3.7. The first figures show an example of what the low-pass filtering was able to do.

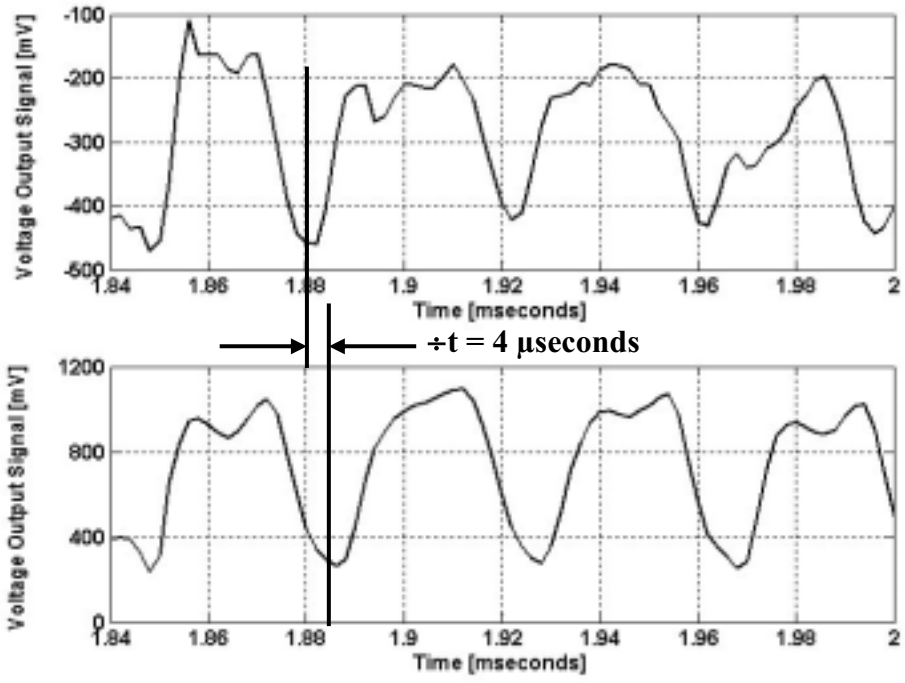

Figure 6.22: A small part of simultaneously captured recordings from sensor No. 6 (upper plot) and sensor No. 8 (lower plot) are shown. The data were collected six hours after production start-up.

The readings shown in Figure 6.22 indicate a strong correlation between the output signals from the two different sensors. The corresponding cross-correlation analysis of these readings is shown in the left-hand diagram in Figure 6.23. The right-hand plot shows the cross-correlation analysis of the whole time series containing 1 MSamples.

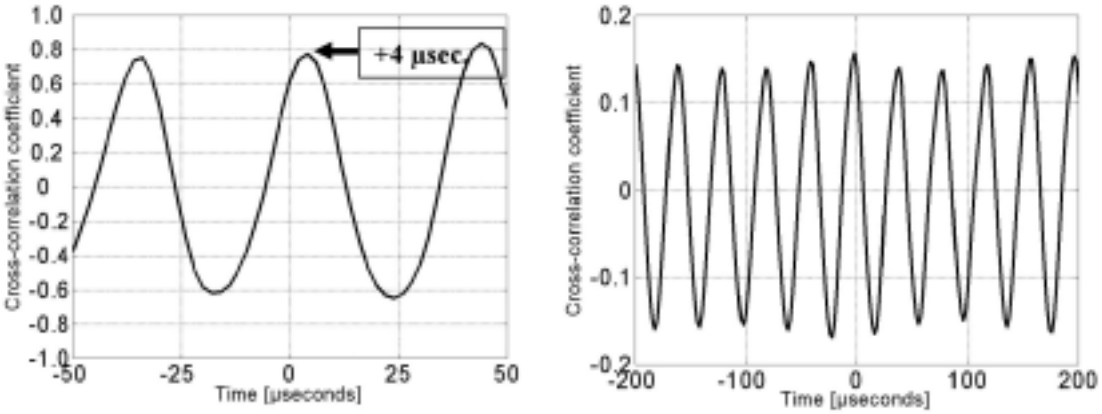

Figure 6.23: The left-hand plot shows the cross-correlation analysis of the short time series (80 samples) as shown in Figure 6.22. The right-hand plot shows a corresponding analysis of the whole time series (1 MSamples).

It is not obvious that the output signal from sensor No. 6 was ahead of the signal from sensor No. 8 by 4 µseconds as the time series (Figure 6.22) and the corresponding cross-correlation analysis (Figure 6.23, left-hand plot) show. This time difference corresponds to a velocity of about 3200 m/s. However, the cross-correlation analysis performed on the whole time series indicates that the output signal from sensor No. 6 lagged behind the readings from sensor No. 8 by 2 µseconds. This gives a pressure wave velocity of about 6400 m/s. Because of the standing waves it is not obvious that the real lag was associated with the coefficient closest to zero. A cross-correlation analysis was performed on the low-pass filtered data to investigate this further. The result from this analysis is shown in Figure 6.24.

In order to put the calculated velocity values in a context it can be mentioned that the velocity of sound in wood along the fibre is found to be in the order of 3000 to 5000 m/s[13], while the velocity across the year-rings are much lower and in the order of 1200 to 1300 m/s[11]. The speed of sound in water is approximately 1500 m/s, while the sound velocity in steel is in the range of 5000 to 6000 m/s. The velocity of sound in saturated water vapour increases from about 400 m/s at a temperature of 100 ∀C to about 530 m/s at a temperature of 200 ∀C. The velocity of the pressure wave propagation in the refiner is dependent on where the wave propagation occurs. In the discs of the refiner it is expected pressure wave propagation comparable with the velocity in steel. The wave propagation between the discs certainly is affected by the assumed inhomogeneous flow patterns. If there is two-phase flow where the steam flow

[13] Handbook of Chemistry and Physics, 31st edition, Chemical Rubber Publishing co. (1949).

is separated from the pulp flow the wave propagation can move with the velocity of steam. A wider range of velocities is expected when the pressure waves propagate through the pulp. Such wave velocities are probably closer to the speed of sound in water than the speed of sound along the fibres of wood.

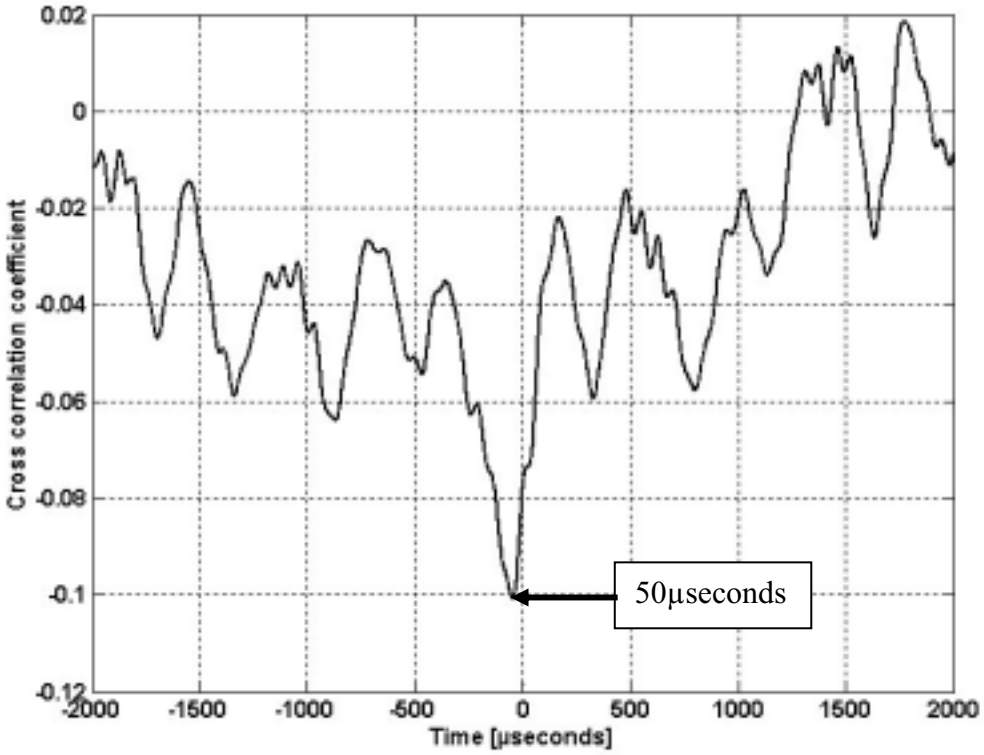

Figure 6.24: The cross-correlation analysis obtained from the low-pass filtered data of the readings shown in Figure 6.22 and the remaining data in that recording is shown.

The cross-correlation analysis made on the low-pass filtered data with a cut-off frequency of 15 kHz, shows that the output signal from sensor No. 6 lagged the readings from sensor No. 8 by 50 µseconds as shown in Figure 6.24. The negative correlation reveals that the output signals were negatively correlated. However, the pressure can still have been positively correlated since the calibration curves from these sensors were in opposite phase as shown in Figures C6 and C7. The time difference corresponding to the highest correlation coefficient indicates that these recordings were correlated by *something* that was moving with a velocity between 250 and 360 m/s. This something was probably not the pulp flow. However, it can have been the pressure wave propagated through the steam or the speed of flexural waves in the stator disc.

The first velocity (250 m/s) is determined based on the radial distance between the two sensors, and the second velocity (360 m/s) is calculated based on the real distance. The reason why the velocities for both the radial distance and the real distance are

determined is to show the difference. It is conceivable that different flow regimes can be present in the refining zone. The pulp flow is expected to mainly follow a radial path outwards influenced by a tangential component due to the rotor movement. However, the pressure waves will propagate in all directions from the point of departure. In addition, it is conceivable that the pulp is flowing in batches or waves because of discontinuous feeding and interruptions made by coarse bars, bolt holes and other effects in the refining zone. The sideband frequencies revealed in the frequency spectra in the previous section imply that the flow patterns are modulated in different ways.

Another result is shown in Figure 6.25. The left-hand plot displays the cross-correlation analysis performed on the output signals from sensors Nos. 4 and 9 during two seconds of the initial chip feeding shown in Figures 6.1 and 6.3. The right-hand plot shows the cross-correlation analysis made on the low-pass filtered data of the same recordings.

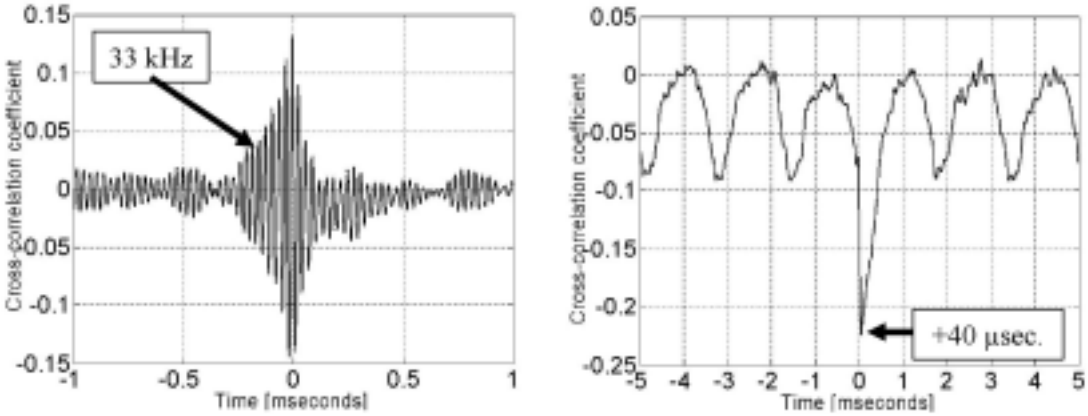

Figure 6.25: Cross-correlation analysis, raw data analysis (left-hand plot) and low-pass filtered data analysis (right-hand plot), made on recordings from sensors Nos. 4 and 9 during the initial chip feeding.

The standing wave pattern shown in the left-hand plot in Figure 6.25 contains a periodicity of 33 kHz (see also Figures F1 and F2). The cross-correlation coefficients are higher to the left from zero lag, which indicates that the readings from sensor No. 9 are ahead of the readings from sensor No. 4. However, in the low-pass filtered data the highest cross-correlation coefficient was found 40 µseconds at the positive part of the time axis as shown in the right-hand plot in Figure 6.25. This means that the readings from sensor No. 4 were ahead of the readings from sensor No. 9. The output signals were negatively correlated. However, the sinusoidal calibration curves were in opposite phase. Consequently the pressure was positively correlated as the average pressures shown in Figure 6.3 reveal. The calculated velocity is found to be approximately 3200 m/s indicating pressure wave propagation outwards in a dense matter.

Besides the clear cross-correlation peak, a clear periodicity was also found in the low-pass filtered data. The periodicity which is clearly evident in Figure 6.25 had a frequency of 600 Hz. This indicates that the output signals were affected by a sideband effect with 600 Hz as the modulation frequency. This frequency may have appeared

from the bolt holes in the plates. In the different frequency spectra shown in Section 6.3, 600 Hz also appears as sideband, especially regarding FFT-analysis of the recordings of sensor No. 4.

In addition to the frequency of 600 Hz shown in Figure 6.25, other typical sideband frequencies are found in the cross-correlation analyses. In Figure 6.26 the frequency of 25 Hz, related to the revolution of the rotor disc, is visible. Figure 6.26 shows the cross-correlation plots of the low-pass filtered output signals from sensors Nos. 4 and 9 captured in the first experimental period. The readings were acquired approximately six hours after the initial chip feeding took place.

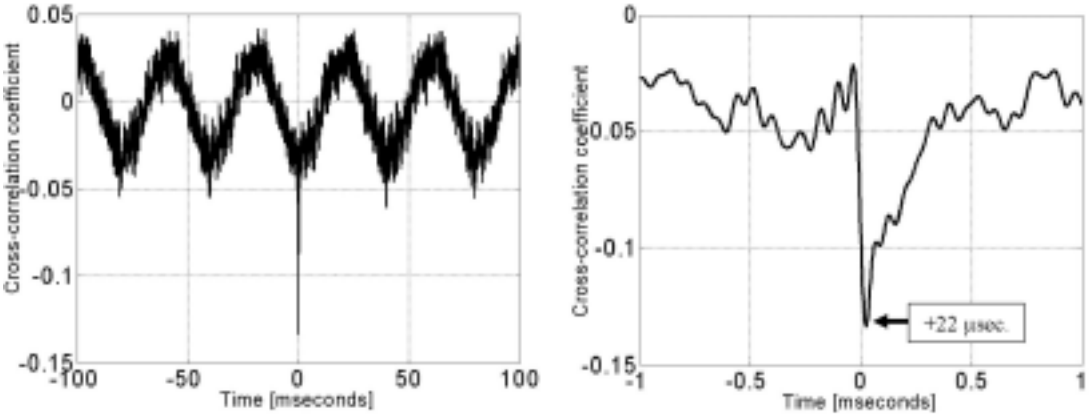

Figure 6.26: Cross-correlation analysis performed on the low-pass filtered data from sensors Nos. 4 and 9 recorded approximately six hours after the initial chip feeding started.

The negative peak in the cross-correlation plots in Figure 6.26 was found 22 μseconds after lag zero. Hence, the readings from sensor No. 4 are ahead of the data from sensor No. 9. The corresponding velocity is found to be close to 6000 m/s. This indicates that the flow propagated from the location of sensor No. 4 towards the outer periphery through the rigid stator disc. Cross-correlation coefficients below –0.06 appear from zero to approximately 250 μseconds as shown in the right-hand plot in Figure 6.26. As 250 μseconds corresponds to a velocity of about 500 m/s, this indicates that the pressure waves were transmitted through the pulp and steam in the plate gap as well.

Other results from the cross-correlation analyses, that have given satisfactorily cross-correlation coefficients, were found in the recordings from the sensors located in the inner square as well. The next two figures display the cross-correlation analyses performed on recordings from sensors located in the intermediate zone.

The low-pass filtering of the recordings from sensors Nos. 7 and 1, shown in Figure 6.27, has not improved the result from the cross-correlation analysis much. The highest cross-correlation coefficient appears at lag zero for the low-pass filtered data and close to the lag zero for the unfiltered data. This indicates that the responses from a common source were measured simultaneously.

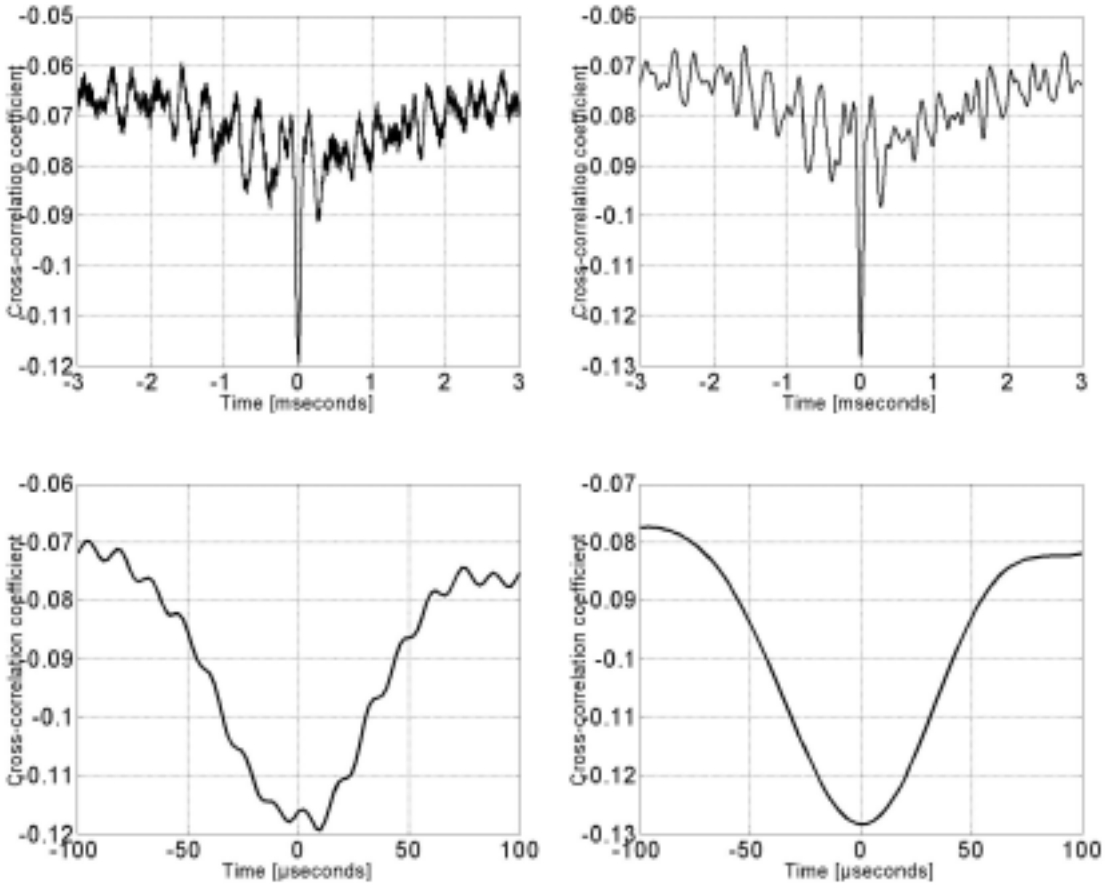

Figure 6.27: Cross-correlation analysis performed on the raw data is shown in the left-hand plots. Similar analysis made on the low-pass filtered data is shown in the right-hand plots. These cross-correlation plots are based on recordings from sensors Nos. 1 and 7 captured approximately five hours after the production start-up.

In the following figure, Figure 6.28, three pairs of plots are shown. The cross-correlation analyses have been made on output signals from sensor No. 4 and sensors Nos. 1, 2 and 7 respectively. Figure 6.28 show the cross-correlation analysis made on the raw data recordings (left-hand plots) and the corresponding low-pass filtered data sets (right-hand plots). These recordings were captured in the first experimental period between 5 and 7 hours after the initial chip feeding started.

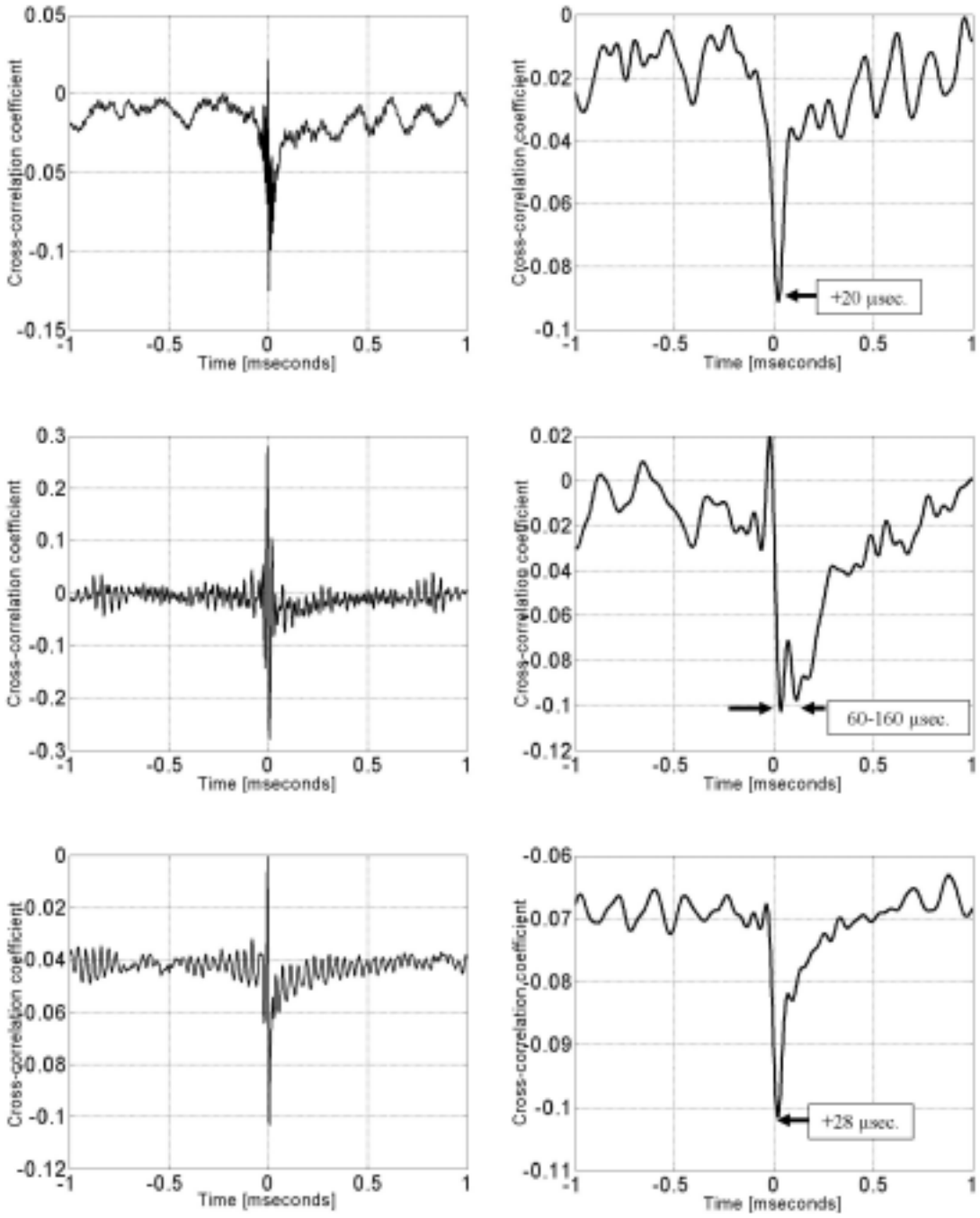

Figure 6.28: Cross-correlation analysis performed on recordings from sensor No. 4 and the following sensors: No. 1 (upper plots), No. 2. (plots in the middle), and No. 7 (lower plots).

The peak in the upper right-hand plot of Figure 6.28 indicates that sensor No. 4 was affected by a common source before this was measured by sensor No. 1. The time difference between the responses was 20 µseconds. The readings from these sensors were negatively correlated, while the pressure signals were positively correlated as

indicated by the sinusoidal calibration curves in Figures C1 and C4. The velocity associated with the time difference is found to be close to 1300 m/s indicating that the pressure wave propagated with a speed close to the speed of sound waves in water.

The readings from sensor No. 4 were ahead of the readings from sensors Nos. 2 and 7 as well. The plots in the middle of Figure 6.28 show the cross-correlation between the recordings from sensors Nos. 4 and 2. The cross-correlation analysis made on the low-pass filtered data is shown in the right-hand plot in the middle. The peak in this plot appears between 60 and 160 μseconds, which give corresponding velocities of 80 to 300 m/s, depending on whether the radial distance or the real distance between the sensors is chosen in the calculation. Readings from sensor No. 2 lagged the readings from sensor No. 4, indicating that the pressure wave propagated towards the inlet of the refiner. The peak in the lower right-hand plot of Figure 6.28 shows that the readings from sensor No. 4 were ahead of the readings from sensor No. 7 by 28 μseconds. The corresponding velocity is found to be 450 m/s when the radial distance is taken into account, while the real length between the locations of the two sensors gives a velocity of about 580 m/s.

6.4.1 Summing up

The main findings in the cross-correlation analyses have shown that:

- The expected velocities related to the pulp flow in the order of 1-30 m/s were not found.
- The highest coefficients in the cross-correlation analyses give indications about pressure wave movements from below 100 m/s to higher than 6000 m/s. The measured velocities indicate that the pressure waves propagated in the disc and through the pulp and steam in the gap between the discs. The high velocities support the assumption that the discs vibrate because of pressure pulses generated by the squeezing of fibres and flocs of fibres between opposite bars on the stator and rotor discs. The reason why no distinct velocities are found regarding pressure wave propagation through the pulp and steam in the gap is probably because of the lack of homogeneous flow patterns in the refining zone.
- The wave propagation seems to have propagated from the intermediate zone (location of sensor No. 4) and in both directions towards the outer periphery (location of sensor No. 9) and the inlet (location of sensors Nos. 1, 2, 7) respectively.
- The cross-correlation coefficients were not very high. Several analyses performed on different recordings from different sensors gave small cross-correlation coefficients. The reason may be related to the large number of samples used in the cross-correlation analyses. However, the long distances between the locations of the individual sensors probably caused the main reason for the relative weak relationship between the different recordings.
- Low-pass filtering gave the opportunity to overcome the lack of distinct peaks in the cross-correlation diagrams due to the standing waves.

6.5 Recalibration of the sensor signals

For some unknown reason, the original calibration data were not valid after the installation of the equipment on site. Possible explanations about the calibration offsets may be found in the fitting of the sensors to the plate, as described in Section 3.3, or in the temperature control of the laser. Both setscrews and epoxy were used to hold the sensor housing tight into the cavity in the plate. Whether the fittings have caused any external stress is not clarified. Temperature variations in the laser driver would certainly give offsets. It is not clarified if any of these effects has caused the observed deviations.

Tests and recalibration using a water pressure chamber were performed at the mill before the plates were installed in the refiner. Still some offsets were observed before the mill start-up. Therefore, it was necessary to make further adjustments to the original calibration curves. The adjustments had to be based on the data from the measurements. The average value and the span of the different time series were mainly used in the determination of the adjusted calibration curves. As support, histograms of different recorded data series and zero-bar pressure measurements were used. For some sensors, which were used to record data during the preheating periods, the refiner's casing pressure could also be used to determine the measured pressure. For instance sensors Nos. 4 and 9 have proved to give valid readings during the preheating periods as shown in Figures 6.3 and 6.4.

The following assessments of the recalibration are concentrated to only one sensor. This choice was assigned sensor No. 4, which was followed up more closely during the experimental periods. A larger amount of recorded data was captured from this sensor than from any other. The calibration curves of the other sensors are displayed in Appendix C. Another approach to the selection of sensor No. 4, as the only sensor that has been investigated more closely regarding the determination of the absolute pressure levels, was that the histograms and frequency spectra from this sensor indicated a dynamic variation level mainly associated with one flange. The recordings spanned the expected range of the sinusoidal calibration curve simultaneously as they showed shapes that can be associated with Gaussian distribution as shown in Figure 6.10. The frequency spectra did not show typical harmonic frequencies either. Thus there has been expected that the signal from sensor No. 4 fluctuated across a top or bottom point of the sinusoidal transfer function curve more seldom. This is of course valid when the distributions were symmetric. The skewed distributions as well as harmonic frequencies as shown in Figure 6.17 clearly indicate that the signals have crossed a maximum or minimum point of the calibration curve. However, this is associated with a level shift in the average pressure. No indications imply that the dynamic pressure variations were changed much. Opposite to the Gaussian distribution, the saddle shaped distributions shown by sensors Nos. 8 and 9 in Figures 6.13 and 6.14 as well as their corresponding frequency spectra containing harmonic frequencies indicate signal fluctuations beyond one single flange. The determination of the absolute pressures for these sensors is more intricate.

6.5.1 Span and noise level detection

Figure 6.29 shows data points corresponding to the calculated average values of 1 MSamples and the corresponding absolute maximum and minimum values for all of the recorded data files using sensor No. 4. These curves in Figure 6.29 roughly consist of 240 data points each. In addition, two other curves are shown in parts of the figure. These curves are associated with the average values of the maximum and minimum readings of a moving average analysis described in Section 3.7. The texts added to Figure 6.29 are labels related to particular periods in the experiment. The results from these periods are discussed in the subsequent sections.

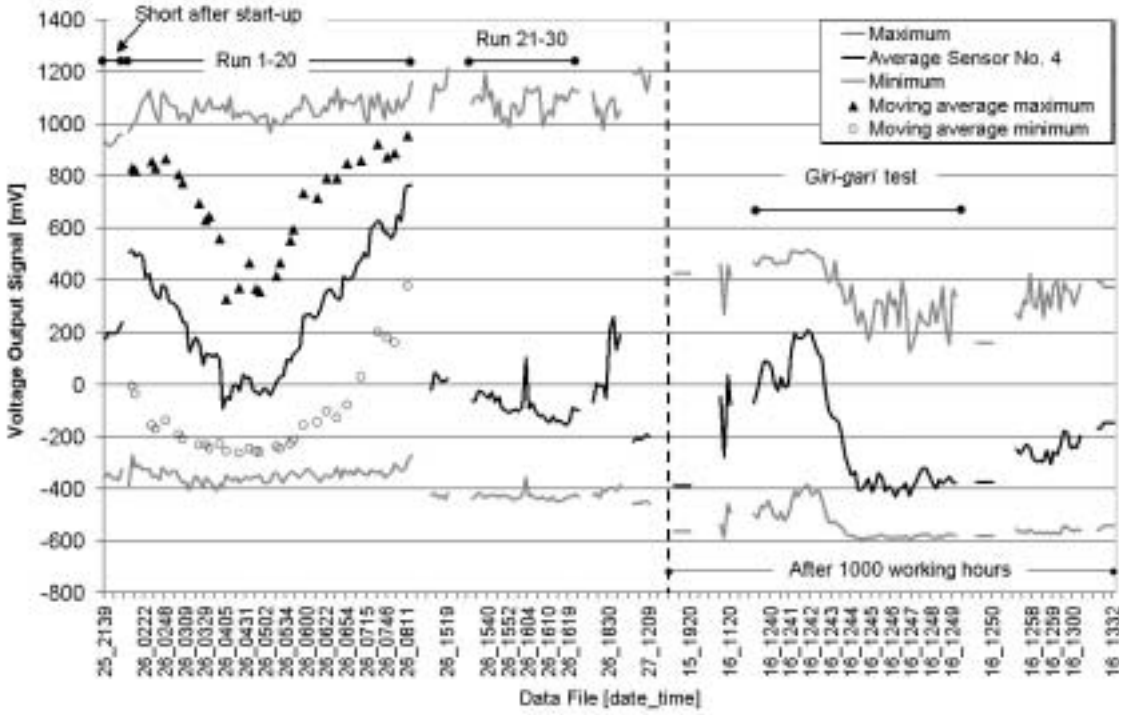

Figure 6.29: Average, maximum and minimum values for sensor No. 4 during the two main data recording periods.

Three particular observations are of special interest regarding the curves in Figure 6.29:

- The span developed from the difference between the absolute maximum and minimum values was high and relatively stable in the first period (0-40 hours after start-up) and smaller after 1000 working hours. Some offsets during the time elapsed can also be observed by for instance looking at the minimum values which have shifted to a lower level in the second experimental period.
- The average maximum and minimum values emanated from the moving average analysis followed the average values.
- The average values mainly represent non-stationary signal behaviour where random fluctuations are suppressed.

The first observation indicates that the pressure variation was smaller when the plates were worn (after 1000 working hours). However, it is not possible to exclude the effect

of pressure pulse damping by built up material in the front of the sensor surface, or by other unknown effects that can have affected the sensor performance after a long period in the harsh environment inside the refiner.

The second observation indicates that the dynamic pressure variations obtained for sensor No. 4 mainly were smaller than one flange.

The third observation is connected to the non-stationary behaviour of the average value. Certainly, there have been process changes that have affected the static pressure level. Some of the non-stationary behaviour of the average values, as shown for the *Giri-gari* test, can positively be connected to the behaviour of the process due to controlled manipulation. The corresponding pressure variations are displayed in Figure 6.6 and further discussed in Section 6.7. The non-stationary signal behaviour is not equally obvious in the periods labelled *Run 1-20* and *Run 21-30*. During these periods the process conditions were changed in steps in a randomized order to avoid time dependence. Thus the underlying process that caused this non-stationary behaviour may have influenced the measurements more than the controlled manipulation of the refiner did. A possible cause may be related to the uneven and unsteady distribution of chips between the two refining zones in the Twin-refiner. The unsteady conditions may lead to a subsequent rotor disc movement. Such behaviour is commonly observed, and it is claimed that such drift is working almost continuously[14]. This phenomenon is further discussed in Section 6.7, while further analyses describing the time dependence are shown in Section 6.6.

In addition to the average values and maximum and minimum values as shown in Figure 6.29, histograms of the recordings were useful in determination of the span of the output signals. Each of the two figures, Figure 6.30 and Figure 6.31, show three histograms of different recordings captured in the two main data recording periods. These reveal the extremities when the distributions of the readings were shifted towards the minimum and maximum of the available output range. In addition, the histograms in the middle of each of the figures show the symmetric distribution when the average of the output signals were located close to the quadrature point i.e. on the middle of a flange of the sinusoidal calibration curve. Figure 6.30 shows histograms from recordings captured in the period labelled *Run 1-20*. The histograms were based on the recordings, which the average values are shown on the rising flange in Figure 6.29. The histograms were represented by a low, middle and high average value. In Figure 6.31 corresponding histograms are shown for the *Giri-gari* test. Each histogram corresponds to a given angle position of one of the two power screws of the load sense conveyor that determine to a certain level the distribution of chips between the two separate refining zones of the Twin refiner. Further results are given in Section 6.7.

[14] Karl Mosbye, Norske Skog Research. Private communication, 2002.

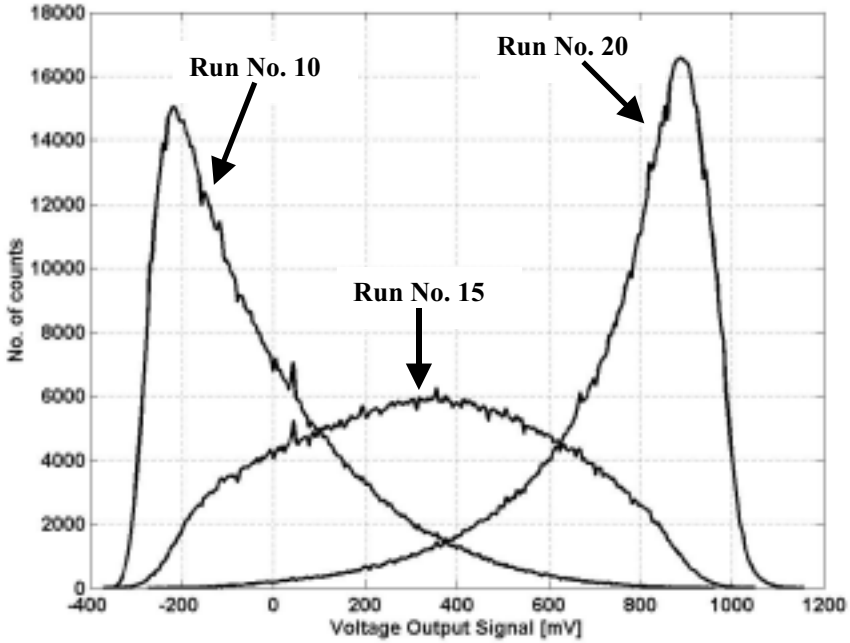

Figure 6.30: Histograms of three recordings from sensor No. 4 captured in the first main period of data recording.

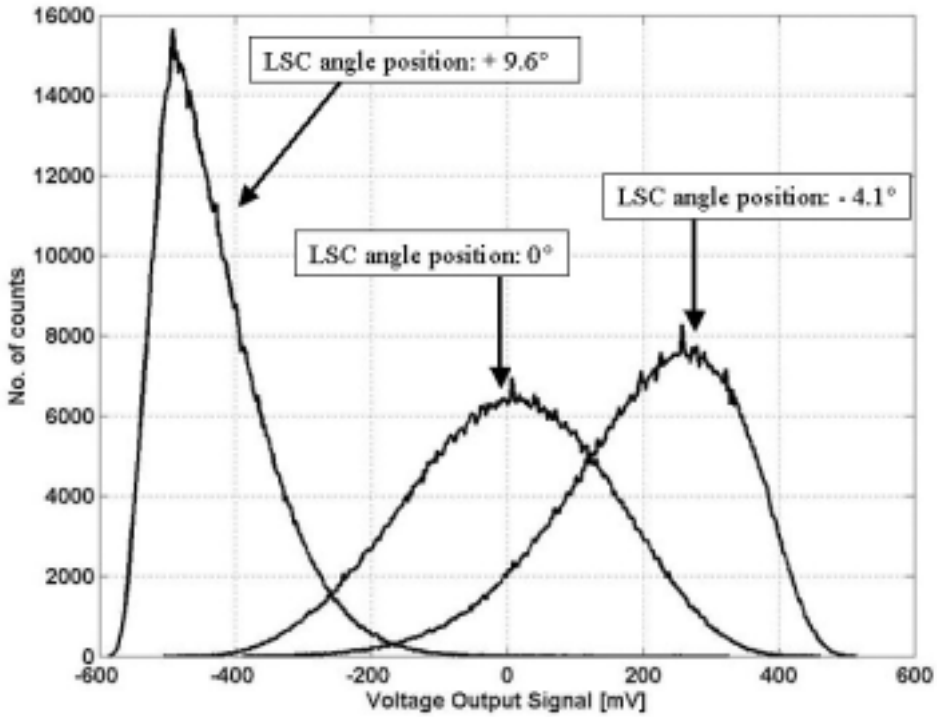

Figure 6.31: Histograms of three recordings from sensor No. 4 captured in the second main period of data recording labelled as Giri-gari test.

The sharp flanges on the histograms lying at the outer edges of Figure 6.30 and on the left-hand side of Figure 6.31 indicate that the output signals corresponding to these histograms have reached the maximum and minimum points of the sinusoidal calibration curve. It is obvious that these output signals were fluctuating across a top or a bottom point of the calibration curve. However, nothing seems to indicate that the output signals shown in these examples were fluctuating across both a minimum and a maximum point in the same time series.

The histograms were useful to determine whether the output signals were fluctuating across a minimum or a maximum point of the calibration curve. However, a visual inspection of the time series as shown in Figures 6.30 and 6.31 was not enough. A more quantitative analysis was made to find a best possible calibration curve. The quantitative analysis was based on a determination of a common maximum and a common minimum value for all of the recordings related to one sensor. It was necessary to split the data material in different periods because of the assumption that an offset had occurred during the time elapsed as revealed in Figure 6.29. Both offset and span deviations from the original calibration were present because the recalibrations of the sensors' output signals were both offset and gain adjusted before the mill start-up. However, since no calibration adjustments were made during the experiment, only offsets should be taken into account when determining the adjusted calibration curves.

It was further assumed that the fringe pattern i.e. the number of pressure units between two adjacent maximum or minimum points in the calibration curve, was maintained and unchanged compared to the original calibration curve. The fringe pattern also describes the sensitivity of the pressure measurements. One period of the sinusoidal calibration curve covered approximately 20 bar. Thus, the span of the output signals associated with one flange corresponded to pressure variations of ± 5 bar.

It is necessary to know the amount of noise when determining of a common maximum and a common minimum value. The absolute maximum and minimum values from each recording did not represent the average maximum and minimum levels. Based on the data recorded at zero bar conditions as shown in Table 6.5 the noise level was determined. The table consists of estimated average and pooled standard deviation values determined from one to nine different recordings, each containing 200 kSamples or 1 MSamples. The amount of noise was calculated as three times the standard deviation of the average value measured when the refiner was unloaded.

Table 6.5: Noise determination: The voltage output signals from the sensors measured at zero bar gauge pressure.

Sensor [No.]	Cold refiner[1] 20∀C Not spinning		Start heating[1] 20∀C Spinning		Warm refiner[1] 75∀C Not spinning		Cold refiner[2] 20∀C Not spinning	
	Ave. [mV]	St.dev. [mV]	Ave. [mV]	St.dev [mV]	Ave. [mV]	St.dev [mV]	Ave. [mV]	St.dev. [mV]
1	281	31	300	24	329	24	364	43
2	-9	34	-19	31	33	30	14	25
4	907	28	871	37	873	28	827	36
5	306	29	320	22	263	16	255	20
6	716	30	648	30	824	35	894	27
7	-118	33	-135	31	173	35	80	26
8	176	30	218	17	184	14	213	10
9	173	29	191	11	223	18	164	8

1 Day 1: Before chip feeding and the unsuccessful start-up.
2 Day 2: Before chip feeding and the production start-up.

Table 6.5 and Figure 6.32 display the output signals at zero bar pressure, captured at different time periods before the production start-up. The last four points in Figure 6.32 are quoted in Table 6.5. The zero bar average values fluctuated more than one standard deviation, which gave an indication of continued offset errors. However, the offsets seem to have decreased as the time elapsed. Possible error sources were:

- Lack of perfect coupling of light into the transmission fibre. Coupling errors could be caused by bad fitting of the connectors when sensor cables were replaced at the two-channel laser driver and amplifier unit. This effect has probably been incorporated in the estimated average and standard deviation values because usually more than one recording has been used to determine these values. Between each recording the sensor cables were usually decoupled and replaced by other sensor cables because the measurements were conducted in turn between the different sensors.
- Laser temperature deviation. Variations in the temperature of the laser driver due to lack of sufficient control, should give even offsets for all of the sensors. However, the amplitude and the direction of the deviation were determined by where on the calibration curve the zero bar pressure was located. It is not obvious that the laser driver has been affected by temperature fluctuations, but it cannot be excluded as a possible error source. Turning off and in turn cooling the laser driver, as shown in Figure 6.32 did not affect the zero bar readings more than before this action was tried. This indicates that the temperature control of the laser driver was sufficient.
- Fitting of the sensor housing into the plate. Use of setscrews and epoxy may have caused unsuspected responses. The outcome did not necessary give an even response from the different sensors. The apparent offset especially between the measurements from the two main data recording periods as shown in Figure 6.29 indicates that the offset was decreasing. After 1000 working hours the offset value had reached a level that approached zero compared to the original calibration points.

It is conceivable that decreasing stress in a structure (sensor housing) caused decreasing offsets. Degraded epoxy after many hours in a harsh environment may have given such effect. Based on the fact that the sensors were mounted into the sensor housing surrounded by a brake fluid to avoid such effects, it is difficult to determine the real cause of the observed offsets. It is important to state that the sensors themselves were not assembled with epoxy.

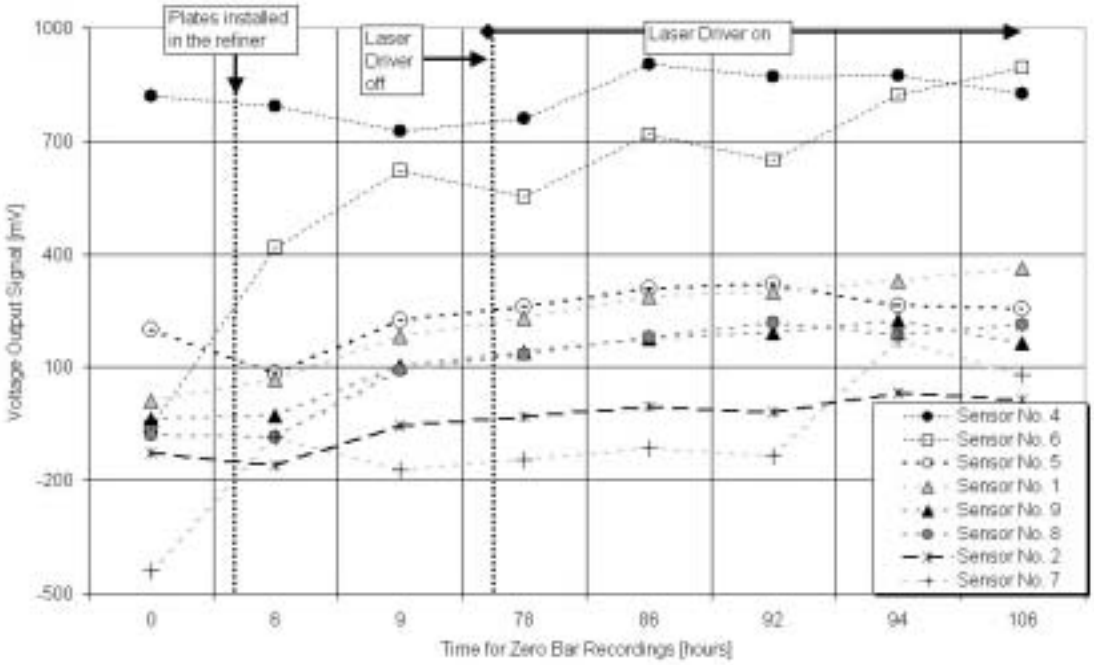

Figure 6.32: Zero bar pressure captured after the last gain and offset adjustment of the sensors' output signals.

The adjustment of the original calibration curve has been based on the quantitative analysis and for some of the sensors, supported by the assumption of known pressure values from the process taken from the mill's DCS. The latter is based on the pressure in the refiner housing during the preheating of the refiner, which was assumed to be approximately the same as the pressure in the refining zone. Table 6.6 gives an overview of the span determination regarding different periods and different methods. The last row in the table shows the corresponding values for the original calibration curve. An explanation of how the quoted values are found is given below.

Table 6.6: Span detection of the voltage output signal from Sensor No. 4.

Period for determination of the adjusted calibration curve	Max. [mV]	Min. [mV]	Span [mV]	Zero bar [mV]
Heating of the refiner 3 data files: 300 x 1 MSamples	940	-240	1180	940 (Day 1) 920 (Day 2)
From start-up until run 20 90 data files: 90 x 1 MSamples	940	-240	1180	830
Moving average 10 run 10 data files: 10 x 1 MSamples	920	-260	1180	830
Run 21-30 36 Data files: 36 x 1 MSamples	980 880	-320 -220	1300 1200	830
After 1000 working hours 11 data files: 100 x 1 MSamples	520	-490	1010	
Original calibration	650	-520	1170	600

- Recordings of the voltage output signal during the preheating of the refiner have revealed signal patterns that were well correlated with the casing pressure. Adjustment of the voltage readings to pressure values were successful using the span and zero bar values as given in row one in Table 6.6. Both Figures 6.3 and 6.4 show pressure readings based on these calibration data.
- In the period from the production start-up, on the second day of data recording, and during the next 10 hours until run No. 20, approximately 90 different recordings each of a length of 1 MSamples were the object of a quantitative analysis. The absolute maximum and minimum values were picked out to determine the span of the adjusted calibration curve. Because of the amount of noise and the risk for outliers, the span was based on the average maximum and minimum values. In addition, the span was reduced with the amount of noise in both ends. The zero bar value was collected from the last zero bar measurement, quoted in Table 6.5.
- The moving average analysis, as quoted in Table 6.7, made on 10 different recordings picked out from the period labelled *Run 1-20* gave almost the same span as the quantitative analysis revealed in previous point.
- The span determination regarding the period labelled *Run 21-30* was based on a quantitative analysis containing 36 data files. While maintaining the earlier determined noise level, the span seems to have increased as shown in the upper row in this section. However, the amount of noise seems to have increased two times the noise level that was first announced. This is indicated through comparing the frequency spectrum in Figure F4 with the corresponding spectrum in Figure 6.10. Consequently the span was reduced from 1300 mV, lower row, to approximately the same level (1200 mV) as obtained in previous periods.
- In the period after 1000 working hours the detectable span was decreased and in addition an offset had occurred. The histogram corresponding to the angle position of + 9.6º of the power screw displayed in Figure 6.31 shows that the output signal was lying close to the bottom of a fringe when the level of the output signal was approximately –500 mV. In Figure 6.30 the corresponding low level was approximately –300 mV. None of the recordings captured in this period gave indications that the readings were lying close to a top of a fringe. Hence, the

maximum value of the span was not reduced corresponding to an assumed contribution from noise. In spite of that, the span was still smaller than in the first main period of data recording. Based on the fact that the gain of the sensor signals was maintained during the period of 1000 working hours, the variation of the output signals, as a measure of the pressure variation, was smaller in the last experimental period. However, it was assumed that the span of the calibration curve was maintained during both experimental periods. Furthermore, it was assumed that only an offset had occurred between the two periods. Since no zero bar measurements were accessible in the second period, a new zero bar value was determined by offset adjustment of the earlier zero bar value.

Table 6.7: Moving average and standard deviation values for sensor No. 4.

Run [No.]	Data File [date_time]	Average [mV]	St.dev. [mV]	Max. [mV]	St.dev. [mV]	Min. [mV]	St.dev. [mV]	Difference max.-min. [mV]
1	26_0225	370	80	860	70	-160	70	1010
2	26_0451	-40	100	360	220	**-260**	**40**	620
3	26_0513	10	80	420	190	-240	30	660
4	26_0748	580	70	890	60	160	170	730
5	26_0723	630	100	**920**	**60**	200	200	730
6	26_0258	280	100	810	100	-200	70	1000
7	26_0703	480	70	860	90	30	140	830
8	26_0536	120	80	600	180	-220	40	810
17	26_0158	490	90	820	50	-40	150	860
18	26_0330	110	140	640	200	-250	60	890

Figure 6.33 shows the calibration curves related to the output signals from sensor No. 4. The original calibration points are shown together with the adjusted calibration curves for both the main data recording periods. Also the calibration points measured in the last calibration test in the water pressure chamber are shown. Calibration curves connected to the other sensors are presented in Appendix C.

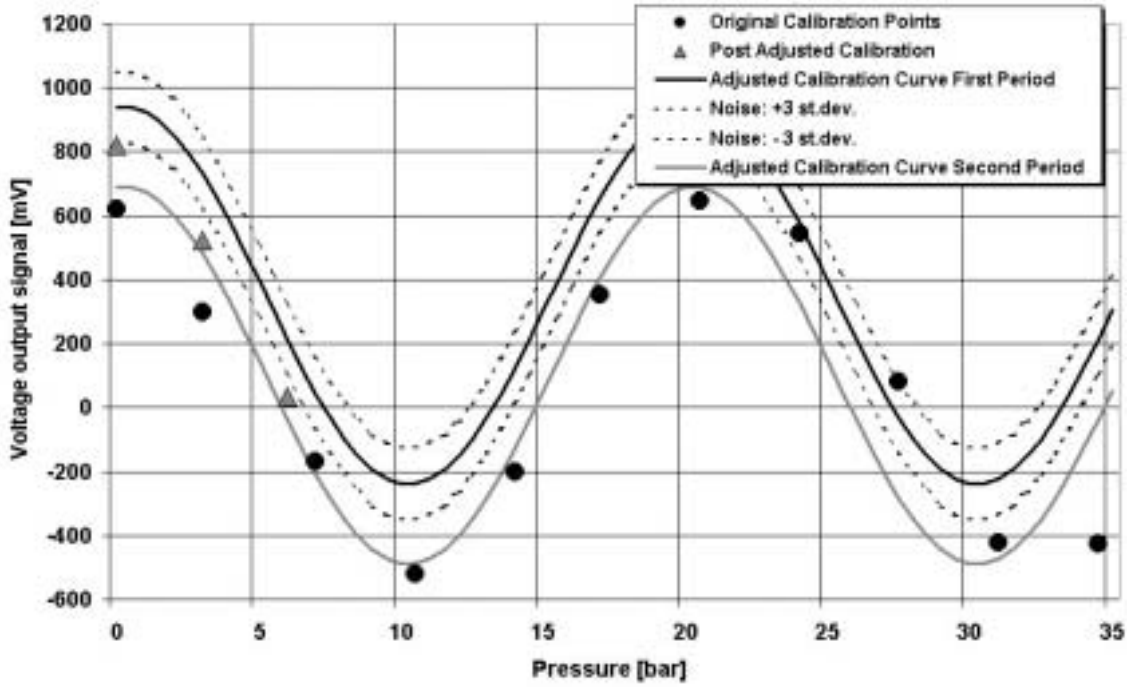

Figure 6.33: Calibration curves for sensor No. 4.

6.5.2 Evaluation of the refining zone pressure level

Theoretical and experimental approach

Based on the uncertainty regarding the sinusoidal calibration curve, it was necessary to evaluate the output signals from the pressure sensors to determine where on the calibration curve the pressure was located. The majority of the histograms as well as the frequency spectra shown in Section 6.3 did not indicate that the dynamic pressure exceeded much more than one flange of the calibration curve. The signals from sensors Nos. 4, 6, 8 and 9 showed large spans indicating large dynamic pressure variations. Frequently pressure variations shown by these sensors probably corresponded to a variation level of approximately ± 5 bar. Even larger pressure peaks have probably been present. Sensors Nos. 8 and 9, with their saddle shaped signal distribution curves, might have had dynamic pressure variations beyond the span of one single flange. This has not been possible to prove despite some efforts to do so, as shown in Section F.3. The output signals from sensors located in the intermediate zone except for sensor No. 4 showed a smaller variation level than the signals from the other sensors. The high frequency pressure variations measured by these sensors were mainly much smaller than a flange. However, some readings as indicated in the histograms seem to have reached high levels with peak-to-peak values corresponding to one flange or more.

The assessment of the absolute pressure levels measured by the sensors was even more difficult. Regarding the refiner there are two *known* pressure levels that can be used in the consideration of the measured pressures. These are the refiner housing pressure and

the saturated water vapour pressure. In addition, earlier experimental results and theoretical assumptions can be used. The following information is considered:

- The valve in the blow line controls the pressure in the refiner housing. The set point for the refiner studied was 4 bar gauge pressure. Supporting information is that the pressure was short-circuited, which means that the inlet and the outlet pressure were lying at the same level. During normal production the average pressure in the refining zone should not drop below the casing pressure. A possible exception might be the pressure readings close to the inlet because relative cold chips and dilution water that feeds in have a cooling effect. During normal operation the dilution water had a temperature of approximately 85 ºC, while the temperature of the chips was approximately 70 ºC.
- If the assumption that saturated water vapour pressure conditions is present, this is a starting point for the refining zone pressure determination. Figure 3.14 shows the relation between the saturated water vapour pressure and the temperature. The temperature varies along the radius of the disc and during different process conditions. Most of the temperature data from the present refiner have been in the range of 160 to 180 ºC corresponding to a saturated water vapour pressure in the order of 5 to 10 bar. Close to the inlet and close to the periphery the steam pressures are probably very close to the casing pressure. It can further be assumed that the measured pressure in the refining zone probably will not drop below the saturated water vapour pressure.
- Since there are no direct comparable previous investigations about the pressure in the refining zone, results from measurements in different types of refiners are considered. Atack and Stationwala (1975) measured the pressure in a 42 inch self-pressurized high-consistency single disc refiner. Pressure peaks up to approximately 7 bar were observed. Their estimates of the average pressure corresponded well with the saturated steam pressure. The results from the study performed in the atmospheric pilot refiner as discussed in Chapter 5 and previously reported as Eriksen (2002), indicated that the average pressure was in the order of 2-5 bar. The corresponding pressure peaks were found up to 60 bar. According to Hietanen (1991) and Caucal *et al.* (1992a) pressure peaks up to 35 bar on the edges of the bars have been reported by Goncharov (1971) from a study in low-consistency refiners. Based on measurements Caucal *et al.* (1992a) calculated the pressure caused by the fibre and pulp in the low-consistency refiner to approximately 8 bar.
- A simplified theoretical approach as discussed in Chapter 3, indicates average pressure measured on the surface of bars of 10-20 bar irrespective of the fibre coverage ratio (*fcr*) i.e. the fraction of the bar intersecting area covered with pulp. However, the pressure peaks measured when pulp is trapped between the sensor surface and a bar on the rotor disc are assumed to be strongly dependent on the fibre coverage ratio. A low fibre coverage ratio of 50-60 % may give average pressure peak values of 20-40 bar as indicated in Figures 3.15 and 3.17. The theoretical approach expected pressure readings that were strongly dependent on the bar pattern on the rotor plates. High and frequent pressure variations could be expected especially if the fibre coverage ratio was high. The saturated water vapour pressure was assumed to be the lower limit. Thus, pressure variations from below 10 bar to above 50 bar could be expected, while the average pressure could be in the order of

10-20 bar. However, the theoretical approach did not include a radial distribution of the pressure. The radial location of the sensors and the amount of pulp in the refining zone are probably crucial factors when determining the pressure levels.

There are insufficient observations of the pressures in the high-consistency refiner to make a good comparison between the theoretical approach and experimental data. In addition, the span in the theoretical approach is wide. Thus the pressure level is the object of speculation. Furthermore, it is not obvious that the measured pressure is in accordance with the real pressure. The measurement technique and the size and location of the sensors in relation to the process medium that creates the pressures are of particular importance. Acoustic resonance that involves effects such as damping or amplifying the true pressure is a factor that should be taken into account.

In this study the sensors were located in a cavity subsurface of a bar. Elastic silicon rubber was deposited on the surface as a protecting layer against wear. The calibration of the sensors included this surface layer, but the original calibration was performed without the plate present. Thus the pre-calibration of the sensors was obtained without considering the effect of location in the plate. However, the static calibration performed on site in the water pressure chamber i.e. post adjusted calibration, did not indicate lack of fit to the original calibration. Figure 6.33 shows that the calibration performed in the water pressure chamber fitted well with the original calibration.

Another question is what happens when the sensors pick up the high frequency pressure pulses? Is it adequate to assume that the measured pressure has reproduced the real pressure? The depth of the cavities between the sensor surface and the plate surface determines the extent of acoustic resonance. The corresponding resonance frequency of the pressure waves within the cavity determines the available frequency range to avoid damping or amplifying the real pressure signal. An operational range that gives a flat transfer function is the optimal solution. The theoretical approach of this theme is based on the Helmholtz resonator theory (Morse and Ingard (1986)). On the assumption that the locations of the sensors did not create any amplitude distortions, it is still a possibility that the measured pressure did not reproduce the real pressure. The operational frequency range of the sensor determines whether the pressure signal is amplified or damped. The natural frequency of the sensor should be much higher than the highest frequency component of the desired signal from the process, to give a flat transfer function and with that avoid such effects. The natural frequency of the fibre-optic sensors used in this study is claimed by the manufacturer of the sensors to be near 75-80 kHz with a frequency response just below that. A report made on similar sensors has revealed a flat response to frequency up to 10 kHz (Murphy (1996)). A dynamic frequency response test was not performed on the sensors used in this study.

One more assessment is related to the size of the sensor. It was desired that the sensor should be as small as possible to measure pressure fluctuations across a bar. The diameter of the sensor was approximately 1 mm. The small size could also be a drawback regarding the measurement of the dynamic pressure. If the particles in the pulp flow were considerably larger than the sensor surface then the surrounding bar area would capture some of the pressure on the particles. This would prevent the sensor from

measuring the real pressure. Flocs as agglomerates of fibres and shives are particles of large sizes. The flexibility and elastic properties of the pulp particles should also be included in this discussion. However, the latter is not considered more thoroughly in this thesis.

The summary of this discussion about possible uncertainties associated with the measurements is that the tests in the water pressure chamber indicated that the static pressure was well reproduced. However, there are still some uncertainties related to the probability of the sensors ability to reproduce the dynamic pressure.

Process data approach

In addition to the theoretical and experimental approach, some process variables were used as support to evaluate the pressure level or at least as support to select which flange on the sinusoidal curve the pressure corresponded to. The measured temperature in the refining zone should give an indication of the pressure level. Figure 6.34 shows the averaged temperatures measured in the two refining zones. The lower line in this figure shows the temperature distribution on the drive side of the refiner, which the pressure sensors were located as well. The average values were based on measurements done in a period of six hours, labelled *Run 1-20*. The measurements started approximately 2 hours after the production start-up. The pressure sensors that were located in approximately the same radial position as the temperature sensors are labelled in the diagram.

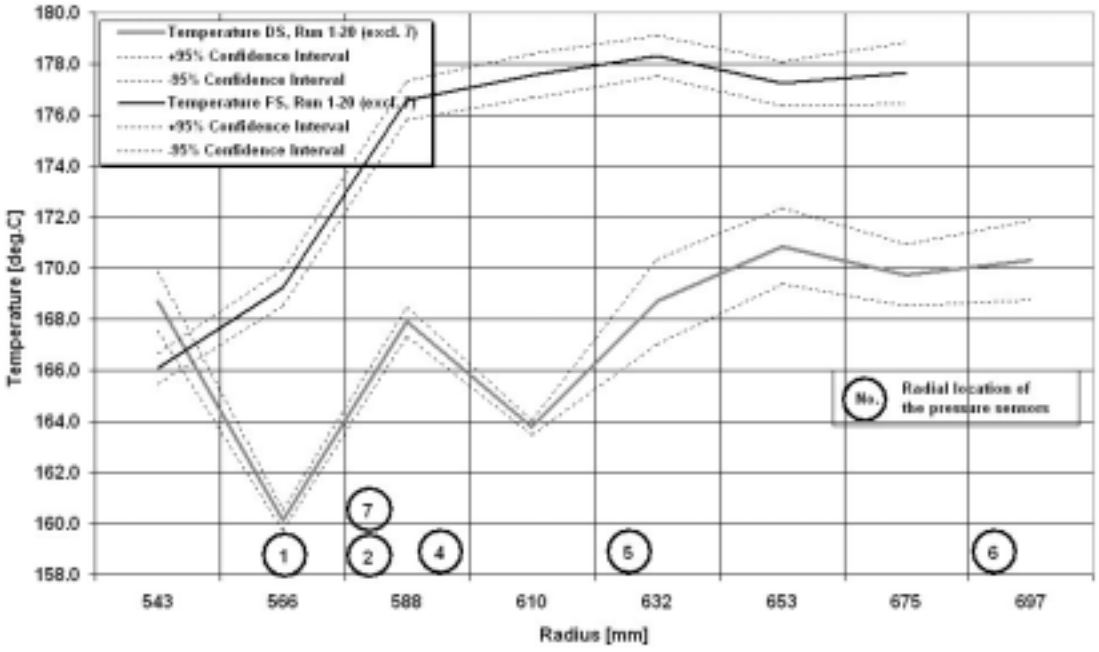

Figure 6.34: The radial distributions of the average temperatures, which were captured between two and eight hours after the production start-up are shown together with the location of the pressure sensors.

The temperature data showed unexpected profiles. The temperature distribution in the refining zone on the front side of the refiner (Figure 6.34) revealed high temperatures in

the outer part of the refining zone. A typical peak temperature was not present. At the drive side, the temperatures were highest in the outer part of the refining zone too. In addition, the distribution did not follow a typical parabolic curve. Mosbye *et al.* (2001) measured the temperatures in the same refiner using the same type of temperature sensors. Their temperature profile showed an expected parabolic form with the maximum temperature located in the intermediate zone as shown in Figure 2.7 as well.

The reason for the discrepancy from an expected temperature distribution was probably due to an imbalance in the refiner. The reason for the imbalance could be process related, refiner related, or any combinations of these. It could be that plates from two different manufacturers were used. The plates had different plate patterns and different tapers. Since the highest temperatures were measured in the fine bar zone, it is reasonable to believe that the main refining action appeared in this part of the refining zone. This is reinforced by the observed vibration and pressure pulse frequencies as shown in Chapter 7. The highest vibration amplitude was found in the fine bar zone (25.2 kHz) when the measurements were performed with new plates. The latter is supported by Strand and Hartler (1985) who claimed that the energy is being applied throughout the entire fine bar section.

Beside the temperature, the motor load and the acceleration variables from the mill's DCS have also been used in the following evaluation. Figures 6.35, 6.36 and 6.37 show values of three estimated parameters from the output signal from sensor No. 4. The estimated parameters are the average value, the standard deviation and the span from 1 MSamples (two seconds) of each recording. Together with these three variables from the pressure recordings, the corresponding average temperature, motor load and acceleration variables are shown. The temperature values were recorded from temperature sensor No. 2 located in the same refining zone, as the pressure sensors were mounted. Temperature sensor No. 2 was located almost in the same radial position as sensor No. 4. The acceleration values were recorded by the internal accelerometer mounted in the stator disc at the drive side of the refiner, where the pressure sensors were located as well. The acceleration is a measure of the vibrations in the refiner. This is used as an indicator of the plate clearance. A high acceleration value indicates a small plate gap and vice versa. The acceleration is measured in the number of g (1 g = 9.8 m/s^2), while the mill's DCS is using per cent (0-100 % = 0-20 g).

The diagrams shown in Figures 6.35, 6.36 and 6.37 are all based on measurements made in the first main period of the experiment. The upper plot in each figure shows the averaged voltage output signals from sensor No. 4 together with the actual process variable. The plots displayed in the middle show the corresponding standard deviation values for the recordings, while the lower plots show the span together with the process variables. Figure 6.35 shows the temperatures together with the variables from sensor No. 4 captured in the period from the production start-up to run No. 20 was performed. The values are averaged corresponding to the same capturing time. Figure 6.36 shows the averaged motor load together with the simultaneously captured pressure signal from all the recordings performed using sensor No. 4 in the first experimental period. Figure 6.37 shows the averaged acceleration values from run 1-30 together with the corresponding variables from sensor No. 4.

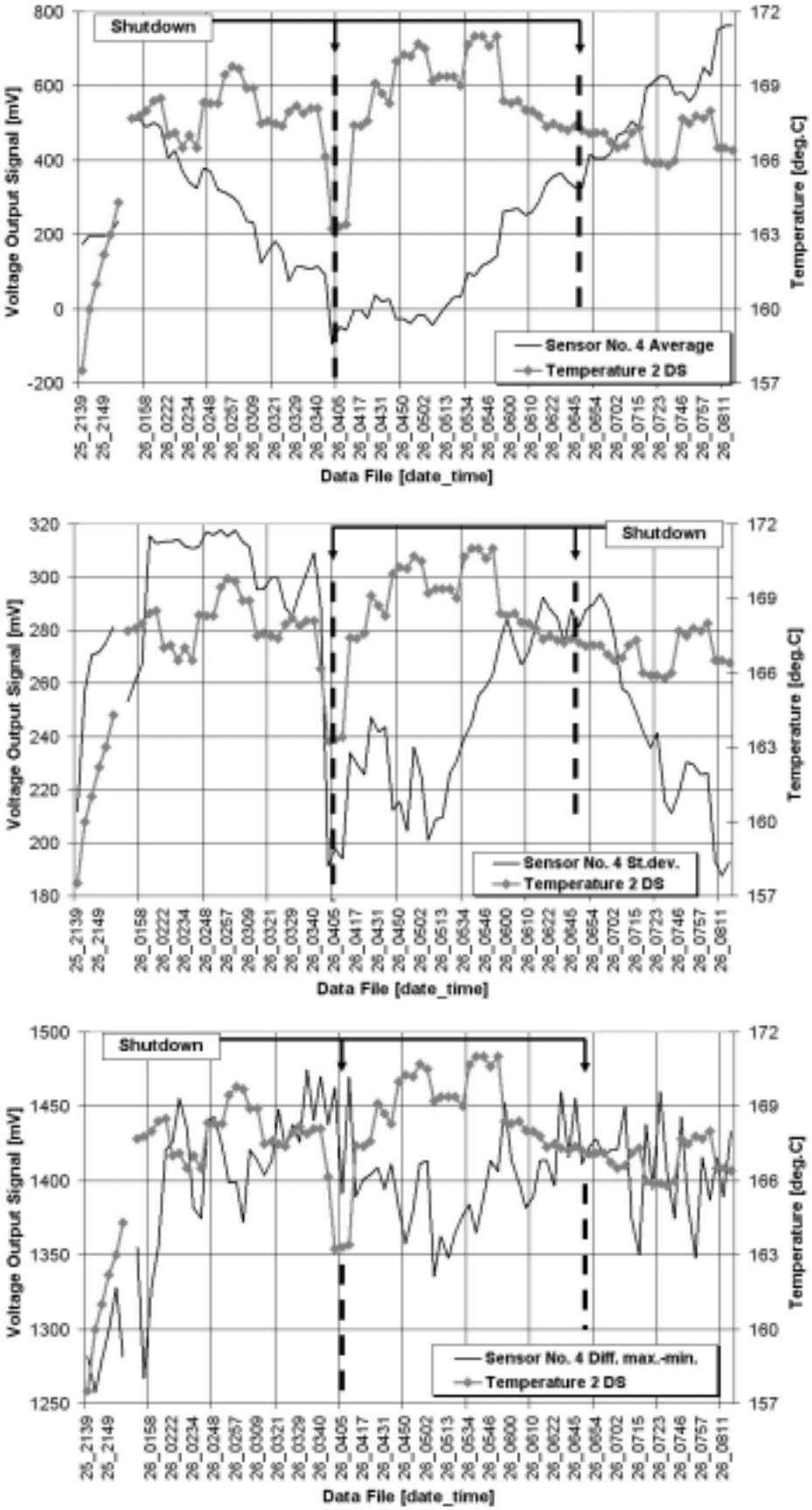

Figure 6.35: Average, standard deviation and span values from sensor No. 4 together with the temperature measured at the same radial position.

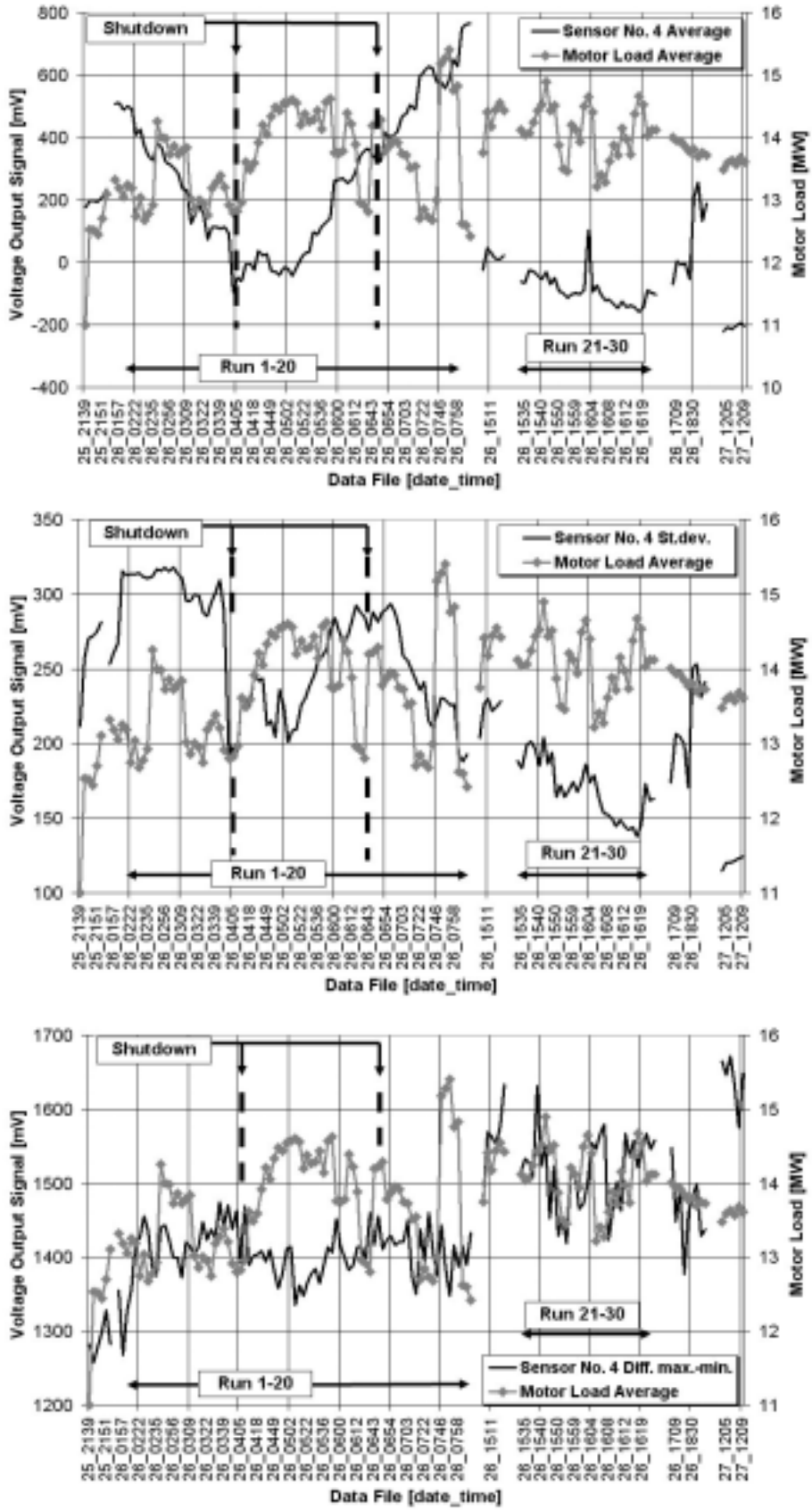

Figure 6.36: Average, standard deviation and span values from sensor No. 4 together with the motor load.

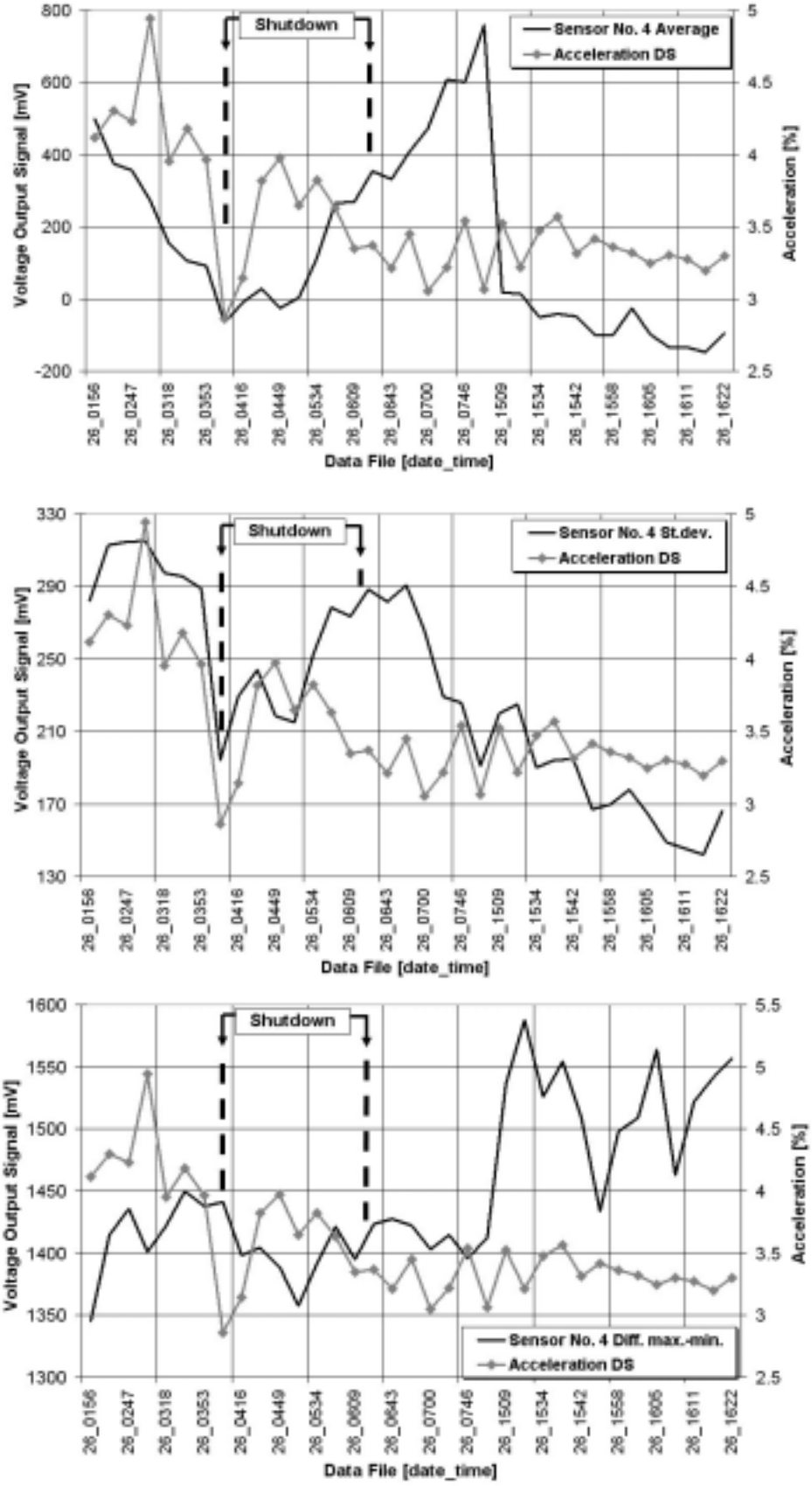

Figure 6.37: Average, standard deviation and span values from sensor No. 4 together with the acceleration values from the same refining zone.

The main assessments made from these diagrams are:

- The standard deviation values of the pressure readings fitted the temperature data to some extent, especially in the first period until the first shutdown, as shown in Figure 6.35, plot in the middle. After the shutdown the standard deviation values seem to be delayed compared with the temperature readings. However, after the first shutdown the average values, upper plot in all three figures, were small indicating that the output signal crossed a minimum of the sinusoidal fringe pattern. This would certainly reduce the standard deviation of the output signals. However, the standard deviation values as a measure of the dynamic range of the output signal, did not reach the same level as before the shutdown, while the temperature increased to a higher level for a short period of approximately one hour.

- The span, i.e. the difference between the maximum and the minimum readings, followed the motor load variable to some extent as shown in the lower plot in Figure 6.36. This was especially so in the first part of the experimental period and in the period labelled *Run 21-30*. It should be remembered that the Twin-refiner has two separate refining zones and that the motor load is dependent on what is happening in both of the refining zones. However, there is reason to believe that the actions that occur in one refining zone can dominate the load, and that such action can switch in turn between the zones as discussed further in Section 6.7.

- The standard deviation values of the pressure signal and the recordings of the acceleration had the same decreasing trend as shown in Figure 6.37, plot in the middle. This indicates decreasing pressure variations and an increasing plate clearance. Probably the rotor disc was moved towards the front side stator disc because of an uneven chip distribution. This probably led to a wider plate gap on the drive side while the disc clearance at the front side became smaller. This hypothesis is supported by investigations of the development of the acceleration and temperature variables related to both of the refining zones as shown in Section 6.6, Figures 6.46 – 6.49. This phenomenon is discussed in Section 6.7. In addition, it can be mentioned that the pressure measurements indicated smaller activity in the refining zone when the plate gap was assumed to be wider. This is shown in Figure F4 where the signal from sensor No. 4 was analysed. No process related frequencies were found in the amplitude spectrum as opposed to earlier observations for instance shown in Figure 6.10.

- It is reasonable to believe that the output signal can be related to different flanges on the sinusoidal calibration curve. This judgement is based on the lack of correlation between the averaged output signal and the process variables. A clearer relationship than shown by the raw data was expected. Shortly after start-up the span and standard deviation values were small as shown in Figure 6.35. This indicates that the dynamic pressure was low, which can also indicate that the average pressure was low. Until the first shutdown the average output signal decreased, which can indicate increasing pressure. This is supported by the high standard deviation values. After this shutdown the voltage output signal increased, while the acceleration and

the standard deviation values decreased as shown in Figure 6.37. This may indicate a decreasing pressure.

Based on these judgements, a diagram of the assumed average pressure signal has been plotted together with the motor load. This is shown in Figure 6.38. Here the average pressure is converted from different flanges of the sinusoidal calibration curve. A corresponding plot containing converted pressure readings from all three flanges are shown in Figure F6. Converted standard deviation values from sensor No. 4 through a linear relationship between pressure and voltage are displayed in Figure 6.39.

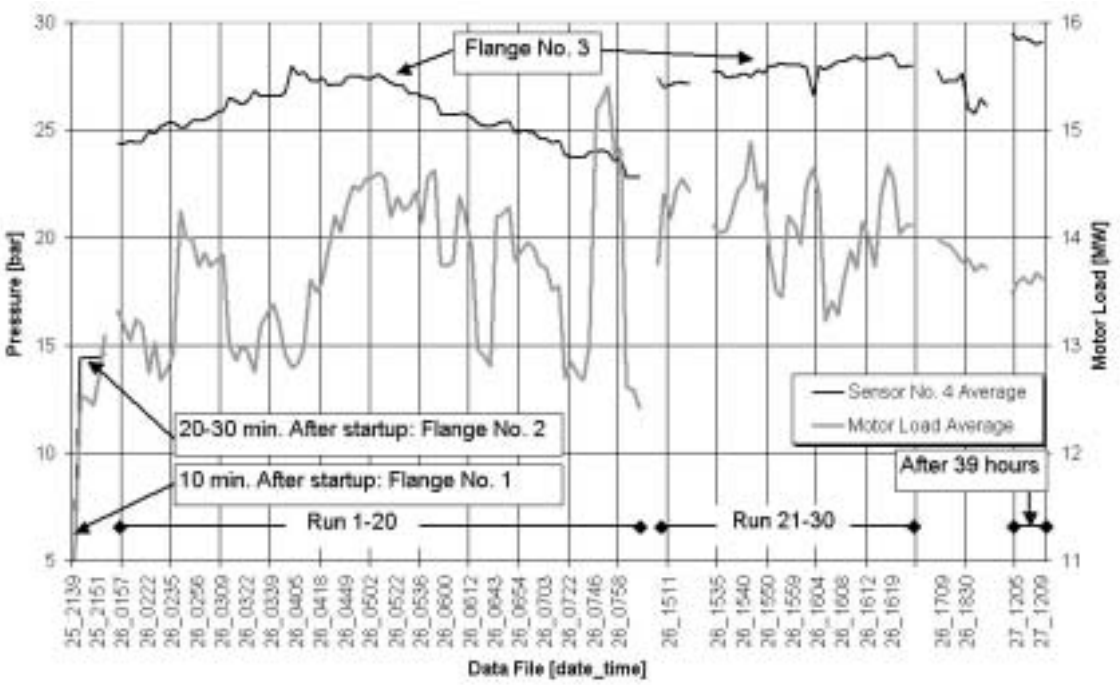

Figure 6.38: Average values from recordings performed by sensor No. 4 converted to pressure through three different flanges of the sinusoidal calibration curve are shown together with corresponding recordings from the motor load.

The following assessments are made, all related to Figure 6.38, about the selection of the flanges:

- The first data file, captured 10 minutes after start-up, was converted through the first flange i.e. the averaged pressure was 7 bar. The corresponding motor load was low, only 11 MW. The hydraulic thrust, i.e. the differential pressure applied on the hydraulic cylinders, was only 96 bar. In addition, it can be assumed that the steam forces were weak because of the low temperature values (approximately 155 ºC corresponding to 4.4 bar saturated water vapour pressure). Temperature readings captured during this production start-up are shown in Figure F7.

- The next four readings were captured approximately 10 minutes later during a period lasting for 10 minutes. Flange number two was selected to represent these readings, which gave average pressures in the order of 14 to15 bar. However, the hydraulic thrust was high. It increased from 110 to 114 bar during this period. The selection of flange number two compared with flange number three was based on the fact that the motor load still was relatively low, and that the pressure converted to flange number two rose in the same manner as the motor load. See also Figure F6. The refiner had probably not reached the heat level to maintain fast water evaporation. The temperature was increasing during this period, but it had not reach more than approximately 165 ºC (6.1 bar) before the last pressure recording was performed. Thus the steam pressure was probably at a relative low level, but certainly enough to keep up the self-pressurization without any additional steam contribution.

- In the period labelled *Run 1-20*, between 4 and 10 hours after the start-up, the process conditions were changed steadily as a consequence of the factorial designed experiment as discussed in Section 6.6. From this period the voltage output signal was converted to pressure according to flange number three. Hence, until the unexpected shutdown after two hours duration, the pressure increased. After the shutdown the pressure slowly decreased.

- After a break of seven hours the next period labelled *Run 21-30* was performed. The pressure readings were still converted through flange number three as the rest of the readings in this diagram, Figure 6.38. The discontinuous pressure readings between the two periods labelled *Run 1-20* and *Run 21-30* produced an uncertainty about the selection of flange. The acceleration values decreased in the last part of the first period (*Run 1-20*). Furthermore, the acceleration was stabilized at a low level during runs 21 to 30. Since the pressure readings decreased as well as the acceleration values, it could be expected that the pressure continued to decrease, or at least was stabilized at a lower level instead of increasing as shown here. If flange number two was selected instead of flange number three, the pressure would followed a slowly decreasing trend between approximately 14 to 13 bar as shown in Figure F6. In addition, the fact that the periodic signal patterns from the recordings performed using sensor No. 4 were strongly damped support the uncertainty about the selection of the third flange as representative for the pressure readings in this period labelled *Run 21-30*. The choice was determined by the last readings, labelled *After 39 hours*.

- The readings after 39 hours were also shown in Figure 6.5 together with simultaneously captured readings from sensor No. 8. The recordings shown in Figure 6.5 were captured during a start-up after a short shutdown. The choice of flanges in this figure resulted in well-correlated pressures from sensors Nos. 4 and 8. Thus, this correlation supports the selection of the third flange in Figure 6.38.

The choice of the third flange that resulted in average pressures between 20-30 bar was made despite the theoretical considerations that expected average pressures between 10-20 bar. However, there are some uncertainties associated with this determination of the pressure levels. The uncertainty was related to both signal offsets and the extent of

data that can have crossed a minimum or maximum point of the sinusoidal calibration curve. The latter make the determination of the average value uncertain. A new or an additional demodulation scheme could have reduced the uncertainty as briefly discussed in Chapter 9.

Other pressure readings that confirm the reliability of the pressure measurements are shown in Section 6.7. In this section pressure data captured during manipulation of the chip distribution to the two refining zones are shown. The responses on the process changes are evidently proven. The voltage output signal from sensor No. 4 was also converted according to the third flange in that section.

The corresponding standard deviation values for the pressure recordings discussed above are shown in Figure 6.39. These values are converted to pressure through an ordinary linear relationship between the voltage readings and the pressure given by the span of one flange in the sinusoidal transfer function curve.

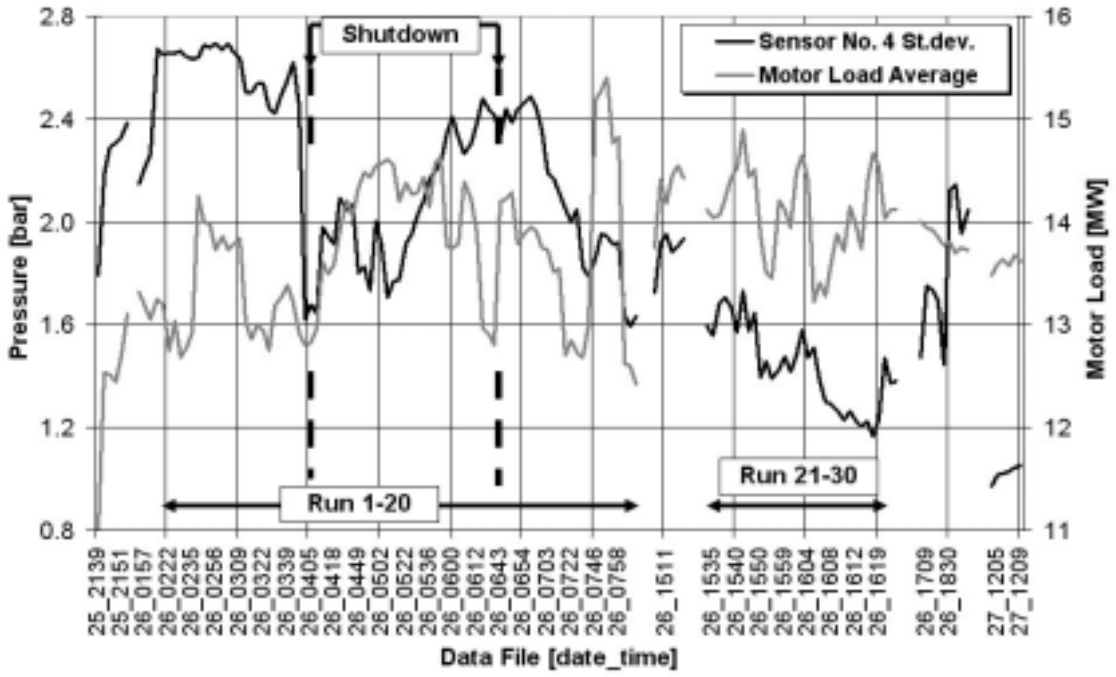

Figure 6.39: Standard deviation values from sensor No. 4 converted to pressure.

6.6 Responses of the factorial designed experiment

The main idea behind the factorial designed experiment was to find relationships between the readings from the pressure sensors and the main process variables as well as the pulp properties. The experiment was conducted in a randomized order to avoid serially correlated errors. Furthermore, the experiment was divided in two individual blocks. The first part of the experiment contained 20 runs performed under different operational conditions. This part started approximately four hours after the production start-up. It lasted for a period of approximately six hours. The second part was conducted after a break of approximately eight hours and lasted for three hours. Meanwhile, the process conditions were changed. Thus, it was necessary to find a new centre point regarding the manipulated variables for the last 10 runs. The change to new centre points involved three of four variables. The production rate and the casing pressure were reduced compared to the corresponding levels in the first period, while the amount of dilution water was increased. The prevailing operational conditions of the process are shown in Table 6.8 and in Figures 6.40 to 6.43.

Compared with the original experimental plan shown in Section 3.6.3, Tables 3.6a and 3.6b, the conducted experiment diverged somewhat. The adjustments of the set points were one of the diverging parts. In addition, one run was not conducted. Run No. 4 was performed with the dilution water flow at a low level instead of at a high level as intended. This run was therefore carried out as a replicate of run No. 9. Thus, a full factorial designed experiment was not accomplished. The following analyses have been based on regression analysis instead of a factorial analysis. However, the two methods give no difference in achieved results.

The following analyses regarding the relationship between the output signals from the pressure sensors and the manipulated variables as well as other process and pulp variables are based on the readings from sensor No. 4. This sensor was chosen because the output signal from this sensor was investigated more thoroughly than the recordings from the other sensors. In addition, more recordings were captured from sensor No. 4 than from any others.

Table 6.8: Manipulated variables during the factorial experiment.

Run order	Hydraulic thrust [bar]	Production [tonnes/day]	Dilution water flow [l/s]	Casing pressure [bar]
1 (CP) [1]	**108.0**	**280**	**1.86**	**4.0**
2	103.9	263	1.71	3.9
3	112.2	296	1.72	4.1
4 (R 9)[2]	**112.2**	**263**	**1.71**	**3.9**
5	102.9	296	2.01	4.1
6 (CP)	**108.0**	**280**	**1.86**	**4.0**
7	103.8	263	1.72	4.1
7	103.9	263	1.73	3.9
8	112.2	296	2.02	4.1
9	**112.2**	**263**	**1.71**	**3.9**
9	**112.2**	**263**	**1.72**	**3.9**
10	103.9	296	1.71	3.9
11	112.2	296	2.02	3.9
12 (CP)	**108.0**	**280**	**1.86**	**4.0**
13	103.9	298	1.71	4.1
14	112.2	263	2.03	4.1
15	112.2	265	1.70	4.1
16 (CP)	**108.0**	**280**	**1.87**	**4.0**
17	103.9	296	2.01	3.9
18	103.9	263	2.01	3.9
19	112.2	296	1.71	3.9
20	103.9	263	2.00	4.1
(21)	111.6	269	2.03	3.8
(22)	107.5	283	2.06	3.9
New CP	**107.5**	**269**	**2.00**	**3.8**
21	**111.6**	269	1.99	3.8
22	107.4	**285**	2.00	3.8
23	107.4	269	**2.17**	3.8
24	107.4	269	1.99	**3.9**
25	**107.4**	**269**	**2.00**	**3.8**
26	107.4	**253**	2.01	3.8
27	**103.3**	269	2.00	3.8
28	**107.5**	**269**	**2.00**	**3.8**
29	107.5	269	**1.85**	3.8
30	107.5	269	2.01	**3.7**
Std. Deviation[3]	**0.04**	**0.4**	**0.02**	**0.02**

1 CP: Centre point
2 R: Replicate.
3 Pooled estimated standard deviation.

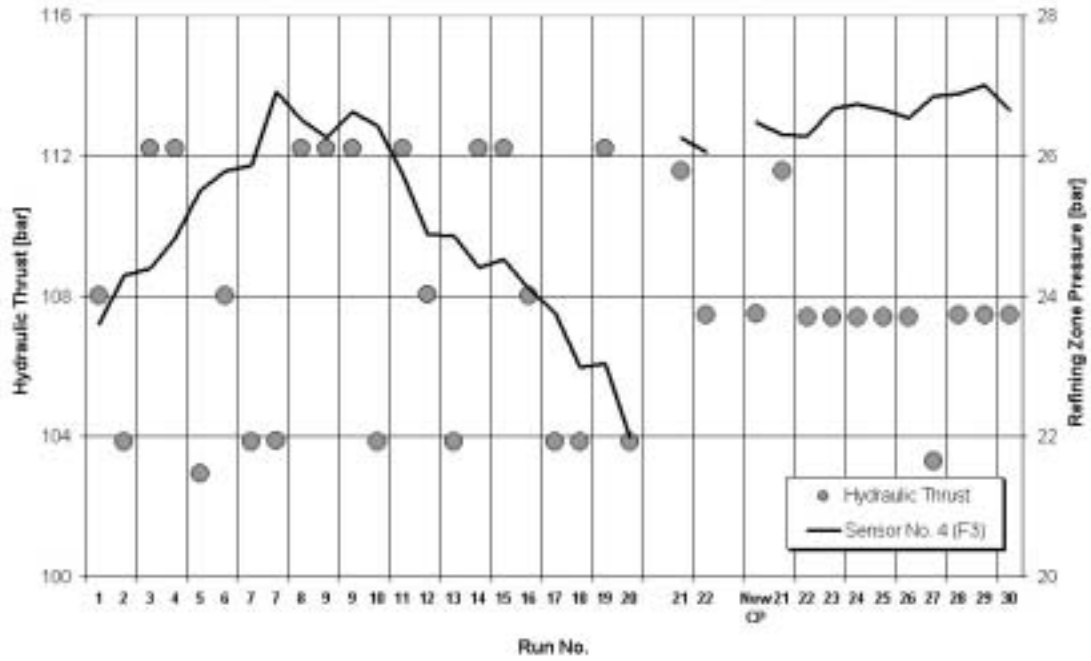

Figure 6.40: The hydraulic thrust as the first manipulated variable of the experiment is shown together with the average pressures recorded by sensor No. 4. The pressures are converted through the third flange of the calibration curve.

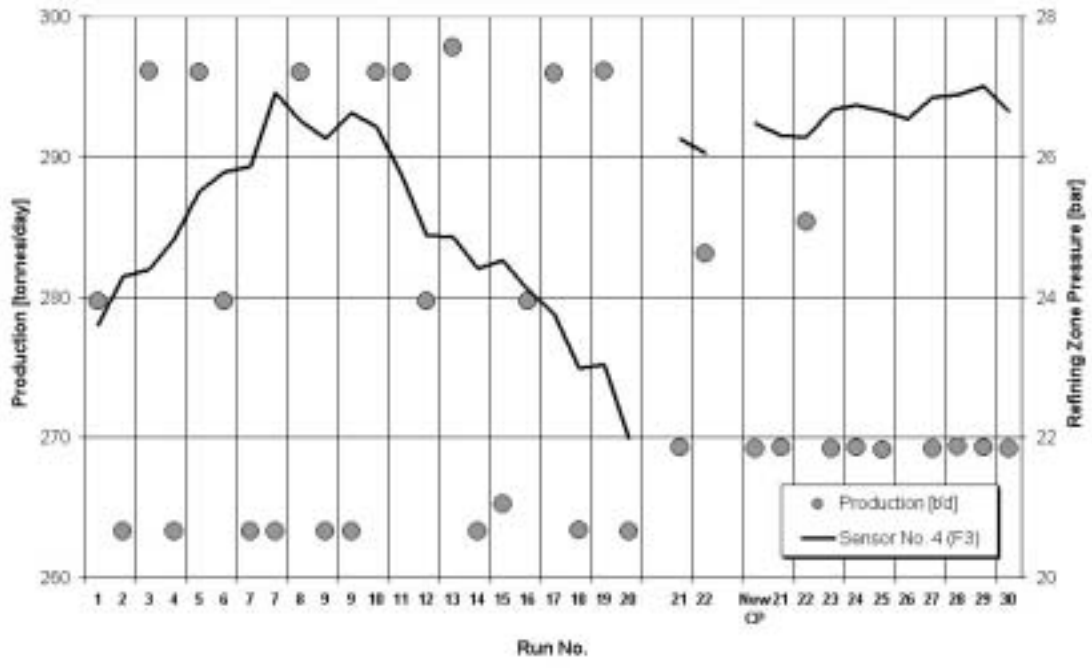

Figure 6.41: The production rate as the second manipulated variable of the experiment is shown together with the average pressures recorded by sensor No. 4.

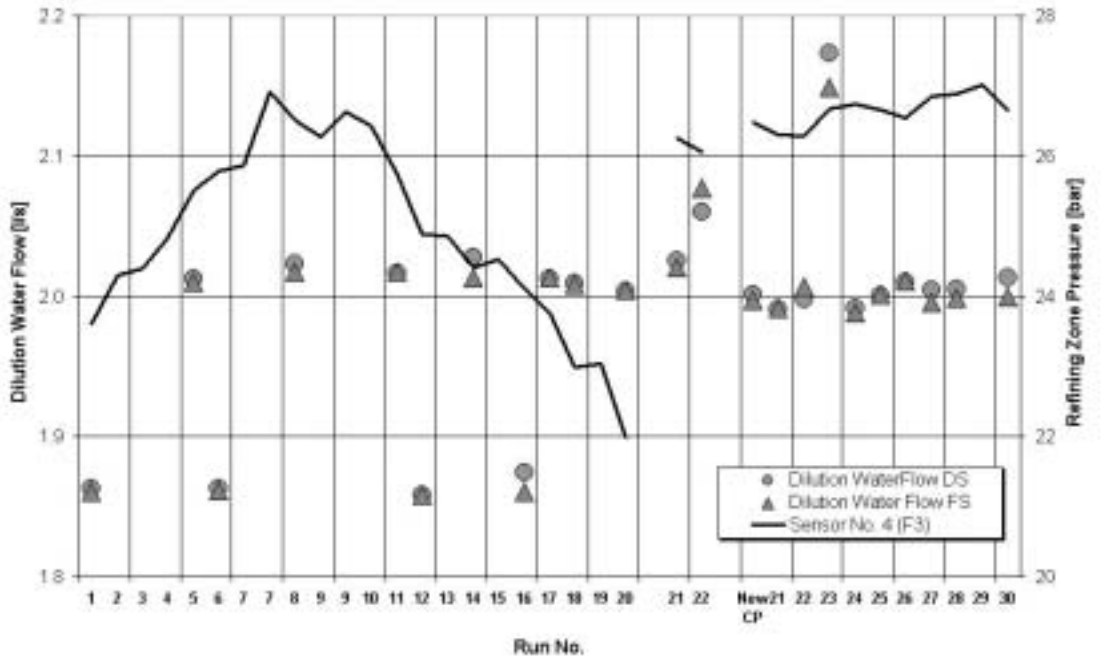

Figure 6.42: The amount of dilution water flow as the third manipulated variable of the experiment is shown together with the average pressures recorded by sensor No. 4.

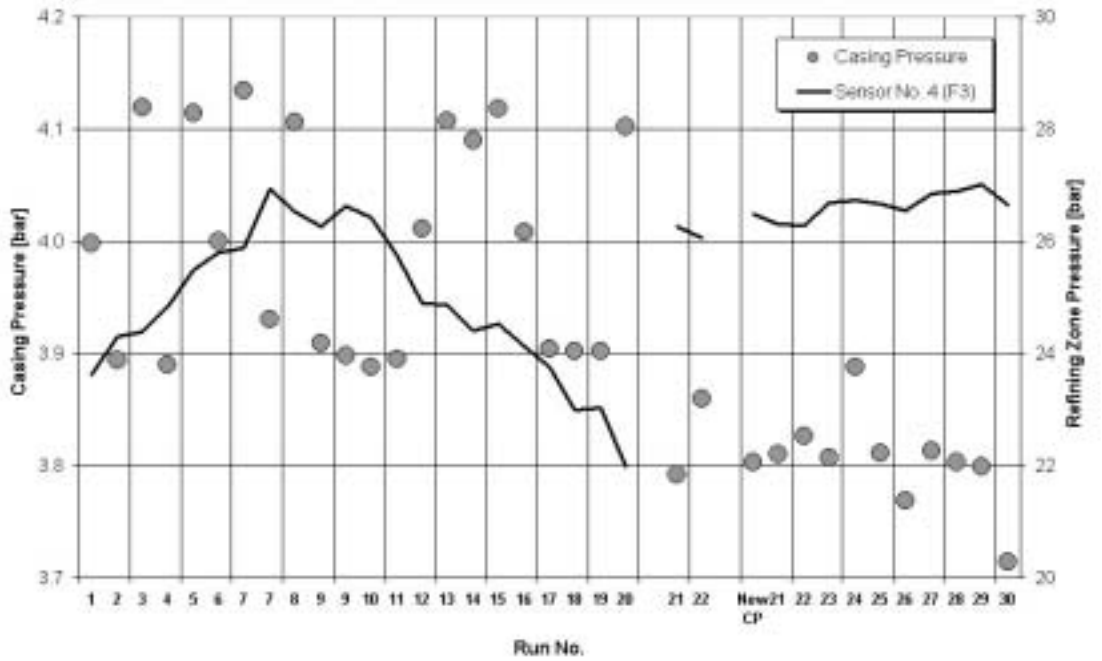

Figure 6.43: The casing pressure as the fourth manipulated variable of the experiment together with the average signals from Sensor No. 4 converted through the third flange of the calibration curve.

6.6.1 Visual inspection of the responses

The responses from some other process variables i.e. acceleration, motor load and temperature, which were recorded during the factorial experiment, are shown in the next figures. The output signal from sensor No. 4 is displayed in Figure 6.44 together with the acceleration variable on the drive side of the refiner. The average pressures have been converted through the third flange of the calibration curve. The standard deviation values from the pressure readings are shown in Figure 6.45. The standard deviation values have been converted to pressure using a simple linear approximation between the pressure and the voltage output signal. This approximation was derived from the span value, which was used in the earlier conversions as discussed in Section 6.5, Table 6.6.

Figure 6.46 shows the motor load together with the acceleration measured at the drive side of the refiner, while Figure 6.47 shows the motor load together with the acceleration on the front side. Linear regressions of the variables are displayed in both figures. The linear regression of the motor load has been made from the four values obtained when the process was operated with equally operating conditions. These four runs are labelled as centre points in Table 6.8. The regressions of the acceleration variables are based on all the averaged values that appeared from run 1-20.

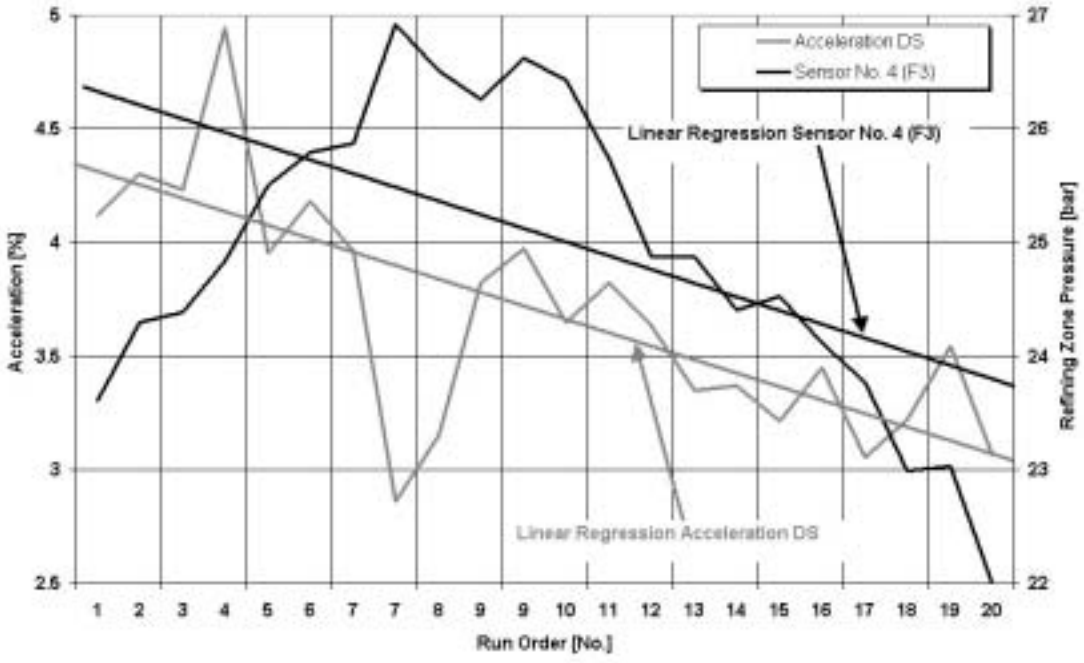

Figure 6.44: The acceleration measured on the drive side of the refiner during the first period (run 1-20) of the experiment is shown together with the average pressures recorded by sensor No. 4. The pressures are converted through the third flange of the calibration curve.

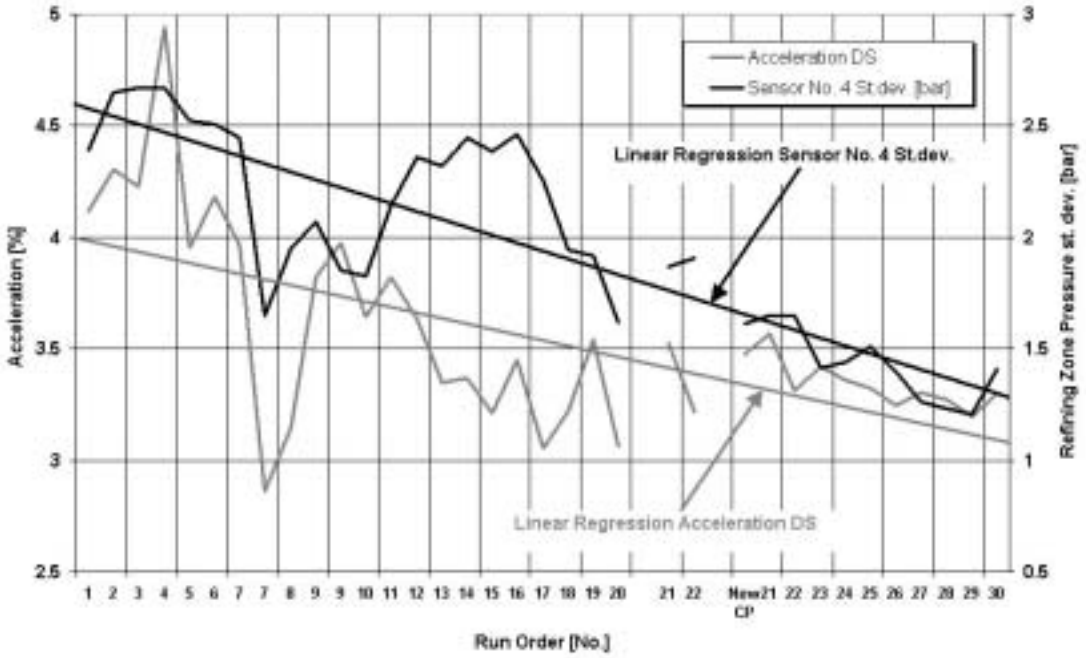

Figure 6.45: The acceleration measured on the drive side of the refiner is shown together with the standard deviation values from sensor No. 4. The standard deviation values are converted to pressure through a linear relationship between the pressure and the voltage readings.

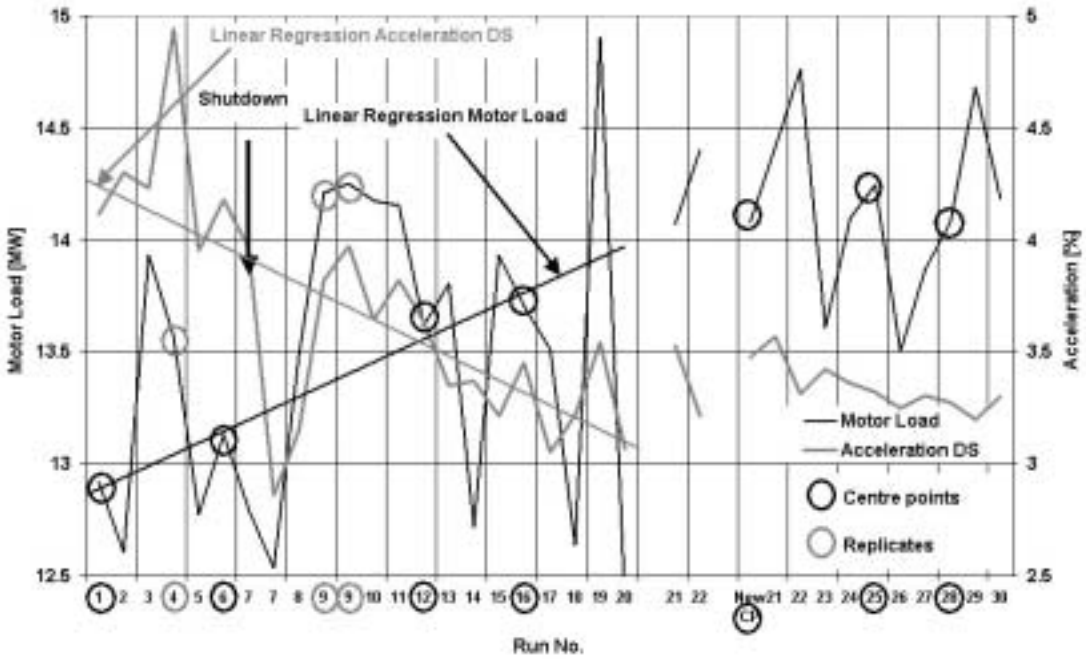

Figure 6.46: The responses from the motor load and the acceleration on the drive side of the refiner recorded during the whole factorial experiment (run 1-30).

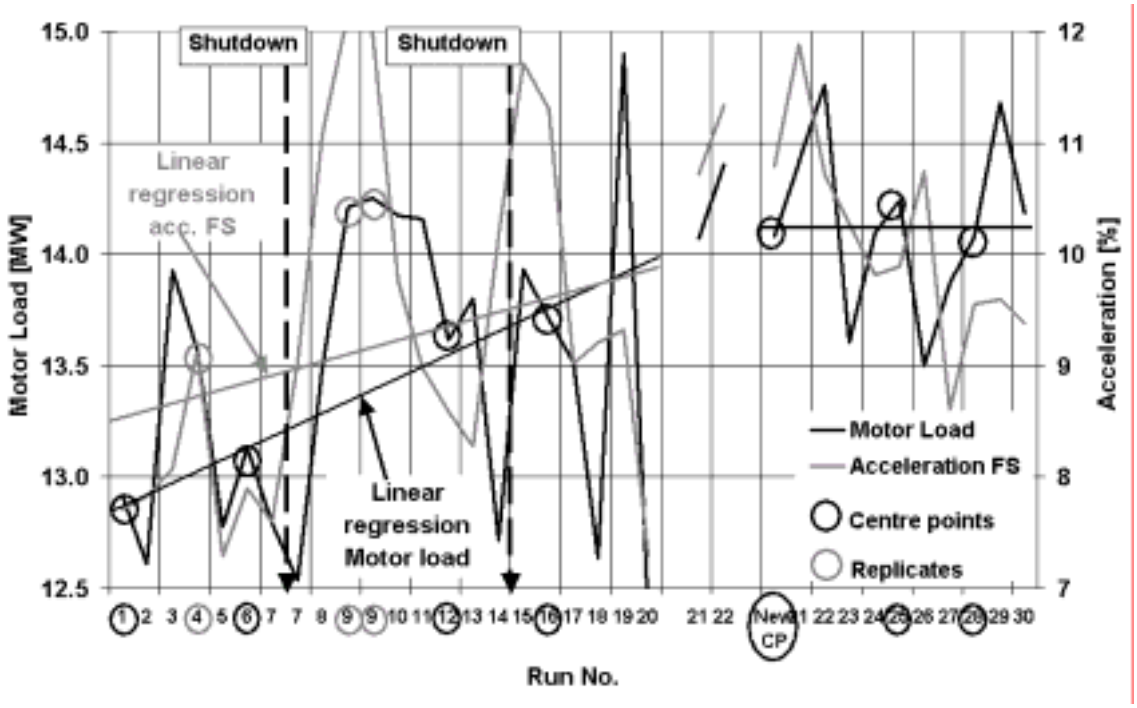

Figure 6.47: The average values of the motor load and acceleration from the front side captured during 30 runs of the factorial experiment.

Additional information about the process behaviour has been found from corresponding analyses of the temperature measurements. Figures 6.48 and 6.49 show the average temperature readings, measured respectively on the drive side and the front side of the refiner, from each run in the first part (run 1-20) of the experiment. The regression lines have been made from the average values obtained from run 1-20 except from the secondary run No. 7. The temperature readings captured during run No. 7 were low compared to the readings from the other runs. Obviously this is because this run was conducted shortly after a start-up. A too high casing pressure caused the corresponding shutdown, which only lasted for a few minutes.

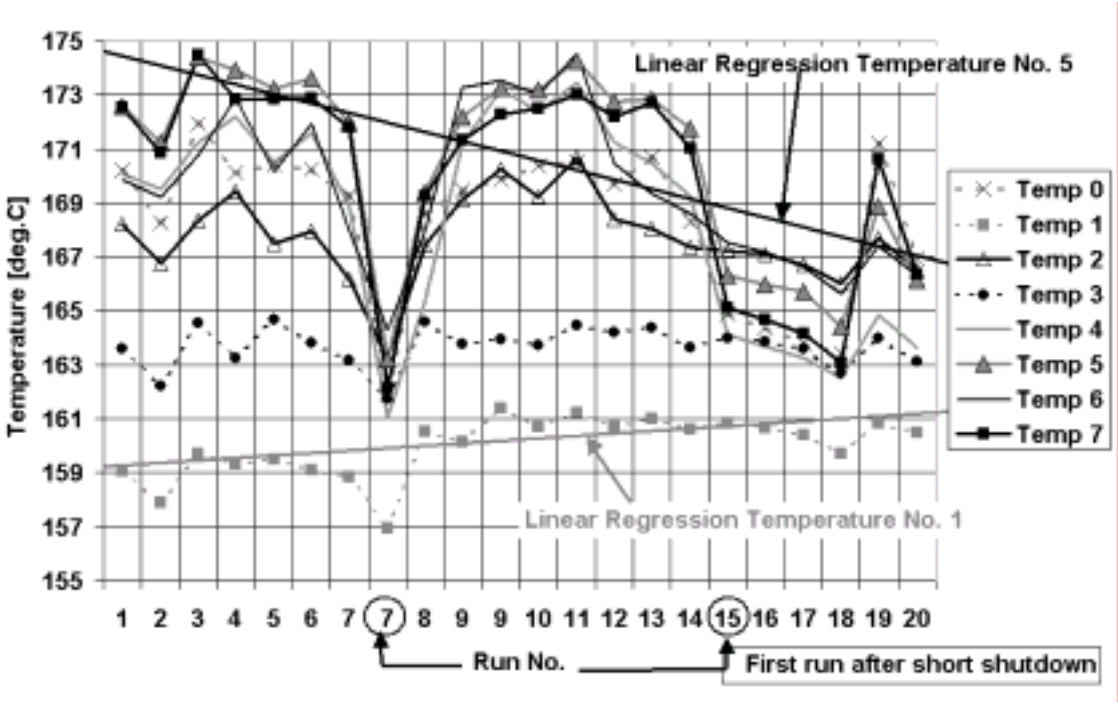

Figure 6.48: The responses from the temperature sensors located on the drive side of the refiner.

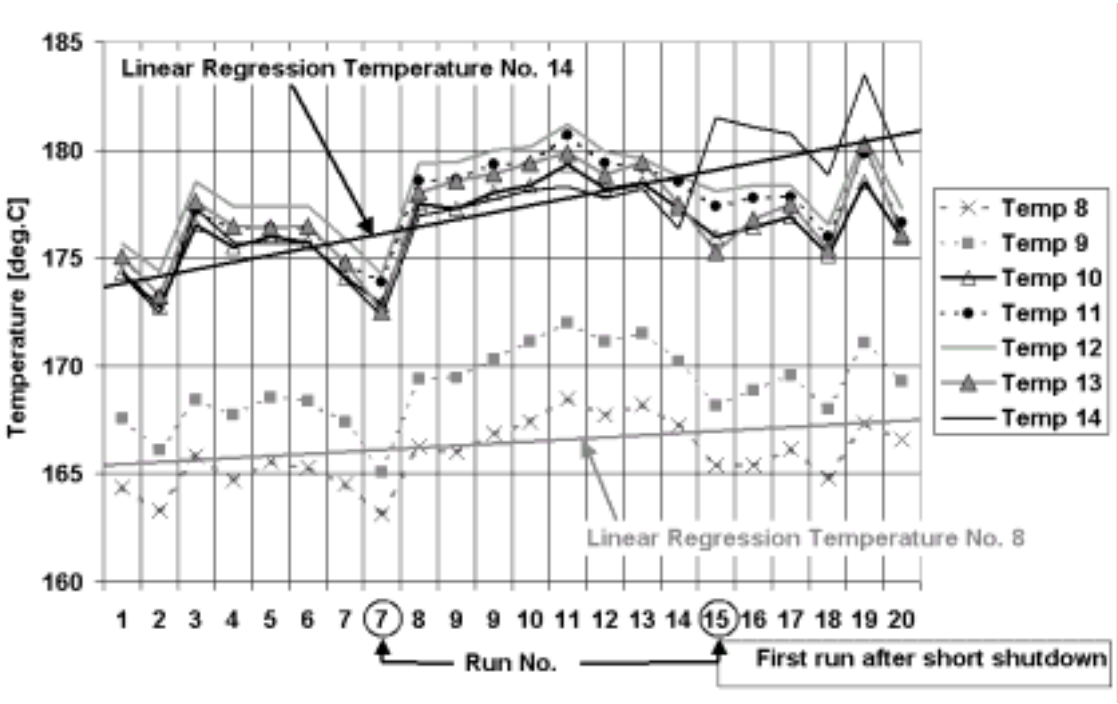

Figure 6.49: The responses from the temperature sensors located on the front side of the refiner.

It is evident from Figures 6.44 to 6.49 that there has been a continuous change in process conditions not related to the experimental design. The responses of the

temperatures, motor load and acceleration signals showed clear signs of time dependency. Some discussion of this is needed before the numerical analysis is considered.

- The motor load increased with time as shown by linear regression between responses from equal process conditions labelled as replicates in Figures 6.46 and 6.47. In the last part of the experiment the motor load associated with the replicated runs were independent on time.
- The acceleration in the front side of the refiner was positively correlated with the motor load as shown in Figure 6.47. The acceleration on the drive side, Figure 6.46, was negatively correlated.
- The temperatures shown in Figures 6.48 and 6.49 were positively correlated with the corresponding acceleration variables on each side of the refiner. The temperature readings from the inner part of the refining zone, (temperature No. 1) on the drive side of the refiner (Figure 6.48), were increasing. Thus, the temperature in this part of the refining zone was negatively correlated with the other temperature variables in the same refining zone.

Different hypotheses or combinations of hypotheses may explain the observed time dependency shortly after the production start-up. The following hypotheses have been formulated:

- The increasing trends of the motor load, acceleration and temperatures measured on the front side of the refiner together with the corresponding decreasing trends of the acceleration and temperatures on the drive side indicate that the process was not stabilized. These trends indicate that the rotor disc moved towards the front side of the refiner. Thus, it is likely that the plate clearance increased on the drive side while the gap decreased on the front side. This assumption is made in spite of the fact that the refiner has a fixed bearing. However, the fixed bearing has some necessary slack. The reason for this apparent rotor movement might be found in an uneven chip distribution between the two refining zones despite the chip-stream splitter being held constant during this experiment. Mosbye *et al.* (2001) showed that the process conditions in the two refining zones could be equalized by adjusting the chip-stream splitter. The influence of the pressure readings while changing the chip-stream splitter device is as well discussed in Section 6.7.

- The increasing trend revealed by the temperatures measured in the inner part of the refining zone, on the drive side of the refiner (Figure 6.48), was opposite to the trends shown by the other temperatures. This probably represented a continued heating of the refiner. The heating of the refiner before the chips were fed in was probably not enough to maintain the temperature in the discs when the relative cold chips (70 ∀C) and dilution water (94 ∀C) were fed in. Before the temperature in the refining zone has been established at a high level, the inner part of the refining zone will be cooled down to a greater extent than the outer part because of the large plate gap and the smaller disc-fibre contact. In the outer part of the refining zone the heating is faster. However, the generated steam in this part of the refining zone

cannot compensate for the temperatures of the large amount of water (approximately 2 l/s per refining zone) and moist chips fed in.

- In addition, the time consumed to fill up the grooves of the new plates by stagnant pulp may be an indirect and additional cause of the observed trends. The time constant regarding the heating of the refiner is not known. Additional temperature readings from the start-up are shown in Figure F7.

- Another reason for the observed temperature trends, that should not be excluded, is that an uneven chip distribution between the two refining zones may occur, despite the stream splitter being held constant. According to Mosbye *et al.* (2001) the temperature distribution and especially the temperatures in the inner and outer parts of the refining zone can vary due to variations in other process variables.

The trend in the pressure signal, both average and standard deviation, as shown in Figures 6.44 and 6.45 followed the corresponding temperature and acceleration variables. This indicates that the pressure readings measured process related influences that happened in the local refining zone. Additional information, as shown in Figure F8, obtained by investigation of the peak frequency (25.2 kHz) development, supports these observations of decreasing trends. However, because of the uncertainty about the determination of the absolute pressures and the corresponding dynamic range, it is difficult to state how valuable the pressure readings have been. In addition, it is not concluded what exact information the pressure sensors have given compared with the other process variables. Since the factorial designed experiment was conducted shortly after the production start-up this has probably reduced the opportunity to extract the expected yield of what an experiment like this could have achieved if it was performed during stabilized operational conditions. The reason why the experiment was started shortly after the production start-up was associated with the uncertainty of the survival of the sensors in the harsh environment. However, the new plates and a relatively cold refiner may not be the whole reason for the time dependencies. The inherent features associated with the two refining zones of the Twin-refiner may mainly have caused these observed conditions. It can be stated that this effect that created the time dependency, was stronger than the effects given by the manipulation of the four process variables.

6.6.2 Regression models – 30 runs

Due to the time dependent instability of the process, very clear relationships from the factorial experiment were not expected. Table 6.9 shows calculated regression coefficients and the R^2 statistic for significant (95 % level) models of responses associated with the four manipulated process variables. The response variables motor load, accelerations and three of the temperatures from both sides of the refiner were investigated. The selected temperatures were from the inner, middle and outer part of the refining zone. In addition, the converted output signal from sensor No. 4 as the average pressures and the corresponding standard deviation values were investigated as response variables.

Table 6.9: Regression coefficients from significant (95 % level) models using the manipulated process variables as input variables.

Response variable	Period	Manipulated variables, X_i				Correlation R^2	[2]Max. R^2
		Hydraulic thrust [bar]	Production [t/d]	Dilution water flow [l/s]	Casing pressure [bar]		
		Coefficients, η_i					
	Run	kW / BAR	kW / t/d	kW / l/s	kW / bar	[%]	[%]
Motor load [kW]	1-30	89	24	-720	-4240	67	95
Motor load [kW]	1-20	101	26	-1950	-2000	81	93
Motor load [kW]	21-30	NS[1]	40	-3160	NS	90	95
Adjusted motor load [kW]	1-20	102	27	-2710	-1760	90	98
	Run	% / BAR	% / t/d	% / l/s	% / bar	[%]	[%]
Acc. FS [%]	1-30	0.24	NS	NS	NS	45	76
	Run	ºC / BAR	ºC / t/d	ºC / l/s	ºC / bar	[%]	[%]
Temp.2 DS [ºC]	1-20	0.23	NS	NS	NS	44	85
Temp.11 FS [ºC]	1-20	0.27	0.065	NS	NS	51	81
	Run	bar / BAR	bar / t/d	bar / l/s	bar / bar	[%]	[%]
Sensor No. 4 average [bar]	1-30	NS	NS	NS	-6	28	87
Sensor No. 4 standard dev. [bar]	1-30	NS	NS	-1	3	55	91

1 NS: Not significant.
2 Maximum possible value of R^2 when pure error is considered (Box and Draper (1987)).

The regression analyses reveal that the motor load was most clearly affected response variable. In addition, when the motor load readings were compensated for the trend shown in Figures 6.46 and 6.47, the regression was further improved. This compensation was based on the assumption that the trend was present during the first part (run 1-20) of the experiment. The motor load values were detrended through the 20 runs as shown in Figure F9.

It was expected that the regression models of the temperatures and the accelerations should have revealed a much higher significance level. Both Mosbye *et al.* (2001) and Engstrand *et al.* (1995) indicated a clear relationship between these variables and other process variables. The regression analyses have indicated (significant on 90 % level)

that the temperatures measured closest to the centre of the refiner were more affected by the amount of chips fed in than the other temperatures. This is in agreement with results reported by Mosbye *et al.* (2001) made in the same refiner and using the same type of temperature sensors as used in this experiment. Furthermore, the hydraulic thrust was the main influencing factor on the temperatures during this factorial experiment. The regression models of temperature No. 11 (front side) and temperature No. 2 (drive side), as shown in Table 6.9, show this. On both sides of the refiner, the temperatures measured in the intermediate zone were the most affected temperatures. The reason why these temperatures were the most affected temperatures may be associated with that higher refining activity was present in the intermediate zones than in the other zones.

The pressure recorded from sensor No. 4 was weakly affected by the manipulated variables. The casing pressure and the dilution water flow-rate were only variables that gave significantly models as shown in Table 6.9. The negative sign of the regression coefficient of the casing pressure in the model of the average pressure was surprising. Increased casing pressure was expected to give increased refining zone pressure. A possible reason for this result may be explained by the sinusoidal relationship between the pressure and the voltage output signals. The pressure converted through the third (decreasing) flange gave this negative relationship. However, a different (increasing) flange would have given a positive relationship. It is further indicated that the standard deviation of the pressure increased when the casing pressure rose, while increased dilution water added gave a reduced standard deviation. The latter is conceivable because more water gives more steam that counteracts the hydraulic forces.

Table 6.10 shows regression coefficients from models of the motor load and the accelerations regressed against temperature variables at different locations in the refining zone. The models were single regression models using only one temperature variable as input variable in each model.

Table 6.10: Regression coefficients from significant (95 % level) models using temperature data as input variable.

Response variable (Period: Run 1-20)	Input variable, X						Correlation R^2
	Temperature 0 DS [°C]	Temperature 2 DS [°C]	Temperature 7 DS [°C]	Temperature 8 FS [°C]	Temperature 11 FS [°C]	Temperature 14 FS [°C]	
	Coefficient, η						
	kW/°C	kW/°C	kW/°C	kW/°C	kW/°C	kW/°C	[%]
Motor load [kW]	*	280	*	*	*	*	43
Motor load [kW]	*	*	*	280	*	*	34
Motor load [kW]	*	*	*	*	270	*	59
Motor load [kW]	*	*	*	*	*	150	37
	Coefficient, η						
	%/°C	%/°C	%/°C	%/°C	%/°C	%/°C	[%]
Acc. DS [%]	0.12	*	*	*	*	*	43
Acc. DS [%]	*	0.18	*	*	*	*	30
Acc. DS [%]	*	*	0.10	*	*	*	54
Acc. FS [%]	*	*	*	*	0.36	*	21

*: Not included in the model.

The regression models and the diagrams in Figures 6.46 - 6.49 show that the motor load, accelerations and temperatures were correlated to some extent. The results displayed in Table 6.10 show that the motor load and the temperature data recorded from the front side of the refiner were correlated irrespective of the location of the temperature sensors. On the drive side, the temperature recordings captured in the intermediate zone (Temperature No. 2) revealed the closest relationship with the motor load. Furthermore, the acceleration on the drive side was closer correlated with the temperature measurements irrespective of radial location than the corresponding variables measured on the front side. However, the acceleration showed a relationship to the temperature measured in the intermediate zone (Temperature No. 11) on the front side. In addition, it can be shown that the acceleration on the front side and the motor load had a closer relationship than the corresponding variable measured on the drive side. This is shown in Figure 6.50.

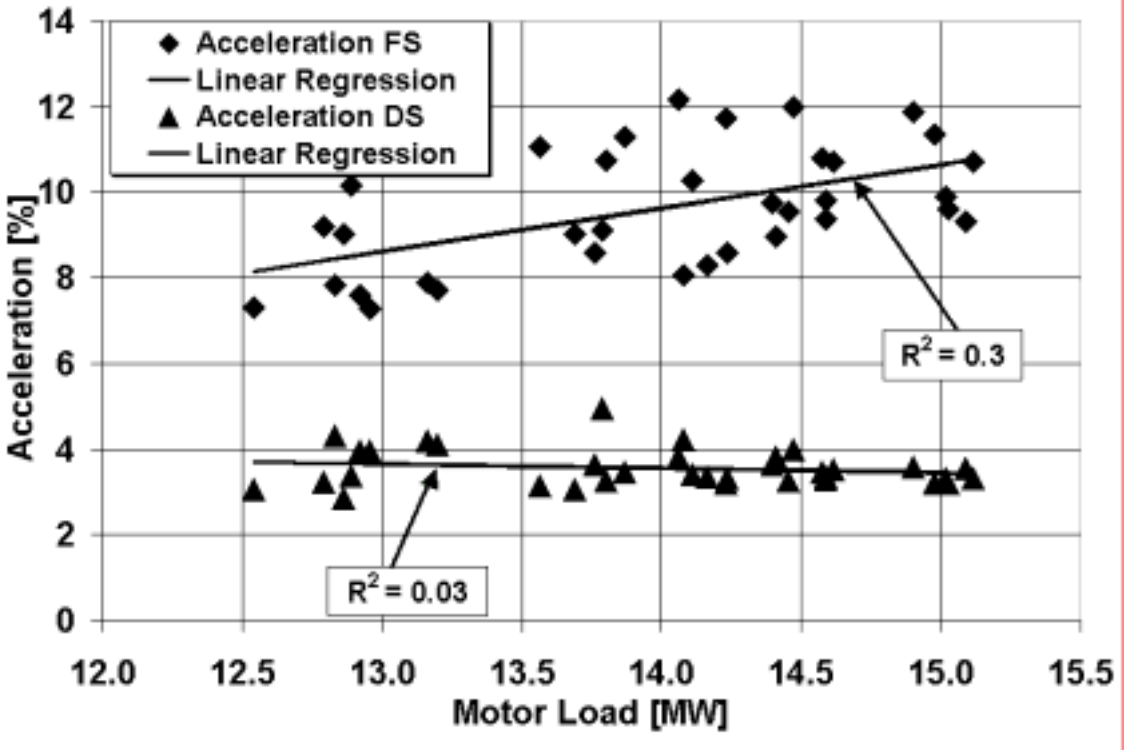

Figure 6.50: The relationships between the motor load and the acceleration variables are shown as they appeared during the factorial designed experiment.

The results in Table 6.10 and in Figure 6.50 support the hypothesis that the rotor was moved towards the front side. Together with the temperature distributions shown in Figure 6.34, which indicated that the temperature profile measured at the front side of the refiner was closer to a typical parabolic curve than the corresponding profile from the drive side, these results indicated that the refining action was unevenly distributed. It is reasonable to believe that the refining actions that occurred on the front side of the refiner during this first experimental period affected the process variables as well as the pulp quality more than the chip treatment on the drive side. Thus this occurred in the *wrong* refining zone, seen from the point of view of the pressure measurements.

6.6.3 Pulp quality data and process data

The sub-factorial designed experiment containing pulp samples was conducted as an integrated part of the whole experiment. 30 pulp samples were collected from 10 different runs. The casing pressure was at a low level except for the two runs, which were centre points. A two level full-factorial design containing three factors and two centre points formed the experimental layout as described in Section 3.6.3. The intention was primarily to investigate if there was any relationship between the pressure measurements and pulp quality variables.

Key figures associated with the input variables of this part of the experiment are shown in Table 6.11.

Table 6.11: Manipulated variables during the experimental part associated with the pulp quality analyses.

Run order	Hydraulic thrust [bar]	Production [tonnes/day]	Dilution water flow [l/s]	Casing pressure [bar]
1 (Centre point)	108	280	1.9	4.0
2	104	263	1.7	3.9
4 (Replicate of No. 9)	112	263	1.7	3.9
6 (Centre point)	108	280	1.9	4.0
9 (Replicate of No. 4)	112	263	1.7	3.9
10	104	296	1.7	3.9
11	112	296	2.0	3.9
17	104	296	2.0	3.9
18	104	263	2.0	3.9
19	112	296	1.7	3.9

A full-factorial experiment was not accomplished because runs Nos. 4 and 9 were conducted under identical operation conditions. Thus, regression analyses were performed when possible relationships between process conditions and pulp quality data were investigated.

Tables 6.12 and 6.13 list some of the most noteworthy pulp quality data, analysed by a PQM-1000 unit. The specific energy consumption for the first stage refiner and the acceleration readings which were collected at the front side of the refiner, are shown together with some of the pulp data.

Table 6.12: Response variables from the pulp quality experiment.

Run order	Specific energy consumption [kWh/t]	Std.dev. [kWh/t]	Freeness (CSF) [ml]	Std.dev. [ml]	Pulp consistency [%]	Std.dev. [%]
1	1110	29	517	0.6	33	10.3
2	1150	35	486	3.8	32	10.6
4	1240	32	435	9.3	44	1.9
6	1130	27	521	7.6	40	2.4
9	**1300**	42	**390**	6.0	**47**	2.0
10	1150	31	481	12.2	44	4.2
11	1150	34	464	2.5	39	0.5
17	1100	30	510	1.0	38	1.7
18	1150	21	461	2.1	34	2.3
19	1210	26	485	7.0	46	6.2

Table 6.13: Response variables from the pulp quality experiment.

Run order	Acc. FS [%]	Std.dev. [kWh/t]	Fibre length [mm]	Std.dev. [mm]	Fibre width [µm]	Std.dev. [µm]	Sum shives [No.]	Std.dev. [No.]
1	7.7	0.4	1.53	0.02	31.61	0.98	3334	195
2	7.8	0.5	1.53	0.03	32.10	0.72	2866	50
4	9.1	0.8	1.53	0.02	32.54	0.65	2380	220
6	7.9	0.5	1.51	0.04	32.75	0.28	3428	84
9	**12.0**	**2.0**	**1.41**	**0.01**	**33.30**	**0.02**	**2301**	**36**
10	9.8	1.2	1.52	0.04	32.52	0.75	3424	215
11	9.0	1.0	1.49	0.02	32.25	0.81	3376	218
17	9.0	1.3	1.52	0.02	32.27	0.15	3986	255
18	9.2	0.6	1.46	0.02	33.14	0.09	3086	12
19	9.3	1.2	1.51	0.01	32.03	0.36	3124	134

Data related to run No. 9 is displayed in bold in Tables 6.12 and 6.13 because these data should have additional attention. The most interesting result from the pulp quality analysis is probably associated with this run. The high acceleration value that appeared on the front side of the refiner during this period gave significantly different pulp quality compared to the other periods. As shown in Figure 6.47 the highest acceleration value appeared when run No. 9 was performed. In addition, the raw data are shown in Figure F10. The operational conditions during this run were as follows: high hydraulic thrust, low production rate, low dilution water flow rate and low casing pressure as shown in Table 6.11. The process responded with high specific energy consumption, while the pulp strongly reduced its freeness, fibre length and shive content. These relationships are shown in Figures 6.51 – 6.53.

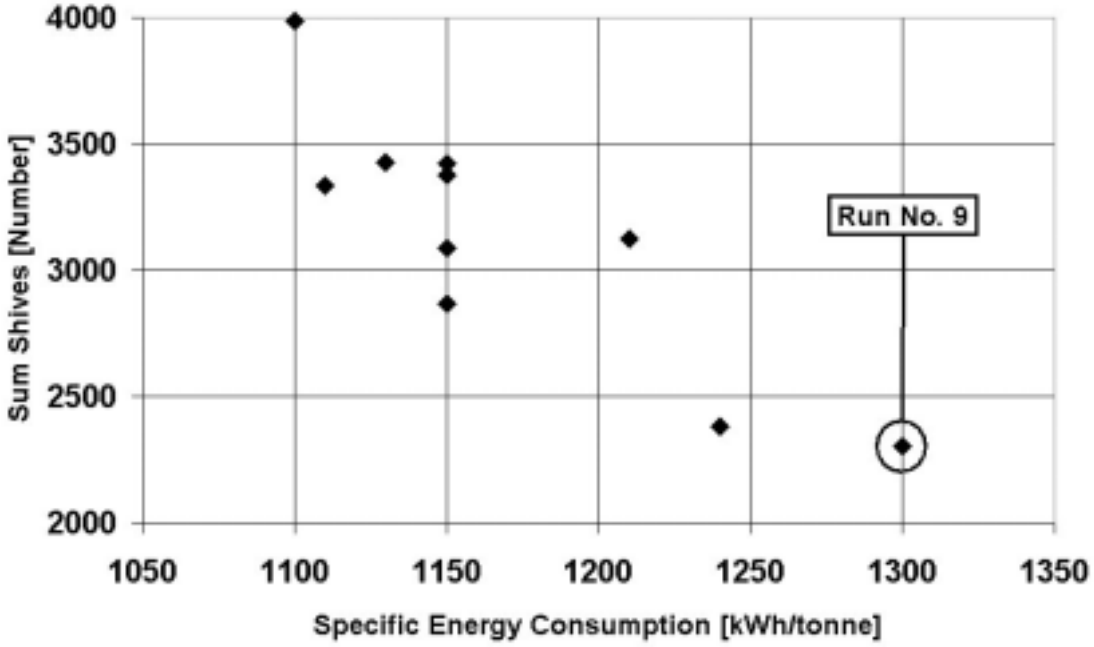

Figure 6.51: The relationship between the number of shives in the pulp and the specific energy consumption.

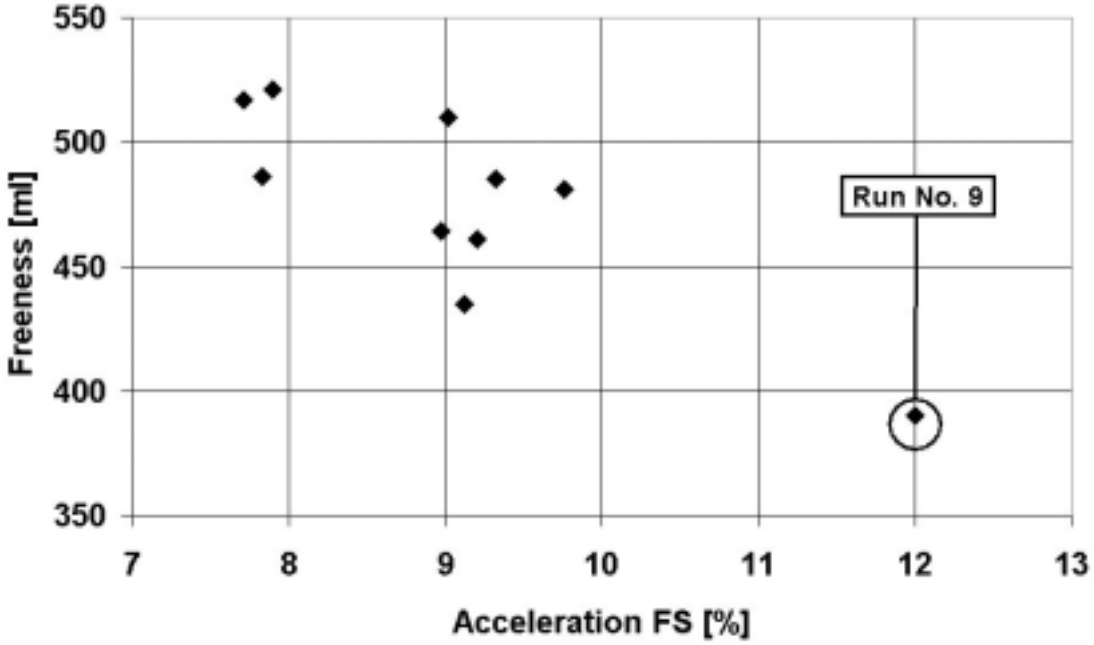

Figure 6.52: The relationship between the freeness and the acceleration on the front side of the refiner.

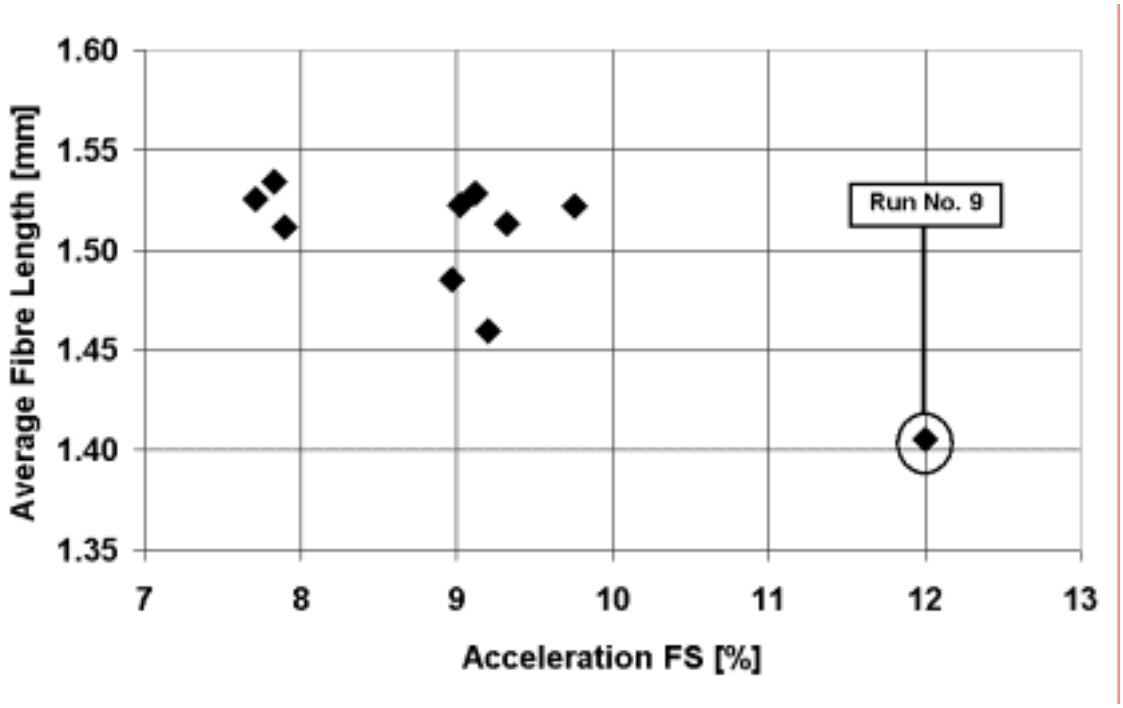

Figure 6.53: The average fibre length was strongly influenced by the high acceleration value during run No. 9.

High acceleration indicates a small plate gap thus a pulp of low freeness could be expected with a considerable degree of fibre shortening and a reduced number of shives. This is supported by a corresponding study by Strand and Mokvist (1987). A similar conclusion was made by Stationwala *et al.* (1994). They claimed that it is mainly when the plate gap becomes excessively small that the fibre shortening takes place. In other studies it is indicated that fibre shortening, after the initial defibration, only occurs to a minor extent during normal operational conditions (Mohlin (1997), Corson (1989), Corson and Ekstam (1993)).

The fibre length distribution measured as fractions of different classes of average length of particles also reflected the fibre shortening. Especially the short fraction between 0.5-1 mm increased while the middle fibre fraction between 1-3 mm decreased as shown in Figure 6.54.

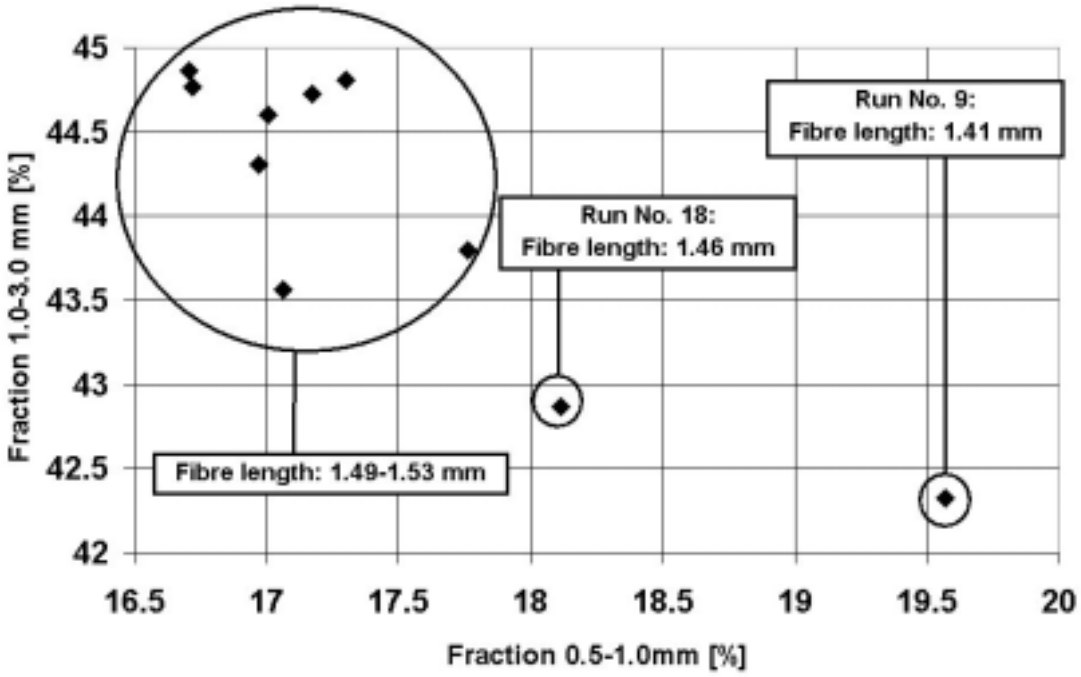

Figure 6.54: The relationship between two of the fractions in the fibre length distribution.

The pressure readings gave no indications about any relationship between this extreme running condition and the pressure. The reason seems to be obvious since the high acceleration values were appearing at the front side of the refiner, while the pressure sensors were mounted in the drive side. These results support the assumption that the refining actions that occurred on the front side of the refiner affected the process variables as well as the pulp quality more than the chip treatment on the drive side.

6.6.4 Regression models – 10 runs

The regression analyses have been investigated for different input variables. Both single and multivariate models have been investigated. First of all the pulp quality variables were tested against the manipulated process variables and the motor load or the specific energy consumption as quoted in Table 6.14. The regression coefficients regarding the motor load are shown for comparison with the corresponding regression analysis made in Section 6.6.2. The difference between these investigations was the amount of data given by the number of runs included in the models.

Further regression analyses were performed between different pulp quality variables. The different shive variables labelled as *SumShives*, *ShortShives*, *WideShives*, *LongShives* and *CoarseShives* were well correlated as expected. Thus, only models of the number of shives (*SumShives*) are shown in Table 6.14. The plots shown in Figures 6.51 - 6.54 reveal that the freeness, the average fibre length, the amount of shive and the fibre length distribution were correlated to some extent.

Table 6.14: Regression coefficients from significant (95 % level) models using the manipulated process variables as input variables.

Response variable	Input variables, X_i					Correlation R^2
	Hydraulic thrust [bar]	Production [t/d]	Dilution water flow [l/s]	Motor load [MW]	Specific energy consumption [kWh/t]	
	Coefficient, η_i					
	kW / BAR	kW / t/d	kW / l/s	kW / MW	KW / kWh/t	[%]
Motor load [kW]	104	32	NS[1]	* [2]	*	79
Adjusted motor load[3] [kW]	104	24	-2820	*	*	91
	ml / BAR	ml / t/d	ml / l/s	ml / MW	Ml / kWh/t	[%]
Freeness (CSF) [ml]	*	*	*	*	-0.57	79
Freeness (CSF) [ml]	*	26	*	-47	*	80
	Coefficient, η_i					
	No. / BAR	No. / t/d	No. / l/s	No. / MW	No. / KWh/t	[%]
Sum Shives [No.]	-56	22	1280	*	*	94
Sum Shives [No.]	*	*	*	*	7.1	76
Sum Shives [No.]	*	38	*	-478	*	94

1 NS: Not significant.
2 Not included in the models.
3 Same adjustment as corresponding variable in Table 6.9.

Tests regarding the relationship between the output signal from pressure sensor No. 4 and different pulp quality variables gave only a weak correlation. For instance, at a 90 % significance level a model could be established between the standard deviations of the pressure readings and the average fibre length and the amount of fibres in the middle fractions, 0.5-1 mm and 1-3 mm.

It can be concluded from Table 6.14 that the freeness variable and the number of remaining shives in the pulp were the two most affected pulp quality variables by the first stage refiner during the prevailing process conditions. The motor load and the production rate were the dominating input variables. That the freeness and the shive content were the most affected pulp variables was expected since the pulp samples were collected in the blow line after the first stage refiner. The main tasks of the first stage refiner are to break down the chips and separate the fibres (Karnis (1994)). However, it was expected even higher degree of relationship between freeness and the manipulated variables. The reason why this was not achieved is assumed to be related to the use of new plates. However, the fact that the experiment was performed shortly after the production start-up, and the indications that the uneven refining conditions between the two refining zones were present, support the reason for the observation of the weak relationships. The first assumption regarding use of new plates is supported by corresponding studies (Lidén (2002), Strand and Mokvist (1987)).

6.7 Chip-stream splitter test

The chip stream splitter test also labelled *Giri-gari* test, was performed to find out how the pressure signals were affected by changes in the amount of chips fed into the refiner. This investigation was carried out in the second main period of data recording after approximately 1000 production hours. The sensors were kept in the plate during this period. The investigations performed during the factorial designed experiment did not reveal any clear relationships between the output signals from the pressure sensors and the process variables. Thus, the chip-stream splitter test was conducted as a complementary study.

This test was based on the fact that the internal position between the two power screws in the load sense conveyor influences the distribution of chips fed into the two refining zones. The angle position between the two power screws was changed in steps i.e. the angle of one of the screws was changed. The other power screw was fixed in one position. Each step corresponded to approximately 1.4∀change of the angular position of the power screw. A simple sketch showing the principle of the screws in the load sense conveyor is displayed in Figure 6.55. A similar manipulation of the process has been described by Mosbye *et al.* (2001). They used temperature measurements to equalize the refining conditions in the two gaps.

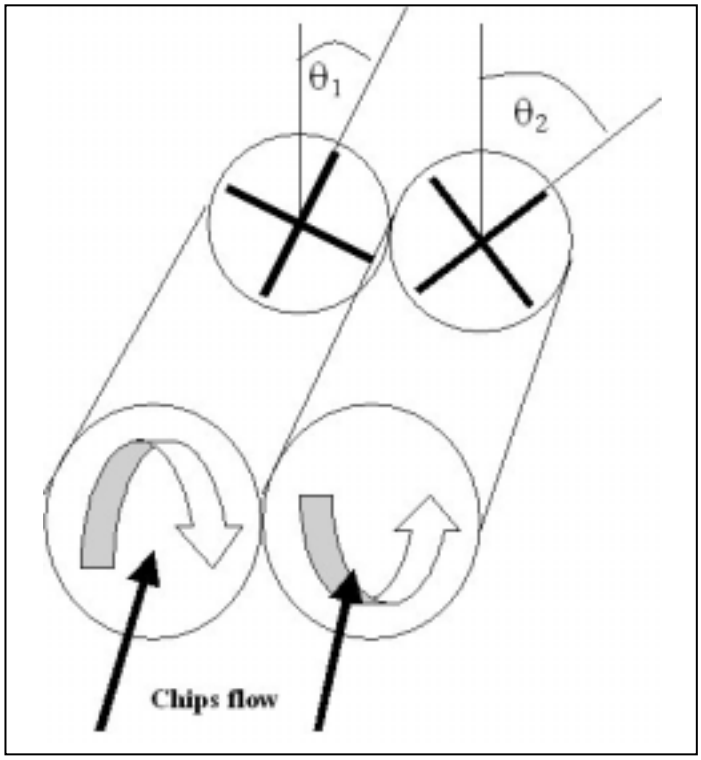

Figure 6.55: A sketch of the principle of the positions of the screws in the load sense conveyor is shown. The angle χ_1 is fixed, while the angle χ_2 is possible to adjust.

Results from this test are shown in Figures 6.56 - 6.60. Data were acquired during a period changing the angular position, ÷χ, of the two screws feeding the refiner from the original position to approximately 4.1∀in one direction and further 13.7∀in the other direction. The voltage output readings from sensor No. 4 were averaged according to one-second windows i.e. 500 kSamples per averaged value. The average values as shown in Figure 6.56 reveal a clear response on the manipulations of the process. The test data shown in this figure represent approximately seven minutes.

The corresponding pressure values converted according to the third flange of the calibration curve, Figure 6.33, are displayed in Figure 6.57, which is the same plot as shown in Figure 6.6. The motor load is shown as well. Thus the result from the chip-stream splitter test showed that the pressure readings from sensor No. 4 were strongly correlated with the motor load and acceleration variables captured from the mill's DCS. The latter is shown in Figure 6.58.

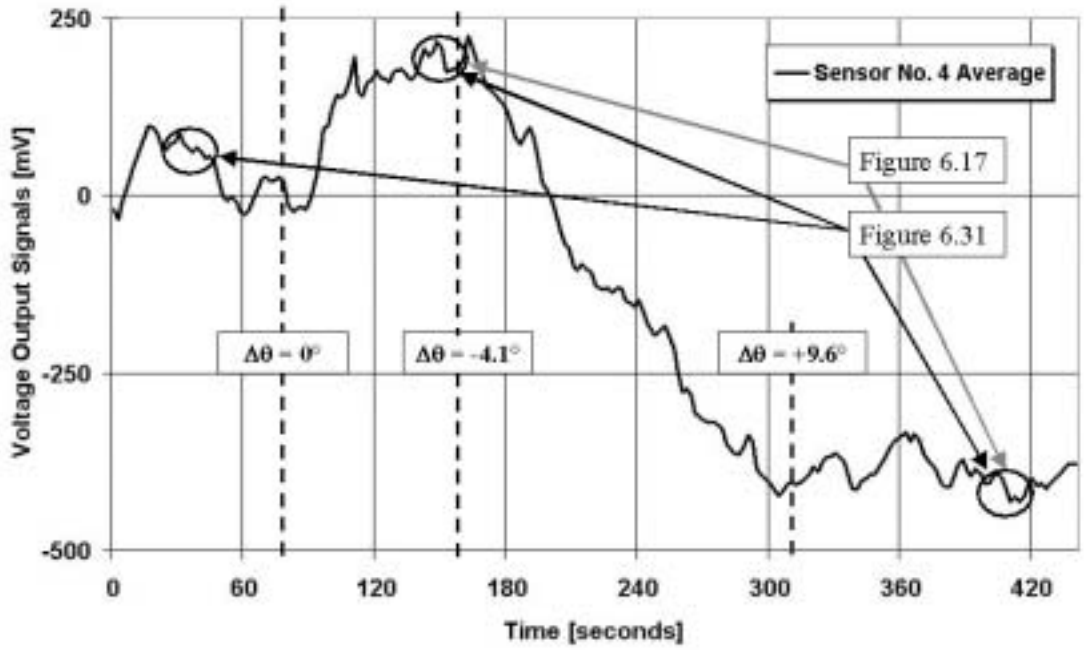

Figure 6.56: Average (one-second window) voltage output data from sensor No. 4 are shown during the test period while changing the difference in angular position of the two screws feeding the refiner.

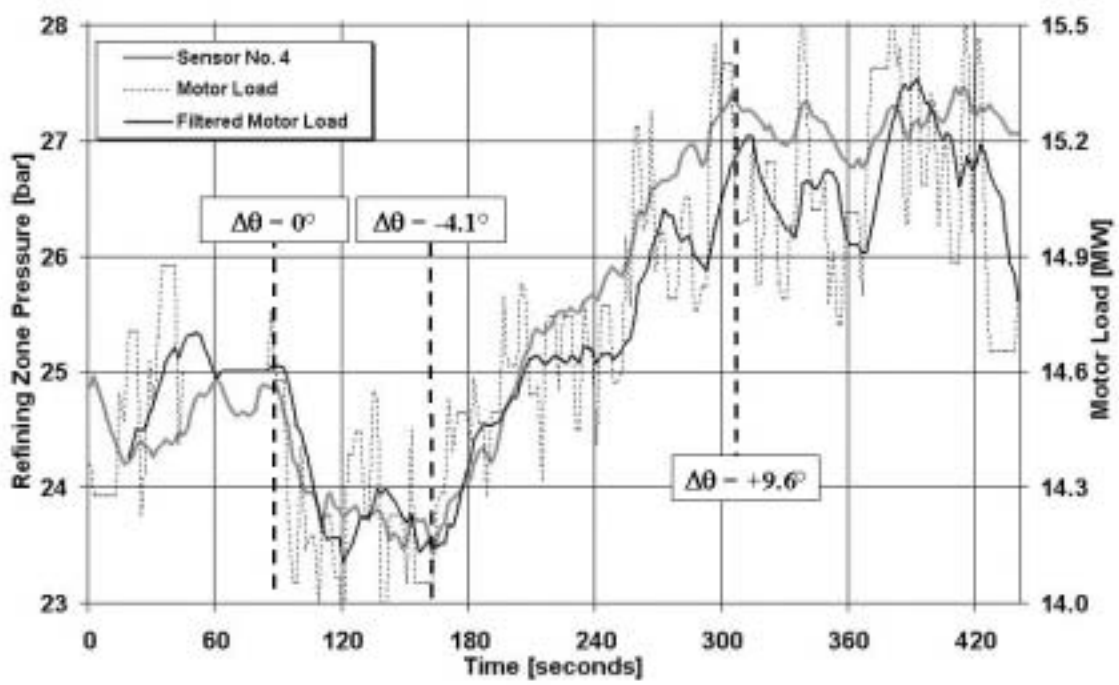

Figure 6.57: The average pressure data, converted through the third flange of the calibration curve are shown together with the motor load.

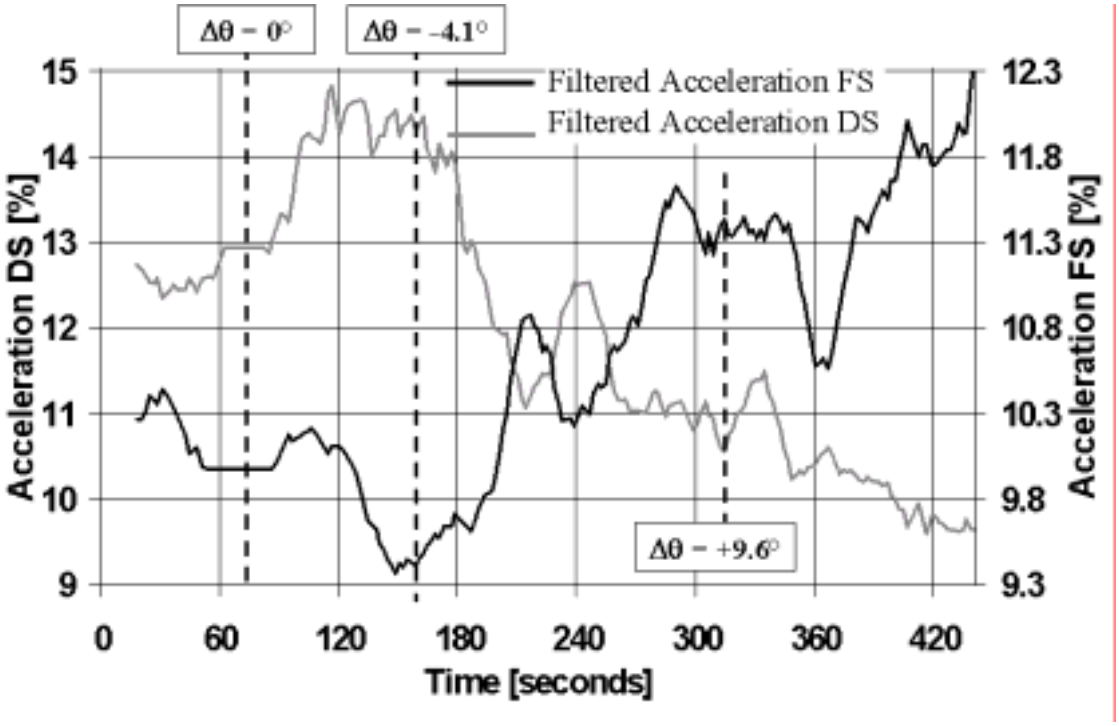

Figure 6.58: Filtered acceleration readings are shown from each side of the refiner as given by the mill's DCS. The signals were captured during the stream splitter test.

The variation recorded by sensor No. 4 indicates a pressure range of approximately 3 bar. The curves in Figure 6.57 show that the pressure readings were highly correlated with the motor load. This is in sharp contrast to the observations made when the plates were new as shown in Sections 6.5 and 6.6. However, this indicates that a large contribution to the variation of the motor load appeared in the refining zone, where the pressure sensors were located. Further indications imply that more energy was applied in the intermediate zone where sensor No. 4 was located compared with the fine bar zone as discussed in Section 6.3.4. A simultaneously captured recording from sensor No. 6, as the readings shown in Figure 6.57, is shown in Figure F11. This plot indicates that the pressure in the outer part of the refining zone was negatively correlated with the pressure measured by sensor No. 4.

The process measurements shown in Figures 6.57 and 6.58 were noisy. Filtering of the raw signals according to the moving average method, improved the readability. However, the raw data from the acceleration variables from each side of the refiner were well correlated as shown in Figure 6.58. The correlation coefficient from the raw data was –0.77. In addition, it should be mentioned that the measured load data from the two power screws of the load sense conveyor had a similar trend as the acceleration signals. This is shown in Figure 6.59. These loads were negatively correlated with the corresponding acceleration signals as shown in Figure 6.60. Furthermore, the load signals were even noisier than the acceleration measurements. The correlation coefficient for the two load signals from the power screws was only -0.2.

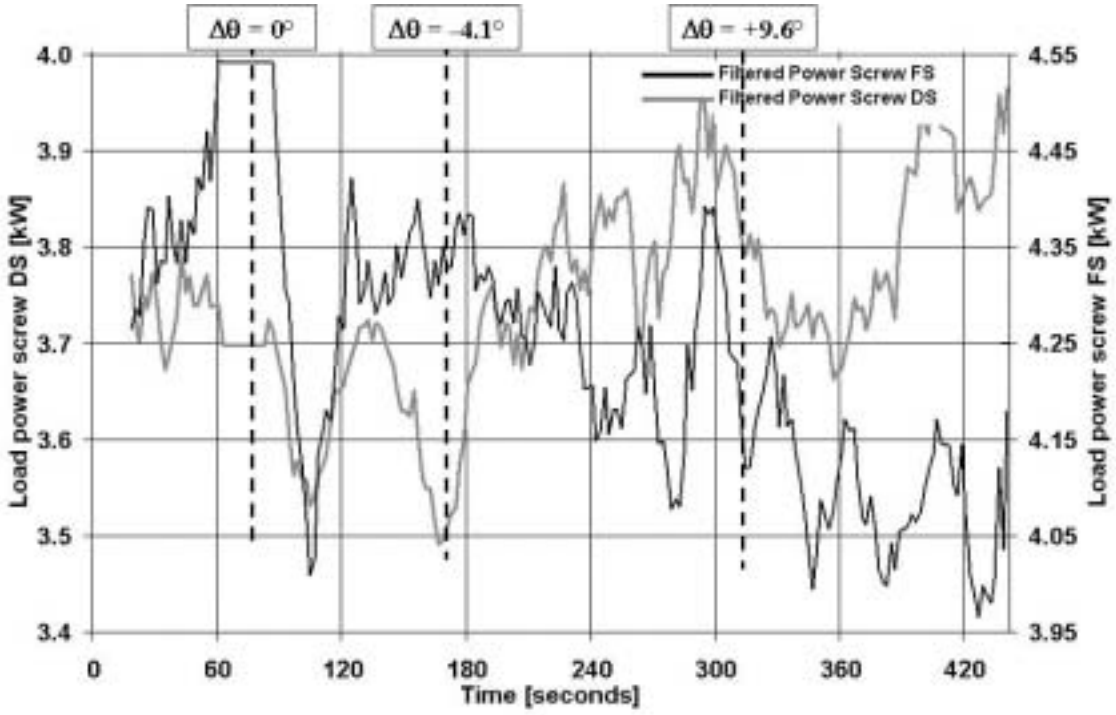

Figure 6.59: The loads from the two power screws of the load sense conveyor, recorded during the chip-stream splitter test, are shown.

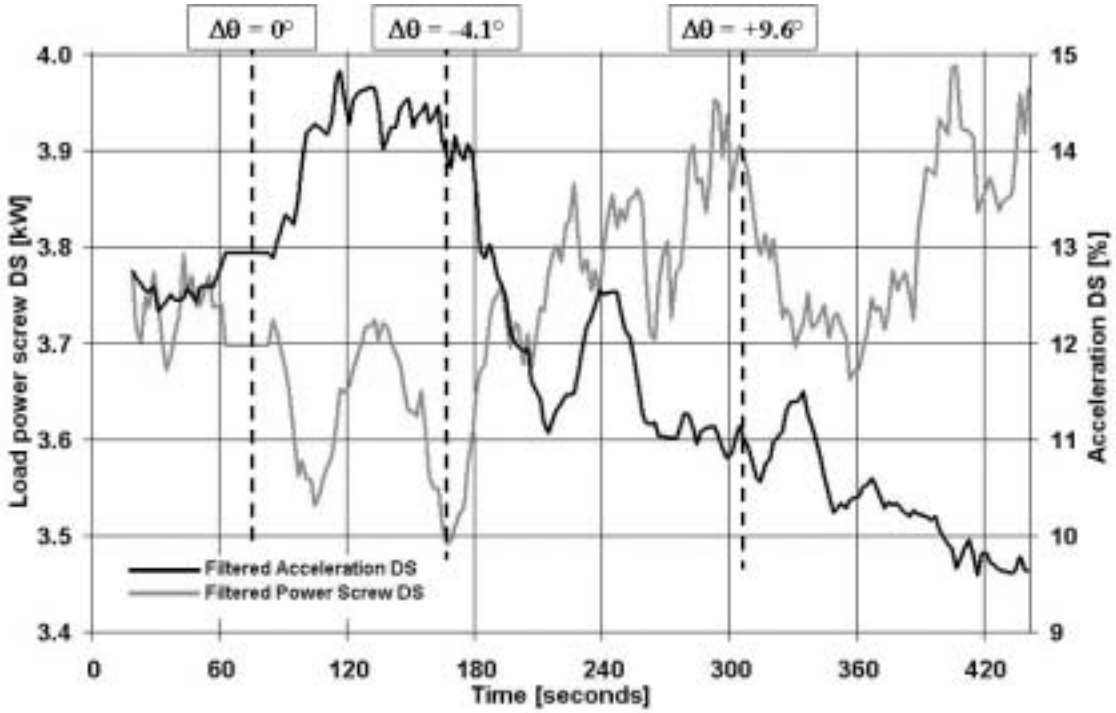

Figure 6.60: The load of the power screw and the acceleration related to the refining zone at the drive side of the refiner recorded during the chip-stream splitter test

The chosen flange of the sinusoidal transfer function curve representing the pressure sensor has given a pressure development, which is directly proportional with the motor load variable as well as the acceleration of the front side of the refiner. Thus, the pressure was negatively correlated with the acceleration on the same side of the refiner, as the pressure sensors were located. It is not obvious that this is correct. Selecting an adjacent flange for the pressure readings the pressure would be negatively correlated with the motor load. However, the pressure measurements reveal a clear relationship to the chip distribution in the Twin refiner and the acceleration variables. The latter is commonly used as indicators of the plate clearance. Thus the pressure measurements seem to give information about the plate clearance as well.

An intuitive explanation of the behaviour of the refiner during this test can be made. It can be concluded that the load of the power screw at the front side was decreasing, while the corresponding acceleration was increasing as shown in Figures 6.58 and 6.59. The opposite effects were revealed at the drive side as shown in Figure 6.60. This might be explained by a smaller amount of chips fed into the refining zone at the front side, which led to a decreasing plate gap in this refining zone. In the drive side where the pressure sensors were located, the reverse action was dominating: more chips were fed in and the plate clearance increased as shown by a decreasing acceleration (Figure 6.58). Since the pressure measured on the drive side of the refiner was closely correlated with the overall motor load (Figure 6.57), it is assumed that the response from the motor load followed the actions that occurred in this refining zone more than the actions on the other side. It indicates that the pressure increased when the refining zone was gradually filled up with pulp.

Mosbye *et al.* (2001) performed a chip-stream splitter experiment in the same refiner to equalize the refining conditions. Here temperature measurements were successfully used to measure the effect of adjusting the split of chips in the stream splitter. Engstrand *et al.* (1995) claimed that the temperature sensors are more sensitive and less noisy compared to the accelerometers when using such measurements to stabilize the refiner by optimizing the split of chips in the load conveyor. The temperature data were not accessible in the present study.

6.8 Time fluctuations of the rotational speed

The main objective of recording the time stamp of the rotating shaft was to get an overview of fluctuations of the rotational velocity. It was assumed that the signal received from each revolution of the rotor disc could support the determination of what was happening across a bar-bar passage. The information from the time stamp was assumed to exactly determine the number of bars passing across the sensor surface. Thus, information could be obtained about periodic variations that appeared across one bar-to-bar passage. However, the supposed analyses of the signals that appeared in a small area as a bar surface have not been included in the present study. This decision was made because of the uncertainties associated with the sinusoidal calibration curves and the great variety of modulated signal patterns. The latter is discussed in Section 6.9.

The recorded signal from the revolution of the shaft and rotor disc was still interesting as a separate study of variations in bar crossing frequency. Thus, the analyses presented in this section were performed to investigate the relationship between the fluctuations of the rotational velocity and the corresponding fluctuations in the bar-crossing frequencies. If the fluctuations in the rotational velocity were significant, and the periodic signal patterns revealed by the pressure sensors were caused by the bar-crossings, then such variations in the bar-crossing frequencies should be detected by the pressure sensors as well. This assumption constituted the basis for the current investigations. It was supported by an earlier experimental study reported by Pettersen and Gunstrøm (1980) as well. They used sound level and vibration measurements in a study of noise and vibrations from grinders. Their results indicated that frequency variations were caused by fluctuations in the rotational velocity of the shaft due to load variations.

6.8.1 Load dependent fluctuations

Two channels on the DAQ-system were used to record the high-frequency signals of the motor load and the time stamp on the refiner shaft. These signals are shown in Figure 6.61 during a start-up sequence. The behaviour of the time stamp signal and the relationship between these signals are displayed as an obvious example in this figure. However, Figure 6.61 has to be looked on as a curiosity, because further processing of the recordings was necessary to achieve the intended results as shown in the following discussion.

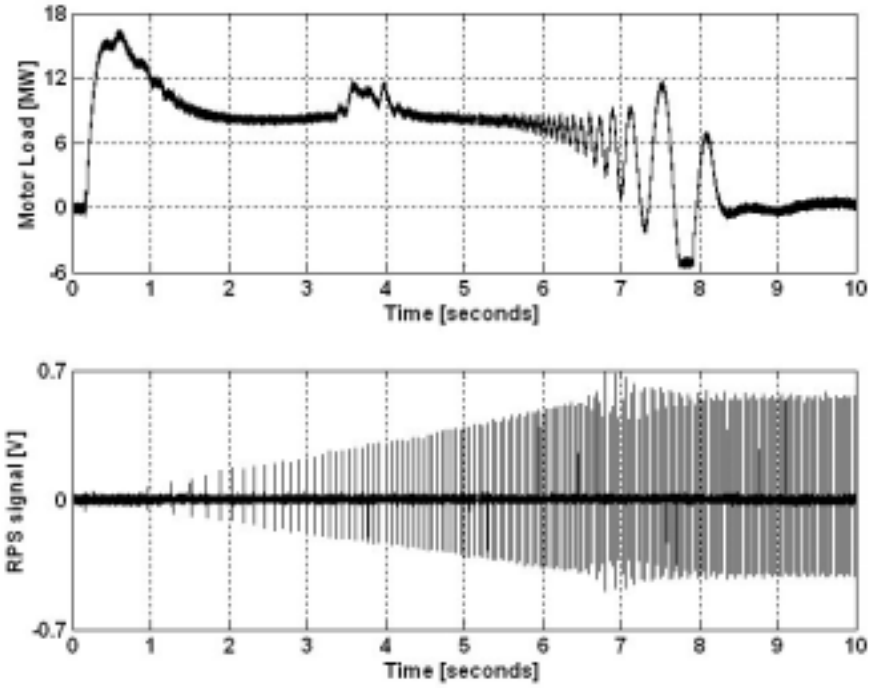

Figure 6.61: High-frequency recordings of the motor load (upper plot) and the refiner shaft revolution (lower plot) are shown during a start-up.

Figure 6.61 shows that the refiner demanded a large amount of power to set the rotor disc in motion. Apparently, it took a lot of time to set the rotor disc in motion. However, the magnetic induction signal was not generated before the shaft obtained a certain speed. This is further revealed by the increasing voltage signal while the time between each revolution rapidly decreased. Additional observation is that the motor load reached negative values after 7-8 seconds. The refiner probably generated power instead of demanding power in parts of this start-up sequence. This assumption is supported by the time stamp measurements, which showed that the speed in this period reached 29 revolutions per second i.e. average value in a 40 millisecond window. The nominal speed corresponding to 25 rps (1500 rmp) was reached after approximately 8.5 seconds simultaneously as the power consumption was stabilized at a low level. This probably occurred simultaneously as the asynchronous start-up sequence was taken over by the synchronous driving mechanism as well.

Figures 6.62 and 6.63 show the post-processed data from the time stamp measurements as explained in Section 3.7. These data were used to explain the behaviour of the rotational velocity of the refiner shaft. The motor load readings were averaged corresponding to the duration of one revolution of the rotor disc (40 milliseconds). The recordings of the time stamp from the shaft were treated such that the time difference between two adjacent revolutions is shown. The whole time series lasted for 2 seconds (50 revolutions).

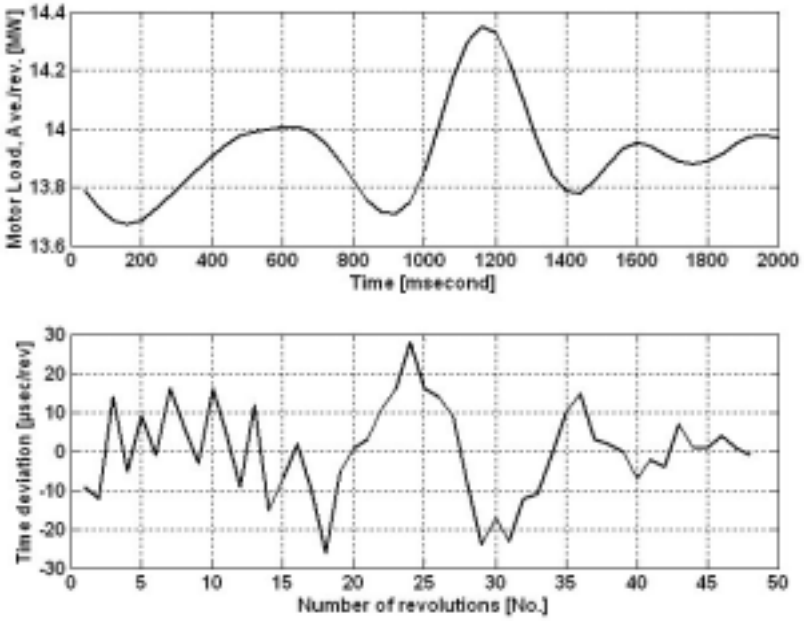

Figure 6.62: The upper plot shows the averaged motor load signal. The lower plot shows the time deviation between two adjacent revolutions. These recordings were captured simultaneously in the first experimental period corresponding to run No. 17 of the factorial experiment.

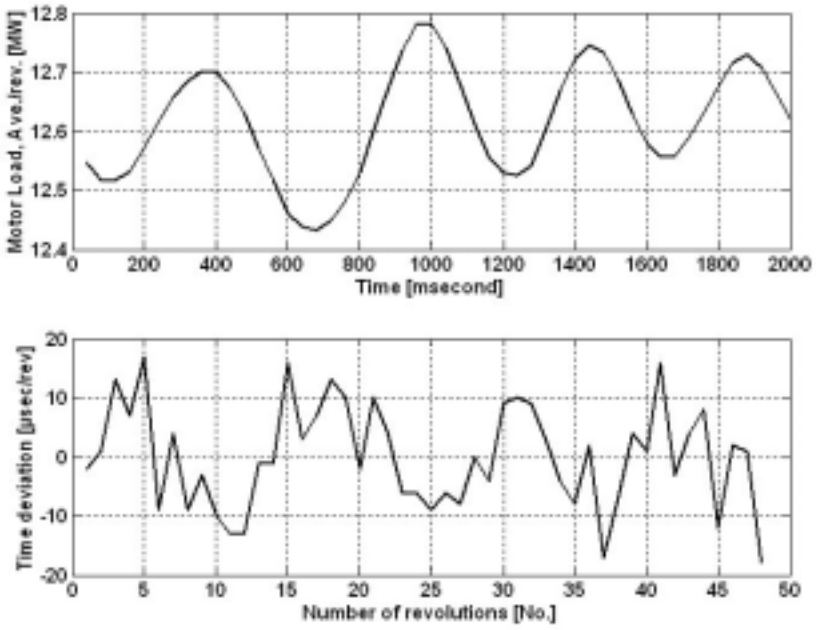

Figure 6.63: The upper plot shows the averaged motor load signal. The lower plot shows the time deviation between two adjacent revolutions. These recordings were captured simultaneously in the first experimental period corresponding to run No. 20 of the factorial experiment.

The findings revealed in Figures 6.62 and 6.63 indicate that the fluctuations in the rotational velocity affected the motor load. The 95 % confidence limits about the mean value were ± 3.3 and ± 2.5 µseconds respectively. The corresponding limits measured when the refiner was unloaded reached ± 1.7 µseconds. Thus, fluctuations outside these limits have been considered affected by other factors such as load variations. The relationship between these signals is clearly visible. As expected, the load lagged behind the rotational speed. In this particular example shown in Figure 6.62, 0.6 MW load variation was caused by 0.15 % (2.3 rpm) change in rotational speed. In addition, results from cross-correlation analyses of the same recordings as shown in Figures 6.62 and 6.63 are shown in Figure 6.64.

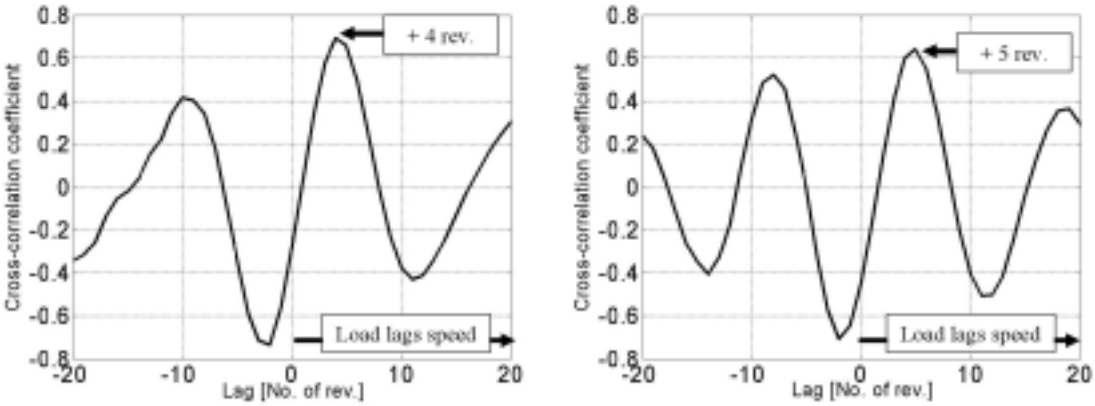

Figure 6.64: Each of the cross-correlation diagrams shown here represents the relationship between the average motor load and the time deviation between adjacent revolutions of the rotor disc captured during run No. 17 (left-hand plot) and during run No. 20 (right-hand plot).

The cross-correlation plots show a periodicity caused by the periodic fluctuations of the signal patterns. Both the negative and the positive correlation coefficient displayed at lags corresponding to respective – 2 revolutions and + 4-5 revolutions were coefficients that could be considered to represent the prevailing process. However, the negative correlation was assumed to be disqualified because of the nature of the process. The negative correlation indicated that higher load lead to faster rotational velocity. In addition, the negative correlation appeared such that the rotational velocity should have lagged behind the motor load. Thus, the positive correlation was considered as the most promising result. It indicated that the load lagged behind the deviation of the rotational speed, and that a decreased rotational speed led to increased load. Hence, the response time of the motor load was approximately 0.2 seconds corresponding to 4-5 revolutions. The response time must be seen in accordance with the high momentum of this process given by the mass of the rotor disc, which is approximately nine metric tonnes. The response time can probably be verified through machine properties. However, such investigations have been considered outside the scope of this thesis.

6.8.2 Bar-to-bar frequency shift

The recorded signal from the magnet attached to the shaft of refiner was used to measure the rotational speed variations and the corresponding fluctuations in the bar crossing frequencies. Thus, determination of these fluctuations has given interesting results. It has been possible to determine the relationship between the periodicities detected by the pressure sensors and by the rotational speed measurements. Such relationship is shown in Figure 6.65 between the observations of the bar crossing frequencies from pressure sensor No. 8 and the calculated bar crossing frequencies from the rotational speed measurements.

The calculated bar-crossing frequencies are based on the indirect measurements of the rotational velocity i.e. the time stamp measurements on the refiner shaft. Equation 6.1

give the bar-crossing frequencies, which are determined by the rotational speed, number of bars per plate (84) at the current location and the number of plates per disc (12).

$$f = a \cdot b \cdot v_{rot.} \qquad (6.1)$$

f : bar-crossing frequency [Hz]
a : number of bars per plate
b : number of plates per revolution
$v_{rot.}$: rotational velocity [rps]

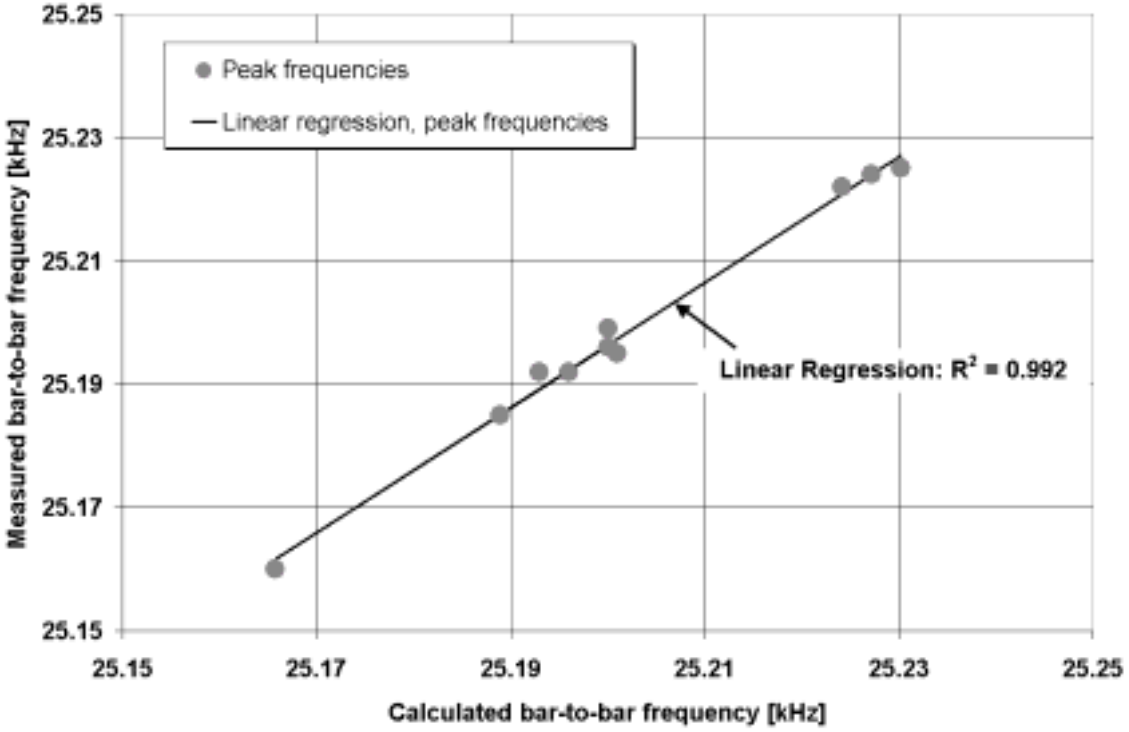

Figure 6.65: The correlation between the calculated and the measured bar-crossing frequency at the location of sensor No. 8 is shown.

The result shown in Figure 6.65 reinforces the validity of the dynamic properties of the pressure measurements. The sensitivity was high since small changes in the rotational velocity were intercepted by the sensors and shown in the frequency analysis. The difference between the maximum and minimum values of the rotational velocity in these 10 data sets was 3.8 rpm, which gave a deviation of approximately 0.3 %. This deviation corresponded to a shift of 64 Hz of the peak frequency related to the bar crossing at the current location in the refining zone. The corresponding amplitude spectra obtained from the recordings that contained the maximum and minimum rotational speeds are shown in Figures 6.66 and 6.67.

The location of sensor No. 8 was approximately at the same radial location as the 25.2 kHz bar crossing frequency was generated. This result is supported by measurements from sensor No. 4 as well. A similar analysis regarding the peak frequency at 25.2 kHz was performed as shown in Figure F12. The peak frequency observed at 25.2 kHz was not the local bar-crossing frequency at the location of sensor No. 4. However, this frequency was clearly visible in the recordings from this sensor as well as from the other sensors. As discussed in, Section 6.3, it is assumed that the discs vibrated due to pulp squeezing between opposite bars at the radial location, which fitted to the bar-crossing frequency of 25.2 kHz. Thus, the other sensors measured these vibrations of the rigid disc independent on their radial location.

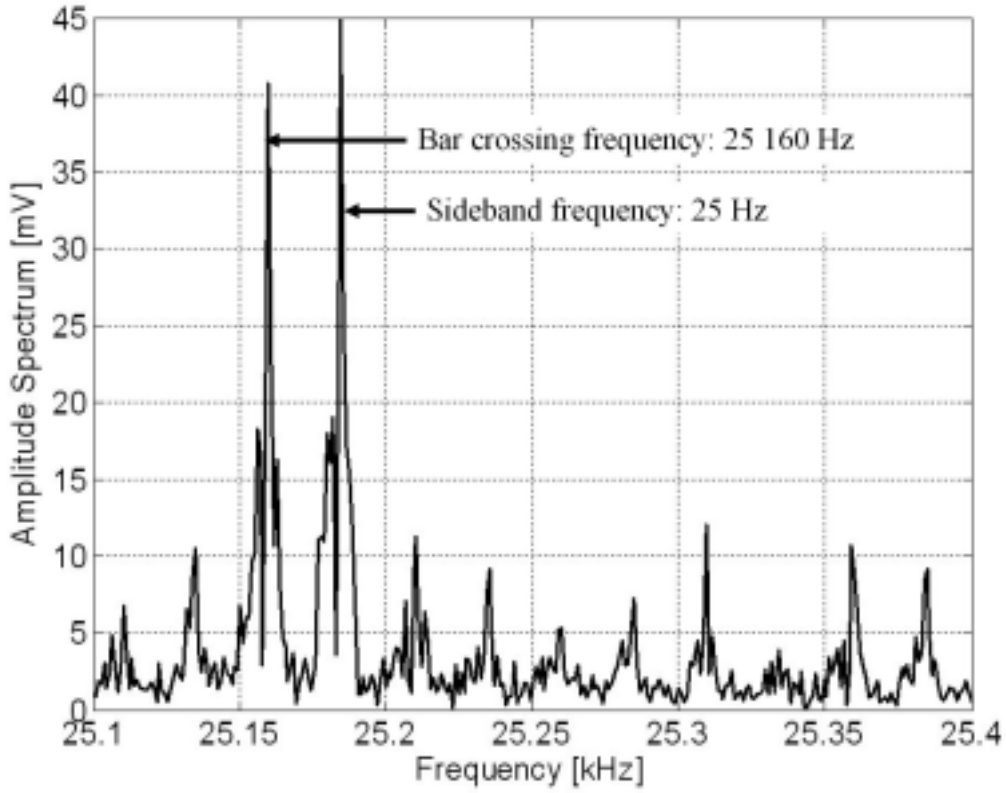

Figure 6.66: A normalized amplitude spectrum from a recording captured by sensor No. 8 is shown. The recording was performed during run No. 9. The corresponding average rotational speed was 24.97 rps.

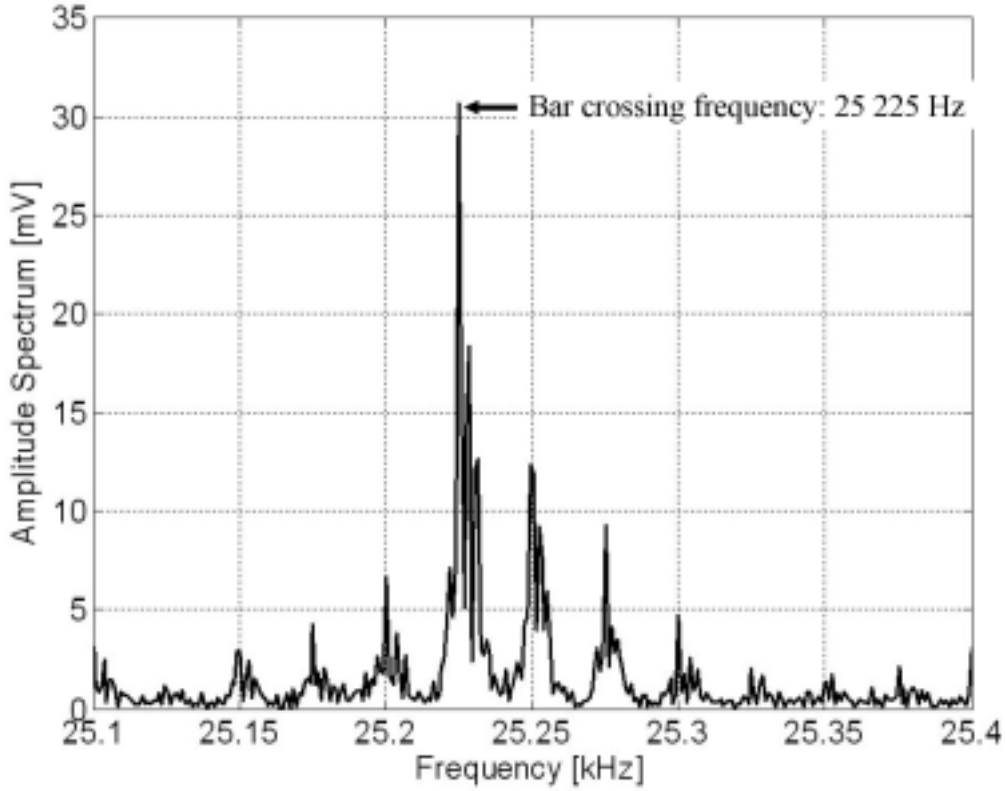

Figure 6.67: A normalized amplitude spectrum from a recording captured by sensor No. 8 is shown. The recording was performed during run No. 19. The corresponding average rotational speed was 25.03 rps.

Figures 6.66 and 6.67 show that additional peak frequencies were present close to the main peak frequency. A constant frequency of 25 Hz separated the additional frequencies. Frequency patterns like these are denoted sideband frequencies. These sideband frequencies were probably present as amplitude modulated signals because of the variation in the rotational speed. Theoretical amplitude modulated signal patterns should give sideband frequencies of equal amplitude separated by two times the modulating frequency, which in this case is the rotational velocity of 25 Hz (Doebelin (1990), Wowk (1991)). In addition, the real bar-crossing frequency should not be seen. This is further discussed in Section 6.9 and particularly shown in Figure 6.72. However, the recorded signals did not consist of theoretical sine waves. Furthermore, the deviation in rotational velocity was not constant. Thus, it is assumed that the side frequencies were sideband frequencies. In addition, it is assumed that the real bar-crossing frequency was present as well. These assumptions are reinforced by the experimental study performed by Pettersen and Gunstrøm (1980). Their results showed the real bar-crossing frequency, and the sideband frequencies related to the rotational frequency and the multiple of this frequency. The amplitudes of the sideband frequencies differed and they reported sideband frequencies that sometimes had higher amplitude values than the amplitude of the bar-crossing frequency. Furthermore, they observed also that the bar crossing frequencies were shifted a few Hertz in either

directions. The authors claimed that this occurred as a result of variations in the rotational velocity due to load variations.

A similar plot as shown in Figures 6.66 and 6.67, showing the bar-crossing frequency at 25.2 kHz and additional sideband frequencies recorded by sensor No. 4, is displayed in Figure 6.68. However, this figure shows in addition to the similarities a difference compared to the other figures. The bar-crossing frequency shown in Figure 6.68 corresponded to the calculated bar-crossing frequency as indicated in Figure F11. In addition, 25 Hz separated the lower sideband frequency from the bar-crossing frequency. The difference was related to the upper sideband frequency, which corresponded to two times the rotational frequency. The reason for this dissimilarity is not clarified. However, it should be remembered that the location of the sensors was different.

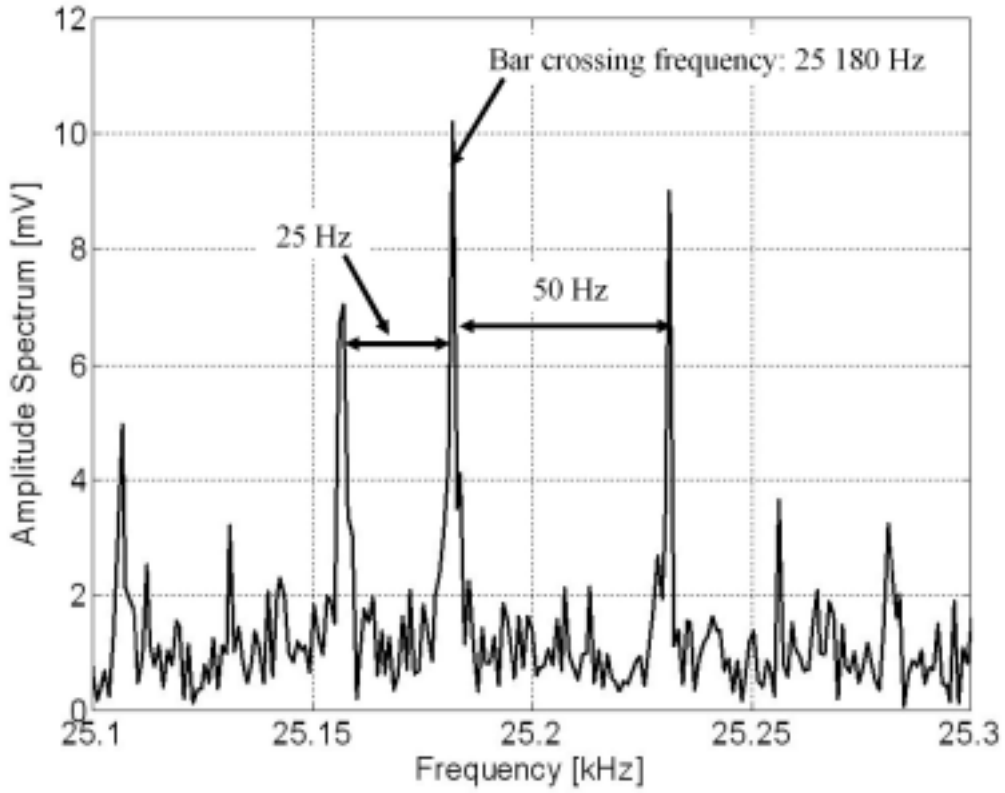

Figure 6.68: The normalized amplitude spectrum from a recording captured by sensor No. 4 during run No. 6 shows the bar crossing frequency at the location of sensor No. 8 and sideband frequencies associated with the rotational speed of the refiner.

6.9 Simulation of sensor signals

The uncertainty regarding the sinusoidal calibration curve has made the determination of pressure levels difficult. Assumptions about the pressure levels have been made using the average values and the span of the voltage output signals as well as considerations about possible relationships to current process variables.

Another approach to explain the behaviour of the raw data is discussed in the following section. Based on observation of the high frequency signal patterns and the corresponding frequency analyses, additional effects have been revealed, such as:

- Sideband frequencies.
- Harmonic frequencies.

The following approach has been performed to investigate the origin of the underlying effects that existed in the raw data. The tool used in this part of the study, to uncover the basic properties, was simulation of suggested signal patterns. Simple simulation and pattern recognition were expected to give indications of the real dynamic behaviour of the pressure signals. The following three approaches were simulated:

- Added signal patterns.
- Amplitude modulated signal patterns.
- Combination of added and amplitude modulated signal patterns.

Some characteristic signal patterns have been revealed through the previous investigations. Among several of them, the high frequency signal with a periodicity of 25.2 kHz has been clearly visible in most of the recordings. This periodicity dominated the recordings from sensor No. 8 during the first part of the experiment. The reason for this was probably that the location of sensor No. 8 fitted to the bar-crossing frequency of 25.2 kHz. The harmonic frequencies of this fundamental frequency, particular 50.4 and 75.6 kHz, have been present as shown in Figure 6.69. These frequencies were also clearly visible in Figure 6.13.

In some recordings the harmonic frequencies dominated even more than the fundamental frequency as shown in Table 6.15. In addition, the sideband frequencies have been present as shown in Figure 6.70. Among the sideband frequencies 25 Hz (rotational velocity), 300 Hz (number of plates or bolt holes in the breaker bar plates, 12 per revolution), 600 Hz (bolt holes in the refiner plates, 24 per revolution) and 1200 Hz (number of bars in the breaker bar plates) have been observed. Which of these sideband frequencies mainly dominated, has not been conclusively proven. Also harmonic frequencies of the sideband frequencies might have appeared instead of one or more of the typical sideband frequencies.

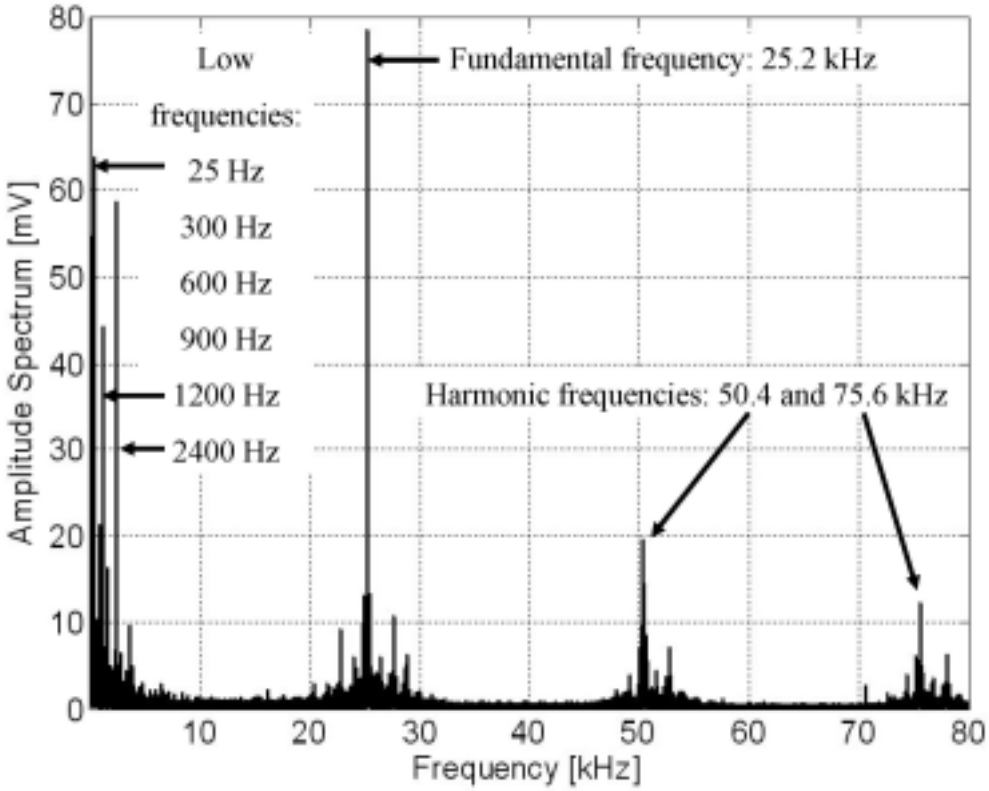

Figure 6.69: Normalized amplitude spectrum showing the fundamental and harmonic frequencies from a recording captured by sensor No. 8 in the first main period of data recording.

Table 6.15: Normalized amplitude spectrum amplitudes from sensor No. 8.

Run	25 Hz	300 Hz	600 Hz	1.2 kHz	2.4 kHz	25.2 kHz	50.4 kHz	75.6 kHz
[No.]	[mV]	[mV]	[mV]	[mV]	[mV]	[mV]	[mV]	[mV]
1	-	16	12	**32**	26	**44**	24	22
2	8	10	8	**22**	20	**64**	12	22
4	-	2	**4**	**4**	-	**32**	-	18
6	2	-	2	**4**	-	14	6	**24**
9	8	6	**14**	-	-	**46**	26	24
10	18	26	26	**54**	48	**70**	28	12
11	18	24	30	24	**72**	**34**	26	-
17	58	48	30	**72**	50	-	46	-
18	40	58	32	56	**68**	18	36	-
19	24	56	36	64	**72**	30	**56**	-

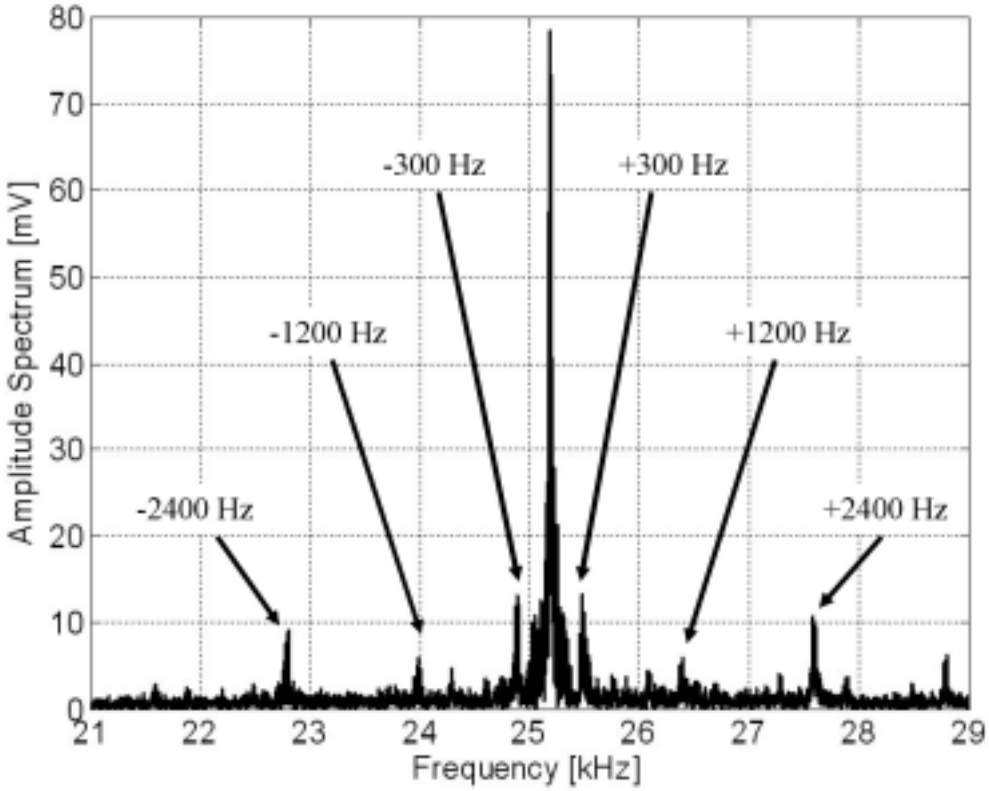

Figure 6.70: The normalized amplitude spectrum shows the fundamental 25.2 kHz frequency and its sideband frequencies. Data were captured by sensor No. 8 in the first main period of data recording.

Results from analyses of the recordings made by sensor No. 8 have been used in the following simulation approaches. However, some restrictions were necessary to maintain a certain overview. The simulations were based on only two main signal patterns. The fundamental frequency of 25.2 kHz was selected as the main signal, while 1200 Hz was chosen as the only sideband frequency. In addition, these signals were assumed to be pure sine waves. The simulations have also been based on the assumption that the pressure signal was operating within a constant range. However, pressure peaks corresponding to more than one flange of the sinusoidal transfer function curve have been simulated as well.

The responses from this simulation approach were first of all results that simulated the voltage output signal appearing as the signal recorded by the data acquisition system. Thus, the simulated pressure signal was passed through the sinusoidal calibration curve of sensor No. 8 as shown in Figure C7 before it ended as a simulated voltage signal.

The equation for the sinusoidal calibration curve is given below as Equation 6.2:

$$V = \frac{V_{High} + V_{Low}}{2} \sin\left(0.2 \pi P - 30 \frac{\pi}{2}\right) + 2 \left(\frac{V_{High} + V_{Low}}{2} - V_{Low}\right) \quad (6.2)$$

V	: Voltage signal [mV]
V_{High}	: Maximum voltage level [mV] (Sensor No. 8: 1100 mV)
V_{Low}	: Minimum voltage level [mV] (Sensor No. 8: 200 mV)
P	: Pressure [bar]

The first simulation approach shows the simple added relationship between the main signal and its sideband signal as is given by Equation 6.3. The next simulation handled multiplied signals, which is the amplitude-modulated case given by Equation 6.4. The third simulation approach combined these two approaches. Thus, the amplitude-modulated signal was added to the signal from the added case as shown by Equation 6.5. The three equations representing the three cases are given below.

- Signal pattern based on added frequencies:

$$P_{add} = \frac{P_{High} + P_{Low}}{2} \sin(2\pi \tau_h t) + P_l \sin(2\pi \tau_l t) + \left(\frac{P_{High} + P_{Low}}{2} - P_{Low}\right) \quad (6.3)$$

- Amplitude-modulated signal pattern:

$$P_{AM} = \frac{P_{High} + P_{Low}}{2} \sin(2\pi \tau_h t) (P_l \sin(2\pi \tau_l t)) + \left(\frac{P_{High} + P_{Low}}{2} - P_{Low}\right) \quad (6.4)$$

- Signal pattern based on the combination of the two previously cases:

$$P_{add2AM} = \frac{P_{High} + P_{Low}}{2} \sin(2\pi \tau_h t) (P_l \sin(2\pi \tau_l t)) + \left(\frac{P_{High} + P_{Low}}{2} - P_{Low}\right) + \frac{P_{High} + P_{Low}}{2} \sin(2\pi \tau_h t) + P_l \sin(2\pi \tau_l t) + \left(\frac{P_{High} + P_{Low}}{2} - P_{Low}\right) \quad (6.5)$$

P_{add}	: Pressure of the added signals [bar]
P_{AM}	: Pressure of the amplitude-modulated signals [bar]
P_{add+AM}	: Pressure of the added and the amplitude-modulated signals [bar]
P_{High}	: Maximum pressure level [mV]
P_{Low}	: Minimum pressure level [mV]
P_l	: Amplitude of the low frequency pressure signal [bar] (2 bar)
τ_h	: Frequency of the high frequency pressure signal [Hz] (25.2 kHz)
τ_l	: Frequency of the low frequency pressure signal [Hz] (1200 Hz)
t	: time [s]

Three selected simulation results are shown in Figures 6.71 – 6.73. Additional results are listed in Table 6.16. Each figure shows three plots associated with the simulated pressure signal (upper plots), the voltage output signal (plots in the middle) and the corresponding normalized amplitude spectrum (lower plots). The figures show the simulated results related to the pressure range between 18-28 bar. The latter is associated with the high frequency (25.2 kHz) pressure variation. In addition, a low frequency (1200 Hz) pressure variation of ± 2 bar is added. In Table 6.16 are results from additional pressure ranges presented as well.

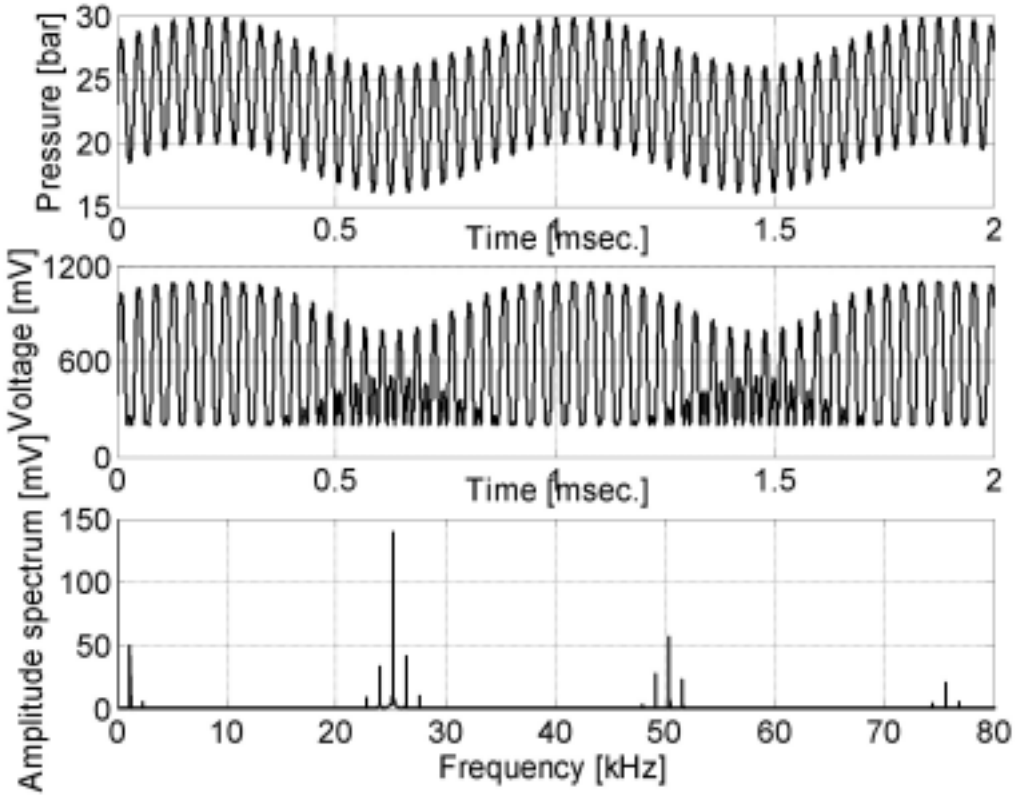

Figure 6.71: Simulation of added signals. Pressure (upper plot), voltage (plot in the middle) and amplitude spectrum (lower plot).

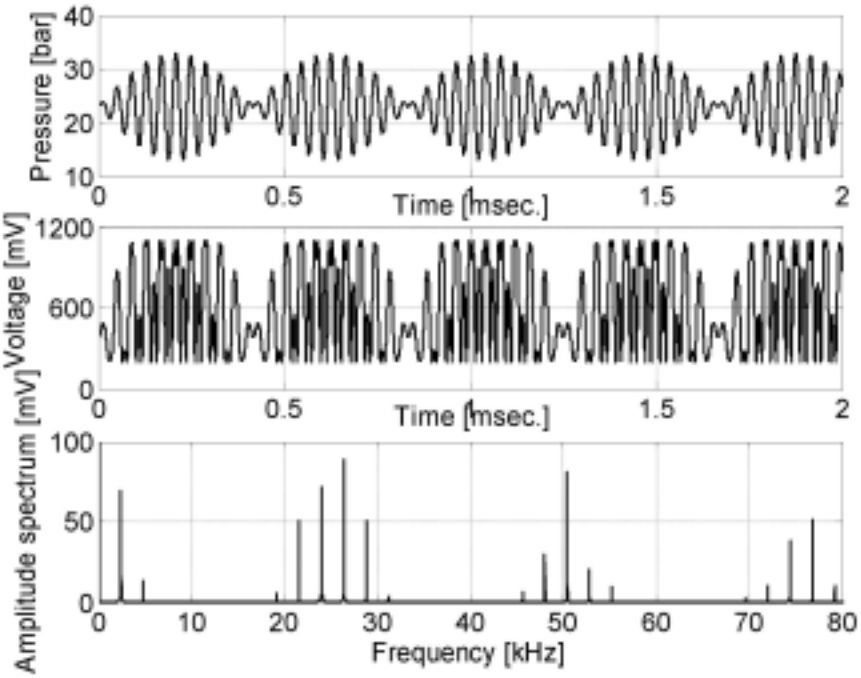

Figure 6.72: Simulation of amplitude-modulated signals. Pressure (upper plot), voltage (plot in the middle) and amplitude spectrum (lower plot).

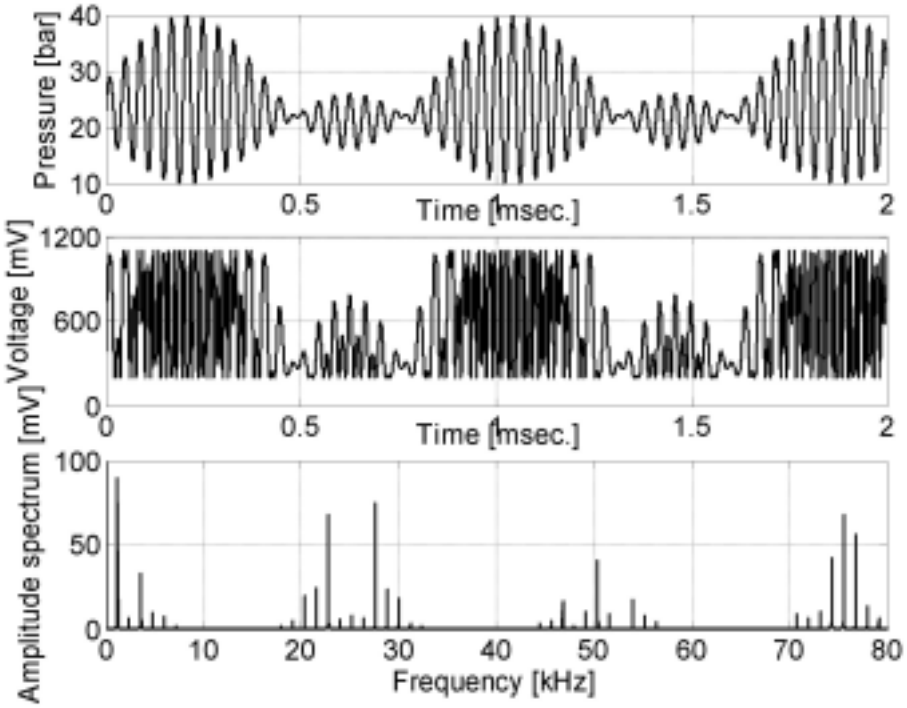

Figure 6.73: Simulation of the combined added and amplitude-modulated signals. Pressure (upper plot), voltage (plot in the middle) and amplitude spectrum (lower plot).

Table 6.16: Peak values obtained from simulated amplitude spectra.

Range [bar]	1200 Hz [mV]	2400 Hz [mV]	3600 Hz [mV]	25.2 Hz [mV]	∂1.2 ∂2.4 kHz [mV]	50.4 kHz [mV]	∂1.2 ∂2.4 kHz [mV]	75.6 kHz [mV]	∂1.2 ∂2.4 kHz [mV]
Add									
24-26	125	-	-	50	- 3	-	-	-	-
20-30	60	1	-	180	- 12	-	30 -	25	- 1
18-28	50	5	1	150	40 10	60	20 2	20	5 1
AM									
24-26	-	-	-	-	50	-	-	-	-
20-30	-	-	-	-	100 60	-	-	-	50 10
18-28	-	70	-	-	80 50	80	- 20	50	- 40
AM+Add									
24-26	120	5	3	50	5 6	6	6 2	1.5	1 0.5
20-30	25	20	10	-	30 100	15	25 5	60	40 5
18-28	90	6	30	8	6 70	40	10 1	70	50 10

The simulation results show that the added signal and the amplitude-modulated signal give few frequencies while the range is connected to one flange of the calibration curve, as shown in the upper rows for each case in Table 6.16. When the range increases the simulated results show a more complex signal pattern. The sinusoidal calibration curve forces the fundamental and the sideband frequencies to harmonic frequencies. These simulations illustrate the uncertainty in the determination of the pressure levels. In addition to these simulation results, two plots are shown in Figures 6.74 and 6.75. The data associated with these figures were captured by sensor No. 8 in the first experimental period. These figures show that a lot of different signal patterns were present in the true recordings.

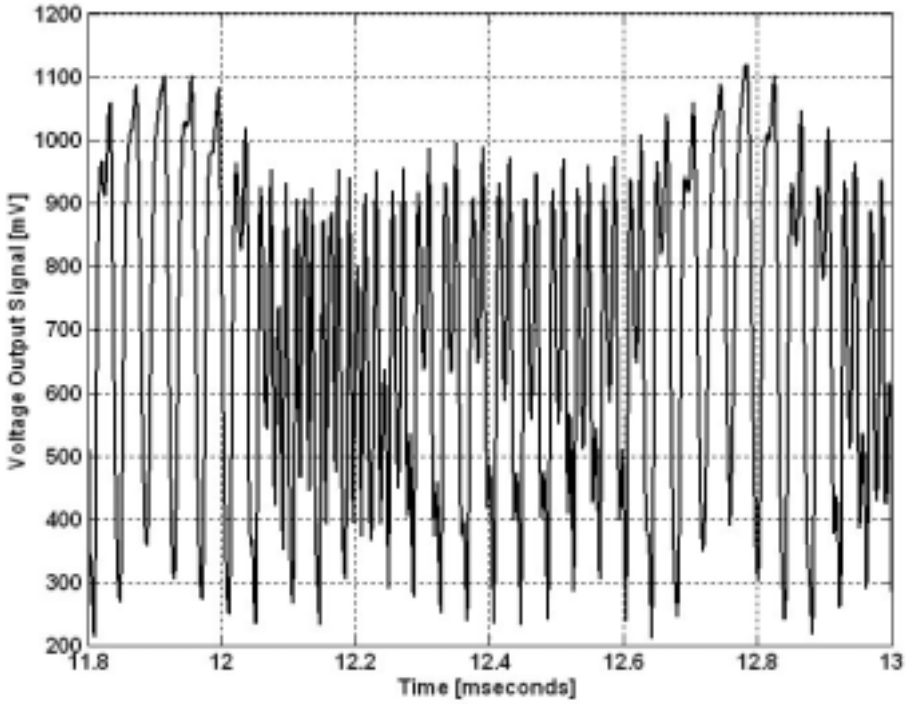

Figure 6.74: A recording from sensor No. 8 during run No. 9 is shown.

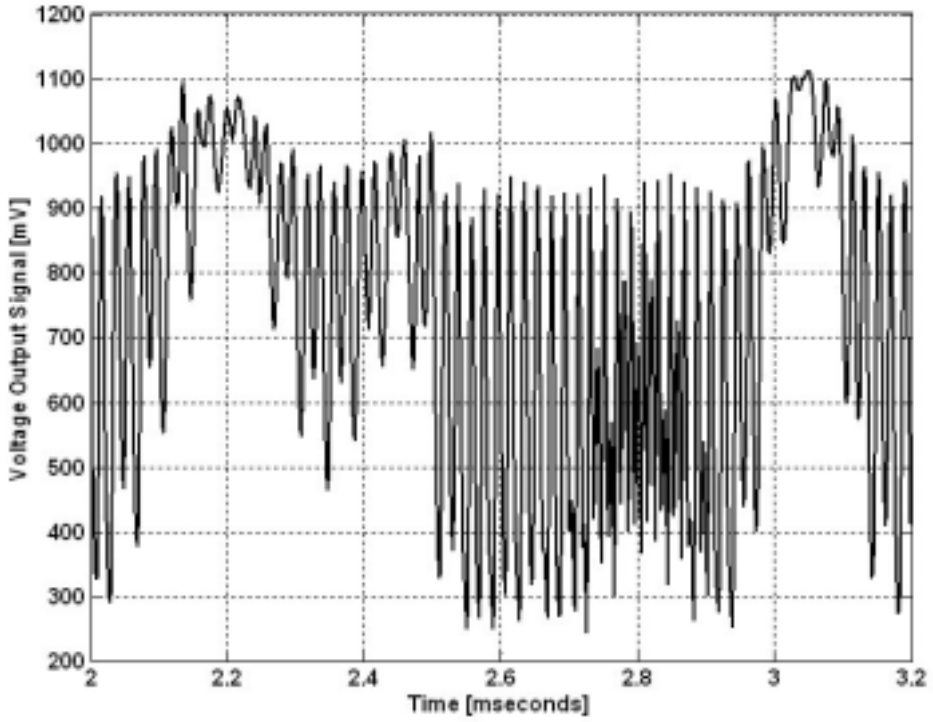

Figure 6.75: A recording from sensor No. 8 during run No. 19 is shown.

Figure 6.74 shows an underlying low-frequency signal pattern that can be related to a sideband effect as shown in the simulation of the added signals. In addition, it is clearly visible that different frequencies were present. The high frequency signals have probably arisen from the folding that occurred when the output signal crossed a minimum or a maximum point of the calibration curve. Figure 6.75 shows two distinct points in the diagram, which have small signal fluctuations. These points were probably caused by a pressure shift corresponding to a voltage signal that was shifted towards maximum of the calibration curve. The underlying cause for this particular effect remains unidentified. However, it is conceivable that some modulating effects were present as shown by similarities in Figures 6.72 and 6.73.

Irrespective of the range of the pressure signals, the responses that were captured by the data acquisition system were modulated because of the non-linear calibration curve. Increasing pressure range that forced the voltage signals across a maximum or a minimum point distorted the signal patterns and created harmonic frequencies. All of that is revealed in the data recorded. The question is how much the signals have been affected. This question remains unanswered. A new detection method or a combination between different detection techniques might solve the pressure determination problem when using interferometer based fibre-optic sensors.

6.10 Concluding remarks

The results shown in the previous sections, show that the dynamic properties of the recordings from the fibre-optic pressure sensors mainly can be explained. The recordings seem to be trustworthy. There has been uncertainty connected to the sinusoidal calibration curves and the determination of the pressure levels. The offsets from the original calibration curves gave additional uncertainty. The determination of the absolute pressures during pulp production has been the greatest weakness of the experiment.

The main findings can be summarized as follows:

- The refining zone pressures followed the casing pressure and the temperatures in the refining zone during the heating of the refiner. Also during a period of initial chip feeding and a subsequent shutdown the average pressure readings followed the casing pressure very well.

- It is indicated that the dynamic behaviour of the refining action, which was measured by the sensors irrespective of radial location, was affected by some common factors. The geometric structure of the plates and particularly of the plates on the rotor disc dominated the pressure signals. This means that the pulp flow was affected by the geometrical structure. Furthermore, the pressure pulses generated vibrations in the discs. These vibrations probably propagated through rigid discs. Thus the sensors located in different radial locations measured pressure variations created by these vibrations. This has been revealed through the frequency analyses, which showed that common frequencies were picked up by the different sensors. In

addition, cross-correlation analyses have indicated that the lag between the sensor signals could be associated with pressure wave propagation through steel.

- The cross-correlation analyses made on the low-pass filtered data gave indications of pressure wave propagation. No pulp flow movement between different sensor locations was obtained. The observed cross-correlation coefficients represented movement velocities in the range of about 100 m/s to more than 6000 m/s. The highest velocity gave indications of wave propagation in steel, while the lower velocities indicated wave propagation through the steam and pulp flow.

- The frequency of 25.2 kHz, associated with a particular bar-to-bar passage in the fine bar zone, was the most dominant frequency in the recordings conducted in the first experimental period. However, during the next 1000 operating hours a change in the periodicity was observed. Here, the frequency of 14.4 kHz associated with the bar crossing in the intermediate zone close to the transition zone between this and the fine bar zone, was more prominent. This strongly indicates that the pulp flow pattern had changed during the time elapsed. The wear of the plates and thus higher load and smaller plate clearance probably caused this shift, which is assumed to be created by changed behaviour of the pulp flow.

- Low frequencies associated with the rotational speed of the refiner, the bars in the breaker bar plates and the bolt holes of the plates were visible in the recordings from the sensors both as single peak frequencies as well as sideband frequencies. It is assumed that these three factors influenced the pulp flow since the pressure readings were significantly affected. The low frequencies appeared as modulated flow patterns probably caused by chip-feed variations due to the inlet zone. Thus the pulp flow may have propagated in waves outwards through the refining zone.

- The span of the output signals from the sensors decreased between the first and second experimental period. Two reasons for this could have been:
  - The pressure pulses were damped because the worn plates did not squeeze the pulp that much. Probable factors may have been rounded edges or serration patterns or a combination of both. Figures G1 – G4 show the serration pattern in the stator plate, which contained the pressure sensors, as well as some of the sensor holes.
  - Damping of the output signals due to full or partial isolation of the sensor surface against the pulp flow. Then pressure pulses had to be transmitted through this packed pulp layer before it reached the sensor surface.

- Determination of the average pressure levels was complicated because of two reasons:
  - The non-linear calibration curves where the relationship between the voltage output signals and the real pressures followed a sinusoidal curve with a periodicity of approximately 20 bar.
  - The pre-installed calibration offsets and the subsequent fluctuations in several zero-bar pressure measurements.

- The average output signals fluctuated more among sensors located in the inner part of the refining zone compared to the data obtained from the sensors located in the fine bar zone. However, the high dynamic pressures dominated the recordings from the sensors located in the outer part of the refining zone in addition to sensor No. 4 due to the smaller plate gap.

- The experimental results indicated that the dynamic range of the output signals usually were within one flange of the calibration curve. This implies that the dynamic pressures mainly were within a range of ± 5 bar. The fast pressure variations were stable at a high level from sensors located in the outer part of the refining zone as well as for sensor No. 4. The inner located sensors measured high-pressure pulses more seldom. The latter was probably a result of a large plate gap. A large plate gap may probably have given minor possibilities for pulp to be squeezed tightly between the sensor surface and the bars on the opposite disc.

- The results from the factorial designed experiment showed that the response variables such as motor load, accelerations and temperatures besides the pressure readings, were time dependent. Thus, it has been assumed that this was the reason for the lack of expected relationships between the response variables and the manipulated variables. The observed time dependency may be explained by uneven refining conditions between the two refining zones, which may have been caused by an uneven chip distribution as well as different plate clearances due to rotor movement. Another suggestion was that the experiment was started too early after the replacement of the plates. New plates and a lack of sufficiently heating may have caused the time dependent observations.

- The expected relationship between the process variables as motor load and acceleration and the pressure readings were confirmed through the chip-stream splitter test conducted in the second experimental period. Both motor load and acceleration were highly correlated with the average pressure.

- The freeness and the number of shives were as expected the most affected pulp quality variables from the pulp sample analyses. The production rate and motor load as input variable gave significantly regression models for these pulp quality variables. The other process variables, among them the pressure readings, did not show any good relationship with the pulp quality variables. The reasons for the weak relationships were probably caused by the uneven refining conditions and that the plates were new.

- Motor load variations have been investigated regarding deviations of the rotational velocity. The variations in rotational speed led to detectable frequency shifts of the bar-crossing frequency. This was properly identified by the analyses of the recordings from the pressure sensors.

- External noise was intercepted by the data acquisition system especially regarding sensors locked to channel A on the amplifier unit. However, the noise does not seem to have influenced the recordings or the data analysis significantly.

CHAPTER 7

RESULTS AND DISCUSSION VIBRATION MEASUREMENTS MILL REFINER

7.1 Introduction

Before the experiment containing the high-frequency pressure sensors was performed, it was expected that periodic signals would appear. The expectations were particularly related to obtaining the bar-crossing frequencies. However, the investigations revealed that irrespective of the radial location of the sensors, common frequencies were clearly visible in the frequency spectra from all of the sensors. The assumption made from these investigations was that pressure pulses generated vibrations in the rigid discs. Hence, all the sensors irrespective of the radial location could measure these vibrations. This assumption had to be investigated more closely. The question was if these vibrations existed, and furthermore, whether these vibrations were detectable using other measurement equipment? Both Strand and Hartler (1985) and Strand and Mokvist (1987) as well as Pettersen and Gunstrøm (1980) indicated that vibration or sound measurement could be used in such investigations.

When the original plates used in the high-frequency pressure experiments were still in the refiner, the first experiment was done based on vibration measurements. The next experiment was performed immediately after the replacement of the original plates. In between and during unloaded and non-spinning conditions, the test to obtain the natural frequency of the refiner was performed. The experimental procedures have been described in Section 3.6.4.

7.2 Vibration measurements before plate change

The vibration measurements gave many of the same peak frequencies in the FFT-analysis as the data recordings from the pressure sensors. This was in agreement with the indications made by Strand and Hartler (1985), Strand and Mokvist (1987) and Pettersen and Gunstrøm (1980). Figure 7.1 shows the amplitude spectra from recordings performed using these two different measurement technologies. The spectrum from the

vibration readings is shown in the upper plot, while the lower spectrum shows the voltage output signal from sensor No. 4. The latter readings were captured during the second experimental period after 1000 working hours. The accelerometers were used one month later after an additional 700 working hours.

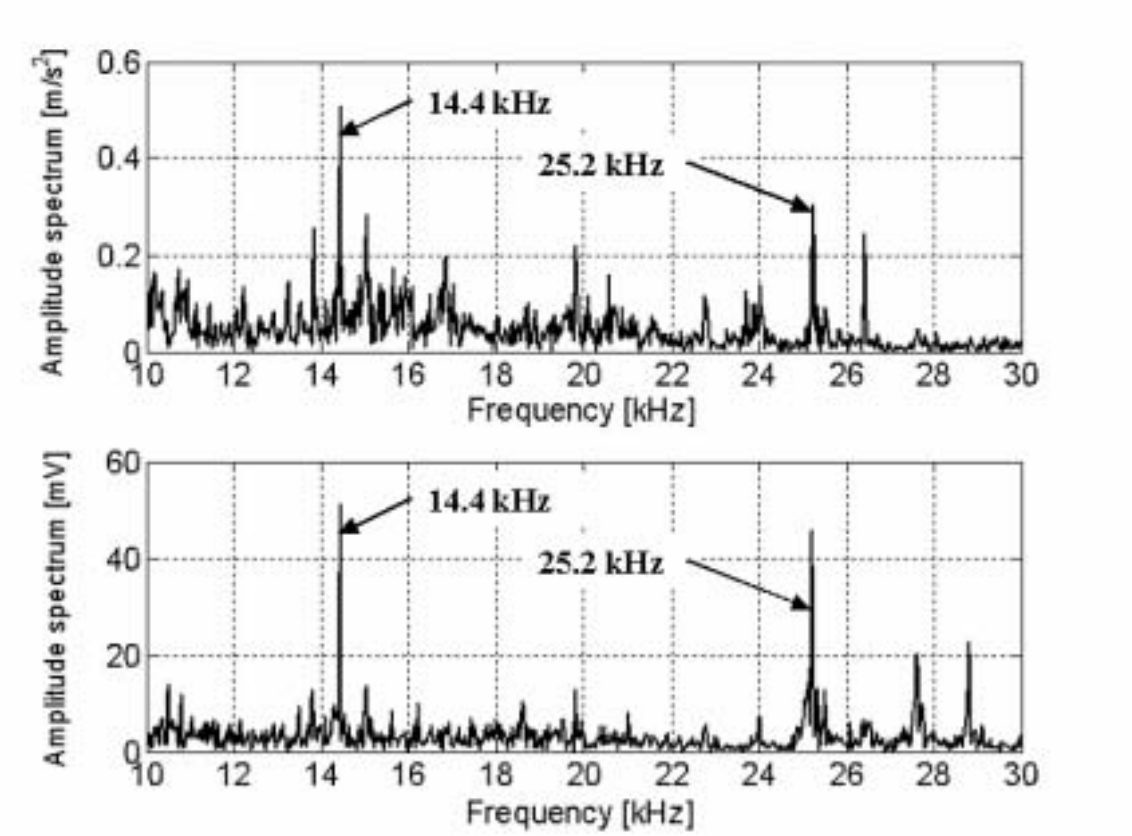

Figure 7.1: Amplitude spectra in the frequency band from 10 to 30 kHz are shown. Upper plot shows the acceleration signal from the refiner using worn plates (1700 hours). The lower plot shows the voltage output signal from sensor No. 4 after 1000 operating hours. Both plots are averaging spectra containing 62 different spectra each.

The spectra shown in Figure 7.1 reveal common peak frequencies in the vibration (upper plot) and pressure (lower plot) measurements. This is in agreement with the indications made by Strand and Mokvist (1987), who claimed that the pressure pulses appearing from the squeezing of pulp between the stator and rotor bars propagate as vibrations in the refiner. The two dominating frequencies of 14.4 and 25.2 kHz found in the data recordings from the pressure sensors were clearly visible also in the amplitude spectra from the vibration measurements. The peak frequency at 14.4 kHz was associated with the bar crossing frequency in the outer part of the intermediate zone. The peak frequency at 25.2 kHz was related to the fine bar zone approximately 80 mm from the periphery and approximately 26 mm outside of the taper break point in the stator plates.

Other common frequencies were found as well in both measurements. The 600 Hz sideband frequencies at both sides of the 14.4 kHz peak frequency as shown as the peaks at 13.8 and 15.0 kHz were clearly visible. In addition, the 1200 Hz sideband frequencies around 25.2 kHz were found. Moreover, the assumed plate periphery frequency of 27.6 kHz was mainly present in the pressure measurements. When averaging more spectra (62 instead of 31) the 27.6 kHz in the amplitude spectrum from the vibration measurement was almost absent. In the frequency spectrum from the pressure sensor both 27.6 and 28.8 kHz had larger amplitude values than the corresponding sideband frequencies. This indicated that these frequencies were the second harmonic frequencies of 13.8 and 14.4 kHz respectively. However, another or additional effect may come from pulp and steam flow activities at the periphery of the plates. The latter effect, if it was present, seems to have affected the vibration measurements in minor extent.

Figures 7.2 and 7.3 show amplitude spectra from additional frequency bands. Figure 7.2 shows the frequency spectrum from 0 to 1 kHz, while Figure 7.3 shows the frequency band from 1 to 10 kHz.

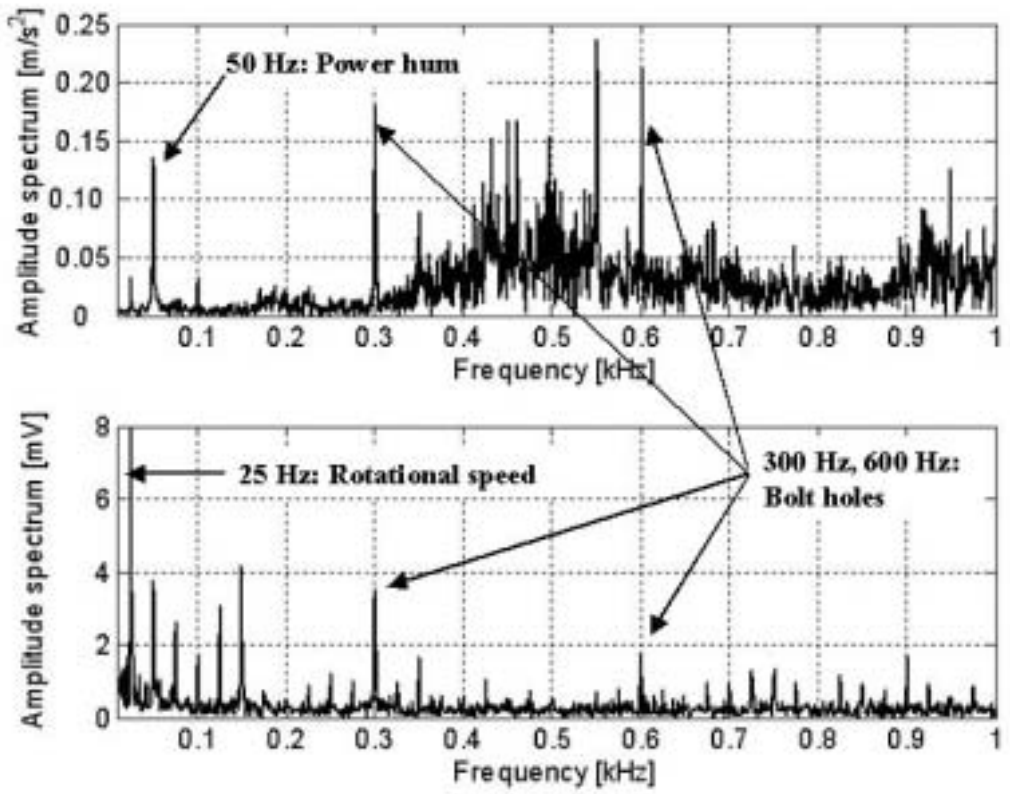

Figure 7.2: Amplitude spectra in the frequency band between 0 to 1 kHz are shown. The vibration is shown in the upper plot, while the pressure signal from sensor No. 4 is shown in the lower plot. Both plots represent one spectrum each containing 2^{19} samples.

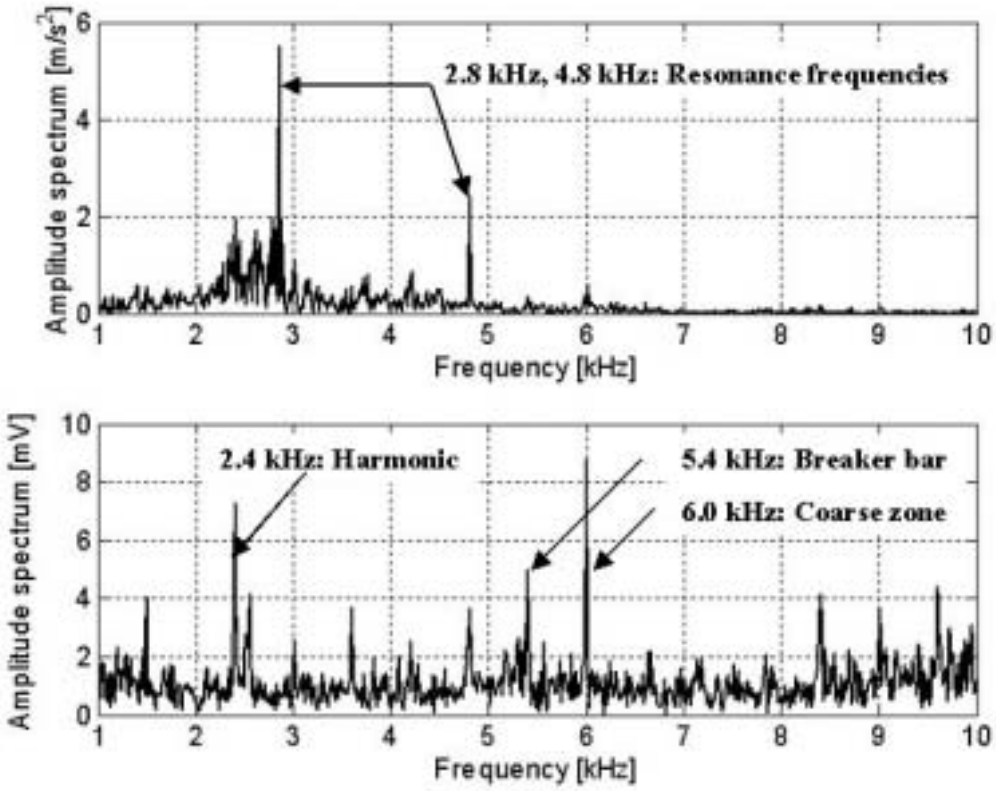

Figure 7.3: Amplitude spectra in the frequency band between 1 to 10 kHz are shown. The upper plot shows the vibration recording, while the lower plot shows one recording from sensor No. 4. Both spectra are averaging spectra from 31 spectra each.

A particular observation is tied to the frequencies of 2.8 and 4.8 kHz as clearly shown in the upper plot in Figure 7.3. These frequencies were probably some of the resonance frequencies in the refiner. The high peak amplitudes compare to the other peak frequencies indicated this. In accordance with Wowk (1991), most metal structural resonance occurs between 100 Hz and 5 kHz. Wowk explained resonance as a condition whereby the driving force applied to a structural part is close to its natural frequency. Thus amplification occurs. The vibration amplitude of a structure excited into resonance can be 10 to 100 times the amplitude of the input force. The amplification is affected by the damping that occurs in the structure. The assumed resonance frequencies as shown in Figure 7.3 have amplitude values up to 10 times the amplitude of the 14.4 kHz signal as shown in Figure 7.1. However, it can be assumed that the driving force that generated the resonance frequencies was less dominating compared with the forces that created the refining zone affected frequencies. The natural frequencies are discussed in Section 7.4.

The lowest frequency (2.8 kHz) may be associated with the resonance frequency of the whole refiner, which represents a coupled system consisting of the drive side, rotor disc and the front side of the refiner. A higher mass reduces the natural frequency of the

system[15]. Using the simple relationship between natural frequency and a spring mass system, the difference in weight corresponding to the two different resonance frequencies was approximately three mass units. The frequency of 4.8 kHz may be associated with the motor side of the refiner solely (one mass unit), while the 2.8 kHz may be associated with the coupled system (three mass units).

The data readings that formed the basis for the frequency spectra in Figures 7.1 to 7.3 were measured by an accelerometer attached to the drive side of the refiner. The presence of the frequency of 4.8 kHz may be associated with periods of smaller coupling efficiency by the pulp between the discs. Furthermore, the smaller amplitude value of the periodicity of 4.8 kHz may be associated with the damping effect related to the pulp between the discs.

7.3 Vibration measurements after plate change

A comparison was made between the amplitude spectra from the vibration measurement performed on the refiner during refining using the stator plates containing the pressure sensors and during refining using another type of refiner plates. This was done to test a hypothesis, which was proposed and associated with the geometrical structures of the plates. It was assumed that different plate patterns would give different frequency patterns in the frequency analyses. The new plates were of the same type as used on the rotor disc in the previous part of the experiment as shown in Figure 3.8. Figures 7.4 and 7.5 show diagrams of the amplitude spectra from recordings captured before and after the plate change.

[15] Undamped natural frequency of a simple spring mass system (Wowk (1991)):

$$\varpi_n \mid \sqrt{\frac{k}{m}};$$

k : spring stiffness
m : mass

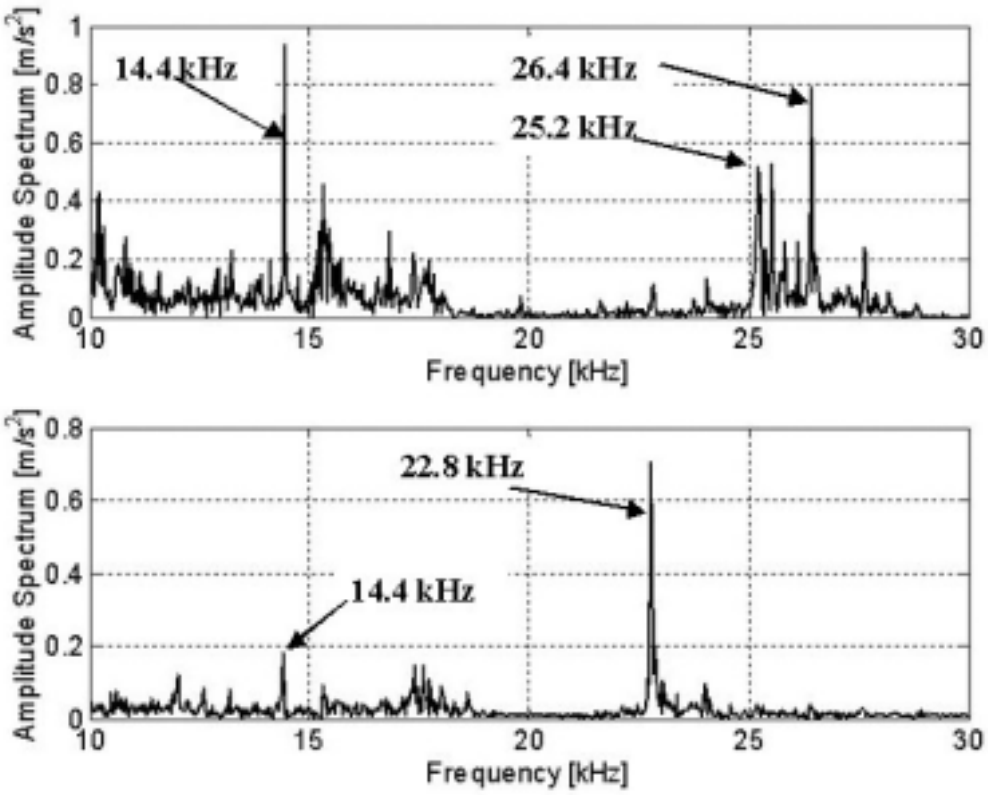

Figure 7.4: **Amplitude spectra in the frequency band from 10 to 30 kHz are shown. The upper plot shows the vibration before replacement of the plates. The lower plot shows the vibration measured after the plate change.**

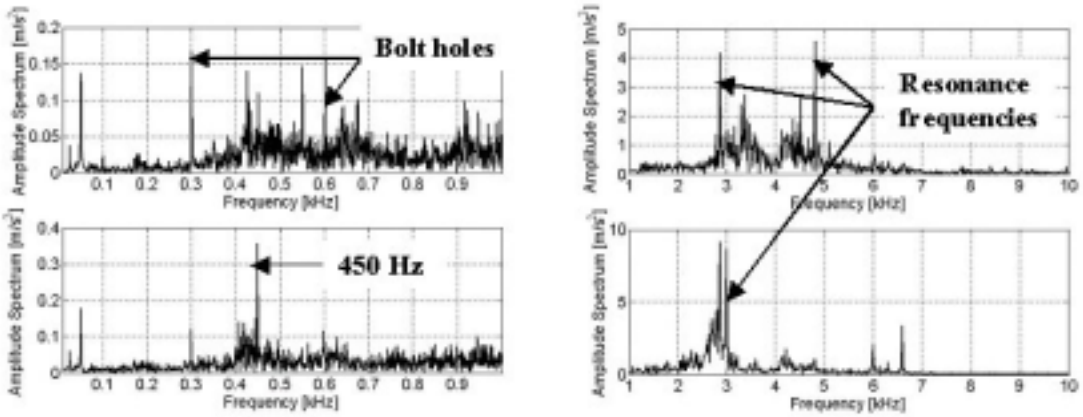

Figure 7.5: **Amplitude spectra in the frequency band from 0 to 1 kHz (left-hand) and in the frequency band from 1 to 10 kHz (right-hand) are shown. The upper plot shows the vibration before replacement of the plates. The lower plot shows the vibration measured after the plate change.**

The comparison between the amplitude spectra in Figure 7.4 shows that the main peak frequencies in the frequency band between 10 and 30 kHz shifted towards a lower frequency. This observation is associated with the change of the main frequency peak in the fine bar zone. The old plates with the pressure sensors installed gave dominating peak frequencies at 25.2 and 26.4 kHz. The new plates gave a plain peak frequency at 22.8 kHz. This indicates that the area where the main pressure pulses occurred was shifted towards the intermediate zone. The shift towards the centre corresponded well with the shift of the taper break point too. The taper break point on the new plates was approximately 10.3 mm closer to the intermediate zone than on the replaced plate set. In addition, the gradient of the taper was smaller at the new plates compared with the replaced ones. This indicates that the pulp flow was resisted earlier in the refining zone because of a more narrow plate gap in the outer part of the refining zone after the plate change. The frequency of 22.8 kHz corresponded to the bar-crossing frequency in the junction between the intermediate and the fine bar pattern zone. However, this frequency represents the area at the fine bar pattern side of the junction approximately 20 mm inside the taper break point. This assumption, about a shift of localization for where the main refining action takes place is dependent on the tapers of the plate, is supported by Miles *et al.* (1980). They claimed that the effect of increasing the taper is seen to be to move the peak pressure outwards.

In addition to the frequency shift in the fine bar zone, some dissimilarities are found in the lower frequency bands as well. This is shown in Figure 7.5. The frequency of 450 Hz was more pronounced after the plate change. The origin of this frequency is not clarified. It was not dominating in the spectra from the recordings captured by the pressure sensors. Thus, this frequency may be related to vibrations created by other factors than the origin of the pressure pulses. The frequency peaks at 6.0 and 6.6 kHz were more pronounced in the measurements recorded after the replacement of the plates. The latter frequency may be a sideband frequency associated with the bolt holes in the plates, while the 6.0 kHz was probably related to the bars in the coarse zone.

These differences and especially the peak frequency shift associated with the fine bar zone indicated that the plate geometry play an important role in the vibrations of the refiner. Because of the common peak frequencies between the pressure measurements and the vibration measurements, it is assumed that the dynamic pressure and the flow pattern of steam and pulp also changes because of the geometrical differences of different types of plates. These measurements and the frequency analyses have strongly enhanced such assumptions. However, there is no evidence in this work that indicates how much these vibrations affected the plate gap. According to Ouellet and Weiss (1994) the axial vibrations resulting from deterministic variations of bar intersecting area and random variations of bar coverage by pulp are probably small. Ohls and Syrjänen (1976) indicated such gap variations in the order of 0.5 μm in an industrial refiner.

7.4 Provoking the natural frequencies

The presence of the frequencies that gave the high amplitudes has been associated with resonance in the refiner house. Several frequencies have been found. Among the most

pronounced were the peak frequencies at 2.8, 3.0, 3.6, 4.2 and 4.8 kHz. According to Wowk (1991), all objects have more than one natural frequency. However, a test was done to examine whether these frequencies had any connection to the natural frequencies of the refiner. The natural frequencies of the refiner were found through provoking resonance in the refiner house.

This test was performed after the replacement of the plates and before the initial chip feeding was started. The test was conducted after the initial heating when the refiner was stopped for recalibration of the plate clearance. The accelerometer was attached to the front side of the refiner in the same position as the measurements during pulp production were captured. Thus, the axial vibrations were measured. A soft hammer was used to provoke the natural frequencies.

Some results of the test are shown in Figure 7.6. The long time series in the upper plot contains 3 MSamples. It shows six following soft-hammer strokes, while the lower plot solely shows the time series of the first stroke containing 3.5 kSamples. The saturation levels due to a very small range in the selected limits of the data acquisition range are clearly visible. In Figure 7.7 the corresponding amplitude spectra are shown. The upper plot is an averaged spectrum from 91 spectra containing 2^{15} samples each. The lower plot shows a single spectrum from 2^{11} samples of the data displayed in the lower plot of Figure 7.6. A natural frequency of about 4.4 kHz was found. This frequency corresponded with the empty non-spinning refiner. The accelerometer was attached at the front side of the refiner. Thus, the result cannot directly be compared with the frequencies shown in Figures 7.3 and 7.5, which were recorded from the drive side.

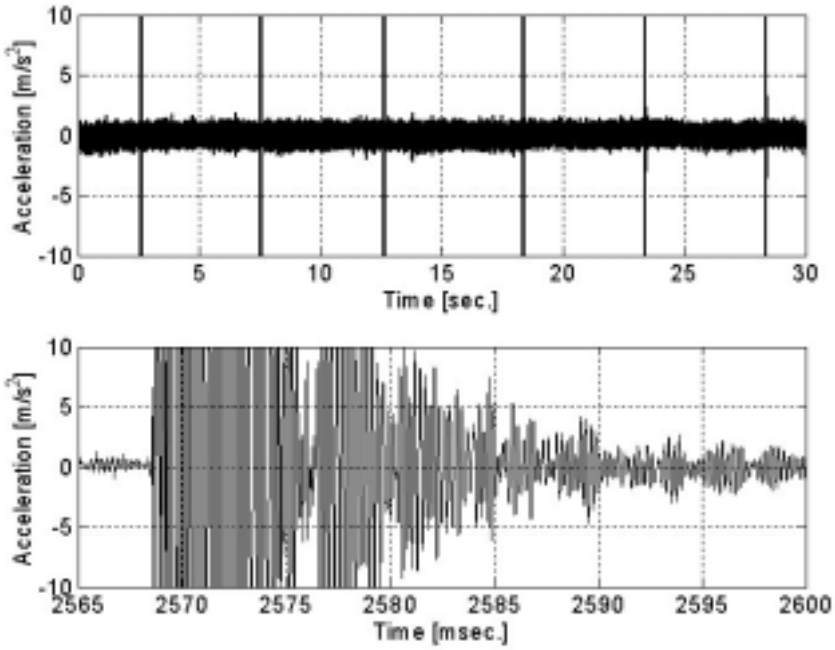

Figure 7.6: Readings from the accelerometer during provoking the natural frequencies are shown. The upper plot shows the responses from six soft-hammer stroke, while the lower plot shows the first response.

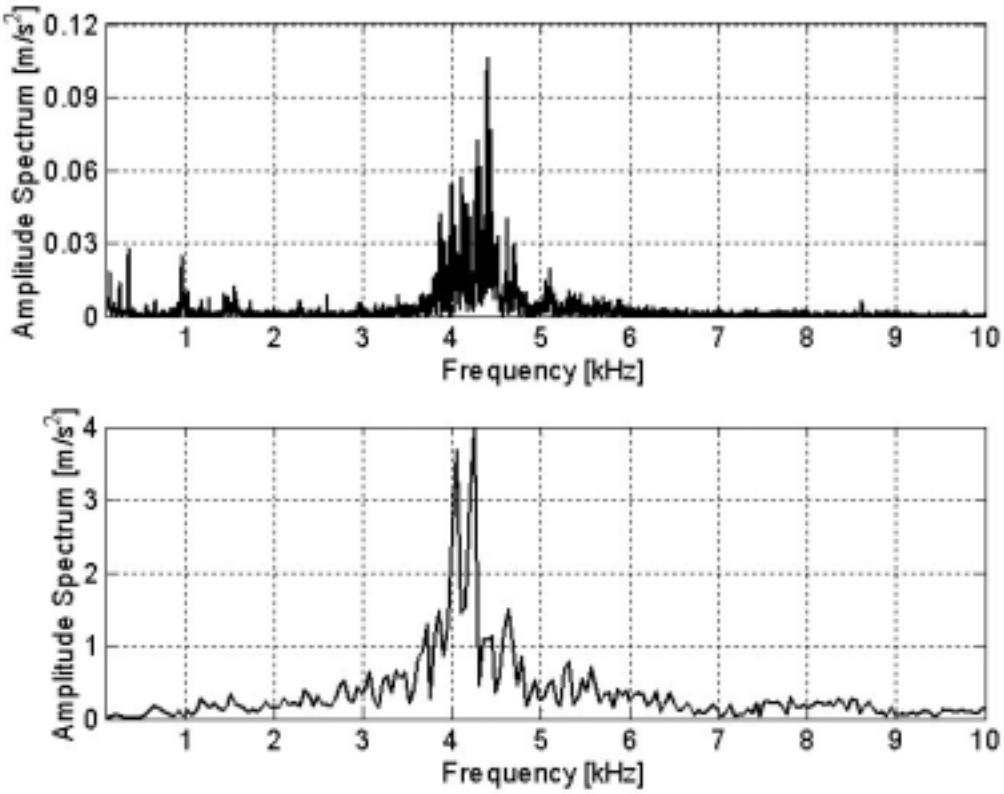

Figure 7.7: Corresponding amplitude spectra from the readings shown in previous figure.

7.5 Concluding remarks

The common frequencies revealed from the vibration measurements and the refining zone pressure measurements gave strong indications that the pressure pulses generated in the refining zone appear as vibrations in the refiner house. These results reinforce the indication made by Strand and Hartler (1985) and Strand and Mokvist (1987) which claimed that vibrations are a direct indicator of the intensity of the pressure pulses resulting from the passing of rotor and stator bars. Pettersen and Gunstrøm (1980) made almost the same statement. They claimed that the noise and the acoustic vibrations from a grinder were generated in the refining zone because of pressure pulses occurred from the passage of the bars on the rotor and the stator.

The differences revealed between the vibrations measurements performed on the refiner while it was equipped with different types of plates reinforce the hypothesis that the plate geometry clearly makes different pulp flow patterns. The vibrations in the refiner were significantly different after the plate change compared with the vibrations that were measured before the plate change. This was especially clear when comparing the vibrations generated in the fine bar zone. The main dominating frequency corresponding to the bar-crossing frequency in the refining zone was shifted towards the intermediate

zone when the new plates with a taper break point closer to the inlet were used. In addition the gradient on the new plates was smaller indicating that the more narrow plate gap forced the main pressure pulses to occur earlier in the refining zone.

The amplitude spectra from the recordings using the pressure sensors did not show any high-peak frequencies that could be associated with the natural frequencies of the refiner. This means that no frequencies were picked up from the refining of pulp that acted as driving forces to set the refiner in resonance. This further indicates that the pressure sensors were unaffected by vibrations operating in resonance. Thus, the pressure sensors were solely measuring the activities in the refining zone. The accelerometers measured process independent vibrations as well as vibrations generated from the refining of pulp. This makes the pressure readings to be better indicators of what is happening in the refining zone compared with the vibration measurements. However, vibration measurements seem to give valuable information about the refining since the pressure pulses generate and transmit vibrations to the refiner house. High-frequency vibration measurements seem to be a mirror image of the pressure pulse frequencies. The amplitude ratio between the pressure pulses and the vibration amplitudes are not yet thoroughly investigated. Further testing is required to determine the benefit of the postulated relationship between the pressure and vibration measurements.

CHAPTER 8

CONCLUSIONS

8.1 General conclusions

Results from high-frequency measurements of pressure and temperature in the refining zone of high-consistency refiners have been presented. It can be concluded that it is possible to establish high-frequency pressure measurements in the refining zone. The fast development within sensor and computer technology has made it possible to achieve measurements that have not been performed earlier. The use of fibre-optic sensor technology in chip refiners has not been reported earlier.

Two mill-scale experiments have been conducted using two different types of pressure sensors: fibre-optic pressure sensors based on extrinsic Fabry-Perot interferometer and piezoresistive temperature and pressure transducers. In addition, an experiment has been performed in a pilot refiner using a single piezoresistive temperature and pressure transducer. The fibre-optic sensors seem to be preferable to the piezoresistive transducers. Reliable measurements were obtained after 1000 operating hours showing that the fibre-optic sensors were working well after long exposure to the harsh environment. The piezoresistive sensors suffered from problems occurring from the wet environment inside the refiner as well as from the electrical dependent circuits and transmission cables. However, the piezoresistive transducer behaved well in the pilot refiner under a less harsh environment.

It has been claimed that there is a relationship between vibrations in the refiner discs and the pressure pulses that are generated from the squeezing of pulp between bars on the rotor and stator disc (Strand and Hartler (1985), Strand and Mokvist (1987)). Nobody has investigated this particular relationship. However, this study strongly indicates that this relationship does exist. Common frequency peaks from two completely different types of measurements are obtained. One of them measured the pressure inside the refining zone, while the other measured the vibrations in the refiner house using external accelerometers. In addition, it is shown that the pressure sensors were not affected by vibrations operating in resonance. This strongly supports the conclusion that the fibre-optic pressure sensors were solely measuring the activities in the refining zone.

Several of the eight fibre-optic sensors used in this study have found common periodic pressure pulses associated with especially one identified bar crossing frequency. This bar crossing frequency appeared from the fine bar zone and gave a distinct peak at 25.2 kHz in the frequency analyses. This common periodicity was clearly observed when the plates were new. Measurements with worn plates gave additional frequencies indicating that the flow pattern had changed during the elapsed time. The presence of the distinct peak frequency of 25.2 kHz indicated that the main pressure pulses were generated in one particular radial location in the refining zone. The pulses probably propagated in the disc so that the whole disc vibrated. Thus the pulp flow through the whole refining zone was affected. The pressure recordings undertaken at different radial locations measured this common influence on the pulp pad, which was predominant compared to the local generated pressure pulses. The local bar crossing frequencies were suppressed and only visible to a minor extent.

Short-term load and rotational speed variations have been identified by frequency analysis of the pressure recordings as well. This reinforces the ability of the sensors to measure high-frequency pressure variations.

Recordings captured during different controlled operating conditions have been used in the investigation of the reliability of the sensors and the relationship between the pressure signals and the process variables. No strong correlations were found between the pressure signals and the process variables shortly after start-up using new plates. Pulp samples collected and analysed did not give any clear relationship between the pressure signals and the pulp data. However, during this period other process disturbances affected the conditions in the refining zone more than the randomized manipulation of the control variables. This was observed as time dependent variations in the pressure recordings as well as several process variables. The most probable disturbance was the amount of chips fed to the refiner and subsequent changes of the plate gap. This is supported by an experiment performed after 1000 working hours, which showed that the pressure amplitude values were sensitive to fluctuations in the amount of chips fed into the refining zone. When changing the amount of chips to the refining zone, the pressure signal was strongly correlated with the process variables motor load and acceleration.

In addition, frequency analyses have showed that the sensors also were affected by frequencies that were related to process conditions in the inner part of the refining zone and the breaker bar section. This was shown both as sideband effects as well as plain peak frequencies. Sideband effects are interpreted as periodic waves of pulp flow propagated through the refining zone. This reinforces the assumption that the amount of chips and the process conditions early in the refining affect the pressure conditions in other parts of the refining zone.

This study indicates that the average pressure in the intermediate zone of the refining zone of mill-scale TMP-refiners can be as high as 20-30 bar. This was somewhat higher than expected from the theoretical considerations. However, the theoretical calculations have some limiting factors, which there are some disagreement in the literature. The area where the energy is applied in the refining zone as well as the tangential friction

coefficient is not clearly determined. Both are included in one of the theoretical approaches. Thus there are some uncertainties associated with the models. However, some uncertainties are related to the determination of the pressure levels for the measurements using the fibre-optic sensors as well. This is mainly due to the lack of well-established demodulation techniques for the sinusoidal relation between the sensor signal and the pressure. This is the greatest weakness in this part of the investigation.

The pressure levels obtained using the piezoresistive sensors were to some extent agreeable with the fibre-optic measurements. However, there was greater uncertainty in the piezoresistive measurements due to probable disturbances related to electromagnetic noise or moisture having a detrimental influence on electric circuits in the sensors. The most interesting results obtained using the piezoresistive sensors in the mill-scale experiment have been observations of process relevant periodic signal patterns.

Stable average pressures between 2 and 4.5 bar were found in the atmospheric pilot refiner during normal operating conditions. In addition, pressure peaks above 10 bar were observed frequently. When the plate gap decreased, the pressure pulses were considerably higher. Pressure peaks up to 60 bar were observed during operation with a small plate clearance. Under such conditions the local bar crossing frequency was clearly visible, not else. Since the local bar crossing frequency did not dominate the periodicities obtained from these recordings, it is assumed that the steam affected the pressure conditions in the refining zone. This is assumed despite the refiner was operating with temperatures below 100 ∀C.

No measurements in this study can confirm that steam is saturated in the refiner. The only reliable results that were obtained came from this part of the study using the combined pressure and temperature measurements in the pilot refiner.

8.2 Piezoresistive sensors – mill-scale experiment

The most convincing results from the mill-scale experiment using four piezoresistive transducers were the peak frequencies obtained from the frequency analyses. Some peak frequencies could be associated to process inherent features. The following recognized frequencies have been found:

- ∉ 25 Hz : Rotational speed of the refiner.
- ∉ 300 Hz : Ribbon feeder or the number of plates in the stator circle.
- ∉ 600 Hz : Bolt holes located close to the radial position of the sensors.
- ∉ 3.0 kHz : The number of bars in the outer part of the breaker bar plates.
- ∉ 5.1 kHz : The number of bars in the coarse zone.
- ∉ 15.6 kHz : The bar-crossing frequency in the intermediate zone.
- ∉ 27.0 kHz : The number of bars in the fine bar zone.
- ∉ Sideband frequencies of ∂ 25 Hz, ∂ 300 Hz, ∂ 600 Hz.

It is unlikely that the peak frequencies were created randomly. It can be assumed that the pressure sensors have responded on the forces acting on the diaphragm. However, it

is not evident that the calibrations of the sensors were trustworthy. The lack of consistent recordings related to influence of noise and saturation effects appearing from the amplifier and the interconnection of the DAQ-systems have been observed. The wet environment may have affected the transducers as well. Thus, some uncertainties can be related to the measurements. Especially the measured pressure levels can be questioned.

8.3 Piezoresistive sensor – pilot-scale experiment

The main results obtained from the pressure and temperature measurements performed in the pilot refiner are presented below:

- Decreasing plate clearance gave significantly increased pressure readings.
- Pressure peaks up to 60 bar were observed at a small plate gap of approximately 0.25 mm.
- During normal operating conditions average pressures between 2 and 4.5 bar were observed, while pressure peaks were frequently found beyond 10 bar.
- High and stable pressure readings indicated that the steam contribution for counteracting the axial thrust should not be ignored. The low-level pressure readings indicated that steam pressure was present to some extent. A possible reason for this may be related to stagnant pulp in the grooves that resisted the steam flow. Thus steam pressure could have been built up in small parts of the outer region of the refining zone. However, an uncertainty associated with the relative large diameter transducer casing as well as the location of the sensor between two bars cannot be excluded as factors that can have been affected by unbalanced forces. Thus an apparent pressure can have been measured.
- Periodic pressure variations identified as out-of tram misalignment have been observed.
- The bar-crossing frequency at 7.15 kHz related to the radial location of the sensor was observed when the plate clearance was small.
- A period of process instability regarding chip-feeding problems was recorded. A plausible explanation of these findings was that too high friction occurred due to small plate clearance, and that the outward driving forces were small because of very dry pulp. Pressures below atmospheric were recorded, as well as unexpectedly high temperature values. The latter might be related to plate touching.
- A relationship between the temperature and pressure signals was obtained. The temperature readings lagged behind the pressure by approximately 50 μseconds. A less clear relationship was found during abnormal running conditions.

8.4 Fibre-optic sensors – mill-scale experiment

The main dynamic properties of the recorded signals from the fibre-optic pressure sensors can be explained. The recordings seem to be trustworthy. However, there have been uncertainties associated with the sinusoidal calibration curves because offsets have been observed. Thus, the determination of the absolute pressure during pulp production has been the greatest weakness in this part of the study.

The main findings can be summarized as follows:

- The pressure readings followed the casing pressure and the temperatures in the refining zone during the preheating. Also during a period of initial chip feeding and a subsequent shutdown, the average pressure readings followed the casing pressure very well.
- The dynamic effects measured by the sensors seem to be affected by some common factors. The geometric design of the plates and particularly of the plates on the rotor disc seems to have dominated the pressure signals. The measurements have indicated that the pressure pulses generated by the bar pattern have propagated in the disc and generated vibrations. These vibrations have probably affected the pulp flow since several sensors, independent of their radial location, have measured the same periodicities. This has been revealed from the frequency analyses. In addition, cross correlation analyses have indicated that the lag between the pressure signals was too small to be caused by any other phenomena than pressure wave propagation. This supports the assumption that the disc was vibrating in axial or flexural motion or a combination of both.
- The frequency of 25.2 kHz, associated with the bar-to-bar passage in the fine bar zone, was the most dominant frequency when the plates were new. The peak frequencies obtained in the frequency spectra were more evenly distributed after 1000 operating hours. The frequency of 14.4 kHz, associated with the bar crossings in the region close to the transition zone between the intermediate and fine bar zones, was more pronounced when the plates were worn. These findings indicate that the pulp flow pattern had changed during the time elapsed, probably because of the wear of the plates.
- The bars in the breaker bar plates and the bolt holes of the plates were clearly visible in the recordings from the sensors. These were observed both as distinct peak frequencies as well as sideband frequencies. It is assumed that these factors associated with the early treatment of the chips influenced the pulp flow through the entire refining zone.
- The span of the output signals decreased between the first and second main period of data recording. Two reasons for that can be:
  - Damping of the output signals according to worn plates.
  - Damping of the output signals due to full or partial isolation of the sensor surface against the pulp flow.
- The average signal from the sensors fluctuated more among sensors located in the inner part of the refining zone compared to the sensors located in the fine bar zone. However, the dynamic pressure was higher in the outer part of the refining zone. This is probably due to the smaller plate gap caused by the tapers of the plates.
- External noise was intercepted by the sensors and especially among sensors locked to channel A on the data acquisition system. The noise does not seem to have affected the results from the analyses significantly.
- The cross-correlation analyses performed on the low-pass filtered data gave indications of pressure wave propagation. No pulp flow movement between different sensors has been visible through the analyses. The observed cross-correlation coefficients represented movement velocities in the range of approximately 100-6000 m/s. The highest velocity has given indications of wave

propagation in steel. The lower velocities indicated wave propagation through the steam and pulp flow.

- Determination of the levels of the average pressures were complicated for two reasons:
  - The non-linear calibration curves where the relationship between the voltage output signal and the pressure followed a sinusoidal curve with a periodicity of approximately 20 bar.
  - The pre-installed calibration offsets and the subsequent fluctuations in several zero-bar measurements. The real mechanism of this abnormal behaviour of the sensor-system remains unidentified. One probable cause has been related to laser temperature fluctuations.
- The experimental results indicated that the dynamic range of the output signals mainly were within one flange of the calibration curve, which implies that the dynamic pressure was in an order of ± 5 bar. The dynamic pressure was stable at a high level among sensors in the outer part of the refining zone as well as for sensor No. 4. The inner located sensors reached high-dynamic pressures more seldom. Some large chip particles squeezed between the sensor surface and the bars on the opposite disc can have caused the highest-pressure peaks. However, the large plate gap probably prevented frequent high-pressure readings. The small size of the fibre-optic sensors might have reduced the ability to read the high pressures as well.
- The results from the factorial designed experiment did not give the expected responses from the manipulated variables. The response variables such as motor load, accelerations and temperatures besides the pressure readings were time dependent despite the experiment being conducted in a randomized order. A reason for this can be that the experiment was started too early after the replacement of the plates. Hence, the refiner was not sufficiently stabilized with regard to plate wear and heating. It has been indicated in this study that inherent fluctuations caused by the chip flow distribution and a subsequent rotor movement have caused such time dependent variations.
- The expected relationship between the process variables and the pressure readings were confirmed through the chip stream splitter test conducted after 1000 working hours. Both the motor load and the acceleration variables were highly correlated with the average pressure.
- The freeness and the number of shives were as expected the most affected pulp quality variables from the pulp sample analyses of the partially factorial experiment. The production rate and the motor load provided significant regression models, while the other process variables, among them the pressure readings, did not show any clear relationship. The reasons for the weak relationships were probably that the start of the experiment was too early and that the plates were new.
- Variations in the rotational speed of the refiner were measured. These corresponded well with variations in the motor load as expected. However, the fibre-optic pressure sensors identified the variations in rotational speed through the corresponding frequency shift of the bar-crossing frequencies. Thus, short-term load and rotational speed variations can be identified by frequency analysis of the pressure recordings.

8.5 Vibration measurements – mill-scale experiment

The common frequencies revealed in the vibration measurements and the refining zone pressure measurements strongly indicated that the pressure pulses generated in the refining zone appeared as vibrations in the refiner housing.

The differences shown by the vibration measurements conducted on various types of plates support the hypothesis that the plate geometry clearly makes different pulp flow patterns. The vibrations in the refiner were significantly different when other plates were used. This was especially clear for the vibrations generated in the fine bar zone. The main dominating frequency corresponding to the bar-crossing frequency in the fine bar zone was shifted towards the intermediate zone when the new plates with a taper break point closer to the inlet were used. In addition, the taper gradient on the new plates was smaller indicating that the narrower plate gap forced the main pressure pulses to occur earlier in the refining zone than was the case with the used plates.

The frequency analyses performed on data from the pressure sensors did not reveal any high peak frequencies that could be associated with the natural frequencies of the refiner. This means that there were not obtained any frequencies from the refining of pulp that could act as driving forces to set the refiner in resonance. This indicates that the pressure sensors were unaffected by the vibrations operating in resonance. While the pressure sensors were solely measuring the activities in the refining zone, the accelerometers measured both the process independent vibrations as well as vibrations generated in the refining zone. This makes the pressure readings as better indicators of the refining actions than the vibration measurements. However, since the pressure pulses seem to generate vibrations in the refiner housing, vibration measurements can provide some valuable information about the refining process.

8.6 Relationship between pressure and the pulp flow activity

Primary goals in studies like this are to arrange improvements in both the pulp quality and the energy efficiency. This can be achieved by improving the control of the refining operation, which will require better understanding of pulp flow behaviour and the refining action between the discs in the refiner. A key factor to gain fundamental knowledge and improve theoretical models of refiner behaviour is the use of suitable measurements, which measures the fundamental variables in the refining zone. Pressure measurements are important for the development of theoretical models that can be used in control strategies.

Theoretical judgements and model considerations are discussed in a minor extent in this thesis. This study has particularly focused on the signal analysis and the reliability of the pressure measurements. It has mainly been an experimental study, which means that assessments are made primarily regarding the recorded data and the related process observations. To summarize what the present pressure measurements have indicated about the pulp flow activity in the refining zone, the following interpretations are done:

- Measured pressure variations seem to have been dominated by fluctuations that were generated in particular parts of the refining zone. These fluctuations propagated as vibrations in the discs. It is not assumed that these vibrations generated large plate gap variations. However, these fluctuations were predominant compared with the local generated pressure pulses. Thus the pressure variations probably propagated through the steam and pulp pad as pressure waves.
- Since the local bar-to-bar passages were visible only to a minor extent, it is conceivable that the pulp pad on the stator side was affected less than the pulp closest to the rotor side by the local bars on the rotor disc. The tapered plate gap due to its width may have prevented disruption of the pulp pad on the stator side where the sensors were located. This assumption is probably close to the concept of gentle refining.
- Steam seems to have a repressive effect on the pressure measurements. This is assumed because there were observed different flow regimes when the refiner was operated under normal conditions compared with the operation during a start-up. Different frequency spectra indicated that the mechanical forces were predominant when the pulp was surrounded by a smaller amount of steam. It is conceivable that the steam and pulp interacts through a two-phase flow. Thus the steam may have a repressive effect on the interaction between the pulp pad and the bar patterns on the discs.
- The high-frequency band between 30-40 kHz as shown in data sets recorded during the initial chip feeding, has been assumed to be associated with the mechanical forces acting on the flocs of fibres. It is indicated that the sizes of the flocs of fibres or the velocities of the fibres moving along the bars have caused such observations.
- Sideband effects have been observed frequently. It is assumed that the pulp flow propagates radially outward in waves caused by low-frequency disturbances from the early stage of chip flow interaction with the refiner. Such disturbances may be associated with the feeding of the refiner, number of ribbons in the feeder and the number of bars in the breaker bar plates.
- There have also been shown that new and worn plates affect the pressure measurements different because of different pulp flow pattern. Refining using new plates indicated that the dominating pressure pulses appeared in the fine bar zone. When the measurements were performed during refining using worn plates, the main refining action appeared in an earlier section of the refining zone. This is agreeable with the corresponding changes in the process variables. The motor load was higher and the plate gap was smaller when the plates were worn. Thus the outward flowing pulp was resisted earlier in the refining zone, and subsequently the main refining action occurred earlier. It is indicated that the energy applied in the outer part of the refining zone was smaller as a consequence of this shift inwards.
- The Twin refiner has revealed that the chip distribution to the two refining zones affected the pressure measurements significantly, and that the pressure measurements were strongly correlated with the process variables such as motor load and acceleration (plate clearance). It is indicated that the influence was stronger in the intermediate zone than in the fine bar zone. This was observed when the plates were partly worn.

CHAPTER 9

PROPOSALS FOR FURTHER WORK

9.1 Introduction

The present study is primarily a matter of scientific interest. Investigations of such areas where prevailing knowledge is limited have led to repeated improvements. For the time being the utility value of this study is limited. The uncertainties related to the determination of the absolute pressure levels using the fibre-optic sensors, as well as the uncertainties regarding the reliability of the piezoresistive sensors have to be solved before further conclusions can be drawn. Another drawback from a practical point of view is the huge amount of data that are generated by such measurements. Improvements in the filtering of data, such that the necessary amount of data can be visualized and stored, are important to make high-speed measurements a practical and useful tool.

This investigation has clearly shown the potential possibilities in high-speed pressure measurements. Future investigations will show how valuable these results have been, and further research is desired. New investigations should be of interest for plate manufacturers and the designers of refiners. Plate geometry improvements as well as improved solutions for chip feeding may be the primary achievements from the use of high-speed pressure measurements inside the refiner. Additionally improvements in operating conditions and the possibilities for making more tailor-made pulp are possible outcome.

The thesis ends by giving a set of proposals for improvements of the prevailing measurement equipment and further interesting investigations.

9.2 Improved detection of the absolute pressure levels

Since the fibre-optic sensor system was primarily a differential rather than an absolute pressure measurement system, improved demodulation techniques are a prerequisite. The fibre-optic sensor manufacturers are working on this approach. The high-speed data recording is one limiting factor. Available demodulation techniques might partly solve the problem already today, but then two separate recording systems have to be used. A high-speed differential pressure reading system that permits fringe counting procedures might be used together with a low-speed data recording system that can read out the absolute pressure levels. However, there will still be uncertainty about which level the pressure is at between each sample being taken with the low-speed data acquisition system.

In addition to an improved demodulation scheme for detection of the absolute pressure levels, it is important to be sure that the average pressure is located close to the quadrature point of the sinusoidal transfer function curve. This ensures the highest sensitivity in the output signals from the interferometric sensor system. This can also be solved today using two separate detection systems. A so-called dual-wavelength sensor system that utilizes two laser-diodes, which have centre wavelengths separated by a given number of nanometers corresponding to a phase shift of $\phi/2$, can be used. This ensures that one of the interference signals backscattered from the Fabry-Perot cavity always is lying at the steepest part of the sinusoidal transfer function curve. Another possibility to avoid the uncertainty associated with the fringe counting is to use a sensor which is stiffer than those used in this study and thus has one sinusoidal period that covers a larger pressure range. However, such system will reduce the high resolution of the pressure measurements.

9.3 Measurements in other types of refiners

The high-speed pressure measurements can certainly be used to develop the theoretical framework of the refining action. However, new investigations should be performed to gain more general knowledge through measurements in different types of refiners. The lack of a consistent relationship between the pressure measurements and the process variables that is revealed in parts of this study may be associated with the complexity of the two refining zones of the Twin refiner. This could probably have been solved by simultaneously measuring the pressure in both refining zones, which would probably lead to some interesting correlations.

Measurements in pure single disc refiners as well as in both refining zones of a conical disc refiner would give additional information. The totally different refining frequencies that appear in double disc refiners compared to single disc refiners would be extremely interesting to observe through high-speed pressure measurements. However, the latter is extremely difficult because of the high frequency recordings so far have been dependent on transmission cables between the sensors and the data acquisition system. Some measurement systems that can handle data recordings in rotating equipment exist and can provide temperature measurements with a moderate sample rate. However, for the

fibre-optic sensor system based on high-frequency data transmission, such approach is even more difficult. Future needs and developments will show if this is possible.

9.4 Measure the effect of other plate geometries

It has been shown that the plate patterns in the refining zone as well as in the breaker bar section affect the pressure readings. Frequency analyses have revealed that periodic signal patterns exist. Several of these periodic signals have been related to the number of bars in different parts of the refiner plates. It is likely that the pulp flow between the discs is affected to a different extent depending on the plate geometries. High-speed measurements of the pressure may be a tool to determine this effect and hence optimize the plate pattern as well as the taper angles. Optimizing the plate patterns can give improved control of the defibration by for instance optimizing the bar-crossing frequencies and the location of the pressure peak.

9.5 Further investigations of pressure and vibrations

It would be interesting to further investigate the relationship between the external vibrations in the refiner housing and the internal pressure pulse variations in the refining zone. High-frequency vibration measurements seem to be a mirror image of the pressure pulse frequencies. However, the amplitude ratio between the pressure pulses and the vibration amplitudes are not yet thoroughly investigated. Further testing is required to determine the benefit of the postulated relationship between the pressure and vibration measurements. Such investigations might lead to information that gives the possibility to read the activity in the refining zone by simple accelerometers or strain gauge measurements from the outside of the refiner.

REFERENCES

Ainsworth, R.W., Miller, R.J., Moss, R.W. and Thorpe, S.J.: *"Unsteady pressure measurement."* Meas. Sci. Technol. 11, pp. 1055-1076, 2000.

Alahautala, T., Vattulainen, J. and Hernberg, R.: *"Quantitative visualisation of pulp refining in a production line refiner."* International Mechanical Pulping Conference, pp. 87-95, 1999.

Alahautala, T., Vattulainen, J. and Hernberg, R.: *"Visualisation of pulp refining in a rotating disk refiner."* XIV IMEKO World Congress, XA, pp. 60-64, 1997.

Alami, R., Boileau, I., Harris, G., Lachaume, J., Karnis, A., Miles, K.B. and Roche, A.: *"Impact of refining intensity on energy reduction in commercial refiners: Effect of primary-stage consistency."* Tappi J., 80 (1), pp. 185-193, 1997.

Alami, R., Boileau, I., Harris, G., Lachaume, J., Karnis, A., Miles, K.B. and Roche, A: *"Evaluation of the impact of refining intensity on energy reduction in commercial size refiners: The effect of primary stage consistency.*" International Mechanical Pulping Conference, pp. 203-211, 1995.

Allison, B.J., Isaksson, A.J. and Karlström, A.: *"Distributed parameter model of a TMP refiner."* Control Systems '96, pp. 113-116, 1996.

Allison, B.J., Isaksson, A.J. and Karlström, A.: *"Grey-Box identification of a TMP refiner."* International Mechanical Pulping Conference, pp. 119-124, 1995.

Allison, B.J., Ciarniello, J., Tessier, P. and Dumont, G.A.: *"Dual adaptive control of chip refiner motor load: industrial results."* Control Systems '94, pp. 289-297, 1994.

Alonso, M. and Finn, E.J.: *"Fundamental university physics. Mechanics and thermodynamics."* Vol. 1, 2nd edition, Addison-Wesley Publishing Company, 538 p., ISBN: 0-201-00161-6, 1980.

Alonso, M. and Finn, E.J.: *"Fundamental university physics. Fields and waves."* Vol. 2, 2nd edition, Addison-Wesley Publishing Company, 658 p., ISBN: 0-201-00162-4, 1983.

Andonovic, I. and Uttamchandani, D.: *"Principles of modern optical systems."* Artech House, 608 p., ISBN: 0-89006-351-6, 1989.

Asplund, A.: *"The origin and development of the Defibrator process."* Svensk Papperstidn., 56 (14), pp. 550-??, 1953.

Atack, D. and Stationwala, M.I.: *"Application of high-speed photography to chip refining."* 19th International Congress on High-Speed Photography and Photonics, pp. 237-245, 1990.

Atack, D., Stationwala, M.I., Huusari, E., Ahlqvist, P., Fontebasso, J. and Perkola, M.: *"High-speed photography of pulp flow patterns in a 5 MW pressurized refiner."* Pap. Puu, 71 (6), pp. 689-695, 1989.

Atack, D., Karnis, A. and Stationwala, M.I.: *"What happens in refining."* International Mechanical Pulping Conference, pp. 115-121, 1983.

Atack, D.: *"Fundamental differences in energy requirement between the mechanical pulping processes."* Svensk Papperstidn., 84 (14), pp. 22-26 , 1981.

Atack, D.: *"Towards a theory of refiner mechanical pulping."* Appita, 34 (3), pp. 223-227, 1980.

Atack, D. and Stationwala, M.I.: *"On the measurement of temperature and pressure in the refining zone of an open discharge refiner."* Transactions of the technical section, CPPA, 1 (3), pp. 71-76, 1975.

Atack, D. and May, W.D.: *"Mechanical reduction of chips by double-disk refining."* Pulp Pap. Mag. Can., 64 (C), pp. T75-T83, 1963.

Baker, C.F.: *"Critical review of refiner theory."* 3rd International Refining Conference, Pira, paper 7, 24 p., 1995.

Batchelor, W.J., Martinez, D.M., Kerekes, R.J. and Ouellet, D.: *"Forces on fibres in low-consistency refining: shear force."* J. Pulp Pap. Sci., 23 (1), pp. J40-J45, 1997.

Becker H., Höglund, H. and Tistad, G.: *"Frequency and temperature in chip refining."* Pap. Puu, 59 (3), pp. 123-130, 1977.

Belleville, C. and Duplain, G.: *"White-light interferometric multimode fiber-optic strain sensor."* Optics Letters, 18 (1), pp. 78-80, 1993.

Bentley, J.P.: *"Principles of measurement systems."* Longman Singapore Publishers Ltd., 3rd edition, 468 p., ISBN: 0-582-23779-3, 1995.

Bhatia, V., Murphy, K.A., Claus, R.O., Tran, T.A. and Greene, J.A.: *"Fiber optic white light interferometry for self-calibrated, absolute strain measurements."* Self-calibrated intelligent optical sensors and systems, SPIE, 2594 (1), pp. 168-177, 1996.

Björkqvist, T., Lautala, P., Saharinen, E., Paulapuro, H., Koskenhely, K. and Lönnberg, B.: "*Behavior of spruce sapwood in mechanical loading."* International Mechanical Pulping Conference, pp. 199-205, 1997.

Box, G.E.P. and Draper N.R.: *"Empirical model-building and response surfaces."* John Wiley & Sons, Inc., 527 p., ISBN: 0-471-81033-9, 1987.

Box, G.E.P., Hunter, W.G. and Hunter J.S.: *"Statistics for experimenters. An introduction to design, data analysis and model building."* John Wiley & Sons, Inc., 628 p., ISBN: 0-471-09315-7, 1978.

Braaten, K.R.: *The impact of site and wood properties on thermo mechanical pulp. Classification of wood for more uniform TMP-quality."* Doctoral thesis, Department of Forest Sciences, Agricultural University of Norway, 27, 137 p., ISBN: 82-575-0297-9, 1996.

Breck, D.H., May, W.D. and Tremblay, M.N.: *"Thermomechanical pulping. A preliminary optimization."* Transactions of the technical section, CPPA, 1 (3), pp. 89-95, 1975.

Caucal G., Chaussy, D. and Renaud, M.: *"Etude Physique et Hydraulique du Raffinage."* Rev. ATIP 45 (5), pp.187-199, 1991.

Caucal G., Chaussy, D. and Renaud, M.: *"Etude Physique et Hydraulique du Raffinage II."* Rev. ATIP, 46 (5), pp.130-138, 1992a.

Caucal G., Chaussy, D. and Renaud, M.: *"Etude Physique et Hydraulique du Raffinage III."* Rev. ATIP, 46 (7), pp.194-199, 1992b.

Choquet, P., Juneau, F. and Dadoun, F.: *"New generation of fiber-optic sensors for dam monitoring."* International Conference on Dam Safety and Monitoring, 10 p., 1999.

Corson, S.R: *"The mechanics of making better pulp with less energy."* Pulp Pap. Int., 39 (5), pp. 61-63, 1997.

Corson, S.R., Wakelin, R.F. and Lloyd, M.D.: *"The furnish development strategies. Part II: Sheet properties."* Pulp Pap. Can., 98 (1), pp. 41-44, 1997.

Corson, S.R., Wakelin, R.F. and Lloyd, M.D.: *"TMP furnish development strategies. Part I: fractionation and long fibre refining."* Pulp Pap. Can., 97 (12), pp. 129-132, 1996.

Corson, S.R. and Ekstam E.I.: *"Intensive refining of radiata pine fibre."* Pap. Puu, 76 (5), pp. 334-339, 1995.

Corson, S.R: *"Aspects of mechanical pulp fibre separation and development in a disc refiner."* International Mechanical Pulping Conference, pp. 1-13, 1989.

Culshaw, B. and Dakin, J.: *"Optical fiber sensors. Systems and applications."* Artech House, 2, ISBN: 0-89006-376-1, 1989.

Dahlsveen, J.: *"Rapid phase transitions – a study of mixing and fragmentation."* Doctoral thesis, Department of Mechanics, Thermo and Fluid Dynamics, Norwegian University of Science and Technology, Trondheim, 16, 182 p., ISBN: 82-471-0382-6, 1999.

Dana, H.R., May, W.D., Miles, K.B. and Newman, B.G.: "*A study of steam flow and self-pressurization in chip refiners."* Transaction of the technical section, CPPA, 1 (3), pp. 82-88, 1975.

Di Ruscio, D. and Holmberg, A.: *"A dynamic model for the pressure and the flow of steam in a TMP Refiner."* Control Systems '96, pp. 107-112, 1996.

Di Ruscio, D.: *"Topics in model based control with application to the thermo mechanical pulping process."* Doctoral thesis, Department of Engineering Cybernetics, The Norwegian Institute of Technology, Trondheim, 46-W, 268 p., ISBN: 82-7119-513-1, 1993.

Doebelin, E.O.: *"Measurement systems. Application and design."* 4th edition, McGraw-Hill Publishing Company, 947 p., ISBN: 0-07-100697-4, 1990.

Dumont, G.A. and Åström, K.J.: *"Wood chip refiner control."* IEEE control system mag., 8 (4), pp. 38-43, 1988.

Dumont, G.A.: *"Self-tuning control of a chip refiner motor load."* Automatica, 18 (3), pp. 307-314, 1982.

Ebeling, K.: *"A critical review of current theories for the refining of chemical pulps."* International Symposium on Fundamental Concepts of Refining, Institute of Paper Chemistry, Appelton, WI, pp. 1-29, 1980.

Elgamel, H.E.: *"Closed-form expressions for the relationships between stress, diaphragm deflection, and resistance change with pressure in silicon piezoresistive pressure sensors."* Sensors and Actuators, A 50, pp. 17-22, 1995.

Engstrand, P., Karlström, A. and Nilsson, L.: *"The impact of chemical addition on refining parameters."* International Mechanical Pulping Conference, pp. 281-286, 1995.

Eriksen, O.: *"High-speed measurements of pressure and temperature in the refining zone of a high-consistency refiner."* 88th Annual Meeting, PAPTAC, pp. C135-C142, 2002.

Eriksen, O.: *"LED-deteksjon av resonansfrekvens til optisk eksitert silisiumresonator."* Cand.scient. (MSc) thesis, Department of Physics, University of Trondheim, Norway, 156 p., 1995.

Fairchild, V.: *"Zooming in the frequency domain."* Electronic Industry, London, UK, (12), 3 p., 1982.

Fan, X., Ouellet, D. and Jeffrey, D.J.: *"A time-dependent model for a single-disc refiner: local density fluctuations."* J. Pulp Pap. Sci., 23 (1), pp. J1-J5, 1997.

Fan, X.: *"Modelling the motion of pulp inside wood-chip disc refiners."* Doctoral thesis, University of Western Ontario, London, Canada, 210 p., ISBN: 0-315-99253-0, 1995.

Fan, X., Jeffrey, D.J. and Ouellet, D.: *"A stochastic model for the residence time of pulp in a single-disc chip refiner."* J. Pulp Pap. Sci., 20 (11), pp. J343-J349, 1994.

Fan, X.: *"Material flow in a wood-chip refiner."* M. Eng. thesis, McGill University, Montreal, Canada, 1987.

Forgacs, O.L.: *"The characterization of mechanical pulps."* Pulp Pap. Mag. Can., 64 (C), pp. T89-T118, 1963.

Fox, T.S., Brodkey, R.S. and Nissan, A.H.: *"Inside a disk refiner."* Tappi, 65 (7), pp. 80-83, 1982.

Fox, T.S., Brodkey, R.S. and Nissan, A.H.: *"High-speed photography of stock transport in a disk refiner."* Tappi, 62 (3), pp. 55-58, 1979.

Frazier, W.C.: *"Applying hydrodynamic bearing theory to the refiner plate-pulp fiber interaction."* International Mechanical Pulping Conference, pp. 55-59, 1985.

Gavelin, G., Borg, O.F. and Sundstedt, K.: *"Mekaniska massor - framställning och användning."* Skogsindustrins Utbildning i Markaryd AB, Sweden, 220 p., ISBN: 91-7322-192-9, 1996.

Gerlach, G., Sager, K. and Nakladal, A.: *"How accurate are measurements with piezoresistive sensors?"* Technisches Messen, 63 (11), pp. 403-412, 1996.

Giertz, H.W.: *"Ännu ett sätt att se på malningsprocessen."*, Norsk Skogindustri, 18 (7), pp. 239-248, 1964.

Goncharov, V.N. and Zyulkov, B.V.: *"Compression characteristics of pulp under kinematic conditions."* Mashiny Oborud. Tsellyul.-Bumazh. Proizv., 2, pp. 62-66, 1974.

Goncharov, V.N.: *"Force factors in a disk refiner and their effect on the beating process."* Bumazh. Prom., 5, pp.12-14, 1971.

Gradin, P.A., Johansson, O., Berg, J-E. and Nyström, S.: *"Measurement of the power distribution in a single-disc refiner."* J. Pulp Pap. Sci., 25 (11), pp. J384-J387, 1999.

Gullichsen, J.: *"Low frequency refining - a new way to make mechanical pulp."* International Mechanical Pulping Conference, pp. 320-342, 1989.

Hattula, T. and Mannström, B.: *"Wood structure as a limiting factor in mechanical pulping."* International Mechanical Pulping Conference, I-1, 1981.

Heikkurinen, A., Vaarasalo, J. and Karnis, A.: *"Effect of initial defiberization on the properties of refiner mechanical pulp."* J. Pulp Pap. Sci., 19 (3), pp. J119-J124, 1993.

Hietanen, S.: *"Effect of control variables and length of refining zone on the refining results with a new pilot refiner."* Pap. Puu, 73 (1), pp. 52-61, 1991.

Hietanen, S. and Ebeling, K.: *"A new hypothesis for the mechanics of refining."* Pap. Puu, 72 (2), pp. 172-179, 1990.

Holmberg, A.: Internal report, Norske Skog, Skogn, Norway, 6 p., 1992.

Härkönen, E. and Tienvieri, T.: *"Energy savings in TMP pulping."* International Mechanical Pulping Conference, pp. 547-555, 2001.

Härkönen, E., Huusari, E. and Ravila P.: *"Residence time of fibre in a single disc refiner."* Pulp Pap. Can., 101 (11), pp. T330-335, 2000.

Härkönen, E., Routtu, S., Routtu, A. and Johansson, O.: *"A theoretical model for a TMP-refiner."* International Mechanical Pulping Conference, pp. 95-102, 1997.

Höglund, H., Back R., Falk, B. and Jackson, M.: *" Thermopulp - a new energy-efficient mechanical pulping process."* Pulp Pap. Can., 98 (6), pp. 82-89, 1997.

Höglund, H., Sohlin, U. and Tistad, G.: *"Physical properties of wood in relation to chip refining."* Tappi, 59 (6), pp. 144-147, 1976.

Höglund, H. and Tistad, G.: *"Energy uptake by wood in the mechanical pulping process."* International Mechanical Pulping Conference, pp. 3.1-3.23, 1973.

Isaksson, A.J., Horch, A., Karlström, A., Allison, B.J. and Nilsson, L.: *"Modelling of mechanical thrust in TMP refiners."* International Mechanical Pulping Conference, pp. 87-93, 1997.

Johansson, O., Hogan, D., Blankenship, D., Snow, E., More, W., Qualls, R., Pugh, K. and Wanderer, M.: *"Improved process optimisation through adjustable refiner plates."* International Mechanical Pulping Conference, pp. 579-589, 2001.

Johnsen, P.O., Skinnarland, I., Helle, T. and Houen, P.J.: *Distribution of lignin and other material on particle surfaces in mechanical pulps."* International Mechanical Pulping Conference, pp. 93-107, 1995.

Kappel, J.: *"Mechanical pulps: from wood to bleached pulp."* TAPPI Press, Atlanta, GA, USA, 396 p., ISBN: 0-89-852-354-0, 1999.

Karnis, A.: *"The mechanism of fibre development in mechanical pulping."* J. Pulp Pap. Sci., 20 (10), pp. J280-J287, 1994.

Karnis, A., Atack, D. and Stationwala, M.I.: *"What happens in refining (Part II)."* International Mechanical Pulping Conference, pp. 35-45, 1985.

Kerekes, R.J.: *"Characterization of pulp refiners by a C-factor."* N. Pulp Pap. J., 5 (1), pp. 3-8, 1990.

Koran, Z.: *"Energy consumption in mechanical fibre separation as a function of temperature."* Transactions of the technical section, CPPA, 7 (2), pp. 40-44, 1981.

Kure, K.A.: *"On the relationship between process input variables and fibre characteristics in termomechanical pulping."* Doctoral thesis, Department of Chemical Engineering, Norwegian University of Science and Technology, 45, 123 p., ISBN: 82-471-0412-1, 1999.

Laine, J.E., MacLeod, J.M., Bolker, H.I. and Goring, D.A.I.: *"Applications of ultrasound in pulp and paper technology."* Pap. Puu, 59 (4a), pp. 235-247, 1977.

Leask, R.A.: *"The theory of chip refining – a status report."* Svensk Papperstidn., 84 (14), pp. 28-35 , 1981.

Leider, P.J. and Nissan, A.H.: *"Understanding the disk refiner. The mechanical treatment of the fibers."* Tappi, 60 (10), pp. 85-89, 1977.

Leider, P.J. and Rihs, J.: *"Understanding the disk refiner. The hydraulic behavior."* Tappi, 60 (9), pp. 98-102, 1977.

Lidén, J.: *"Models for control of TMP quality for a local primary refiner system."* FSCN-report R-0221 (abstract), Mid-Sweden University, 2002.

Luhde, V.F.: *"The influence of conventional and disk refined groundwood processes on wood defibration."* Das Papier, 16 (11), pp. 655-663, 1962.

Lunan, W.E., Miles, K.B. and May, W.D.: *"The effect of differential pressure on energy consumption in thermomechanical pulping."* International Mechanical Pulping Conference, pp. 241-247, 1983.

MacDonald, J.E. and Guthrie Jr., J.J.: *"Chip mass flow meter."* International Mechanical Pulping Conference, pp.187-192, 1987.

Martinez, D.M., Batchelor, W.J., Kerekes, R.J. and Ouellet, D.: *"Forces on fibres in low-consistency refining: normal force."* J. Pulp Pap. Sci., 23 (1), pp. J11-J17, 1997.

Martinez, D.M. and Kerekes, R.J.: *"Forces on fibres in low-consistency refining."* TAPPI, 77 (12), pp. 119-123, 1994.

May, W.D.: *"The Miles and May model – a presentation."* The Marcus Wallenberg Foundation Symposia, Stockholm, Sweden, pp. 1-14, 1998.

May, W.D., McRae, M.R., Miles, K.B. and Lunan, W.E.: *"An approach to the measurement of pulp residence time in a chip refiner."* J. Pulp Pap. Sci., 14 (3), pp. J47-J53, 1988.

May, W.D., Miles, K.B. and Jefferys, R.C.: *"The measurement of temperature in a chip refiner."* International Mechanical Pulping Conference, pp.13.1-13.31, 1973.

May, W.D.: *"The measurement of disc misalignment in refiners."* Pulp Pap. Mag. Can., 71 (15), pp. T319-T328, 1970.

Miles, K.B.: *"The essence of high consistency refining."* The Marcus Wallenberg Foundation Symposia, Stockholm, Sweden, pp. 20-30, 1998.

Miles, K.B. and Karnis, A.: *"Wood characteristics and energy consumption in refiner pulps."* J. Pulp Pap. Sci., 21 (11), pp. J383-J389, 1995.

Miles, K.B. and May, W.D.: *"Predicting the performance of a chip refiner: A constitutive approach."* International Mechanical Pulping Conference, pp.295-301, 1991.

Miles, K.B.: *"A simplified method for calculating the residence time and refining intensity in a chip refiner."* Pap. Puu, 73 (9), pp. 852-857, 1991.

Miles, K.B., May, W.D. and Karnis, A.: *"Refining intensity, energy consumption, and pulp quality in two-stage chip refining."* Tappi J., 86 (3), pp. 221-230, 1991.

Miles, K.B. and May, W.D.: *"The flow of pulp in chip refiners."* J. Pulp Pap. Sci., 16 (2), pp. J63-J71, 1990.

Miles, K.B., Dana, H.R. and May, W.D.: *"The flow of steam in chip refiners."* International Symposium on Fundamental Concepts of Refining, Institute of Paper Chemistry, Appelton, WI, pp. 30-42, 1980.

Miles, K.B. and May, W.D.: *"Dynamic disc misalignment in a chip refiner."* International Mechanical Pulping Conference, pp.29.1-29.24, 1977.

Mohlin, U.B.: *"Fibre development during mechanical pulp refining."* J. Pulp Pap. Sci., 23 (1), pp. J28-J33, 1997.

Morse, P.M. and Ingard, K.U.: *"Theoretical acoustics."* Princeton University Press, Princeton, N.J., USA, 927 p., ISBN: 0-691-08425-4, 1986.

Mosbye, K., Kure, K.A., Fuglem, G. and Johansson, O.: *"Use of refining zone temperature measurements for refiner control."* International Mechanical Pulping Conference, pp. 481-488, 2001.

Meller, S.A.: *"Extrinsic Fabry-Perot Interferometer system using wavelength modulated source."* MSc. Elect. Eng. thesis, Virginia Polytechnic Institute and State University, Blacksburg, VA., USA, 52 p., 1996.

Murphy, K.A.: *"Practical applications of Extrinsic Fabry Perot Interferometric (EFPI) sensors."* Fiber Optic and Laser Sensors XIV, SPIE, 2839 (10), pp. 82-92, 1996.

Murphy, K.A., Gunther, M.F., May, R.G., Claus, R.O., Tran, T.A., Greene, J.A. and Duncan, P.G.: *"EFPI sensor manufacturing and applications."* Smart Structures and Materials, SPIE, 2721 (5), pp. 476-482, 1996.

Murton, K., Duffy, G. and Corson S.R.: *"Pulp residence time influence on refining intensity and pulp quality."* 56th Appita Annual Conference, pp. 185-193, 2002.

Newman, B.G., Stationwala, M.I. and Atack, D.: *"Analysis of steam flow in disc refining."* International Mechanical Pulping Conference, pp.60-67, 1985.

Nakladal, A. and Sager, K.: *"Influence of humidity and moisture on the stability of piezoresistive sensors."* Technisches Messen, 60 (10), pp. 338-388, 1993.

Nordman, L., Levlin, J-E., Makkonen, T. and Jokisalo, H.: *"Conditions in an LC-refiner as observed by physical measurements."* Pap. Puu, 63 (4), pp. 169-180, 1981.

Ohls, P-E. and Syrjänen, A.: *"The importance of disc parallelism in single rotating disc refiners."* Tappi, 59 (1), pp. 100-103, 1976.

Ouellet, D., Bennington, C.P.J. and Potkins, D.: *"Wood comminution and material flow in a laboratory chip refiner."* 81st Annual Meeting, CPPA, pp. B187-B194, 1995a.

Ouellet, D., Bennington, C.P.J., Senger, J.J., Borisoff, J.F. and Matiskainen, J.M.: *"Measurement of pulp residence time in a high consistency refiner."* International Mechanical Pulping Conference, pp.171-176, 1995b.

Ouellet, D. and Weiss, R.: *"Modeling of the nonlinear, axial vibrations of the rotor assembly in a disc refiner."* J. Pulp Pap. Sci., 20 (9), pp. J259-J265, 1994.

Page, D.H.: *"The beating of chemical pulps – the action and the effects."* 9th Fundamental Research Symposium, "Fundamentals of Papermaking", pp. 1-38, 1989.

Pearson, A.J.: *"A unified theory of refining."* Pulp and Paper Technology Series, TAPPI/CPPA, 6, pp. 187-219, ISBN: 0-919893-79-1, 1990.

Petrusewicz, S.A. and Longmore, D.K.: *"Noise and vibration control for industrialists."* Scientific Books Ltd., London, UK, 284 p., ISBN: 0-236-17704-4, 1974.

Pettersen, G.W. and Gunstrøm, A.: *"Maleorganer og støy."* SCAN report, 235, PFI, Oslo, Norway, 57 p., 1980.

Reme, P.A.: *"Some effects of wood characteristics and the pulping process on mechanical pulp fibres."* Doctoral thesis, Department of Chemical Engineering, Norwegian University of Science and Technology, 21, 120 p., ISBN: 82-7984-042-7, 2000.

Reme, P.A., Helle, T. and Johnsen, P.O.: *"Fibre characteristics of various mechanical pulp grades."* International Mechanical Pulping Conference, pp. 297-307, 1997.

Rydholm, S.A.: *"Pulping processes."* Interscience Publishers, John Wiley & Sons, Inc., New York, USA, 1269 p., ISBN: 0-471-74793-9, 1965.

Sabourin, M., Vaughn, J., Frith, M., Lauritzen, J., Wiseman, N. and Fraser, T.: *"Characterization of paper properties from spruce and pine thermomechanical pulps – effect of refining intensity."* 88th Annual Meeting, PAPTAC, pp. C125-C134, 2002.

Sabourin, M., Wiseman, N. and Vaughn, J.: *"Refining theory considerations for assessing pulp properties in the commercial manufacture of TMP."* 55th Appita Annual Conference, pp. 195-204, 2001.

Sabourin, M., Xu, E., Cort, B., Boileau, I. and Waller, A.: *"Optimizing residence time, temperature and speed to improve TMP pulp properties and reduce energy."* Pulp Pap. Can., 98 (4), pp. T111-118, 1997.

Sager, K., Gerlach, G., Nakladal, A. and Schroth, A.: *"Ambient humidity and moisture – a decisive failure source in piezoresistive sensors."* Sensors and Actuators A 46-47, pp. 171-175, 1995.

Salmén, N.L., Dumail, J.F. and Uhmeier, A.: *"Compression behaviour of wood in relation to mechanical pulping."* International Mechanical Pulping Conference, pp. 207-211, 1997.

Salmén, N.L., Fellers, C. and Tigerström, A.: *"The effect of loading mode on the energy consumption during mechanical treatment of wood."* International Mechanical Pulping Conference, pp. 109-114, 1983.

Salmén, N.L. and Fellers, C.: *"The effect of loading mode on the energy consumption during mechanical treatment of wood."* Transactions of the technical section, CPPA, 8 (4), pp. TR93-TR99, 1982.

Senger J.J. and Ouellet, D.: *"Factors affecting the shear forces in high-consistency refining."* J. Pulp Pap. Sci., 28 (11), pp. 364-369, 2002.

Senger J.J. and Ouellet, D.: *"Factors affecting the shear forces in high-consistency refining."* International Mechanical Pulping Conference, pp. 531-545, 2001.

Senger J.J., Ouellet, D. and Bennington, C.P.J.: *"Effects of pulp furnish and refiner speed on residence time in a high-consistency refiner."* Tappi J., 81 (4), pp. 152-158, 1998.

Shah, S.J.: *"Field wiring and noise considerations for analog signals."* Application Note 025, National Instruments Corp., 21 p., 2000.

Singh, R.P. and Shukla, A.: *"A critical evaluation of the performance of optical fiber sensors for monitoring dynamic strains."* Journal of Testing and Evaluation, JTEVA, 24 (5), pp. 295-301, 1996.

Smith, S. W.: *"The scientist and engineer's guide to digital signal processing."* 2nd Edition, California Technical Publishing, San Diego, CA, USA, 643 p., ISBN: 0-9660176-6-8, 1999.

Stationwala, M.I., Miles, K.B. and Karnis, A.: *"Effect of feed rate on refining."* 80th Annual Meeting, CPPA, pp. A109-A113, 1994.

Stationwala, M.I., Miles, K.B. and Karnis, A.: *"The effect of first-stage refining conditions on pulp properties and energy consumption."* J. Pulp Pap. Sci., 19 (1), pp. J12-J18, 1993.

Stationwala, M.I., Atack, D. and Karnis, A.: *"Distribution and motion of pulp fibres on refiner bar surface."* J. Pulp Pap. Sci., 18 (4), pp. J131-J137, 1992.

Stationwala, M.I., Atack, D., Wood, J.R., Wild, D.J. and Karnis, A.: *"The effect of control variables on refining zone conditions and pulp properties."* Pap. Puu, 73 (1), pp. 62-69, 1991.

Stationwala, M.I. and Atack, D.: *"On the measurement of plate separation in a double-rotating disc refiner and analysis of its variation."* Pap. Puu, 62 (1), pp. 4-12, 1980.

Stationwala, M.I., Atack, D., Wood, J.R., Wild, D.J. and Karnis, A.: *"The effect of control variables on refining zone conditions and pulp properties."* International Mechanical Pulping Conference, pp. 93-109, 1979.

Stevens, W.V.: *"Pulp and Paper Manufacture. Stock preparation, Ch. X: Refining."* 3rd Edition, TAPPI/CPPA, Atlanta, GA, USA, Vol. 6, pp. 187-219, ISBN: 0-919893-04-x, (1983-), 1992.

Strand, B.C. and Mokvist, A.: *"Control and optimization of conical disc refiners."* International Mechanical Pulping Conference, pp.11-18, 1987.

Strand, B.C. and Hartler, N.: *"Modelling and optimization of full scale chip refining."* International Mechanical Pulping Conference, pp.46-54, 1985.

Sundholm, J.: *"Mechanical pulping."* Papermaking Science and Technology (5), Finnish Paper Engineers' Association and TAPPI, Fapet Oy, Helsinki, Finland, 427 p., ISBN: 952-5216-05-5, 1999.
Chapter 4, authors: L. Salmén, M. Lucander, E. Härkönen and J. Sundholm.
Chapter 7, authors: T. Tienvieri, E. Huusari, J. Sundholm, P. Vourio, J. Kortelainen, H. Nystedt and A. Artamo.

Sundholm, J., Heikkurinen, A. and Mannström, B.: *"The role of rate of rotation and frequency in refiner mechanical pulping."* International Mechanical Pulping Conference, pp. 45-51, 1987.

Sutinen, R. and Joensuu, I.: *" Experiences of TMP refiner control based on an in-line consistency measurement."* 50th Appita Annual Conference, pp. 547-552, 1996.

Thiruvengadaswamy, R. and Ouellet, D.: *"On the generation of structural damage in wood by cyclic compressive loading."* International Mechanical Pulping Conference, pp. 183-197, 1997.

Tyrväinen, J.: *"Newsgrade TMP from three different Norway Spruce (Picea Abies) wood assortments in mill-scale."* Pulp Pap. Can., 98 (10), pp. T376-T385, 1997.

Tyrväinen, J.: *"Influence of seasonal wood variation on TMP properties, bleach consumption and newsprint runnability."* International Mechanical Pulping Conference, pp. 213-225, 1997.

Tyrväinen, J.: *"Wood and fiber properties of Norway Spruce and its suitability for thermomechanical pulping."* Society of Forest Science, Finnish Forest Research Institute, Helsinki, Finland, 155 p., ISBN: 951-40-1479-0, 1995a.

Tyrväinen, J.: *"The influence of wood properties on the quality of TMP made from Norway Spruce (Picea abies) - wood from old-growth forests, first-thinnings, and sawmill chips."* International Mechanical Pulping Conference, pp. 23-34, 1995b.

Wei, W.W.S.: *"Time series analysis. Univariate and multivariate methods."* Addison-Wesley Publishing Company, 478 p., ISBN: 0-201-15911-2, 1994.

Welch, L.V.S.: *"Low consistency refining of mechanical pulps."* Doctoral thesis, Department of Chemical Engineering, The University of British Columbia, 131 p., 1999.

Wowk, V.: *"Machinery vibration: measurement and analysis."* McGraw-Hill Inc., New York, USA, 325 p., ISBN: 0-07-071936-5, 1991.

Wultsch, F. and Flucher, W.: *"The Escher-Wyss small refiner as a standard test apparatus for modern stock preparation plants."* Das Papier, 12 (13/14), pp. 334-342, 1958.

APPENDIX

A

CALIBRATION TESTS PIEZORESISTIVE SENSORS MILL REFINER

A.1 Water and dry heat chamber tests

Two tests were performed to check the temperature response from the transducers both under wet and dry conditions. Two transducers were attached on top of a water boiler containing some 1.5 litres of water. The starting temperature was 21.5∀C. The CAN-A data acquisition unit recorded the temperature responses and the pressure signals during the heating. A sample rate of 50 Samples/s was used. Another temperature response test was performed in a dry heat chamber (Termax), while the temperature was raised from 100∀C to approximately 170∀C. These data were recorded with a sample rate of 10 Sample/s. A calibrated temperature sensor, Digitherm Universal mkIII from Kone-May Instrumentation, Inc., was used to supervise the temperature development.

The results from these tests are shown in Tables A1 and A2. Figures A1 and A2 show the response from one transducer in each test respectively. The transducers are labelled sensor A and sensor B. None of these were used in the first mill-scale experiment.

Table A1: Water boiling test.

Temperature [∀C]	**Standard deviation [∀C]**	
	Sensor A	**Sensor B**
21.5	∂ 0.30	∂ 0.17
100	∂ 0.51	∂ 0.56
Measured sensitivity [mV/∀C] Original sensitivity [mV/∀C]	4.222 4.024	4.063 3.613
Pressure [bar]	0 ∂ 0.04	0 ∂ 0.11

URN:NBN:no-6437

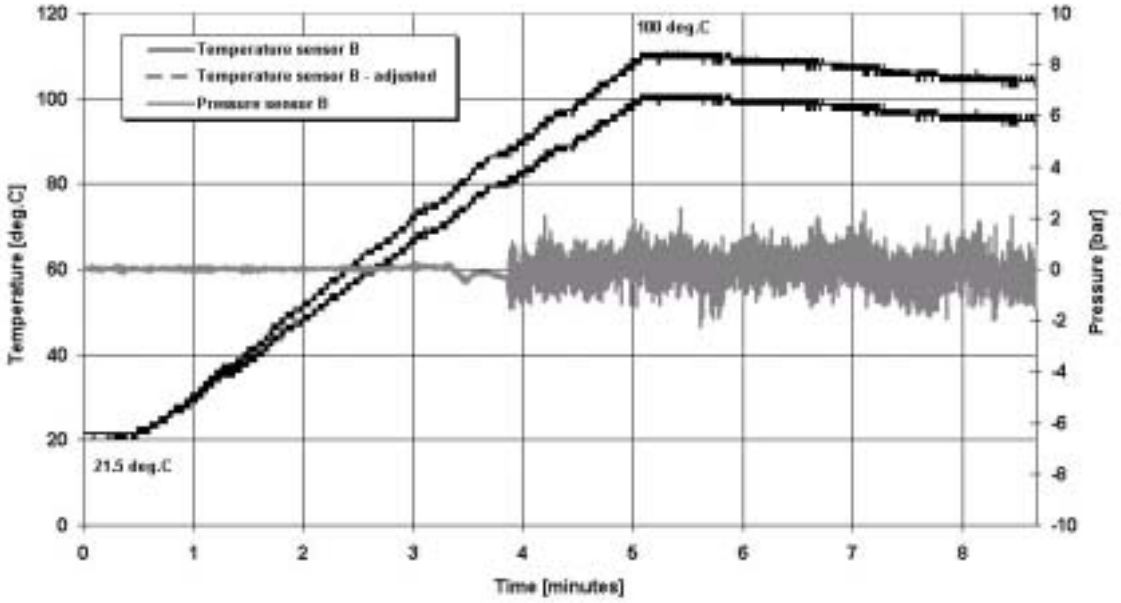

Figure A1: Temperature and pressure data recorded by sensor B are shown. It was captured when a calibration test in a water boiler was performed. Original and adjusted temperature sensitivity data were used to fit each of the curves.

Table A2: Dry heat chamber test.

Temperature [∀C]	**Standard deviation [∀C]**	
	Sensor A	**Sensor B**
100.9	∂ 0.56	∂ 0.62
124.4	∂ 0.48	∂ 0.52
149.2	∂ 0.80	∂ 0.50
158.3	∂ 0.55	∂ 0.26
165.0	∂ 0.54	∂ 0.74
Measured sensitivity [mV/∀C] Original sensitivity [mV/∀C]	4.393 4.024	3.157 3.613
Pressure [bar] (all data) Pressure [bar] (after stabilizing)	14.1 ∂ 10.2 0 ∂ 0.04	0 ∂ 0.52

URN:NBN:no-6437

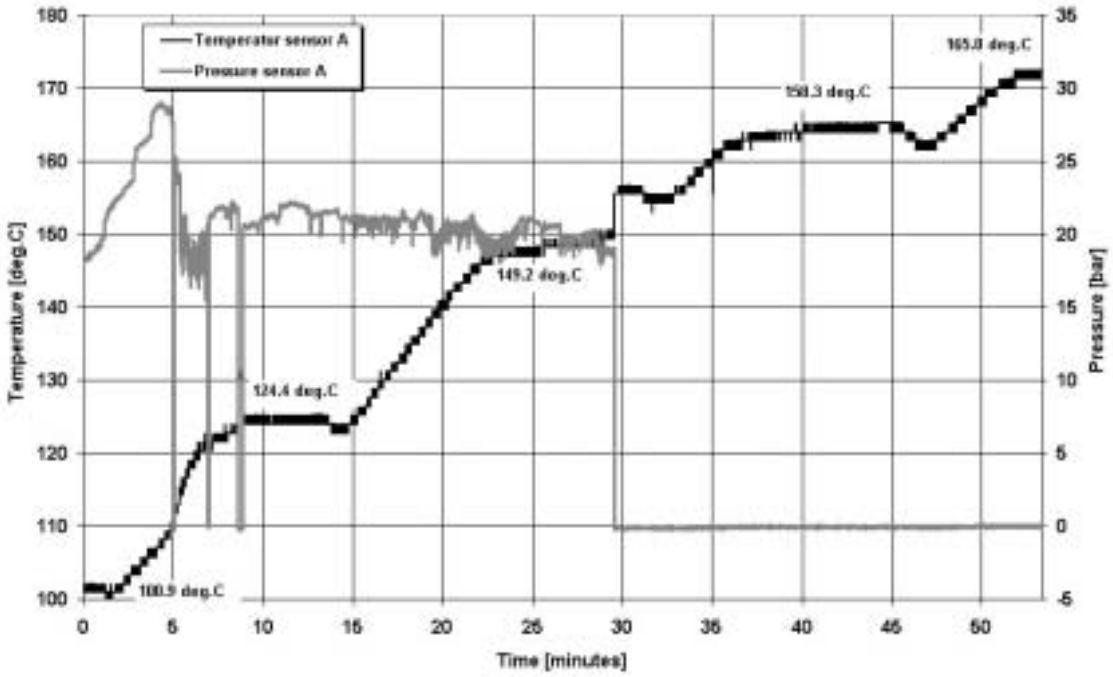

Figure A2: Temperature and pressure data recorded by sensor A are shown. It was captured when a calibration test in a dry heat chamber was performed. Original sensitivity data were used to fit the temperature curve.

The measured temperature signals gave expected responses of the two different heating processes. However, the results deviated somewhat from the original sensitivity data as shown in Tables A1 and A2. The increasing variation of the pressure output signal shown in Figure A1 was not expected. Even more alarming was the pressure output signal shown in Figure A2. Here, the output signal was totally outside the expected range in the first half of the recorded time series. The other transducer, sensor B, had a large standard deviation value, but the average value did not deviate from the expected zero bar gauge pressure. It is reasonable to believe that the water and steam caused the increased degree of variation and the out-of-range signal pattern. The heating and water evaporation in the dry heat chamber, which was performed after the boiling water test, had probably restored the transducer's operational behaviour as shown in the last part of Figure A2. In addition, it should be mentioned that both transducers broke down during the subsequent calibration test, probably because of the exposure to the water and steam in the boiling water test.

A.2 Pressure and temperature chamber test

A calibration test of the five original Kulite transducers was undertaken in a pressure and temperature chamber at the SINTEF Petroleum Research Institute in Trondheim. The calibration set-up consisted of a heating chamber and a hydraulic system as shown in Figure A3. Each transducer was connected to the hydraulic system by a conical holding screw. A Teflon ferrule was laid between the transducer and the holding screw.

The pressure was raised stepwise between approximately 7 and 32 bar. The temperature in the chamber was raised to approximately 180∀C. The CAN-A data acquisition unit with a sample rate of 10 Samples/s was used to record the response signals.

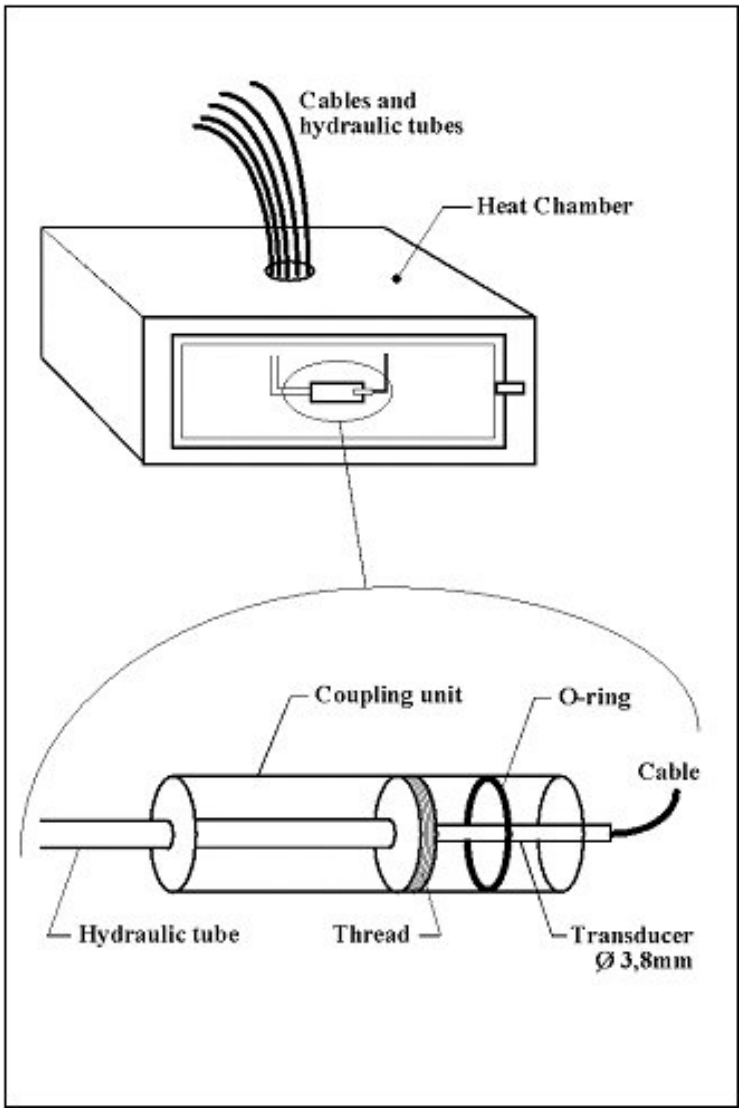

Figure A3: The calibration test set-up in a pressure and temperature chamber consisted of a heating chamber where the hydraulic pressure system and the connected transducers were inherent parts.

The results from the test performed in the pressure and temperature chamber are shown in Table A3 and in Figure A4. Only the transducers labelled sensors Nos. 1 and 2 showed the expected development during this calibration test. The three other broke down. A possible cause for this break down is probably due to the water exposures in earlier laboratory tests.

Table A3: Dry heat chamber test.

Pressure [bar]	Pressure [bar]	
	Sensor No. 1	Sensor No. 2
6.87	6.87 ∂ 0.03	6.87 ∂ 0.02
11.78	11.82 ∂ 0.04	11.78 ∂ 0.03
16.69	16.73 ∂ 0.05	16.66 ∂ 0.04
Original sensitivity [mV/bar]	2.456	2.411
Temperature [∀C] 80	79.7 ∂ 0.6	79.4 ∂ 0.7

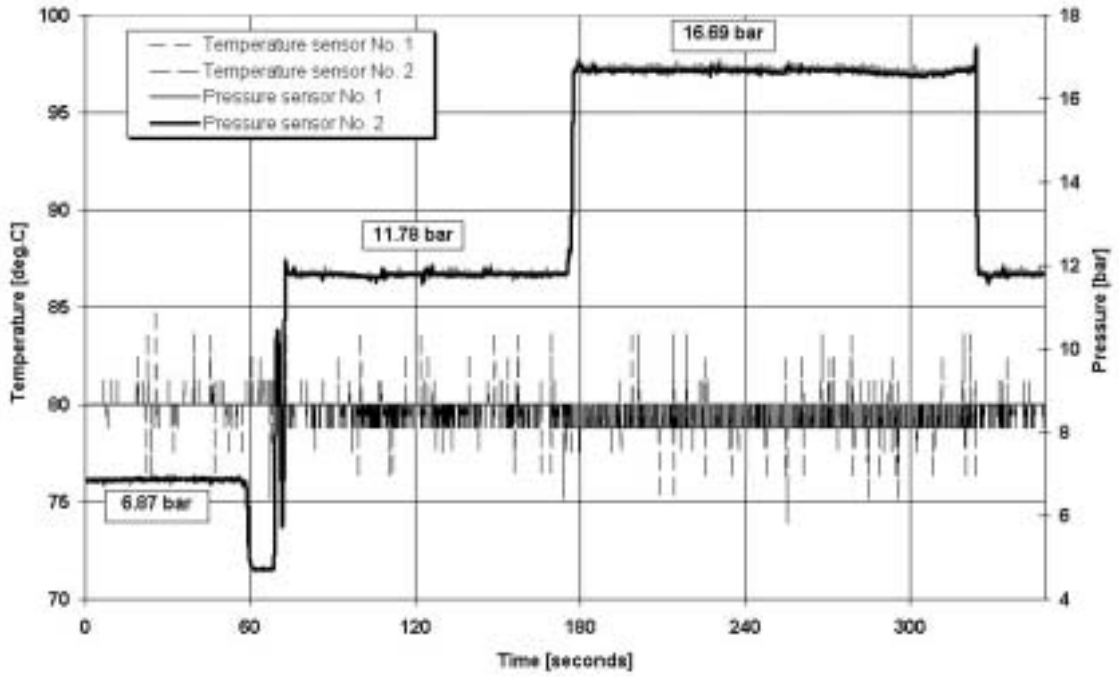

Figure A4: The responses of the transducers, sensors Nos. 1 and 2, during one period of the calibration test in the combined pressure and temperature chamber.

A.3 Dynamic-response test

The dynamic-response test was made in a laboratory test rig as shown in Figure A5. This is based on a test rig proposed by Dahlsveen (1999). The test rig used in the present study consisted of a small chest, 180 litres, filled with water, and a pipe, and a weight for generating pressure waves. The transducers were installed in the refiner plate, which was laid on the bottom of the filled water chest. The pipe with a diameter of 0.1 metre, sufficiently large to cover the area where the transducers were mounted, was clamped over this area on the test plate. The height of the pipe was approximately

3 metres. A weight of two-three kilograms was dropped at different heights. When the weight stroke the bottom surface of a floating bucket at the water surface a pressure wave was generated. The transducers and the measurement system measured this wave. The original high-speed data acquisition card should be used in this test, but failed. The CAN-A data acquisition unit recorded the responses at a sample rate of 500 Hz, which was a too small sampling rate to determine the frequency response of the measurement system. However, the results from this test during five drops of the weight, performed before 100 seconds had passed, are shown in Figures A6 to A8.

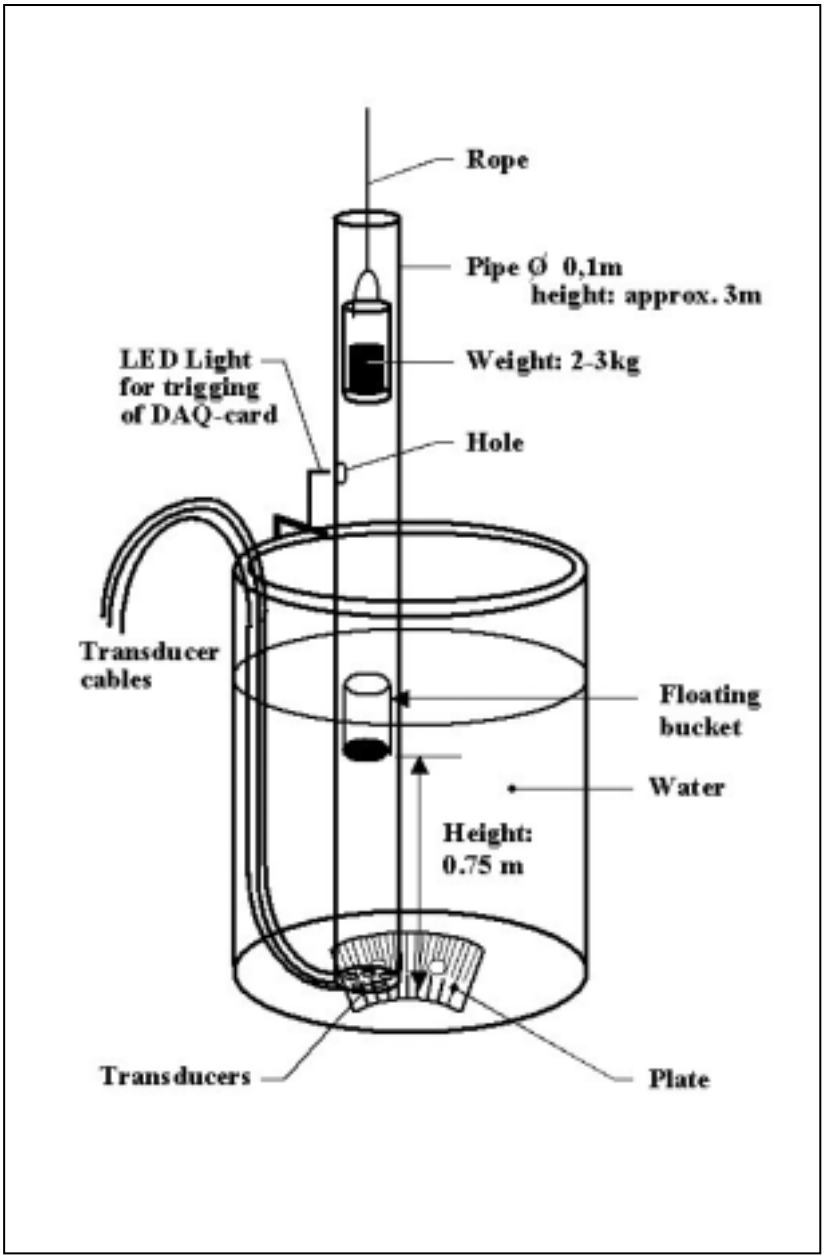

Figure A5: A sketch of the falling weight test rig and the measurement set-up, which should be used to determine the frequency response of the measurement system.

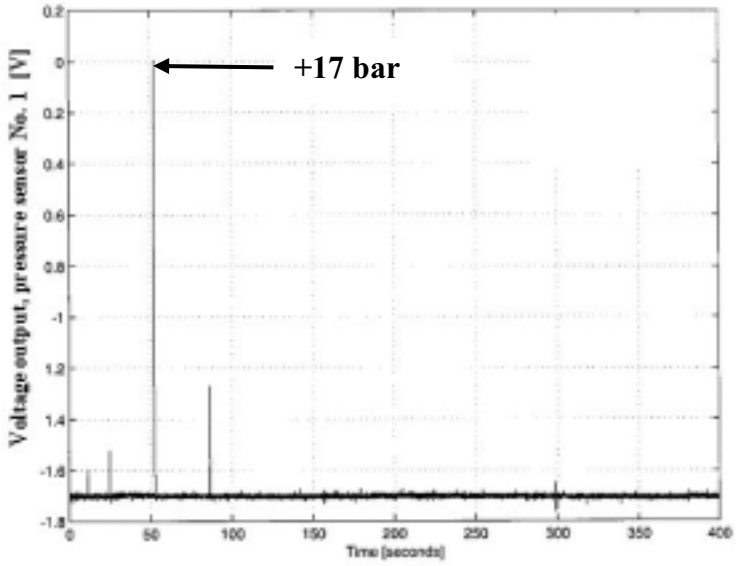

Figure A6: Pressure signals from sensor No. 1 during five drops of the falling weight from different heights in the dynamic-response test.

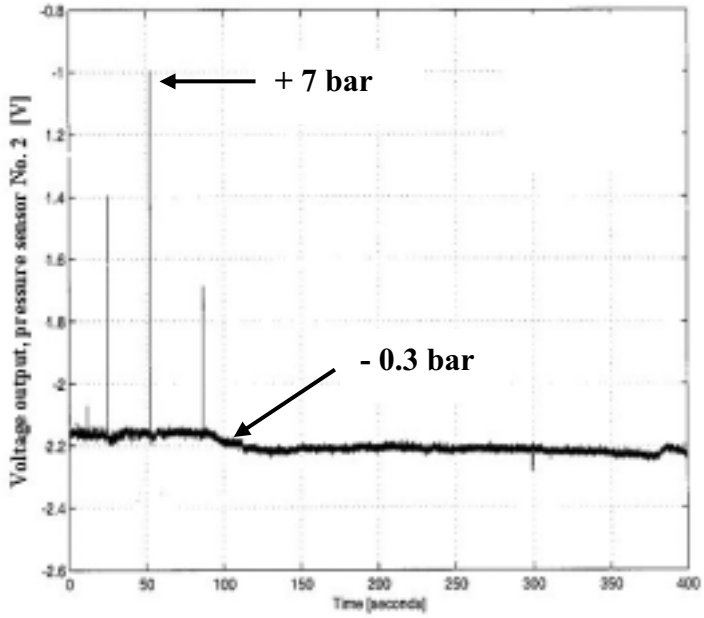

Figure A7: Pressure signals from sensor No. 2 during five drops of the falling weight from different heights in the dynamic-response test.

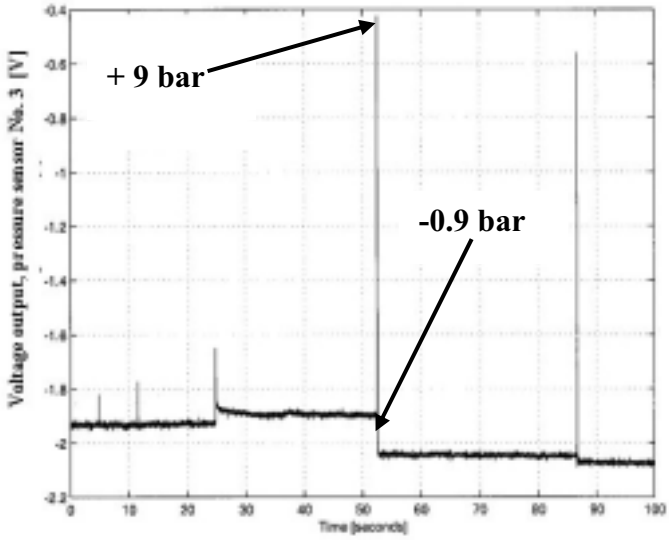

Figure A8: Pressure signals from sensor No. 3, mounted flush to the surface of a bar, during five drops of the falling weight from different heights in the dynamic-response test.

The test rig functioned as expected. The Kulite transducers responded on the falling weight. However, the transducers responded differently in this test. All of the transducers recorded the pressure waves, but at different peak levels. Another observation was that the low level (static pressure) at stable conditions changed during the test period. Especially the signal from one of the transducers, sensor No. 3, fluctuated corresponding to more than 1 bar pressure change as shown in Figure A8. However, sensor No. 1 was very stable as shown in Figure A6. The Presens transducer was also tested. It gave no response during the test. The reason was probably due to the water exposure and the poorly protected connection area for the cable ends.

APPENDIX

B

CALIBRATION TESTS PIEZORESISTIVE SENSOR PILOT REFINER

B.1 Dry heat chamber test

Several temperature response tests were performed in a dry heat chamber (Termax), to investigate the temperature sensitivity data of the transducer. The result from one test shows an increase in temperature from approximately 20 to 125∀C. This is shown in Table B1 and Figure B1. The data were recorded with a sample rate of 10 Sample/s. A calibrated temperature sensor, Digitherm Universal mkIII from Kone-May Instrumentation, Inc., was used to supervise the temperature development.

Table B1: Dry heat chamber test.

Temperature [∀C]	Measurements	
	Temperature [∀C]	**Pressure [bar]**
23	23.7 ∂ 0.35	0.02 ∂ 0.02
50	48.8 ∂ 0.5	0.12 ∂ 0.02
75	75.7 ∂ 0.5	0.08 ∂ 0.02
105	105.2 ∂ 0.5	-0.07 ∂ 0.02
125	124.9 ∂ 0.4	-0.16 ∂ 0.02
Measured sensitivity Original sensitivity	3.15 [mV/∀C] 3.44 [mV/∀C]	3.45 [mV/bar]

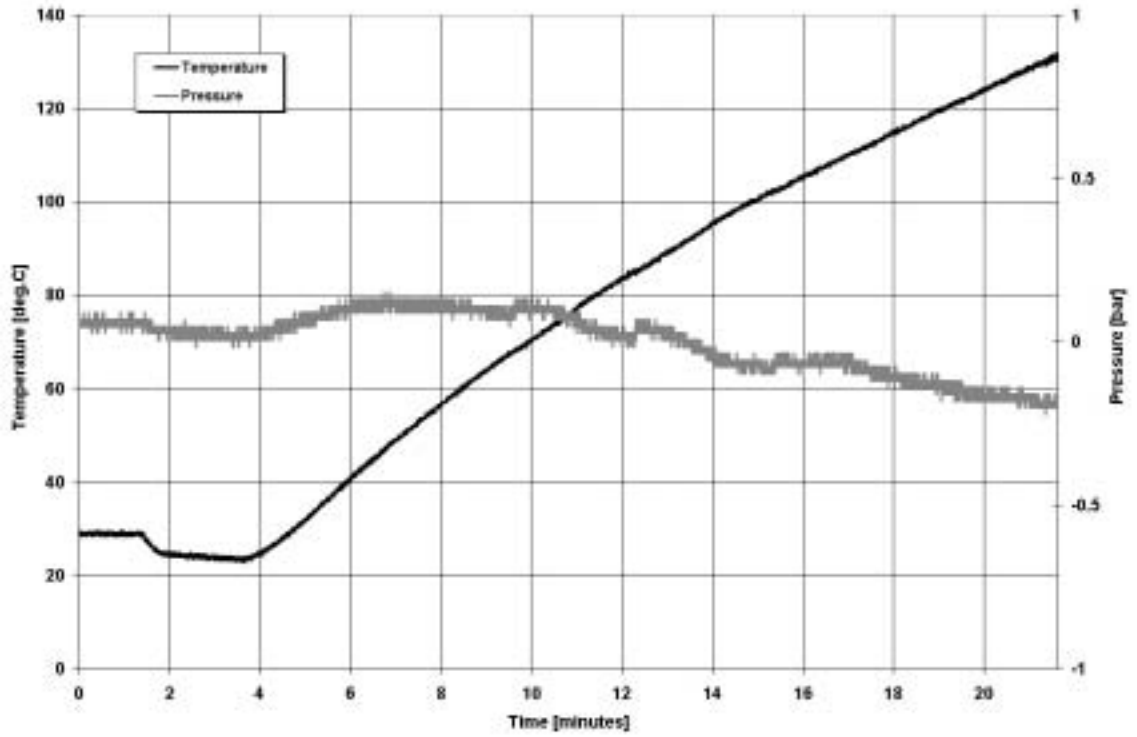

Figure B1: Temperature and pressure data recorded by the combined temperature and pressure transducer, which was used in the pilot-scale experiment. It was captured when a calibration test in a dry heat chamber was performed. Adjusted temperature sensitivity data was used to fit the temperature curve.

B.2 Dynamic-response test

The dynamic-response test was made in the same laboratory test rig as shown in Figure A5. The only differences between this test and the previous test were that the weight was increased to approximately four kilograms and the high-speed data acquisition card was used to measure the response. The result from one of several tests is shown in Figures B2 and B3. The sample rate of the present test was 1 MSamples/s.

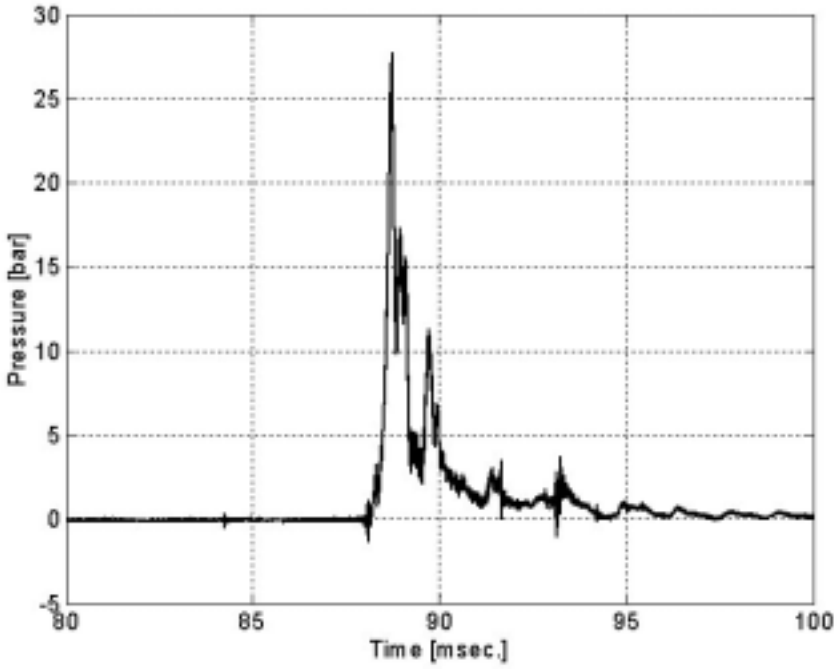

Figure B2: **The pressure response from the transducer, which was used in the pilot-scale experiment, is shown. The response occurred approximately 90 milliseconds after the trigger was activated by the falling weight.**

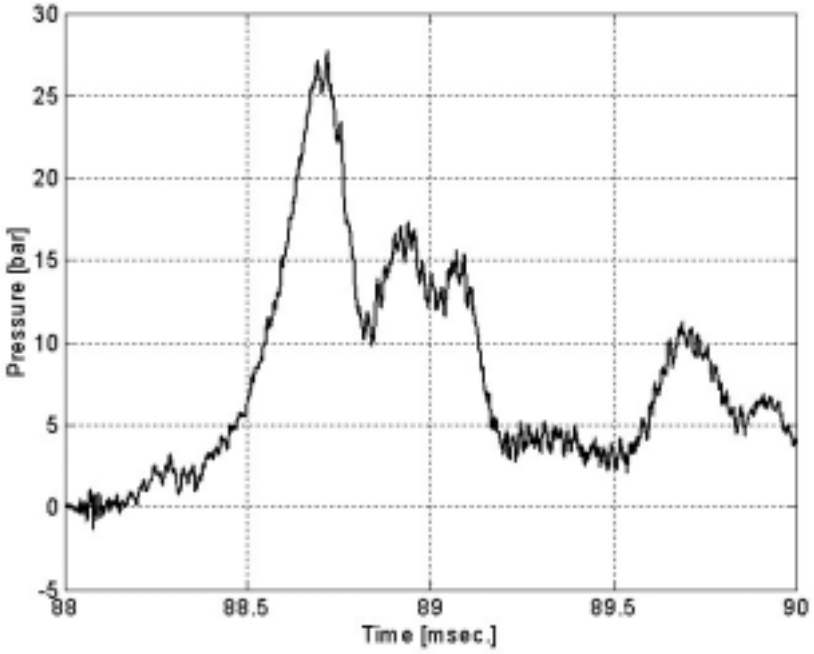

Figure B3: **This is a part of the response curve as shown in Figure B2.**

The result from the dynamic-response test showed that the transducer responded well on the applied pressure wave. The time between the trigger was activated to the response was visible is associated with two different processes. A main part of this time corresponded to the movement of the falling weight before it hit the metallic surface of the floating bucket. The rest of the time corresponded to the wave propagation through the water filled tube and the response time of the measurement system. Without examine the different processes in detail the measurement indicated that the falling weight had a speed of 5-6 m/s, while the wave propagation through the water moved with a speed in the order of 300 to 400 m/s. A pressure wave speed of approximately 1500 m/s could be expected. However, the design of the test rig with a small diameter tube keeping the water closed from the surrounding water in the chest had probably a large damping effect of the pressure wave. This is supported by a similar study reported by Dahlsveen (1999).

The frequency response of the measurement system has not been investigated closely because the response curve indicated that the apparent pure impulse was not as pure as expected. The response time from the pressure readings started to increase to the pressure reached the highest level was too long (0.7 millisecond). Assuming a second order system activated by a pure impulse (Dirac pulse), this gives a low bandwidth in the order of a few kHz. It is assumed that the response time would be shorter under ideal conditions (Dirac pulse), and that the bandwidth of the system was limited by the bandwidth of the amplifier, which was claimed to be 100 kHz by the manufacturer. The natural frequency of the pressure sensor was in the order of 1 MHz. Furthermore, it is claimed that piezoresisitive pressure sensors have a second order transfer function with a small damping ratio. The bandwidth is expected to be high (a few hundred kHz), apart from sensors that have a protecting screen of holes or mesh (below 100 kHz) (Ainsworth *et al.* (2000)). A screen did not protect the present sensor.

Based on the study of the response curves, it is assumed that the test rig was not well fitted for investigations of the dynamic behaviour of the measurement system. Additional effects like reflections from the tube wall probably affected the pressure wave propagation through the water filled tube. Probably, the excitation of a pure pressure wave was not present as well.

APPENDIX

C

CALIBRATION CURVES FIBRE-OPTIC SENSORS

C.1 Sensor No. 1

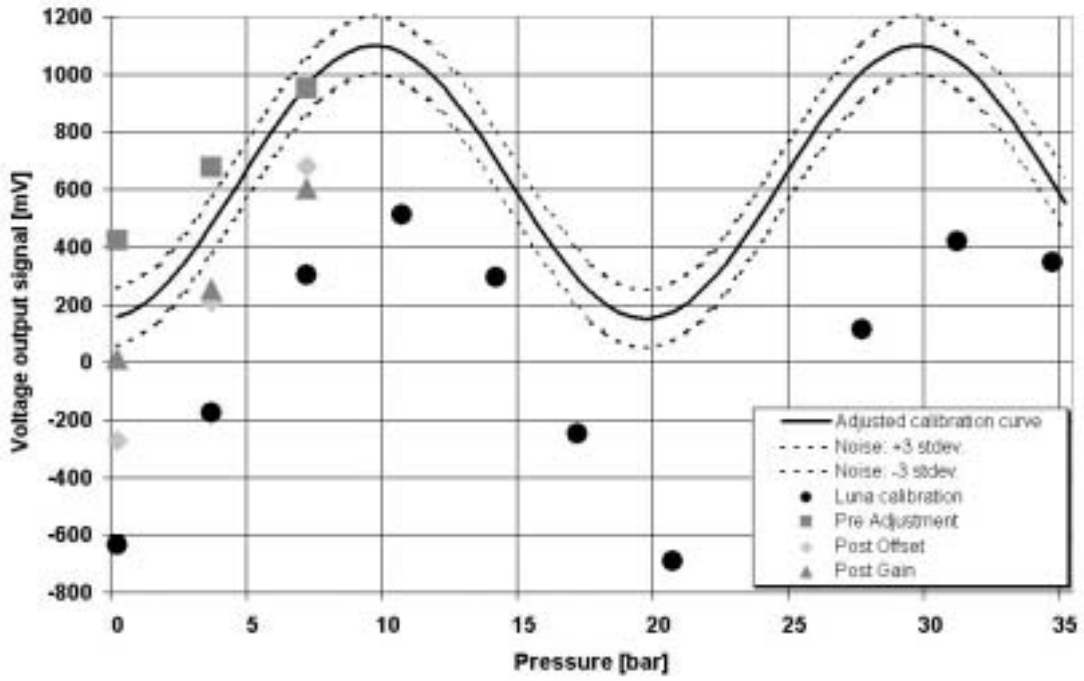

Figure C1: Calibration curves obtained for sensor No. 1.

URN:NBN:no-6437

C.2 Sensor No. 2

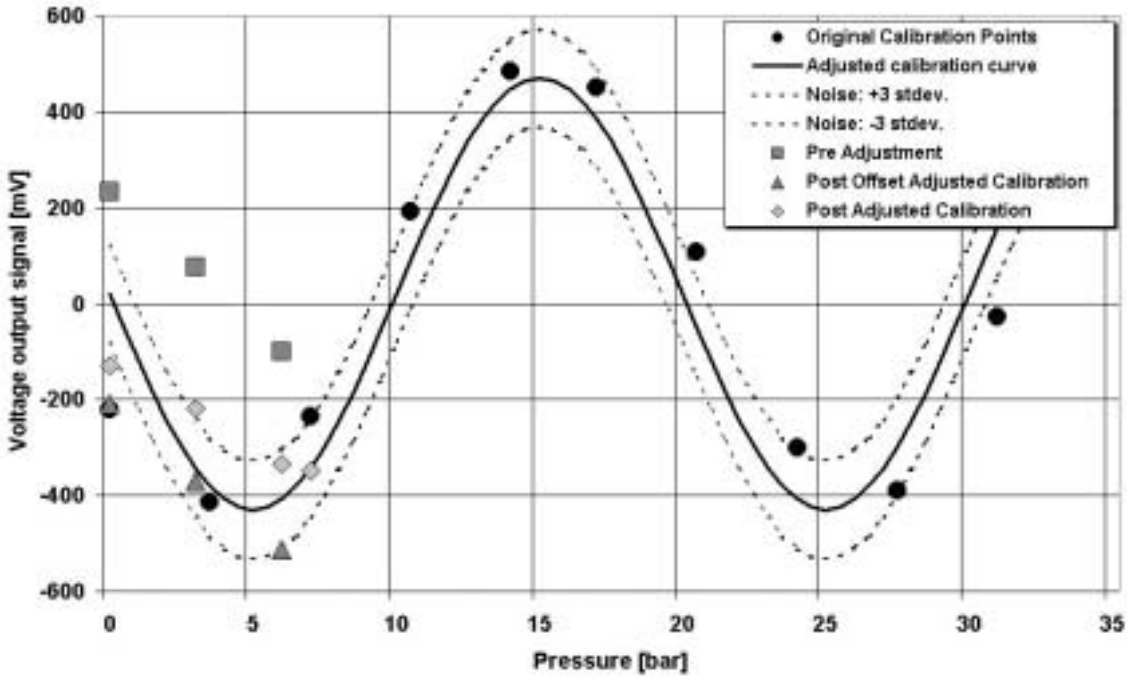

Figure C2: Calibration curves obtained for sensor No. 2.

C.3 Sensor No. 7

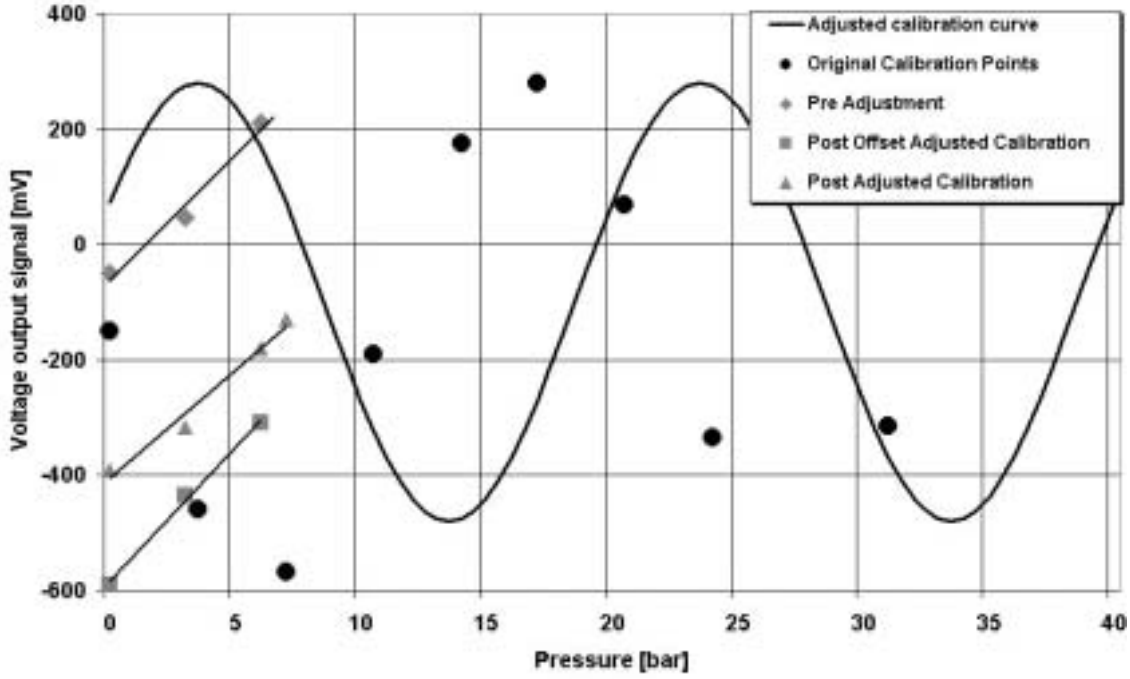

Figure C3: Calibration curves obtained for sensor No. 7.

C.4 Sensor No. 4

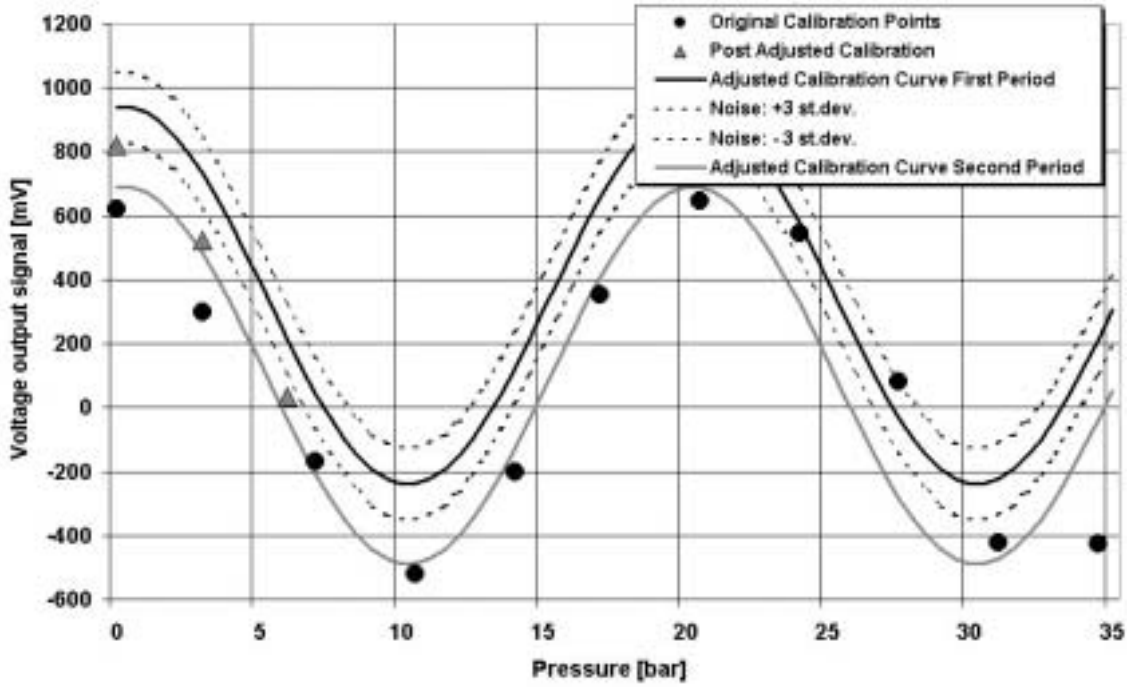

Figure C4: Calibration curves obtained for sensor No. 4.

C.5 Sensor No. 5

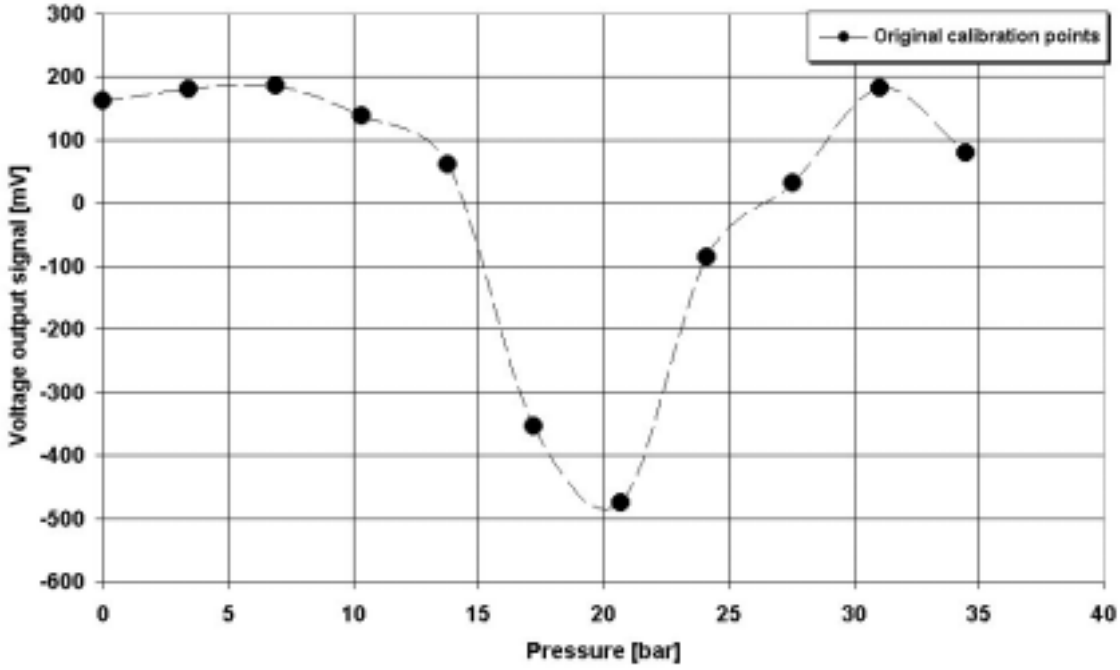

Figure C5: Calibration curves obtained for sensor No. 5.

URN:NBN:no-6437

C.6 Sensor No. 6

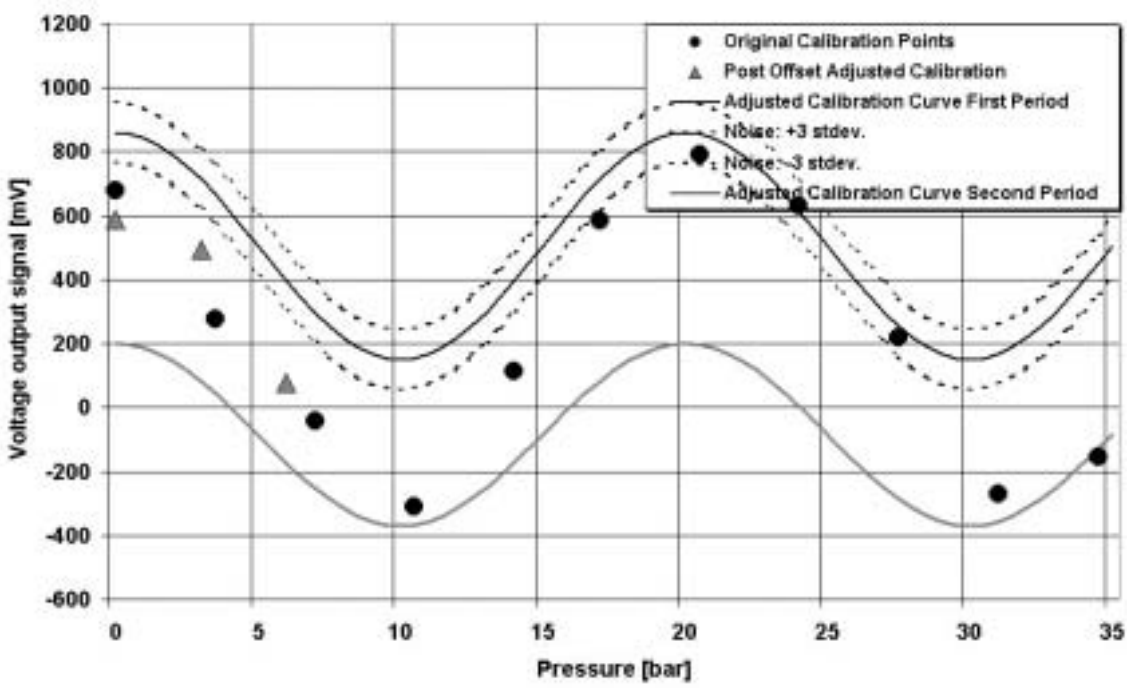

Figure C6: Calibration curves obtained for sensor No. 6.

C.7 Sensor No. 8

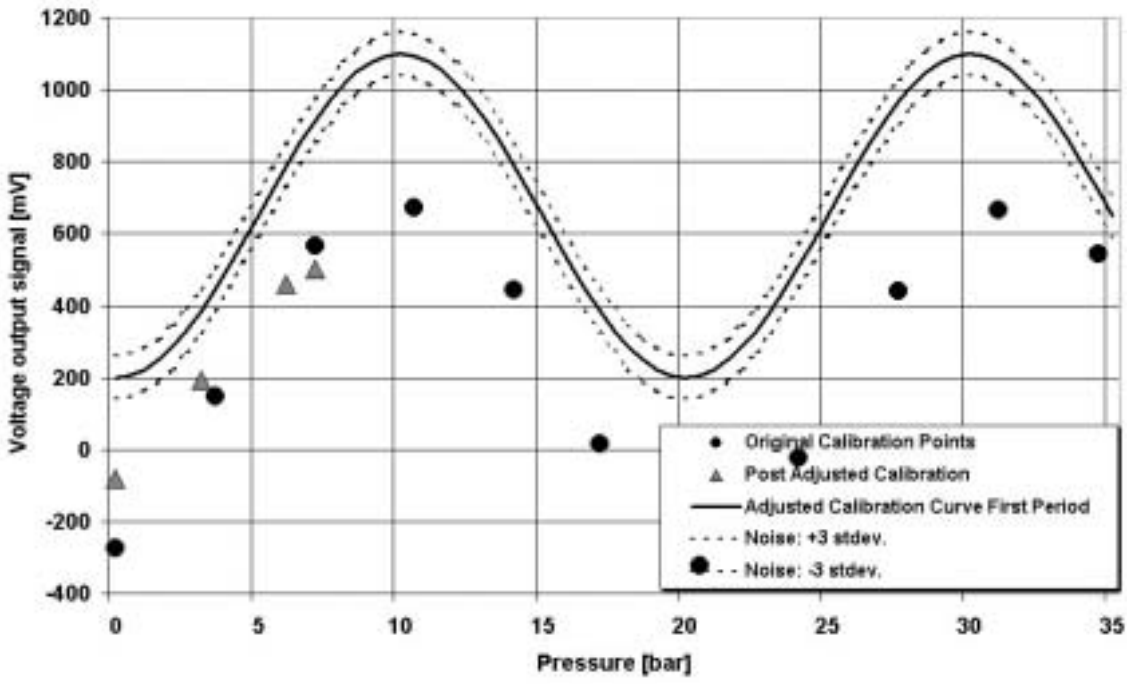

Figure C7: Calibration curves obtained for sensor No. 8.

URN:NBN:no-6437

C.8 Sensor No. 9

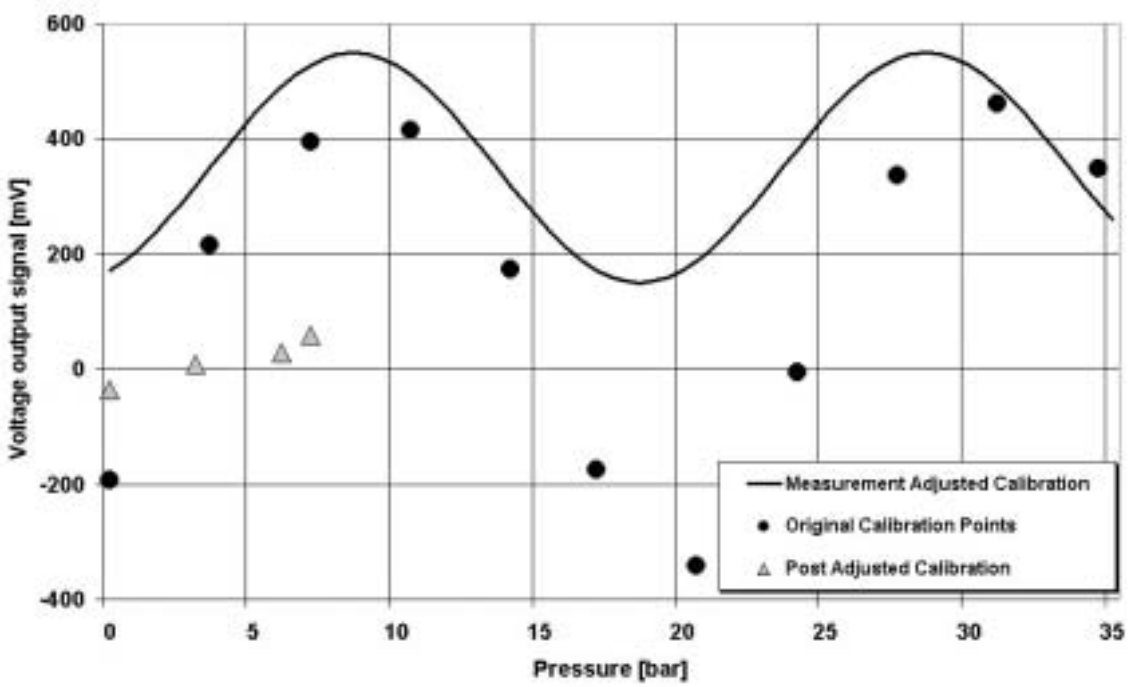

Figure C8: Calibration curves obtained for sensor No. 9.

APPENDIX

D

CALIBRATION TESTS EXTERNAL ACCELEROMETERS

D.1 Brüel & Kjær 4384 - 1390386

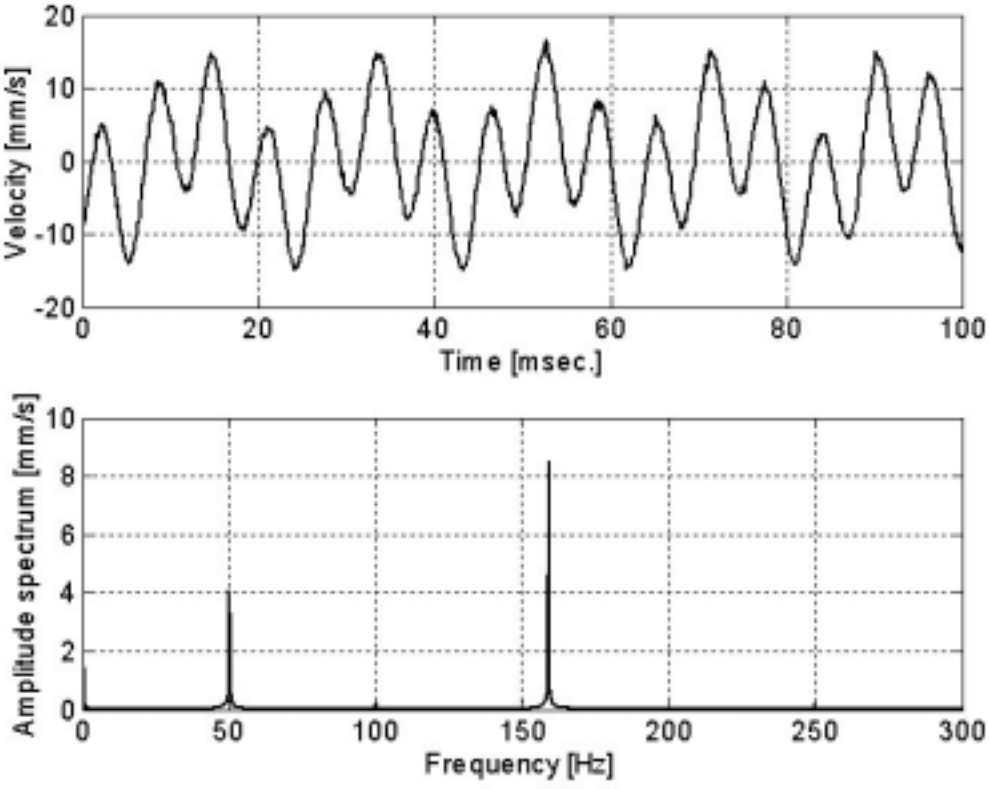

Figure D1: Calibration curves obtained for accelerometer No. 1.

URN:NBN:no-6437

D.2 Brüel & Kjær 4384 - 1390387

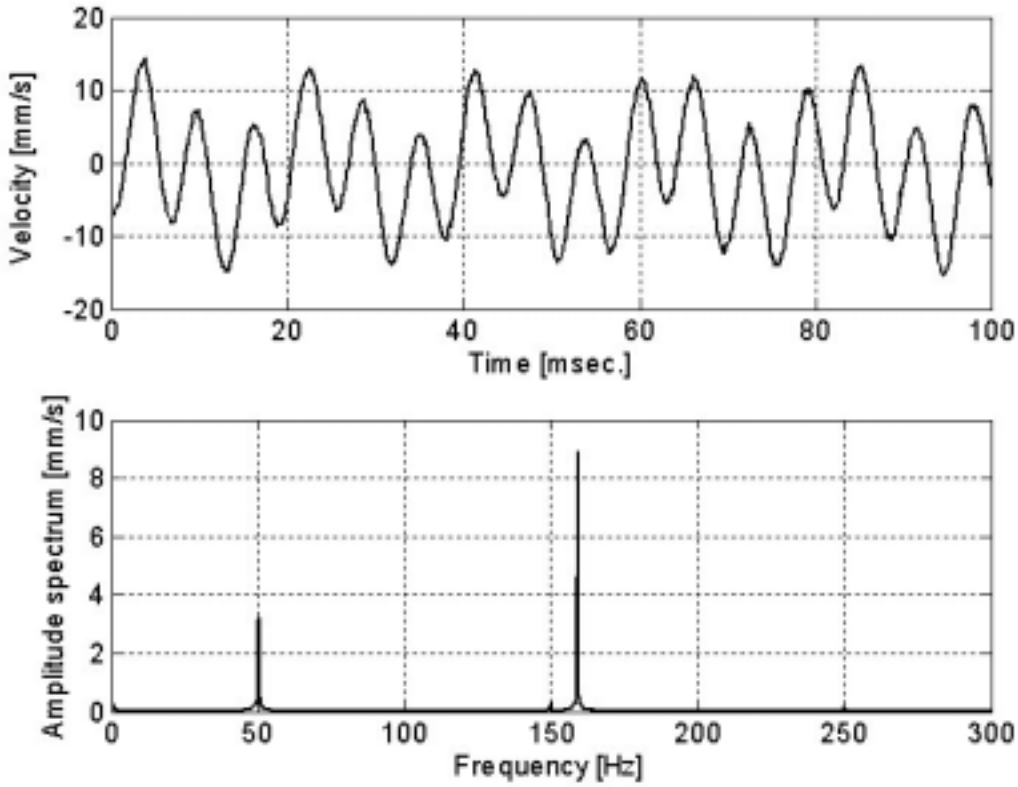

Figure D2: Calibration curves obtained for accelerometer No. 2.

URN:NBN:no-6437

APPENDIX

E

FACTORIAL DESIGNED EXPERIMENT

E.1 Central composite design

The design shown in Table 3.6a shows the experimental conditions chosen for the four manipulated process variables. It is a second order composite design in coded variables. The coded levels are obtained by the relationship between the real levels as shown in Table 3.6b and the difference between them. Second order design is valuable when checking for curvature in the response surface. This second order design comprises of the following parts:

- Cube points: 16 runs given by a 2^4 factorial design (first order).
- Star or axial points: 8 runs given by 2 runs per variable (second order).
- Centre points: 6 runs (4 runs related to the cube and 2 runs related to the star).

Basic features with the design are the choice of the levels of the manipulated variables and the incorporation of the centre points. These features can be explained in the following manner:

- The design is orthogonal (the sum of the multiplication of the levels of all the variables at each run is zero). This ensures that the regression coefficients are uncorrelated. It gives greater precision of the estimates of the coefficients i.e. the confidence intervals are smaller than for non-orthogonal designs.
- The axial points are face centred i.e. their levels (positions) are lying at the cube points. However, to ensure proper rotability they should have been spherically distributed about the designs origin. For this design their levels should have been 2 according to the coded variables. The face centred value is an appropriate choice when the cube points are at the operational limits of the process. Rotability provides the desirable property of constant variance at all points that are equidistant from the design centre. In addition, the axial points give efficient estimates of the quadratic terms in a second order model.
- Centre point responses are valuable to estimate the error variance independent of the model. This is ensured if the centre points are genuine replicates made at an identical set of manipulated variables. With genuine replicates means that they are run in randomised order such that they are subjected to all the sources of error that beset runs made at different conditions.

The experimental set-up was organized in randomized order as shown in Chapter 6, Table 6.8 as opposed to the standard order design shown in Table 3.6a. Randomizing avoids correlated errors between the recordings.

E.2 Analysis techniques

The results of the analysis of the central composite design are comparable with results from regression analysis. The factorial analysis gives the effect, average difference in response, when the manipulating variable is changed from the low level to the high level. However, the regression analysis shows the change of the response variable for one unit change of the manipulated variables.

The central composite designed experiment could be analysed using response surface methodology as briefly described next:

- The factorial part (run 1-20) as a first order system allowing the mean, the main effects and interaction effects to be calculated in addition to the variance given from the replicated centre points runs. These effects are shown in Equation (E-1) – (E-5):

  Mean:

  $$\hat{E}_M = \bar{y} \qquad \text{(E-1)}$$

  $\bar{y}$: Average of all the response values.

  Main effect:

  $$\hat{E}_{Xi} = \bar{y}_{Xi2} - \bar{y}_{Xi4} \qquad \text{(E-2)}$$

  X_i : Manipulating variable No. i.

  y_{xi+} : Average of the response values from the runs where the refiner was operated at the high level of the manipulated variables.

  y_{xi-} : Average of the response values from the runs where the refiner was operated at the low level of the manipulating variable.

  Interaction effect:

  $$\hat{E}_{X1\Delta X2} = \bar{y}_{(X1\Delta X2)2} - \bar{y}_{(X1\Delta X2)4} \qquad \text{(E-3)}$$

  $y_{x1\,x2+}$: Average of the response values corresponding to the high level derived from the multiplication of the coded variables *x1* and *x2*.

  $y_{x1\,x2-}$: Average of the response values corresponding to the low level derived from the multiplication of the coded variables *x1* and *x2*.

Sample variance:

$$\hat{\omega}_y^2 = \frac{\sum_{i=1}^{n} (y_{CPi} - \bar{y}_{CP})}{(n-1)} \qquad \text{(E-4)}$$

CP : centre points (replicated runs).
n : the number of replicated runs.

Variance of each effect:

$$\hat{\omega}_E^2 = \frac{4 \cdot \hat{\omega}_y^2}{N} \qquad \text{(E-5)}$$

N : the number of runs in the factorial (first order) design.

The axial points (run 21-30) determine the second order terms. In addition, they can be used in an extended determination of the sample variance through a pooled estimate of the variances obtained for the replicated runs in each of the periods denoted cube and star.

APPENDIX

F

ADDITIONAL RESULTS MILL-SCALE EXPERIMENT FIBRE-OPTIC SENSORS

F.1 Initial chip feeding

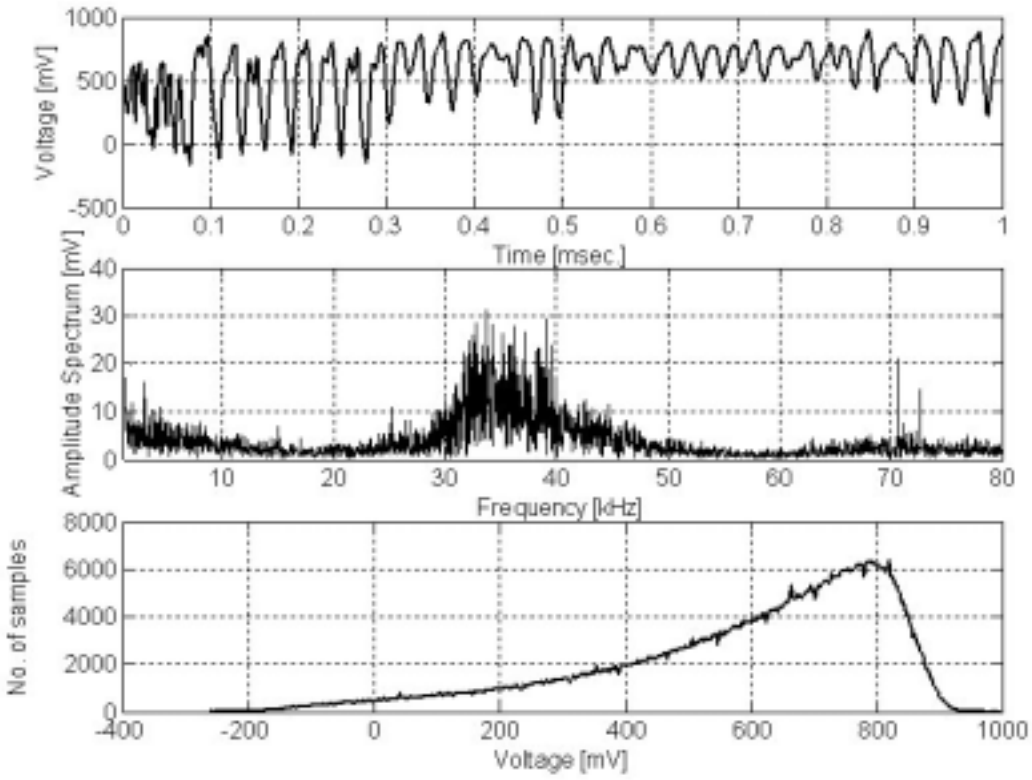

Figure F1: **Voltage output signal from Sensor No. 4 captured between 110 and 112 seconds of the recording shown in Figure 6.3.**

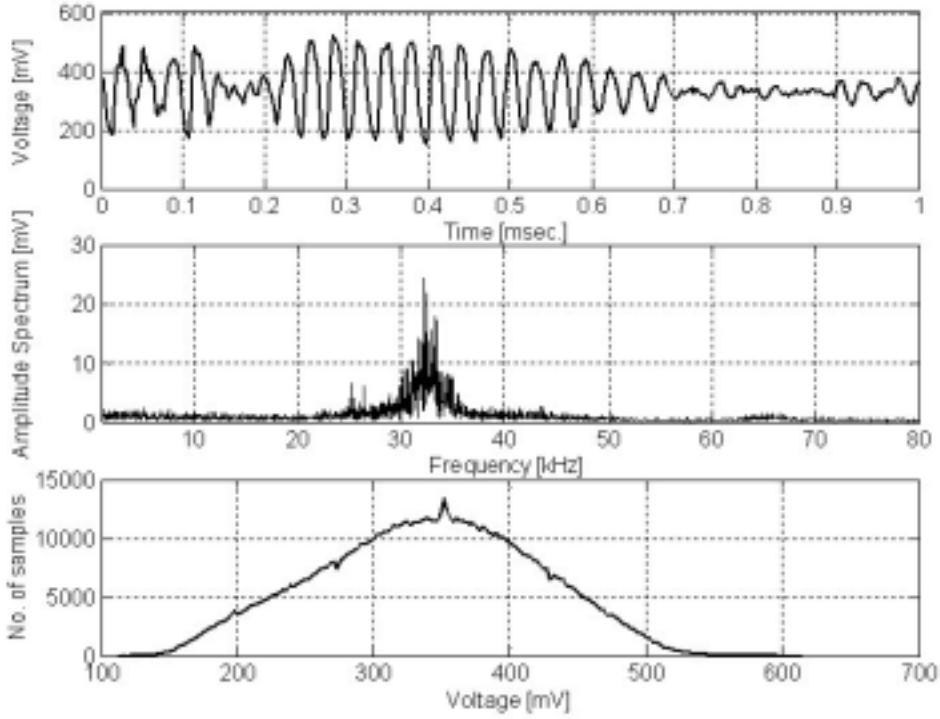

Figure F2: Voltage output signal from Sensor No. 9 captured between 110 and 112 seconds of the recording shown in Figure 6.3.

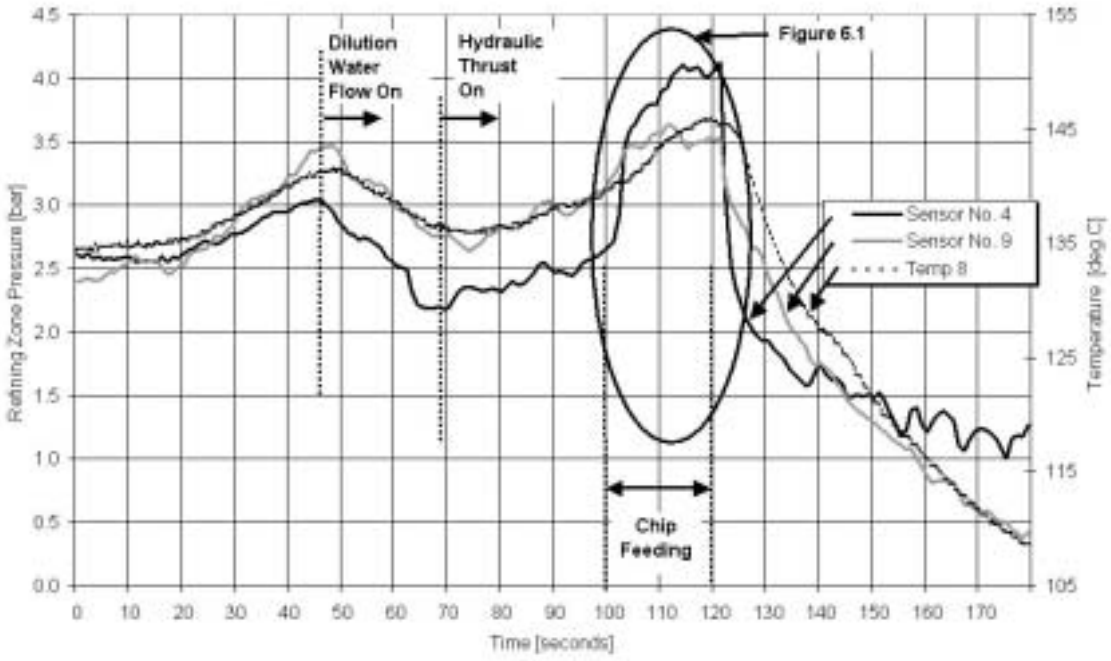

Figure F3: Pressures from by sensor No. 4 and No. 9 as shown in Figure 6.3, are shown together with the signal from temperature sensor No. 8 (DS).

F.2 Recalibration of sensor signals - noise

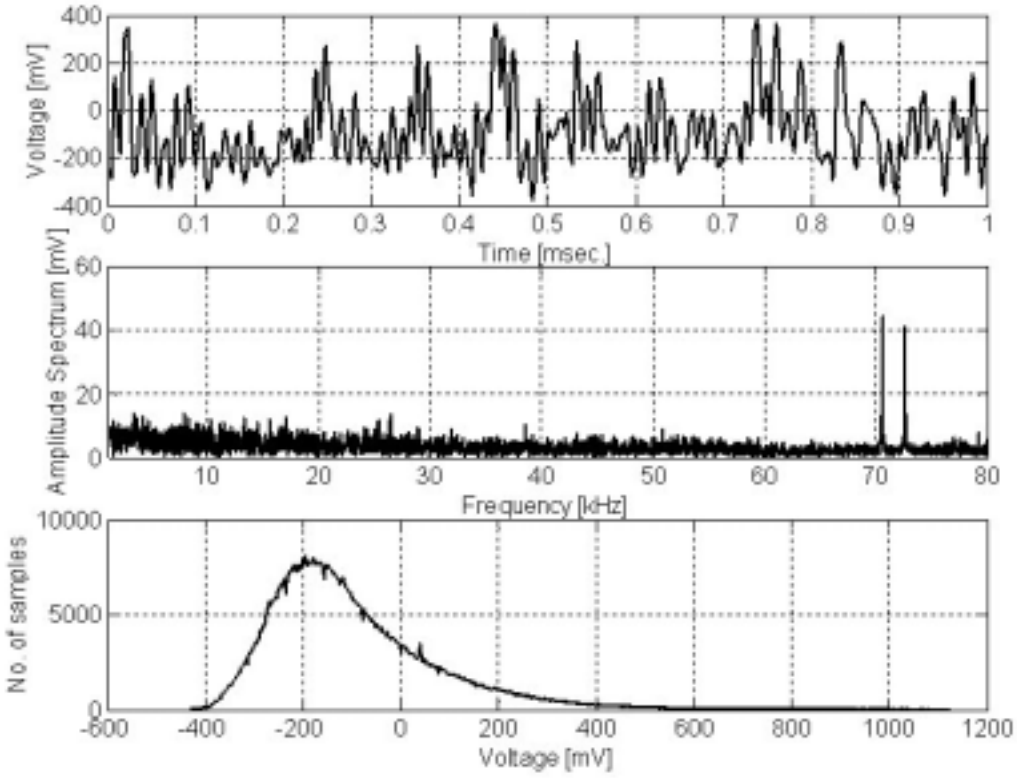

Figure F4: Voltage output signal from Sensor No. 4 captured as run No. 30 in the first experimental period is shown. The periodicity in the recording was dominated by noise frequencies at 70.6 and 72.6 kHz.

F.3 Normalization of histograms

Normalization of the histograms corresponding to the recordings from the fibre-optic sensor has been tested. This analysis was made to assess the shape of the histogram of the output signals. The distortion of the pressure signal through the sinusoidal transfer function curve should be accounted. Normalization accounts for the sinusoidal shape and straighten out the response curve. The following steps were performed:

- The ordinary histogram was normalized such that the sum of all the values in the re-arranged histogram was equal to one. In other words, the histogram was re-arranged to an approximate probability mass function (pmf).
- A normalized histogram, probability mass function, of a pure sine wave (sinusoidal transfer function curve) was made based on the recalibrated data of the sinusoidal transfer function of the selected sensor. This histogram was assigned the same resolution (number of bins, equal to mainly one LSB) as the histogram of the recordings.

- The two normalized curves with the same voltage resolution and the same total area were divided (one value of the histogram of the recordings divided by the corresponding value of the sinusoidal based histogram).

The result from this procedure was expected to be a normalized histogram (pmf) of a signal that had a linear transfer function. One example is given in Figure F5. A pronounced saddle shaped histogram could be expected to occur from a signal that crossed both the maximum and minimum points of the sinusoidal calibration curve. However, an extremely periodic signal would also give a saddle shaped histogram. Through considering the changed shape of the normalized histogram compared to the original histogram, it was assumed that the number of samples that could have crossed a maximum or minimum point of the calibration curve could be determined. However, the offsets regarding the calibration of the sensors made it difficult to exactly determine the calibration curve. Further discussions about this analysis were therefore ended.

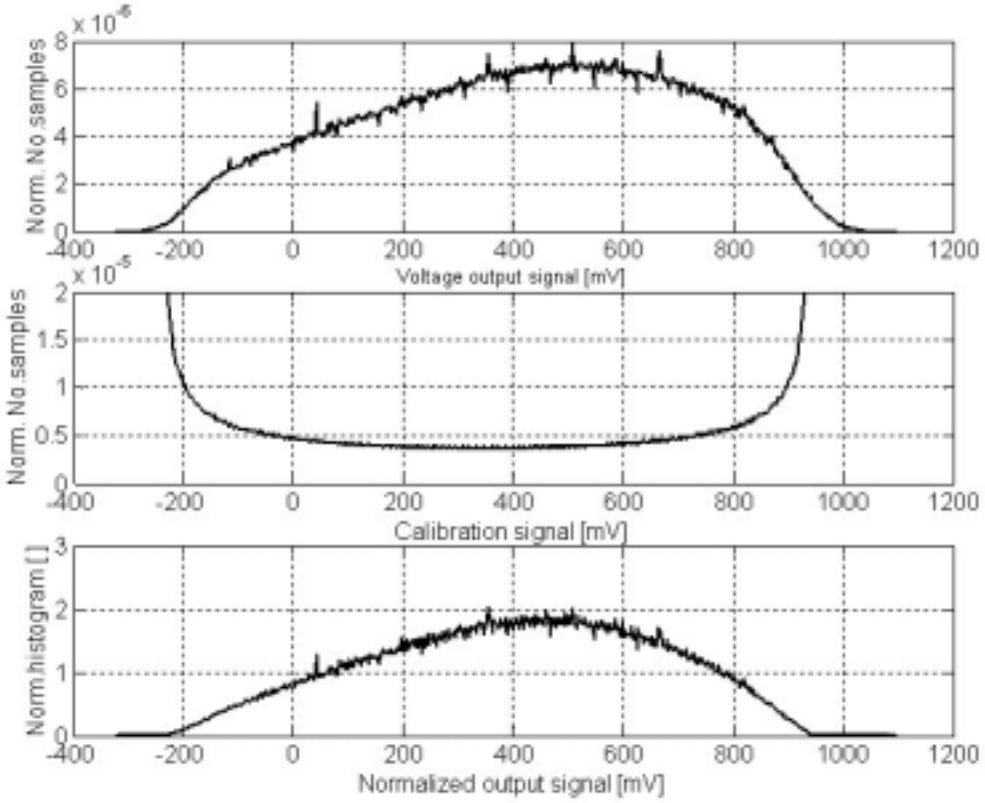

Figure F5: Normalized histogram of the recording from Sensor No. 4 shown in Figure 6.10. The histogram representing the sinusoidal calibration curve, plot in the middle, is based on data from Table 6.6.

F.4 Recalibration of sensor signals – selection of flange

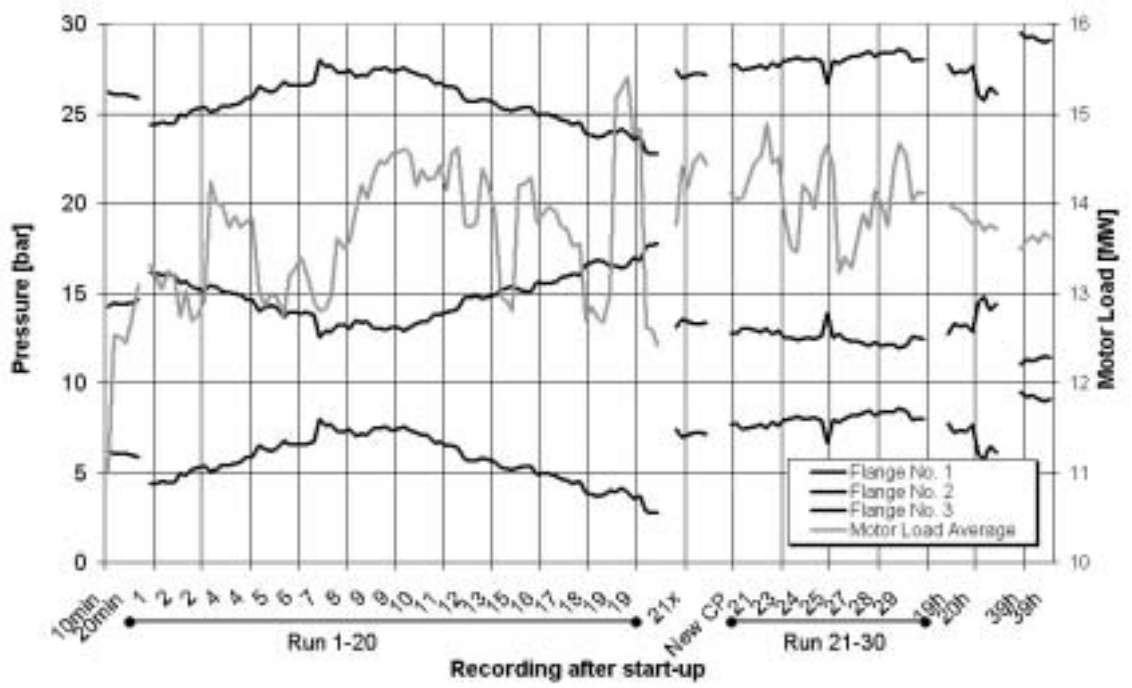

Figure F6: **Average values from recordings performed by sensor No. 4 converted to pressure through three different flanges of the sinusoidal calibration curve are shown together with corresponding recordings from the motor load.**

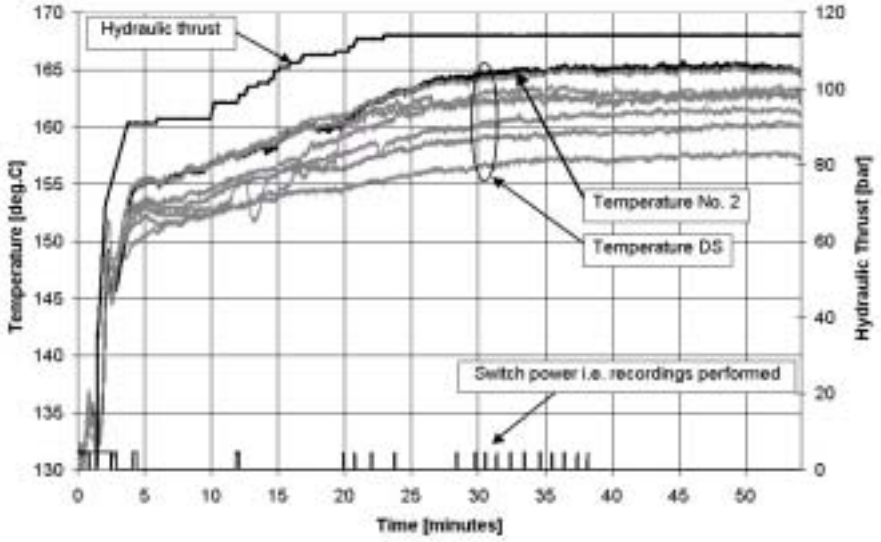

Figure F7: **Temperature readings captured from the drive side during a production start-up are shown together with corresponding data from the hydraulic thrust and the power switch. The latter shows when the pressure recordings were performed.**

F.5 Responses of the factorial designed experiment

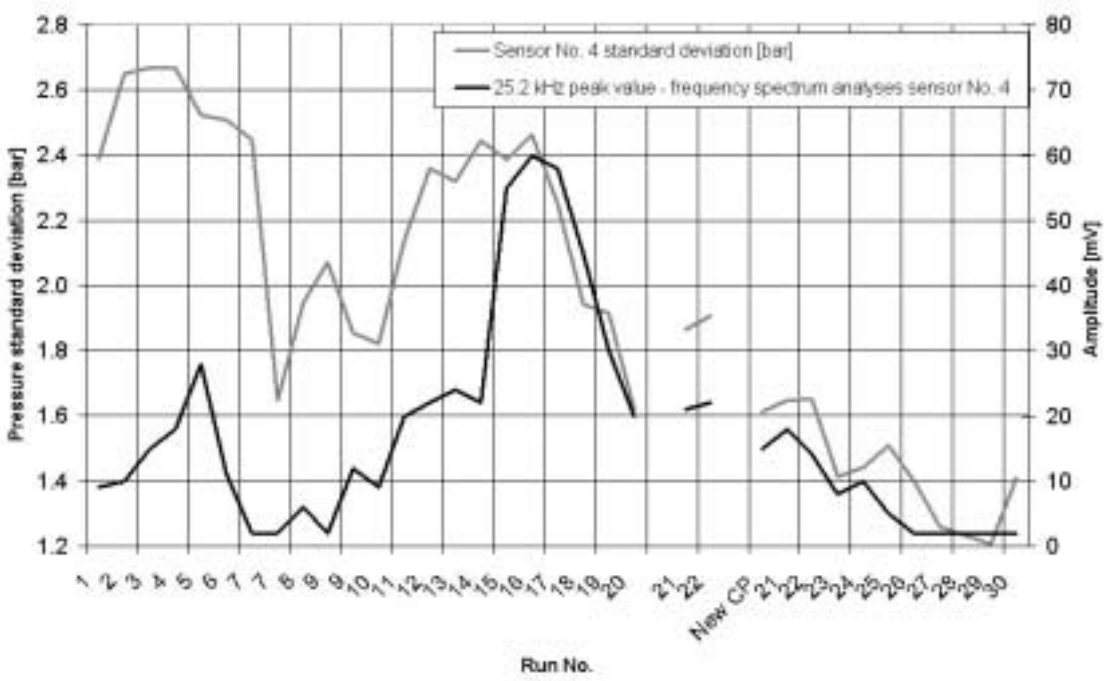

Figure F8: **The development of the peak frequency at 25.2 kHz appearing from recordings captured by sensor No. 4 is shown. Frequency analyses were performed on data sets from the factorial designed experiment.**

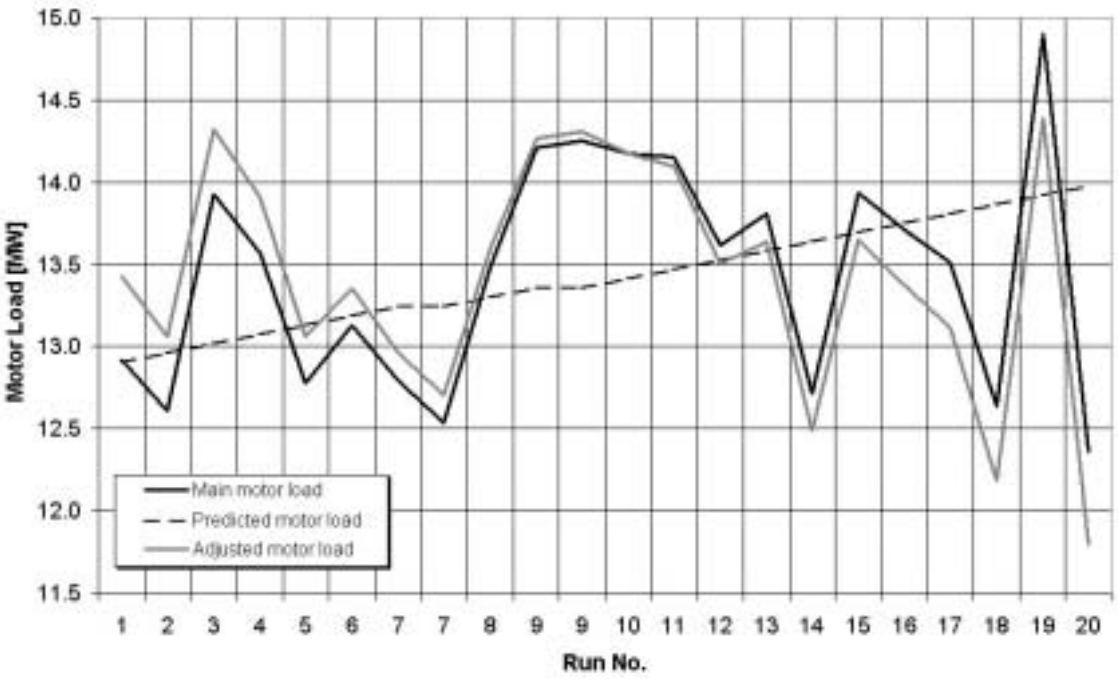

Figure F9: **The adjusted motor load values due to the trend revealed in Figures 6.46 and 6.47 are shown.**

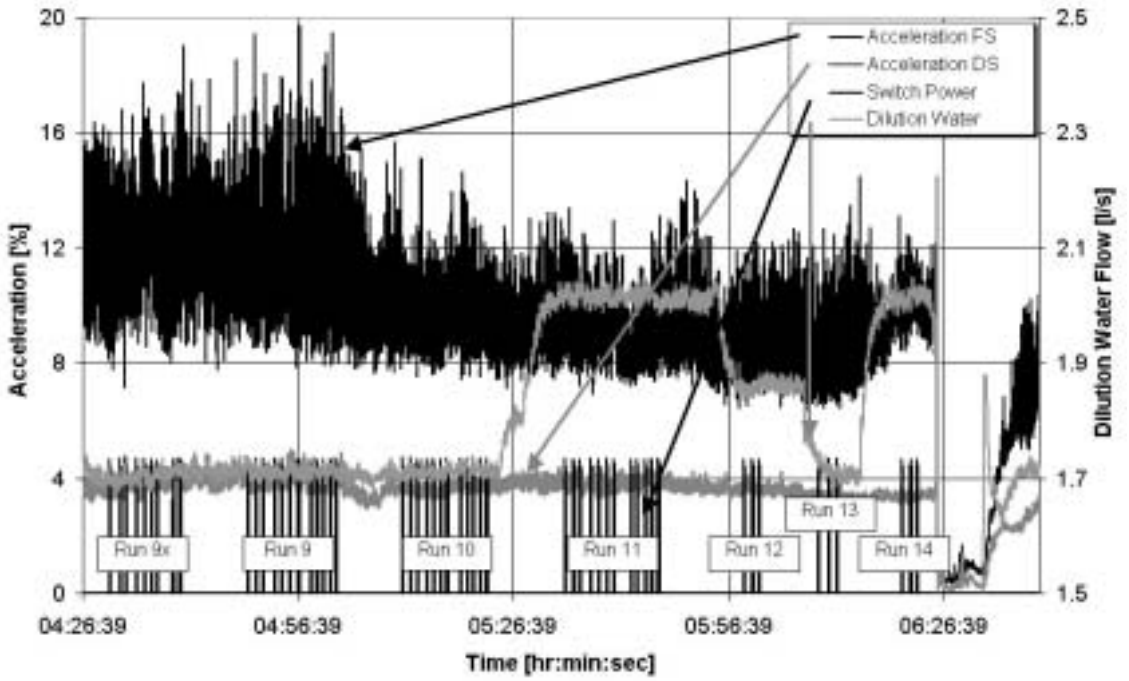

Figure F10: The raw data readings from the acceleration measured on the front side during run No. 9, are shown together with the acceleration measured on the drive side and the dilution water flow rate and the switch power.

F.6 Chip-stream splitter test

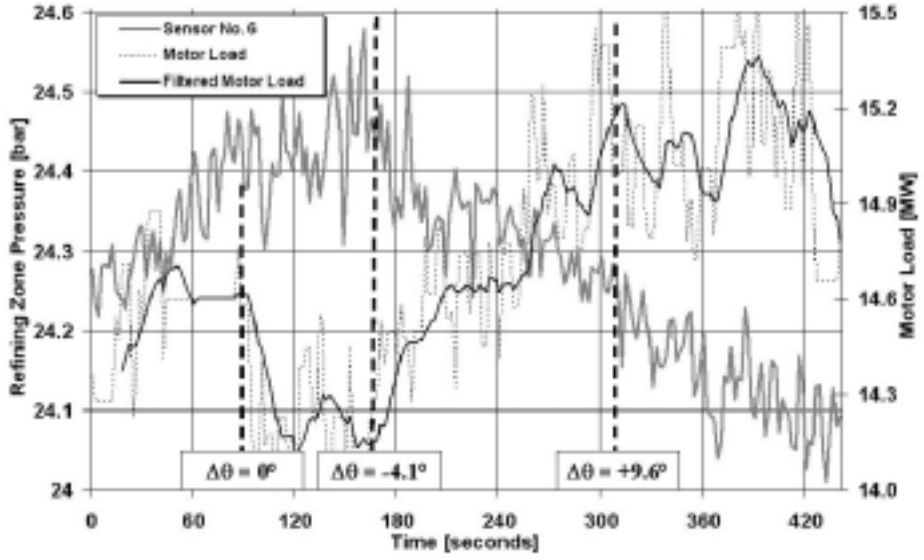

Figure F.11: The average pressure data from sensor No. 6, converted through the third flange of the calibration curve and the motor load.

F.7 Time fluctuations of the rotational speed

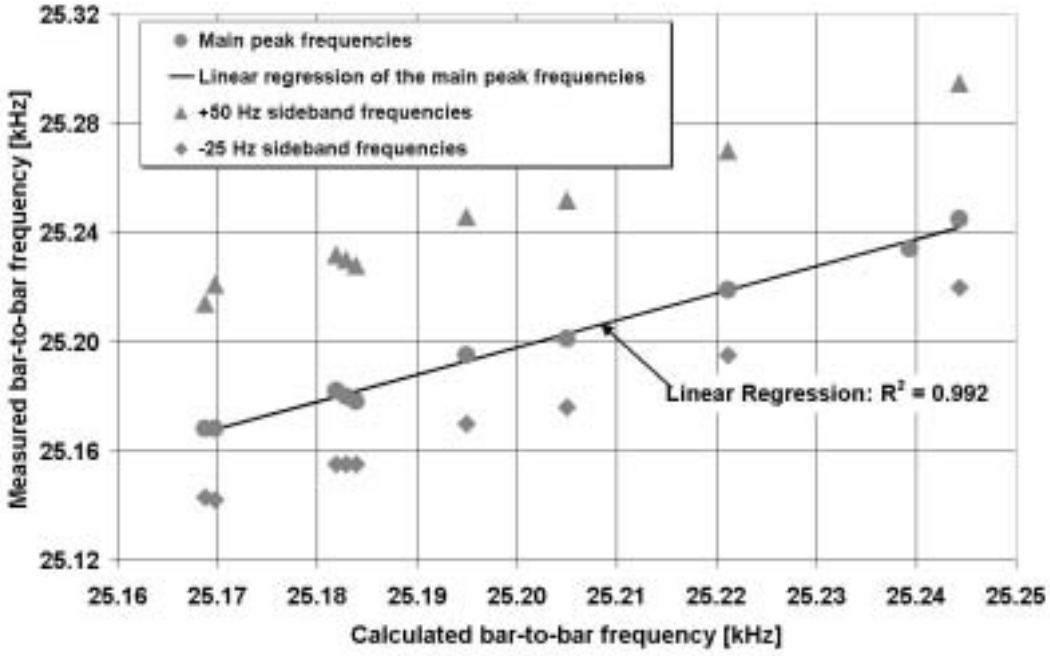

Figure F12: The correlation between the calculated and the measured bar crossing frequency of 25.2 kHz at the location of sensor No. 4 was high.

APPENDIX G

PICTURES OF THE REPLACED PLATE AND SENSOR HOLES

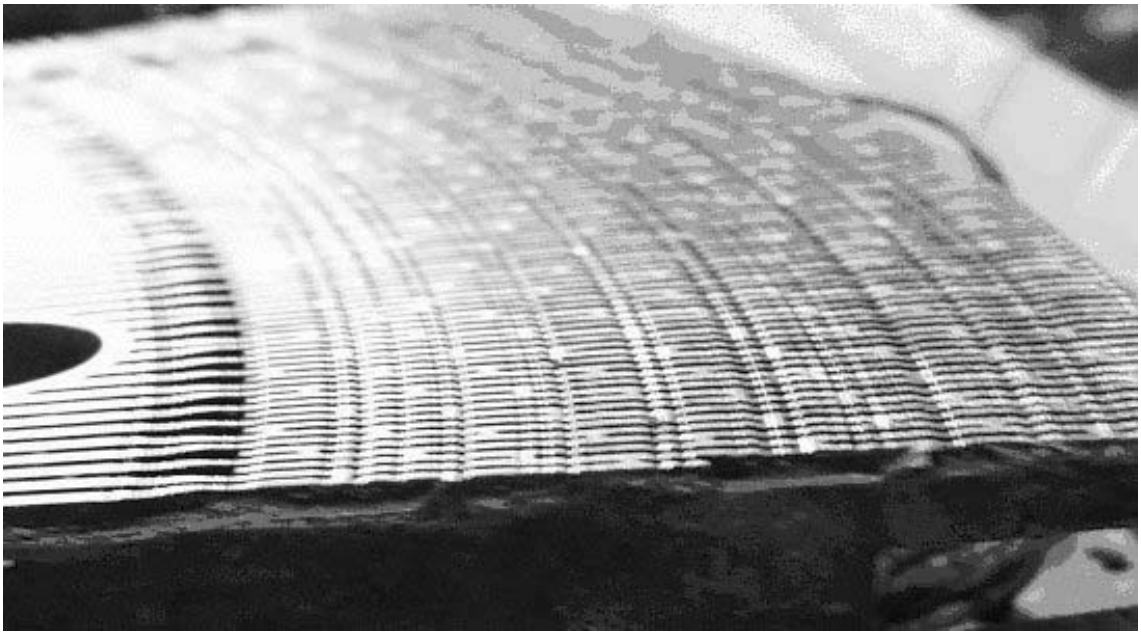

Figure G1: **The replaced plate containing the fibre-optic sensors is shown. The serration wear pattern is clearly visible after approximately 1700 working hours.**

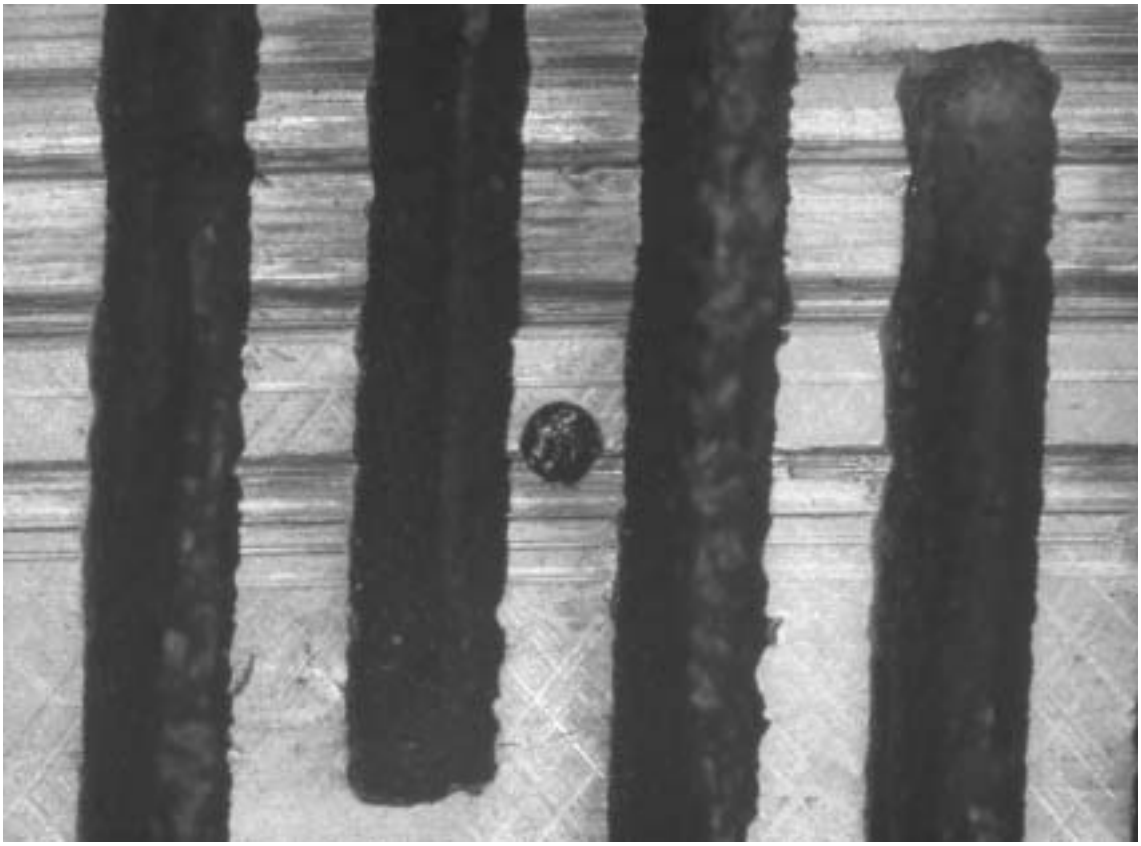

Figure G2: Sensor No. 9 was installed in this hole in one bar in the fine bar zone. The wear across the hole is clearly visible as shown in Figure G3 too.

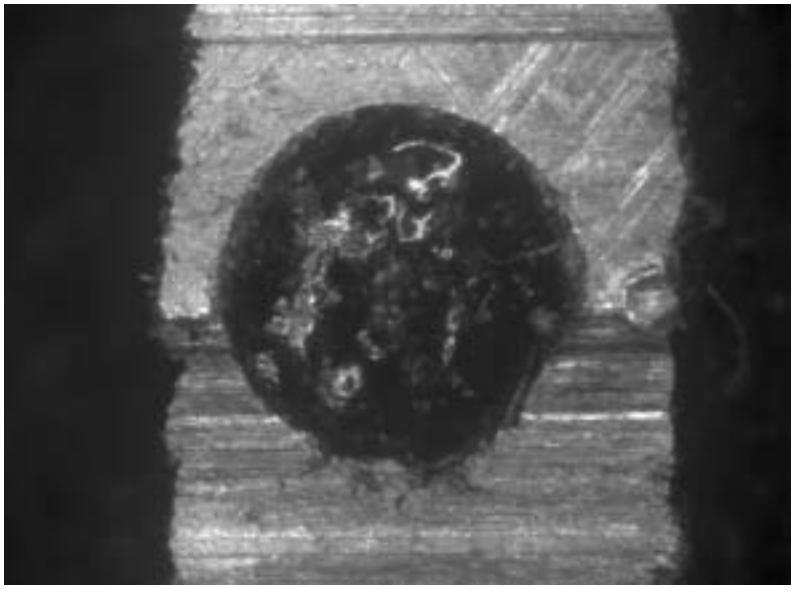

Figure G3: The wear across the hole where sensor No. 9 was mounted is shown. In addition, it was revealed that carbonised material filled the hole.

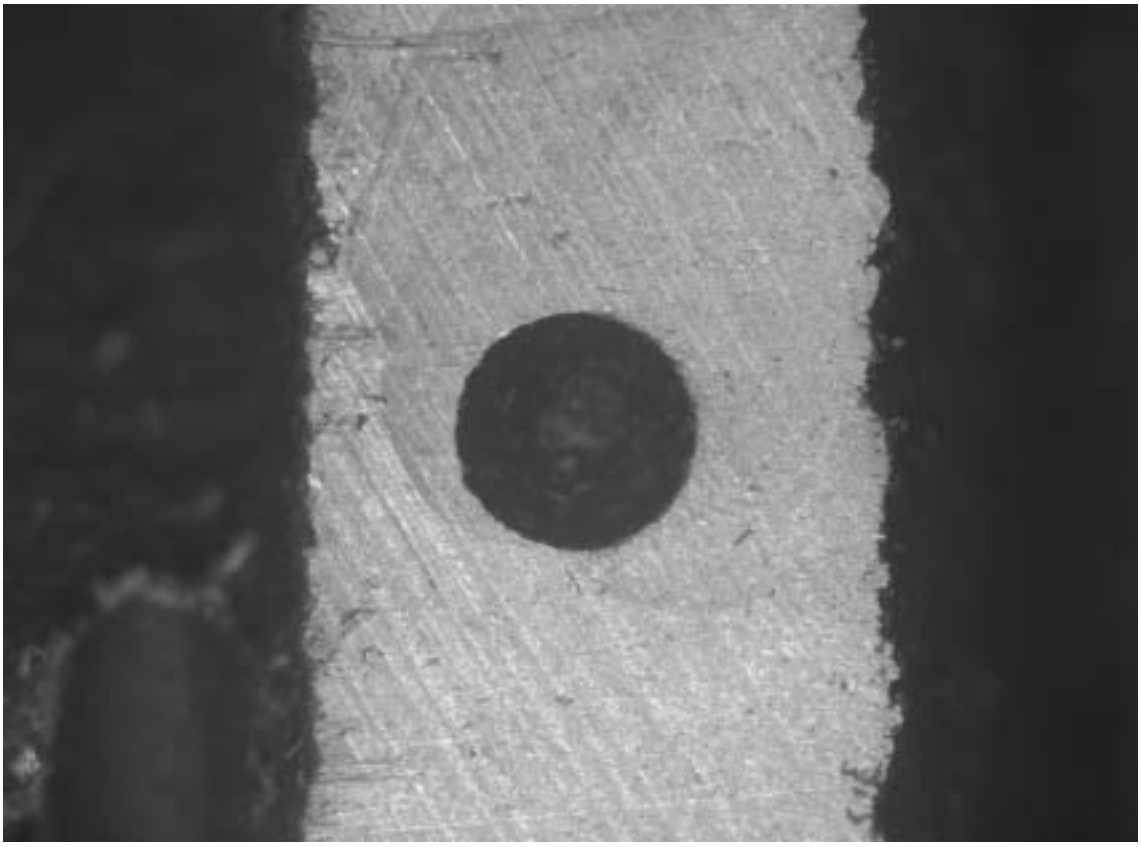

Figure G4: The wear around the holes located in the intermediate zone was almost absent. Here is one of the five holes in the intermediate zone shown after the plate was replaced.